CHAPTER 1
INTRODUCTION

1.1 GEOTECHNICAL EARTHQUAKE ENGINEERING

Geotechnical earthquake engineering can be defined as that subspecialty within the field of geotechnical engineering which deals with the design and construction of projects in order to resist the effects of earthquakes. Geotechnical earthquake engineering requires an understanding of basic geotechnical principles as well as geology, seismology, and earthquake engineering. In a broad sense, *seismology* can be defined as the study of earthquakes. This would include the internal behavior of the earth and the nature of seismic waves generated by the earthquake.

The first step in geotechnical earthquake engineering is often to determine the dynamic loading from the anticipated earthquake (the anticipated earthquake is also known as the *design earthquake*). For the analysis of earthquakes, the types of activities that may need to be performed by the geotechnical engineer include the following:

- Investigating the possibility of liquefaction at the site (Chap. 6). Liquefaction can cause a complete loss of the soil's shear strength, which could result in a bearing capacity failure, excessive settlement, or slope movement.
- Calculating the settlement of the structure caused by the anticipated earthquake (Chap. 7).
- Checking the design parameters for the foundation, such as the bearing capacity and allowable soil bearing pressures, to make sure that the foundation does not suffer a bearing capacity failure during the anticipated earthquake (Chap. 8).
- Investigating the stability of slopes for the additional forces imposed during the design earthquake. In addition, the lateral deformation of the slope during the anticipated earthquake may need to be calculated (Chap. 9).
- Evaluating the effect of the design earthquake on the stability of retaining walls (Chap. 10).
- Analyzing other possible earthquake effects, such as surface faulting and resonance of the structure (Chap. 11).
- Developing site improvement techniques to mitigate the effects of the anticipated earthquake. Examples include ground stabilization and groundwater control (Chap. 12).
- Determining the type of foundation, such as a shallow or deep foundation, that is best suited for resisting the effects of the design earthquake (Chap. 13).
- Assisting the structural engineer by investigating the effects of ground movement due to seismic forces on the structure and by providing design parameters or suitable structural systems to accommodate the anticipated displacement (Chap. 13).

In many cases, the tasks listed above may be required by the building code or other regulatory specifications (Chap. 14). For example, the *Uniform Building Code* (1997), which is the building code required for construction in California, states (code provision submitted by the author, adopted in May 1994):

> The potential for soil liquefaction and soil strength loss during earthquakes shall be evaluated during the geotechnical investigation. The geotechnical report shall assess potential consequences of any liquefaction and soil strength loss, including estimation of differential settlement, lateral movement or reduction in foundation soil-bearing capacity, and discuss mitigating measures. Such measures shall be given consideration in the design of the building and may include, but are not limited to, ground stabilization, selection of appropriate foundation type and depths, selection of appropriate structural systems to accommodate anticipated displacement or any combination of these measures.

The intent of this building code requirement is to obtain an estimate of the foundation displacement caused by the earthquake-induced soil movement. In terms of accuracy of the calculations used to determine the earthquake-induced soil movement, Tokimatsu and Seed (1984) conclude:

> It should be recognized that, even under static loading conditions, the error associated with the estimation of settlement is on the order of ±25 to 50%. It is therefore reasonable to expect less accuracy in predicting settlements for the more complicated conditions associated with earthquake loading.…In the application of the methods, it is essential to check that the final results are reasonable in light of available experience.

1.2 ENGINEERING GEOLOGY

An *engineering geologist* is an individual who applies geologic data, principles, and interpretation so that geologic factors affecting the planning, design, construction, and maintenance of civil engineering works are properly recognized and utilized (*Geologist and Geophysicist Act* 1986). In some areas of the United States, there may be minimal involvement of engineering geologists except for projects involving such items as rock slopes or earthquake fault studies. In other areas of the country, such as California, the geotechnical investigations are usually performed jointly by the geotechnical engineer and the engineering geologist. The majority of geotechnical reports include both engineering and geologic aspects of the project, and the report is signed by both the geotechnical engineer and the engineering geologist.

The primary duty of the engineering geologist is to determine the location of faults, investigate the faults in terms of being either active or inactive, and evaluate the historical records of earthquakes and their impact on the site. These studies by the engineering geologist will help to define the design earthquake parameters, such as the peak ground acceleration and magnitude of the anticipated earthquake. The primary duty of the geotechnical engineer is to determine the response of soil and rock materials for the design earthquake and to provide recommendations for the seismic design of the structure.

1.3 GEOTECHNICAL ENGINEERING TERMS

Like most fields, geotechnical engineering has its own unique terms and definitions. Appendix A presents a glossary, which has been divided into five different parts, as follows:

Glossary 1: Field Testing Terminology
Glossary 2: Laboratory Testing Terminology
Glossary 3: Terminology for Engineering Analysis and Computations
Glossary 4: Compaction, Grading, and Construction Terminology
Glossary 5: Earthquake Terminology

1.4 SYMBOLS AND UNITS

A list of symbols is provided at the beginning of most chapters. An attempt has been made to select those symbols most frequently listed in standard textbooks and used in practice. Units that are used is this book consist of the following:

1. International System of Units (SI).
2. Inch-pound units (I-P units), which is also frequently referred to as the U.S. Customary System (USCS) units. Appendix C presents factors that can be used to convert USCS values into SI units.

In some cases, figures have been reproduced that use the old metric system (e.g., stress in kilograms per centimeter squared). These figures have not been revised to reflect SI units.

1.5 BOOK OUTLINE

Part 1 of the book, which consists of Chaps. 2 through 4, presents a brief discussion of basic earthquake principles, common earthquake effects, and structural damage caused by earthquakes. Numerous photographs are used in these three chapters in order to show the common types of earthquake effects and damage.

Part 2 of the book deals with the essential geotechnical earthquake engineering analyses, as follows:

- Field exploration (Chap. 5)
- Liquefaction (Chap. 6)
- Settlement of structures (Chap. 7)
- Bearing capacity (Chap. 8)
- Slope stability (Chap. 9)
- Retaining walls (Chap. 10)
- Other earthquake effects (Chap. 11)

Part 3 of the book (Chaps. 12 and 13) presents commonly used site improvement methods and foundation alternatives. Part 4 (Chap. 14) presents a brief introduction to building codes as they pertain to geotechnical earthquake engineering.

As mentioned in Sec. 1.3, a glossary in included in App. A. Other items are presented in the appendices:

- Data from the EQSEARCH, EQFAULT, and FRISKSP computer programs (App. B)
- Conversion factors (App. C)

- Example of the portion of the geotechnical report dealing with earthquake engineering (App. D)
- Solution to problems (App. E)
- References (App. F)

P · A · R · T · 1

INTRODUCTION TO EARTHQUAKES

CHAPTER 2

BASIC EARTHQUAKE PRINCIPLES

The following notation is used in this chapter:

SYMBOL	*DEFINITION*
a_{max}	Maximum horizontal acceleration at the ground surface (also known as the peak ground acceleration)
A	Maximum trace amplitude recorded by a Wood-Anderson seismograph
A'	Maximum ground displacement in micrometers
A_f	Area of the fault plane
A_0	Maximum trace amplitude for the smallest recorded earthquake (A_0 = 0.001 mm)
D	Average displacement of the ruptured segment of the fault
g	Acceleration of gravity
M_L	Local magnitude of the earthquake
M_0	Seismic moment of the earthquake
M_s	Surface wave magnitude of the earthquake
M_w	Moment magnitude of the earthquake
Δ	Epicentral distance to the seismograph, measured in degrees
μ	Shear modulus of the material along the fault plane

2.1 PLATE TECTONICS

The theory of plate tectonics in the 1960s has helped immeasurably in the understanding of earthquakes. According to the plate tectonic theory, the earth's surface contains tectonic plates, also known as lithosphere plates, with each plate consisting of the crust and the more rigid part of the upper mantle. Figure 2.1 shows the locations of the major tectonic plates, and the arrows indicate the relative directions of plate movement. Figure 2.2 shows the locations of the epicenters of major earthquakes. In comparing Figs. 2.1 and 2.2, it is evident that the locations of the great majority of earthquakes correspond to the boundaries between plates. Depending on the direction of movement of the plates, there are three types of plate boundaries: divergent boundary, convergent boundary, and transform boundary.

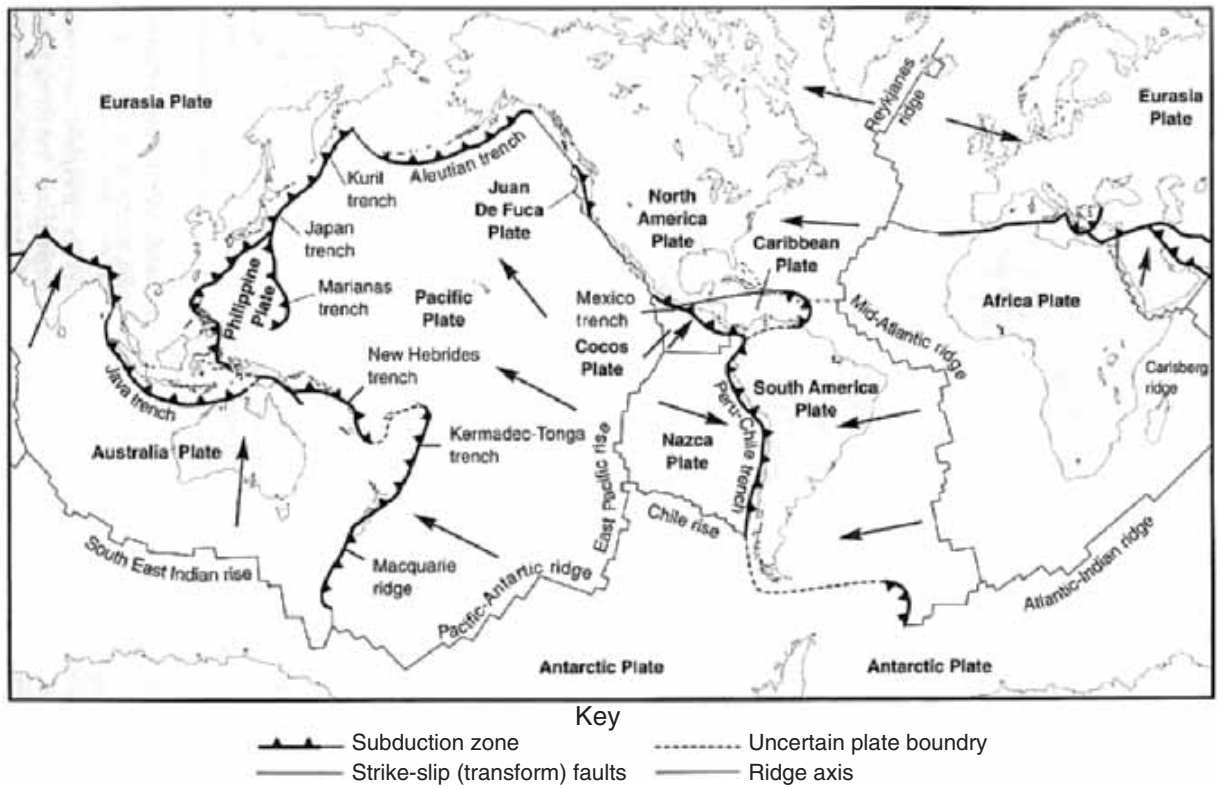

FIGURE 2.1 The major tectonic plates, mid-oceanic ridges, trenches, and transform faults of the earth. Arrows indicate directions of plate movement. (*Developed by Fowler 1990, reproduced from Kramer 1996.*)

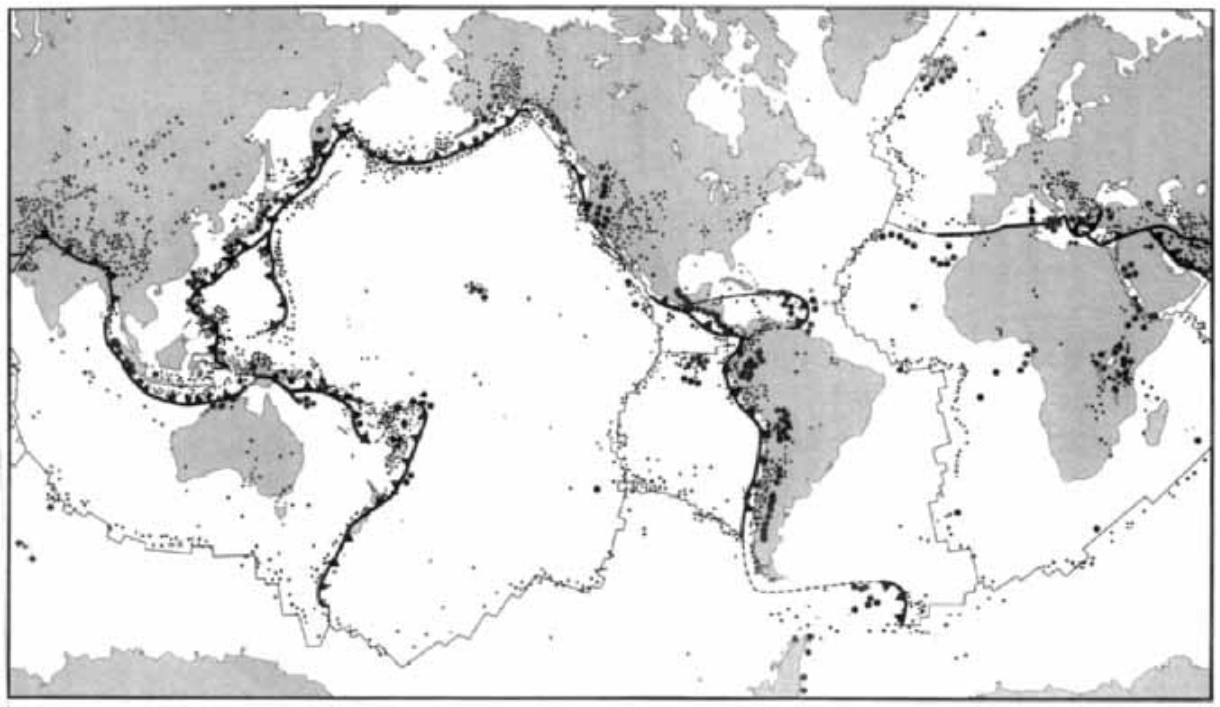

FIGURE 2.2 Worldwide seismic activity, where the dots represent the epicenters of significant earthquakes. In comparing Figs. 2.1 and 2.2, the great majority of the earthquakes are located at the boundaries between plates. (*Developed by Bolt 1988, reproduced from Kramer 1996.*)

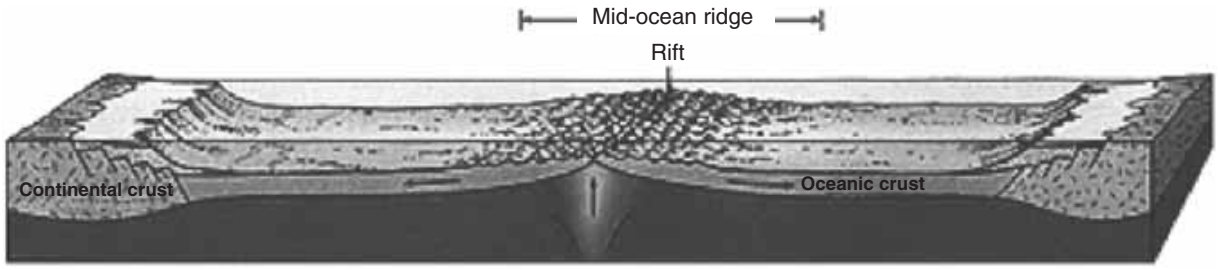

FIGURE 2.3 Illustration of a divergent boundary (seafloor spreading). (*From USGS.*)

Divergent Boundary. This occurs when the relative movement of two plates is away from each other. The upwelling of hot magma that cools and solidifies as the tectonic plates move away from each other forms spreading ridges. Figure 2.3 illustrates seafloor spreading and the development of a mid-ocean ridge. An example of a spreading ridge is the mid-Atlantic ridge (see Fig. 2.1). Earthquakes on spreading ridges are limited to the ridge crest, where new crust is being formed. These earthquakes tend to be relatively small and occur at shallow depths (Yeats et al. 1997).

When a divergent boundary occurs within a continent, it is called *rifting*. Molten rock from the asthenosphere rises to the surface, forcing the continent to break and separate. Figure 2.4 illustrates the formation of a continental rift valley. With enough movement, the rift valley may fill with water and eventually form a mid-ocean ridge.

Convergent Boundary. This occurs when the relative movement of the two plates is toward each other. The amount of crust on the earth's surface remains relatively constant, and therefore when a divergent boundary occurs in one area, a convergent boundary must occur in another area. There are three types of convergent boundaries: oceanic-continental subduction zone, oceanic-oceanic subduction zone, and continent-continent collision zone.

1. *Oceanic-continental subduction zone:* In this case, one tectonic plate is forced beneath the other. For an oceanic subduction zone, it is usually the denser oceanic plate that will subduct beneath the less dense continental plate, such as illustrated in Fig. 2.5. A deep-sea trench forms at the location where one plate is forced beneath the other. Once the subducting oceanic crust reaches a depth of about 60 mi (100 km), the crust begins to melt and some of this magma is pushed to the surface, resulting in volcanic eruptions (see Fig. 2.5). An example of an oceanic-continental subduction zone is seen at the Peru-Chile trench (see Fig. 2.1).

2. *Oceanic-oceanic subduction zone:* An oceanic-oceanic subduction zone often results in the formation of an island arc system, such as illustrated in Fig. 2.6. As the subducting oceanic crust meets with the asthenosphere, the newly created magma rises to the surface and forms volcanoes. The volcanoes may eventually grow tall enough to form a chain of islands. An eexample of an oceanic-oceanic subjection zone is the Aleutian Island chain (see Fig. 2.1).

The earthquakes related to subduction zones have been attributed to four different conditions (Christensen and Ruff 1988):

- Shallow interplate thrust events caused by failure of the interface between the down-going plate and the overriding plate.
- Shallow earthquakes caused by deformation within the upper plate.
- Earthquakes at depths from 25 to 430 mi (40 to 700 km) within the down-going plate.

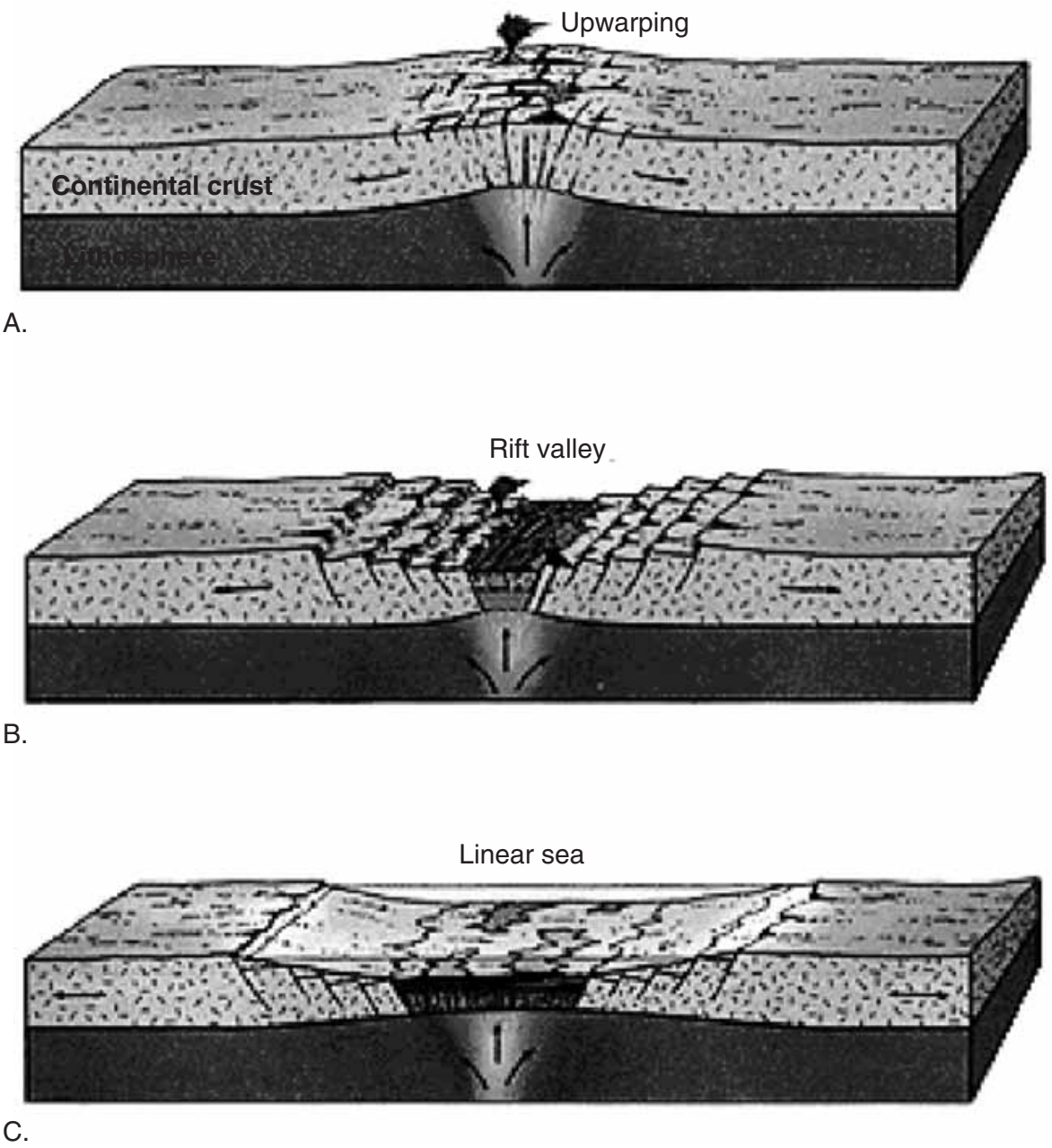

FIGURE 2.4 Illustration of a divergent boundary (rift valley). (A) The upwarping of the ground surface, (B) the rift valley development, and (C) flooding to form a linear sea. (*From USGS.*)

- Earthquakes that are seaward of the trench, caused mainly by the flexing of the downgoing plate, but also by compression of the plate.

In terms of the seismic energy released at subduction zones, it has been determined that the largest earthquakes and the majority of the total seismic energy released during the past century have occurred as shallow earthquakes at subduction zone–plate boundaries (Pacheco and Sykes 1992).

3. *Continent-continent collision zone:* The third type of convergent boundary is the continent-continent collision zone, which is illustrated in Fig. 2.7. This condition occurs when two continental plates collide with each other, causing the two masses to squeeze, fold, deform, and thrust upward. According to Yeats et al. (1997), the Himalaya Mountains

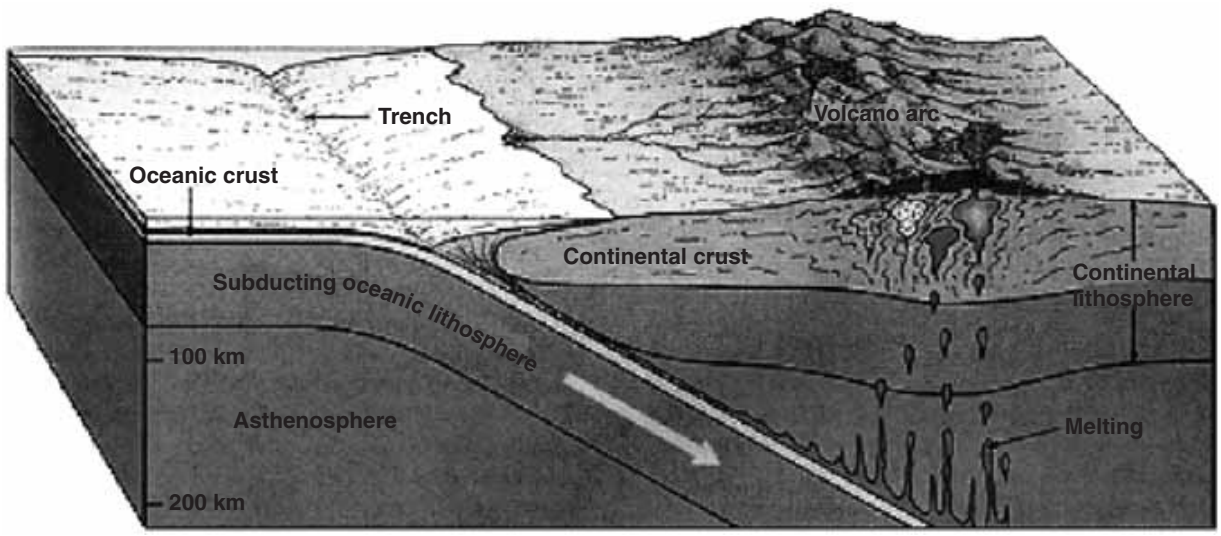

FIGURE 2.5 Illustration of a convergent boundary (oceanic-continental subduction zone). (*From USGS.*)

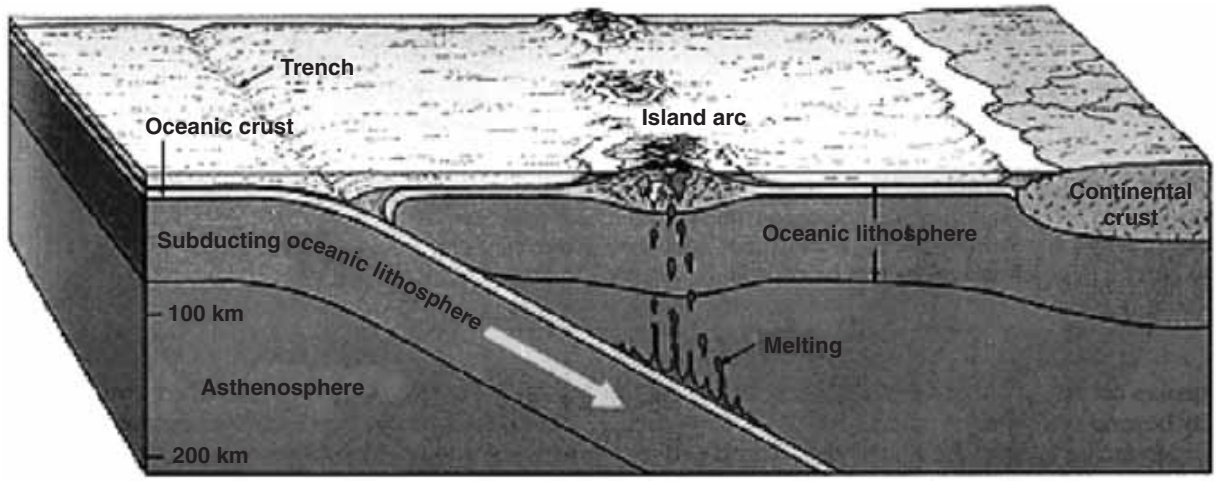

FIGURE 2.6 Illustration of a convergent boundary (oceanic-oceanic subduction zone). (*From USGS.*)

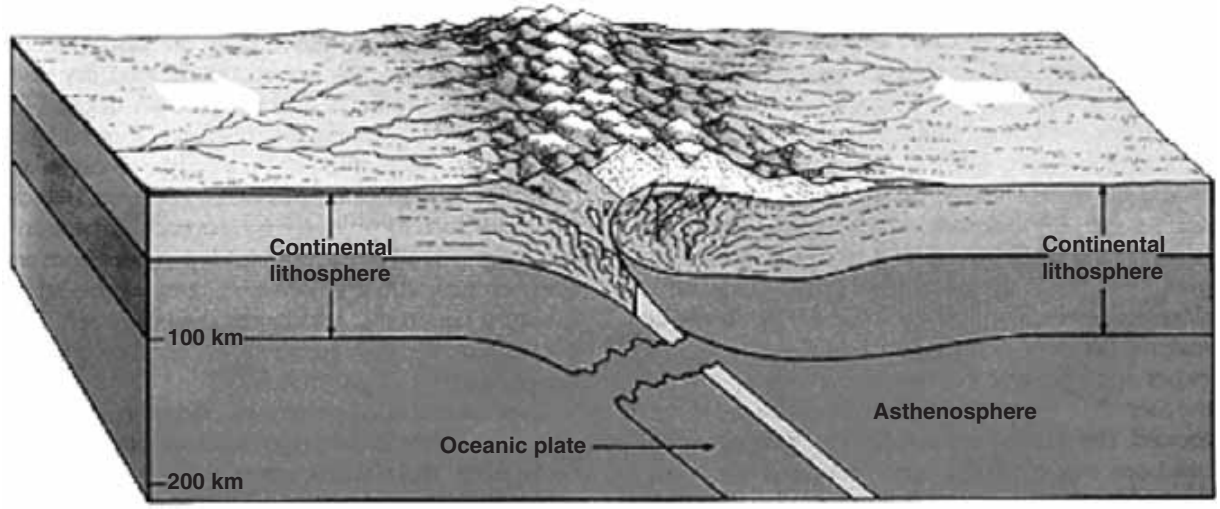

FIGURE 2.7 Illustration of a convergent boundary (continent-continent collision zone). (*From USGS.*)

mark the largest active continent-continent collision zone on earth. They indicate that the collision between the Indian subcontinent and the Eurasia plate began in early tertiary time, when the northern edge of the Indian plate was thrust back onto itself, with the subsequent uplifting of the Himalaya Mountains.

Transform Boundary. A transform boundary, or transform fault, involves the plates sliding past each other, without the construction or destruction of the earth's crust. When the relative movement of two plates is parallel to each other, strike-slip fault zones can develop at the plate boundaries. *Strike-slip faults* are defined as faults on which the movement is parallel to the strike of the fault; or in other words, there is horizontal movement that is parallel to the direction of the fault.

California has numerous strike-slip faults, with the most prominent being the San Andreas fault. Figure 2.8 shows that large earthquakes have occurred on or near the San Andreas fault, and Fig. 2.9 presents an example of the horizontal movement along this fault (1906 San Francisco earthquake). Since a boundary between two plates occurs in California, it has numerous earthquakes and the highest seismic hazard rating in the continental United States (see Fig. 2.10).

The theory of plate tectonics is summarized in Table 2.1. This theory helps to explain the location and nature of earthquakes. Once a fault has formed at a plate boundary, the shearing resistance for continued movement of the fault is less than the shearing resistance

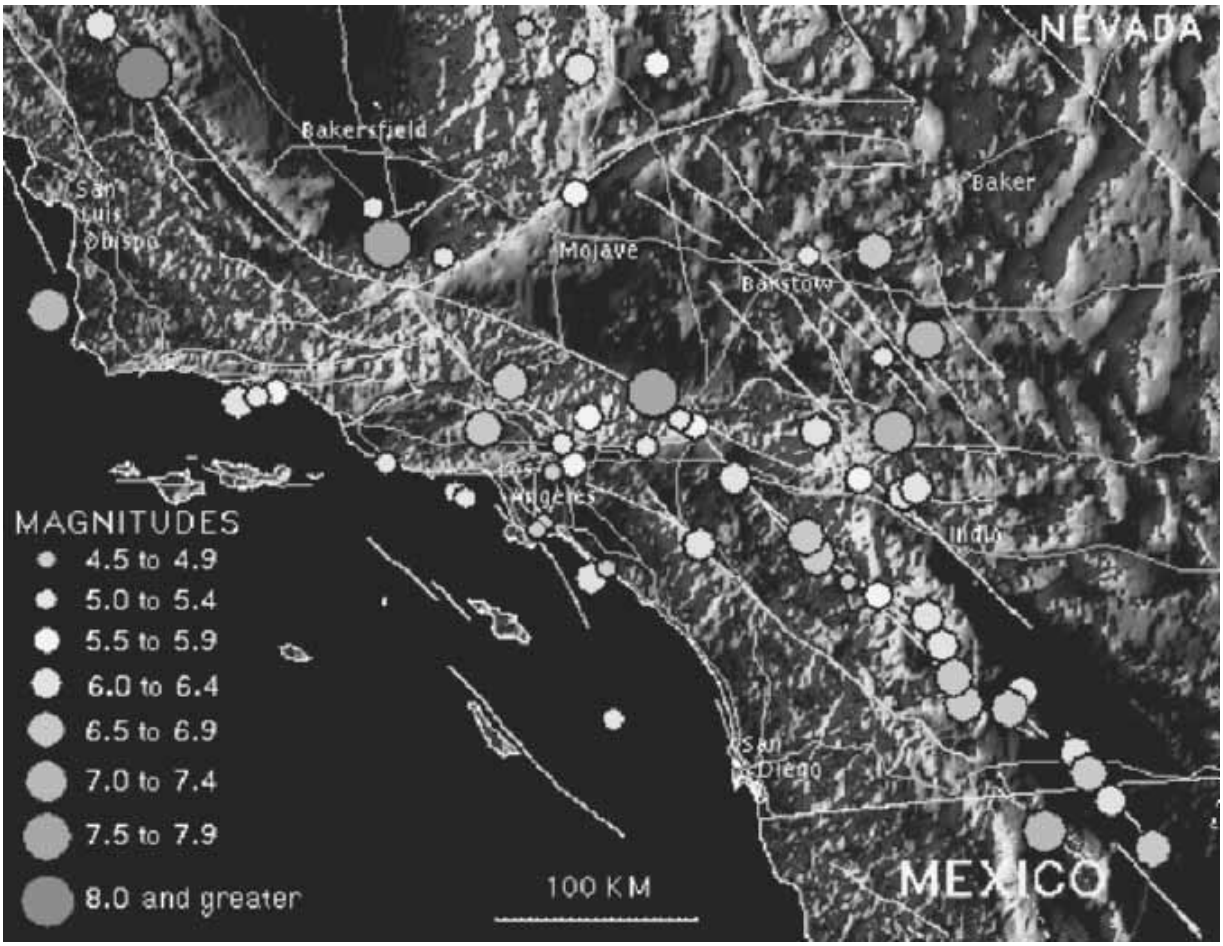

FIGURE 2.8 Epicenters of historic earthquakes (1812–1996). The map does not show all the epicenters of earthquakes with magnitude greater than 4.5, but rather is meant as an overview of large and destructive, fairly recent, or unusual earthquakes. Also shown are the traces of major faults. The magnitudes indicated are generally moment magnitude M_w for earthquakes above magnitude 6 and local magnitude M_L for earthquakes below magnitude 6 and for earthquakes which occurred before 1933. (*Source: USGS.*)

FIGURE 2.9 San Francisco earthquake, 1906. The fence has been offset 8.5 ft by the San Andreas fault displacement. The location is 0.5 mi northwest of Woodville, Marin County, California. (*Photograph courtesy of USGS.*)

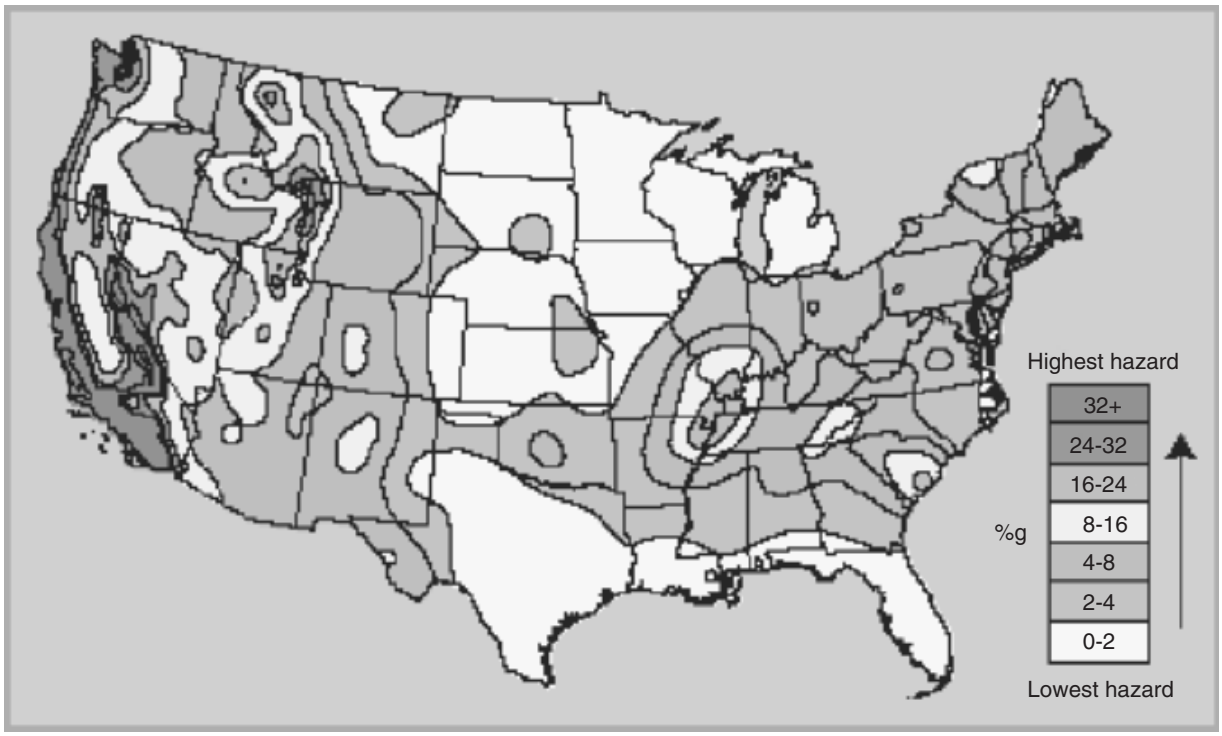

FIGURE 2.10 Seismic hazard map for the continental United States. The map indicates the lowest versus highest seismic hazard areas. (*Source: USGS.*)

TABLE 2.1 Summary of Plate Tectonics Theory

Plate boundary type	Type of plate movement	Categories	Types of earthquakes	Examples
Divergent boundary	Relative movement of the two plates is away from each other.	Seafloor spreading ridge (Fig. 2.3)	Earthquakes on spreading ridges are limited to the ridge crest, where new crust is being formed. These earthquakes tend to be relatively small and occur at shallow depths.	Mid-Atlantic ridge
		Continental rift valley (Fig. 2.4)	Earthquakes generated along normal faults in the rift valley.	East African rift
Convergent boundary	Relative movement of the two plates is toward each other.	Oceanic-continental subduction zone (Fig. 2.5)	1. Shallow interplate thrust events caused by failure of the interface between the down-going plate and the overriding plate. 2. Shallow earthquakes caused by deformation within the upper plate.	Peru-Chile trench
		Oceanic-oceanic subduction zone (Fig. 2.6)	3. Earthquakes at depths from 25 to 430 mi (40 to 700 km) within the down-going plate. 4. Earthquakes that are seaward of the trench, caused mainly by the flexing of the down-going plate, but also by compression of the plate.	Aleutian Island chain
		Continent-continent collision zone (Fig. 2.7)	Earthquakes generated at the collision zone, such as at reverse faults and thrust faults.	Himalaya Mountains
Transform boundary	Plates slide past each other, without the construction or destruction of the earth's crust.	Strike-slip fault zones (Fig. 2.9)	Earthquakes often generated on strike-slip faults.	San Andreas fault

required to fracture new intact rock. Thus faults at the plate boundaries that have generated earthquakes in the recent past are likely to produce earthquakes in the future. This principle is the basis for the development of seismic hazard maps, such as shown in Fig. 2.10.

The theory of plate tectonics also helps explain such geologic features as the islands of Hawaii. The islands are essentially large volcanoes that have risen from the ocean floor. The volcanoes are believed to be the result of a thermal plume or "hot spot" within the mantle, which forces magna to the surface and creates the islands. The thermal plume is believed to be relatively stationary with respect to the center of the earth, but the Pacific plate is moving to the northwest. Thus the islands of the Hawaiian chain to the northwest are progressively older and contain dormant volcanoes that have weathered away. Yeats et al. (1997) use an analogy of the former locations of the Pacific plate with respect to the plume as being much like a piece of paper passed over the flame of a stationary candle, which shows a linear pattern of scorch marks.

2.1.1 Types of Faults

A fault is defined as a fracture or a zone of fractures in rock along which displacement has occurred. The fault length can be defined as the total length of the fault or fault zone. The fault length could also be associated with a specific earthquake, in which case it would be defined as the actual rupture length along a fault or fault zone. The rupture length could be determined as the distance of observed surface rupture.

In order to understand the terminology associated with faults, the terms "strike" and "dip" must be defined. The "strike" of a fault plane is the azimuth of a horizontal line drawn on the fault plane. The dip is measured in a direction perpendicular to the strike and is the angle between the inclined fault plane and a horizontal plane. The strike and dip provide a description of the orientation of the fault plane in space. For example, a fault plane defined as N70W 50NE would indicate a strike of N70W (North 70° West) and a dip of 50NE (50° to the Northeast).

Typical terms used to describe different types of faults are as follows:

- Strike-Slip Fault: During the discussion of the transform boundary in Section 2.1, a strike-slip fault was defined as a fault on which the movement is parallel to the strike of the fault. A strike-slip fault is illustrated in Fig. 2.11.

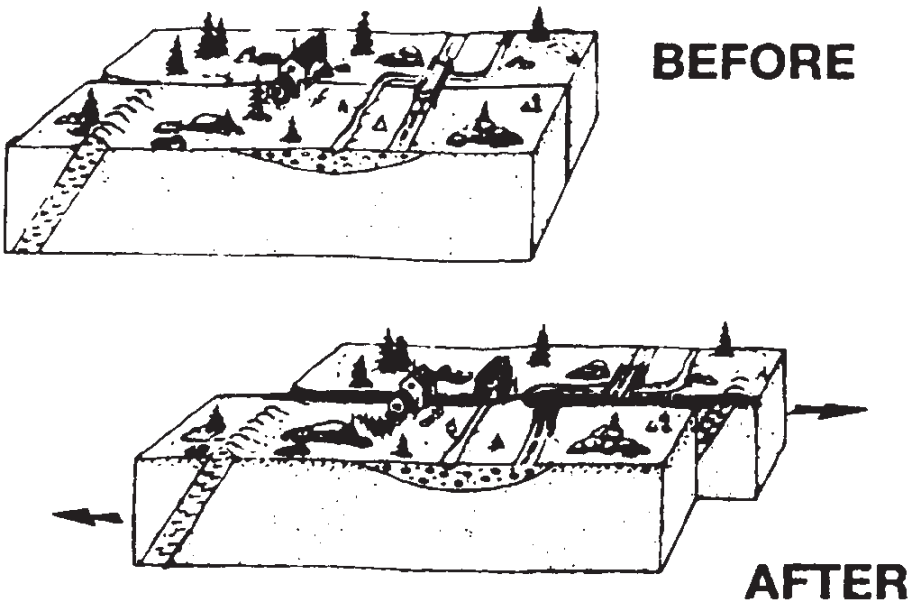

FIGURE 2.11 Illustration of a strike-slip fault. (*From Namson and Davis 1988.*)

- Transform Fault: A fault that is located at a transform boundary (see Section 2.1). Yeats et al. (1997) define a transform fault as a strike-slip fault of plate-boundary dimensions that transforms into another plate-boundary structure at its terminus.
- Normal Fault: Figure 2.12 illustrates a normal fault. The "hangingwall" is defined as the overlying side of a nonvertical fault. Thus, in Figure 2.12, the "hangingwall" block is that part of the ground on the right side of the fault and the "footwall" block is that part of the ground on the left side of the fault. A normal fault would be defined as a fault where the hangingwall block has moved downward with respect to the footwall block.
- Reverse Fault: Figure 2.13 illustrates a reverse fault. A reverse fault would be defined as a fault where the hangingwall block has moved upward with respect to the footwall block.
- Thrust Fault: A thrust fault is defined as a reverse fault where the dip is less than or equal to 45°.
- Blind Fault: A blind fault is defined as a fault that has never extended upward to the ground surface. Blind faults often terminate in the upward region of an anticline.
- Blind Thrust Fault: A blind reverse fault where the dip is less than or equal to 45°.
- Longitudinal Step Fault: A series of parallel faults. These parallel faults develop when the main fault branches upward into several subsidiary faults.
- Dip-Slip Fault: A fault which experiences slip only in the direction of its dip, or in other words, the movement is perpendicular to the strike. Thus a fault could be described as a "dip-slip normal fault," which would indicate that it is a normal fault (see Fig. 2.12) with the slip only in the direction of its dip.
- Oblique-Slip Fault: A fault which experiences components of slip in both its strike and dip directions. A fault could be described as a "oblique-slip normal fault," which would indicate that it is a normal fault (see Fig. 2.12) with components of slip in both the strike and dip directions.
- Fault Scarp: This generally only refers to a portion of the fault that has been exposed at

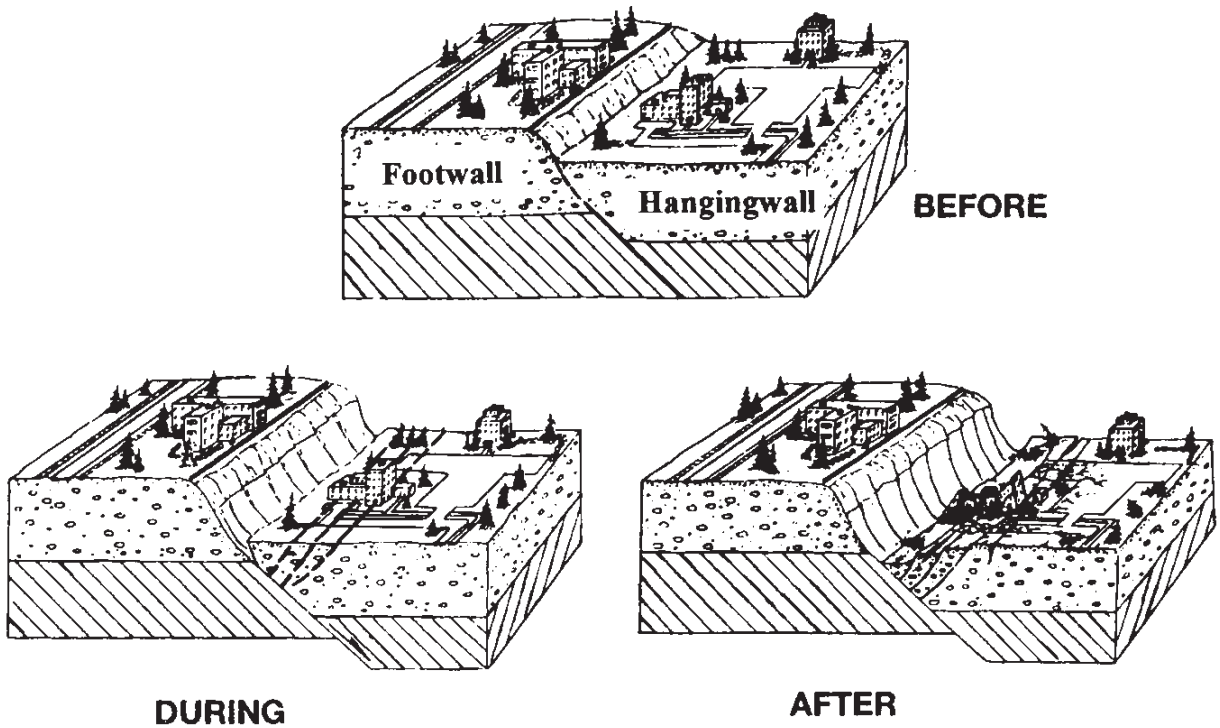

FIGURE 2.12 Illustration of a normal fault. For a normal fault, the hangingwall block has moved downward with respect to the footwall block. (*Adapted from Namson and Davis 1988.*)

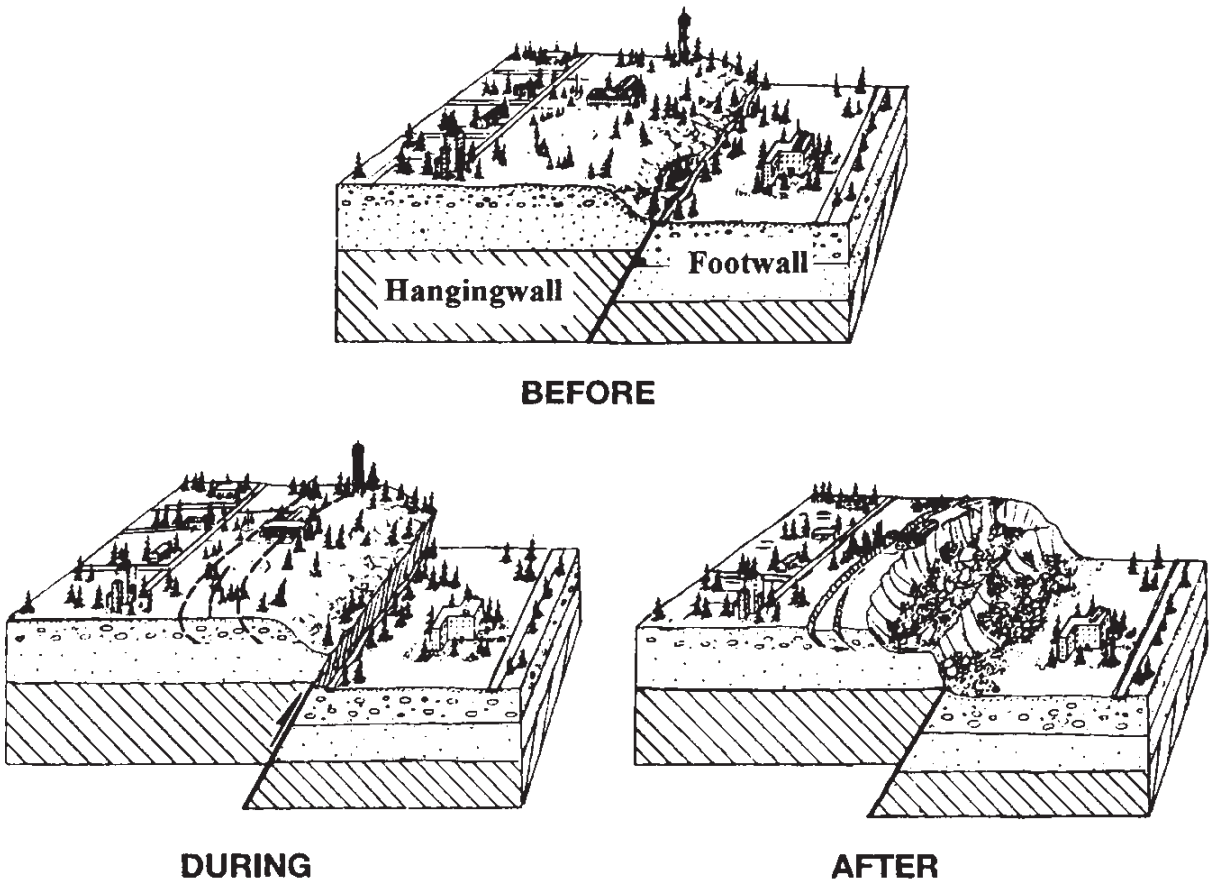

FIGURE 2.13 Illustration of a reverse fault. For a reverse fault, the hangingwall block has moved upward with respect to the footwall block. (*Adapted from Namson and Davis 1988.*)

ground surface due to ground surface fault rupture. The exposed portion of the fault often consists of a thin layer of "fault gouge," which is a clayey seam that has formed during the slipping or shearing of the fault and often contains numerous slickensides.

2.2 SEISMOGRAPH

Most earthquakes are caused by the release of energy due to sudden displacements on faults. This is not to imply that all ground movement of a fault will produce an earthquake. For example, there can be fault creep, where the ground movement is unaccompanied by an earthquake. The major earthquake is characterized by the buildup of stress and then the sudden release of this stress as the fault ruptures.

A *seismograph* is an instrument that records, as a function of time, the motion of the earth's surface due to the seismic waves generated by the earthquake. The actual record of ground shaking from the seismograph, known as a *seismogram,* can provide information about the nature of the earthquake.

The simplest seismographs can consist of a pendulum or a mass attached to a spring, and they are used to record the horizontal movement of the ground surface. For the pendulum-type seismograph, a pen is attached to the bottom of the pendulum, and the pen is in contact with a chart that is firmly anchored to the ground. When the ground shakes during an earthquake, the chart moves, but the pendulum and its attached pen tend to remain more or less stationary because of the effects of inertia. The pen then traces the horizontal movement between the relatively stationary pendulum and the moving chart. After the ground

shaking has ceased, the pendulum will tend to return to a stable position, and thus could indicate false ground movement. Therefore a pendulum damping system is required so that the ground displacements recorded on the chart will produce a record that is closer to the actual ground movement.

Much more sophisticated seismographs are presently in use. For example, the engineer is often most interested in the peak ground acceleration a_{max} during the earthquake. An *accelerograph* is defined as a low-magnification seismograph that is specially designed to record the ground acceleration during the earthquake. Most modern accelerographs use an electronic transducer that produces an output voltage which is proportional to the acceleration. This output voltage is recorded and then converted to acceleration and plotted versus time, such as shown in Fig. 2.14. Note that the velocity and displacement plots in Fig. 2.14 were produced by integrating the acceleration.

The data in Fig. 2.14 were recorded during the February 9, 1971, San Fernando earthquake. The three plots indicate the following:

1. *Acceleration versus time:* The acceleration was measured in the horizontal direction. In Fig. 2.14, the maximum value of the horizontal acceleration a_{max}, which is also commonly referred to as the *peak ground acceleration,* is equal to 250 cm/s^2 (8.2 ft/s^2). The peak ground acceleration for this earthquake occurs at a time of about 13 s after the start of the record.

Since the acceleration due to earth's gravity g is 981 cm/s^2, the peak ground acceleration can be converted to a fraction of earth's gravity. This calculation is performed by dividing 250 cm/s^2 by 981 cm/s^2; or the peak ground acceleration a_{max} is equal to 0.255g.

2. *Velocity versus time:* By integrating the horizontal acceleration, the horizontal velocity versus time was obtained. In Fig. 2.14, the maximum horizontal velocity at ground surface v_{max} is equal to 30 cm/s (1.0 ft/s). The maximum velocity at ground surface for this earthquake occurs at a time of about 10 s after the start of the record.

3. *Displacement versus time:* The third plot in Fig. 2.14 shows the horizontal displacement at ground surface versus time. This plot was obtained by integrating the horizontal velocity data. In Fig. 2.14, the maximum horizontal displacement at ground surface is 14.9 cm (5.9 in). The maximum displacement at ground surface for this earthquake occurs at a time of about 10 s after the start of the record.

2.3 SEISMIC WAVES

The acceleration of the ground surface, such as indicated by the plot shown in Fig. 2.14, is due to various seismic waves generated by the fault rupture. There are two basic types of seismic waves: body waves and surface waves. P and S waves are both called body waves because they can pass through the interior of the earth. Surface waves are only observed close to the surface of the earth, and they are subdivided into Love waves and Rayleigh waves. Surface waves result from the interaction between body waves and the surficial earth materials. The four types of seismic waves are further discussed below:

1. *P wave (body wave):* The P wave is also known as the primary wave, compressional wave, or longitudinal wave. It is a seismic wave that causes a series of compressions and dilations of the materials through which it travels. The P wave is the fastest wave and is the first to arrive at a site. Being a compression-dilation type of wave, P waves can travel through both solids and liquids. Because soil and rock are relatively resistant to compression-dilation effects, the P wave usually has the least impact on ground surface movements.

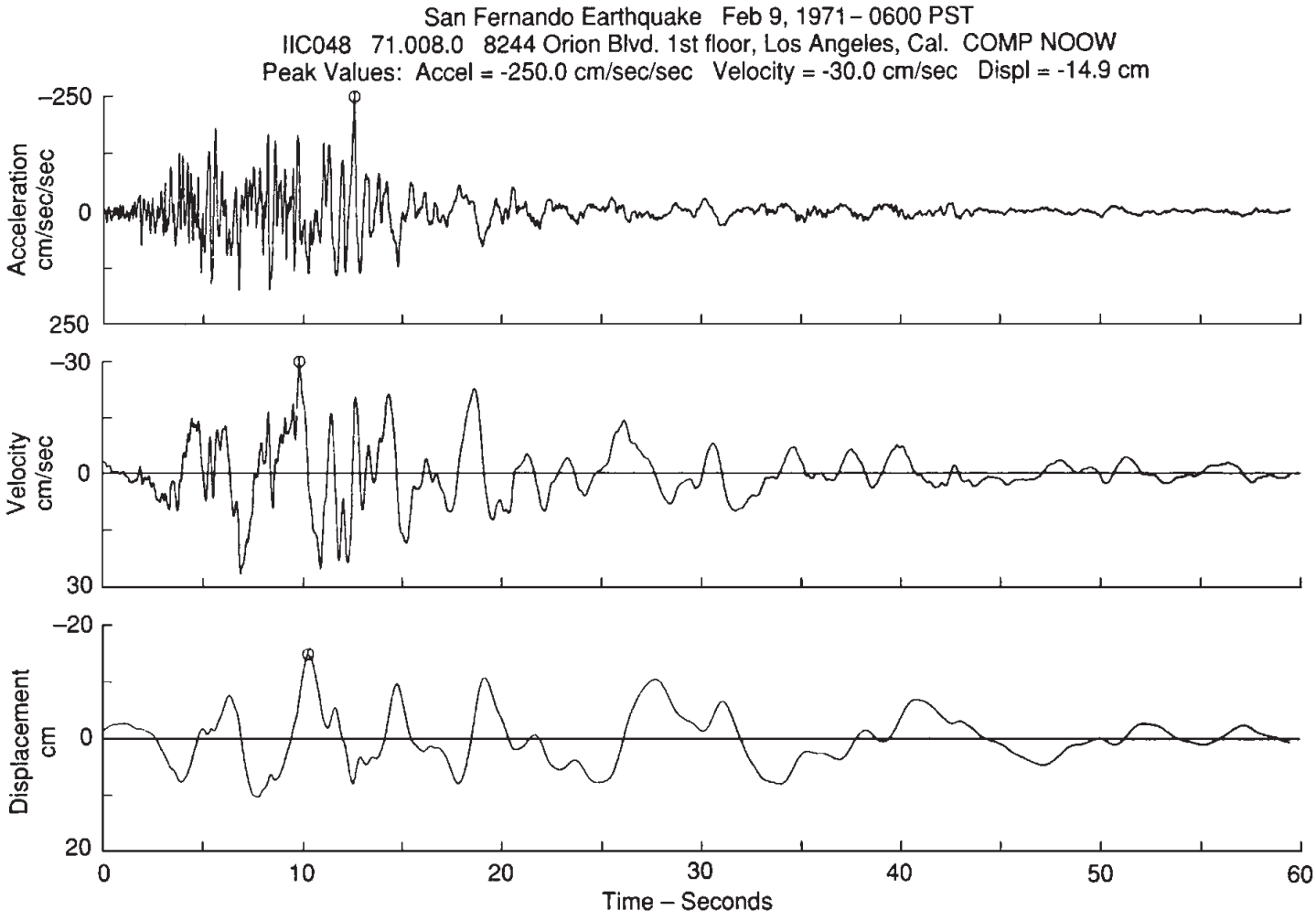

FIGURE 2.14 Acceleration, velocity, and displacement versus time recorded during the San Fernando earthquake. (*Data record from California Institute of Technology 1971, reproduced from Krinitzsky et al. 1993.*)

2. *S wave (body wave):* The S wave is also known as the secondary wave, shear wave, or transverse wave. The S wave causes shearing deformations of the materials through which it travels. Because liquids have no shear resistance, S waves can only travel through solids. The shear resistance of soil and rock is usually less than the compression-dilation resistance, and thus an S wave travels more slowly through the ground than a P wave. Soil is weak in terms of its shear resistance, and S waves typically have the greatest impact on ground surface movements.

3. *Love wave (surface wave):* Love waves are analogous to S waves in that they are transverse shear waves that travel close to the ground surface (Yeats et al. 1997).

4. *Rayleigh wave (surface wave):* Rayleigh waves have been described as being similar to the surface ripples produced by a rock thrown into a pond. These seismic waves produce both vertical and horizontal displacement of the ground as the surface waves propagate outward.

Generally, there is no need for the engineer to distinguish between the different types of seismic waves that could impact the site. Instead, the combined effect of the waves in terms of producing a peak ground acceleration a_{max} is of primary interest. However, it is important to recognize that the peak ground acceleration will be most influenced by the S waves and, in some cases, by surface waves. For example, Kramer (1996) states that at distances greater than about twice the thickness of the earth's crust, surface waves, rather than body waves, will produce peak ground motions.

2.4 MAGNITUDE OF AN EARTHQUAKE

There are two basic ways to measure the strength of an earthquake: (1) based on the earthquake magnitude and (2) based on the intensity of damage. *Magnitude* measures the amount of energy released from the earthquake, and *intensity* is based on the damage to buildings and reactions of people. This section discusses earthquake magnitude, and Sec. 2.5 discusses the intensity of the earthquake.

There are many different earthquake magnitude scales used by seismologists. This section discusses three of the more commonly used magnitude scales.

2.4.1 Local Magnitude Scale M_L

In 1935, Professor Charles Richter, from the California Institute of Technology, developed an earthquake magnitude scale for shallow and local earthquakes in southern California. This magnitude scale has often been referred to as the *Richter magnitude scale.* Because this magnitude scale was developed for shallow and local earthquakes, it is also known as the *local magnitude scale* M_L. This magnitude scale is the best known and most commonly used magnitude scale. The magnitude is calculated as follows (Richter 1935, 1958):

$$M_L = \log A - \log A_0 = \log A/A_0 \tag{2.1}$$

where M_L = local magnitude (also often referred to as Richter magnitude scale)
A = maximum trace amplitude, mm, as recorded by a standard Wood-Anderson seismograph that has a natural period of 0.8 s, a damping factor of 80%, and a static magnification of 2800. The maximum trace amplitude must be that amplitude that would be recorded if a Wood-Anderson seismograph were

located on firm ground at a distance of exactly 100 km (62 mi) from the epicenter of the earthquake. Charts and tables are available to adjust the maximum trace amplitude for the usual case where the seismograph is not located exactly 100 km (62 mi) from the epicenter.

A_o = 0.001 mm. The zero of the local magnitude scale was arbitrarily fixed as an amplitude of 0.001 mm, which corresponded to the smallest earthquakes then being recorded.

As indicated above, Richter (1935) designed the magnitude scale so that a magnitude of 0 corresponds to approximately the smallest earthquakes then being recorded. There is no upper limit to the Richter magnitude scale, although earthquakes over an M_L of 8 are rare. Often the data from Wood-Anderson siesmographs located at different distances from the epicenter provide different values of the Richter magnitude. This is to be expected because of the different soil and rock conditions that the seismic waves travel through and because the fault rupture will not release the same amount of energy in all directions.

Since the Richter magnitude scale is based on the logarithm of the maximum trace amplitude, there is a 10-times increase in the amplitude for an increase in 1 unit of magnitude. In terms of the energy released during the earthquake, Yeats et al. (1997) indicate that the increase in energy for an increase of 1 unit of magnitude is roughly 30-fold and is different for different magnitude intervals.

For the case of small earthquakes (that is, $M_L < 6$), the center of energy release and the point where the fault rupture begins are not far apart. But in the case of large earthquakes, these points may be very far apart. For example, the Chilean earthquake of 1960 had a fault rupture length of about 600 mi (970 km), and the epicenter was at the northern end of the ruptured zone which was about 300 mi (480 km) from the center of the energy release (Housner 1963, 1970). This increased release of energy over a longer rupture distance resulted in both a higher peak ground acceleration a_{max} and a longer duration of shaking. For example, Table 2.2 presents approximate correlations between the local magnitude M_L and the peak ground acceleration a_{max}, duration of shaking, and modified Mercalli intensity level (discussed in Sec. 2.5) near the vicinity of the fault rupture. At distances farther from the epicenter or location of fault rupture, the intensity will decrease but the duration of ground shaking will increase.

TABLE 2.2 Approximate Correlations between Local Magnitude M_L and Peak Ground Acceleration a_{max}, Duration of Shaking, and Modified Mercalli Level of Damage near Vicinity of Fault Rupture

Local magnitude M_L	Typical peak ground acceleration a_{max} near the vicinity of the fault rupture	Typical duration of ground shaking near the vicinity of the fault rupture	Modified Mercalli intensity level near the vicinity of the fault rupture (see Table 2.3)
≤2	—	—	I–II
3	—	—	III
4	—	—	IV–V
5	0.09g	2 s	VI–VII
6	0.22g	12 s	VII–VIII
7	0.37g	24 s	IX–X
≥8	≥0.50g	≥34 s	XI–XII

Sources: Yeats et al. 1997, Gere and Shah 1984, and Housner 1970.

2.4.2 Surface Wave Magnitude Scale M_s

The surface wave magnitude scale is based on the amplitude of surface waves having a period of about 20 s. The surface wave magnitude scale M_s is defined as follows (Gutenberg and Richter 1956):

$$M_s = \log A' + 1.66 \log \Delta + 2.0 \tag{2.2}$$

where M_s = surface wave magnitude scale
A' = maximum ground displacement, μm
Δ = epicentral distance to seismograph measured in degrees (360° corresponds to circumference of earth)

The surface wave magnitude scale has an advantage over the local magnitude scale in that it uses the maximum ground displacement, rather than the maximum trace amplitude from a standard Wood-Anderson seismograph. Thus any type of seismograph can be used to obtain the surface wave magnitude. This magnitude scale is typically used for moderate to large earthquakes, having a shallow focal depth, and the seismograph should be at least 1000 km (622 mi) from the epicenter.

2.4.3 Moment Magnitude Scale M_w

The moment magnitude scale has become the more commonly used method for determining the magnitude of large earthquakes. This is because it tends to take into account the entire size of the earthquake. The first step in the calculation of the moment magnitude is to calculate the seismic moment M_0. The seismic moment can be determined from a seismogram using very long-period waves for which even a fault with a very large rupture area appears as a point source (Yeats et al. 1997). The seismic moment can also be estimated from the fault displacement as follows (Idriss 1985):

$$M_0 = \mu A_f D \tag{2.3}$$

where M_0 = seismic moment, N · m
μ = shear modulus of material along fault plane, N/m^2. The shear modulus is often assumed to be 3×10^{10} N/m^2 for surface crust and 7×10^{12} N/m^2 for mantle.
A_f = area of fault plane undergoing slip, m^2. This can be estimated as the length of surface rupture times the depth of the aftershocks.
D = average displacement of ruptured segment of fault, m. Determining the seismic moment works best for strike-slip faults where the lateral displacement on one side of fault relative to the other side can be readily measured.

In essence, to determine the seismic moment requires taking the entire area of the fault rupture surface A_f times the shear modulus μ in order to calculate the seismic force (in newtons). This force is converted to a moment by multiplying the seismic force (in newtons) by the average slip (in meters), in order to calculate the seismic moment (in newton-meters).

Engineers may have a hard time visualizing the seismic moment. The reason is because the seismic force and the moment arm are in the same direction. In engineering, a moment is calculated as the force times the moment arm, and the moment arm is always perpendicular (not parallel) to the force. Setting aside the problems with the moment arm, the seismic moment does consider the energy radiated from the entire fault, rather than the energy

from an assumed point source. Thus the seismic moment is a more useful measure of the strength of an earthquake.

Kanamori (1977) and Hanks and Kanamori (1979) introduced the moment magnitude M_w scale, in which the magnitude is calculated from the seismic moment by using the following equation:

$$M_w = -6.0 + 0.67 \log M_0 \tag{2.4}$$

where M_w = moment magnitude of earthquake
M_0 = seismic moment of earthquake, N · m. The seismic moment is calculated from Eq. (2.3).

2.4.4 Comparison of Magnitude Scales

Figure 2.15 shows the approximate relationships between several different earthquake magnitude scales. When we view the data shown in Fig. 2.15, it would appear that there is an exact relationship between the moment magnitude M_w and the other various magnitude

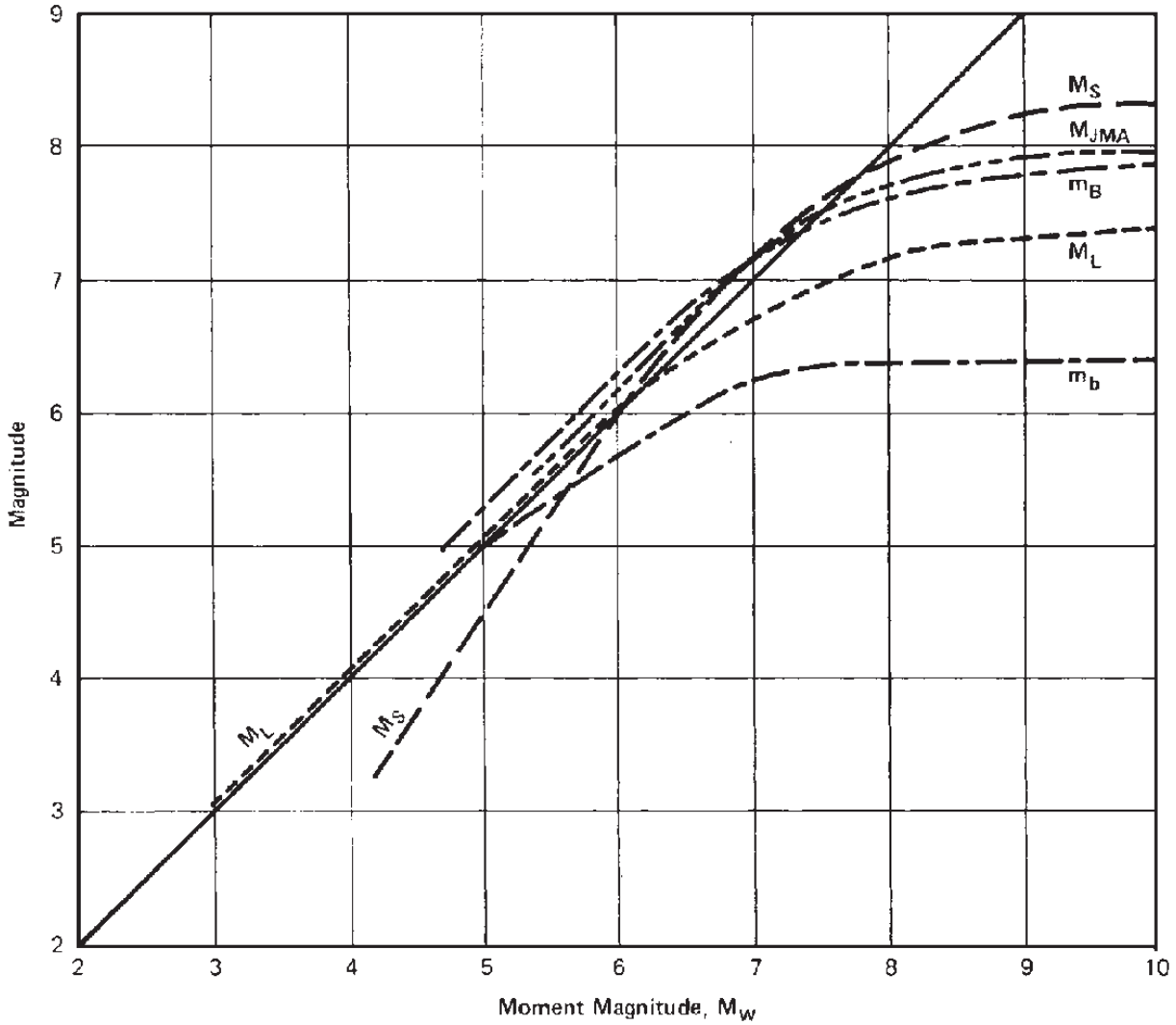

FIGURE 2.15 Approximate relationships between the moment magnitude scale M_w and other magnitude scales. Shown are the short-period body wave magnitude scale m_b, the local magnitude scale M_L, the long-period body wave magnitude scale m_B, the Japan Meteorological Agency magnitude scale M_{JMA} and the surface-wave magnitude scale M_S. (*Developed by Heaton et al. 1982, reproduced from Idriss 1985.*)

scales. But in comparing Eqs. (2.1) and (2.4), it is evident that these two equations cannot be equated. Therefore, there is not an exact and unique relationship between the maximum trace amplitude from a standard Wood-Anderson seismograph [Eq. (2.1)] and the seismic moment [Eq. (2.4)]. The lines drawn in Fig. 2.15 should only be considered as approximate relationships, representing a possible wide range in values.

Given the limitations of Fig. 2.15, it could still be concluded that the local magnitude M_L, the surface wave magnitude scale M_s, and moment magnitude M_w scales are reasonably close to one another below a value of about 7. At high magnitude values, the moment magnitude M_w tends to significantly deviate from these other two magnitude scales.

Note in Fig. 2.15 that the various relationships tend to flatten out at high moment magnitude values. Yeats et al. (1997) state that these magnitude scales are "saturated" for large earthquakes because they cannot distinguish the size of earthquakes based simply on the maximum trace amplitude recorded on the seismogram. Saturation appears to occur when the ruptured fault dimension becomes much larger than the wavelength of seismic waves that are used in measuring the magnitude (Idriss 1985). As indicated in Fig. 2.15, the local magnitude scale becomes saturated at an M_L of about 7.3.

2.4.5 Summary

In summary, seismologists use a number of different magnitude scales. While any one of these magnitude scales may be utilized, an earthquake's magnitude M is often reported without reference to a specific magnitude scale. This could be due to many different reasons, such as these:

1. *Closeness of the scales:* As discussed in Sec. 2.4.4, the local magnitude M_L, the surface wave magnitude M_s, and moment magnitude M_w scales are reasonably close to one another below a value of about 7. Thus as a practical matter, there is no need to identify the specific magnitude scale.

2. *Average value:* An earthquake's magnitude may be computed in more than one way at each seismic station that records the event. These different estimates often vary by as much as one-half a magnitude unit, and the final magnitude M that is reported can be the average of many estimates.

3. *Preseismograph event:* For earthquakes before the advent of the seismograph, the magnitude M of the earthquake is a rough estimate based on historical accounts of damage. In these cases, it would be impractical to try to determine the magnitude for each of the different magnitude scales.

4. *Lack of seismograph data:* Even after the advent of the seismograph, there may still be limited data available for many parts of the world. For example, Hudson (1970) states that not a single ground acceleration measurement was obtained for the earthquakes in Mexico (1957), Chile (1960), Agadir (1960), Iran (1962), Skopje (1963), and Alaska (1964). With only limited data, the earthquake magnitude is often an estimate based on such factors as type of damage, extent of damage, and observations concerning any surface fault rupture.

At high magnitude values, it is often desirable to determine or estimate the earthquake magnitude based on the moment magnitude M_w scale. This is because M_w tends to significantly deviate from the other magnitude scales at high magnitude values and M_w appears to better represent the total energy released by very large earthquakes. Thus for very large earthquakes, the moment magnitude scale M_w would seem to be the most appropriate magnitude scale. In terms of moment magnitude M_w, the top five largest earthquakes in the world for the past century are as follows (USGS 2000a):

Ranking	Location	Year	Moment magnitude M_w
1	Chile	1960	9.5
2	Alaska	1964	9.2
3	Russia	1952	9.0
4	Ecuador	1906	8.8
5	Japan	1958	8.7

2.5 INTENSITY OF AN EARTHQUAKE

The intensity of an earthquake is based on the observations of damaged structures and the presence of secondary effects, such as earthquake-induced landslides, liquefaction, and ground cracking. The intensity of an earthquake is also based on the degree to which the earthquake was felt by individuals, which is determined through interviews.

The intensity of the earthquake may be easy to determine in an urban area where there is a considerable amount of damage, but could be very difficult to evaluate in rural areas. The most commonly used scale for the determination of earthquake intensity is the *modified Mercalli intensity scale,* which is presented in Table 2.3. As indicated in Table 2.3, the intensity ranges from an earthquake that is not felt (I) up to an earthquake that results in total destruction (XII). In general, the larger the magnitude of the earthquake, the greater the area affected by the earthquake and the higher the intensity level. Figures 2.16 to 2.18 present the locations of U.S. earthquakes causing VI to XII levels of damage according to the modified Mercalli intensity scale. Table 2.2 presents an approximate correlation between the local magnitude M_L and the modified Mercalli intensity scale.

A map can be developed that contains contours of equal intensity (called *isoseisms*). Such a map is titled an intensity map or an isoseismal map, and an example is presented in Fig. 2.19. The intensity will usually be highest in the general vicinity of the epicenter or at the location of maximum fault rupture, and the intensity progressively decreases as the distance from the epicenter or maximum fault rupture increases. There can be numerous exceptions to this rule. For example, the epicenter of the 1985 Michoacan earthquake was about 350 km (220 mi) from Mexico City, yet there were buildings that collapsed at the Lake Zone district. This was due to the underlying thick deposit of soft clay that increased the peak ground acceleration and the site period, resulting in resonance for the taller buildings. This effect of local soil and geologic conditions on the earthquake intensity is further discussed in Sec. 5.6.

The modified Mercalli intensity scale can also be used to illustrate the anticipated damage at a site due to a future earthquake. For example, Fig. 2.20 shows the estimated intensity map for San Francisco and the surrounding areas, assuming there is a repeat of the 1906 earthquake. It is predicted that there will be extreme damage along the San Andreas fault as well as in those areas underlain by the San Francisco Bay mud.

2.6 PROBLEMS

The problems have been divided into basic categories as indicated below:

Identification of Faults

2.1 The engineering geologist has determined that a fault plane is oriented 5NW 34W. The engineering geologist also discovered a fault scarp, and based on a trench excavated

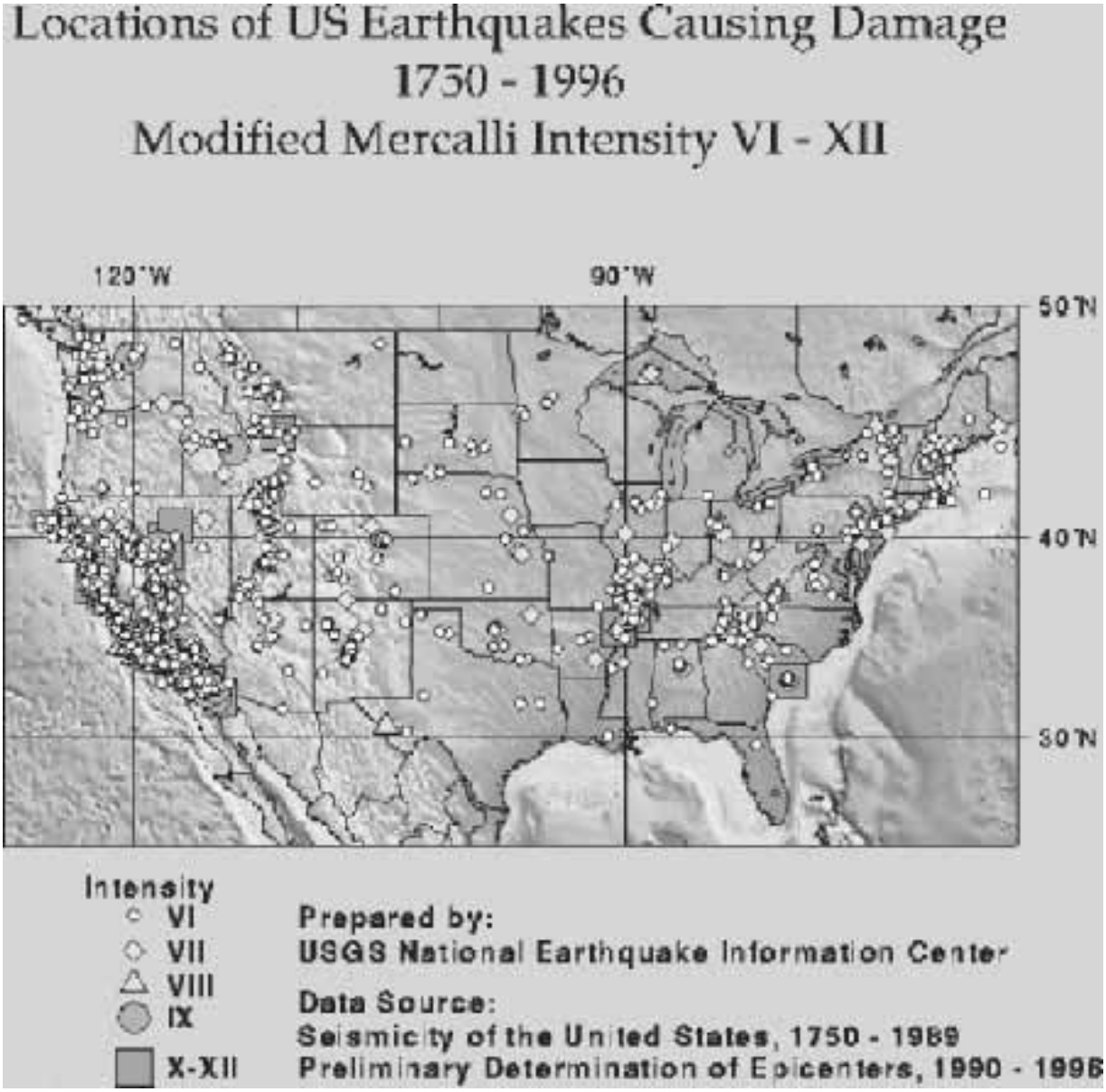

FIGURE 2.16 Locations of continental U.S. earthquakes causing damage from 1750 to 1996 and having a modified Mercalli intensity of VI to XII. (*Prepared by USGS National Earthquake Information Center.*)

across the scarp, the hangingwall block has moved upward with respect to the footwall block. In addition, the surface faulting appears to have occurred solely in the dip direction. Based on this data, determine the type of fault. *Answer:* dip-slip thrust fault.

2.2 Figure 2.21 shows the displacement of rock strata caused by the Carmel Valley Fault, located at Torry Pines, California. Based on the displacement of the hangingwall as compared to the footwall, what type of fault is shown in Figure 2.21. *Answer:* normal fault.

Earthquake Magnitude

2.3 Assume that the displacement data shown in Fig. 2.14 represents the trace data from a standard Wood-Anderson seismograph and that the instrument is exactly 100 km from the epicenter. Based on these assumptions, determine the Richter magnitude. *Answer:* $M_L = 5.2$.

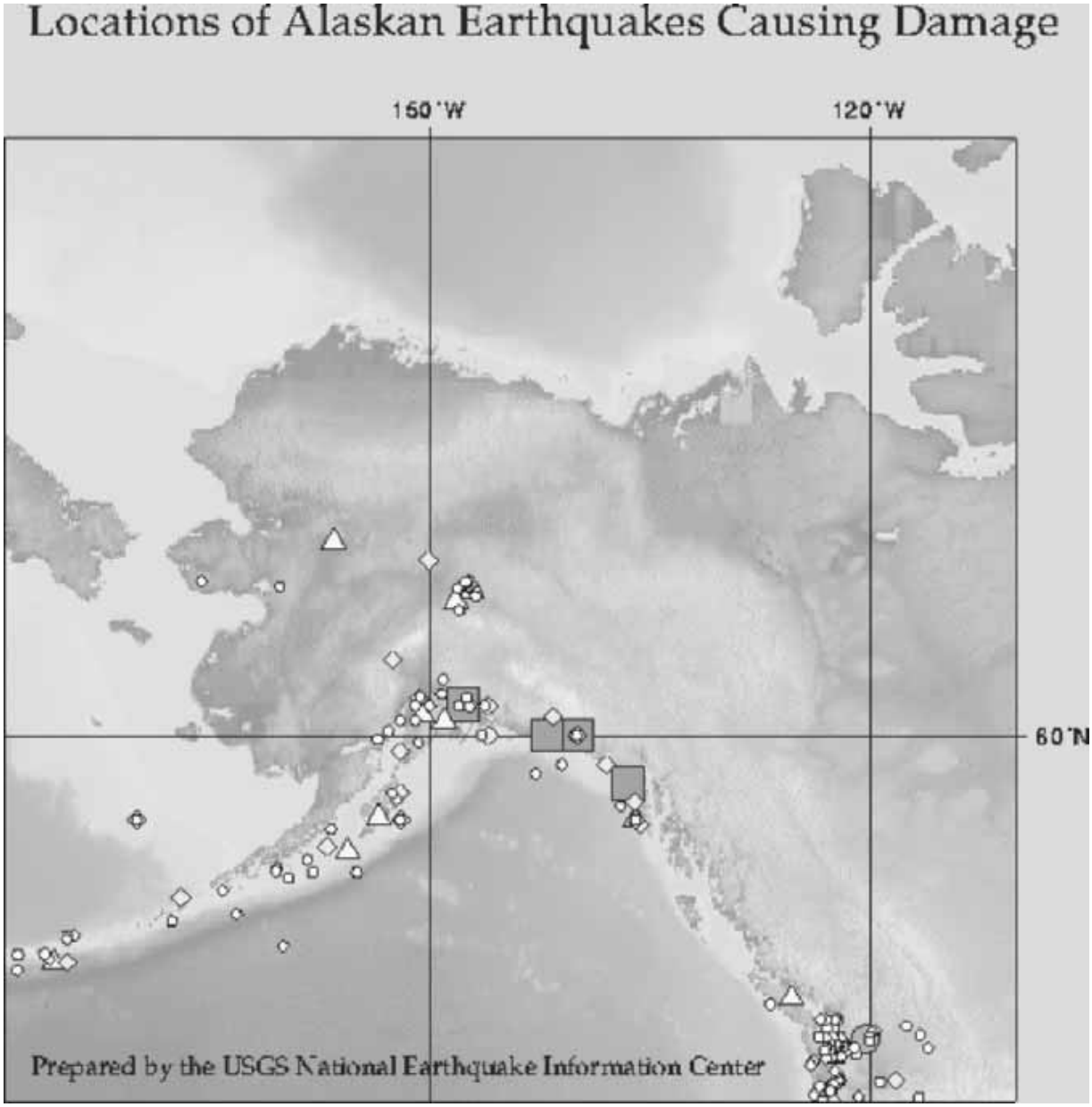

FIGURE 2.17 Locations of Alaskan earthquakes causing damage from 1750 to 1996 and having a modified Mercalli intensity of VI to XII. See Fig. 2.16 for intensity legend. (*Prepared by USGS National Earthquake Information Center.*)

2.4 Assume that a seismograph, located 1200 km from the epicenter of an earthquake, records a maximum ground displacement of 15.6 mm for surface waves having a period of 20 seconds. Based on these assumptions, determine the surface wave magnitude. *Answer:* $M_s = 7.9$.

2.5 Assume that during a major earthquake, the depth of fault rupture is estimated to be 15 km, the length of surface faulting is determined to be 600 km, and the average slip along the fault is 2.5 m. Based on these assumptions, determine the moment magnitude. Use a shear modulus equal to 3×10^{10} N/m^2. *Answer:* $M_w = 8.0$.

Earthquake Intensity

2.6 Suppose that you are considering buying an house located in Half Moon Bay, California. The house can be classified as a well-designed frame structure. For a repeat of

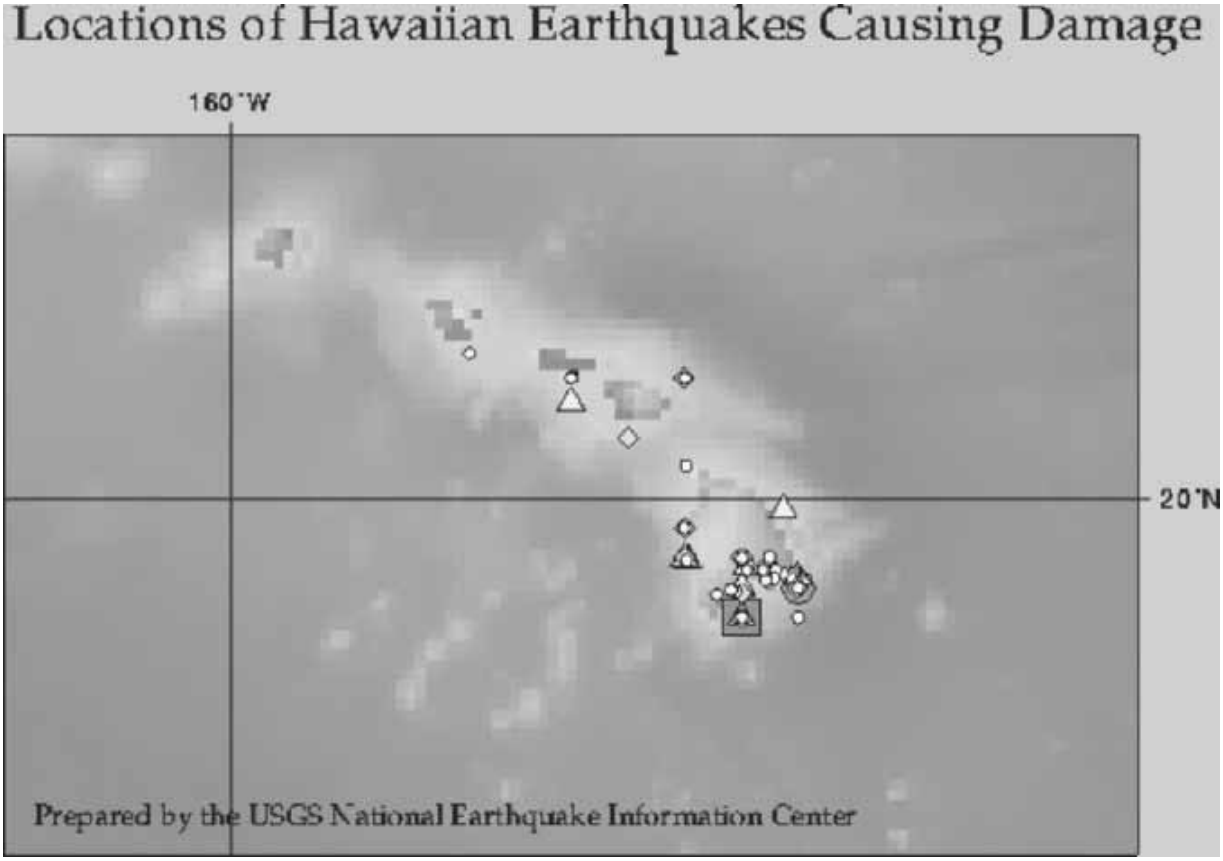

FIGURE 2.18 Locations of Hawaiian earthquakes causing damage from 1750 to 1996 and having a modified Mercalli intensity of VI to XII. See Fig. 2.16 for intensity legend. (*Prepared by USGS National Earthquake Information Center.*)

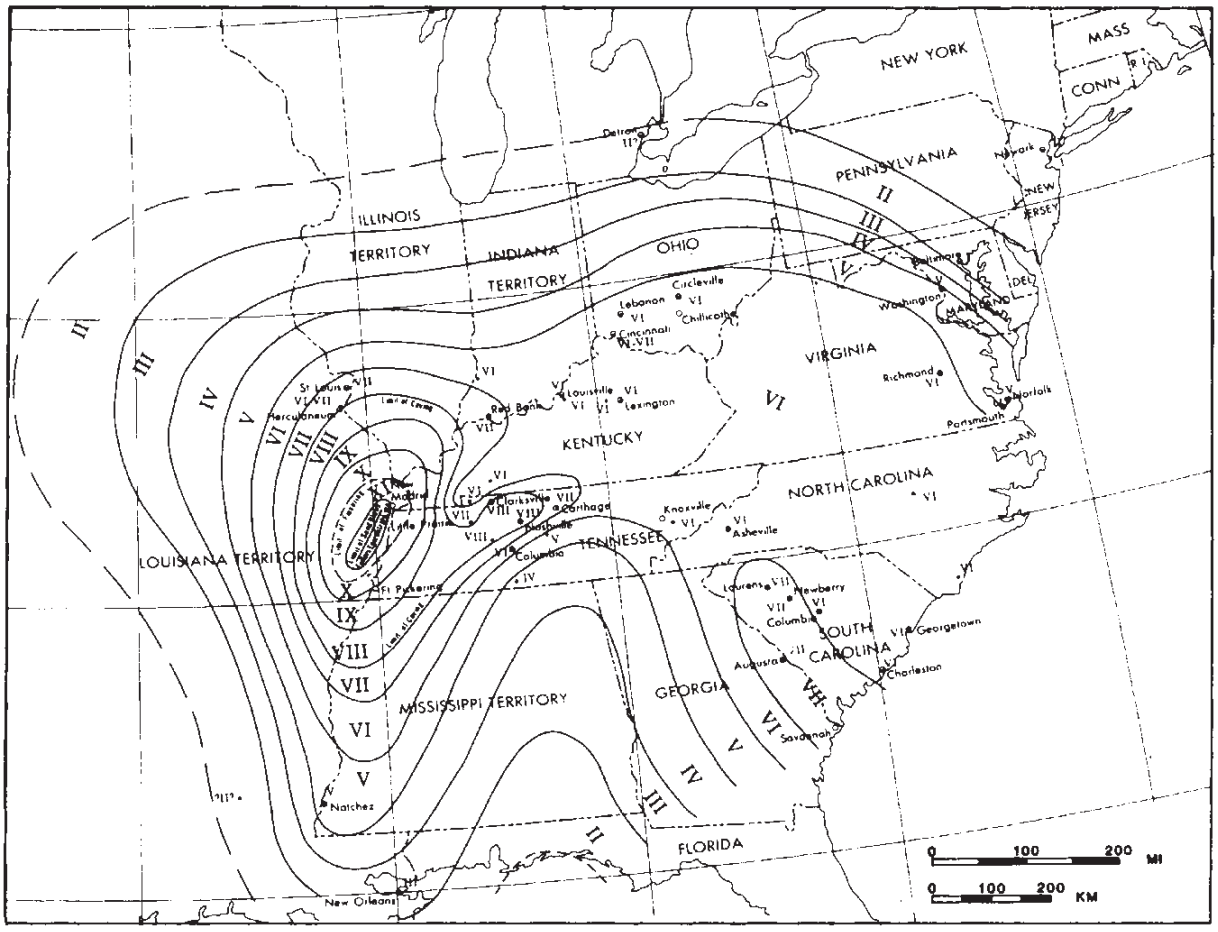

FIGURE 2.19 Intensity map for the New Madrid earthquake of December 16, 1811. (*Developed by Stearns and Wilson 1972, reproduced from Krinitzsky et al. 1993.*)

the 1906 San Francisco earthquake, what type of damage would be expected for this house? *Answer:* Based on Fig. 2.20, you should expect a modified Mercalli level of damage of IX, which corresponds to heavy damage. Per Table 2.3, at a level of IX, well-designed frame structures are thrown out of plumb.

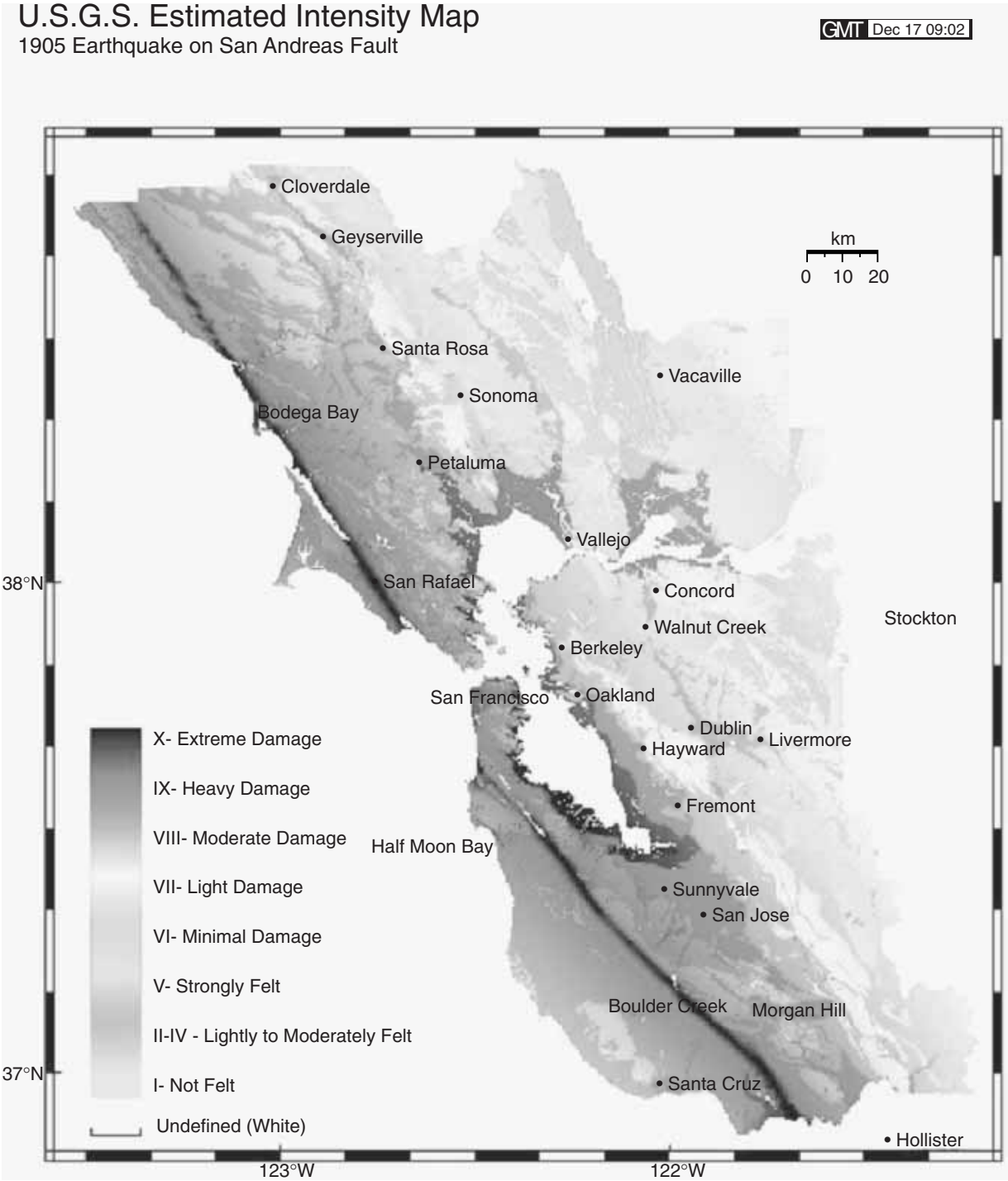

FIGURE 2.20 USGS estimated intensity map for a repeat of the 1906 San Francisco earthquake. (*Prepared by USGS.*)

FIGURE 2.21 Figure for Prob. 2.2.

TABLE 2.3 Modified Mercalli Intensity Scale

Intensity level	Reaction of observers and types of damage
I	Reactions: Not felt except by a very few people under especially favorable circumstances. Damage: No damage.
II	Reactions: Felt only by a few persons at rest, especially on upper floors of buildings. Many people do not recognize it as an earthquake. Damage: No damage. Delicately suspended objects may swing.
III	Reactions: Felt quite noticeably indoors, especially on upper floors of buildings. The vibration is like the passing of a truck, and the duration of the earthquake may be estimated. However, many people do not recognize it as an earthquake. Damage: No damage. Standing motor cars may rock slightly.
IV	Reactions: During the day, felt indoors by many, outdoors by a few. At night, some people are awakened. The sensation is like a heavy truck striking the building. Damage: Dishes, windows, and doors are disturbed. Walls make a creaking sound. Standing motor cars rock noticeably.
V	Reactions: Felt by nearly everyone, many awakened.

TABLE 2.3 Modified Mercalli Intensity Scale (*Continued*)

Intensity level	Reaction of observers and types of damage
	Damage: Some dishes, windows, etc., broken. A few instances of cracked plaster and unstable objects overturned. Disturbances of trees, poles, and other tall objects sometimes noticed. Pendulum clocks may stop.
VI	Reactions: Felt by everyone. Many people are frightened and run outdoors. Damage: There is slight structural damage. Some heavy furniture is moved, and there are a few instances of fallen plaster or damaged chimneys.
VII	Reactions: Everyone runs outdoors. Noticed by persons driving motor cars. Damage: Negligible damage in buildings of good design and construction, slight to moderate damage in well-built ordinary structures, and considerable damage in poorly built or badly designed structures. Some chimneys are broken.
VIII	Reactions: Persons driving motor cars are disturbed. Damage: Slight damage in specially designed structures. Considerable damage in ordinary substantial buildings, with partial collapse. Great damage in poorly built structures. Panel walls are thrown out of frame structures. There is the fall of chimneys, factory stacks, columns, monuments, and walls. Heavy furniture is overturned. Sand and mud are ejected in small amounts, and there are changes in well-water levels.
IX	Damage: Considerable damage in specially designed structures. Well-designed frame structures are thrown out of plumb. There is great damage in substantial buildings with partial collapse. Buildings are shifted off of their foundations. The ground is conspicuously cracked, and underground pipes are broken.
X	Damage: Some well-built wooden structures are destroyed. Most masonry and frame structures are destroyed, including the foundations. The ground is badly cracked. There are bent train rails, a considerable number of landslides at river banks and steep slopes, shifted sand and mud, and water is splashed over their banks.
XI	Damage: Few, if any, masonry structures remain standing. Bridges are destroyed, and train rails are greatly bent. There are broad fissures in the ground, and underground pipelines are completely out of service. There are earth slumps and land slips in soft ground.
XII	Reactions: Waves are seen on the ground surface. The lines of sight and level are distorted. Damage: Total damage with practically all works of construction greatly damaged or destroyed. Objects are thrown upward into the air.

CHAPTER 3
COMMON EARTHQUAKE EFFECTS

3.1 INTRODUCTION

This chapter deals with common earthquake damage due to tectonic surface processes and secondary effects. Section 3.2 deals with ground surface fault rupture, which is also referred to as *surface rupture*. Section 3.3 discusses regional subsidence, which often occurs at a rift valley, subduction zone, or an area of crust extension. Surface faulting and regional subsidence are known as tectonic surface processes.

Secondary effects are defined as nontectonic surface processes that are directly related to earthquake shaking (Yeats et al. 1997). Examples of secondary effects are liquefaction, earthquake-induced slope failures and landslides, tsunamis, and seiches. These secondary effects are discussed in Secs. 3.4 to 3.6.

3.2 SURFACE RUPTURE

3.2.1 Description

Most earthquakes will not create ground surface fault rupture. For example, there is typically an absence of surface rupture for small earthquakes, earthquakes generated at great depths at subduction zones, and earthquakes generated on blind faults. Krinitzsky et al. (1993) state that fault ruptures commonly occur in the deep subsurface with no ground breakage at the surface. They further state that such behavior is widespread, accounting for all earthquakes in the central and eastern United States.

On the other hand, large earthquakes at transform boundaries will usually be accompanied by ground surface fault rupture on strike-slip faults. An example of ground surface fault rupture of the San Andreas fault is shown in Fig. 2.9. Figures 2.11 to 2.13 also illustrate typical types of damage directly associated with the ground surface fault rupture. Two other examples of surface fault rupture are shown in Figs. 3.1 and 3.2.

Fault displacement is defined as the relative movement of the two sides of a fault, measured in a specific direction (Bonilla 1970). Examples of very large surface fault rupture are the 11 m (35 ft) of vertical displacement in the Assam earthquake of 1897 (Oldham 1899) and the 9 m (29 ft) of horizontal movement during the Gobi-Altai earthquake of 1957

FIGURE 3.1 Surface fault rupture associated with the El Asnam (Algeria) earthquake on October 10, 1980. (*Photograph from the Godden Collection, EERC, University of California, Berkeley.*)

(Florensov and Solonenko 1965). The length of the fault rupture can be quite significant. For example, the estimated length of surface faulting in the 1964 Alaskan earthquake varied from 600 to 720 km (Savage and Hastie 1966, Housner 1970).

3.2.2 Damage Caused by Surface Rupture

Surface fault rupture associated with earthquakes is important because it has caused severe damage to buildings, bridges, dams, tunnels, canals, and underground utilities (Lawson et al. 1908, Ambraseys 1960, Duke 1960, California Department of Water Resources 1967, Bonilla 1970, Steinbrugge 1970).

There were spectacular examples of surface fault rupture associated with the Chi-chi (Taiwan) earthquake on September 21, 1999. According to seismologists at the U.S. Geological Survey, National Earthquake Information Center, Golden, Colorado, the tectonic environment near Taiwan is unusually complicated. They state (USGS 2000a):

> Tectonically, most of Taiwan is a collision zone between the Philippine Sea and Eurasian plates. This collision zone is bridged at the north by northwards subduction of the Philippine Sea plate beneath the Ryuku arc and, at the south, an eastwards thrusting at the Manila trench. The northern transition from plate collision to subduction is near the coastal city of Hualien, located at about 24 degrees north, whereas the southern transition is 30–50 kilometers south of Taiwan.

With a magnitude of 7.6, the earthquake was the strongest to hit Taiwan in decades and was about the same strength as the devastating tremor that killed more than 17,000 people

FIGURE 3.2 Surface fault rupture associated with the Izmit (Turkey) earthquake on August 17, 1999. (*Photograph by Tom Fumal, USGS.*)

in Turkey a month before. The earthquake also triggered at least five aftershocks near or above magnitude 6. The epicenter of the earthquake was in a small country town of Chi-chi (located about 90 mi south of Taipei). Surface fault rupture associated with this Taiwan earthquake caused severe damage to civil engineering structures, as discussed below:

- *Dam failure:* Figures 3.3 and 3.4 show two views of the failure of a dam located northeast of Tai-Chung, Taiwan. This dam was reportedly used to supply drinking water for the surrounding communities. The surface fault rupture runs through the dam and caused the southern end to displace upward about 9 to 10 m (30 to 33 ft) as compared to the northern end. This ground fault displacement is shown in the close-up view in Fig. 3.4. Note in this figure that the entire length of fence on the top of the dam was initially at the same elevation prior to the earthquake.
- *Kuang Fu Elementary School:* Figures 3.5 and 3.6 show damage to the Kuang Fu Elementary School, located northeast of Tai-Chung, Taiwan. The Kuang Fu Elementary School was traversed by a large fault rupture that in some locations caused a ground displacement of as much as 3 m (10 ft), as shown in Fig. 3.5.

FIGURE 3.3 Overview of a dam damaged by surface fault rupture associated with the Chi-chi (Taiwan) earthquake on September 21, 1999. (*Photograph from the Taiwan Collection, EERC, University of California, Berkeley.*)

FIGURE 3.4 Close-up view of the location of the dam damaged by surface fault rupture associated with the Chi-chi (Taiwan) earthquake on September 21, 1999. Note in this figure that the entire length of fence on the top of the dam was initially at the same elevation prior to the earthquake. (*Photograph from the Taiwan Collection, EERC, University of California, Berkeley.*)

FIGURE 3.5 Overview of damage to the Kuang Fu Elementary School by surface fault rupture associated with the Chi-chi (Taiwan) earthquake on September 21, 1999. (*Photograph from the Taiwan Collection, EERC, University of California, Berkeley.*)

FIGURE 3.6 Portion of a building that remained standing at the Kuang Fu Elementary School. This portion of the building was directly adjacent to the surface fault rupture associated with the Chi-chi (Taiwan) Earthquake on September 21, 1999. Note in this figure that the ground was actually compressed together adjacent to the footwall side of the fault rupture. (*Photograph from the Taiwan Collection, EERC, University of California, Berkeley.*)

Figure 3.6 shows a building at the Kuang Fu Elementary School that partially collapsed. The portion of the building that remained standing is shown in Fig. 3.6. This portion of the building is immediately adjacent to the surface fault rupture and is located on the footwall side of the fault. Note in Fig. 3.6 that the span between the columns was actually reduced by the fault rupture. In essence, the ground was compressed together adjacent to the footwall side of the fault rupture.

- *Wu-His (U-Shi) Bridge:* Figure 3.7 shows damage to the second bridge pier south of the abutment of the new Wu-His (U-Shi) Bridge in Taiwan. At this site, surface fault rupturing was observed adjacent to the bridge abutment. Note in Fig. 3.7 that the bridge pier was literally sheared in half.
- *Retaining wall north of Chung-Hsing (Jung Shing) in Taiwan:* Figure 3.8 shows damage to a retaining wall and adjacent building. At this site, the surface fault rupture caused both vertical and horizontal displacement of the retaining wall.
- *Collapsed bridge north of Fengyuen:* Figures 3.9 to 3.11 show three photographs of the collapse of a bridge just north of Fengyuen, Taiwan. The bridge generally runs in a north-south direction, with the collapse occurring at the southern portion of the bridge.

  The bridge was originally straight and level. The surface fault rupture passes underneath the bridge and apparently caused the bridge to shorten such that the southern spans were shoved off their supports. In addition, the fault rupture developed beneath one of the piers, resulting in its collapse. Note in Fig. 3.11 that there is a waterfall to the east of the bridge. The fault rupture that runs underneath the bridge caused this displacement and development of the waterfall. The waterfall is estimated to be about 9 to 10 m (30 to 33 ft) in height.

  Figure 3.12 shows a close-up view of the new waterfall created by the surface fault rupture. This photograph shows the area to the east of the bridge. Apparently the dark

FIGURE 3.7 Close-up view of bridge pier (Wu-His Bridge) damaged by surface fault rupture associated with the Chi-chi (Taiwan) earthquake on September 21, 1999. (*Photograph from the Taiwan Collection, EERC, University of California, Berkeley.*)

FIGURE 3.8 Retaining wall located north of Chung-Hsing (Jung Shing). At this site, the surface fault rupture associated with the Chi-chi (Taiwan) earthquake on September 21, 1999, has caused both vertical and horizontal displacement of the retaining wall. (*Photograph from the Taiwan Collection, EERC, University of California, Berkeley.*)

FIGURE 3.9 Collapsed bridge north of Fengyuen caused by surface fault rupture associated with the Chi-chi (Taiwan) earthquake on September 21, 1999. (*Photograph from the USGS Earthquake Hazards Program, NEIC, Denver.*)

FIGURE 3.10 Another view of the collapsed bridge north of Fengyuen caused by surface fault rupture associated with the Chi-chi (Taiwan) earthquake on September 21, 1999. (*Photograph from the USGS Earthquake Hazards Program, NEIC, Denver.*)

rocks located in front of the waterfall are from the crumpling of the leading edge of the thrust fault movement.

- *Roadway damage:* The final photograph of surface fault rupture from the Chi-chi (Taiwan) earthquake is shown in Fig. 3.13. In addition to the roadway damage, such surface faulting would shear apart any utilities that happened to be buried beneath the roadway.

In addition to surface fault rupture, such as described above, there can be ground rupture away from the main trace of the fault. These ground cracks could be caused by many different factors, such as movement of subsidiary faults, auxiliary movement that branches off from the main fault trace, or ground rupture caused by the differential or lateral movement of underlying soil deposits.

As indicated by the photographs in this section, structures are unable to resist the shear movement associated with surface faulting. One design approach is to simply restrict construction in the active fault shear zone. This is discussed further in Sec. 11.2.

3.3 REGIONAL SUBSIDENCE

In addition to the surface fault rupture, another tectonic effect associated with the earthquake could be uplifting or regional subsidence. For example, at continent-continent

FIGURE 3.11 Another view of the collapsed bridge north of Fengyuen caused by surface fault rupture associated with the Chi-chi (Taiwan) earthquake on September 21, 1999. Note that the surface faulting has created the waterfall on the right side of the bridge. (*Photograph from the USGS Earthquake Hazards Program, NEIC, Denver.*)

collision zones (Fig. 2.7), the plates collide into one another, causing the ground surface to squeeze, fold, deform, and thrust upward.

Besides uplifting, there could also be regional subsidence associated with the earthquake. There was extensive damage due to regional subsidence during the August 17, 1999, Izmit earthquake in Turkey. Concerning this earthquake, the USGS (2000a) states:

> The Mw 7.4 [moment magnitude] earthquake that struck western Turkey on August 17, 1999 occurred on one of the world's longest and best studied strike-slip faults: the east-west trending North Anatolian fault. This fault is very similar to the San Andreas Fault in California.
>
> Turkey has had a long history of large earthquakes that often occur in progressive adjacent earthquakes. Starting in 1939, the North Anatolian fault produced a sequence of major earthquakes, of which the 1999 event is the 11th with a magnitude greater than or equal to 6.7. Starting with the 1939 event in western Turkey, the earthquake locations have moved both eastward and westward. The westward migration was particularly active and ruptured 600 km of contiguous fault between 1939 and 1944. This westward propagation of earthquakes then slowed and ruptured an additional adjacent 100 km of fault in events in 1957 and 1967, with separated activity further west during 1963 and 1964. The August 17, 1999 event fills in a 100 to 150 km long gap between the 1967 event and the 1963 and 1964 events.

The USGS also indicated that the earthquake originated at a depth of 17 km (10.5 mi) and caused right-lateral strike-slip movement on the fault. Preliminary field studies found that the earthquake produced at least 60 km (37 mi) of surface rupture and right-lateral offsets as large as 2.7 m (9 ft).

FIGURE 3.12 Close-up view of the waterfall shown in Fig. 3.11. The waterfall was created by the surface fault rupture associated with the Chi-chi (Taiwan) earthquake on September 21, 1999, and has an estimated height of 9 to 10 m. (*Photograph from the USGS Earthquake Hazards Program, NEIC, Denver.*)

As described above, the North Anatolian fault is predominantly a strike-slip fault due to the Anatolian plate shearing past the Eurasian plate. But to the west of Izmit, there is a localized extension zone where the crust is being stretched apart and has formed the Gulf of Izmit. An extension zone is similar to a rift valley. It occurs when a portion of the earth's crust is stretched apart and a graben develops. A *graben* is defined as a crustal block that has dropped down relative to adjacent rocks along bounding faults. The down-dropping block is usually much longer than its width, creating a long and narrow valley.

The city of Golcuk is located on the south shore of the Gulf of Izmit. It has been reported that during the earthquake, 2 mi (3 km) of land along the Gulf of Izmit subsided at least 3

FIGURE 3.13 Surface fault rupture and roadway damage associated with the Chi-chi (Taiwan) earthquake on September 21, 1999. (*Photograph from the USGS Earthquake Hazards Program, NEIC, Denver.*)

m (10 ft). Water from the Gulf of Izmit flooded inland, and several thousand people drowned or were crushed as buildings collapsed in Golcuk. Figures 3.14 to 3.18 show several examples of the flooded condition associated with the regional subsidence along the extension zone.

It is usually the responsibility of the engineering geologist to evaluate the possibility of regional subsidence associated with extension zones and rift valleys. For such areas, special foundation designs, such as mat slabs, may make the structures more resistant to the regional tectonic movement.

FIGURE 3.14 Flooding caused by regional subsidence associated with the Izmit (Turkey) earthquake on August 17, 1999. (*Photograph from the Izmit Collection, EERC, University of California, Berkeley.*)

FIGURE 3.15 Flooding caused by regional subsidence associated with the Izmit (Turkey) earthquake on August 17, 1999. (*Photograph from the Izmit Collection, EERC, University of California, Berkeley.*)

FIGURE 3.16 Flooding caused by regional subsidence associated with the Izmit (Turkey) earthquake on August 17, 1999. (*Photograph from the Izmit Collection, EERC, University of California, Berkeley.*)

FIGURE 3.17 Flooding caused by regional subsidence associated with the Izmit (Turkey) earthquake on August 17, 1999. (*Photograph from the Izmit Collection, EERC, University of California, Berkeley.*)

CHAPTER 4
EARTHQUAKE STRUCTURAL DAMAGE

4.1 INTRODUCTION

As discussed in Chap. 3, the actual rupture of the ground due to fault movement could damage a structure. Secondary effects, such as the liquefaction of loose granular soil, slope movement or failure, and inundation from a tsunami, could also cause structural damage. This chapter discusses some of the other earthquake-induced effects or structural conditions that can result in damage.

Earthquakes throughout the world cause a considerable amount of death and destruction. Earthquake damage can be classified as being either structural or non-structural. For example, the Federal Emergency Management Agency (1994) states:

> Damage to buildings is commonly classified as either structural or non-structural. Structural damage means the building's structural support has been impaired. Structural support includes any vertical and lateral force resisting systems, such as the building frames, walls, and columns. Non-structural damage does not affect the integrity of the structural support system. Examples of non-structural damage include broken windows, collapsed or rotated chimneys, and fallen ceilings. During an earthquake, buildings get thrown from side to side, and up and down. Heavier buildings are subjected to higher forces than lightweight buildings, given the same acceleration. Damage occurs when structural members are overloaded, or differential movements between different parts of the structure strain the structural components. Larger earthquakes and longer shaking durations tend to damage structures more. The level of damage resulting from a major earthquake can be predicted only in general terms, since no two buildings undergo the exact same motions during a seismic event. Past earthquakes have shown us, however, that some buildings are likely to perform more poorly than others.

There are four main factors that cause structural damage during an earthquake:

1. *Strength of shaking:* For small earthquakes (magnitude less than 6), the strength of shaking decreases rapidly with distance from the epicenter of the earthquake. According to the USGS (2000a), the strong shaking along the fault segment that slips during an earthquake becomes about one-half as strong at a distance of 8 mi, one-quarter as strong at a distance of 17 mi, one-eighth as strong at a distance of 30 mi, and one-sixteenth as strong at a distance of 50 mi.

In the case of a small earthquake, the center of energy release and the point where slip begins are not far apart. But in the case of large earthquakes, which have a significant length of fault rupture, these two points may be hundreds of miles apart. Thus for large earthquakes, the strength of shaking decreases in a direction away from the fault rupture.

2. *Length of shaking:* The length of shaking depends on how the fault breaks during the earthquake. For example, the maximum shaking during the Loma Prieta earthquake lasted only 10 to 15 s. But during other magnitude earthquakes in the San Francisco Bay area, the shaking may last 30 to 40 s. The longer the ground shakes, the greater the potential for structural damage. In general, the higher the magnitude of an earthquake, the longer the duration of the shaking ground (see Table 2.2).

3. *Type of subsurface conditions:* Ground shaking can be increased if the site has a thick deposit of soil that is soft and submerged. Many other subsurface conditions can cause or contribute to structural damage. For example, as discussed in Sec. 3.4, there could be structural damage due to liquefaction of loose submerged sands.

4. *Type of building:* Certain types of buildings and other structures are especially susceptible to the side-to-side shaking common during earthquakes. For example, sites located within approximately 10 mi (16 km) of the epicenter or location of fault rupture are generally subjected to rough, jerky, high-frequency seismic waves that are often more capable of causing short buildings to vibrate vigorously. For sites located at greater distance, the seismic waves often develop into longer-period waves that are more capable of causing high-rise buildings and buildings with large floor areas to vibrate vigorously (Federal Emergency Management Agency 1994).

Much as diseases will attack the weak and infirm, earthquakes damage those structures that have inherent weaknesses or age-related deterioration. Those buildings that are not reinforced, poorly constructed, weakened from age or rot, or underlain by soft or unstable soil are most susceptible to damage. This chapter discusses some of these susceptible structures.

4.2 EARTHQUAKE-INDUCED SETTLEMENT

Those buildings founded on solid rock are least likely to experience earthquake-induced differential settlement. However, buildings on soil could be subjected to many different types of earthquake-induced settlement. As discussed in Chap. 3, a structure could settle or be subjected to differential movement from the following conditions:

Tectonic Surface Effects

- Surface fault rupture, which can cause a structure that straddles the fault to be displaced vertically and laterally.
- Regional uplifting or subsidence associated with the tectonic movement.

Liquefaction

- Liquefaction-induced settlement.
- Liquefaction-induced ground loss below the structure, such as the loss of soil through the development of ground surface sand boils.
- Liquefaction-induced bearing capacity failure. Localized liquefaction could also cause limited punching-type failure of individual footings.
- Liquefaction-induced flow slides.
- Liquefaction-induced localized or large-scale lateral spreading.

Seismic-Induced Slope Movement

- Seismic-induced slope movement or failure (Tables 3.1 and 3.2).

- Seismic-induced landslide movement or failure.
- Slumping or minor shear deformations of embankments.

Tsunami or Seiche

- Settlement directly related to a tsunami or seiche. For example, the tsunami could cause erosion of the soil underneath the foundation, leading to settlement of the structure. An example of this condition is shown in Figs. 4.1 and 4.2.

Two additional conditions can cause settlement of a structure:

1. *Volumetric compression, also known as cyclic soil densification:* This type of settlement is due to ground shaking that causes the soil to compress, which is often described as *volumetric compression* or *cyclic soil densification.* An example would be the settlement of dry and loose sands that densify during the earthquake, resulting in ground surface settlement.

2. *Settlement due to dynamic loads caused by rocking:* This type of settlement is due to dynamic structural loads that momentarily increase the foundation pressure acting on the soil. The soil will deform in response to the dynamic structural load, resulting in settlement of the building. This settlement due to dynamic loads is often a result of the structure rocking back and forth.

These two conditions can also work in combination and cause settlement of the foundation. Settlement due to volumetric compression and rocking settlement are discussed in Secs. 7.4 and 7.5.

FIGURE 4.1 Overview of damage caused by a tsunami generated during the Prince William Sound earthquake in Alaska on March 27, 1964. Note the tilted tower in the background. (*Photograph from the Steinbrugge Collection, EERC, University of California, Berkeley.*)

FIGURE 4.2 Close-up view of the tilted tower shown in Fig. 4.1. The tilting of the tower was caused by the washing away of soil due to a tsunami generated during the Prince William Sound earthquake in Alaska on March 27, 1964. (*Photograph from the Steinbrugge Collection, EERC, University of California, Berkeley.*)

4.3 TORSION

Torsional problems develop when the center of mass of the structure is not located at the center of its lateral resistance, which is also known as the center of rigidity. A common example is a tall building that has a first-floor area consisting of a space that is open and supports the upper floors by the use of isolated columns, while the remainder of the first-floor area contains solid load-bearing walls that are interconnected. The open area having isolated columns will typically have much less lateral resistance than that part of the floor containing the interconnected load-bearing walls. While the center of mass of the building may be located at the midpoint of the first-floor area, the center of rigidity is offset toward the area containing the interconnected load-bearing walls. During the earthquake, the center of mass will twist about the center of rigidity, causing torsional forces to be induced into the building frame.

An example is shown in Figs. 4.3 and 4.4. The two views are inside the Hotel Terminal and show the collapse of the second story due to torsional shear failure of the second-floor columns during the Gualan earthquake in Guatemala on February 4, 1976. This torsional failure has been described as follows (EERC 2000):

> Figure 4.3 is a view inside Hotel Terminal showing the collapse of the second story due to shear failure of the second-floor columns. Note the significant lateral displacement (interstory drift to the right) due to the torsional rotation of the upper part of the building.
>
> Figure 4.4 is a close-up of one of the collapsed columns of Hotel Terminal. Note that the upper floor has displaced to the right and dropped, and the top and bottom sections of the column are now side-by-side. Although the columns had lateral reinforcement (ties), these were

FIGURE 4.3 Torsional failure of the second story of the Hotel Terminal. The torsional failure occurred during the Gualan earthquake in Guatemala on February 4, 1976. (*Photograph from the Godden Collection, EERC, University of California, Berkeley.*)

FIGURE 4.4 Close-up view of a collapsed second-story column at the Hotel Terminal. Note that the upper floor has displaced to the right and dropped, and the top and bottom sections of the column are now side by side. The torsional failure occurred during the Gualan earthquake in Guatemala on February 4, 1976. (*Photograph from the Godden Collection, EERC, University of California, Berkeley.*)

not enough and at inadequate spacing to resist the shear force developed due to the torsional moment which originated in the second story. This failure emphasizes the importance of avoiding large torsional forces and the need for providing an adequate amount of transverse reinforcement with proper detailing.

4.4 SOFT STORY

4.4.1 Definition and Examples

A *soft story,* also known as a *weak story,* is defined as a story in a building that has substantially less resistance, or stiffness, than the stories above or below it. In essence, a soft story has inadequate shear resistance or inadequate ductility (energy absorption capacity) to resist the earthquake-induced building stresses. Although not always the case, the usual location of the soft story is at the ground floor of the building. This is because many buildings are designed to have an open first-floor area that is easily accessible to the public. Thus the first floor may contain large open areas between columns, without adequate shear resistance. The earthquake-induced building movement also causes the first floor to be subjected to the greatest stress, which compounds the problem of a soft story on the ground floor.

Concerning soft stories, the National Information Service for Earthquake Engineering (2000) states:

> In shaking a building, an earthquake ground motion will search for every structural weakness. These weaknesses are usually created by sharp changes in stiffness, strength and/or ductility, and the effects of these weaknesses are accentuated by poor distribution of reactive masses. Severe structural damage suffered by several modern buildings during recent earthquakes illustrates the importance of avoiding sudden changes in lateral stiffness and strength. A typical example of the detrimental effects that these discontinuities can induce is seen in the case of buildings with a "soft story." Inspection of earthquake damage as well as the results of analytical studies have shown that structural systems with a soft story can lead to serious problems during severe earthquake ground shaking. [Numerous examples] illustrate such damage and therefore emphasize the need for avoiding the soft story by using an even distribution of flexibility, strength, and mass.

The following are five examples of buildings having a soft story on the ground floor:

1. *Chi-chi earthquake in Taiwan on September 21, 1999:* In Taiwan, it is common practice to have an open first-floor area by using columns to support the upper floors. In some cases, the spaces between the columns are filled in with plate-glass windows in order to create ground-floor shops. Figure 4.5 shows an example of this type of construction and the resulting damage caused by the Chi-chi earthquake.

2. *Northridge earthquake in California on January 17, 1994:* Many apartment buildings in southern California contain a parking garage on the ground floor. To provide an open area for the ground-floor parking area, isolated columns are used to support the upper floors. These isolated columns often do not have adequate shear resistance and are susceptible to collapse during an earthquake. For example, Figs. 4.6 and 4.7 show the collapse of an apartment building during the Northridge earthquake caused by the weak shear resistance of the first-floor garage area.

3. *Loma Prieta earthquake in California on October 19, 1989:* Another example of a soft story due to a first-floor garage area is shown in Fig. 4.8. The four-story apartment building was located on Beach Street, in the Marina District, San Francisco. The first-floor

FIGURE 4.5 Damage due to a soft story at the ground floor. The damage occurred during the Chi-chi earthquake in Taiwan on September 21, 1999. (*Photograph from the USGS Earthquake Hazards Program, NEIC, Denver.*)

garage area, with its large open areas, had inadequate shear resistance and was unable to resist the earthquake-induced building movements.

4. *Izmit earthquake in Turkey on August 17, 1999:* Details concerning this earthquake have been presented in Sec. 3.3. In terms of building conditions, it has been stated (Bruneau 1999):

> A typical reinforced concrete frame building in Turkey consists of a regular, symmetric floor plan, with square or rectangular columns and connecting beams. The exterior enclosure as well as interior partitioning are of non-bearing unreinforced brick masonry infill walls. These walls contributed significantly to the lateral stiffness of buildings during the earthquake and, in many instances, controlled the lateral drift and resisted seismic forces elastically. This was especially true in low-rise buildings, older buildings where the ratio of wall to floor area was very high, and buildings located on firm soil. Once the brick infills failed, the lateral strength and stiffness had to be provided by the frames alone, which then experienced significant inelasticity in the critical regions. At this stage, the ability of reinforced concrete columns,

FIGURE 4.6 Building collapse caused by a soft story due to the parking garage on the first floor. The building collapse occurred during the Northridge earthquake in California on January 17, 1994.

FIGURE 4.7 View inside the collapsed first-floor parking garage (the arrows point to the columns). The building collapse occurred during the Northridge earthquake in California on January 17, 1994.

FIGURE 4.8 Damage caused by a soft story due to a parking garage on the first floor. The damage occurred during the Loma Prieta earthquake in California on October 17, 1989. (*Photograph from the Loma Prieta Collection, EERC, University of California, Berkeley.*)

beams, and beam-column joints to sustain deformation demands depended on how well the seismic design and detailing requirements were followed both in design and in construction.

A large number of residential and commercial buildings were built with soft stories at the first-floor level. First stories are often used as stores and commercial areas, especially in the central part of cities. These areas are enclosed with glass windows, and sometimes with a single masonry infill at the back. Heavy masonry infills start immediately above the commercial floor. During the earthquake, the presence of a soft story increased deformation demands very significantly, and put the burden of energy dissipation on the first-story columns. Many failures and collapses can be attributed to the increased deformation demands caused by soft stories, coupled with lack of deformability of poorly designed columns. This was particularly evident on a commercial street where nearly all buildings collapsed towards the street.

Examples of this soft story condition are shown in Figs. 4.9 and 4.10.

5. *El Asnam earthquake in Algeria on October 10, 1980:* An interesting example of damage due to a soft story is shown in Fig. 4.11 and described below (National Information Service for Earthquake Engineering 2000):

Although most of the buildings in this new housing development [see Fig. 4.11] remained standing after the earthquake, some of them were inclined as much as 20 degrees and dropped up to 1 meter, producing significant damage in the structural and non-structural elements of the first story. The reason for this type of failure was the use of the "Vide Sanitaire," a crawl space about 1 meter above the ground level. This provides space for plumbing and ventilation under the first floor slab and serves as a barrier against transmission of humidity from the ground to the first floor. Unfortunately, the way that the vide sanitaires were constructed created a soft story with inadequate shear resistance. Hence the stubby columns in this crawl space were sheared off by the inertia forces induced by the earthquake ground motion.

Although the above five examples show damage due to a soft story located on the first floor or lowest level of the building, collapse at other stories can also occur depending on

FIGURE 4.9 Damage caused by a soft story at the first-floor level. The damage occurred during the Izmit earthquake in Turkey on August 17, 1999. (*Photograph by Mehmet Celebi, USGS.*)

the structural design. For example, after the Kobe earthquake in Japan on January 17, 1995, it was observed that there were a large number of 20-year and older high-rise buildings that collapsed at the fifth floor. The cause was apparently an older version of the building code that allowed a weaker superstructure beginning at the fifth floor.

While damage and collapse due to a soft story are most often observed in buildings, they can also be developed in other types of structures. For example, Figs. 4.12 and 4.13 show an elevated gas tank that was supported by reinforced concrete columns. The lower level containing the concrete columns behaved as a soft story in that the columns were unable to provide adequate shear resistance during the earthquake.

Concerning the retrofitting of a structure that has a soft story, the National Information Service for Earthquake Engineering (2000) states:

> There are many existing buildings in regions of high seismic risk that, because of their structural systems and/or of the interaction with non-structural components, have soft stories with either inadequate shear resistance or inadequate ductility (energy absorption capacity) in the event of being subjected to severe earthquake ground shaking. Hence they need to be retrofitted. Usually the most economical way of retrofitting such a building is by adding proper shear walls or bracing to the soft stories.

4.4.2 Pancaking

Pancaking occurs when the earthquake shaking causes a soft story to collapse, leading to total failure of the overlying floors. These floors crush and compress together such that the

FIGURE 4.10 Building collapse caused by a soft story at the first-floor level. The damage occurred during the Izmit earthquake in Turkey on August 17, 1999. (*Photograph by Mehmet Celebi, USGS.*)

FIGURE 4.11 Building tilting and damage caused by a soft story due to a ground-floor crawl space. The damage occurred during the El Asnam earthquake in Algeria on October 10, 1980. (*Photograph from the Godden Collection, EERC, University of California, Berkeley.*)

FIGURE 4.12 Overview of a collapsed gas storage tank, located at a gas storage facility near Sabanci Industrial Park, Turkey. The elevated gas storage tank collapsed during the Izmit earthquake in Turkey on August 17, 1999. (*Photograph from the Izmit Collection, EERC, University of California, Berkeley.*)

FIGURE 4.13 Close-up view of the columns that had supported the elevated gas storage tank shown in Fig. 4.12. The columns did not have adequate shear resistance and were unable to support the gas storage tank during the Izmit earthquake in Turkey on August 17, 1999. (*Photograph from the Izmit Collection, EERC, University of California, Berkeley.*)

final collapsed condition of the building consists of one floor stacked on top of another, much like a stack of pancakes.

Pancaking of reinforced concrete multistory buildings was common throughout the earthquake-stricken region of Turkey due to the Izmit earthquake on August 17, 1999. Examples of pancaking caused by this earthquake are shown in Figs. 4.14 to 4.16. Concerning the damage caused by the Izmit earthquake, Bruneau (1999) states:

> Pancaking is attributed to the presence of "soft" lower stories and insufficiently reinforced connections at the column-beam joints. Most of these buildings had a "soft" story—a story with most of its space unenclosed—and a shallow foundation and offered little or no lateral resistance to ground shaking. As many as 115,000 of these buildings—some engineered, some not—were unable to withstand the strong ground shaking and were either badly damaged or collapsed outright, entombing sleeping occupants beneath the rubble. Partial collapses involved the first two stories. The sobering fact is that Turkey still has an existing inventory of several hundred thousand of these highly vulnerable buildings. Some will need to undergo major seismic retrofits; others will be demolished.

Another example of pancaking is shown in Fig. 4.17. The site is located in Mexico City, and the damage was caused by the Michoacan earthquake in Mexico on September 19, 1985. Note in Fig. 4.17 that there was pancaking of only the upper several floors of the parking garage. The restaurant building that abutted the parking garage provided additional lateral support, which enabled the lower three floors of the parking garage to resist the earthquake shaking. The upper floors of the parking garage did not have this additional lateral support and thus experienced pancaking during the earthquake.

FIGURE 4.14 Pancaking of a building during the Izmit earthquake in Turkey on August 17, 1999. (*Photograph by Mehmet Celebi, USGS.*)

FIGURE 4.15 Pancaking of a building, which also partially crushed a bus, during the Izmit earthquake in Turkey on August 17, 1999. (*Photograph from the Izmit Collection, EERC, University of California, Berkeley.*)

FIGURE 4.16 Pancaking of a building, during the Izmit earthquake in Turkey on August 17, 1999. Note that the center of the photograph shows a hole that was excavated through the pancaked building in order to rescue the survivors. (*Photograph from the Izmit Collection, EERC, University of California, Berkeley.*)

FIGURE 4.17 Pancaking of the upper floors of a parking garage during the Michoacan earthquake in Mexico on September 19, 1985. Note that the restaurant building provided additional lateral support which enabled the lower three floors of the parking garage to resist the collapse. (*Photograph from the Steinbrugge Collection, EERC, University of California, Berkeley.*)

4.4.3 Shear Walls

Many different types of structural systems can be used to resist the inertia forces in a building that are induced by the earthquake ground motion. For example, the structural engineer could use braced frames, moment-resisting frames, and shear walls to resist the lateral earthquake-induced forces. Shear walls are designed to hold adjacent columns or vertical support members in place and then transfer the lateral forces to the foundation. The forces resisted by shear walls are predominately shear forces, although a slender shear wall could also be subjected to significant bending (Arnold and Reitherman 1982).

Figure 4.18 shows the failure of a shear wall at the West Anchorage High School caused by the Prince William Sound earthquake in Alaska on March 27, 1964. Although the shear wall shown in Fig. 4.18 contains four small windows, often a shear wall is designed and constructed as a solid and continuous wall, without any window or door openings. The X-shaped cracks between the two lower windows in Fig. 4.18 are 45° diagonal tension cracks,

FIGURE 4.18 Damage to a shear wall at the West Anchorage High School caused by the Prince William Sound earthquake in Alaska on March 27, 1964. (*Photograph from the Steinbrugge Collection, EERC, University of California, Berkeley.*)

which are typical and characteristic of earthquake-induced damage. These diagonal tension cracks are formed as the shear wall moves back and forth in response to the earthquake ground motion.

Common problems with shear walls are that they have inadequate strength to resist the lateral forces and that they are inadequately attached to the foundation. For example, having inadequate shear walls on a particular building level can create a soft story. A soft story could also be created if there is a discontinuity in the shear walls from one floor to the other, such as a floor where its shear walls are not aligned with the shear walls on the upper or lower floors.

Even when adequately designed and constructed, shear walls will not guarantee the survival of the building. For example, Fig. 4.19 shows a comparatively new building that was proclaimed as "earthquake-proof" because of the box-type construction consisting of numerous shear walls. Nevertheless, the structure was severely damaged because of earthquake-induced settlement of the building.

4.4.4 Wood-Frame Structures

It is generally recognized that single-family wood-frame structures that include shear walls in their construction are very resistant to collapse from earthquake shaking. This is due to several factors, such as their flexibility, strength, and light dead loads, which produce low earthquake-induced inertia loads. These factors make the wood-frame construction much better at resisting shear forces and hence more resistant to collapse.

There are exceptions to the general rule that wood-frame structures are resistant to collapse. For example, in the 1995 Kobe earthquake, the vast majority of deaths were due to

FIGURE 4.19 A comparatively new building that was proclaimed as "earthquake-proof" because of the box-type construction consisting of numerous shear walls. Nevertheless, the structure was severely damaged because of earthquake-induced settlement of the building during the Bucharest earthquake on March 4, 1977. (*Photograph from the Steinbrugge Collection, EERC, University of California, Berkeley.*)

the collapse of one- and two-story residential and commercial wood-frame structures. More than 200,000 houses, about 10 percent of all houses in the Hyogo prefecture, were damaged, including more than 80,000 collapsed houses, 70,000 severely damaged, and 7000 consumed by fire. The collapse of the houses has been attributed to several factors, such as (EQE Summary Report, 1995):

- Age-related deterioration, such as wood rot, that weakened structural members.
- Post and beam construction that often included open first-floor areas (i.e., a soft first floor), with few interior partitions that were able to resist lateral earthquake loads.
- Weak connections between the walls and the foundation.
- Inadequate foundations that often consisted of stones or concrete blocks.

- Poor soil conditions consisting of thick deposits of soft or liquefiable soil that settled during the earthquake. Because of the inadequate foundations, the wood-frame structures were unable to accommodate the settlement.
- Inertia loads from heavy roofs that exceeded the lateral earthquake load-resisting capacity of the supporting walls. The heavy roofs were created by using thick mud or heavy tile and were used to resist the winds from typhoons. However, when the heavy roofs collapsed during the earthquake, they crushed the underlying structure.

4.5 POUNDING DAMAGE

Pounding damage can occur when two buildings are constructed close to each other and, as they rock back-and-forth during the earthquake, they collide into each other. Even when two buildings having dissimilar construction materials or different heights are constructed adjacent to each other, it does not necessarily mean that they will be subjected to pounding damage. For example, as shown in Fig. 4.17, the restaurant that was constructed adjacent to the parking garage actually provided lateral support to the garage and prevented the three lower levels from collapsing.

In the common situation for pounding damage, a much taller building, which has a higher period and larger amplitude of vibration, is constructed against a squat and short building that has a lower period and smaller amplitude of vibration. Thus during the earthquake, the buildings will vibrate at different frequencies and amplitudes, and they can collide with each other. The effects of pounding can be especially severe if the floors of one building impact the other building at different elevations, so that, for example, the floor of one building hits a supporting column of an adjacent building.

Figure 4.20 shows an example of pounding damage to the Anchorage-Westward Hotel caused by the Prince William Sound earthquake in Alaska on March 27, 1964. Although not evident in the photograph, the structure shown on the right half of the photograph is a 14-story hotel. The structure visible on the left half of Fig. 4.20 is the hotel ballroom. The pounding damage occurred at the junction of the 14-story hotel and the short and squat ballroom. Note in Fig. 4.20 that the main cracking emanates from the upper left corner of the street-level doorway. The doorway is a structural weak point, which has been exploited during the side-to-side shaking during the earthquake.

Another example of pounding damage and eventual collapse is shown in Fig. 4.21. The buildings were damaged during the Izmit earthquake in Turkey on August 17, 1999. As shown in Fig. 4.21, the pounding damage was accompanied by the collapse of the two buildings into each other.

It is very difficult to model the pounding effects of two structures and hence design structures to resist such damage. As a practical matter, the best design approach to prevent pounding damage is to provide sufficient space between the structures to avoid the problem. If two buildings must be constructed adjacent to each other, then one design feature should be to have the floors of both buildings at the same elevations, so that the floor of one building does not hit a supporting column of an adjacent building.

4.51 Impact Damage from Collapse of Adjacent Structures

Similar to pounding damage, the collapse of a building can affect adjacent structures. For example, Fig. 4.22 shows a building that has lost a corner column due to the collapse of an adjacent building during the Izmit Earthquake in Turkey on August 17, 1999. The buildings were under construction at the time of the earthquake. Note that the roof of the col-

FIGURE 4.20 Pounding damage to the Anchorage-Westward Hotel caused by the Prince William Sound earthquake in Alaska on March 27, 1964. The building on the right half of the photograph is the 14-story hotel, while the building visible on the left half of the photograph is the ballroom. (*Photograph from the Steinbrugge Collection, EERC, University of California, Berkeley.*)

lapsed building now rests on the third story corner of the standing building.

Since the geotechnical engineer and engineering geologist are usually required to discuss any "earthquake hazards" that could affect the planned construction, it may be appropriate for them to evaluate possible collapse of adjacent buildings founded on poor soil or susceptible to geologic hazards.

4.5.2 Asymmetry

Similar to pounding damage, buildings that are asymmetric, such as T- or L-shaped buildings, can experience damage as different parts of the building vibrate at different frequencies and amplitudes. This difference in movement of different parts of the building is due to the relative stiffness of each portion of the building. For example, for the T-shaped build-

FIGURE 4.21 Another example of pounding damage and eventual collapse caused by the Izmit earthquake in Turkey on August 17, 1999. (*Photograph from the Izmit Collection, EERC, University of California, Berkeley.*)

ing, the two segments that make up the building are usually much more stiff in their long directions, then across the segments. Thus damage tends to occur where the two segments of the T join together.

4.6 RESONANCE OF THE STRUCTURE

Resonance is defined as a condition in which the period of vibration of the earthquake-induced ground shaking is equal to the natural period of vibration of the building. When resonance occurs, the shaking response of the building is enhanced, and the amplitude of vibration of the building rapidly increases. Tall buildings, bridges, and other large structures respond most to ground shaking that has a high period of vibration, and small structures respond most to low-period shaking. For example, a rule of thumb is that the period of vibration is about equal to 0.1 times the number of stories in a building. Thus a 10-story

FIGURE 4.22 The building shown has lost a corner column due to the collapse of an adjacent building during the Izmit earthquake in Turkey on August 17, 1999. Note that the roof of the collapsed building now rests on the third-story corner of the standing building. (*Photograph from the Izmit Collection, EERC, University of California, Berkeley.*)

building would have a natural period of vibration of about 1 s, and if the earthquake-induced ground motion also has a period of vibration of about 1 s, then resonance is expected to occur for the 10-story building.

A response spectrum can be used to directly assess the nature of the earthquake ground motion on the structure. A response spectrum is basically a plot of the maximum displacement, velocity, or acceleration versus the natural period of a single-degree-of-freedom system. Different values of system damping can be used, and thus a family of such curves could be obtained. This information can then be used by the structural engineer in the design of the building. The response spectrum is discussed further in Sec. 11.5.

4.6.1 Soft Ground Effects

If the site is underlain by soft ground, such as a soft and saturated clay deposit, then there could be an increased peak ground acceleration a_{max} and a longer period of vibration of the ground. The following two examples illustrate the effect of soft clay deposits.

Michoacan Earthquake in Mexico on September 19, 1985. There was extensive damage to Mexico City caused by the September 19, 1985, Michoacan earthquake. The greatest damage in Mexico City occurred to those buildings underlain by 125 to 164 ft (39 to 50 m) of soft clays, which are within the part of the city known as the Lake Zone (Stone et al. 1987). Because the epicenter of the earthquake was so far from Mexico City, the peak ground acceleration a_{max} recorded in the foothills of Mexico City (rock site) was about

FIGURE 4.23 Building collapse in Mexico City caused by the Michoacan earthquake in Mexico on September 19, 1985. (*Photograph from the Steinbrugge Collection, EERC, University of California, Berkeley.*)

FIGURE 4.24 Building collapse in Mexico City caused by the Michoacan earthquake in Mexico on September 19, 1985. (*Photograph from the Steinbrugge Collection, EERC, University of California, Berkeley.*)

0.04*g*. However, at the Lake Zone, the peak ground accelerations a_{max} were up to 5 times greater than at the rock site (Kramer 1996). In addition, the characteristic site periods were estimated to be 1.9 to 2.8 s (Stone et al. 1987). This longer period of vibration of the ground tended to coincide with the natural period of vibration of the taller buildings in the 5- to 20-story range. The increased peak ground acceleration and the effect of resonance caused either collapse or severe damage of these taller buildings, such as shown in Figs. 4.23 and 4.25. To explain this condition of an increased peak ground acceleration and a longer period of surface vibration, an analogy is often made between the shaking of these soft clays and the shaking of a bowl of jelly.

Loma Prieta Earthquake in San Francisco Bay Area on October 17, 1989. A second example of soft ground effects is the Loma Prieta earthquake on October 17, 1989. Figure 4.26 presents the ground accelerations (east-west direction) at Yerba Buena Island and at Treasure Island (R. B. Seed et al. 1990). Both sites are about the same distance from the epicenter of the Loma Prieta earthquake. However, the Yerba Buena Island seismograph is located directly on a rock outcrop, while the Treasure Island seismograph is underlain by

FIGURE 4.25 Building damage and tilting in Mexico City caused by the Michoacan earthquake in Mexico on September 19, 1985. (*Photograph from the Steinbrugge Collection, EERC, University of California, Berkeley.*)

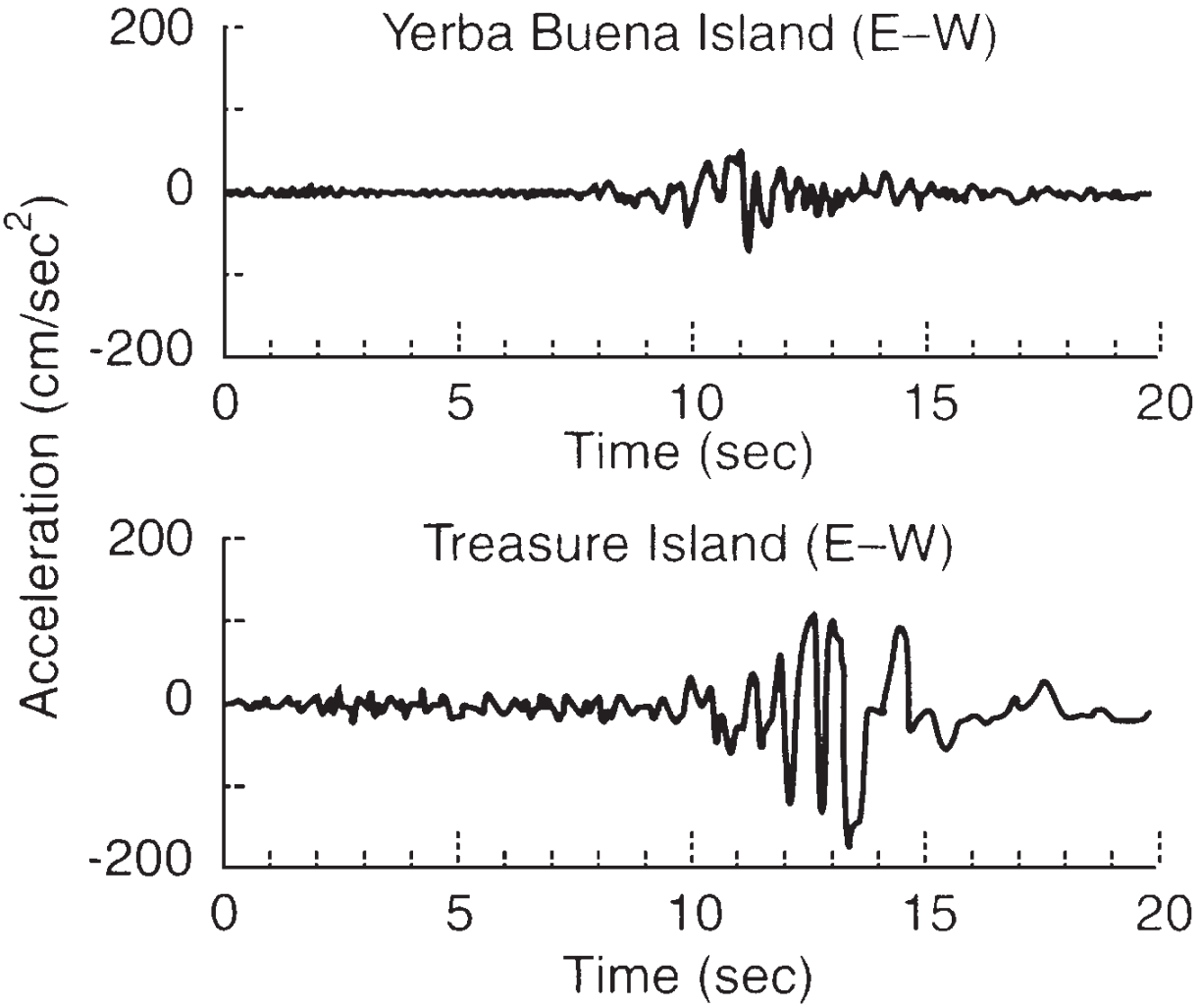

FIGURE 4.26 Ground surface acceleration in the east-west direction at Yerba Buena Island and at Treasure Island for the Loma Prieta earthquake in California on October 17, 1989. (*From Seed et al. 1990.*)

45 ft (13.7 m) of loose sandy soil over 55 ft (16.8 m) of San Francisco Bay mud (a normally consolidated silty clay). Note the significantly different ground acceleration plots for these two sites. The peak ground acceleration in the east-west direction at Yerba Buena Island was only 0.06*g*, while at Treasure Island the peak ground acceleration in the east-west direction was 0.16*g* (Kramer 1996). Thus the soft clay site had a peak ground acceleration that was 2.7 times that of the hard rock site.

The amplification of the peak ground acceleration by soft clay also contributed to damage of structures throughout the San Francisco Bay area. For example, the northern portion of the Interstate 880 highway (Cypress Street Viaduct) that collapsed was underlain by the San Francisco Bay mud (see Figs. 4.27 to 4.29). The southern portion of the Interstate 880 highway was not underlain by the bay mud, and it did not collapse.

As these two examples illustrate, local soft ground conditions can significantly increase the peak ground acceleration a_{max} by a factor of 3 to 5 times. The soft ground can also increase the period of ground surface shaking, leading to resonance of taller structures. The geotechnical engineer and engineering geologist will need to evaluate the possibility of increasing the peak ground acceleration a_{max} and increasing the period of ground shaking for sites that contain thick deposits of soft clay. This is discussed further in Sec. 5.6.

FIGURE 4.27 Overview of the collapse of the Cypress Street Viaduct caused by the Loma Prieta earthquake in California on October 17, 1989. (*From USGS.*)

FIGURE 4.28 Close-up view of the collapse of the Cypress Street Viaduct caused by the Loma Prieta earthquake in California on October 17, 1989. (*From USGS.*)

FIGURE 4.29 Close-up view of the collapse of the Cypress Street Viaduct caused by the Loma Prieta earthquake in California on October 17, 1989. (*From USGS.*)

P · A · R · T · 2

GEOTECHNICAL EARTHQUAKE ENGINEERING ANALYSES

CHAPTER 5

SITE INVESTIGATION FOR GEOTECHNICAL EARTHQUAKE ENGINEERING

The following notation is used in this chapter:

SYMBOL	*DEFINITION*
a_{max}	Peak ground acceleration
c	Cohesion based on a total stress analysis
c'	Cohesion based on an effective stress analysis
C_b	Borehole diameter correction
C_N	Correction factor to account for the overburden pressure
C_r	Rod length correction
D	Inside diameter of the SPT sampler
D_r	Relative density
e	Void ratio of soil
e_{max}	Void ratio corresponding to loosest possible state of soil
e_{min}	Void ratio corresponding to densest possible state of soil
E_m	Hammer efficiency
F	Outside diameter of the SPT sampler
FS_L	Factor of safety against liquefaction
g	Acceleration of gravity
h	Depth below ground surface
N	Measured SPT blow count (that is, N value in blows per foot)
N_{60}	N value corrected for field testing procedures
$(N_1)_{60}$	N value corrected for field testing procedures and overburden pressure
q_c	Cone resistance
q_{c1}	Cone resistance corrected for overburden pressure
r_u	Pore water pressure ratio
s_u	Undrained shear strength of soil
S_t	Sensitivity of cohesive soil
u	Pore water pressure
Z	Seismic zone factor
ϕ	Friction angle of sand (Sec. 5.4)
ϕ	Friction angle based on a total stress analysis (Sec. 5.5)
ϕ'	Friction angle based on an effective stress analysis
ϕ_r'	Drained residual friction angle
γ_t	Total unit weight of soil

σ	Total stress
σ'	Effective stress ($\sigma' = \sigma - u$)
σ_{v0}'	Vertical effective stress

5.1 INTRODUCTION

Part 2 of the book describes the different types of geotechnical earthquake engineering analyses. Specific items that are included in Part 2 are as follows:

- Site investigation for geotechnical earthquake engineering (Chap. 5)
- Liquefaction (Chap. 6)
- Settlement of structures (Chap. 7)
- Bearing capacity (Chap. 8)
- Slope stability (Chap. 9)
- Retaining walls (Chap. 10)
- Other earthquake effects (Chap. 11)

It is important to recognize that without adequate and meaningful data from the site investigation, the engineering analyses presented in the following chapters will be of doubtful value and may even lead to erroneous conclusions. In addition, when performing the site investigation, the geotechnical engineer may need to rely on the expertise of other specialists. For example, as discussed in this chapter, geologic analyses are often essential for determining the location of active faults and evaluating site-specific impacts of the design earthquake.

The purpose of this chapter is to discuss the site investigation that may be needed for geotechnical earthquake engineering analyses. The focus of this chapter is on the information that is needed for earthquake design, and not on the basic principles of subsurface exploration and laboratory testing. For information on standard subsurface exploration and laboratory testing, see Day (1999, 2000).

In terms of the investigation for assessing seismic hazards, *Guidelines for Evaluating and Mitigating Seismic Hazards in California* (Division of Mines and Geology 1997) states: "the working premise for the planning and execution of a site investigation within seismic hazard zones is that the suitability of the site should be demonstrated. This premise will persist until either: (a) the site investigation satisfactorily demonstrates the absence of liquefaction or landslide hazard, or (b) the site investigation satisfactorily defines the liquefaction or landslide hazard and provides a suitable recommendation for its mitigation." Thus the purpose of the site investigation should be to demonstrate the absence of seismic hazards or to adequately define the seismic hazards so that suitable recommendations for mitigation can be developed. The scope of the site investigation is discussed next.

5.1.1 Scope of the Site Investigation

The scope of the site investigation depends on many different factors such as the type of facility to be constructed, the nature and complexity of the geologic hazards that could impact the site during the earthquake, economic considerations, level of risk, and specific requirements such as local building codes or other regulatory specifications. The most

rigorous geotechnical earthquake investigations would be required for critical facilities. For example, the Federal Emergency Management Agency (1994) states:

> Critical facilities are considered parts of a community's infrastructure that must remain operational after an earthquake, or facilities that pose unacceptable risks to public safety if severely damaged. Essential facilities are needed during an emergency, such as hospitals, fire and police stations, emergency operation centers and communication centers. High-risk facilities, if severely damaged, may result in a disaster far beyond the facilities themselves. Examples include nuclear power plants, dams and flood control structures, freeway interchanges and bridges, industrial plants that use or store explosives, toxic materials or petroleum products. High-occupancy facilities have the potential of resulting in a large number of casualties or crowd control problems. This category includes high-rise buildings, large assembly facilities, and large multifamily residential complexes. Dependent care facilities house populations with special evacuation considerations, such as preschools and schools, rehabilitation centers, prisons, group care homes, and nursing and convalescent homes. Economic facilities are those facilities that should remain operational to avoid severe economic impacts, such as banks, archiving and vital record keeping facilities, airports and ports, and large industrial and commercial centers.
>
> It is essential that critical facilities designed for human occupancy have no structural weaknesses that can lead to collapse. The Federal Emergency Management Agency has suggested the following seismic performance goals for health care facilities:
>
> 1. The damage to the facilities should be limited to what might be reasonably expected after a destructive earthquake and should be repairable and not life-threatening.
> 2. Patients, visitors, and medical, nursing, technical and support staff within and immediately outside the facility should be protected during an earthquake.
> 3. Emergency utility systems in the facility should remain operational after an earthquake.
> 4. Occupants should be able to evacuate the facility safely after an earthquake.
> 5. Rescue and emergency workers should be able to enter the facility immediately after an earthquake and should encounter only minimum interference and danger.
> 6. The facility should be available for its planned disaster response role after an earthquake.

As previously mentioned, in addition to the type of facility, the scope of the investigation may be dependent on the requirements of the local building codes or other regulatory specifications. Prior to initiating a site investigation for seismic hazards, the geotechnical engineer and engineering geologist should obtain the engineering and geologic requirements of the governing review agency. For example, *Guidelines for Evaluating and Mitigating Seismic Hazards in California* (Division of Mines and Geology 1997) states that geotechnical engineers and engineering geologists:

> May save a great deal of time (and the client's money), and possibly misunderstandings, if they contact the reviewing geologist or engineer at the initiation of the investigation. Reviewers typically are familiar with the local geology and sources of information and may be able to provide additional guidance regarding their agency's expectations and review practices. Guidelines for geologic or geotechnical reports have been prepared by a number of agencies and are available to assist reviewers in their evaluation of reports. Distribution of copies of written policies and guidelines adopted by the agency usually alerts the applicants and consultants about procedures, report formats, and levels of investigative detail that will expedite review and approval of the project.

The scope of the investigation for geotechnical earthquake engineering is usually divided into two parts: (1) the screening investigation and (2) the quantitative evaluation of the seismic hazards (Division of Mines and Geology 1997). These two items are individually discussed in the next two sections.

5.2 SCREENING INVESTIGATION

The first step in geotechnical earthquake engineering is to perform a screening investigation. The purpose of the screening investigation is to assess the severity of the seismic hazards at the site, or in other words to screen out those sites that do not have seismic hazards. If it can be clearly demonstrated that a site is free of seismic hazards, then the quantitative evaluation could be omitted. On the other hand, if a site is likely to have seismic hazards, then the screening investigation can be used to define those hazards before proceeding with the quantitative evaluation.

An important consideration for the screening investigation is the effect that the new construction will have on potential seismic hazards. For example, as a result of grading or construction at the site, the groundwater table may be raised or adverse bedding planes may be exposed that result in a landslide hazard. Thus when a screening investigation is performed, both the existing condition and the final constructed condition must be evaluated for seismic hazards. Another important consideration is off-site seismic hazards. For example, the city of Yungay was devastated by an earthquake-induced debris avalanche that originated at a source located many miles away, as discussed in Sec. 3.5.2 (see Fig. 3.44).

The screening investigation should be performed on both a regional and a site-specific basis. The first step in the screening investigation is to review available documents, such as the following:

1. *Preliminary design information:* The documents dealing with preliminary design and proposed construction of the project should be reviewed. For example, the structural engineer or architect may have design information, such as the building location, size, height, loads, and details on proposed construction materials and methods. Preliminary plans may even have been developed that show the proposed construction.

2. *History of prior site development:* If the site had prior development, it is also important to obtain information on the history of the site. The site could contain old deposits of fill, abandoned septic systems and leach fields, buried storage tanks, seepage pits, cisterns, mining shafts, tunnels, and other artificial and subsurface works that could impact the proposed development. There may also be old reports that document seismic hazards at the site.

3. *Seismic history of the area:* There may be many different types of documents and maps that provide data on the seismic history of the area. For example, there may be seismic history information on the nature of past earthquake-induced ground shaking. This information could include the period of vibration, ground acceleration, magnitude, and intensity (isoseismal maps) of past earthquakes. This data can often be obtained from seismology maps and reports that illustrate the differences in ground shaking intensity based on geologic type; 50-, 100-, and 250-year acceleration data; and type of facilities or landmarks.

Geographical maps and reports are important because they can identify such items as the pattern, type, and movement of nearby potentially active faults or fault systems, and the distance of the faults to the area under investigation. Historical earthquake records should also be reviewed to determine the spatial and temporal distribution of historic earthquake epicenters.

4. *Aerial photographs and geologic maps:* During the screening investigation, the engineering geologist and geotechnical engineer should check aerial photographs and geologic maps. Aerial photographs and geologic maps can be useful in identifying existing and potential slope instability, fault ground rupture, liquefaction, and other geologic hazards. The type of observed features includes headwall scarps, debris chutes, fissures,

grabens, and sand boils. By comparing older aerial photographs with newer ones, the engineering geologist can also observe any artificial or natural changes that have occurred at the site.

Geologic reports and maps can be especially useful to the geotechnical engineer and engineering geologist because they often indicate seismic hazards such as faults and landslides. Geologic reports and maps may indicate the geometry of the fault systems, the subsoil profile, and the amplification of seismic waves due to local conditions, which are important factors in the evaluation of seismic risk. For example, Fig. 5.1 presents a portion of a geologic map, and Fig. 5.2 shows cross sections through the area shown in Fig. 5.1 (from Kennedy 1975). Note that the geologic map and cross sections indicate the location of several faults and the width of the faults, and often state whether the faults are active or inactive. For example, Fig. 5.2 shows the Rose Canyon fault zone, an active fault having a ground shear zone about 300 m (1000 ft) wide. The cross sections in Fig. 5.2 also show fault-related displacement of various rock layers.

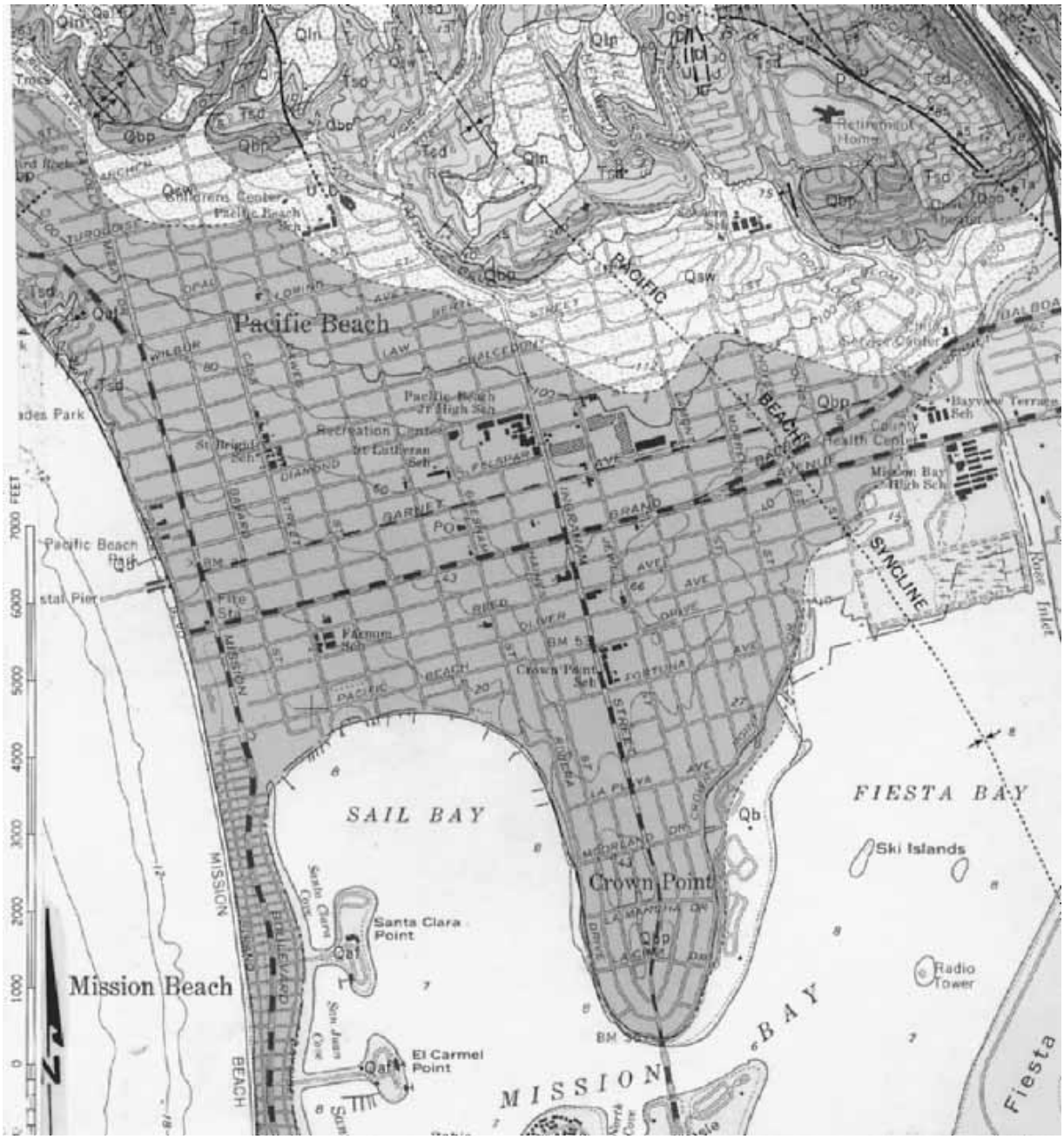

FIGURE 5.1 Geologic map. (*From Kennedy 1975.*)

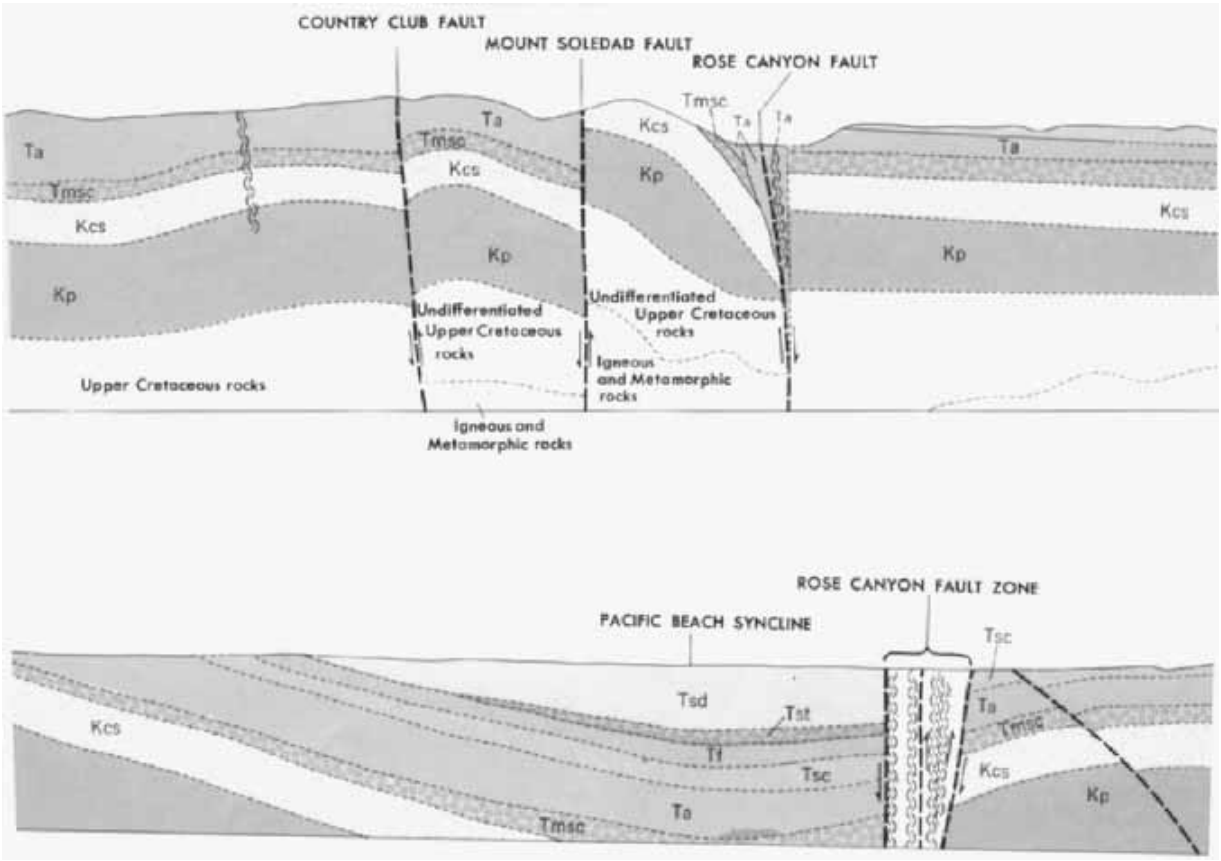

FIGURE 5.2 Geologic cross sections. (*From Kennedy 1975.*)

A major source for geologic maps in the United States is the U.S. Geological Survey (USGS). The USGS prepares many different geologic maps, books, and charts; a list of USGS publications is provided in *Index of Publications of the Geological Survey* (USGS 1997). The USGS also provides an *Index to Geologic Mapping in the United States,* which shows a map of each state and indicates the areas where a geologic map has been published.

5. *Special study maps:* For some areas, special study maps may have been developed that indicate local seismic hazards. For example, Fig. 5.3 presents a portion of the Seismic Safety Study (1995) that shows the location of the Rose Canyon fault zone. Special study maps may also indicate other geologic and seismic hazards, such as potentially liquefiable soil, landslides, and abandoned mines.

6. *Topographic maps:* Both old and recent topographic maps can provide valuable site information. Figure 5.4 presents a portion of the topographic map for the Encinitas Quadrangle, California (USGS 1975). As shown in Fig. 5.4, the topographic map is drawn to scale and shows the locations of buildings, roads, freeways, train tracks, and other civil engineering works as well as natural features such as canyons, rivers, lagoons, sea cliffs, and beaches. The topographic map in Fig. 5.4 even shows the locations of sewage disposal ponds, and water tanks; and by using different colors and shading, it indicates older versus newer development. But the main purpose of the topographic map is to indicate ground surface elevations or elevations of the seafloor, such as shown in Fig. 5.4. This information can be used to determine the major topographic features at the site and to evaluate potential seismic hazards.

7. *Building codes or other regulatory specifications:* A copy of the most recently adopted local building code should be reviewed. Investigation and design requirements for ordinary structures, critical facilities, and lifelines may be delineated in building codes or

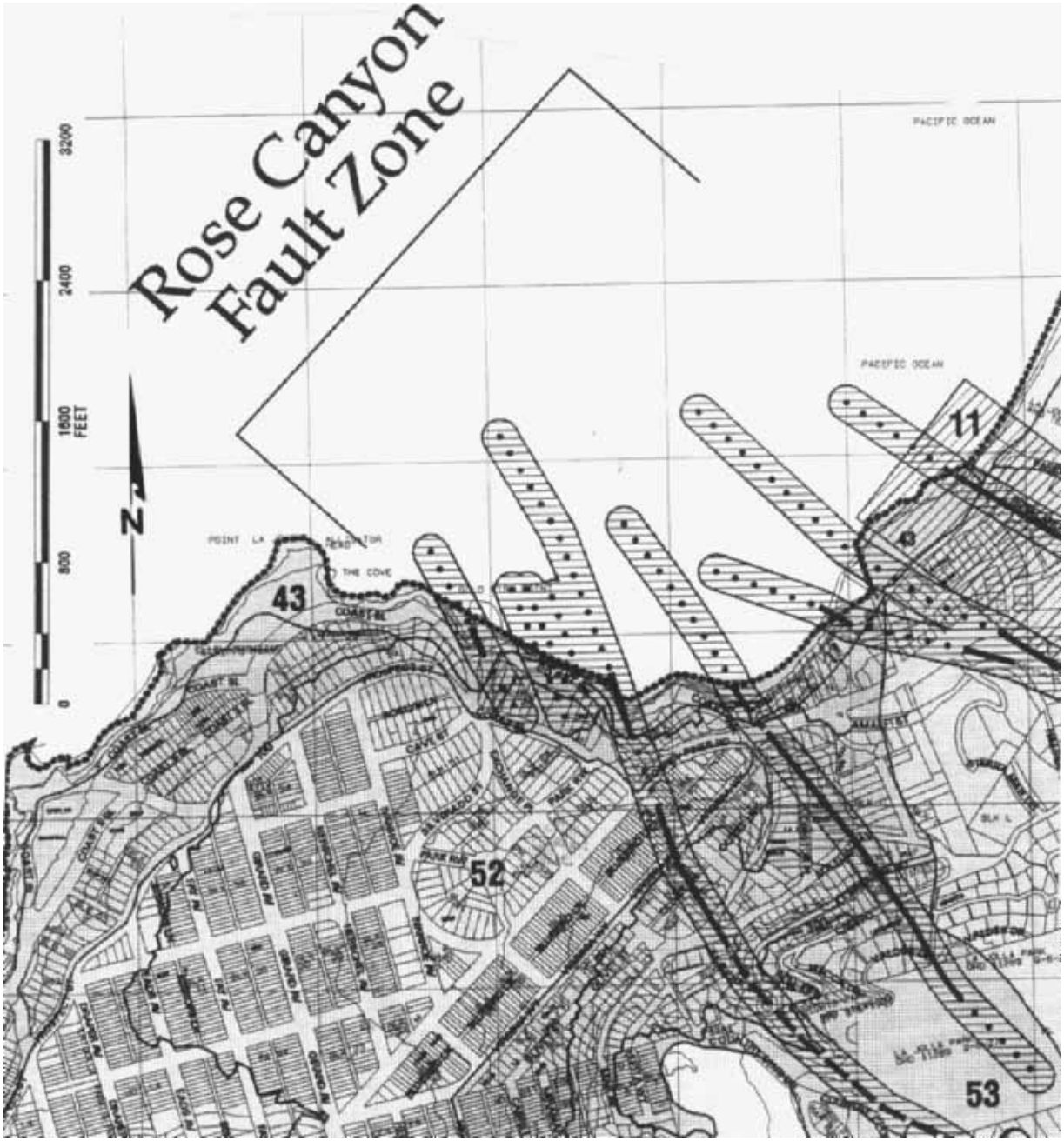

FIGURE 5.3 Portion of Seismic Safety Study, 1995. (*Developed by the City of San Diego.*)

other regulatory documents. For example, the *Uniform Building Code* (1997) provides seismic requirements that have been adopted by many building departments in the United States. These seismic code specifications have also been incorporated into the building codes in other countries.

8. *Other available documents:* There are many other types of documents and maps that may prove useful during the screening investigation. Examples include geologic and soils engineering maps and reports used for the development of adjacent properties (often available at the local building department), water well logs, and agricultural soil survey reports.

After the site research has been completed, the next step in the screening investigation is a field reconnaissance. The purpose is to observe the site conditions and document any recent changes to the site that may not be reflected in the available documents. The field reconnaissance should also be used to observe surface features and other details that may not be readily evident from the available documents. Once the site research and field recon-

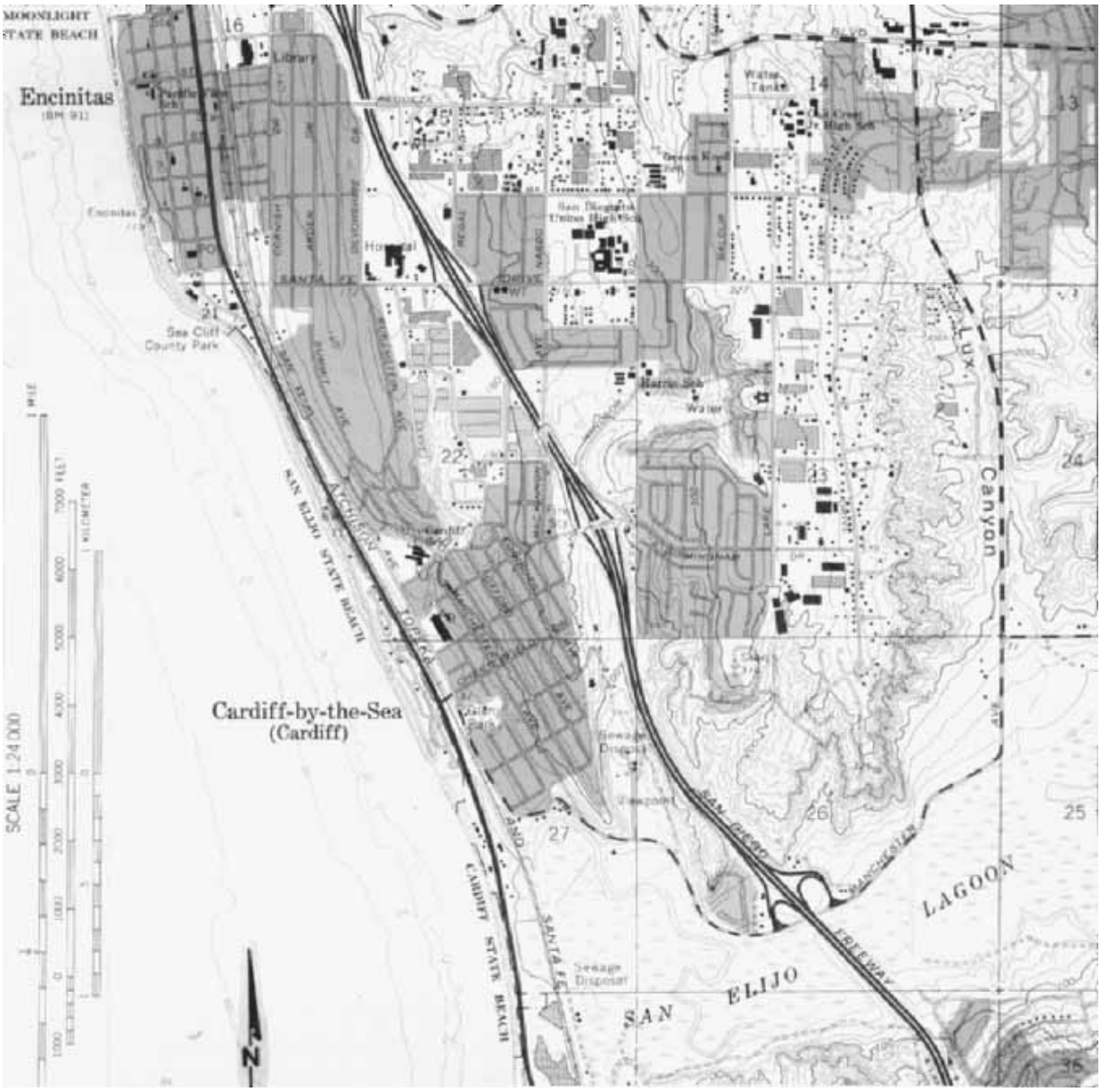

FIGURE 5.4 Topographic map. (*From USGS 1975.*)

naissance are completed, the engineering geologist and geotechnical engineer can then complete the screening investigation. The results should either clearly demonstrate the lack of seismic hazards or indicate the possibility of seismic hazards, in which case a quantitative evaluation is required.

It should be mentioned that even if the result of the screening investigation indicates no seismic hazards, the governing agency might not accept this result for critical facilities. It may still require that subsurface exploration demonstrate the absence of seismic hazards for critical facilities.

5.3 QUANTITATIVE EVALUATION

The purpose of the quantitative evaluation is to obtain sufficient information on the nature and severity of the seismic hazards so that mitigation recommendations can be developed. The quantitative evaluation consists of the following:

- *Geologic mapping:* The first step is to supplement the results of the field reconnaissance (see Sec. 5.2) with geologic mapping, which can be used to further identify such features as existing landslides and surficial deposits of unstable soil.
- *Subsurface exploration:* The results of the screening investigation and geologic mapping are used to plan the subsurface exploration, which could consist of the excavation of borings, test pits, or trenches. During the subsurface exploration, soil samples are often retrieved from the excavations. Field testing could also be performed in the excavations. Subsurface exploration is discussed in Sec. 5.4.
- *Laboratory testing:* The purpose of the laboratory testing is to determine the engineering properties of the soil to be used in the seismic hazard analyses. Laboratory testing is discussed in Sec. 5.5.
- *Engineering and geologic analyses:* An important parameter for the engineering and geologic analysis of seismic hazards is the peak ground acceleration. This is discussed in Sec. 5.6.
- *Report preparation:* The results of the screening investigation and quantitative evaluation are often presented in report form that describes the seismic hazards and presents the geologic and geotechnical recommendations. Section 5.7 presents guidelines on the report content for seismic hazards.

5.4 SUBSURFACE EXPLORATION

There are many different aspects of subsurface exploration. The most important part of the subsurface exploration typically consists of the excavation of borings, test pits, and trenches. Soil samples are usually retrieved from these excavations and then tested in the laboratory to determine their engineering properties. In addition, field tests, such as the standard penetration test (SPT) or cone penetration test (CPT) could also be performed. These aspects of the subsurface exploration are individually discussed in the following sections. In addition, App. A (Glossary 1) presents a list of field testing terms and definitions.

5.4.1 Borings, Test Pits, and Trenches

Objectives of the Excavations. The main objectives of the borings, test pits, and trenches are to determine the nature and extent of the seismic hazards. In this regard, the Division of Mines and Geology (1997) states:

> The subsurface exploration should extend to depths sufficient to expose geologic and subsurface water conditions that could affect slope stability or liquefaction potential. A sufficient quantity of subsurface information is needed to permit the engineering geologist and/or civil engineer to extrapolate with confidence the subsurface conditions that might affect the project, so that the seismic hazard can be properly evaluated, and an appropriate mitigation measure can be designed by the civil engineer. The preparation of engineering geologic maps and geologic cross sections is often an important step into developing an understanding of the significance and extent of potential seismic hazards. These maps and/or cross sections should extend far enough beyond the site to identify off-site hazards and features that might affect the site.

Excavation Layout. The required number and spacing of borings, test pits, and trenches for a particular project must be based on judgment and experience. Obviously the more test excavations that are performed, the more knowledge will be obtained about the subsurface

conditions and the seismic hazards. This can result in a more economical foundation design and less risk of the project being impacted by geologic and seismic hazards.

In general, boring layouts should not be random. Instead, if an approximate idea of the location of the proposed structure is known, then the borings should be concentrated in that area. For example, borings could be drilled at the four corners of a proposed building, with an additional (and deepest) boring located at the center of the proposed building. If the building location is unknown, then the borings should be located in lines, such as across the valley floor, in order to develop soil and geologic cross sections.

If geologic or seismic hazards may exist outside the building footprint, then they should also be investigated with borings. For example, if there is an adjacent landslide or fault zone that could impact the site, then it will also need to be investigated with subsurface exploration.

Some of the factors that influence the decisions on the number and spacing of borings include the following:

- *Relative costs of the investigation:* The cost of additional borings must be weighed against the value of additional subsurface information.
- *Type of project:* A more detailed and extensive subsurface investigation is required for an essential facility as compared to a single-family dwelling.
- *Topography (flatland versus hillside):* A hillside project usually requires more subsurface investigation than a flatland project because of the slope stability requirements.
- *Nature of soil deposits (uniform versus erratic):* Fewer borings may be needed when the soil deposits are uniform as compared to erratic deposits.
- *Geologic and seismic hazards:* The more known or potential geologic and seismic hazards at the site, the greater the need for subsurface exploration.
- *Access:* In many cases, the site may be inaccessible, and access roads will have to be constructed. Creating access roads throughout the site can be expensive and disruptive and may influence decisions on the number and spacing of borings.
- *Government or local building department requirements:* For some projects, there may be specifications on the required number and spacing of borings.

Often a preliminary subsurface plan is developed to perform a limited number of exploratory borings. The purpose is just to obtain a rough idea of the soil, rock, and groundwater conditions and the potential geologic and seismic hazards at the site. Then once the preliminary subsurface data are analyzed, additional borings as part of a detailed seismic exploration are performed. The detailed subsurface exploration can be used to better define the soil profile, explore geologic and seismic hazards, and obtain further data on the critical subsurface conditions and seismic hazards that will likely have the greatest impact on the design and construction of the project.

Depth of Excavations. In terms of the depth of the subsurface exploration, R. B. Seed (1991) states:

> Investigations should extend to depths below which liquefiable soils cannot reasonably be expected to occur (e.g., to bedrock, or to hard competent soils of sufficient geologic age that possible underlying units could not reasonably be expected to pose a liquefaction hazard). At most sites where soil is present, such investigation will require either borings or trench/test pit excavation. Simple surface inspection will suffice only when bedrock is exposed over essentially the full site, or in very unusual cases when the local geology is sufficiently well-documented as to fully ensure the complete lack of possibility of occurrence of liquefiable soils (at depth) beneath the exposed surface soil unit(s).

Down-Hole Logging. For geologic hazards such as landslides, a common form of subsurface exploration is large-diameter bucket-auger borings that are down-hole logged by the geotechnical engineer or engineering geologist. Figure 5.5 shows a photograph of the top of the boring with the geologist descending into the hole in a steel cage. Note in Fig. 5.5 that a collar is placed around the top of the hole to prevent loose soil or rocks from being accidentally knocked down the hole. The process of down-hole logging is a valuable technique because it allows the geotechnical engineer or engineering geologist to observe the subsurface materials as they exist in place. Usually the process of excavation of the boring smears the side of the hole, and the surface must be chipped away to observe intact soil or rock. Going down-hole is dangerous because of the possibility of a cave-in of the hole as well as "bad air" (presence of poisonous gases or lack of oxygen) and should only be attempted by an experienced geotechnical engineer or engineering geologist.

The down-hole observation of soil and rock can lead to the discovery of important geologic and seismic hazards. For example, Figs. 5.6 and 5.7 provide an example of the type of conditions observed down-hole. Figure 5.6 shows a knife that has been placed in an open fracture in bedrock. The open fracture in the rock was caused by massive landslide movement. Figure 5.7 is a side view of the same condition.

Trench Excavations. Backhoe trenches are an economical means of performing subsurface exploration. The backhoe can quickly excavate the trench, which can then be used to observe and test the in situ soil. In many subsurface explorations, backhoe trenches are used to evaluate near-surface and geologic conditions (i.e., up to 15 ft deep), with borings being used to investigate deeper subsurface conditions. Backhoe trenches are especially useful for performing fault studies. For example, Figs. 5.8 and 5.9 show two views of the excava-

FIGURE 5.5 Down-hole logging. Note that the arrow points to the top of the steel cage used for the down-hole logging.

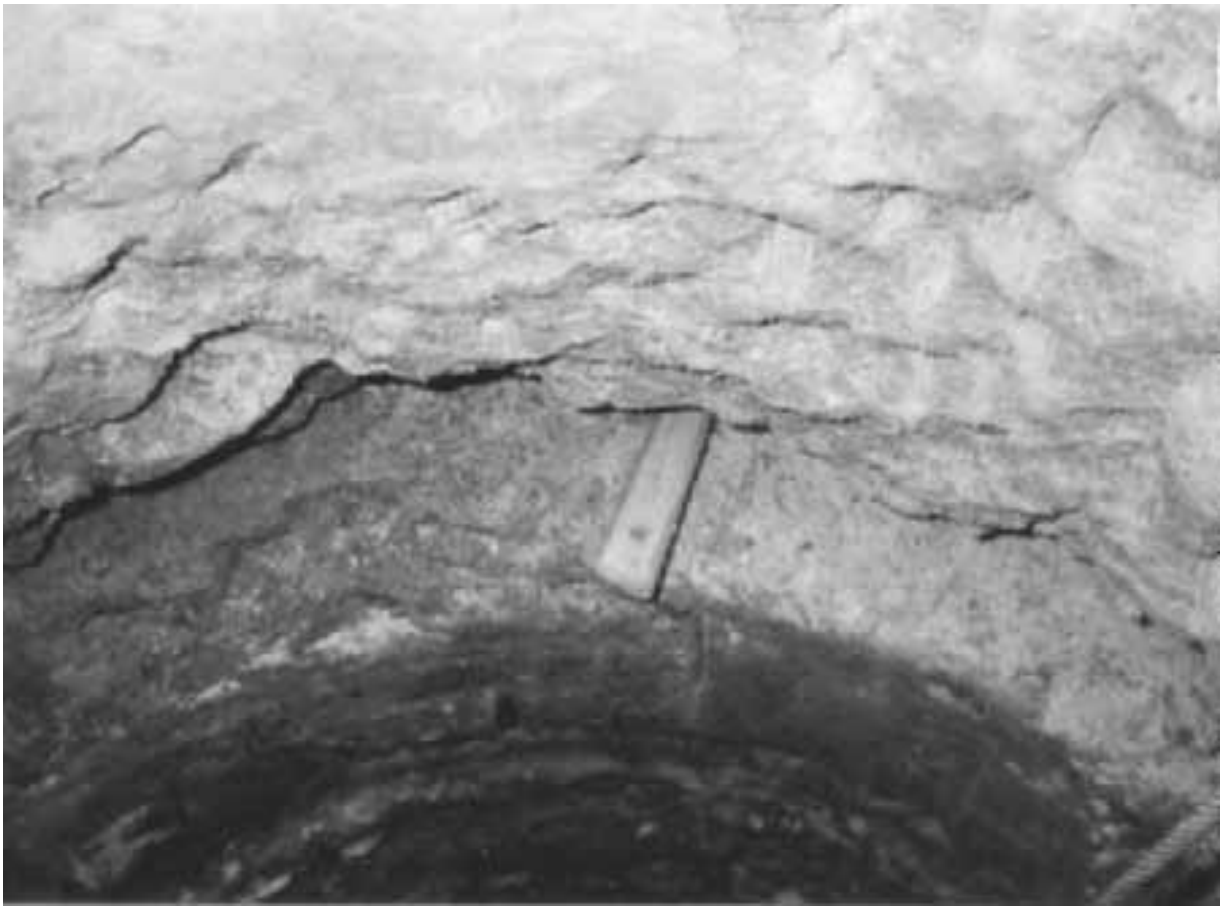

FIGURE 5.6 Knife placed in an open fracture in bedrock caused by landslide movement. The photograph was taken down-hole in a large-diameter auger boring.

FIGURE 5.7 Side view of the condition shown in Fig. 5.6.

FIGURE 5.8 Backhoe trench for a fault study.

tion of a trench that is being used to investigate the possibility of an on-site active fault. Figure 5.9 is a close-up view of the conditions in the trench and shows the fractured and disrupted nature of the rock. Note in Fig. 5.9 that metal shoring has been installed to prevent the trench from caving in. Often the fault investigations are performed by the engineering geologist with the objective of determining if there are active faults that cross the site. In addition, the width of the shear zone of the fault can often be determined from the trench excavation studies. If there is uncertainty as to whether a fault is active, then often datable material must be present in the trench excavation in order to determine the date of the most recent fault movement. Krinitzsky et al. (1993) present examples of datable materials, as follows:

- Displacements of organic matter or other datable horizons across faults
- Sudden burials of marsh soils
- Killed trees
- Disruption of archaeological sites
- Liquefaction intrusions cutting older liquefaction

5.4.2 Soil Sampling

To study the potential seismic hazards of a soil deposit, the ideal situation would be to obtain an undisturbed soil specimen, apply the same stress conditions that exist in the field, and then subject the soil specimen to the anticipated earthquake-induced cyclic shear stress. The resulting soil behavior could then be used to evaluate the seismic hazards. The disadvantages of this approach are that undisturbed soil specimens and sophisticated laboratory equipment would be required. Usually in engineering practice, this approach is not practical or is too expensive, and other options are used as described below.

FIGURE 5.9 Close-up view of trench excavation.

Cohesive Soils. Although undisturbed cohesive soil samples can often be obtained during the subsurface exploration, the usual approach in practice is to obtain the soil engineering properties from standard laboratory tests. In terms of the undrained shear strength of the soil, the unconfined compression test (ASTM D 2166-98, 2000) or the consolidated undrained triaxial compression test (ASTM D 4767-95, 2000) is usually performed. Typically standard soil sampling practices, such as the use of thin-walled Shelby tubes, are used to obtain undisturbed cohesive soil specimens (see Day 1999). Section 5.5.1 describes the interpretation of this data for use in geotechnical earthquake engineering analyses.

Granular Soils. There are three different methods that can be used to obtain undisturbed soil specimens of granular soil (Poulos et al. 1985, Ishihara 1985, Hofmann et al. 2000):

1. *Tube sampling:* Highly sophisticated techniques can be employed to obtain undisturbed soil specimens from tube samplers. For example, a fixed-piston sampler consists of a piston that is fixed at the bottom of the borehole by a rod that extends to the ground surface. A thin-walled tube is then pushed into the ground past the piston, while the piston rod is held fixed.

Another approach is to temporarily lower the groundwater table in the borehole and allow the water to drain from the soil. The partially saturated soil will then be held together by capillarity, which will enable the soil strata to be sampled. When brought to the ground surface, the partially saturated soil specimen is frozen. Because the soil is only partially saturated, the volume increase of water as it freezes should not significantly disturb the soil structure. The frozen soil specimen is then transported to the laboratory for testing.

Although the soil specimen may be considered to be an undisturbed specimen, there could still be disruption of the soil structure during all phases of the sampling operation. The greatest disturbance will probably occur during the physical pushing of the sampler into the soil.

2. *Block sampling:* Another approach for near-surface soil is to temporarily lower the groundwater table. Then a test pit or trench is excavated into the soil. Because the groundwater table has been lowered, the partially saturated soil will be held together by capillarity. A block sample is then cut from the sides of the test pit or trench, and the block sample is transported to the laboratory for testing.

If the soil does not have enough capillarity to hold itself together, then this method will not work. In addition, the soil could be disturbed due to stress relief when making the excavation or when extracting the soil specimen.

3. *Freezing technique:* The essential steps in the freezing technique are to first freeze the soil and then cut or core the frozen soil from the ground. The freezing is accomplished by installing pipes in the ground and then circulating ethanol and crushed dry ice or liquid nitrogen through the pipes. Because water increases in volume upon freezing, it is important to establish a slow freezing front so that the freezing water can slowly expand and migrate out of the soil pores. This process can minimize the sample disturbance associated with the increase in volume of freezing water.

From a practical standpoint, the three methods described above are usually not economical for most projects. Thus laboratory testing is not practical, and the analyses of earthquake hazards (such as liquefaction) are normally based on field testing that is performed during the subsurface exploration. The two most commonly used field tests are the standard penetration test (SPT) and the cone penetration test (CPT), as discussed in the next two sections.

5.4.3 Standard Penetration Test

Test Procedure. The standard penetration test can be used for all types of soil, but in general the SPT should only be used for granular soils (Coduto 1994). The SPT can be especially valuable for clean sand deposits where the sand falls or flows out from the sampler when retrieved from the ground. Without a soil sample, other types of tests, such as the standard penetration test, must be used to assess the engineering properties of the sand. Often when a borehole is drilled, if subsurface conditions indicate a sand stratum and sampling tubes come up empty, the sampling gear can be quickly changed to perform standard penetration tests.

The standard penetration test consists of driving a thick-walled sampler into the granular soil deposit. The test parameters are as follows:

- *Sampler:* Per ASTM D 1586-99 (2000), the SPT sampler must have an inside barrel diameter $D = 3.81$ cm (1.5 in) and an outside diameter $F = 5.08$ cm (2 in), as shown in Fig. 5.10.
- *Driving hammer:* The SPT sampler is driven into the sand by using a 63.5-kg (140-lb) hammer falling a distance of 0.76 m (30 in).
- *Driving distance:* The SPT sampler is driven a total of 45 cm (18 in), with the number of blows recorded for each 15-cm (6-in) interval.
- *N value:* The *measured SPT N value* (blows per foot) is defined as the penetration resistance of the soil, which equals the sum of the number of blows required to drive the SPT

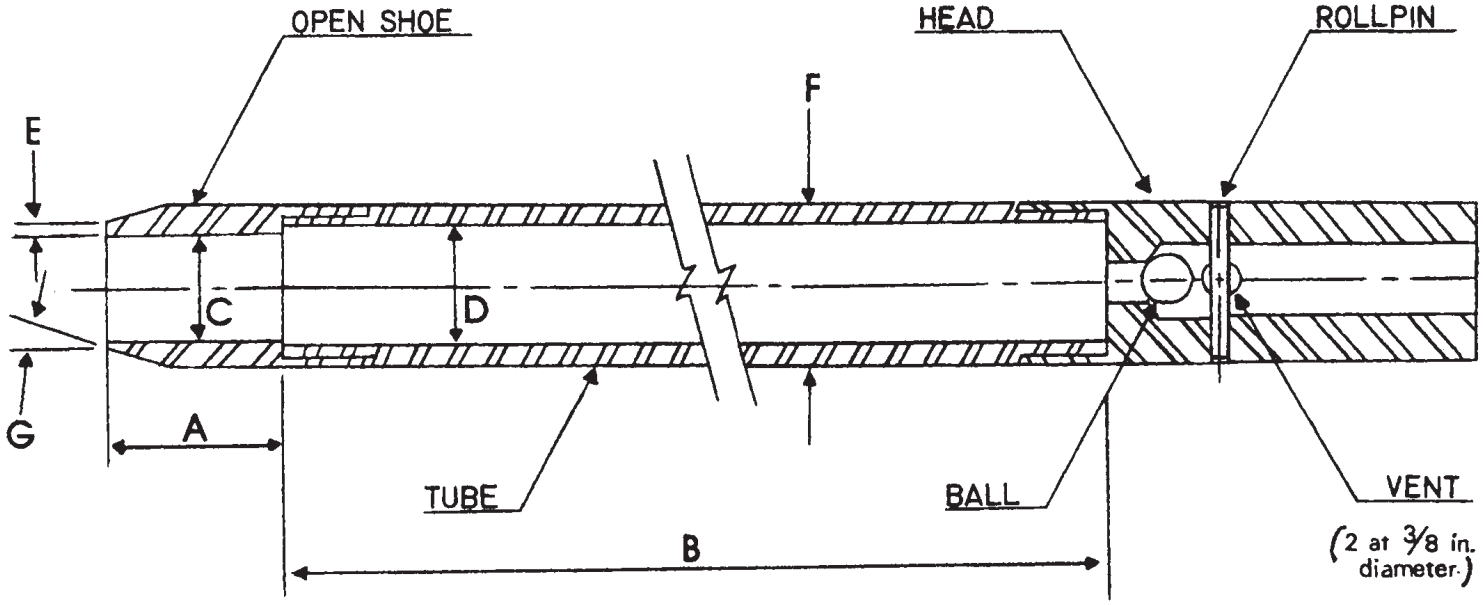

A = 1.0 to 2.0 in. (25 to 50 mm)
B = 18.0 to 30.0 in. (0.457 to 0.762 m)
C = 1.375± 0.005 in. (34.93 ± 0.13 mm)
D = 1.50 ± 0.05 – 0.00 in. (38.1 ± 1.3 – 0.0 mm)
E = 0.10 ± 0.02 in. (2.54 ± 0.25 mm)
F = 2.00 ± 0.05 – 0.00 in. (50.8 ± 1.3 – 0.0 mm)
G = 16.0° to 23.0°

FIGURE 5.10 Standard penetration test sampler. (*Reprinted with permission from the American Society for Testing and Materials 2000.*)

sampler over the depth interval of 15 to 45 cm (6 to 18 in). The reason the number of blows required to drive the SPT sampler for the first 15 cm (6 in) is not included in the N value is that the drilling process often disturbs the soil at the bottom of the borehole, and the readings at 15 to 45 cm (6 to 18 in) are believed to be more representative of the in situ penetration resistance of the granular soil.

Factors That Could Affect the Test Results. The measured SPT N value can be influenced by the type of soil, such as the amount of fines and gravel-size particles in the soil. Saturated sands that contain appreciable fine soil particles, such as silty or clayey sands, could give abnormally high N values if they have a tendency to dilate or abnormally low N values if they have a tendency to contract during the undrained shear conditions associated with driving the SPT sampler. Gravel-size particles increase the driving resistance (hence increased N value) by becoming stuck in the SPT sampler tip or barrel.

A factor that could influence the measured SPT N value is groundwater. It is important to maintain a level of water in the borehole at or above the in situ groundwater level. This is to prevent groundwater from rushing into the bottom of the borehole, which could loosen the granular soil and result in low measured N values.

Besides the soil and groundwater conditions described above, many different testing factors can influence the accuracy of the SPT readings. For example, the measured SPT N value could be influenced by the hammer efficiency, the rate at which the blows are applied, the borehole diameter, and the rod lengths. The different factors that can affect the standard penetration test results are presented in Table 5.1.

Corrections for Testing and Overburden Pressure. Corrections can be applied to the test results to compensate for the testing procedures (Skempton 1986):

$$N_{60} = 1.67 E_m C_b C_r N \tag{5.1}$$

where N_{60} = standard penetration test N value corrected for field testing procedures
E_m = hammer efficiency (for U.S. equipment, E_m is 0.6 for a safety hammer and 0.45 for a doughnut hammer)
C_b = borehole diameter correction (C_b = 1.0 for boreholes of 65- to 115-mm diameter, 1.05 for 150-mm diameter, and 1.15 for 200-mm diameter hole)
C_r = rod length correction (C_r = 0.75 for up to 4 m of drill rods, 0.85 for 4 to 6 m of drill rods, 0.95 for 6 to 10 m of drill rods, and 1.00 for drill rods in excess of 10 m)
N = measured standard penetration test N value

For many geotechnical earthquake engineering evaluations, such as liquefaction analysis, the standard penetration test N_{60} value [Eq. (5.1)] is corrected for the vertical effective stress σ'_{v0}. When a correction is applied to the N_{60} value to account for the vertical effective pressure, these values are referred to as $(N_1)_{60}$ values. The procedure consists of multiplying the N_{60} value by a correction C_N in order to calculate the $(N_1)_{60}$ value. Figure 5.11 presents a chart that is commonly used to obtain the correction factor C_N. Another option is to use the following equation:

$$(N_1)_{60} = C_N N_{60} = (100/\sigma'_{v0})^{0.5} N_{60} \tag{5.2}$$

where $(N_1)_{60}$ = standard penetration test N value corrected for both field testing procedures and overburden pressure
C_N = correction factor to account for overburden pressure. As indicated in Eq. (5.2), C_N is approximately equal to $(100/\sigma'_{v0})^{0.5}$, where σ'_{v0} is the vertical

effective stress, also known as the effective overburden pressure, in kilopascals. Suggested maximum values of C_N range from 1.7 to 2.0 (Youd and Idriss 1997, 2001) .

N_{60} = standard penetration test N value corrected for field testing procedures. Note that N_{60} is calculated by using Eq. (5.1).

Correlations between SPT Results and Soil Properties. Commonly used correlations between the SPT results and various soil properties are as follows:

- *Table 5.2:* This table presents a correlation between the measured SPT N value (blows per foot) and the density condition of a clean sand deposit. Note that this correlation is

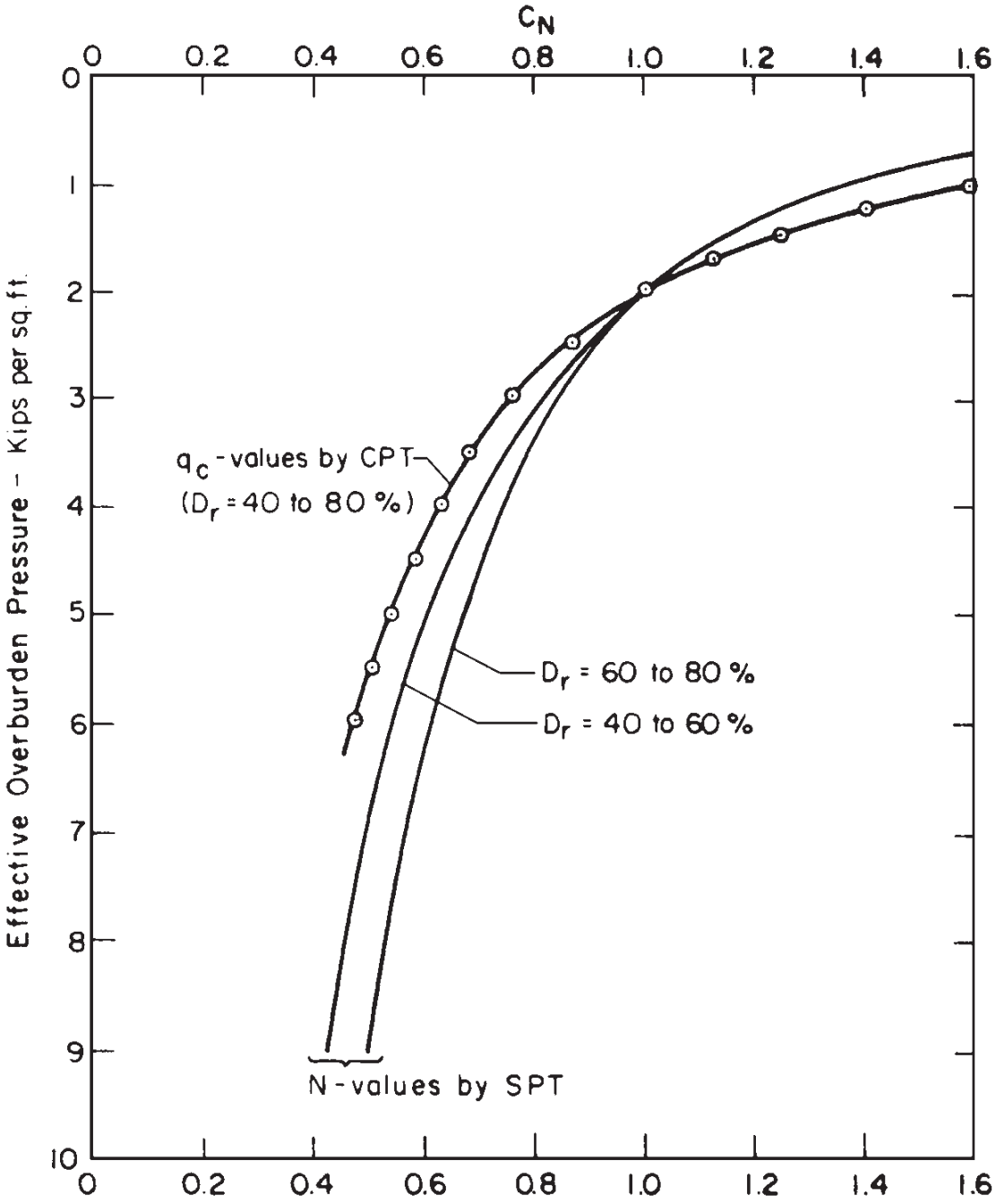

FIGURE 5.11 Correction factor C_N used to adjust the standard penetration test N value and cone penetration test q_c value for the effective overburden pressure. The symbol D_r refers to the relative density of the sand. (*Reproduced from Seed et al. 1983, with permission from the American Society of Civil Engineers.*)

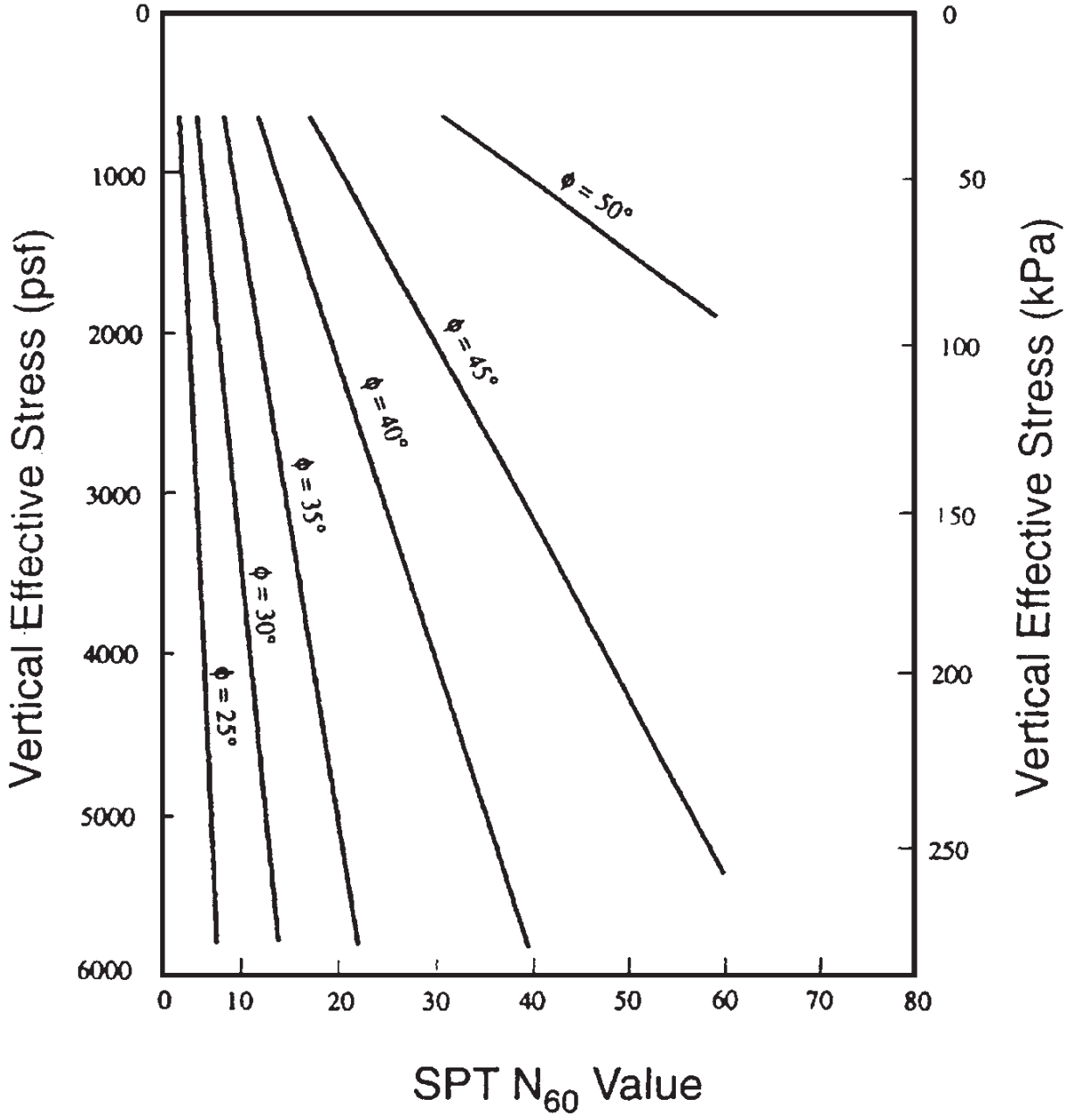

FIGURE 5.12 Empirical correlation between the standard penetration test N_{60} value, vertical effective stress, and friction angle for clean quartz sand deposits. (*Adapted from de Mello 1971, reproduced from Coduto 1994.*)

very approximate and the boundaries between different density conditions are not as distinct as implied by the table. As indicated in Table 5.2, if it only takes 4 blows or less to drive the SPT sampler, then the sand should be considered to be very loose and could be subjected to significant settlement due to the weight of a structure or due to earthquake shaking. On the other hand, if it takes more than 50 blows to drive the SPT sampler, then the sand is considered to be in a very dense condition and would be able to support high bearing loads and would be resistant to settlement from earthquake shaking.

- *Table 5.3:* This table is based on the work by Tokimatsu and Seed (1987) and is similar to Table 5.2, except that it provides a correlation between $(N_1)_{60}$ and the relative density.

- *Figure 5.12:* This figure is based on the work by de Mello (1971) and presents an empirical correlation between the standard penetration test N_{60} value [Eq. (5.1)], the vertical effective stress σ'_{v0}, and the friction angle ϕ of clean, quartz sand.

Popularity of SPT Test. Even with the limitations and all the corrections that must be applied to the measured *N* value, the standard penetration test is probably the most widely used field test in the United States. This is because it is relatively easy to use, the test is economical compared to other types of field testing, and the SPT equipment can be quickly adapted and included as part of almost any type of drilling rig.

5.4.4 Cone Penetration Test

The idea for the cone penetration test is similar to the standard penetration test except that instead of driving a thick-walled sampler into the soil, a steel cone is pushed into the soil. There are many different types of cone penetration devices, such as the mechanical cone, mechanical-friction cone, electric cone, and piezocone (see App. A, Glossary 1, for descriptions). The simplest type of cone is shown in Fig. 5.13 (from ASTM D 3441-98, 2000). First the cone is pushed into the soil to the desired depth (initial position), and then a force is applied to the inner rods which moves the cone downward into the extended position. The force required to move the cone into the extended position (Fig. 5.13) divided by the horizontally projected area of the cone is defined as the *cone resistance* q_c. By continually repeating the two-step process shown in Fig. 5.13, the cone resistance data are obtained at increments of depth. A continuous record of the cone resistance versus depth can be obtained by using the electric cone, where the cone is pushed into the soil at a rate of 10 to 20 mm/s (2 to 4 ft/min).

Figure 5.14 (adapted from Robertson and Campanella 1983) presents an empirical correlation between the cone resistance q_c, vertical effective stress, and friction angle ϕ of clean, quartz sand. Note that Fig. 5.14 is similar in appearance to Fig. 5.12, which should be the case because both the SPT and the CPT involve basically the same process of forcing an object into the soil and then measuring the resistance of the soil to penetration by the object.

For many geotechnical earthquake engineering evaluations, such as liquefaction analysis, the cone penetration test q_c value is corrected for the vertical effective stress σ'_{v0}. When a correction is applied to the q_c value to account for the vertical effective pressure, these values are referred to as q_{c1} values. The procedure consists of multiplying the q_c value by a correction C_N in order to calculate the q_{c1} value. Figure 5.11 presents a chart that is commonly used to obtain the correction factor C_N. Another option is to use the following equation:

$$q_{c1} = C_N q_c = \frac{1.8 q_c}{0.8 + \sigma'_{v0}/100} \tag{5.3}$$

where q_{c1} = corrected CPT tip resistance (corrected for overburden pressure)
C_N = correction factor to account for overburden pressure. As indicated in Eq. (5.3), C_N is approximately equal to $1.8/(0.8 + \sigma'_{v0}/100)$, where σ'_{v0} is the vertical effective stress in kilopascals.
q_c = cone penetration tip resistance

A major advantage of the cone penetration test is that by using the electric cone, a continuous subsurface record of the cone resistance q_c can be obtained. This is in contrast to

TABLE 5.1 Factors That Can Affect the Standard Penetration Test Results

Factors that can affect the standard penetration test results	Comments
Inadequate cleaning of the borehole	SPT is only partially made in original soil. Sludge may be trapped in the sampler and compressed as the sampler is driven, increasing the blow count. This may also prevent sample recovery.
Not seating the sampler spoon on undisturbed material	Incorrect *N* value is obtained.
Driving of the sample spoon above the bottom of the casing	The *N* value is increased in sands and reduced in cohesive soil.
Failure to maintain sufficient hydrostatic head in boring	The water table in the borehole must be at least equal to the piezometric level in the sand; otherwise the sand at the bottom of the borehole may be transformed to a loose state.
Attitude of operators	Blow counts for the same soil using the same rig can vary, depending on who is operating the rig and perhaps the mood of operator and time of drilling.
Overdriven sample	Higher blow counts usually result from overdriven sampler.
Sampler plugged by gravel	Higher blow counts result when gravel plugs the sampler. The resistance of loose sand could be highly overestimated.
Plugged casing	High *N* values may be recorded for loose sand when sampling below the groundwater table. Hydrostatic pressure causes sand to rise and plug the casing.
Overwashing ahead of casing	Low blow count may result for dense sand since sand is loosened by overwashing.
Drilling method	Drilling technique (e.g., cased holes versus mud-stabilized holes) may result in different *N* values for the same soil.
Not using the standard hammer drop	Energy delivered per blow is not uniform. European countries have adopted an automatic trip hammer not currently in use in North America.
Free fall of the drive weight is not attained	Using more than 1.5 turns of rope around the drum and/or using wire cable will restrict the fall of the drive weight.
Not using the correct weight	Driller frequently supplies drive hammers with weights varying from the standard by as much as 10 lb.
Weight does not strike the drive cap concentrically	Impact energy is reduced, increasing the *N* value.
Not using a guide rod	Incorrect *N* value is obtained.
Not using a good tip on the sampling spoon	If the tip is damaged and reduces the opening or increases the end area, the *N* value can be increased.

TABLE 5.1 Factors That Can Affect the Standard Penetration Test Results (*Continued*)

Factors that can affect the standard penetration test results	Comments
Use of drill rods heavier than standard	With heavier rods, more energy is absorbed by the rods, causing an increase in the blow count.
Not recording blow counts and penetration accurately	Incorrect *N* values are obtained.
Incorrect drilling	The standard penetration test was originally developed from wash boring techniques. Drilling procedures which seriously disturb the soil will affect the *N* value, for example, drilling with cable tool equipment.
Using large drill holes	A borehole correction is required for large-diameter boreholes. This is because larger diameters often result in a decrease in the blow count.
Inadequate supervision	Frequently a sampler will be impeded by gravel or cobbles, causing a sudden increase in blow count. This is often not recognized by an inexperienced observer. Accurate recording of drilling sampling and depth is always required.
Improper logging of soils	The sample is not described correctly.
Using too large a pump	Too high a pump capacity will loosen the soil at the base of the hole, causing a decrease in blow count.

Source: NAVFAC DM-7.1 (1982).

TABLE 5.2 Correlation between Uncorrected SPT *N* Value and Density of Clean Sand

Uncorrected *N* value (blows per foot)	Sand density	Relative density D_r, percent
0–4	Very loose condition	0–15
4–10	Loose condition	15–35
10–30	Medium condition	35–65
30–50	Dense condition	65–85
Over 50	Very dense condition	85–100

Note: Relative density $D_r = 100(e_{max} - e)/(e_{max} - e_{min})$, where e_{max} = void ratio corresponding to the loosest possible state of the soil, usually obtained by pouring the soil into a mold of known volume (ASTM D 4254-96, 2000), e_{min} = void ratio corresponding to the densest possible state of the soil, usually obtained by vibrating the soil particles into a dense state (ASTM D 4253-96, 2000), and e = the natural void ratio of the soil.

Sources: Terzaghi and Peck (1967) and Lambe and Whitman (1969).

TABLE 5.3 Correlation between $(N_1)_{60}$ and Density of Sand

$(N_1)_{60}$ (blows per foot)	Sand density	Relative density D_r, percent
0–2	Very loose condition	0–15
2–5	Loose condition	15–35
5–20	Medium condition	35–65
20–35	Dense condition	65–85
Over 35	Very dense condition	85–100

Source: Tokimatsu and Seed (1987).

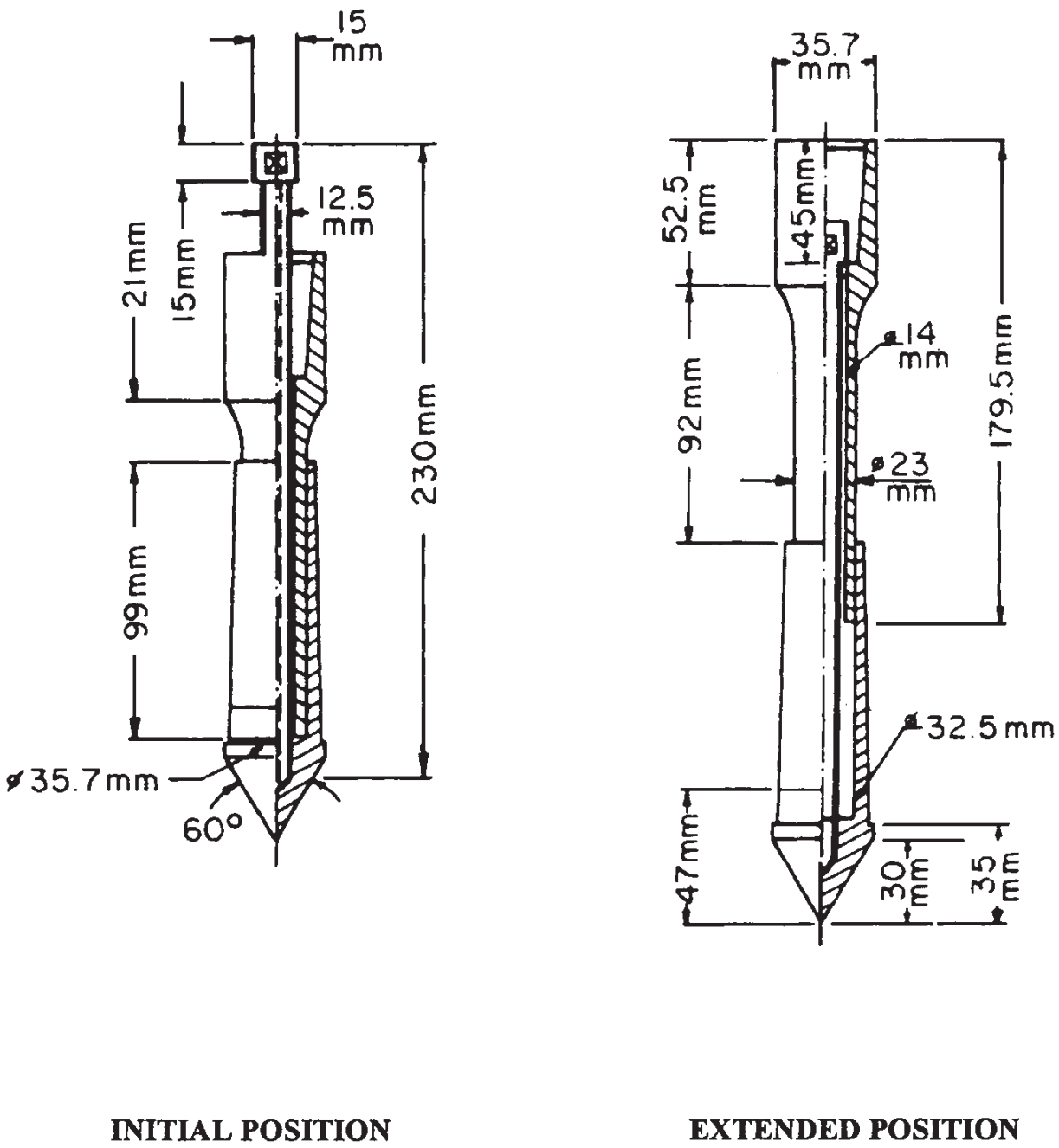

FIGURE 5.13 Example of mechanical cone penetrometer tip (Dutch mantle cone). (*Reprinted with permission from the American Society for Testing and Materials 2000.*)

the standard penetration test, which obtains data at intervals in the soil deposit. Disadvantages of the cone penetration test are that soil samples cannot be recovered and special equipment is required to produce a steady and slow penetration of the cone. Unlike the SPT, the ability to obtain a steady and slow penetration of the cone is not included as part of conventional drilling rigs. Because of these factors, in the United States, the CPT is used less frequently than the SPT.

5.5 LABORATORY TESTING

As discussed in Sec. 5.4.2, soil engineering properties that are used in earthquake analyses are usually obtained from field tests (SPT and CPT) or from standard laboratory tests (see Day

CHAPTER 6
LIQUEFACTION

The following notation is used in this chapter:

SYMBOL	*DEFINITION*
a	Acceleration
a_{max}	Maximum horizontal acceleration at ground surface (also known as peak ground acceleration)
C_b	Borehole diameter correction
C_N, C_v	Correction factor to account for overburden pressure
C_r	Rod length correction
CRR	Cyclic resistance ratio
CSR, SSR	Cyclic stress ratio, also known as the seismic stress ratio
D_r	Relative density
e_i	Initial void ratio
E_m	Hammer efficiency
F	Horizontal earthquake force
FS	Factor of safety against liquefaction
g	Acceleration of gravity
k_0	Coefficient of lateral earth pressure at rest
LL	Liquid limit
m	Mass of the soil column
M_L	Local magnitude of earthquake
M_s	Surface wave magnitude of earthquake
M_w	Moment magnitude of earthquake
N_{60}	N value corrected for field testing procedures
$(N_1)_{60}$	N value corrected for field testing procedures and overburden pressure
q_{c1}	Cone resistance corrected for overburden pressure
r_d	Depth reduction factor
u_e	Excess pore water pressure
V_s	Shear wave velocity measured in field
V_{s1}	Shear wave velocity corrected for overburden pressure
w	Water content
W	Weight of soil column
z	Depth below ground surface
γ_t	Total unit weight of soil
σ_{dc}	Cyclic deviator stress (cyclic triaxial test)
σ_{v0}	Total vertical stress
σ'_0	Effective confining pressure
σ'_{v0}	Vertical effective stress
τ_{cyc}	Uniform cyclic shear stress amplitude of earthquake
τ_d	Cyclic shear stress
τ_{max}	Maximum shear stress

6.1 INTRODUCTION

This chapter deals with the liquefaction of soil. An introduction to liquefaction was presented in Sec. 3.4. The concept of liquefaction was first introduced by Casagrande in the late 1930s (also see Casagrande 1975).

As mentioned in Sec. 3.4, the typical subsurface soil condition that is susceptible to liquefaction is a loose sand, which has been newly deposited or placed, with a groundwater table near ground surface. During an earthquake, the application of cyclic shear stresses induced by the propagation of shear waves causes the loose sand to contract, resulting in an increase in pore water pressure. Because the seismic shaking occurs so quickly, the cohesionless soil is subjected to an undrained loading (total stress analysis). The increase in pore water pressure causes an upward flow of water to the ground surface, where it emerges in the form of mud spouts or sand boils. The development of high pore water pressures due to the ground shaking and the upward flow of water may turn the sand into a liquefied condition, which has been termed *liquefaction.* For this state of liquefaction, the effective stress is zero, and the individual soil particles are released from any confinement, as if the soil particles were floating in water (Ishihara 1985).

Structures on top of the loose sand deposit that has liquefied during an earthquake will sink or fall over, and buried tanks will float to the surface when the loose sand liquefies (Seed 1970). Section 3.4 has shown examples of damage caused by liquefaction. Sand boils, such as shown in Fig. 3.19, often develop when there has been liquefaction at a site.

After the soil has liquefied, the excess pore water pressure will start to dissipate. The length of time that the soil will remain in a liquefied state depends on two main factors: (1) the duration of the seismic shaking from the earthquake and (2) the drainage conditions of the liquefied soil. The longer and the stronger the cyclic shear stress application from the earthquake, the longer the state of liquefaction persists. Likewise, if the liquefied soil is confined by an upper and a lower clay layer, then it will take longer for the excess pore water pressures to dissipate by the flow of water from the liquefied soil. After the liquefaction process is complete, the soil will be in a somewhat denser state.

This chapter is devoted solely to *level-ground liquefaction.* Liquefaction can result in ground surface settlement (Sec. 7.2) or even a bearing capacity failure of the foundation (Sec. 8.2). Liquefaction can also cause or contribute to lateral movement of slopes, which is discussed in Secs. 9.4 and 9.5.

6.2 LABORATORY LIQUEFACTION STUDIES

The liquefaction of soils has been extensively studied in the laboratory. There is a considerable amount of published data concerning laboratory liquefaction testing. This section presents examples of laboratory liquefaction data from Ishihara (1985) and Seed and Lee (1965).

6.2.1 Laboratory Data from Ishihara

Figures 6.1 and 6.2 (from Ishihara 1985) present the results of laboratory tests performed on hollow cylindrical specimens of saturated Fuji River sand tested in a torsional shear test apparatus. Figure 6.1 shows the results of laboratory tests on a saturated sand having a medium density (D_r = 47 percent), and Fig. 6.2 shows the results of laboratory tests on a saturated sand in a dense state (D_r = 75 percent). Prior to the cyclic shear testing, both soil specimens were subjected to an effective confining pressure σ_0' of 98 kN/m^2 (2000 lb/ft^2). The saturated sand specimens were then subjected to undrained conditions during the application of the cyclic shear stress. Several different plots are shown in Figs. 6.1 and 6.2, as follows:

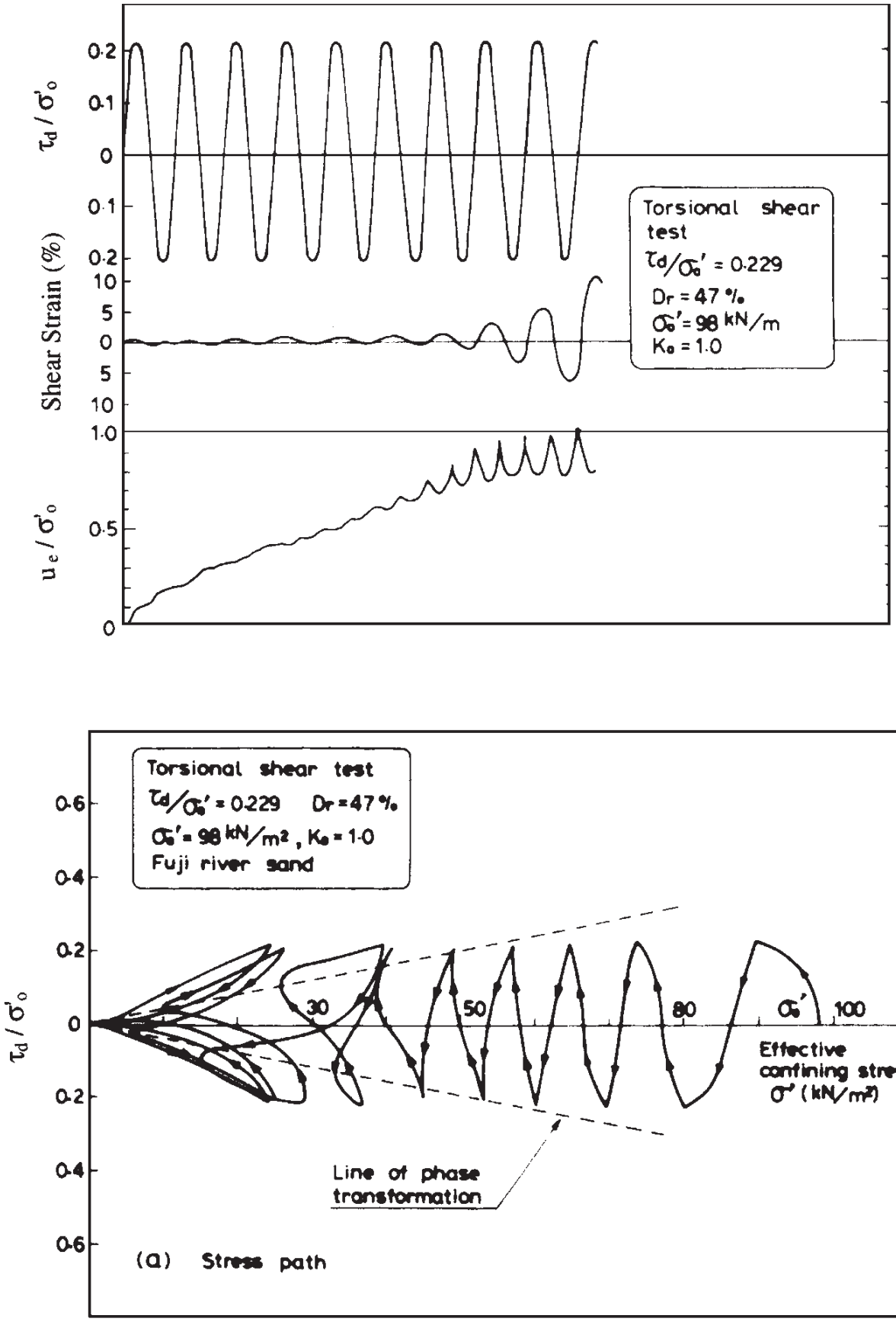

FIGURE 6.1 Laboratory test data from cyclic torsional shear tests performed on Fuji River sand having a medium density (D_r = 47 percent). (*Reproduced from Ishihara 1985.*)

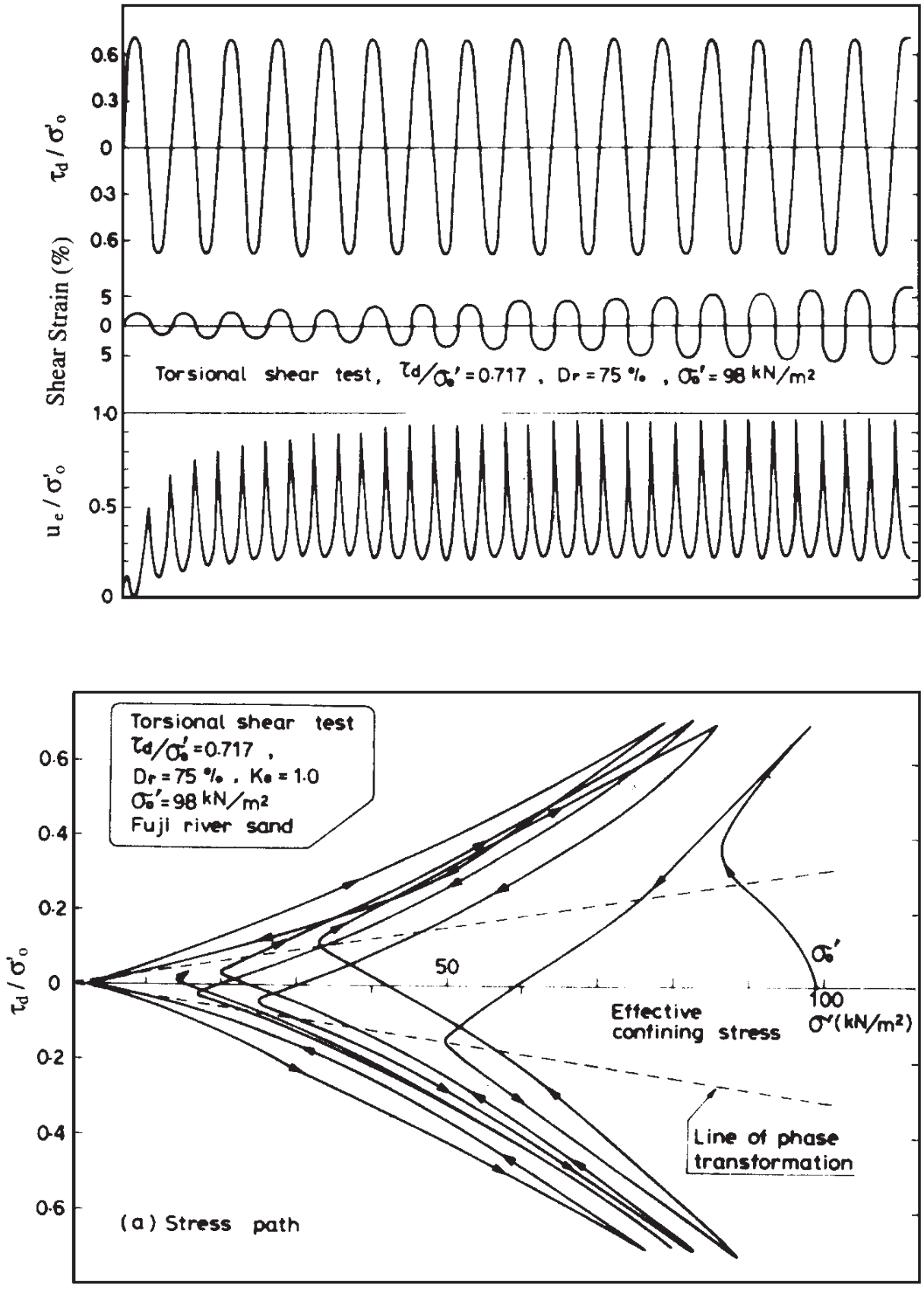

FIGURE 6.2 Laboratory test data from cyclic torsional shear tests performed on Fuji River sand having a dense state (D_r = 75 percent). (*Reproduced from Ishihara 1985.*)

1. *Plot of normalized cyclic shear stress* τ_d/σ_0': The uppermost plot shows the constant-amplitude cyclic shear stress that is applied to the saturated sand specimens. The applied cyclic shear stress has a constant amplitude and a sinusoidal pattern. The constant-amplitude cyclic shear stress τ_d has been normalized by dividing it by the initial effective confining pressure σ_0'. Note in Figs. 6.1 and 6.2 that the sand having a medium density (D_r = 47 percent) was subjected to a much lower constant-amplitude cyclic stress than the dense sand (D_r = 75 percent); that is, $\tau_d/\sigma_0' = 0.229$ for the sand having a medium density and $\tau_d/\sigma_0' = 0.717$ for the sand in a dense state.

2. *Plot of percent shear strain:* This plot shows the percent shear strain as the constant-amplitude cyclic shear stress is applied to the soil specimen. Note that for the sand having a medium density (D_r = 47 percent) there is a sudden and rapid increase in shear strain as high as 20 percent. For the dense sand (D_r = 75 percent), there is not a sudden and dramatic increase in shear strain, but rather the shear strain slowly increases with applications of the cyclic shear stress.

3. *Plot of normalized excess pore water pressure* u_e/σ_0': The normalized excess pore water pressure is also known as the *cyclic pore pressure ratio.* Because the soil specimens were subjected to undrained conditions during the application of the cyclic shear stress, excess pore water pressures u_e will develop as the constant-amplitude cyclic shear stress is applied to the soil. The excess pore water pressure u_e has been normalized by dividing it by the initial effective confining pressure σ_0'. When the excess pore water pressure u_e becomes equal to the initial effective confining pressure σ_0', the effective stress will become zero. Thus the condition of zero effective stress occurs when the ratio u_e/σ_0' is equal to 1.0. Note in Fig. 6.1 that the shear strain dramatically increases when the effective stress is equal to zero. As previously mentioned, liquefaction occurs when the effective stress becomes zero during the application of cyclic shear stress. Thus, once the sand having a medium density (D_r = 47 percent) liquefies, there is a significant increase in shear strain.

For the dense sand (D_r = 75 percent), u_e/σ_0' also becomes equal to 1.0 during the application of the cyclic shear stress. But the dense sand does not produce large shear displacements. This is because on reversal of the cyclic shear stress, the dense sand tends to dilate, resulting in an increased undrained shear resistance. Although the dense sand does reach a liquefaction state (that is, $u_e/\sigma_0' = 1.0$), it is only a momentary condition. Thus, this state has been termed *peak cyclic pore water pressure ratio of 100 percent with limited strain potential* (Seed 1979a). This state is also commonly referred to as *cyclic mobility* (Casagrande 1975, Castro 1975). The term *cyclic mobility* can be used to describe a state where the soil may only momentarily liquefy, with a limited potential for undrained deformation.

4. *Stress paths:* The lower plot in Figs. 6.1 and 6.2 shows the stress paths during application of the constant-amplitude cyclic shear stress. For the sand having a medium density (D_r = 47 percent), there is a permanent loss in shear strength as the stress path moves to the left with each additional cycle of constant-amplitude shear stress.

For the dense sand (Fig. 6.2), there is not a permanent loss in shear strength during the application of additional cycles of constant-amplitude shear stress. Instead, the stress paths tend to move up and down the shear strength envelope as the cycles of shear stress are applied to the soil.

It should be recognized that earthquakes will not subject the soil to uniform constant-amplitude cyclic shear stresses such as shown in the upper plot of Figs. 6.1 and 6.2. Nevertheless, this type of testing provides valuable insight into soil behavior.

In summary, the test results shown in Figs. 6.1 and 6.2 indicate that the sand having a medium density (D_r = 47 percent) has a sudden and dramatic increase in shear strain when the soil liquefies (i.e., when u_e/σ_0' becomes equal to 1.0). If the sand had been tested in a

loose or very loose state, the loss of shear strength upon liquefaction would be even more sudden and dramatic. For loose sand, this initial liquefaction when u_e/σ_0' becomes equal to 1.0 coincides with the contraction of the soil structure, subsequent liquefaction, and large deformations. As such, for loose sands, the terms *initial liquefaction* and *liquefaction* have been used interchangeably.

For dense sands, the state of initial liquefaction ($u_e/\sigma_0' = 1.0$) does not produce large deformations because of the dilation tendency of the sand upon reversal of the cyclic stress. However, there could be some deformation at the onset of initial liquefaction, which is commonly referred to as cyclic mobility.

6.2.2 Laboratory Data from Seed and Lee

Figure 6.3 (from Seed and Lee 1965) shows a summary of laboratory data from cyclic triaxial tests performed on saturated specimens of Sacramento River sand. Cylindrical sand specimens were first saturated and subjected in the triaxial apparatus to an isotropic effective confining pressure of 100 kPa (2000 lb/ft^2). The saturated sand specimens were then subjected to undrained conditions during the application of the cyclic deviator stress in the triaxial apparatus (see Sec. 5.5.2 for discussion of cyclic triaxial test).

Numerous sand specimens were prepared at different void ratios (e_i = initial void ratio). The sand specimens were subjected to different values of cyclic deviator stress σ_{dc}, and the number of cycles of deviator stress required to produce initial liquefaction and 20 percent axial strain was recorded. The laboratory data shown in Fig. 6.3 indicate the following:

1. For sand having the same initial void ratio e_i and same effective confining pressure, the higher the cyclic deviator stress σ_{dc}, the lower the number of cycles of deviator stress required to cause initial liquefaction.
2. Similar to item 1, for a sand having the same initial void ratio e_i and same effective confining pressure, the cyclic deviator stress σ_{dc} required to cause initial liquefaction will decrease as the number of cycles of deviator stress is increased.
3. For sand having the same effective confining pressure, the denser the soil (i.e., the lower the value of the initial void ratio), the greater the resistance to liquefaction. Thus a dense soil will require a higher cyclic deviator stress σ_{dc} or more cycles of the deviator stress in order to cause initial liquefaction, as compared to the same soil in a loose state.
4. Similar to item 3, the looser the soil (i.e., the higher the value of the initial void ratio), the lower the resistance to liquefaction. Thus a loose soil will require a lower cyclic deviator stress σ_{dc} or fewer cycles of the deviator stress in order to cause initial liquefaction, as compared to the same soil in a dense state.

6.3 MAIN FACTORS THAT GOVERN LIQUEFACTION IN THE FIELD

There are many factors that govern the liquefaction process for in situ soil. Based on the results of laboratory tests (Sec. 6.2) as well as field observations and studies, the most important factors that govern liquefaction are as follows:

1. *Earthquake intensity and duration:* In order to have liquefaction of soil, there must be ground shaking. The character of the ground motion, such as acceleration and duration of shaking, determines the shear strains that cause the contraction of the soil particles and the development of excess pore water pressures leading to liquefaction. The

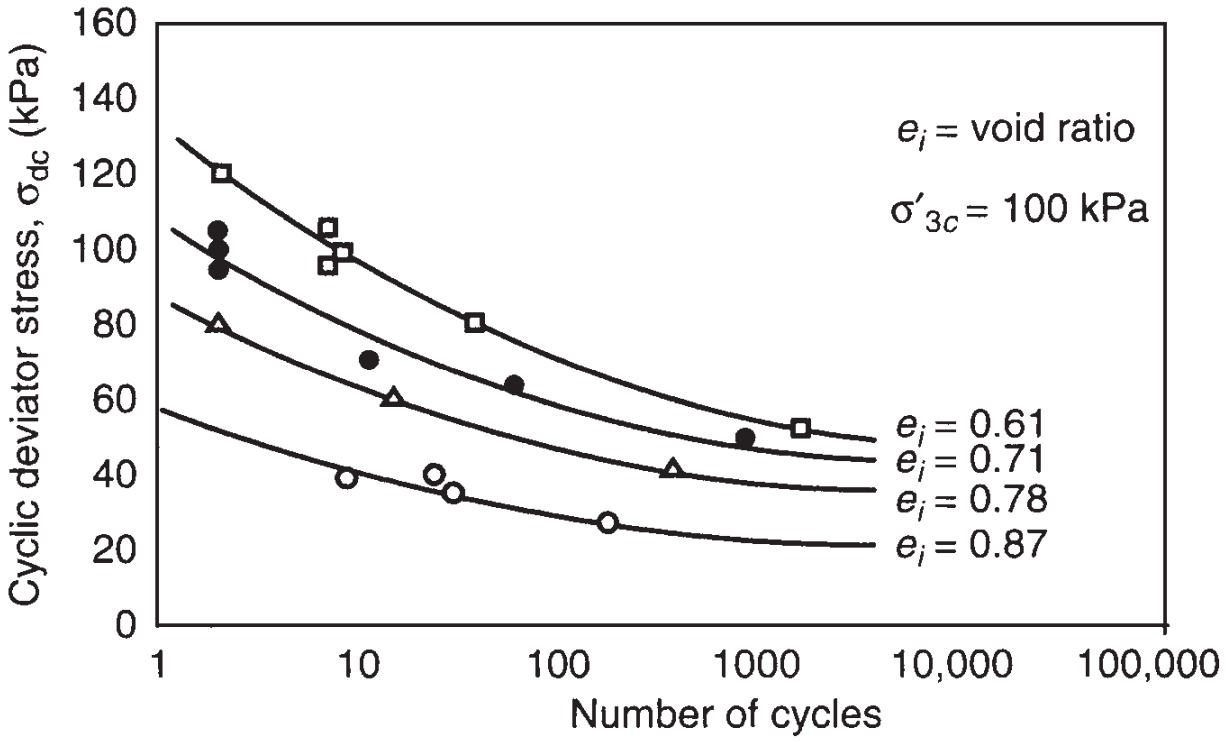

FIGURE 6.3 Laboratory test data from cyclic triaxial tests performed on Sacramento River sand. The plotted data represent the cyclic deviator stress versus number of cycles of deviator stress required to cause initial liquefaction and 20 percent axial strain. (*Initially developed by Seed and Lee 1965, reproduced from Kramer 1996.*)

most common cause of liquefaction is due to the seismic energy released during an earthquake. The potential for liquefaction increases as the earthquake intensity and duration of shaking increase. Those earthquakes that have the highest magnitude will produce both the largest ground acceleration and the longest duration of ground shaking (see Table 2.2).

Although data are sparse, there would appear to be a shaking threshold that is needed to produce liquefaction. These threshold values are a peak ground acceleration a_{max} of about $0.10g$ and local magnitude M_L of about 5 (National Research Council 1985, Ishihara 1985). Thus, a liquefaction analysis would typically not be needed for those sites having a peak ground acceleration a_{max} less than $0.10g$ or a local magnitude M_L less than 5.

Besides earthquakes, other conditions can cause liquefaction, such as subsurface blasting, pile driving, and vibrations from train traffic.

2. *Groundwater table:* The condition most conducive to liquefaction is a near-surface groundwater table. Unsaturated soil located above the groundwater table will not liquefy. If it can be demonstrated that the soils are currently above the groundwater table and are highly unlikely to become saturated for given foreseeable changes in the hydrologic regime, then such soils generally do not need to be evaluated for liquefaction potential.

At sites where the groundwater table significantly fluctuates, the liquefaction potential will also fluctuate. Generally, the historic high groundwater level should be used in the liquefaction analysis unless other information indicates a higher or lower level is appropriate (Division of Mines and Geology 1997).

Poulos et al. (1985) state that liquefaction can also occur in very large masses of sands or silts that are dry and loose and loaded so rapidly that the escape of air from the voids is restricted. Such movement of dry and loose sands is often referred to as *running soil* or *running ground.* Although such soil may flow as liquefied soil does, in this text, such soil deformation will not be termed liquefaction. It is best to consider that liquefaction only occurs for soils that are located below the groundwater table.

3. *Soil type:* In terms of the soil types most susceptible to liquefaction, Ishihara (1985) states: "The hazard associated with soil liquefaction during earthquakes has been known to be encountered in deposits consisting of fine to medium sand and sands containing low-plasticity fines. Occasionally, however, cases are reported where liquefaction apparently occurred in gravelly soils."

Thus, the soil types susceptible to liquefaction are nonplastic (cohesionless) soils. An approximate listing of cohesionless soils from least to most resistant to liquefaction is clean sands, nonplastic silty sands, nonplastic silt, and gravels. There could be numerous exceptions to this sequence. For example, Ishihara (1985, 1993) describes the case of tailings derived from the mining industry that were essentially composed of ground-up rocks and were classified as rock flour. Ishihara (1985, 1993) states that the rock flour in a water-saturated state did not possess significant cohesion and behaved as if it were a clean sand. These tailings were shown to exhibit as low a resistance to liquefaction as clean sand.

Seed et al. (1983) stated that based on both laboratory testing and field performance, the great majority of cohesive soils will not liquefy during earthquakes. Using criteria originally stated by Seed and Idriss (1982) and subsequently confirmed by Youd and Gilstrap (1999), in order for a cohesive soil to liquefy, it must meet *all* the following three criteria:

- The soil must have less than 15 percent of the particles, based on dry weight, that are finer than 0.005 mm (i.e., percent finer at 0.005 mm $<$ 15 percent).
- The soil must have a liquid limit (LL) that is less than 35 (that is, LL $<$ 35).
- The water content w of the soil must be greater than 0.9 of the liquid limit [that is, $w > 0.9$ (LL)].

If the cohesive soil does not meet all three criteria, then it is generally considered to be not susceptible to liquefaction. Although the cohesive soil may not liquefy, there could still be a significant undrained shear strength loss due to the seismic shaking.

4. *Soil relative density D_r:* Based on field studies, cohesionless soils in a loose relative density state are susceptible to liquefaction. Loose nonplastic soils will contract during the seismic shaking which will cause the development of excess pore water pressures. As indicated in Sec. 6.2, upon reaching initial liquefaction, there will be a sudden and dramatic increase in shear displacement for loose sands.

For dense sands, the state of initial liquefaction does not produce large deformations because of the dilation tendency of the sand upon reversal of the cyclic shear stress. Poulos et al. (1985) state that if the in situ soil can be shown to be dilative, then it need not be evaluated because it will not be susceptible to liquefaction. In essence, dilative soils are not susceptible to liquefaction because their undrained shear strength is greater than their drained shear strength.

5. *Particle size gradation:* Uniformly graded nonplastic soils tend to form more unstable particle arrangements and are more susceptible to liquefaction than well-graded soils. Well-graded soils will also have small particles that fill in the void spaces between the large particles. This tends to reduce the potential contraction of the soil, resulting in less excess pore water pressures being generated during the earthquake. Kramer (1996) states that field evidence indicates that most liquefaction failures have involved uniformly graded granular soils.

6. *Placement conditions or depositional environment:* Hydraulic fills (fill placed under water) tend to be more susceptible to liquefaction because of the loose and segregated soil structure created by the soil particles falling through water. Natural soil deposits formed in lakes, rivers, or the ocean also tend to form a loose and segregated soil structure and are more susceptible to liquefaction. Soils that are especially susceptible to liquefaction are formed in lacustrine, alluvial, and marine depositional environments.

7. *Drainage conditions:* If the excess pore water pressure can quickly dissipate, the soil may not liquefy. Thus highly permeable gravel drains or gravel layers can reduce the liquefaction potential of adjacent soil.

8. *Confining pressures:* The greater the confining pressure, the less susceptible the soil is to liquefaction. Conditions that can create a higher confining pressure are a deeper groundwater table, soil that is located at a deeper depth below ground surface, and a surcharge pressure applied at ground surface. Case studies have shown that the possible zone of liquefaction usually extends from the ground surface to a maximum depth of about 50 ft (15 m). Deeper soils generally do not liquefy because of the higher confining pressures.

This does not mean that a liquefaction analysis should not be performed for soil that is below a depth of 50 ft (15 m). In many cases, it may be appropriate to perform a liquefaction analysis for soil that is deeper than 50 ft (15 m). An example would be sloping ground, such as a sloping berm in front of a waterfront structure or the sloping shell of an earth dam (see Fig. 3.38). In addition, a liquefaction analysis should be performed for any soil deposit that has been loosely dumped in water (i.e., the liquefaction analysis should be performed for the entire thickness of loosely dumped fill in water, even if it exceeds 50 ft in thickness). Likewise, a site where alluvium is being rapidly deposited may also need a liquefaction investigation below a depth of 50 ft (15 m). Considerable experience and judgment are required in the determination of the proper depth to terminate a liquefaction analysis.

9. *Particle shape:* The soil particle shape can also influence liquefaction potential. For example, soils having rounded particles tend to densify more easily than angular-shape soil particles. Hence a soil containing rounded soil particles is more susceptible to liquefaction than a soil containing angular soil particles.

10. *Aging and cementation:* Newly deposited soils tend to be more susceptible to liquefaction than older deposits of soil. It has been shown that the longer a soil is subjected to a confining pressure, the greater the liquefaction resistance (Ohsaki 1969, Seed 1979a, Yoshimi et al. 1989). Table 6.1 presents the estimated susceptibility of sedimentary deposits to liquefaction versus the geologic age of the deposit.

The increase in liquefaction resistance with time could be due to the deformation or compression of soil particles into more stable arrangements. With time, there may also be the development of bonds due to cementation at particle contacts.

11. *Historical environment:* It has also been determined that the historical environment of the soil can affect its liquefaction potential. For example, older soil deposits that have already been subjected to seismic shaking have an increased liquefaction resistance compared to a newly formed specimen of the same soil having an identical density (Finn et al. 1970, Seed et al. 1975).

Liquefaction resistance also increases with an increase in the overconsolidation ratio (OCR) and the coefficient of lateral earth pressure at rest k_0 (Seed and Peacock 1971, Ishihara et al. 1978). An example would be the removal of an upper layer of soil due to erosion. Because the underlying soil has been preloaded, it will have a higher overconsolidation ratio and it will have a higher coefficient of lateral earth pressure at rest k_0. Such a soil that has been preloaded will be more resistant to liquefaction than the same soil that has not been preloaded.

12. *Building load:* The construction of a heavy building on top of a sand deposit can decrease the liquefaction resistance of the soil. For example, suppose a mat slab at ground surface supports a heavy building. The soil underlying the mat slab will be subjected to shear stresses caused by the building load. These shear stresses induced into the soil by the building load can make the soil more susceptible to liquefaction. The reason is that a smaller additional shear stress will be required from the earthquake in order to cause contraction and hence liquefaction of the soil. For level-ground liquefaction discussed in this chapter, the effect of the building load is ignored. Although building loads are not considered in the liquefaction analysis in this chapter, the building loads must be included in all liquefaction-induced settlement, bearing capacity, and stability analyses, as discussed in Chaps. 7 through 9.

In summary, the site conditions and soil type most susceptible to liquefaction are as follows:

Site Conditions

- Site that is close to the epicenter or location of fault rupture of a major earthquake
- Site that has a groundwater table close to ground surface

Soil Type Most Susceptible to Liquefaction for Given Site Conditions

- Sand that has uniform gradation and rounded soil particles, very loose or loose density state, recently deposited with no cementation between soil grains, and no prior preloading or seismic shaking

6.4 LIQUEFACTION ANALYSIS

6.4.1 Introduction

The first step in the liquefaction analysis is to determine if the soil has the ability to liquefy during an earthquake. As discussed in Sec. 6.3 (item number 3), the vast majority of soils that are susceptible to liquefaction are cohesionless soils. Cohesive soils should not be considered susceptible to liquefaction unless they meet all three criteria listed in Sec. 6.3 (see item 3, soil type).

The most common type of analysis to determine the liquefaction potential is to use the standard penetration test (SPT) (Seed et al. 1985, Stark and Olson 1995). The analysis is based on the simplified method proposed by Seed and Idriss (1971). This method of liquefaction analysis proposed by Seed and Idriss (1971) is often termed the *simplified procedure.* This is the most commonly used method to evaluate the liquefaction potential of a site. The steps are as follows:

1. *Appropriate soil type:* As discussed above, the first step is to determine if the soil has the ability to liquefy during an earthquake. The soil must meet the requirements listed in Sec. 6.3 (item 3).

2. *Groundwater table:* The soil must be below the groundwater table. The liquefaction analysis could also be performed if it is anticipated that the groundwater table will rise in the future, and thus the soil will eventually be below the groundwater table.

3. *CSR induced by earthquake:* If the soil meets the above two requirements, then the simplified procedure can be performed. The first step in the simplified procedure is to determine the cyclic stress ratio (CSR) that will be induced by the earthquake (Sec. 6.4.2).

A major unknown in the calculation of the CSR induced by the earthquake is the peak horizontal ground acceleration a_{max} that should be used in the analysis. The peak horizontal ground acceleration is discussed in Sec. 5.6. Threshold values needed to produce liquefaction are discussed in Sec. 6.3 (item 1). As previously mentioned, a liquefaction analysis would typically not be needed for those sites having a peak ground acceleration a_{max} less than $0.10g$ or a local magnitude M_L less than 5.

4. *CRR from standard penetration test:* By using the standard penetration test, the cyclic resistance ratio (CRR) of the in situ soil is then determined (Sec. 6.4.3). If the CSR induced by the earthquake is greater than the CRR determined from the standard penetration test, then it is likely that liquefaction will occur during the earthquake, and vice versa.

5. *Factor of safety* (FS): The final step is to determine the factor of safety against liquefaction (Sec. 6.4.4), which is defined as FS = CRR/CSR.

TABLE 6.1 Estimated Susceptibility of Sedimentary Deposits to Liquefaction during Strong Seismic Shaking Based on Geologic Age and Depositional Environment

Type of deposit	General distribution of cohesionless sediments in deposits	Likelihood that cohesionless sediments, when saturated, would be susceptible to liquefaction (by age of deposit)			
		<500 years	Holocene	Pleistocene	Pre-Pleistocene
(*a*) Continental deposits					
Alluvial fan and plain	Widespread	Moderate	Low	Low	Very low
Delta and fan-delta	Widespread	High	Moderate	Low	Very low
Dunes	Widespread	High	Moderate	Low	Very low
Marine terrace/plain	Widespread	Unknown	Low	Very low	Very low
Talus	Widespread	Low	Low	Very low	Very low
Tephra	Widespread	High	High	Unknown	Unknown
Colluvium	Variable	High	Moderate	Low	Very low
Glacial till	Variable	Low	Low	Very low	Very low
Lacustrine and playa	Variable	High	Moderate	Low	Very low
Loess	Variable	High	High	High	Unknown
Floodplain	Locally variable	High	Moderate	Low	Very low
River channel	Locally variable	Very high	High	Low	Very low
Sebka	Locally variable	High	Moderate	Low	Very low
Residual soils	Rare	Low	Low	Very low	Very low
Tuff	Rare	Low	Low	Very low	Very low
(*b*) Coastal zone					
Beach—large waves	Widespread	Moderate	Low	Very low	Very low
Beach—small waves	Widespread	High	Moderate	Low	Very low
Delta	Widespread	Very high	High	Low	Very low
Estuarine	Locally variable	High	Moderate	Low	Very low
Foreshore	Locally variable	High	Moderate	Low	Very low
Lagoonal	Locally variable	High	Moderate	Low	Very low
(*c*) Artificial					
Compacted fill	Variable	Low	Unknown	Unknown	Unknown
Uncompacted fill	Variable	Very high	Unknown	Unknown	Unknown

Source: Data from Youd and Hoose (1978), reproduced from R. B. Seed (1991).

6.4.2 Cyclic Stress Ratio Caused by the Earthquake

If it is determined that the soil has the ability to liquefy during an earthquake and the soil is below or will be below the groundwater table, then the liquefaction analysis is performed. The first step in the simplified procedure is to calculate the cyclic stress ratio, also commonly referred to as the *seismic stress ratio* (*SSR*), that is caused by the earthquake.

To develop the CSR earthquake equation, it is assumed that there is a level ground surface and a soil column of unit width and length, and that the soil column will move horizontally as a rigid body in response to the maximum horizontal acceleration a_{max} exerted by the earthquake at ground surface. Figure 6.4 shows a diagram of these assumed conditions. Given these assumptions, the weight W of the soil column is equal to $\gamma_t z$, where γ_t = total

unit weight of the soil and z = depth below ground surface. The horizontal earthquake force F acting on the soil column (which has a unit width and length) is:

$$F = ma = \left(\frac{W}{g}\right)a = \left(\frac{\gamma_t z}{g}\right)a_{\max} = \sigma_{vo}\left(\frac{a_{\max}}{g}\right) \tag{6.1}$$

where F = horizontal earthquake force acting on soil column that has a unit width and length, lb or kN
m = total mass of soil column, lb or kg, which is equal to W/g
W = total weight of soil column, lb or kN. For the assumed unit width and length of soil column, the total weight of the soil column is $\gamma_t z$.
γ_t = total unit weight of soil, lb/ft^3 or kN/m^3.
z = depth below ground surface of soil column, as shown in Fig. 6.4.
a = acceleration, which in this case is the maximum horizontal acceleration at ground surface caused by the earthquake ($a = a_{\max}$), ft/s^2 or m/s^2
$a_{\max}$ = maximum horizontal acceleration at ground surface that is induced by the earthquake, ft/s^2 or m/s^2. The maximum horizontal acceleration is also commonly referred to as the peak ground acceleration (see Sec. 5.6).
σ_{v0} = total vertical stress at bottom of soil column, lb/ft^2 or kPa. The total vertical stress = $\gamma_t z$.

As shown in Fig. 6.4, by summing forces in the horizontal direction, the force F acting on the rigid soil element is equal to the maximum shear force at the base on the soil element. Since the soil element is assumed to have a unit base width and length, the maximum shear force F is equal to the maximum shear stress $\tau_{\max}$, or from Eq. (6.1):

$$\tau_{\max} = F = \sigma_{v0}\left(\frac{a_{\max}}{g}\right) \tag{6.2}$$

Dividing both sides of the equation by the vertical effective stress σ'_{vo} gives

$$\frac{\tau_{\max}}{\sigma'_{v0}} = \left(\frac{\sigma_{v0}}{\sigma'_{v0}}\right)\left(\frac{a_{\max}}{g}\right) \tag{6.3}$$

Since the soil column does not act as a rigid body during the earthquake, but rather the soil is deformable, Seed and Idriss (1971) incorporated a depth reduction factor r_d into the right side of Eq. (6.3), or

$$\frac{\tau_{\max}}{\sigma'_{v0}} = r_d\left(\frac{\sigma_{v0}}{\sigma'_{v0}}\right)\left(\frac{a_{\max}}{g}\right) \tag{6.4}$$

For the simplified method, Seed et al. (1975) converted the typical irregular earthquake record to an equivalent series of uniform stress cycles by assuming the following:

$$\tau_{\text{cyc}} = 0.65\tau_{\max} \tag{6.5}$$

where τ_{cyc} = uniform cyclic shear stress amplitude of the earthquake (lb/ft^2 or kPa).

In essence, the erratic earthquake motion was converted to an equivalent series of uniform cycles of shear stress, referred to as τ_{cyc}. By substituting Eq. (6.5) into Eq. (6.4), the earthquake-induced cyclic stress ratio is obtained.

$$\text{CSR} = \frac{\tau_{\text{cyc}}}{\sigma'_{v0}} = 0.65r_d\left(\frac{\sigma_{v0}}{\sigma'_{v0}}\right)\left(\frac{a_{\max}}{g}\right) \tag{6.6}$$

where CSR = cyclic stress ratio (dimensionless), also commonly referred to as seismic stress ratio

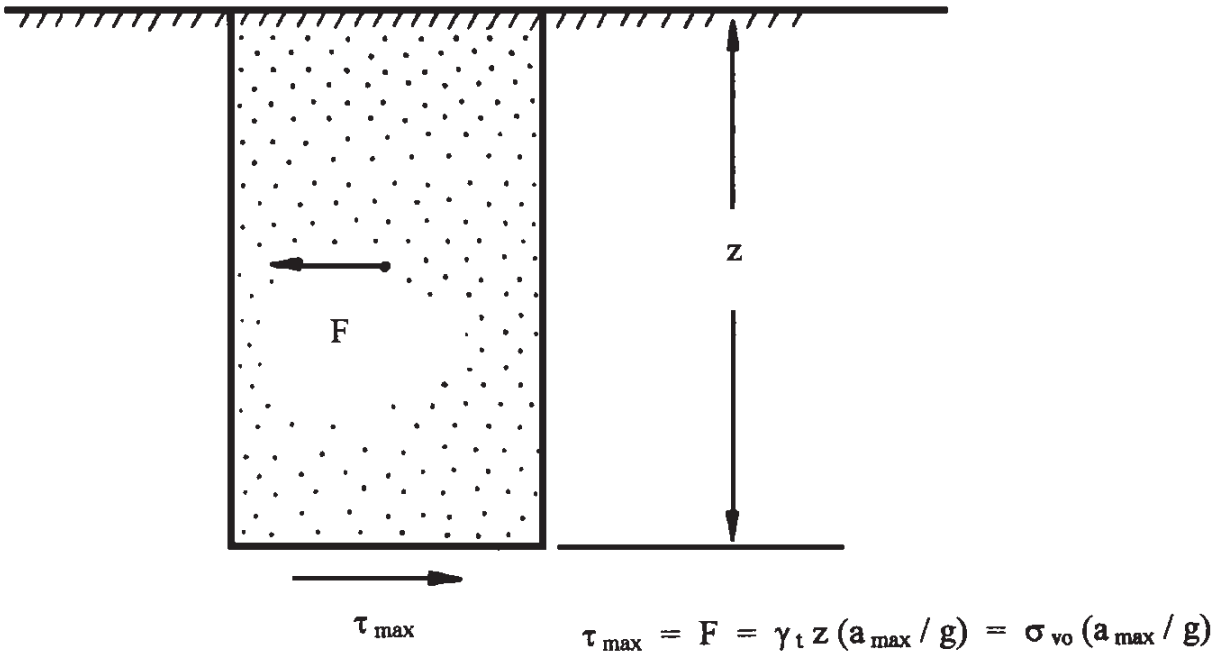

FIGURE 6.4 Conditions assumed for the derivation of the CSR earthquake equation.

a_{max} = maximum horizontal acceleration at ground surface that is induced by the earthquake, ft/s^2 or m/s^2, also commonly referred to as the peak ground acceleration (see Sec. 5.6)
g = acceleration of gravity (32.2 ft/s^2 or 9.81 m/s^2)
σ_{v0} = total vertical stress at a particular depth where the liquefaction analysis is being performed, lb/ft^2 or kPa. To calculate total vertical stress, total unit weight γ_t of soil layer (s) must be known
σ'_{v0} = vertical effective stress at that same depth in soil deposit where σ_{v0} was calculated, lb/ft^2 or kPa. To calculate vertical effective stress, location of groundwater table must be known
r_d = depth reduction factor, also known as stress reduction coefficient (dimensionless)

As previously mentioned, the depth reduction factor was introduced to account for the fact that the soil column shown in Fig. 6.4 does not behave as a rigid body during the earthquake. Figure 6.5 presents the range in values for the depth reduction factor r_d versus depth below ground surface. Note that with depth, the depth reduction factor decreases to account for the fact that the soil is not a rigid body, but is rather deformable. As indicated in Fig. 6.5, Idriss (1999) indicates that the values of r_d depend on the magnitude of the earthquake. As a practical matter, the r_d values are usually obtained from the curve labeled "Average values by Seed & Idriss (1971)" in Fig. 6.5.

Another option is to assume a linear relationship of r_d versus depth and use the following equation (Kayen et al. 1992):

$$r_d = 1 - 0.012z \tag{6.7}$$

where z = depth in meters below the ground surface where the liquefaction analysis is being performed (i.e., the same depth used to calculate σ_{v0} and σ'_{v0}).

For Eq. (6.6), the vertical total stress σ_{v0} and vertical effective stress σ'_{v0} can be readily calculated using basic geotechnical principles. Equation (6.7) or Fig. 6.5 could be used to determine the depth reduction factor r_d. Thus all parameters in Eq. (6.6) can be readily calculated, except for the peak ground acceleration a_{max}, which is discussed in Sec. 5.6.

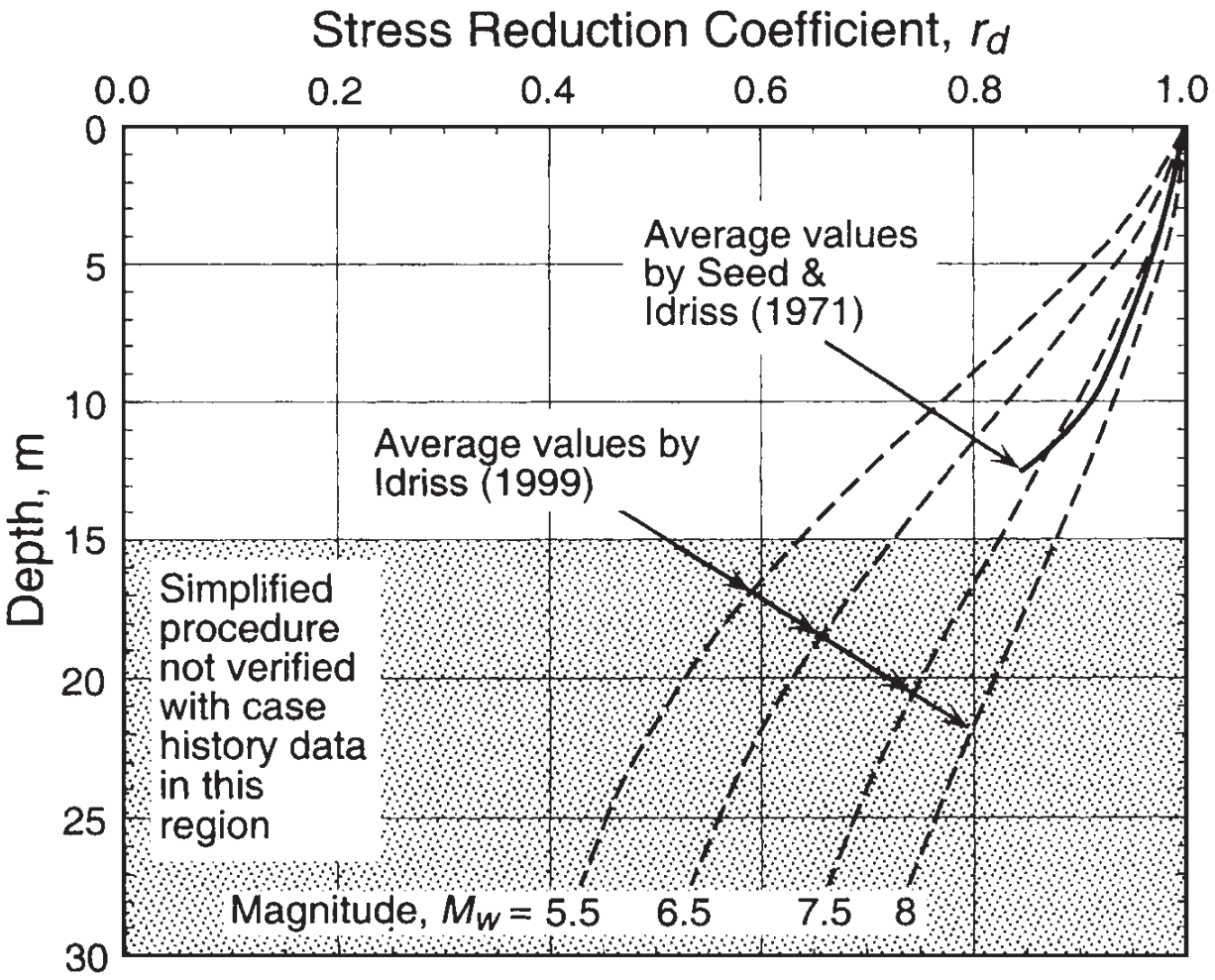

FIGURE 6.5 Reduction factor r_d versus depth below level or gently sloping ground surfaces. (*From Andrus and Stokoe 2000, reproduced with permission from the American Society of Civil Engineers.*)

6.4.3 Cyclic Resistance Ratio from the Standard Penetration Test

The second step in the simplified procedure is to determine the cyclic resistance ratio of the in situ soil. The cyclic resistance ratio represents the liquefaction resistance of the in situ soil. The most commonly used method for determining the liquefaction resistance is to use the data obtained from the standard penetration test. The standard penetration test is discussed in Sec. 5.4.3. The advantages of using the standard penetration test to evaluate the liquefaction potential are as follows:

1. *Groundwater table:* A boring must be excavated in order to perform the standard penetration test. The location of the groundwater table can be measured in the borehole. Another option is to install a piezometer in the borehole, which can then be used to monitor the groundwater level over time.

2. *Soil type:* In clean sand, the SPT sampler may not be able to retain a soil sample. But for most other types of soil, the SPT sampler will be able to retrieve a soil sample. The soil sample retrieved in the SPT sampler can be used to visually classify the soil and to estimate the percent fines in the soil. In addition, the soil specimen can be returned to the laboratory, and classification tests can be performed to further assess the liquefaction susceptibility of the soil (see item 3, Sec. 6.3).

3. *Relationship between N value and liquefaction potential:* In general, the factors that increase the liquefaction resistance of a soil will also increase the $(N_1)_{60}$ from the standard penetration test [see Sec. 5.4.3 for the procedure to calculate $(N_1)_{60}$]. For example, a

well-graded dense soil that has been preloaded or aged will be resistant to liquefaction and will have high values of $(N_1)_{60}$. Likewise, a uniformly graded soil with a loose and segregated soil structure will be more susceptible to liquefaction and will have much lower values of $(N_1)_{60}$.

Based on the standard penetration test and field performance data, Seed et al. (1985) concluded that there are three approximate potential damage ranges that can be identified:

$(N_1)_{60}$	Potential damage
0–20	High
20–30	Intermediate
>30	No significant damage

As indicated in Table 5.3, an $(N_1)_{60}$ value of 20 is the approximate boundary between the medium and dense states of the sand. Above an $(N_1)_{60}$ of 30, the sand is in either a dense or a very dense state. For this condition, initial liquefaction does not produce large deformations because of the dilation tendency of the sand upon reversal of the cyclic shear stress. This is the reason that such soils produce no significant damage, as indicated by the above table.

Figure 6.6 presents a chart that can be used to determine the cyclic resistance ratio of the in situ soil. This figure was developed from investigations of numerous sites that had liquefied or did not liquefy during earthquakes. For most of the data used in Fig. 6.6, the earthquake magnitude was close to 7.5 (Seed et al. 1985). The three lines shown in Fig. 6.6 are for soil that contains 35, 15, or ≤5 percent fines. The lines shown in Fig. 6.6 represent approximate dividing lines, where data to the left of each individual line indicate field liquefaction, while data to the right of the line indicate sites that generally did not liquefy during the earthquake.

Use Fig. 6.6 to determine the cyclic resistance ratio of the in situ soil, as follows:

1. *Standard penetration test $(N_1)_{60}$ value:* Note in Fig. 6.6 that the horizontal axis represents data from the standard penetration test, which must be expressed in terms of the $(N_1)_{60}$ value. In the liquefaction analysis, the standard penetration test N_{60} value [Eq. (5.1)] is corrected for the overburden pressure [see Eq. (5.2)]. As discussed in Sec. 5.4.3, when a correction is applied to the N_{60} value to account for the effect of overburden pressure, this value is referred to as $(N_1)_{60}$.

2. *Percent fines:* Once the $(N_1)_{60}$ value has been calculated, the next step is to determine or estimate the percent fines in the soil. For a given $(N_1)_{60}$ value, soils with more fines have a higher liquefaction resistance. Figure 6.6 is applicable for nonplastic silty sands or for plastic silty sands that meet the criteria for cohesive soils listed in Sec. 6.3 (see item 3, soil type).

3. *Cyclic resistance ratio for an anticipated magnitude 7.5 earthquake:* Once the $(N_1)_{60}$ value and the percent fines in the soil have been determined, then Fig. 6.6 can be used to obtain the cyclic resistance ratio of the soil. To use Fig. 6.6, the figure is entered with the corrected standard penetration test $(N_1)_{60}$ value from Eq. (5.2), and then by intersecting the appropriate fines content curve, the cyclic resistance ratio is obtained.

As shown in Fig. 6.6, for a magnitude 7.5 earthquake, clean sand will not liquefy if the $(N_1)_{60}$ value exceeds 30. For an $(N_1)_{60}$ value of 30, the sand is in either a dense or a very dense state (see Table 5.3). As previously mentioned, dense sands will not liquefy because they tend to dilate during shearing.

4. *Correction for other magnitude earthquakes:* Figure 6.6 is for a projected earthquake that has a magnitude of 7.5. The final factor that must be included in the analysis is

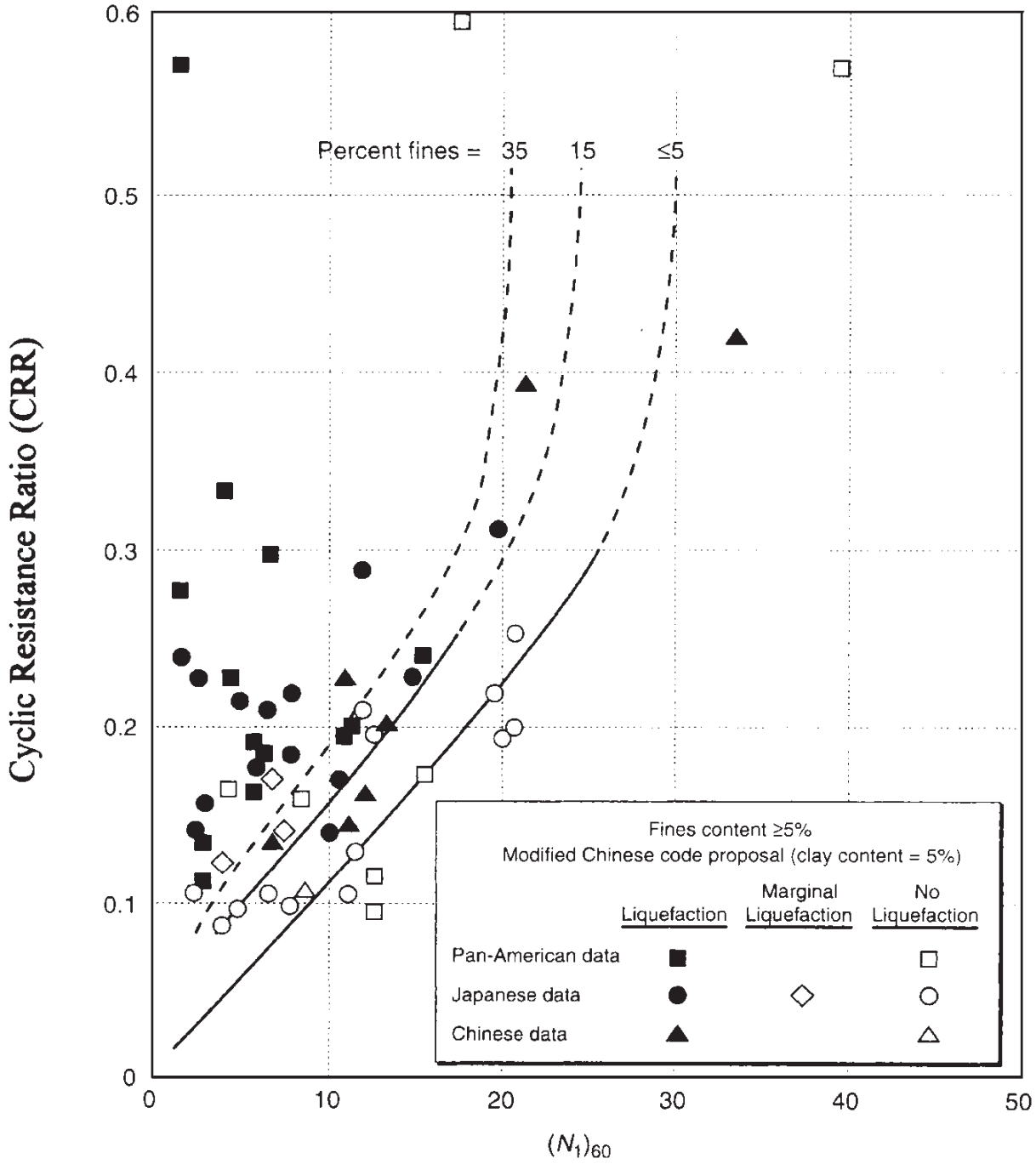

FIGURE 6.6 Plot used to determine the cyclic resistance ratio for clean and silty sands for $M = 7.5$ earthquakes. (*After Seed et al. 1985, reprinted with permission of the American Society of Civil Engineers.*)

the magnitude of the earthquake. As indicated in Table 2.2, the higher the magnitude of the earthquake, the longer the duration of ground shaking. A higher magnitude will thus result in a higher number of applications of cyclic shear strain, which will decrease the liquefaction resistance of the soil. Figure 6.6 was developed for an earthquake magnitude of 7.5; and for other different magnitudes, the CRR values from Fig. 6.6 would be multiplied by the magnitude scaling factor indicated in Table 6.2. Figure 6.7 presents other suggested magnitude scaling factors.

As discussed in Sec. 2.4.4, it could be concluded that the local magnitude M_L, the surface wave magnitude M_s, and moment magnitude M_w scales are reasonably close to one another below a value of about 7. Thus for a magnitude of 7 or below, any one of these magnitude scales can be used to determine the magnitude scaling factor. At high magnitude val-

TABLE 6.2 Magnitude Scaling Factors

Anticipated earthquake magnitude	Magnitude scaling factor (MSF)
8½	0.89
7½	1.00
6¾	1.13
6	1.32
5¼	1.50

Note: To determine the cyclic resistance ratio of the in situ soil, multiply the magnitude scaling factor indicated above by the cyclic resistance ratio determined from Fig. 6.6.

Source: Seed et al. (1985).

ues, the moment magnitude M_w tends to significantly deviate from the other magnitude scales, and the moment magnitude M_w should be used to determine the magnitude scaling factor from Table 6.2 or Fig. 6.7.

Two additional correction factors may need to be included in the analysis. The first correction factor is for the liquefaction of deep soil layers (i.e., depths where $\sigma'_{v0} > 100$ kPa, in which liquefaction has not been verified by the Seed and Idriss simplified procedure, see Youd and Idriss 2001). The second correction factor is for sloping ground conditions, which is discussed in Sec. 9.4.2.

As indicated in Secs. 4.6.1 and 5.6.4, both the peak ground acceleration a_{max} and the length of ground shaking increase for sites having soft, thick, and submerged soils. In a sense, the earthquake magnitude accounts for the increased shaking at a site; that is, the higher the magnitude, the longer the ground is subjected to shaking. Thus for sites having soft, thick, and submerged soils, it may be prudent to increase both the peak ground acceleration a_{max} and the earthquake magnitude to account for local site effects.

6.4.4 Factor of Safety against Liquefaction

The final step in the liquefaction analysis is to calculate the factor of safety against liquefaction. If the cyclic stress ratio caused by the anticipated earthquake [Eq. (6.6)] is greater than the cyclic resistance ratio of the in situ soil (Fig. 6.6), then liquefaction could occur during the earthquake, and vice versa. The factor of safety against liquefaction (FS) is defined as follows:

$$\text{FS} = \frac{\text{CRR}}{\text{CSR}} \tag{6.8}$$

The higher the factor of safety, the more resistant the soil is to liquefaction. However, soil that has a factor of safety slightly greater than 1.0 may still liquefy during an earthquake. For example, if a lower layer liquefies, then the upward flow of water could induce liquefaction of the layer that has a factor of safety slightly greater than 1.0.

In the above liquefaction analysis, there are many different equations and corrections that are applied to both the cyclic stress ratio induced by the anticipated earthquake and the cyclic resistance ratio of the in situ soil. For example, there are four different corrections (that is, E_m, C_b, C_r, and σ'_{v0}) that are applied to the standard penetration test N value in order to calculate the $(N_1)_{60}$ value. All these different equations and various corrections may provide the engineer with a sense of high accuracy, when in fact the entire analysis is only a gross approximation. The analysis should be treated as such, and engineering experience

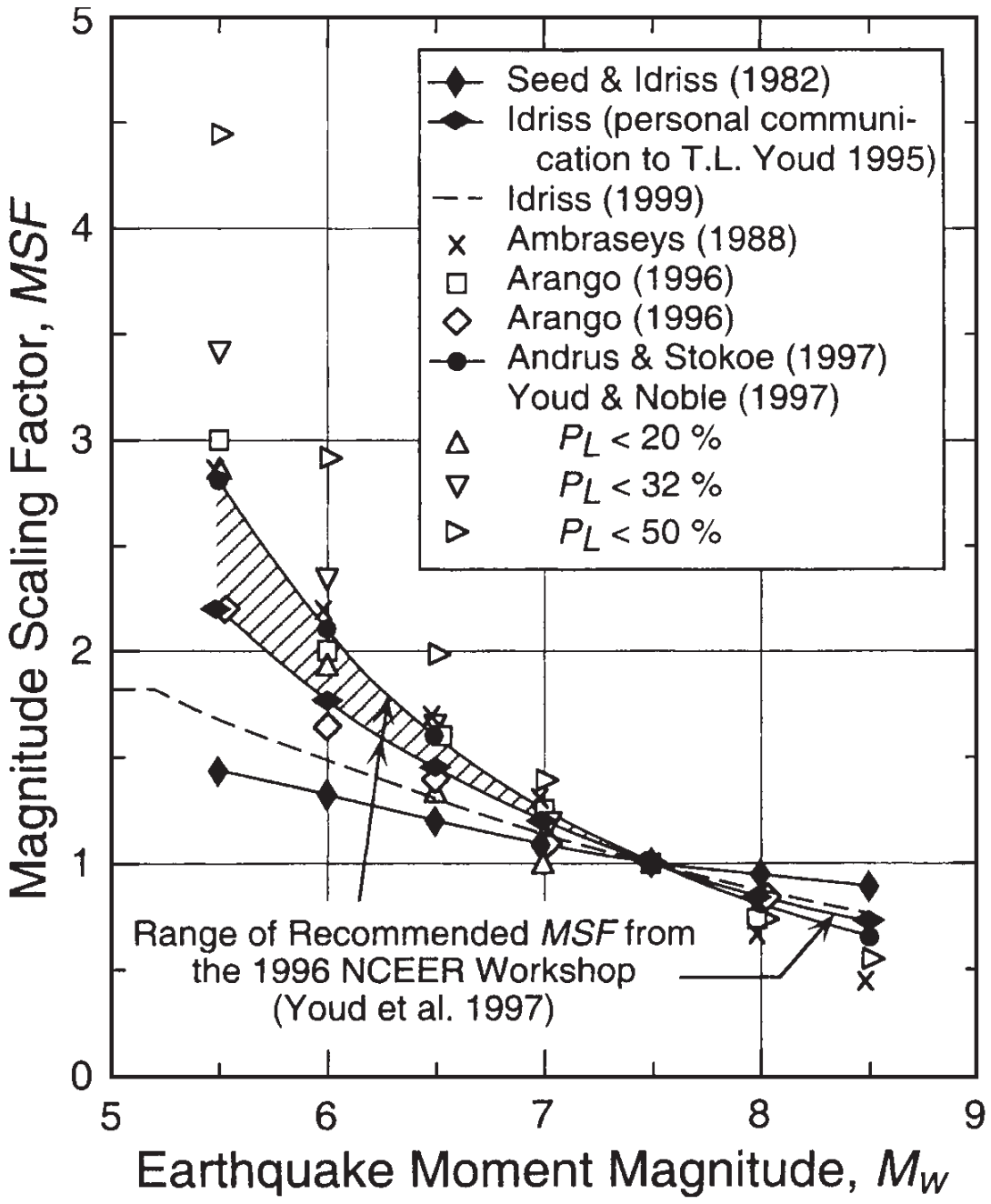

FIGURE 6.7 Magnitude scaling factors derived by various investigators. (*From Andrus and Stokoe 2000, reprinted with permission of the American Society of Civil Engineers.*)

and judgment are essential in the final determination of whether a site has liquefaction potential.

6.4.5 Example Problem

The following example problem illustrates the procedure that is used to determine the factor of safety against liquefaction: It is planned to construct a building on a cohesionless sand deposit (fines $<$ 5 percent). There is a nearby major active fault, and the engineering geologist has determined that for the anticipated earthquake, the peak ground acceleration a_{max} will be equal to 0.40g. Assume the site conditions are the same as stated in Problems 5.2 and 5.3, that is, a level ground surface with the groundwater table located 1.5 m below ground surface and the standard penetration test performed at a depth of 3 m. Assuming an antici-

pated earthquake magnitude of 7.5, calculate the factor of safety against liquefaction for the saturated clean sand located at a depth of 3 m below ground surface.

Solution. Per Probs. 5.2 and 5.3, $\sigma'_{v0} = 43$ kPa and $(N_1)_{60} = 7.7$. Using the soil unit weights from Prob. 5.2, we have

$$\sigma_{v0} = (1.5 \text{ m})\,(18.9 \text{ kN/m}^3) + (1.5 \text{ m})\,(9.84 + 9.81 \text{ kN/m}^3) = 58 \text{ kPa}$$

Using Eq. (6.7) with $z = 3$ m gives $r_d = 0.96$. Use the following values:

$$r_d = 0.96$$

$$\frac{\sigma_{v0}}{\sigma'_{v0}} = \frac{58}{43} = 1.35$$

$$\frac{a_{\max}}{g} = 0.40$$

And inserting the above values into Eq. (6.6), we see that the cyclic stress ratio due to the anticipated earthquake is 0.34.

The next step is to determine the cyclic resistance ratio of the in situ soil. Entering Fig. 6.6 with $(N_1)_{60} = 7.7$ and intersecting the curve labeled less than 5 percent fines, we find that the cyclic resistance ratio of the in situ soil at a depth of 3 m is 0.09.

The final step is to calculate the factor of safety against liquefaction by using Eq. (6.8):

$$\text{FS} = \frac{\text{CRR}}{\text{CSR}} = \frac{0.09}{0.34} = 0.26$$

Based on the factor of safety against liquefaction, it is probable that during the anticipated earthquake the in situ sand located at a depth of 3 m below ground surface will liquefy.

6.4.6 Cyclic Resistance Ratio from the Cone Penetration Test

As an alternative to using the standard penetration test, the cone penetration test can be used to determine the cyclic resistance ratio of the in situ soil. The first step is to determine the corrected CPT tip resistance q_{c1} by using Eq. (5.3). Then Fig. 6.8 can be used to determine the cyclic resistance ratio of the in situ soil. The final step is to determine the factor of safety against liquefaction by using Eq. (6.8).

Note that Fig. 6.8 was developed for an anticipated earthquake that has a magnitude of 7.5. The magnitude scaling factors in Table 6.2 or Fig. 6.7 can be used if the anticipated earthquake magnitude is different from 7.5. Figure 6.8 also has different curves that are to be used depending on the percent fines in the soil (F.C. = percent fines in the soil). For a given q_{c1} value, soils with more fines have a higher cyclic resistance ratio. Figure 6.9 presents a chart that can be used to assess the liquefaction of clean gravels (5 percent or less fines) and silty gravels.

6.4.7 Cyclic Resistance Ratio from the Shear Wave Velocity

The shear wave velocity of the soil can also be used to determine the factor of safety against liquefaction. The shear wave velocity can be measured in situ by using several different geophysical techniques, such as the uphole, down-hole, or cross-hole methods. Other methods that can be used to determine the in situ shear wave velocity include the seismic cone penetrometer and suspension logger (see Woods 1994).

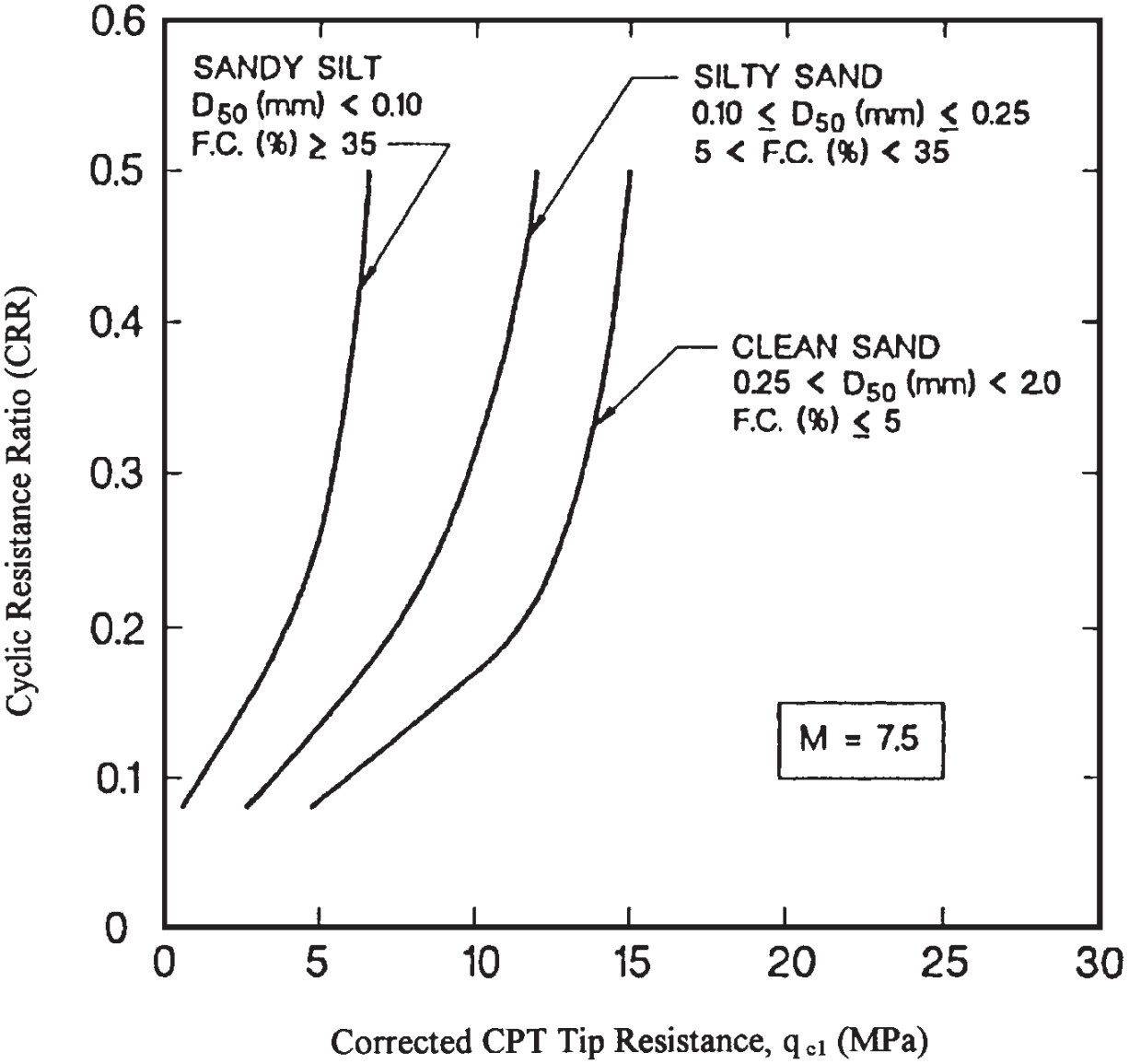

FIGURE 6.8 Relationship between cyclic resistance ratio (CRR) and corrected CPT tip resistance values for clean sand, silty sand, and sandy silt for $M = 7.5$ earthquakes. (*From Stark and Olson 1995, reprinted with permission of the American Society of Civil Engineers.*)

Much like the SPT and CPT, the shear wave velocity is corrected for the overburden pressure by using the following equation (Sykora 1987, Robertson et al. 1992):

$$V_{s1} = V_s C_v = V_s \left(\frac{100}{\sigma'_{v0}} \right)^{0.25} \tag{6.9}$$

where V_{s1} = corrected shear wave velocity (corrected for overburden pressure)
C_v = correction factor to account for overburden pressure. As indicated in the above equation, C_v is approximately equal to $(100/\sigma'_{v0})^{0.25}$, where σ'_{v0} is the vertical effective stress, kPa
V_s = shear wave velocity measured in field

When the shear wave velocity is used to determine the cyclic resistance ratio, Fig. 6.10 is used instead of Figs. 6.6 and 6.8. The curves in Fig. 6.10 are based on field performance data (i.e., sites with liquefaction versus no liquefaction). Figure 6.10 is entered with the corrected shear wave velocity V_{s1} from Eq. (6.9), and then by intersecting the appropriate fines content

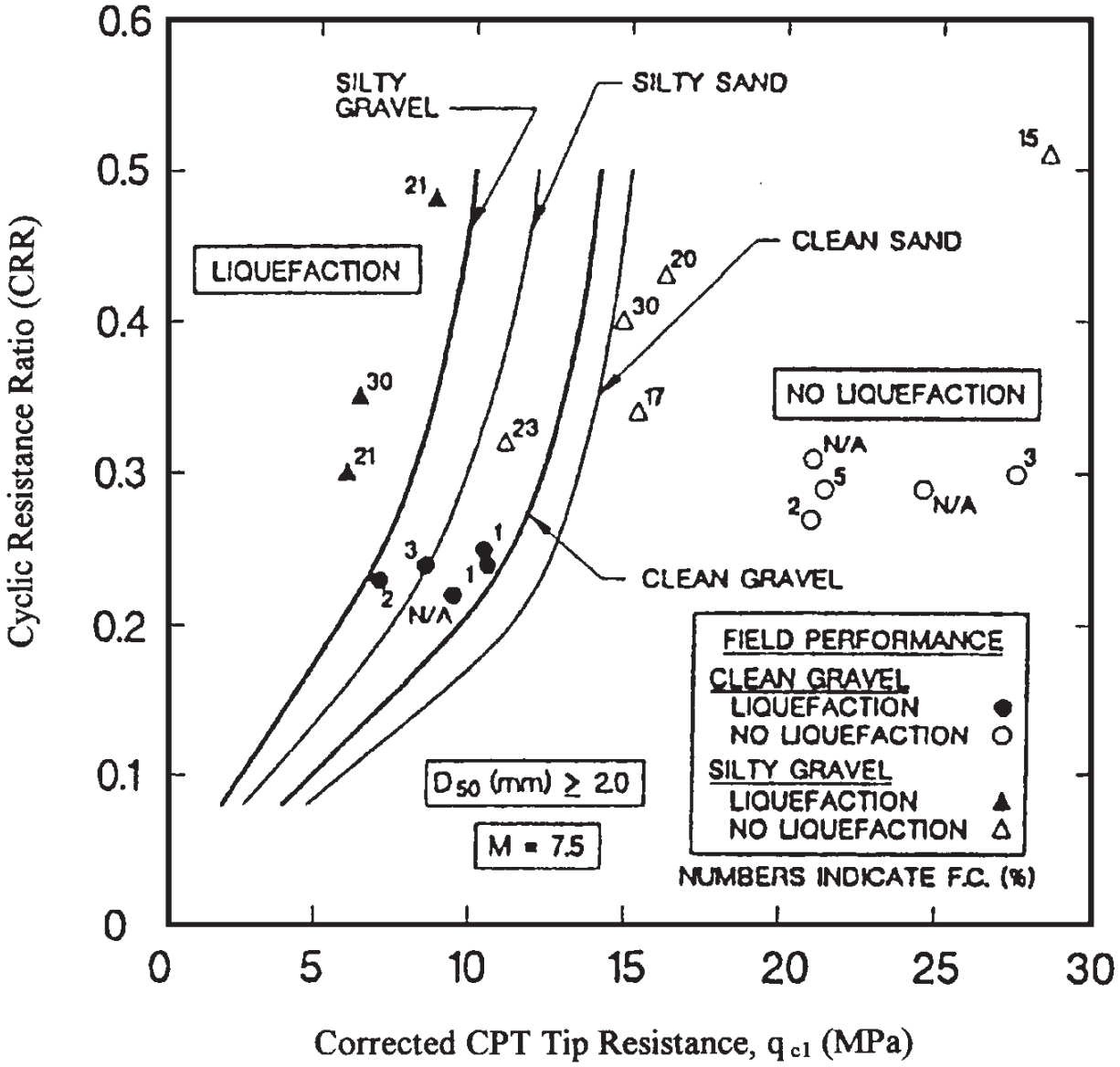

FIGURE 6.9 Relationship between cyclic resistance ratio and corrected CPT tip resistance values for clean gravel and silty gravel for $M = 7.5$ earthquakes. (*From Stark and Olson 1995, reprinted with permission of the American Society of Civil Engineers.*)

curve, the cyclic resistance ratio is obtained. The factor of safety against liquefaction is then calculated by using Eq. (6.8) (or FS = CRR/CSR). Note that Fig. 6.10 was developed for a moment magnitude M_w earthquake of 7.5. The magnitude scaling factors in Table 6.2 or Fig. 6.7 can be used if the anticipated earthquake magnitude is different from 7.5.

An advantage of using the shear wave velocity to determine the factor of safety against liquefaction is that it can be used for very large sites where an initial evaluation of the liquefaction potential is required. Disadvantages of this method are that soil samples are often not obtained as part of the testing procedure, thin strata of potentially liquefiable soil may not be identified, and the method is based on small strains of the soil, whereas the liquefaction process actually involves high strains.

In addition, as indicated in Fig. 6.10, there are few data to accurately define the curves above a CRR of about 0.3. Furthermore, the curves are very steep above a shear wave velocity of 200 m/s, and a small error in measuring the shear wave velocity could result in a significant error in the factor of safety. For example, an increase in shear wave velocity from 190 to 210 m/s will essentially double the CRR. Because of the limitations of this method, it is best to use the shear wave velocity as a supplement for the SPT and CPT methods.

6.5 REPORT PREPARATION

The results of the liquefaction analysis will often need to be summarized in report form for review by the client and governing agency. A listing of the information that should be included in the report, per the *Guidelines for Evaluating and Mitigating Seismic Hazards in California* (Division of Mines and Geology 1997), is as follows:

- If methods other than the standard penetration test (ASTM D 1586-99) and cone penetration test (ASTM D 3441-98) are used, include a description of pertinent equipment and procedural details of field measurements of penetration resistance (i.e., borehole type, hammer type and drop mechanism, sampler type and dimensions, etc.).
- Include boring logs that show raw (unmodified) N values if SPTs are performed or CPT probe logs showing raw q_c values and plots of raw sleeve friction if CPTs are performed.
- Provide an explanation of the basis and methods used to convert raw SPT, CPT, and/or other nonstandard data to "corrected" and "standardized" values [e.g., Eqs. (5.2) and (5.3)].
- Tabulate and/or plot the corrected SPT or corrected CPT values that were used in the liquefaction analysis.
- Provide an explanation of the method used to develop estimates of the design earthquake-induced cyclic stress ratio [e.g., CSR from Eq. (6.6)].
- Similarly, provide an explanation of the method used to develop estimates of the cyclic resistance ratio of the in situ soil (e.g., CRR from Figs. 6.6 to 6.9).
- Determine factors of safety against liquefaction for the design earthquake [e.g. Eq. (6.8)].
- Show the factors of safety against liquefaction at various depths and/or within various potentially liquefiable soil units.
- State conclusions regarding the potential for liquefaction and its likely impact on the proposed project.
- If needed, provide a discussion of mitigation measures necessary to reduce potential damage caused by liquefaction to an acceptable level of risk.
- For projects where remediation has been performed, show criteria for SPT-based or CPT-based acceptable testing that will be used to demonstrate that the site has had satisfactory remediation (see example in Fig. 6.11).

An example of a geotechnical engineering report that includes the results of the liquefaction analysis is provided in App. D.

6.6 PROBLEMS

The problems have been divided into basic categories as indicated below:

Soil Type versus Liquefaction Potential

6.1 Figure 6.12 shows laboratory classification data for eight different soils. Note in Fig. 6.12 that W_l is the liquid limit, W_p is the plastic limit, and PI is the plasticity index of the soil. Based on the soil properties summarized in Fig. 6.12, determine if each soil could be susceptible to liquefaction. *Answer:* Soil types 1 through 4 and 7 could be susceptible to liquefaction: soil types 5, 6, and 8 are not susceptible to liquefaction.

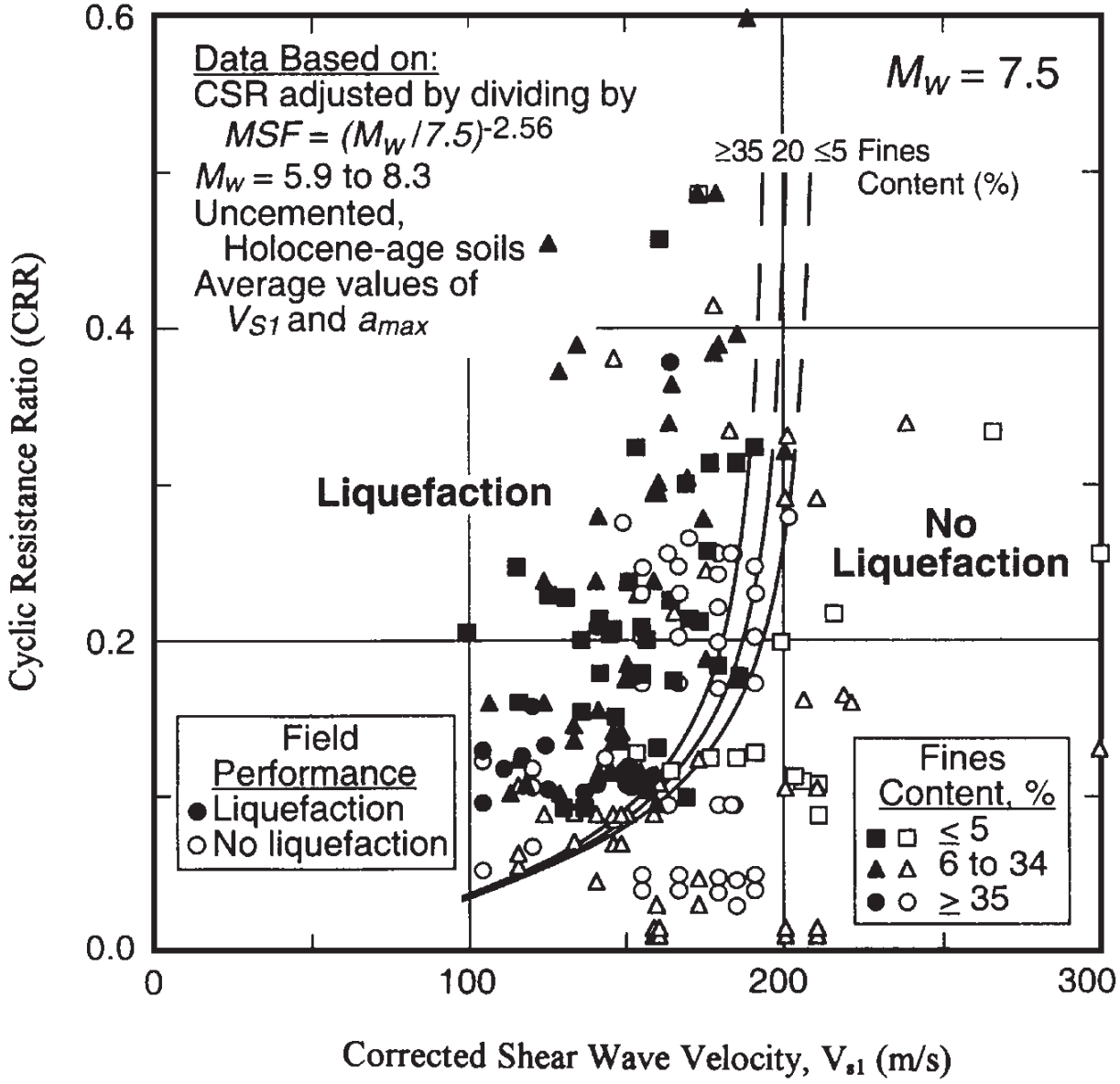

FIGURE 6.10 Relationship between cyclic resistance ratio and corrected shear wave velocity for clean sand, silty sand, and sandy silt for $M = 7.5$ earthquakes. (*From Andrus and Stokoe 2000, reprinted with permission of the American Society of Civil Engineers.*)

Factor of Safety against Liquefaction

6.2 Use the data from the example problem in Sec. 6.4.5, but assume that there is a vertical surcharge pressure applied at ground surface that equals 20 kPa. Determine the cyclic stress ratio induced by the design earthquake. *Answer:* CSR = 0.31.

6.3 Use the data from the example problem in Sec. 6.4.5, but assume that $a_{max}/g = 0.1$ and the sand contains 15 percent nonplastic fines. Calculate the factor of safety against liquefaction. *Answer:* See Table 6.3.

6.4 Use the data from the example problem in Sec. 6.4.5, but assume that $a_{max}/g = 0.2$ and the earthquake magnitude $M = 5¼$. Calculate the factor of safety against liquefaction. *Answer:* See Table 6.3.

6.5 Use the data from the example problem in Sec. 6.4.5, but assume at a depth of 3 m that $q_c = 3.9$ MPa. Calculate the factor of safety against liquefaction. *Answer:* See Table 6.3.

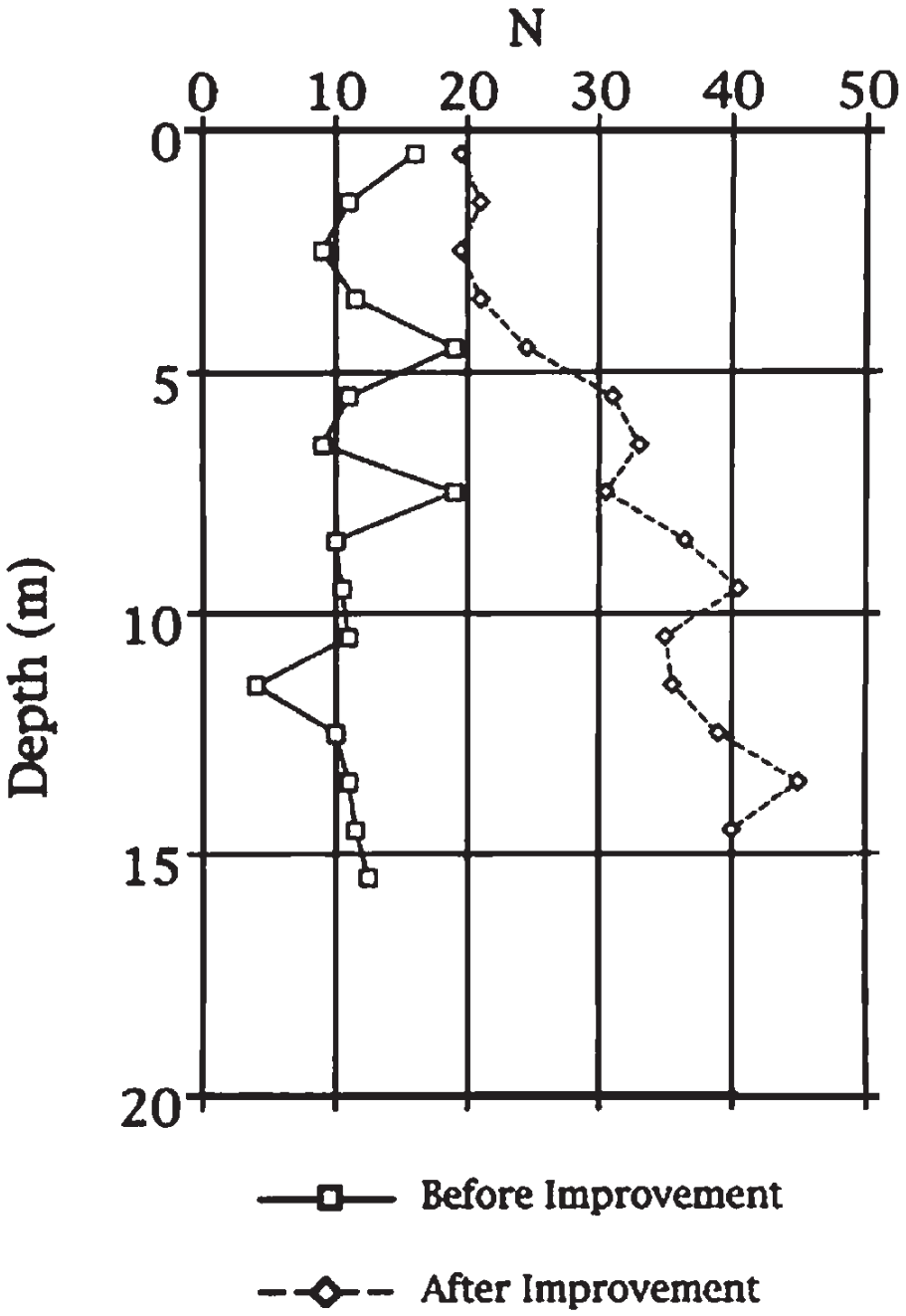

FIGURE 6.11 Pre- and posttreatment standard penetration resistance profiles at a warehouse site. (*Reproduced from the Kobe Geotechnical Collection, EERC, University of California, Berkeley.*)

6.6 Use the data from the example problem in Sec. 6.4.5, but assume that the shear wave velocity $V_s = 150$ m/s. Calculate the factor of safety against liquefaction. *Answer:* See Table 6.3.

6.7 Use the data from the example problem in Sec. 6.4.5, but assume that the soil type is crushed limestone (i.e., soil type 1, see Fig. 6.12) and at a depth of 3 m, $q_{c1} = 5.0$ MPa. Calculate the factor of safety against liquefaction. *Answer:* See Table 6.3.

6.8 Use the data from the example problem in Sec. 6.4.5, but assume that the soil type is silty gravel (i.e., soil type 2, see Fig. 6.12) and at a depth of 3 m, $q_{c1} = 7.5$ MPa. Calculate the factor of safety against liquefaction. *Answer:* See Table 6.3.

6.9 Use the data from the example problem in Sec. 6.4.5, but assume that the soil type is gravelly sand (i.e., soil type 3, see Fig. 6.12) and at a depth of 3 m, $q_{c1} = 14$ MPa. Calculate the factor of safety against liquefaction. *Answer:* See Table 6.3.

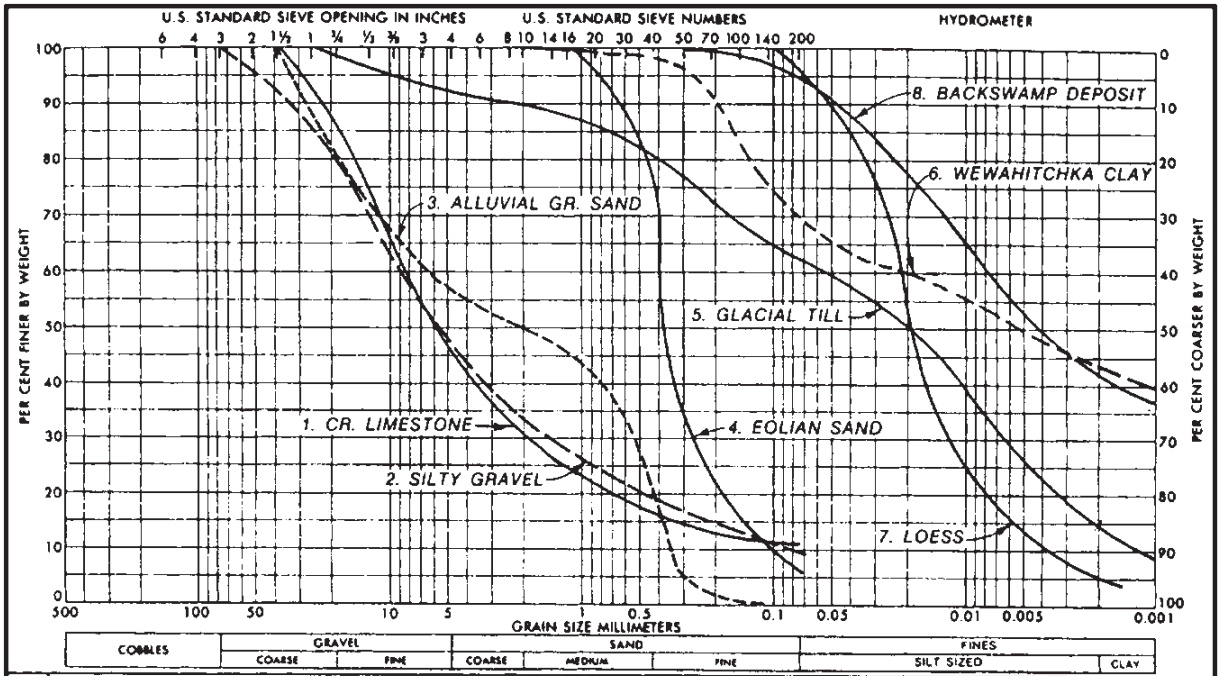

NO.	SOIL DESCRIPTION	W_l	W_p	PI	NO.	SOIL DESCRIPTION	W_l	W_p	PI
1	CRUSHED LIMESTONE, TENNESSEE	18	11	7	5	GLACIAL TILL, ILLINOIS	25	15	10
2	SILTY GRAVEL FROM WEATHERED GABBRO, OMAN	23	20	3	6	WEWAHITCHKA SANDY CLAY, FLORIDA	85	25	41
3	ALLUVIAL GRAVELLY SAND, MISSISSIPPI	-	-	-	7	LOESS, MISSISSIPPI	29	24	5
4	EOLIAN SAND, OMAN	-	-	-	8	BACKSWAMP DEPOSIT, MISSISSIPPI RIVER	59	18	41

FIGURE 6.12 Grain size curves and Atterberg limits test data for eight different soils. (*From Rollings and Rollings 1996, reproduced with permission of McGraw-Hill, Inc.*)

6.10 Use the data from the example problem in Sec. 6.4.5, but assume that the soil type is eolian sand (i.e., soil type 4, see Fig. 6.12). Calculate the factor of safety against liquefaction. *Answer:* See Table 6.3.

6.11 Use the data from the example problem in Sec. 6.4.5, but assume that the soil type is noncemented loess (i.e., soil type 7, see Fig. 6.12). Calculate the factor of safety against liquefaction. *Answer:* See Table 6.3.

Subsoil Profiles

6.12 Figure 6.13 shows the subsoil profile at Kawagishi-cho in Niigata. Assume a level-ground site with the groundwater table at a depth of 1.5 m below ground surface; the medium sand and medium-fine sand have less than 5 percent fines; the total unit weight γ_t of the soil above the groundwater table is 18.3 kN/m^3; and the buoyant unit weight γ_b of the soil below the groundwater table is 9.7 kN/m^3.

The standard penetration data shown in Fig. 6.13 are uncorrected N values. Assume a hammer efficiency E_m of 0.6 and a boring diameter of 100 mm, and the length of drill rods is equal to the depth of the SPT test below ground surface. The earthquake conditions are a peak ground acceleration a_{max} of 0.16g and a magnitude of 7.5. Using the standard penetration test data, determine the factor of safety against liquefaction versus depth. *Answer:* See App. E for the solution and Fig. 6.14 for a plot of the factor of safety against liquefaction versus depth.

6.13 In Fig. 6.13, assume the cyclic resistance ratio (labeled *cyclic strength* in Fig. 6.13) for the soil was determined by modeling the earthquake conditions in the laboratory (i.e., the amplitude and number of cycles of the sinusoidal load are equivalent to $a_{max} = 0.16g$ and magnitude = 7.5). Using the laboratory cyclic strength tests performed on large-diameter samples, determine the factor of safety against liquefaction versus depth. *Answer:* See

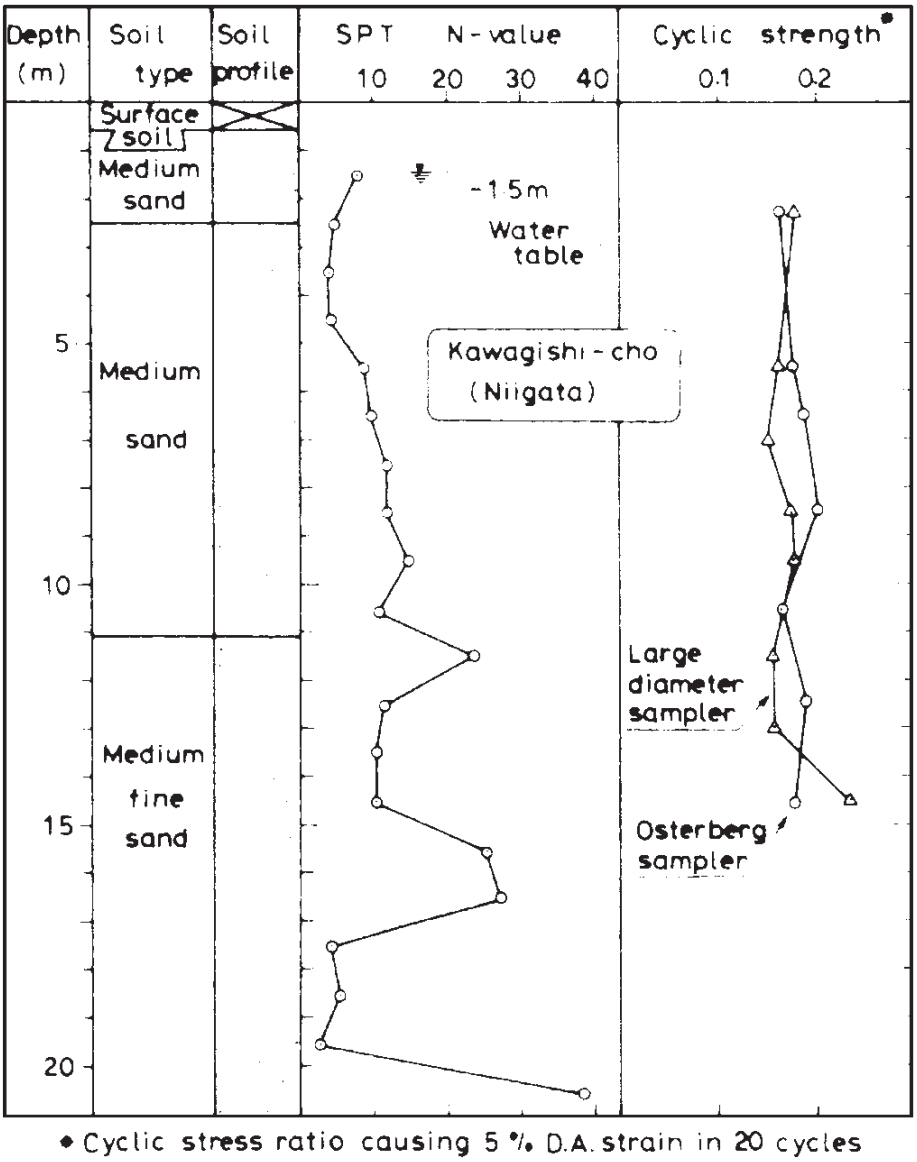

FIGURE 6.13 Subsoil profile, Kawagishi-cho, Niigata. (*Reproduced from Ishihara 1985.*)

App. E for the solution and Fig. 6.14 for a plot of the factor of safety against liquefaction versus depth.

6.14 Based on the results from Probs. 6.12 and 6.13, what zones of soil will liquefy during the earthquake? *Answer:* Per Fig. 6.14, the standard penetration test data indicate that there are three zones of liquefaction from about 2 to 11 m, 12 to 15 m, and 17 to 20 m below ground surface. Per Fig. 6.14, the laboratory cyclic strength tests indicate that there are two zones of liquefaction from about 6 to 8 m and 10 to 14 m below ground surface.

6.15 Figure 6.15 shows the subsoil profile at a sewage disposal site in Niigata. Assume a level-ground site with the groundwater table at a depth of 0.4 m below ground surface, the medium to coarse sand has less than 5 percent fines, the total unit weight γ_t of the soil above the groundwater table is 18.3 kN/m^3, and the buoyant unit weight γ_b of the soil below the groundwater table is 9.7 kN/m^3.

The standard penetration data shown in Fig. 6.15 are uncorrected N values. Assume a hammer efficiency E_m of 0.6 and a boring diameter of 100 mm, and the length of drill rods is equal to the depth of the SPT test below ground surface. The earthquake conditions are a peak ground acceleration a_{max} of 0.16g and a magnitude of 7.5. Using the standard penetration test data, determine the factor of safety against liquefaction versus depth. *Answer:*

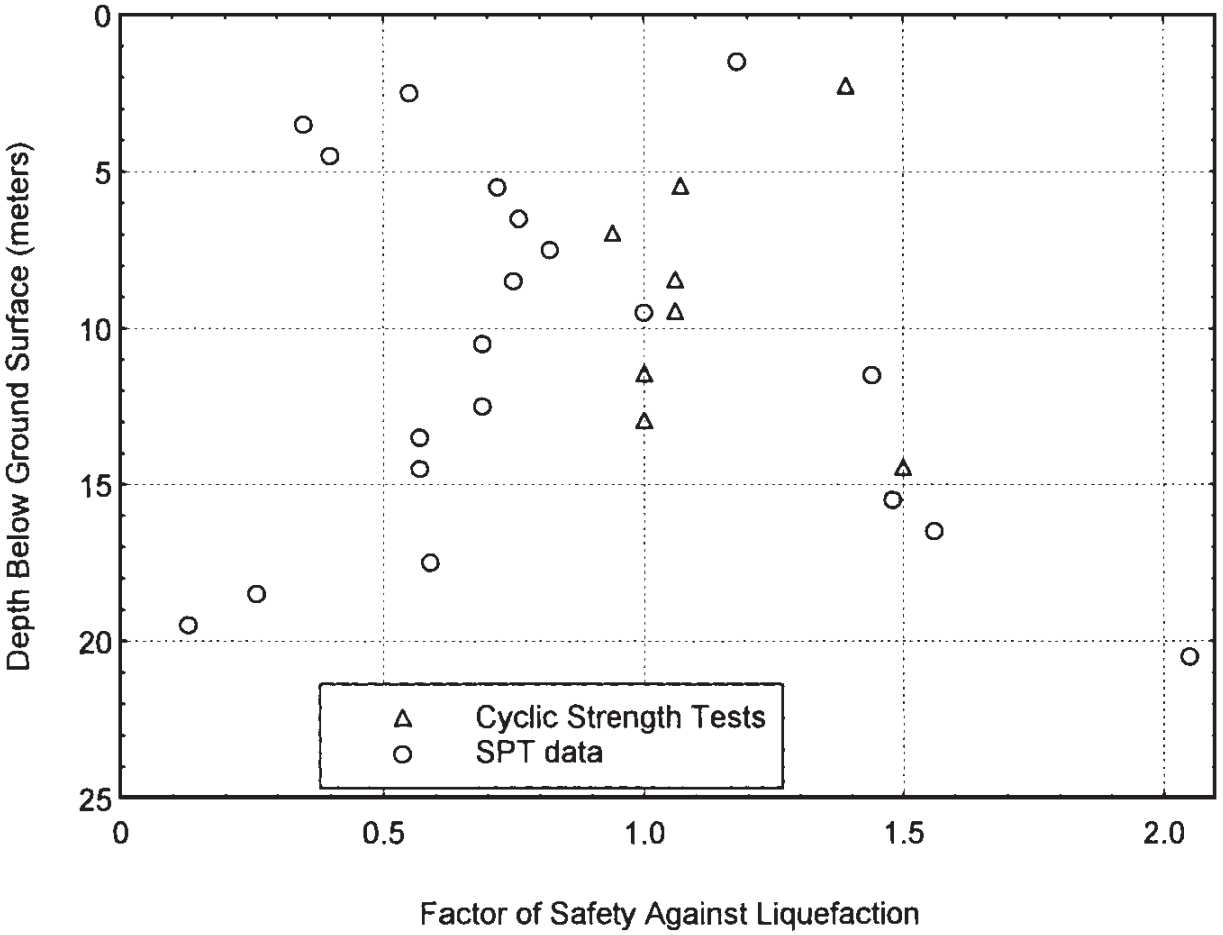

FIGURE 6.14 Solution plot for Probs. 6.12 and 6.13.

See App. E for the solution and Fig. 6.16 for a plot of the factor of safety against liquefaction versus depth.

6.16 In Fig. 6.15, assume the cyclic resistance ratio (labeled *cyclic strength* in Fig. 6.15) for the soil was determined by modeling the earthquake conditions in the laboratory (i.e., the amplitude and number of cycles of the sinusoidal load are equivalent to $a_{max} = 0.16g$ and magnitude = 7.5). Using the laboratory cyclic strength tests performed on block samples, determine the factor of safety against liquefaction versus depth. *Answer:* See App. E for the solution and Fig. 6.16 for a plot of the factor of safety against liquefaction versus depth.

6.17 Based on the results from Probs. 6.15 and 6.16, what zones of soil would be most likely to liquefy? *Answer:* Per Fig. 6.16, the standard penetration test data indicate that there are two zones of liquefaction from about 1.2 to 6.7 m and from 12.7 to 13.7 m below ground surface. Per Fig. 6.16, the laboratory cyclic strength tests indicate that the soil has a factor of safety against liquefaction in excess of 1.0.

Remediation Analysis

6.18 Figure 6.11 presents "before improvement" and "after improvement" standard penetration resistance profiles at a warehouse site. Assume a level-ground site with the groundwater table at a depth of 0.5 m below ground surface, the soil type is a silty sand with an average of 15 percent fines, the total unit weight γ_t of the soil above the groundwater table is 18.9 kN/m^3, and the buoyant unit weight γ_b of the soil below the groundwater table is 9.8 kN/m^3. Neglect any increase in unit weight of the soil due to the improvement process.

The standard penetration data shown in Fig. 6.11 are uncorrected N values. Assume a hammer efficiency E_m of 0.6 and a boring diameter of 100 mm, and the length of drill rods is equal to the depth of the SPT test below ground surface. The design earthquake condi-

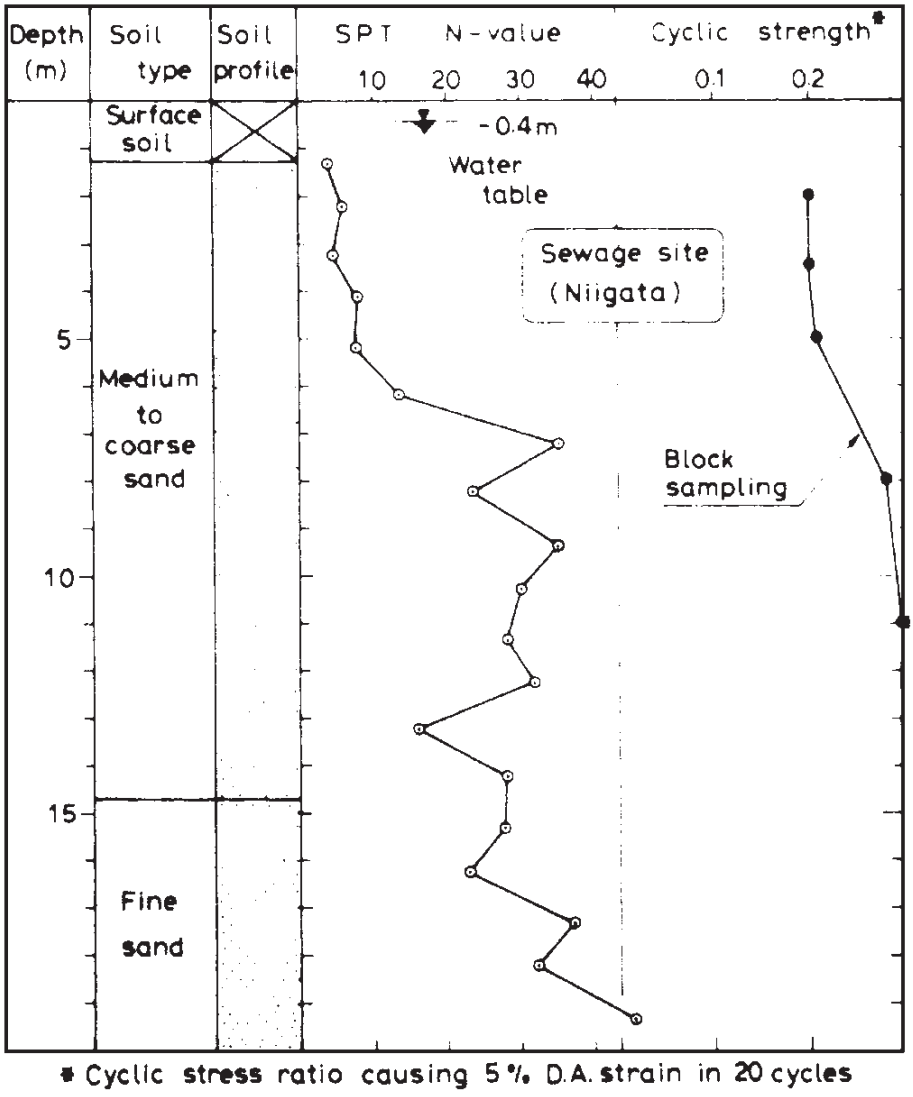

FIGURE 6.15 Subsoil profile, sewage site, Niigata. (*Reproduced from Ishihara 1985.*)

tions are a peak ground acceleration a_{max} of 0.40g and moment magnitude M_w of 8.5. Determine the factor of safety against liquefaction for the before-improvement and after-improvement conditions. Was the improvement process effective in reducing the potential for liquefaction at the warehouse site? *Answer:* See App. E for the solution and Fig. 6.17 for a plot of the factor of safety against liquefaction versus depth. Since the after improvement factor of safety against liquefaction exceeds 1.0 for the design earthquake, the improvement process was effective in eliminating liquefaction potential at the site.

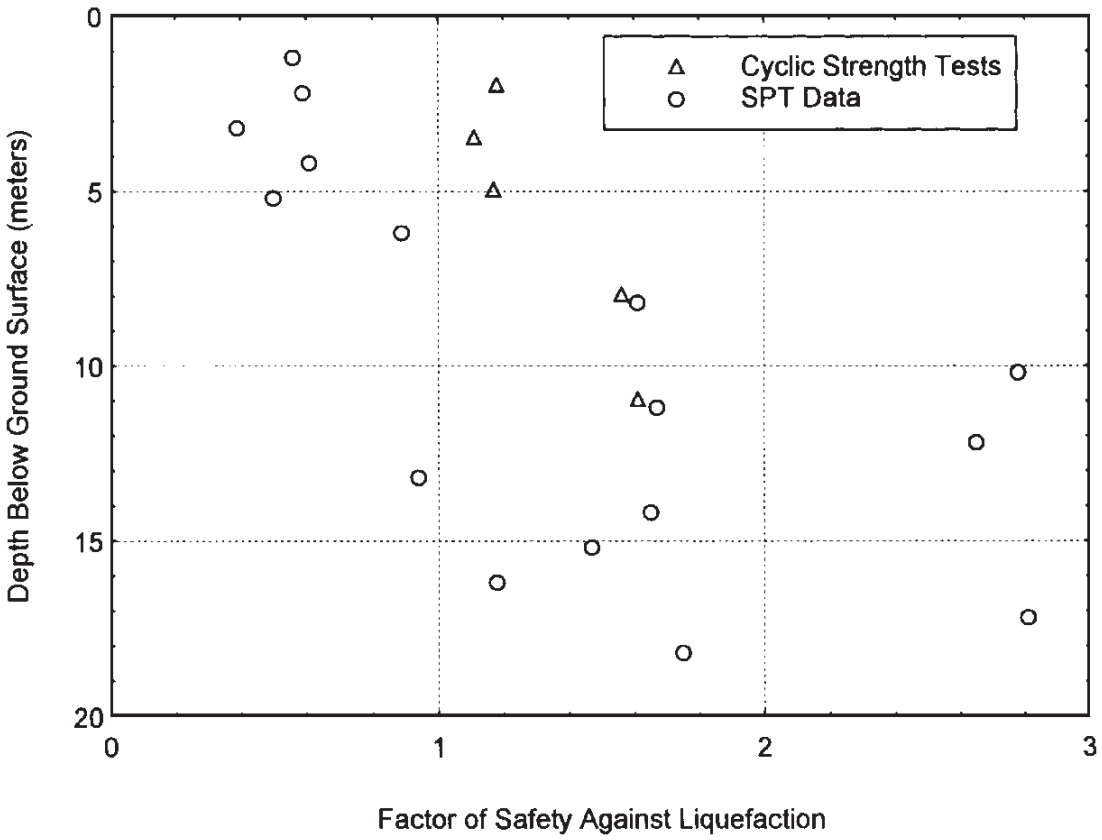

FIGURE 6.16 Solution plot for Probs. 6.15 and 6.16.

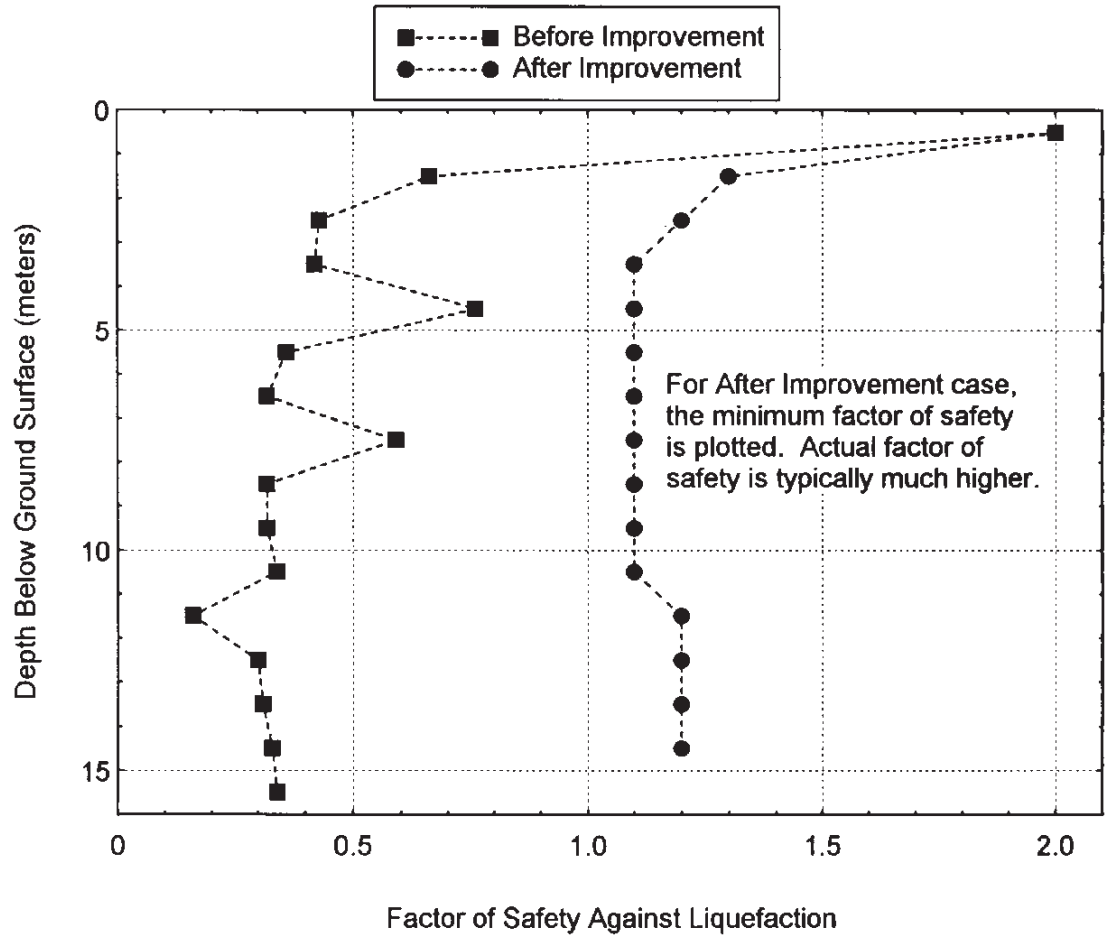

FIGURE 6.17 Solution plot for Prob. 6.18.

TABLE 6.3 Summary of Answers for Probs. 6.3 to 6.11

Problem no.	Soil type	a_{max}/g	Earthquake magnitude	$(N_1)_{60}$ blows/ft; q_{c1}, MPa; V_{s1}, m/s	Cyclic stress ratio	Cyclic resistance ratio	FS = CRR/CSR
Section 6.4.5	Clean sand	0.40	7½	7.7 blows/ft	0.34	0.09	0.26
Problem 6.3	Sand—15% fines	0.10	7½	7.7 blows/ft	0.084	0.14	1.67
Problem 6.4	Clean sand	0.20	5¼	7.7 blows/ft	0.17	0.14	0.82
Problem 6.5	Clean sand	0.40	7½	5.8 MPa	0.34	0.09	0.26
Problem 6.6	Clean sand	0.40	7½	185 m/s	0.34	0.16	0.47
Problem 6.7	Crushed limestone	0.40	7½	5.0 MPa	0.34	0.18	0.53
Problem 6.8	Silty gravel	0.40	7½	7.5 MPa	0.34	0.27	0.79
Problem 6.9	Clean gravelly sand	0.40	7½	14 MPa	0.34	0.44	1.29
Problem 6.10	Eolian sand	0.40	7½	7.7 blows/ft	0.34	0.09	0.26
Problem 6.11	Loess	0.40	7½	7.7 blows/ft	0.34	0.18	0.53

Note: See App. E for solutions.

CHAPTER 7
EARTHQUAKE-INDUCED SETTLEMENT

The following notation is used in this chapter:

SYMBOL	*DEFINITION*
$a_{\max}$, a_p	Maximum horizontal acceleration at ground surface (also known as peak ground acceleration)
CSR	Cyclic stress ratio
D_r	Relative density
E_m	Hammer efficiency
F	Lateral force reacting to earthquake-induced base shear
FS, FS_L	Factor of safety against liquefaction
g	Acceleration of gravity
G_{eff}	Effective shear modulus at induced strain level
$G_{\max}$	Shear modulus at a low strain level
H	Initial thickness of soil layer
H_1	Thickness of surface layer that does not liquefy
H_2	Thickness of soil layer that will liquefy during earthquake
ΔH	Change in height of soil layer
k_0	Coefficient of earth pressure at rest
N_{corr}	Value added to $(N_1)_{60}$ to account for fines in soil
N	Uncorrected SPT blow count (blows per foot)
N_1	Japanese standard penetration test value for Fig. 7.1
$(N_1)_{60}$	N value corrected for field testing procedures and overburden pressure
OCR	Overconsolidation ratio = $\sigma'_{vm}/\sigma'_{v0}$
q_{c1}	Cone resistance corrected for overburden pressure
r_d	Depth reduction factor
u_e	Excess pore water pressure
V	Base shear induced by earthquake
Δ	Earthquake-induced maximum differential settlement of foundation
ε_v	Volumetric strain
γ_{eff}	Effective shear strain

γ_{max}	Maximum shear strain
γ_t	Total unit weight of soil
ρ_{max}	Earthquake-induced total settlement of foundation
σ_{v0}	Total vertical stress
σ'_m	Mean principal effective stress
σ'_{vm}	Maximum past pressure, also known as preconsolidation pressure
σ'_{v0}	Vertical effective stress
σ'_1	Major principal effective stress
σ'_2	Intermediate principal effective stress
σ'_3	Minor principal effective stress
$\Delta\sigma_v$	Increase in foundation pressure due to earthquake
τ_{cyc}	Uniform cyclic shear stress amplitude of earthquake
τ_{eff}	Effective shear stress induced by earthquake
τmax	Maximum shear stress induced by earthquake

7.1 INTRODUCTION

As discussed in Sec. 4.2, those buildings founded on solid rock are least likely to experience earthquake-induced differential settlement. However, buildings on soil could be subjected to many different types of earthquake-induced settlement. This chapter deals with only settlement of soil for a level-ground surface condition. The types of earthquake-induced settlement discussed in this chapter are as follows:

- *Settlement versus the factor of safety against liquefaction (Sec. 7.2):* This section discusses two methods that can be used to estimate the ground surface settlement for various values of the factor of safety against liquefaction (FS). If FS is less than or equal to 1.0, then liquefaction will occur, and the settlement occurs as water flows from the soil in response to the earthquake-induced excess pore water pressures. Even for FS greater than 1.0, there could still be the generation of excess pore water pressures and hence settlement of the soil. However, the amount of settlement will be much greater for the liquefaction condition compared to the nonliquefied state.
- *Liquefaction-induced ground damage (Sec. 7.3):* There could also be liquefaction-induced ground damage that causes settlement of structures. For example, there could be liquefaction-induced ground loss below the structure, such as the loss of soil through the development of ground surface sand boils. The liquefied soil could also cause the development of ground surface fissures that cause settlement of structures.
- *Volumetric compression (Sec. 7.4):* Volumetric compression is also known as *soil densification.* This type of settlement is due to ground shaking that causes the soil to compress together, such as dry and loose sands that densify during the earthquake.
- *Settlement due to dynamic loads caused by rocking (Sec. 7.5):* This type of settlement is due to dynamic structural loads that momentarily increase the foundation pressure acting on the soil. The soil will deform in response to the dynamic structural load, resulting in settlement of the building. This settlement due to dynamic loads is often a result of the structure rocking back and forth.

The usual approach for settlement analyses is to first estimate the amount of earthquake-induced total settlement ρ_{max} of the structure. Because of variable soil conditions and structural loads, the earthquake-induced settlement is rarely uniform. A common assumption is that the maximum differential settlement Δ of the foundation will be equal to 50 to 75 percent of ρ_{max} (that is, $0.5\rho_{max} \leq \Delta \leq 0.75\rho_{max}$). If the anticipated total settlement ρ_{max} and/or the maximum differential settlement Δ is deemed to be unacceptable, then soil improvement or the construction of a deep foundation may be needed. Chapters 12 and 13 deal with mitigation measures such as soil improvement or the construction of deep foundations.

7.2 SETTLEMENT VERSUS FACTOR OF SAFETY AGAINST LIQUEFACTION

7.2.1 Introduction

This section discusses two methods that can be used to estimate the ground surface settlement for various values of the factor of safety against liquefaction. A liquefaction analysis (Chap. 6) is first performed to determine the factor of safety against liquefaction. If FS is less than or equal to 1.0, then liquefaction will occur, and the settlement occurs as water flows from the soil in response to the earthquake-induced excess pore water pressures. Even for FS greater than 1.0, there could still be the generation of excess pore water pressures and hence settlement of the soil. However, the amount of settlement will be much greater for the liquefaction condition compared to the nonliquefied state.

This section is solely devoted to an estimation of ground surface settlement for various values of the factor of safety. Other types of liquefaction-induced movement, such as bearing capacity failures, flow slides, and lateral spreading, are discussed in Chaps. 8 and 9.

7.2.2 Methods of Analysis

Method by Ishihara and Yoshimine (1992). Figure 7.1 shows a chart developed by Ishihara and Yoshimine (1992) that can be used to estimate the ground surface settlement of saturated clean sands for a given factor of safety against liquefaction. The procedure for using Fig. 7.1 is as follows:

1. *Calculate the factor of safety against liquefaction* FS_L*:* The first step is to calculate the factor of safety against liquefaction, using the procedure outlined in Chap. 6 [i.e., Eq. (6.8)].

2. *Soil properties:* The second step is to determine one of the following properties: relative density D_r of the in situ soil, maximum shear strain to be induced by the design earthquake γ_{max}, corrected cone penetration resistance q_{c1} kg/cm^2, or Japanese standard penetration test N_1 value.

Kramer (1996) indicates that the Japanese standard penetration test typically transmits about 20 percent more energy to the SPT sampler, and the equation $N_1 = 0.83(N_1)_{60}$ can be used to convert the $(N_1)_{60}$ value to the Japanese N_1 value. However, R. B. Seed (1991) states that Japanese SPT results require corrections for blow frequency effects and hammer release, and that these corrections are equivalent to an overall effective energy ratio E_m of 0.55 (versus $E_m = 0.60$ for U.S. safety hammer). Thus R. B. Seed (1991) states that the $(N_1)_{60}$ values should be increased by about 10 percent (that is, 0.6/0.55) when using Fig. 7.1 to estimate volumetric compression, or $N_1 = 1.10(N_1)_{60}$. As a practical matter, it can be

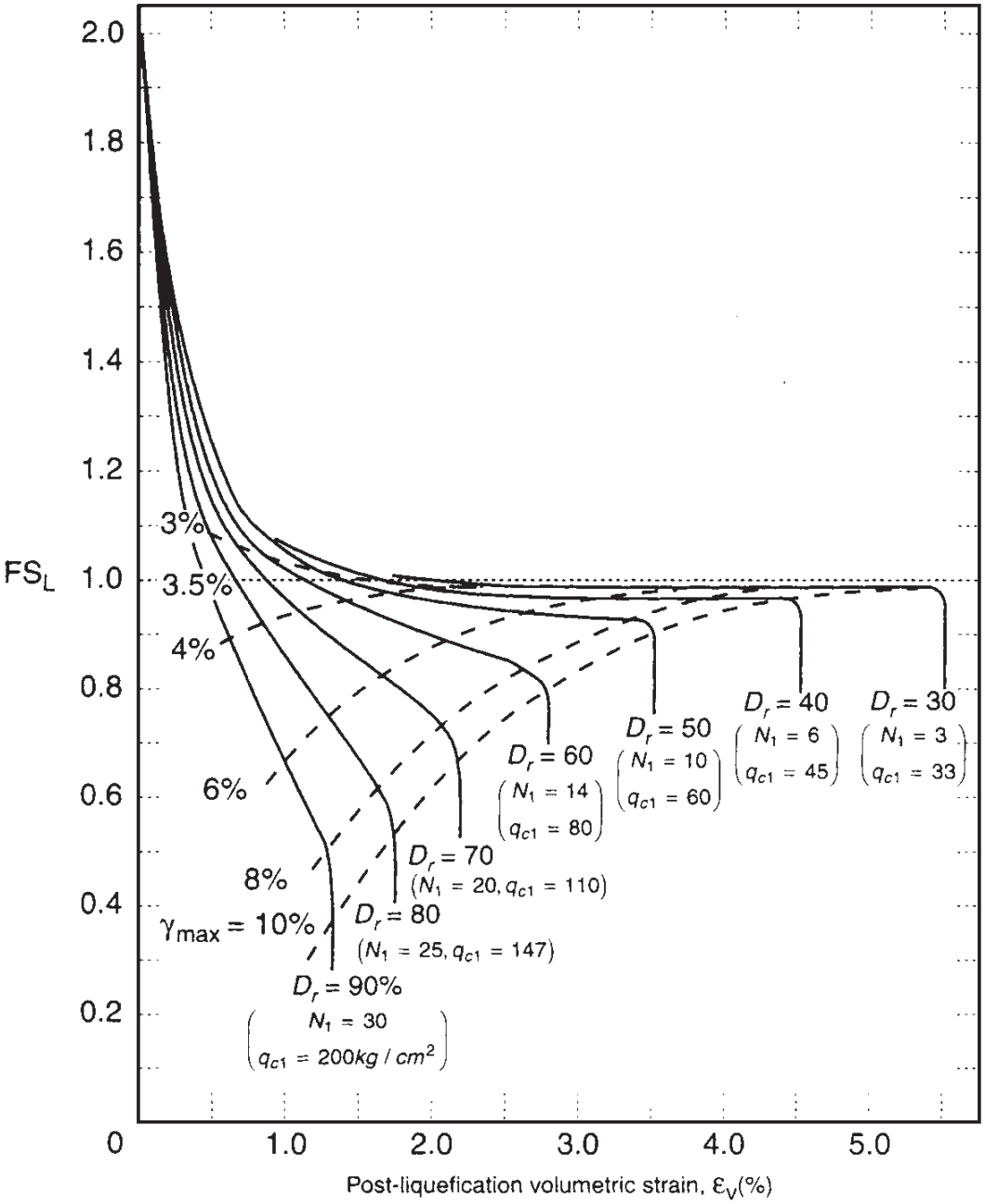

FIGURE 7.1 Chart for estimating the ground surface settlement of clean sand as a function of the factor of safety against liquefaction FS_L. To use this figure, one of the following properties must be determined: relative density D_r of the in situ soil, maximum shear strain to be induced by the design earthquake γ_{max}, corrected cone penetration resistance q_{c1} (kg/cm^2), or Japanese standard penetration test N_1 value. For practical purposes, assume the Japanese standard penetration test N_1 value is equal to the $(N_1)_{60}$ value from Eq. (5.2). (*Reproduced from Kramer 1996, originally developed by Ishihara and Yoshimine 1992.*)

assumed that the Japanese N_1 value is approximately equivalent to the $(N_1)_{60}$ value calculated from Eq. (5.2) (Sec. 5.4.3).

3. *Volumetric strain:* In Fig. 7.1, enter the vertical axis with the factor of safety against liquefaction, intersect the appropriate curve corresponding to the Japanese N_1 value [assume Japanese $N_1 = (N_1)_{60}$ from Eq. (5.2)], and then determine the volumetric strain ε_v from the horizontal axis. Note in Fig. 7.1 that each N_1 curve can be extended straight downward to obtain the volumetric strain for very low values of the factor of safety against liquefaction.

4. *Settlement:* The settlement of the soil is calculated as the volumetric strain, expressed as a decimal, times the thickness of the liquefied soil layer.

Note in Fig. 7.1 that the volumetric strain can also be calculated for clean sand that has a factor of safety against liquefaction in excess of 1.0. For FS_L greater than 1.0 but less than 2.0, the contraction of the soil structure during the earthquake shaking results in excess pore water pressures that will dissipate and cause a smaller amount of settlement. At FS_L equal to or greater than 2.0, Fig. 7.1 indicates that the volumetric strain will be essentially equal to zero. This is because for FS_L higher than 2.0, only small values of excess pore water pressures u_e will be generated during the earthquake shaking (i.e., see Fig. 5.15).

Method by Tokimatsu and Seed (1984, 1987). Figure 7.2 shows a chart developed by Tokimatsu and Seed (1984, 1987) that can be used to estimate the ground surface settlement of saturated clean sands. The solid lines in Fig. 7.2 represent the volumetric strain for liquefied soil (i.e., factor of safety against liquefaction less than or equal to 1.0). Note that the solid line labeled 1 percent volumetric strain in Fig. 7.2 is similar to the dividing line in Fig. 6.6 between liquefiable and nonliquefiable clean sand.

The dashed lines in Fig. 7.2 represent the volumetric strain for a condition where excess pore water pressures are generated during the earthquake, but the ground shaking is not sufficient to cause liquefaction (that is, FS $>$ 1.0). This is similar to the data in Fig. 7.1, in that

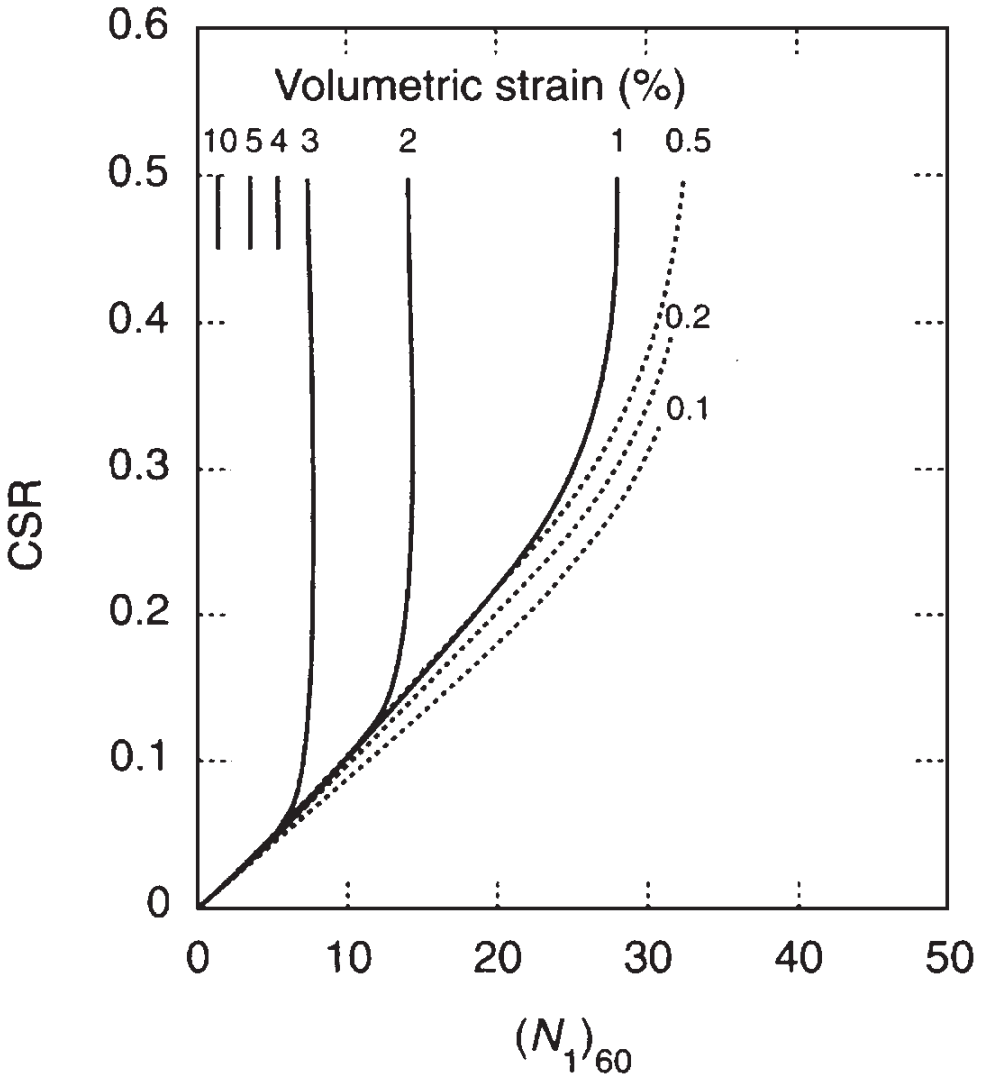

FIGURE 7.2 Chart for estimating the ground surface settlement of clean sand for factor of safety against liquefaction less than or equal to 1.0 (solid lines) and greater than 1.0 (dashed lines). To use this figure, the cyclic stress ratio from Eq. (6.6) and the $(N_1)_{60}$ value from Eq. (5.2) must be determined. (*Reproduced from Kramer 1996, originally developed by Tokimatsu and Seed 1984.*)

the contraction of the soil structure during the earthquake shaking could cause excess pore water pressures that will dissipate and result in smaller amounts of settlement. Thus by using the dashed lines in Fig. 7.2, the settlement of clean sands having a factor of safety against liquefaction in excess of 1.0 can also be calculated.

The procedure for using Fig. 7.2 is as follows:

1. *Calculate the cyclic stress ratio:* The first step is to calculate the cyclic stress ratio (CSR) by using Eq. (6.6). Usually a liquefaction analysis (Chap. 6) is first performed, and thus the value of CSR should have already been calculated.

2. *Adjusted CSR value:* Figure 7.2 was developed for a magnitude 7.5 earthquake. Tokimatsu and Seed (1987) suggest that the cyclic stress ratio calculated from Eq. (6.6) be adjusted if the magnitude of the anticipated earthquake is different from 7.5. The corrected CSR value is obtained by dividing the CSR value from Eq. (6.6) by the magnitude scaling factor from Table 6.2. The chart in Fig. 7.2 is entered on the vertical axis by using this corrected CSR value.

As will be illustrated by the following example problem, applying an earthquake magnitude correction factor to the cyclic stress ratio is usually unnecessary. The reason is that once liquefication has occurred, a higher magnitude earthquake will not result in any additional settlement of the liquefied soil. Thus as a practical matter, the chart in Fig. 7.2 can be entered on the vertical axis with the CSR value from Eq. (6.6).

3. $(N_1)_{60}$ *value:* Now calculate the $(N_1)_{60}$ value [Eq. (5.2), see Sec. 5.4.3]. Usually a liquefaction analysis (Chap. 6) is first performed, and thus the value of $(N_1)_{60}$ should have already been calculated.

4. *Volumetric strain:* In Fig. 7.2, the volumetric strain is determined by entering the vertical axis with the CSR from Eq. (6.6) and entering the horizontal axis with the $(N_1)_{60}$ value from Eq. (5.2).

5. *Settlement:* The settlement of the soil is calculated as the volumetric strain, expressed as a decimal, times the thickness of the liquefied soil layer.

Example Problem. This example problem illustrates the procedure used to determine the ground surface settlement of soil using Figs. 7.1 and 7.2.

Use the data from the example problem in Sec. 6.4.5. Assume that the liquefied soil layer is 1.0 m thick. As indicated in Sec. 6.4.5, the factor of safety against liquefaction is 0.26, and the calculated value of $(N_1)_{60}$ determined at a depth of 3 m below ground surface is equal to 7.7.

- *Solution using Fig. 7.1:* For Fig. 7.1, assume that the Japanese N_1 value is approximately equal to the $(N_1)_{60}$ value from Eq. (5.2), or use Japanese $N_1 = 7.7$. The Japanese N_1 curves labeled 6 and 10 are extended straight downward to FS = 0.26, and then by extrapolating between the curves for an N_1 value of 7.7, the volumetric strain is equal to 4.1 percent. Since the in situ liquefied soil layer is 1.0 m thick, the ground surface settlement of the liquefied soil is equal to 1.0 m times 0.041, or a settlement of 4.1 cm.
- *Solution using Fig. 7.2:* Per the example problem in Sec. 6.4.5, the cyclic stress ratio from Eq. (6.6) is equal to 0.34, and the calculated value of $(N_1)_{60}$ determined at a depth of 3 m below ground surface is equal to 7.7. Entering Fig. 7.2 with CSR = 0.34 and $(N_1)_{60} = 7.7$, the volumetric strain is equal to 3.0 percent. Since the in situ liquefied soil layer is 1.0 m thick, the ground surface settlement of the liquefied soil is equal to 1.0 m times 0.030, or a settlement of 3.0 cm.

Suppose instead of assuming the earthquake will have a magnitude of 7.5, the example problem is repeated for a magnitude $5^1/_4$ earthquake. As indicated in Table 6.2, the

magnitude scaling factor = 1.5, and thus the corrected CSR is equal to 0.34 divided by 1.5, or 0.23. Entering Fig. 7.2 with the modified CSR = 0.23 and $(N_1)_{60}$ = 7.7, the volumetric strain is still equal to 3.0 percent. Thus, provided the sand liquefies for both the magnitude 5¼ and magnitude 7.5 earthquakes, the settlement of the liquefied soil is the same.

- *Summary of values:* Based on the two methods, the ground surface settlement of the 1.0-m-thick liquefied sand layer is expected to be on the order of 3 to 4 cm.

Silty Soils. Figures 7.1 and 7.2 were developed for clean sand deposits (fines ≤ 5 percent). For silty soils, R. B. Seed (1991) suggests that the most appropriate adjustment is to increase the $(N_1)_{60}$ values by adding the values of N_{corr} indicated below:

Percent fines	N_{corr}
≤5	0
10	1
25	2
50	4
75	5

7.2.3 Limitations

The methods presented in Figs. 7.1 and 7.2 can only be used for the following cases:

- *Lightweight structures:* Settlement of lightweight structures, such as wood-frame buildings bearing on shallow foundations
- *Low net bearing stress:* Settlement of any other type of structure that imparts a low net bearing pressure onto the soil
- *Floating foundation:* Settlement of floating foundations, provided the zone of liquefaction is below the bottom of the foundation and the floating foundation does not impart a significant net stress upon the soil
- *Heavy structures with deep liquefaction:* Settlement of heavy structures, such as massive buildings founded on shallow foundations, provided the zone of liquefaction is deep enough that the stress increase caused by the structural load is relatively low
- *Differential settlement:* Differential movement between a structure and adjacent appurtenances, where the structure contains a deep foundation that is supported by strata below the zone of liquefaction

The methods presented in Figs. 7.1 and 7.2 cannot be used for the following cases:

- *Foundations bearing on liquefiable soil:* Do not use Figs. 7.1 and 7.2 when the foundation is bearing on soil that will liquefy during the design earthquake. Even lightly loaded foundations will sink into the liquefied soil.
- *Heavy buildings with underlying liquefiable soil:* Do not use Figs. 7.1 and 7.2 when the liquefied soil is close to the bottom of the foundation and the foundation applies a large net load onto the soil. In this case, once the soil has liquefied, the foundation load will cause it to punch or sink into the liquefied soil. There could even be a bearing capacity type of failure. Obviously these cases will lead to settlement well in excess of the values obtained from Figs. 7.1 and 7.2. It is usually very difficult to determine the settlement for these conditions, and the best engineering solution is to provide a sufficiently high static

factor of safety so that there is ample resistance against a bearing capacity failure. This is discussed further in Chap. 8.

- *Buoyancy effects:* Consider possible buoyancy effects. Examples include buried storage tanks or large pipelines that are within the zone of liquefied soil. Instead of settling, the buried storage tanks and pipelines may actually float to the surface when the ground liquefies.
- *Sloping ground condition:* Do not use Figs. 7.1 and 7.2 when there is a sloping ground condition. If the site is susceptible to liquefaction-induced flow slide or lateral spreading, the settlement of the building could be well in excess of the values obtained from Figs. 7.1 and 7.2. This is discussed further in Chap. 9.
- *Liquefaction-induced ground damage:* The calculations using Figs. 7.1 and 7.2 do not include settlement that is related to the loss of soil through the development of ground surface sand boils or the settlement of shallow foundations caused by the development of ground surface fissures. These types of settlement are discussed in the next section.

7.3 LIQUEFACTION-INDUCED GROUND DAMAGE

7.3.1 Types of Damage

As previously mentioned, there could also be liquefaction-induced ground damage that causes settlement of structures. This liquefaction-induced ground damage is illustrated in Fig. 7.3. As shown, there are two main aspects to the ground surface damage:

1. *Sand boils:* There could be liquefaction-induced ground loss below the structure, such as the loss of soil through the development of ground surface sand boils. Often a line of sand boils, such as shown in Fig. 7.4, is observed at ground surface. A row of sand boils often develops at the location of cracks or fissures in the ground.
2. *Surface fissures:* The liquefied soil could also cause the development of ground surface fissures which break the overlying soil into blocks that open and close during the earthquake. Figure 7.5 shows the development of one such fissure. Note in Fig. 7.5 that liquefied soil actually flowed out of the fissure.

The liquefaction-induced ground conditions illustrated in Fig. 7.3 can damage all types of structures, such as buildings supported on shallow foundations, pavements, flatwork, and utilities. In terms of the main factor influencing the liquefaction-induced ground dam-

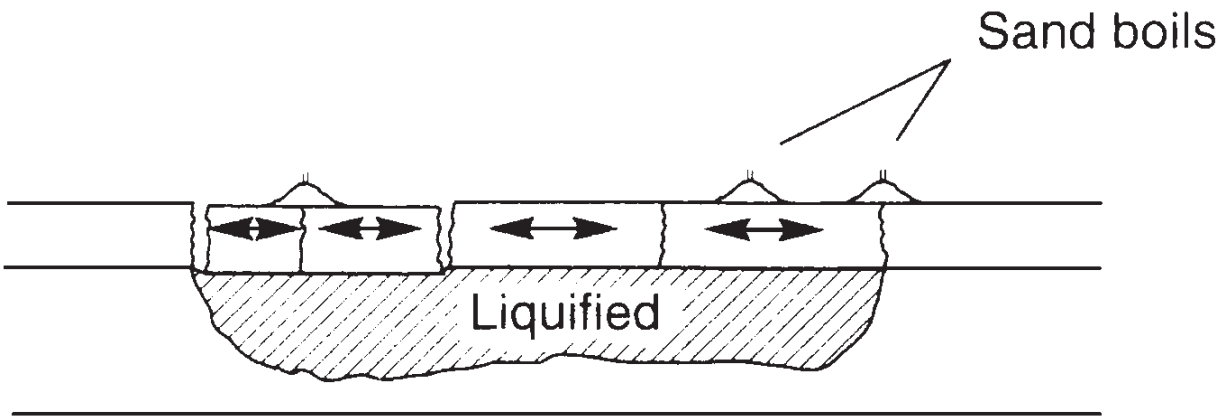

FIGURE 7.3 Ground damage caused by the liquefaction of an underlying soil layer. (*Reproduced from Kramer 1996, originally developed by Youd 1984.*)

FIGURE 7.4 Line of sand boils caused by liquefaction during the Niigata (Japan) earthquake of June 16, 1964. (*Photograph from the Steinbrugge Collection, EERC, University of California, Berkeley.*)

age, Ishihara (1985) states:

> One of the factors influencing the surface manifestation of liquefaction would be the thickness of a mantle of unliquefied soils overlying the deposit of sand which is prone to liquefaction. Should the mantle near the ground surface be thin, the pore water pressure from the underlying liquefied sand deposit will be able to easily break through the surface soil layer, thereby bringing about the ground rupture such as sand boiling and fissuring. On the other hand, if the mantle of the subsurface soil is sufficiently thick, the uplift force due to the excess water pressure will not be strong enough to cause a breach in the surface layer, and hence, there will be no surface manifestation of liquefaction even if it occurs deep in the deposit.

7.3.2 Method of Analysis

Based on numerous case studies, Ishihara (1985) developed a chart (Fig. 7.6*a*) that can be used to determine the thickness of the unliquefiable soil surface layer H_1 in order to prevent damage due to sand boils and surface fissuring. Three different situations were used by

FIGURE 7.5 Surface fissure caused by the Izmit earthquake in Turkey on August 17, 1999. Note that liquefied soil flowed out of the fissure. (*Photograph from the Izmit Collection, EERC, University of California, Berkeley.*)

Ishihara (1985) in the development of the chart, and they are shown in Fig. 7.6*b*.

Since it is very difficult to determine the amount of settlement due to liquefaction-induced ground damage (Fig. 7.3), one approach is to ensure that the site has an adequate surface layer of unliquefiable soil by using Fig. 7.6. If the site has an inadequate surface layer of unliquefiable soil, then mitigation measures such as the placement of fill at ground surface, soil improvement, or the construction of deep foundations may be needed (Chaps. 12 and 13).

To use Fig. 7.6, the thickness of layers H_1 and H_2 must be determined. Guidelines are as follows:

1. *Thickness of the unliquefiable soil layer* H_1: For two of the three situations in Fig. 7.6*b,* the unliquefiable soil layer is defined as that thickness of soil located above the groundwater table. As previously mentioned in Sec. 6.3, soil located above the groundwater table will not liquefy.

One situation in Fig. 7.6*b* is for a portion of the unliquefiable soil below the groundwater table. Based on the case studies, this soil was identified as unliquefiable cohesive soil (Ishihara 1985). As a practical matter, it would seem the "unliquefiable soil" below the

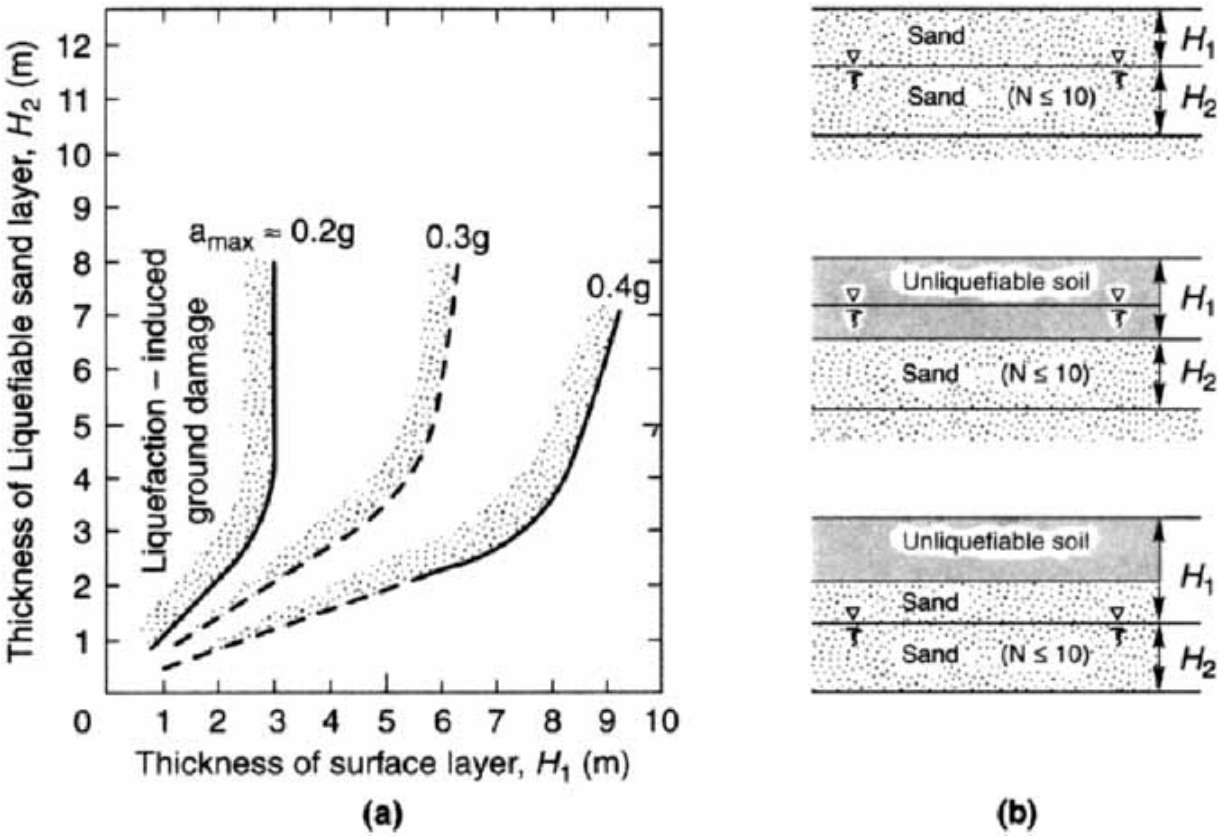

FIGURE 7.6 (*a*) Chart that can be used to evaluate the possibility of liquefaction-induced ground damage based on H_1, H_2, and the peak ground acceleration a_{max}. (*b*) Three situations used for the development of the chart, where H_1 = thickness of the surface layer that will not liquefy during the earthquake and H_2 = thickness of the liquefiable soil layer. (*Reproduced from Kramer 1996, originally developed by Ishihara 1985.*)

groundwater table that is used to define the layer thickness H_1 would be applicable for any soil that has a factor of safety against liquefaction in excess of 1.0. However, if the factor of safety against liquefaction is only slightly in excess of 1.0, it could still liquefy due to the upward flow of water from layer H_2. Considerable experience and judgment are required in determining the thickness H_1 of the unliquefiable soil when a portion of this layer is below the groundwater table.

2. *Thickness of the liquefied soil layer* H_2: Note in Fig. 7.6*b* that for all three situations, the liquefied sand layer H_2 has an uncorrected N value that is less than or equal to 10. These N value data were applicable for the case studies evaluated by Ishihara (1985). It would seem that irrespective of the N value, H_2 could be the thickness of the soil layer which has a factor of safety against liquefaction that is less than or equal to 1.0.

7.3.3 Example Problem

This example problem illustrates the use of Fig. 7.6. Use the data from Prob. 6.15, which deals with the subsurface conditions shown in Fig. 6.15 for the sewage disposal site. Based on the standard penetration test data, the zone of liquefaction extends from a depth of 1.2 to 6.7 m below ground surface. Assume the surface soil (upper 1.2 m) shown in Fig. 6.15 consists of an unliquefiable soil. Using a peak ground acceleration a_{max} of 0.20*g,* will there be liquefaction-induced ground damage at this site?

Solution. Since the zone of liquefaction extends from a depth of 1.2 to 6.7 m, the thickness of the liquefiable sand layer H_2 is equal to 5.5 m. By entering Fig. 7.6 with $H_2 = 5.5$ m and intersecting the $a_{max} = 0.2g$ curve, the minimum thickness of the surface layer H_1 needed to prevent surface damage is 3 m. Since the surface layer of unliquefiable soil is only 1.2 m thick, there will be liquefaction-induced ground damage.

Some appropriate solutions would be as follows: (1) At ground surface, add a fill layer that is at least 1.8 m thick, (2) densify the sand and hence improve the liquefaction resistance of the upper portion of the liquefiable layer, or (3) use a deep foundation supported by soil below the zone of liquefaction.

7.4 VOLUMETRIC COMPRESSION

7.4.1 Main Factors Causing Volumetric Compression

Volumetric compression is also known as soil densification. This type of settlement is due to earthquake-induced ground shaking that causes the soil particles to compress together. Noncemented cohesionless soils, such as dry and loose sands or gravels, are susceptible to this type of settlement. Volumetric compression can result in a large amount of ground surface settlement. For example, Grantz et al. (1964) describe an interesting case of ground vibrations from the 1964 Alaskan earthquake that caused 0.8 m (2.6 ft) of alluvium settlement.

Silver and Seed (1971) state that the earthquake-induced settlement of dry cohesionless soil depends on three main factors:

1. *Relative density D_r of the soil:* The looser the soil, the more susceptible it is to volumetric compression. Those cohesionless soils that have the lowest relative densities will be most susceptible to soil densification. Often the standard penetration test is used to assess the density condition of the soil.
2. *Maximum shear strain γ_{max} induced by the design earthquake:* The larger the shear strain induced by the earthquake, the greater the tendency for a loose cohesionless soil to compress. The amount of shear strain will depend on the peak ground acceleration a_{max}. A higher value of a_{max} will lead to a greater shear strain of the soil.
3. *Number of shear strain cycles:* The more cycles of shear strain, the greater the tendency for the loose soil structure to compress. For example, it is often observed that the longer a loose sand is vibrated, the greater the settlement. The number of shear strain cycles can be related to the earthquake magnitude. As indicated in Table 2.2, the higher the earthquake magnitude, the longer the duration of ground shaking.

In summary, the three main factors that govern the settlement of loose and dry cohesionless soil are the relative density, amount of shear strain, and number of shear strain cycles. These three factors can be accounted for by using the standard penetration test, peak ground acceleration, and earthquake magnitude.

7.4.2 Simple Settlement Chart

Figure 7.7 presents a simple chart that can be used to estimate the settlement of dry sand (Krinitzsky et al. 1993). The figure uses the standard penetration test N value and the peak ground acceleration a_p to calculate the earthquake-induced volumetric strain (that is, $\Delta H/H$, expressed as a percentage). Figure 7.7 accounts for two of the three main factors causing

volumetric compression: the looseness of the soil based on the standard penetration test and the amount of shear strain based on the peak ground acceleration a_p.

Note in Fig. 7.7 that the curves are labeled in terms of the uncorrected N values. As a practical matter, the curves should be in terms of the standard penetration test $(N_1)_{60}$ values [i.e., Eq. (5.2), Sec. 5.4.3]. This is because the $(N_1)_{60}$ value more accurately represents the density condition of the sand. For example, given two sand layers having the same uncorrected N value, the near-surface sand layer will be in a much denser state than the sand layer located at a great depth.

To use Fig. 7.7, both the $(N_1)_{60}$ value of the sand and the peak ground acceleration a_p must be known. Then by entering the chart with the a_p/g value and intersecting the desired $(N_1)_{60}$ curve, the volumetric strain ($\Delta H/H$, expressed as a percentage) can be determined. The volumetric compression (i.e., settlement) is then calculated by multiplying the volumetric strain, expressed as a decimal, by the thickness of the soil layer H.

7.4.3 Method by Tokimatsu and Seed

A much more complicated method for estimating the settlement of dry sand has been proposed by Tokimatsu and Seed (1987), based on the prior work by Seed and Silver (1972) and Pyke et al. (1975). The steps in using this method are as follows:

1. *Determine the earthquake-induced effective shear strain* γ_{eff}. The first step is to determine the shear stress induced by the earthquake and then to convert this shear stress to an effective shear strain γ_{eff}. Using Eq. (6.6) and deleting the vertical effective stress σ'_{v0} from both sides of the equation gives

$$\tau_{\text{cyc}} = 0.65 r_d \sigma_{v0} (a_{\max}/g) \tag{7.1}$$

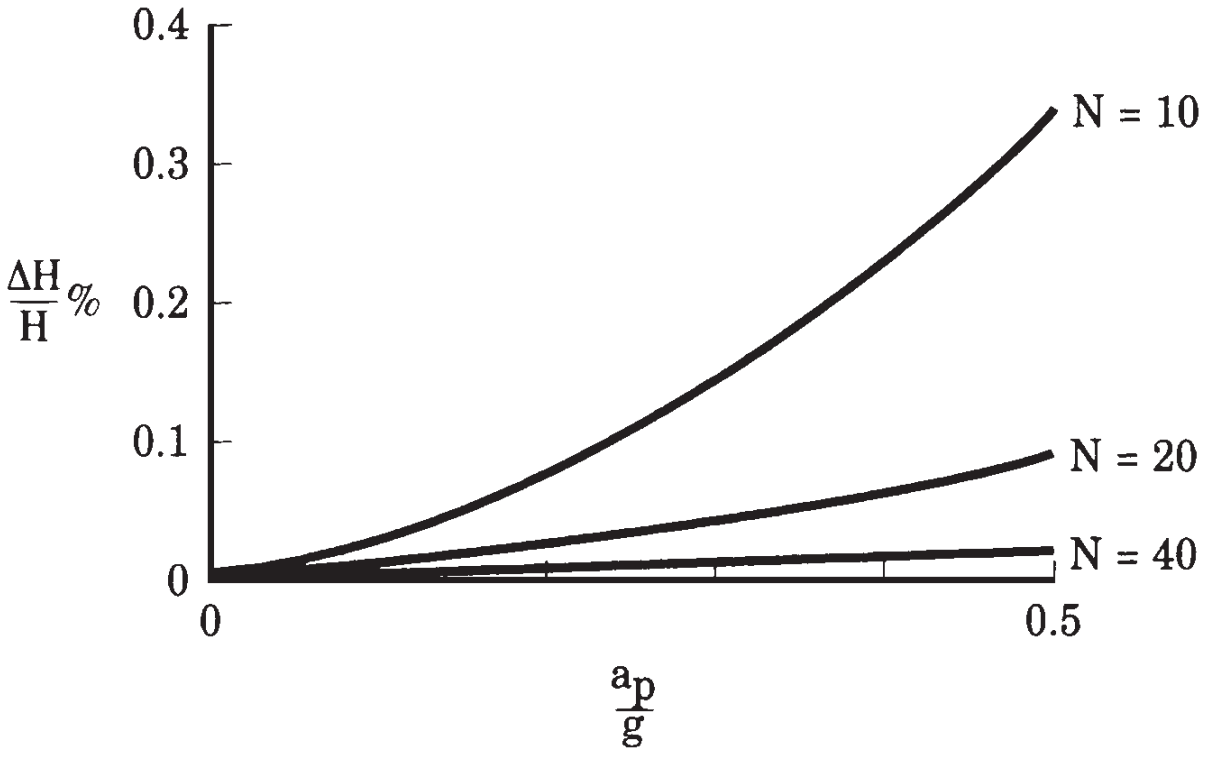

FIGURE 7.7 Simple chart that can be used to determine the settlement of dry sand. In this figure, use the peak ground acceleration a_p and assume that N refers to $(N_1)_{60}$ values from Eq. (5.2). (*Reproduced from Krinitzsky et al. 1993, with permission from John Wiley & Sons.*)

where τ_{cyc} = uniform cyclic shear stress amplitude of the earthquake
r_d = depth reduction factor, also known as *stress reduction coefficient* (dimensionless). Equation (6.7) or Fig. 6.5 can be used to obtain the value of r_d.
σ_{v0} = total vertical stress at a particular depth where the settlement analysis is being performed, lb/ft^2 or kPa. To calculate total vertical stress, total unit weight γ_t of soil layer (s) must be known.
a_{max} = maximum horizontal acceleration at ground surface that is induced by the earthquake, ft/s^2 or m/s^2, which is also commonly referred to as the peak ground acceleration (see Sec. 5.6)
g = acceleration of gravity (32.2 ft/s^2 or 9.81 m/s^2)

As discussed in Chap. 6, Eq. (7.1) was developed by converting the typical irregular earthquake record to an equivalent series of uniform stress cycles by assuming that $\tau_{cyc} = 0.65\tau_{max}$, where τ_{max} is equal to the maximum earthquake-induced shear stress. Thus τ_{cyc} is the amplitude of the uniform stress cycles and is considered to be the effective shear stress induced by the earthquake (that is, $\tau_{eff} = \tau_{cyc}$). To determine the earthquake-induced effective shear strain, the relationship between shear stress and shear strain can be utilized:

$$\tau_{cyc} = \tau_{eff} = \gamma_{eff} G_{eff} \tag{7.2}$$

where τ_{eff} = effective shear stress induced by the earthquake, which is considered to be equal to the amplitude of uniform stress cycles used to model earthquake motion ($\tau_{cyc} = \tau_{eff}$), lb/ft^2 or kPa
γ_{eff} = effective shear strain that occurs in response to the effective shear stress (dimensionless)
G_{eff} = effective shear modulus at induced strain level, lb/ft^2 or kPa

Substituting Eq. (7.2) into (7.1) gives

$$\gamma_{eff} G_{eff} = 0.65 r_d \sigma_{v0} (a_{max}/g) \tag{7.3}$$

And finally, dividing both sides of the equation by G_{max}, which is defined as the shear modulus at a low strain level, we get as the final result

$$\gamma_{eff} \left(\frac{G_{eff}}{G_{max}} \right) = 0.65 r_d \left(\frac{\sigma_{v0}}{G_{max}} \right) \left(\frac{a_{max}}{g} \right) \tag{7.4}$$

Similar to the liquefaction analysis in Chap. 6, all the parameters on the right side of the equation can be determined except for G_{max}. Based on the work by Ohta and Goto (1976) and Seed et al. (1984, 1986), Tokimatsu and Seed (1987) recommend that the following equation be used to determine G_{max}:

$$G_{max} = 20{,}000 \, [(N_1)_{60}]^{0.333} \, (\sigma'_m)^{0.50} \tag{7.5}$$

where G_{max} = shear modulus at a low strain level, lb/ft^2
$(N_1)_{60}$ = standard penetration test N value corrected for field testing procedures and overburden pressure [i.e., Eq. (5.2)]
σ'_m = mean principal effective stress, defined as the average of the sum of the three principal effective stresses, or $(\sigma_1' + \sigma_2' + \sigma_3')/3$. For a geostatic condition and a sand deposit that has not been preloaded (i.e., OCR = 1.0), the coefficient

of earth pressure at rest $k_0 \cong 0.5$. Thus the value of $\sigma'_m \cong 0.67\sigma\sigma'_{v0}$. Note in Eq. (7.5) that the value of σ'_m must be in terms of pounds per square foot.

After the value of G_{max} has been determined from Eq. (7.5), the value of γ_{eff} (G_{eff} /G_{max}) can be calculated by using Eq. (7.4). To determine the effective shear strain γ_{eff} of the soil, Fig. 7.8 is entered with the value of $\gamma_{eff}(G_{eff}/G_{max})$ and upon intersecting the appropriate value of mean principal effective stress (σ'_m in ton/ft^2), the effective shear strain γ_{eff} is obtained from the vertical axis.

2. *Determine the volumetric strain* ε_v. Figure 7.9 can be used to determine the volumetric strain ε_v of the soil. This figure was developed for cases involving 15 equivalent uniform strain cycles, which is representative of a magnitude 7.5 earthquake. In Fig. 7.9, the cyclic shear strain γ_{cyc} is equivalent to the effective shear strain γ_{eff} calculated from step 1, except that the cyclic shear strain γ_{cyc} is expressed as a percentage ($\%\gamma_{cyc} = 100\ \gamma_{eff}$). To determine the volumetric strain ε_v in percent, either the relative density D_r of the in situ soil or data from the standard penetration test must be known. For Fig. 7.9, assume the N_1 in the figure refers to $(N_1)_{60}$ values from Eq. (5.2).

To use Fig. 7.9, first convert γ_{eff} from step 1 to percent cyclic shear strain ($\%\gamma_{cyc} = 100\gamma_{eff}$). Then enter the horizontal axis with percent γ_{cyc}, and upon intersecting the relative

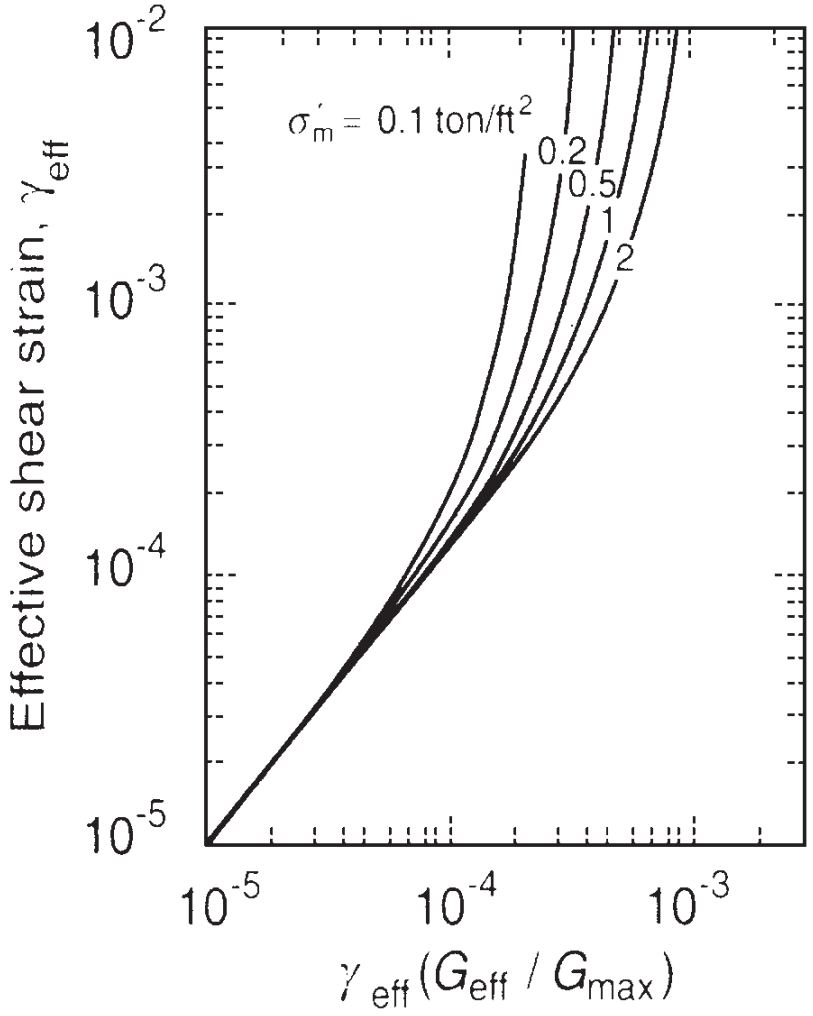

FIGURE 7.8 Plot that is used to estimate the effective shear strain γ_{eff} for values of $\gamma_{eff}(G_{eff}/G_{max})$ from Eq. (7.4) and the mean principal effective stress σ'_m. (*Reproduced from Tokimatsu and Seed 1987, with permission from the American Society of Civil Engineers.*)

density D_r curve or the $(N_1)_{60}$ curve, the value of the volumetric strain ε_v is obtained from the vertical axis.

3. *Multidirectional shear:* The development of Fig. 7.9 was based on unidirectional simple shear conditions, or in other words, shear strain in only one direction. However, actual earthquake shaking conditions are multidirectional, where the soil is strained back and forth. Based on unidirectional and multidirectional tests, Pyke et al. (1975) conclude that "the settlements caused by combined horizontal motions are about equal to the sum of the settlements caused by the components acting alone." Therefore, the unidirectional volumetric strains determined from Fig. 7.9 must be doubled to account for the multidirectional shaking effects of the earthquake.

4. *Magnitude of the earthquake:* Figure 7.9 was developed for a magnitude 7.5 earthquake (that is, 15 cycles at $0.65\tau_{max}$). Table 7.1 presents the volumetric strain ratio that can be used to determine the volumetric strain ε_v for different-magnitude earthquakes. The procedure is to multiply the volumetric strain ε_v from step 3 by the volumetric strain ratio VSR from Table 7.1.

Note that the volumetric strain ratio is similar in concept to the magnitude scaling factor (MSF) in Table 6.2. It would seem that the volumetric strain ratio in Table 7.1 should be equal to the inverse of the magnitude scaling factors in Table 6.2 (that is, VSR = 1.0/MSF). However, they do not equate because the correction in Table 7.1 is made for volumetric strain, while the correction in Table 6.2 is made for shear stress.

5. *Settlement:* Because of the variations in soil properties with depth, the soil profile should be divided into several different layers. The volumetric strain from step 4 is then calculated for each layer. The settlement for each layer is the volumetric strain, expressed as a decimal, times the thickness of the layer. The total settlement is calculated as the sum of the settlement calculated for each soil layer.

Section 7.4.4 presents an example problem illustrating the various steps outlined above. This method proposed by Tokimatsu and Seed (1987) is most applicable for dry sands that

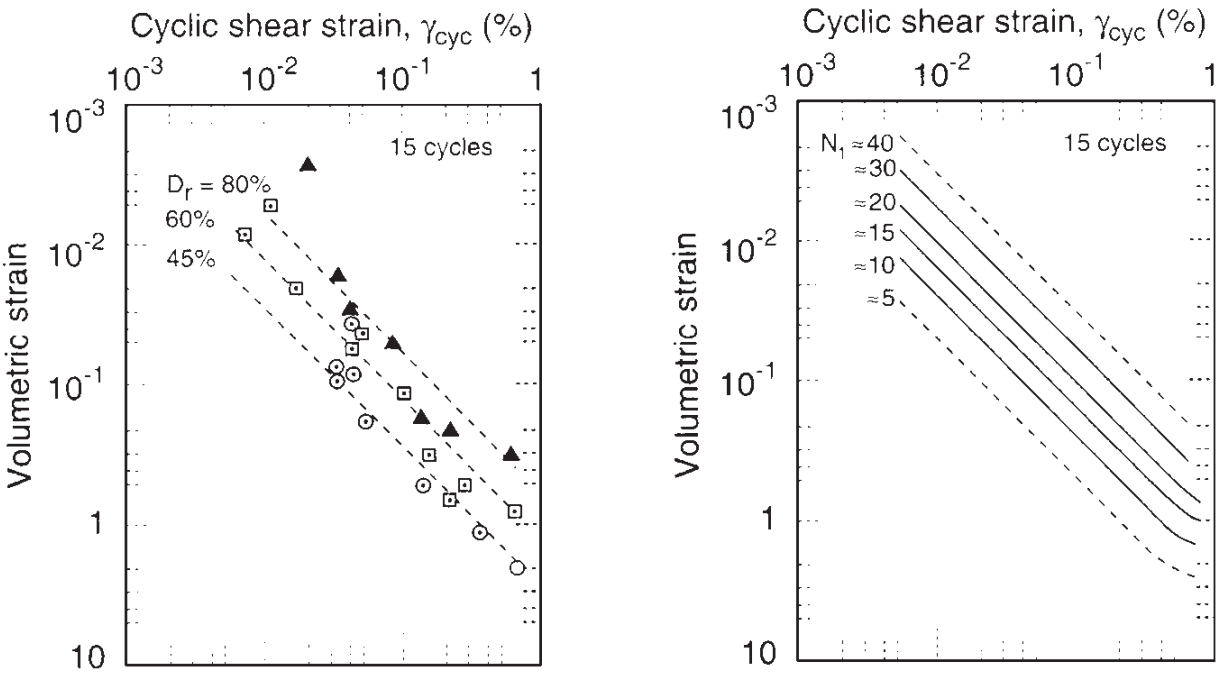

FIGURE 7.9 Plots that can be used to estimate the volumetric strain ε_v based on the cyclic shear strain γ_{cyc} and relative density D_r or N_1 value. Assume that N_1 in this figure refers to the $(N_1)_{60}$ values from Eq. (5.2). (*Reproduced from Tokimatsu and Seed 1987, with permission from the American Society of Civil Engineers.*)

TABLE 7.1 Earthquake Magnitude versus Volumetric Strain Ratio for Dry Sands

Earthquake magnitude	Number of representative cycles at $0.65\tau_{max}$	Volumetric strain ratio
8½	26	1.25
7½	15	1.00
6¾	10	0.85
6	5	0.60
5¼	2–3	0.40

Notes: To account for the earthquake magnitude, multiply the volumetric strain ε_v from Fig. 7.9 by the VSR. Data were obtained from Tokimatsu and Seed (1987).

have 5 percent or less fines. For dry sands (i.e., water content = 0 percent), capillary action does not exist between the soil particles. As the water content of the sand increases, capillary action produces a surface tension that holds together the soil particles and increases their resistance to earthquake-induced volumetric settlement. As a practical matter, clean sands typically have low capillarity and thus the method by Tokimatsu and Seed (1987) could also be performed for damp and moist sands.

For silty soils, R. B. Seed (1991) suggests that the most appropriate adjustment is to increase the $(N_1)_{60}$ values by adding the values of N_{corr} indicated in Sec. 7.2.2.

7.4.4 Example Problem

Silver and Seed (1972) investigated a 50-ft- (15-m-) thick deposit of dry sand that experienced about 2½ in (6 cm) of volumetric compression caused by the San Fernando earthquake of 1971. They indicated that the magnitude 6.6 San Fernando earthquake subjected the site to a peak ground acceleration a_{max} of $0.45g$. The sand deposit has a total unit weight $\gamma_t = 95$ lb/ft^3 (15 kN/m^3) and an average $(N_1)_{60} = 9$. Estimate the settlement of this 50-ft- (15-m-) thick sand deposit using the methods outlined in Secs. 7.4.2 and 7.4.3.

Solution Using Fig. 7.7. As shown in Fig. 7.7, the volumetric compression rapidly increases as the $(N_1)_{60}$ value decreases. Since the peak ground acceleration $a_p = 0.45g$, the horizontal axis is entered at 0.45. For an $(N_1)_{60}$ value of 9, the volumetric strain $\Delta H/H$ is about equal to 0.35 percent. The ground surface settlement is obtained by multiplying the volumetric strain, expressed as a decimal, by the thickness of the sand layer, or 0.0035×50 ft = 0.18 ft or 2.1 in (5.3 cm).

Solution Using the Tokimatsu and Seed (1987) Method. Table 7.2 presents the solution using the Tokimatsu and Seed (1987) method as outlined in Sec. 7.4.3. The steps are as follows:

1. *Layers:* The soil was divided into six layers.
2. *Thickness of the layers:* The upper two layers are 5.0 ft (1.5 m) thick, and the lower four layers are 10 ft (3.0 m) thick.
3. *Vertical effective stress:* For dry sand, the pore water pressures are zero and the vertical effective stress σ'_{v0} is equal to the vertical total stress σ_v. This stress was calculated by multiplying the total unit weight ($\gamma_t = 95$ lb/ft^3) by the depth to the center of each layer.

TABLE 7.2 Settlement Calculations Using the Tokimatsu and Seed (1987) Method

Layer number	Layer thickness, ft	$\sigma'_{v0} = \sigma_v$, lb/ft^2	$(N_1)_{60}$	G_{max} [Eq. (7.5)] kip/ft^2	$\gamma_{eff}(G_{eff}/G_{max})$ [Eq. (7.4)]	γ_{eff} (Fig. 7.8)	$\%\gamma_{cyc} = 100\gamma_{eff}$	ε_v (Fig. 7.9)	Multi-directional shear = $2\varepsilon_v$	Multiply by VSR	Settlement, in
(1)	(2)	(3)	(4)	(5)	(6)	(7)	(8)	(9)	(10)	(11)	(12)
1	5	238	9	517	1.3×10^{-4}	5×10^{-4}	5×10^{-2}	0.14	0.28	0.22	0.13
2	5	713	9	896	2.3×10^{-4}	1.0×10^{-3}	1.0×10^{-1}	0.29	0.58	0.46	0.28
3	10	1425	9	1270	3.1×10^{-4}	1.3×10^{-3}	1.3×10^{-1}	0.40	0.80	0.64	0.77
4	10	2375	9	1630	3.9×10^{-4}	1.4×10^{-3}	1.4×10^{-1}	0.43	0.86	0.69	0.83
5	10	3325	9	1930	4.4×10^{-4}	1.3×10^{-3}	1.3×10^{-1}	0.40	0.80	0.64	0.77
6	10	4275	9	2190	4.8×10^{-4}	1.3×10^{-3}	1.3×10^{-1}	0.40	0.80	0.64	0.77

Total = 3.5 in

4. $(N_1)_{60}$ *values:* As previously mentioned, the average $(N_1)_{60}$ value for the sand deposit was determined to be 9.
5. G_{max}: Equation (7.5) was used to calculate the value of G_{max}. It was assumed that the mean principal effective stress σ'_m was equal to $0.65\sigma'_{v0}$. Note that G_{max} is expressed in terms of kips per square foot (ksf) in Table 7.2.
6. *Equation (7.4):* The value of $\gamma_{eff}(G_{eff}/G_{max})$ was calculated by using Eq. (7.4). A peak ground acceleration a_{max} of $0.45g$ and a value of r_d from Eq. (6.7) were used in the analysis.
7. *Effective shear strain* γ_{eff}: Based on the values of $\gamma_{eff}(G_{eff}/G_{max})$ and the mean principal effective stress (σ'_m in ton/ft^2), Fig. 7.8 was used to obtain the effective shear strain.
8. *Percent cyclic shear strain* $\%\gamma_{cyc}$: The percent cyclic shear strain was calculated as γ_{eff} times 100.
9. *Volumetric strain* ε_v*:* Entering Fig. 7.9 with the percent cyclic shear strain and using $(N_1)_{60} = 9$, the percent volumetric strain ε_v was obtained from the vertical axis.
10. *Multidirectional shear:* The values of percent volumetric strain ε_v from step 9 were doubled to account for the multidirectional shear.
11. *Earthquake magnitude:* The earthquake magnitude is equal to 6.6. Using Table 7.1, the volumetric strain ratio is approximately equal to 0.8. To account for the earthquake magnitude, the percent volumetric strain ε_v from step 10 was multiplied by the VSR.
12. *Settlement:* The final step was to multiply the volumetric strain ε_v from step 11, expressed as a decimal, by the layer thickness. The total settlement was calculated as the sum of the settlement from all six layers (i.e., total settlement = 3.5 in).

Summary of Values. Based on the two methods, the ground surface settlement of the 50-ft- (15-m-) thick sand layer is expected to be on the order of 2 to 3½ in (5 to 9 cm). As previously mentioned, the actual settlement as reported by Seed and Silver (1972) was about 2½ in (6 cm).

7.4.5 Limitations

The methods for the calculation of volumetric compression as presented in Sec. 7.4 can only be used for the following cases:

- *Lightweight structures:* Settlement of lightweight structures, such as wood-frame buildings bearing on shallow foundations
- *Low net bearing stress:* Settlement of any other type of structure that imparts a low net bearing pressure onto the soil
- *Floating foundation:* Settlement of floating foundations, provided the floating foundation does not impart a significant net stress upon the soil
- *Heavy structures with deep settlement:* Settlement of heavy structures, such as massive buildings founded on shallow foundations, provided the zone of settlement is deep enough that the stress increase caused by the structural load is relatively low
- *Differential settlement:* Differential movement between a structure and adjacent appurtenances, where the structure contains a deep foundation that is supported by strata below the zone of volumetric compression

The methods for the calculation of volumetric compression as presented in Sec. 7.4 cannot be used for the following cases:

- *Heavy buildings bearing on loose soil:* Do not use the methods when the foundation applies a large net load onto the loose soil. In this case, the heavy foundation will punch downward into the loose soil during the earthquake. It is usually very difficult to determine the settlement for these conditions, and the best engineering solution is to provide a sufficiently high static factor of safety so that there is ample resistance against a bearing capacity failure. This is further discussed in Chap. 8.
- *Sloping ground condition:* These methods will underestimate the settlement for a sloping ground condition. The loose sand may deform laterally during the earthquake, and the settlement of the building could be well in excess of the calculated values.

7.5 SETTLEMENT DUE TO DYNAMIC LOADS CAUSED BY ROCKING

Details on this type of settlement are as follows:

- *Settlement mechanism:* This type of settlement is caused by dynamic structural loads that momentarily increase the foundation pressure acting on the soil, such as illustrated in Fig. 7.10. The soil will deform in response to the dynamic structural load, resulting in settlement of the building. This settlement due to dynamic loads is often a result of the structure rocking back and forth.
- *Vulnerable soil types:* Both cohesionless soil and cohesive soil are susceptible to rocking settlement. For cohesionless soils, loose sands and gravels are prone to rocking settlement. In addition, rocking settlement and volumetric compression (Sec. 7.4) often work in combination to cause settlement of the structure.

  Cohesive soils can also be susceptible to rocking settlement. The types of cohesive soils most vulnerable are normally consolidated soils (OCR = 1.0), such as soft clays and organic soils. There can be significant settlement of foundations on soft saturated clays and organic soils because of undrained plastic flow when the foundations are overloaded during the seismic shaking. Large settlement can also occur if the existing vertical effective stress σ'_{v0} plus the dynamic load $\Delta\sigma_v$ exceeds the maximum past pressure σ'_{vm} of the cohesive soil, or $\sigma'_{v0} + \Delta\sigma_v > \sigma'_{vm}$.

  Another type of cohesive soil that can be especially vulnerable to rocking settlement is sensitive clays. These soils can lose a portion of their shear strength during the cyclic loading. The higher the sensitivity, the greater the loss of shear strength for a given shear strain.
- *Susceptible structures:* Lightly loaded structures would be least susceptible to rocking settlement. On the other hand, tall and heavy buildings that have shallow foundations bearing on vulnerable soils would be most susceptible to this type of settlement.
- *Example:* Figure 7.11 presents an example of damage caused by rocking settlement. The rocking settlement occurred to a tall building located in Mexico City. The rocking settlement was caused by the September 19, 1985, Michoacan earthquake, which is described in Sec. 4.6.1.

In terms of the analysis for rocking settlement, R. B. Seed (1991) states:

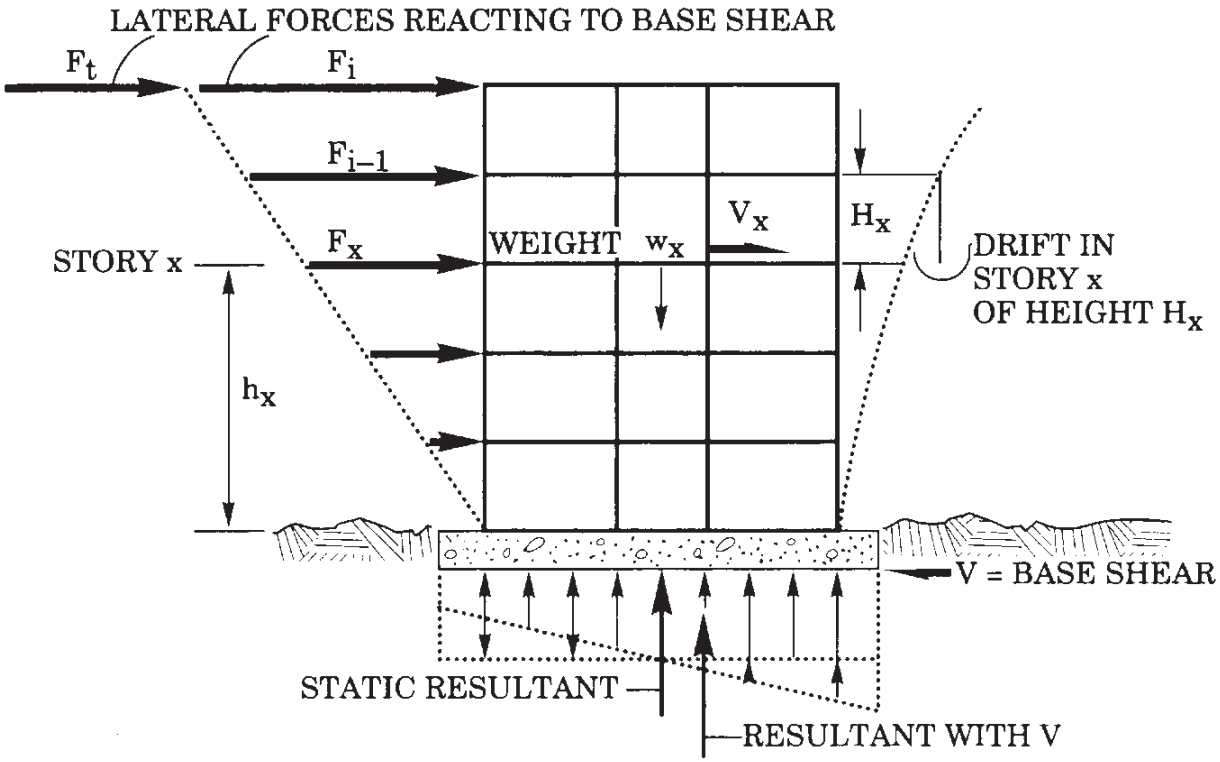

FIGURE 7.10 Diagram illustrating lateral forces *F* in response to the base shear *V* caused by the earthquake. Note that the uniform static bearing pressure is altered by the earthquake such that the pressure is increased along one side of the foundation. (*Reproduced from Krinitzsky et al. 1993, with permission from John Wiley & Sons.*)

Vertical accelerations during earthquake seldom produce sufficient vertical thrust to cause significant foundation settlements. Horizontal accelerations, on the other hand, can cause "rocking" of a structure, and the resulting structural overturning moments can produce significant cyclic vertical thrusts on the foundation elements. These can, in turn, result in cumulative settlements, with or without soil liquefaction or other strength loss. This is generally a potentially serious concern only for massive, relatively tall structures. Structures on deep foundations are not necessarily immune to this hazard; structures founded on "friction piles" (as opposed to more solidly-based end-bearing piles) may undergo settlements of up to several inches or more in some cases. It should be noted that the best engineering solution is generally simply to provide a sufficiently high static factor of safety in bearing in order to allow for ample resistance to potential transient seismic loading.

As indicated above, the best engineering solution is to provide a sufficiently high factor of safety against a bearing capacity failure, which is discussed in Chap. 8.

7.6 PROBLEMS

The problems have been divided into basic categories as indicated below:

Liquefaction-Induced Settlement

7.1 Use the data from the example problem in Sec. 7.2.2, but assume that $a_{max}/g = 0.1$ and the sand contains 15 percent nonplastic fines. Calculate the settlement, using Figs. 7.1 and 7.2. *Answer:* See Table 7.3.

FIGURE 7.11 Settlement caused by the building rocking back and forth during the Michoacan earthquake in Mexico on September 19, 1985. (*Photograph from the Steinbrugge Collection, EERC, University of California, Berkeley.*)

7.2 Use the data from the example problem in Sec. 7.2.2, but assume that $a_{max}/g = 0.2$ and the earthquake magnitude $M = 5¼$. Calculate the liquefaction-induced settlement, using Figs. 7.1 and 7.2. *Answer:* See Table 7.3.

7.3 Use the data from the example problem in Sec. 7.2.2, but assume at a depth of 3 m that $q_c = 3.9$ MPa. Calculate the liquefaction-induced settlement, using Figs. 7.1 and 7.2. *Answer:* See Table 7.3.

7.4 Use the data from the example problem in Sec. 7.2.2, but assume that the shear wave velocity $V_s = 150$ m/s. Calculate the liquefaction-induced settlement, using Figs. 7.1 and 7.2. *Answer:* See Table 7.3.

7.5 Use the data from the example problem in Sec. 7.2.2, but assume that the soil type is crushed limestone (i.e., soil type 1, see Fig. 6.12) and at a depth of 3 m, $q_{c1} = 5.0$ MPa. Calculate the liquefaction-induced settlement, using Figs. 7.1 and 7.2. *Answer:* See Table 7.3.

7.6 Use the data from the example problem in Sec. 7.2.2, but assume that the soil type is silty gravel (i.e., soil type 2, see Fig. 6.12) and at a depth of 3 m, $q_{c1} = 7.5$ MPa. Calculate the liquefaction-induced settlement, using Figs. 7.1 and 7.2. *Answer:* See Table 7.3.

TABLE 7.3 Summary of Answers for Probs. 7.1 to 7.9

Problem no.	Soil type	a_{max}/g	Earthquake magnitude	$(N_1)_{60}$ bl./ft q_{c1}, MPa V_{s1}, m/s	Cyclic stress ratio (CSR)	Cyclic resistance ratio (CRR)	FS = CRR / CSR	Settlement, cm (Fig. 7.1)	Settlement, cm (Fig. 7.2)
Section 7.2.2	Clean sand	0.40	$7^1/_2$	7.7 blows/ft	0.34	0.09	0.26	4.1	3.0
Problem 7.1	Sand—15% fines	0.10	$7^1/_2$	7.7 blows/ft	0.084	0.14	1.67	0.15	0.15
Problem 7.2	Clean sand	0.20	$5^1/_4$	7.7 blows/ft	0.17	0.14	0.82	4.1	2.9
Problem 7.3	Clean sand	0.40	$7^1/_2$	5.8 MPa	0.34	0.09	0.26	3.6	3.0
Problem 7.4	Clean sand	0.40	$7^1/_2$	185 m/s	0.34	0.16	0.47	2.8	2.1
Problem 7.5	Crushed limestone	0.40	$7^1/_2$	5.0 MPa	0.34	0.18	0.53	4.2	3.1
Problem 7.6	Silty gravel	0.40	$7^1/_2$	7.5 MPa	0.34	0.27	0.79	3.0	2.2
Problem 7.7	Gravelly sand	0.40	$7^1/_2$	14 MPa	0.34	0.44	1.29	0.3	1.2
Problem 7.8	Eolian sand	0.40	$7^1/_2$	7.7 blows/ft	0.34	0.09	0.26	4.1	3.0
Problem 7.9	Loess	0.40	$7^1/_2$	7.7 blows/ft	0.34	0.18	0.53	3.0	2.3

Note: See App. E for solutions.

7.7 Use the data from the example problem in Sec. 7.2.2, but assume that the soil type is gravelly sand (i.e., soil type 3, see Fig. 6.12) and at a depth of 3 m, $q_{c1} = 14$ MPa. Calculate the settlement, using Figs. 7.1 and 7.2. *Answer:* See Table 7.3.

7.8 Use the data from the example problem in Sec. 7.2.2, but assume that the soil type is eolian sand (i.e., soil type 4, see Fig. 6.12). Calculate the liquefaction-induced settlement, using Figs. 7.1 and 7.2. *Answer:* See Table 7.3.

7.9 Use the data from the example problem in Sec. 7.2.2, but assume that the soil type is noncemented loess (i.e., soil type 7, see Fig. 6.12). Calculate the liquefaction-induced settlement, using Figs. 7.1 and 7.2. *Answer:* See Table 7.3.

7.10 Assume a site has clean sand and a groundwater table near ground surface. The following data are determined for the site:

Layer depth, m	Cyclic stress ratio	$(N_1)_{60}$
2–3	0.18	10
3–5	0.20	5
5–7	0.22	7

Using Figs. 7.1 and 7.2, calculate the total liquefaction-induced settlement of these layers caused by a magnitude 7.5 earthquake. *Answer:* Per Fig. 7.1, 22 cm; per Fig. 7.2, 17 cm.

Liquefaction-Induced Settlement, Subsoil Profiles

7.11 Use the data from Prob. 6.12 and the subsoil profile shown in Fig. 6.13. Ignore any possible settlement of the soil above the groundwater table (i.e., ignore settlement from ground surface to a depth of 1.5 m). Also ignore any possible settlement of the soil located below a depth of 21 m. Using Figs. 7.1 and 7.2, calculate the earthquake-induced settlement of the sand located below the groundwater table. *Answer:* Per Fig. 7.1, 61 cm; per Fig. 7.2, 53 cm.

7.12 Use the data from Prob. 6.15 and the subsoil profile shown in Fig. 6.15. Ignore any possible settlement of the surface soil (i.e., ignore settlement from ground surface to a depth of 1.2 m). Also ignore any possible settlement of soil located below a depth of 20 m. Using Figs. 7.1 and 7.2, calculate the earthquake-induced settlement of the sand located below the groundwater table. *Answer:* Per Fig. 7.1, 22 cm; per Fig. 7.2, 17 cm.

7.13 Figure 7.12 shows the subsoil profile at the Agano River site in Niigata. Assume a level-ground site with the groundwater table at a depth of 0.85 m below ground surface. The medium sand, medium to coarse sand, and coarse sand layers have less than 5 percent fines. The fine to medium sand layers have an average of 15 percent fines. The total unit weight γ_t of the soil above the groundwater table is 18.5 kN/m^3, and the buoyant unit weight γ_b of the soil below the groundwater table is 9.8 kN/m^3.

The standard penetration data shown in Fig. 7.12 are uncorrected N values. Assume a hammer efficiency E_m of 0.6 and a boring diameter of 100 mm; and the length of drill rods is equal to the depth of the SPT below ground surface. The design earthquake conditions are a peak ground acceleration a_{max} of 0.20g and magnitude of 7.5. Based on the standard penetration test data and using Figs. 7.1 and 7.2, calculate the earthquake-induced settlement of the soil located at a depth of 0.85 to 15.5 m below ground surface. *Answer:* Per Fig. 7.1, 30 cm; per Fig. 7.2, 24 cm.

7.14 Figure 7.13 shows the subsoil profile at a road site in Niigata. Assume a level-ground site with the groundwater table at a depth of 2.5 m below ground surface. Also assume that all the soil types located below the groundwater table meet the criteria for potentially liquefiable soil. The medium sand layers have less than 5 percent fines, the

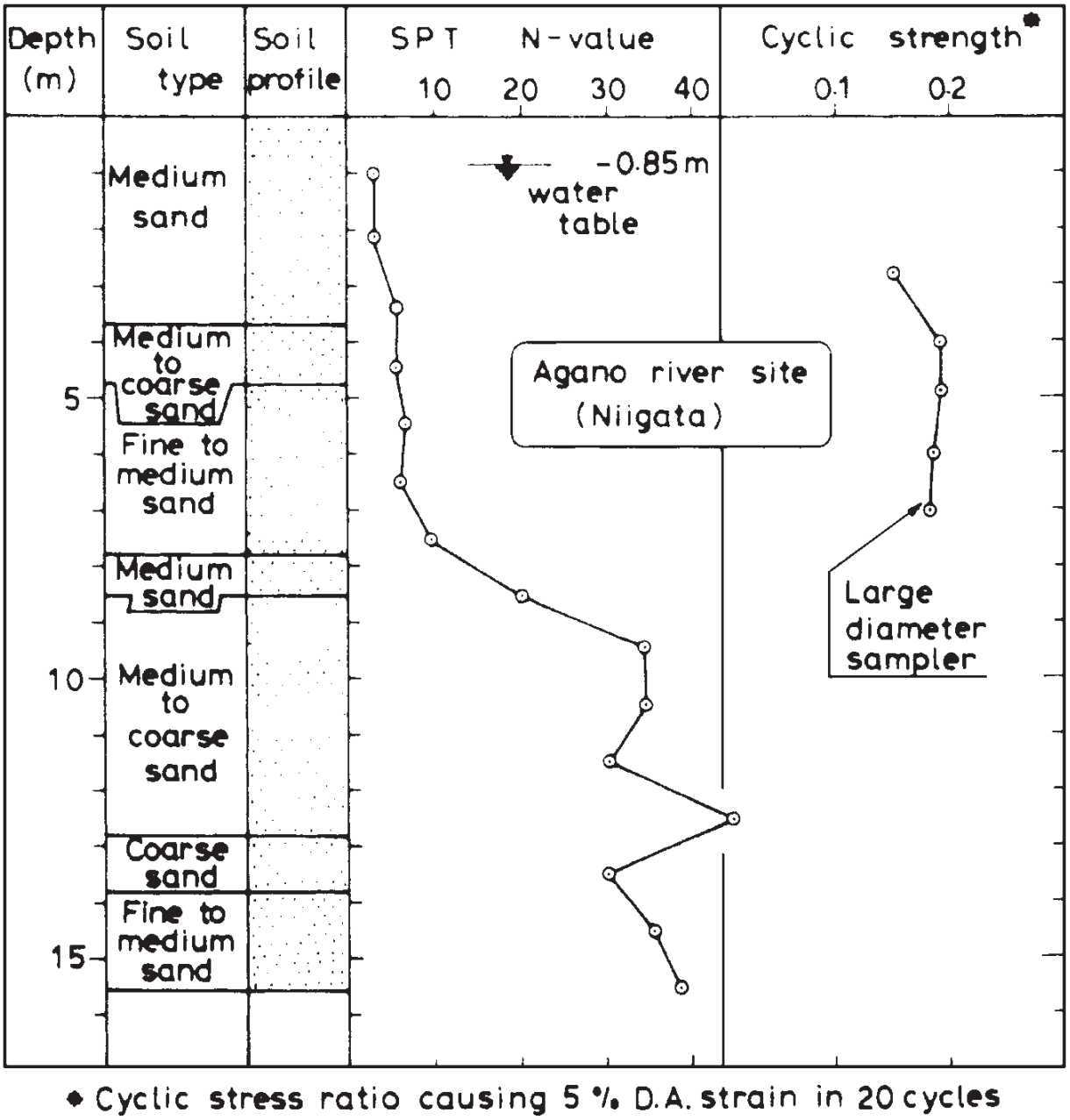

FIGURE 7.12 Subsoil profile, Agano River site, Niigata. (*Reproduced from Ishihara, 1985.*)

sandy silt layer has 50 percent fines, and the silt layers have 75 percent fines. The total unit weight γ_t of the soil above the groundwater table is 18.5 kN/m^3, and the buoyant unit weight γ_b of the soil below the groundwater table is 9.8 kN/m^3.

The standard penetration data shown in Fig. 7.13 are uncorrected N values. Assume a hammer efficiency E_m of 0.6 and a boring diameter of 100 mm; and the length of drill rods is equal to the depth of the SPT below ground surface. The design earthquake conditions are a peak ground acceleration a_{max} of 0.20g and magnitude of 7.5. Based on the standard penetration test data and using Figs. 7.1 and 7.2, calculate the earthquake-induced settlement of the soil located at a depth of 2.5 to 15 m below ground surface. *Answer:* Per Fig. 7.1, 34 cm; per Fig. 7.2, 27 cm.

7.15 Use the data from Prob. 6.18 and Fig. 6.11. Based on Figs. 7.1 and 7.2, calculate the earthquake-induced settlement of the soil located at a depth of 0.5 to 16 m below ground surface for the before-improvement and after-improvement conditions. *Answers:* Before

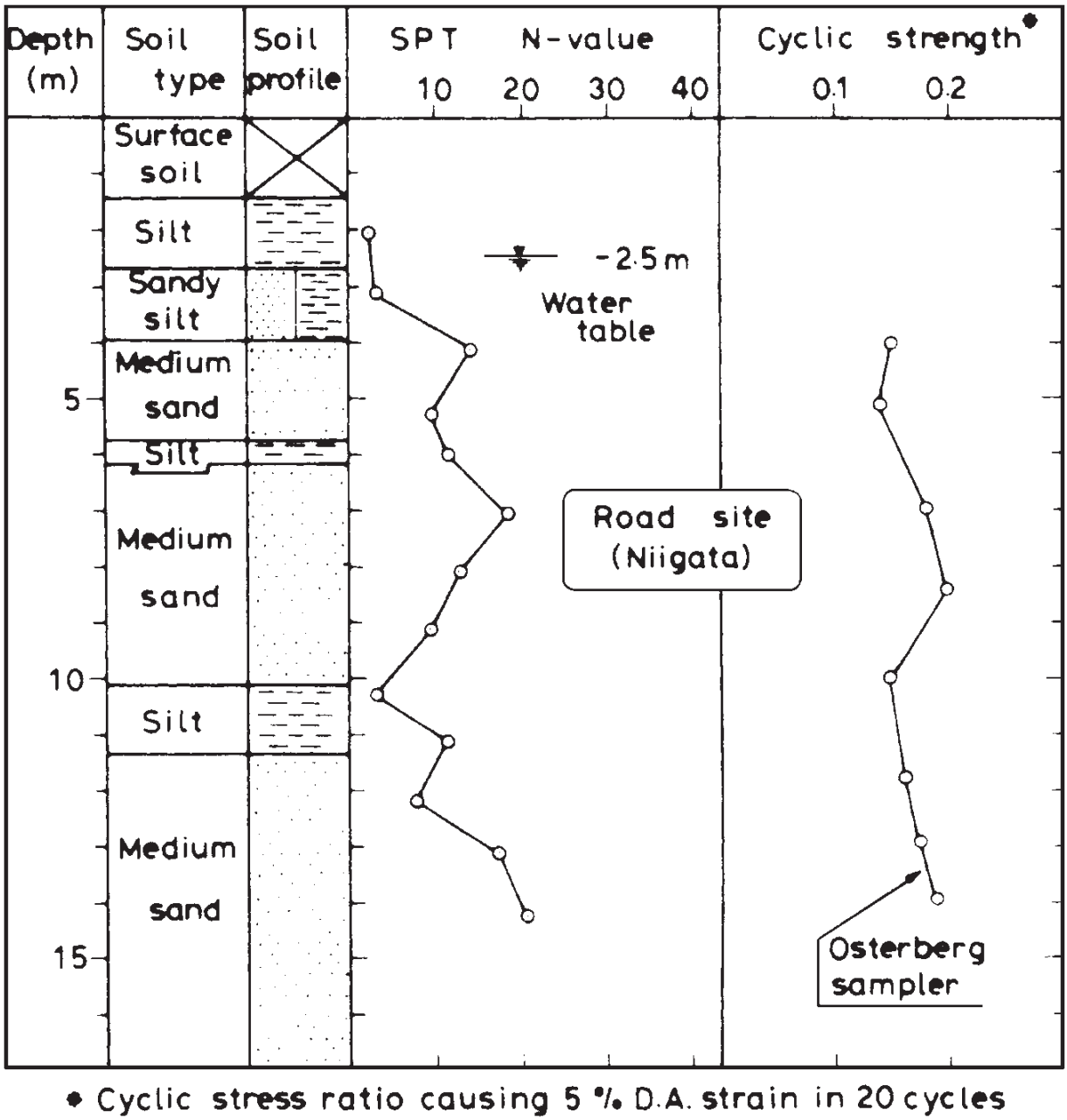

FIGURE 7.13 Subsoil profile, road site, Niigata. (*Reproduced from Ishihara, 1985.*)

improvement: per Fig. 7.1, 45 cm; per Fig. 7.2, 35 cm. After improvement: per Fig. 7.1, 0.3 cm; and per Fig. 7.2, 2.7 cm.

7.16 Use the data from Prob. 6.12 and Fig. 6.13. Assume that there has been soil improvement from ground surface to a depth of 15 m, and for the zone of soil having soil improvement (0 to 15-m depth), the factor of safety against liquefaction is greater than 2.0. A mat foundation for a heavy building will be constructed such that the bottom of the mat is at a depth of 1.0 m. The mat foundation is 20 m long and 10 m wide, and according to the structural engineer, the foundation will impose a net stress of 50 kPa onto the soil (the 50 kPa includes earthquake-related seismic load). Calculate the earthquake-induced settlement of the heavy building, using Figs. 7.1 and 7.2. *Answer:* Per Fig. 7.1, 17 cm; per Fig. 7.2, 19 cm.

7.17 Use the data from Prob. 6.15 and Fig. 6.15. A sewage disposal tank will be installed at a depth of 2 to 4 m below ground surface. Assuming the tank is empty at the

time of the design earthquake, calculate the liquefaction-induced settlement of the tank. *Answer:* Since the tank is in the middle of a liquefied soil layer, it is expected that the empty tank will not settle, but rather will float to the ground surface.

Liquefaction-Induced Ground Damage

7.18 A soil deposit has a 6-m-thick surface layer of unliquefiable soil underlain by a 4-m-thick layer that is expected to liquefy during the design earthquake. The design earthquake has a peak ground acceleration a_{max} equal to 0.40g. Will there be liquefaction-induced ground damage for this site? *Answer:* Based on Fig. 7.6, liquefaction-induced ground damage is expected for this site.

7.19 Use the data from Prob. 6.12 and Fig. 6.13. Assume that the groundwater table is unlikely to rise above its present level. Using a peak ground acceleration a_{max} equal to 0.20g and the standard penetration test data, will there be liquefaction-induced ground damage for this site? *Answer:* Based on Fig. 7.6, liquefaction-induced ground damage is expected for this site.

7.20 Use the data from Prob. 7.13 and Fig. 7.12. Assume that the groundwater table is unlikely to rise above its present level. Using a peak ground acceleration a_{max} equal to 0.20g and the standard penetration test data, determine the minimum thickness of a fill layer that must be placed at the site in order to prevent liquefaction-induced ground damage for this site. *Answer:* Based on Fig. 7.6, minimum thickness of fill layer = 2.2 m.

7.21 Use the data from Prob. 7.14 and Fig. 7.13. Assume that the groundwater table is unlikely to rise above its present level. Using a peak ground acceleration a_{max} equal to 0.20g and the standard penetration test data, will there be liquefaction-induced ground damage for this site? *Answer:* The solution depends on the zone of assumed liquefaction (see App. E).

Volumetric Compression

7.22 Solve the example problem in Sec. 7.4.4, using the Tokimatsu and Seed (1987) method and assuming that the 50-ft-thick deposit of sand has $(N_1)_{60} = 5$. *Answer:* 11 in (28 cm).

7.23 Solve the example problem in Sec. 7.4.4, using the Tokimatsu and Seed (1987) method and the chart shown in Fig. 7.7, assuming that the 50-ft-thick deposit of sand has $(N_1)_{60} = 15$. *Answer:* Using the Tokimatsu and Seed (1987) method, settlement = 1.3 in (3.3 cm). Using the chart shown in Fig. 7.7, settlement = 0.9 in (2 cm).

7.24 Solve the example problem in Sec. 7.4.4, using the Tokimatsu and Seed (1987) method and the chart shown in Fig. 7.7, assuming that the 50-ft-thick deposit of sand will be subjected to a peak ground acceleration of 0.20g and the earthquake magnitude = 7.5. *Answer:* Using the Tokimatsu and Seed (1987) method, settlement = 0.9 in (2.3 cm). Using the chart shown in Fig. 7.7, settlement = 0.6 in (1.5 cm).

7.25 Solve the example problem in Sec. 7.4.4, using the Tokimatsu and Seed (1987) method and assuming that the 50-ft-thick deposit of sand has $(N_1)_{60} = 5$, a peak ground acceleration of 0.20g, and the earthquake magnitude = 7.5. *Answer:* Settlement = 2 in (5 cm).

CHAPTER 8

BEARING CAPACITY ANALYSES FOR EARTHQUAKES

The following notation is used in this chapter:

SYMBOL	*DEFINITION*
B	Width of footing
B'	Reduced footing width to account for eccentricity of load
c	Cohesion based on total stress analysis
c'	Cohesion based on effective stress analysis
D_f	Depth below ground surface to bottom of footing
D_r	Relative density
e	Eccentricity of vertical load Q
e_1, e_2	Eccentricities along and across footing (Fig. 8.9)
FS	Factor of safety
H_1	Thickness of surface layer that does not liquefy
k_0	Coefficient of earth pressure at rest
L	Length of footing
L'	Reduced footing length to account for eccentricity of load
N	Measured SPT blow count (N value in blows per foot)
N_c, N_γ, N_q	Dimensionless bearing capacity factors
$(N_1)_{60}$	N value corrected for field testing procedures and overburden pressure
P, Q	Footing load
q_{all}	Allowable bearing pressure
q_{ult}	Ultimate bearing capacity
q'	Largest bearing pressure exerted by eccentrically loaded footing
q''	Lowest bearing pressure exerted by eccentrically loaded footing
Q_{ult}	Load causing a bearing capacity failure
r_u	Pore water pressure ratio
R	Shear resistance of soil
s_u	Undrained shear strength of soil
S_t	Sensitivity of soil
T	Vertical distance from bottom of footing to top of liquefied soil layer
u_e	Excess pore water pressure generated during earthquake
w_l	Liquid limit
w_p	Plastic limit
ϕ	Friction angle based on total stress analysis
ϕ'	Friction angle based on effective stress analysis
γ_b	Buoyant unit weight of saturated soil below groundwater table
γ_t	Total unit weight of soil

σ'	Initial effective stress acting on shear surface
σ_h	Horizontal total stress
σ'_h	Horizontal effective stress
σ_v	Vertical total stress
σ'_{vm}	Maximum past pressure, also known as preconsolidation pressure
σ'_{v0}	Vertical effective stress
τ_f	Shear strength of soil

8.1 INTRODUCTION

8.1.1 General, Punching, and Local Shear

A *bearing capacity failure* is defined as a foundation failure that occurs when the shear stresses in the soil exceed the shear strength of the soil. For both the static and seismic cases, bearing capacity failures of foundations can be grouped into three categories, (Vesic 1963, 1967, 1975):

1. *General shear (Fig. 8.1):* As shown in Fig. 8.1, a general shear failure involves total rupture of the underlying soil. There is a continuous shear failure of the soil (solid lines) from below the footing to the ground surface. When the load is plotted versus settlement of the footing, there is a distinct load at which the foundation fails (solid circle), and this is designated Q_{ult}. The value of Q_{ult} divided by the width B and length L of the footing is considered to be the *ultimate bearing capacity* q_{ult} of the footing. The ultimate bearing capacity has been defined as the bearing stress that causes a sudden catastrophic failure of the foundation (Lambe and Whitman 1969).

Note in Fig. 8.1 that a general shear failure ruptures and pushes up the soil on both sides of the footing. For actual failures in the field, the soil is often pushed up on only one side of the footing with subsequent tilting of the structure. A general shear failure occurs for soils that are in a dense or hard state.

2. *Punching shear (Fig. 8.2):* As shown in Fig. 8.2, a punching shear failure does not develop the distinct shear surfaces associated with a general shear failure. For punching shear, the soil outside the loaded area remains relatively uninvolved, and there is minimal movement of soil on both sides of the footing.

The process of deformation of the footing involves compression of soil directly below the footing as well as the vertical shearing of soil around the footing perimeter. As shown in Fig. 8.2, the load-settlement curve does not have a dramatic break, and for punching shear, the bearing capacity is often defined as the first major nonlinearity in the load-settlement curve (open circle). A punching shear failure occurs for soils that are in a loose or soft state.

3. *Local shear failure (Fig. 8.3):* As shown in Fig. 8.3, local shear failure involves rupture of the soil only immediately below the footing. There is soil bulging on both sides of the footing, but the bulging is not as significant as in general shear. Local shear failure can be considered as a transitional phase between general shear and punching shear. Because of the transitional nature of local shear failure, the bearing capacity could be defined as the first major nonlinearity in the load-settlement curve (open circle) or at the point where the settlement rapidly increases (solid circle). A local shear failure occurs for soils that are in a medium or firm state.

Table 8.1 presents a summary of the type of bearing capacity failure that would most likely develop based on soil type and soil properties.

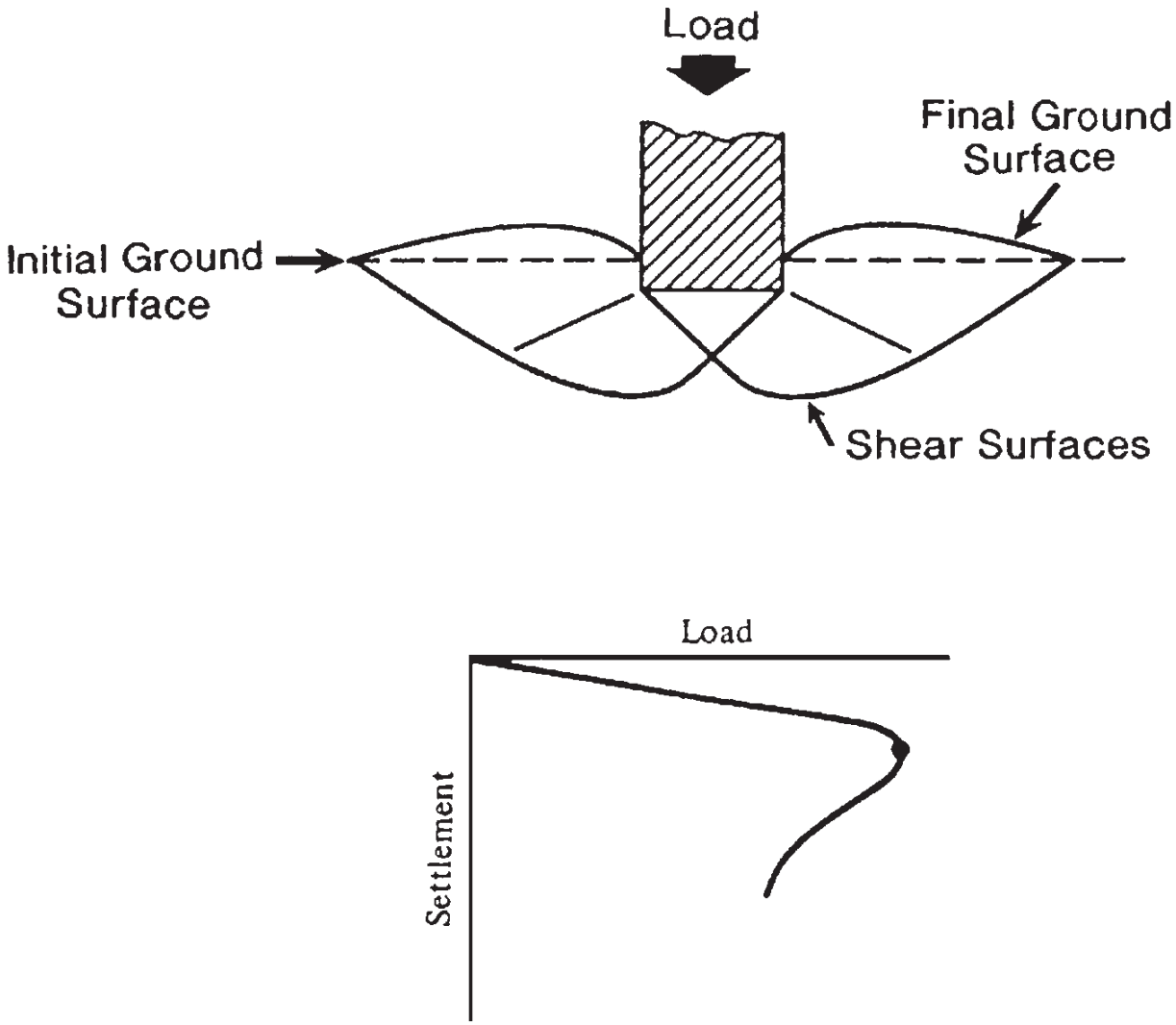

FIGURE 8.1 General shear foundation failure. (*After Vesic 1963.*)

8.1.2 Bearing Capacity Failures

Compared to the number of structures damaged by earthquake-induced settlement, there are far fewer structures that have earthquake-induced bearing capacity failures. This is because of the following factors:

1. *Settlement governs:* The foundation design is based on several requirements. Two of the main considerations are that (1) settlement due to the building loads must not exceed tolerable values and (2) there must be an adequate factor of safety against a bearing capacity failure. In most cases, settlement governs and the foundation bearing pressures recommended by the geotechnical engineer are based on limiting the amount of expected settlement due to the static or seismic cases. In other cases where the settlement is too high, the building is often constructed with a deep foundation, which also reduces the possibility of a bearing capacity failure.

2. *Extensive studies:* There have been extensive studies of both static and seismic bearing capacity failures, which have led to the development of bearing capacity equations that are routinely used in practice to determine the ultimate bearing capacity of the foundation.

3. *Factor of safety:* To determine the allowable bearing pressure q_{all}, the ultimate bearing capacity q_{ult} is divided by a factor of safety. The normal factor of safety used for static bearing capacity analyses is 3. For the evaluation of the bearing capacity for seismic

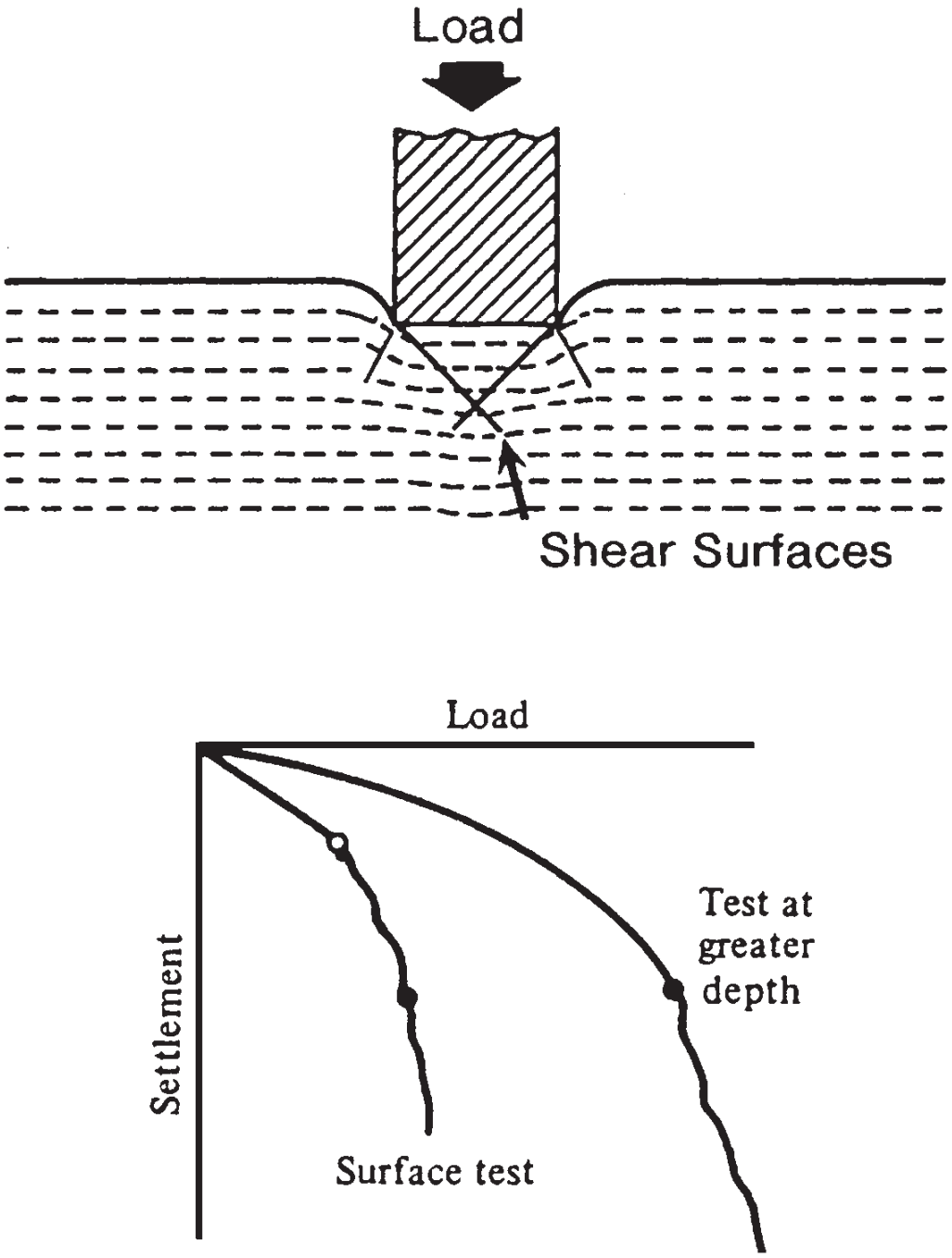

FIGURE 8.2 Punching shear foundation failure. (*After Vesic 1963.*)

analysis, the factor of safety is often in the range of 5 to 10 (Krinitzsky et al. 1993). These are high factors of safety compared to other factors of safety, such as only 1.5 for slope stability analyses (Chap. 9).

4. *Minimum footing sizes:* Building codes often require minimum footing sizes and embedment depths. Larger footing sizes will lower the bearing pressure on the soil and reduce the potential for static or seismic bearing capacity failures.

5. *Allowable bearing pressures:* In addition, building codes often have maximum allowable bearing pressures for different soil and rock conditions. Table 8.2 presents maximum allowable bearing pressures based on the *Uniform Building Code* (Table 18-I-A, 1997). Especially in the case of dense or stiff soils, these allowable bearing pressures often have adequate factors of safety for both static and seismic cases.

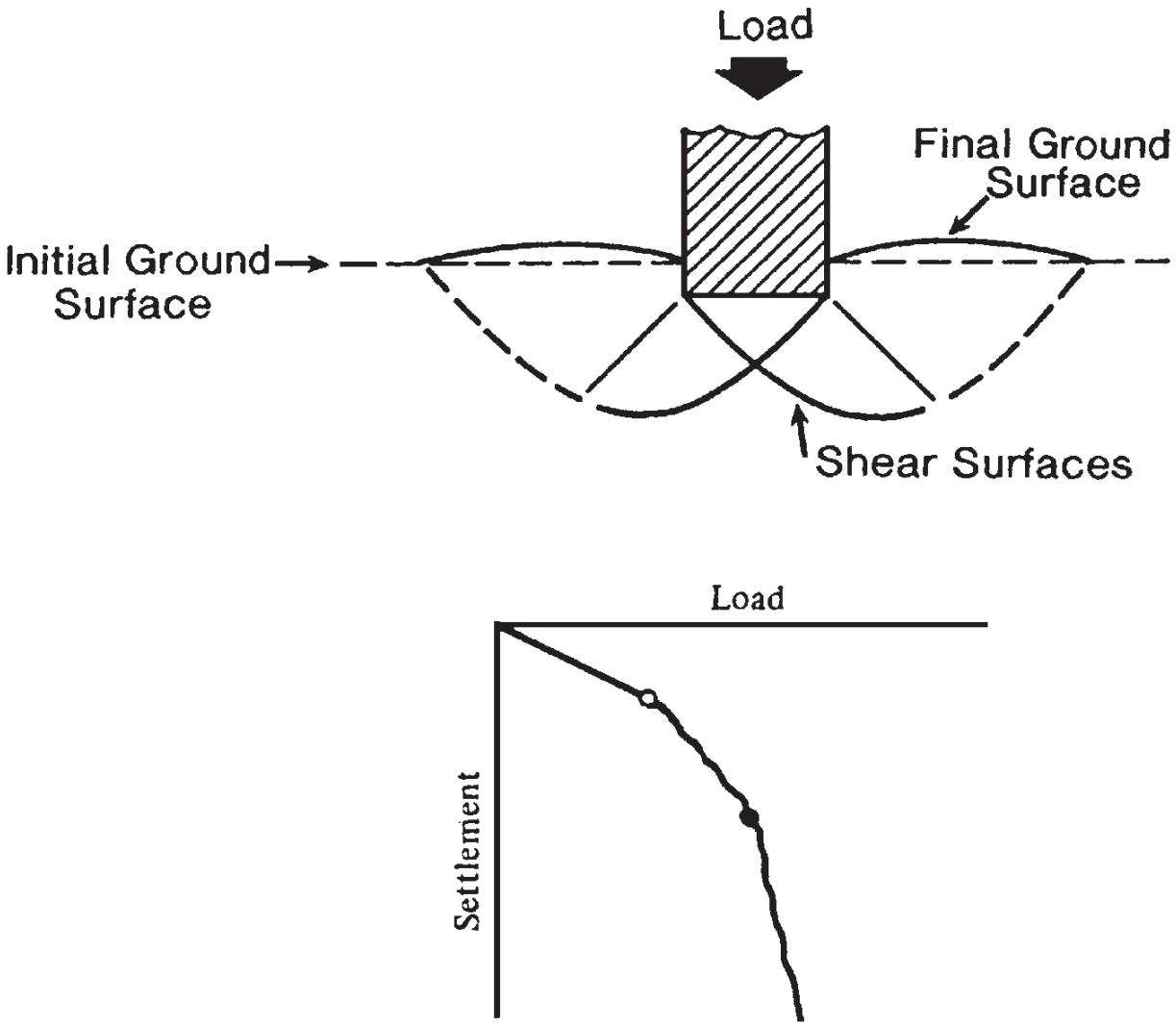

FIGURE 8.3 Local shear foundation failure. (*After Vesic 1963.*)

6. *Footing dimensions:* Usually the structural engineer will determine the size of the footing by dividing the maximum footing load by the allowable bearing pressure. Typically the structural engineer uses values of dead, live, and seismic loads that also contain factors of safety. For example, the live load may be from the local building code, which specifies minimum live load requirements for specific building uses (e.g., see Table 16-A, *Uniform Building Code,* 1997). Thus the load that is used to proportion the footing also contains a factor of safety, which is in addition to the factor of safety that was used to determine the allowable bearing pressure.

The documented cases of bearing capacity failures during earthquakes indicate that usually the following three factors (separately or in combination) are the cause of the failure:

1. *Soil shear strength:* Common problems include an overestimation of the shear strength of the underlying soil. Another common situation leading to a bearing capacity failure is the loss of shear strength during the earthquake, because of the liquefaction of the soil or the loss of shear strength for sensitive clays.
2. *Structural load:* Another common problem is that the structural load at the time of the bearing capacity failure was greater than that assumed during the design phase. This can often occur when the earthquake causes rocking of the structure, and the resulting structural overturning moments produce significant cyclic vertical thrusts on the foundation elements and underlying soil.

TABLE 8.1 Summary of Type of Bearing Capacity Failure versus Soil Properties

	Cohesionless soil (e.g., sands)			Cohesive soil (e.g., clays)	
Type of bearing capacity failure	Density condition	Relative density D_r, percent	$(N_1)_{60}$	Consistency	Undrained shear strength s_u
General shear failure (Fig. 8.1)	Dense to very dense	65–100	>20	Very stiff to hard	>2000 lb/ft^2 (>100 kPa)
Local shear failure (Fig. 8.3)	Medium	35–65	5–20	Medium to stiff	500–2000 lb/ft^2 (25–100 kPa)
Punching shear failure (Fig. 8.2)	Loose to very loose	0–35	<5	Soft to very soft	<500 lb/ft^2 (<25 kPa)

3. *Change in site conditions:* An altered site can produce a bearing capacity failure. For example, if the groundwater table rises, then the potential for liquefaction is increased. Another example is the construction of an adjacent excavation, which could result in a reduction in support and a bearing capacity failure.

The most common cause of a seismic bearing capacity failure is liquefaction of the underlying soil. Section 3.4.2 presents an introduction to bearing capacity failures caused by liquefaction during the earthquake. Figures 3.20 to 3.22 show examples of bearing capacity failures caused by the Niigata earthquake on June 16, 1964. Figure 8.4 shows a bearing capacity failure due to liquefaction during the Izmit earthquake in Turkey on August 17, 1999. Another example is shown in Fig. 8.5, where rather than falling over, the building has literally punched downward into the liquefied soil.

Although bearing capacity failures related to liquefaction of underlying soils are most common, there could also be localized failures due to punching shear when the footing is overloaded, such as by the building's rocking back and forth. Figure 8.6 presents an example of a punching-type failure. The building foundation shown in Fig. 8.6 was constructed of individual spread footings that were interconnected with concrete tie beams. The building collapsed during the Caracas earthquake in Venezuela on July 29, 1967, and when the foundation was exposed, it was discovered that the spread footings had punched downward into the soil. Note in Fig. 8.6 that the tie beam at the center of the photograph was bent and pulled downward when the footing punched into the underlying soil.

8.1.3 Shear Strength

Because the bearing capacity failure involves a shear failure of the underlying soil (Figs. 8.1 to 8.3), the analysis will naturally include the shear strength of the soil (Sec. 5.5.1). As shown in Figs. 8.1 to 8.3, the depth of the bearing capacity failure tends to be rather shallow. For static bearing capacity analyses, it is often assumed that the soil involved in the bearing capacity failure can extend to a depth equal to B (footing width) below the bottom of the footing. However, for cases involving earthquake-induced liquefaction failures or punching shear failures, the depth of soil involvement could exceed the footing width. For buildings with numerous spread footings that occupy a large portion of the building area, the individual pressure bulbs from each footing may combine, and thus the entire width of the building could be involved in a bearing capacity failure.

Either a total stress analysis or an effective stress analysis must be used to determine the bearing capacity of a foundation. These two types of analyses are discussed in Sec. 5.5.1. Table 5.4 presents a summary of the type of analyses and the shear strength parameters that should be used for the bearing capacity analyses.

FIGURE 8.4 The building suffered a liquefaction-induced bearing capacity failure during the Izmit earthquake in Turkey on August 17, 1999. (*Photograph from the Izmit Collection, EERC, University of California, Berkeley.*)

8.1.4 One-Third Increase in Bearing Pressure for Seismic Conditions

When the recommendations are presented for the allowable bearing pressures at a site, it is common practice for the geotechnical engineer to recommend that the allowable bearing pressure be increased by a factor of one-third when performing seismic analyses. For example, in soil reports, it is commonly stated: "For the analysis of earthquake loading, the allowable bearing pressure and passive resistance may be increased by a factor of one-third." The rational behind this recommendation is that the allowable bearing pressure has an ample factor of safety, and thus for seismic analyses, a lower factor of safety would be acceptable.

Usually the above recommendation is appropriate for the following materials:

1. Massive crystalline bedrock and sedimentary rock that remains intact during the earthquake
2. Dense to very dense granular soil
3. Heavily overconsolidated cohesive soil, such as very stiff to hard clays

These materials do not lose shear strength during the seismic shaking, and therefore an increase in bearing pressure is appropriate.

A one-third increase in allowable bearing pressure should not be recommended for the following materials:

1. Foliated or friable rock that fractures apart during the earthquake
2. Loose soil subjected to liquefaction or a substantial increase in excess pore water pressure
3. Sensitive clays that lose shear strength during the earthquake
4. Soft clays and organic soils that are overloaded and subjected to plastic flow

These materials have a reduction in shear strength during the earthquake. Since the materials are weakened by the seismic shaking, the static values of allowable bearing pres-

FIGURE 8.5 The building suffered a liquefaction-induced punching shear failure during the Izmit earthquake in Turkey on August 17, 1999. (*Photograph from the Izmit Collection, EERC, University of California, Berkeley.*)

sure should not be increased for the earthquake analyses. In fact, the allowable bearing pressure may actually have to be reduced to account for the weakening of the soil during the earthquake. The remainder of this chapter deals with the determination of the bearing capacity of soils that are weakened by seismic shaking.

8.2 BEARING CAPACITY ANALYSES FOR LIQUEFIED SOIL

8.2.1 Introduction

Section 8.2 deals with the bearing capacity of foundations underlain by liquefied soil. The liquefaction analysis presented in Chap. 6 can be used to determine those soil layers that will liquefy during the design earthquake.

Table 8.3 summarizes the requirements and analyses for soil susceptible to liquefaction. The steps are as follows:

FIGURE 8.6 The building foundation shown above was constructed of individual footings that were interconnected with concrete tie beams. The building collapsed during the Caracas earthquake in Venezuela on July 29, 1967. When the foundation was exposed, it was discovered that the spread footings had punched downward into the soil. Note that the tie beam at the center of the photograph was bent and pulled downward when the footing punched into the underlying soil. (*Photograph from the Steinbrugge Collection, EERC, University of California, Berkeley.*)

1. *Requirements:* The first step is to determine whether the two requirements listed in Table 8.3 are met. If these two requirements are not met, then the foundation is susceptible to failure during the design earthquake, and special design considerations, such as the use of deep foundations or soil improvement, are required.

2. *Settlement analysis:* Provided that the two design requirements are met, the next step is to perform a settlement analysis using Figs. 7.1 and 7.2. Note that in some cases, the settlement analysis is unreliable (e.g., heavy buildings with an underlying liquefied soil layer close to the bottom of the foundation).

3. *Bearing capacity analysis:* There are two different types of bearing capacity analysis that can be performed. The first deals with a shear failure where the footing punches into the liquefied soil layer (Sec. 8.2.2). The second case uses the traditional Terzaghi bearing

TABLE 8.2 Allowable Bearing Pressures

Material type	Allowable bearing pressure*	Maximum allowable bearing pressure†
Massive crystalline bedrock	4,000 lb/ft^2 (200 kPa)	12,000 lb/ft^2 (600 kPa)
Sedimentary and foliated rock	2,000 lb/ft^2 (100 kPa)	6,000 lb/ft^2 (300 kPa)
Gravel and sandy gravel (GW, GP)‡	2,000 lb/ft^2 (100 kPa)	6,000 lb/ft^2 (300 kPa)
Nonplastic soil: sands, silty gravel, and nonplastic silt (GM, SW, SP, SM)‡	1,500 lb/ft^2 (75 kPa)	4,500 lb/ft^2 (220 kPa)
Plastic soil: silts and clays (ML, MH, SC, CL, CH)‡	1,000 lb/ft^2 (50 kPa)	3,000 lb/ft^2 (150 kPa)§

*Minimum footing width and embedment depth equal 1 ft (0.3 m).

†An increase of 20 percent of the allowable bearing pressure is allowed for each additional 1 ft (0.3 m) of width or depth up to the maximum allowable bearing pressures listed in the rightmost column. An exception is plastic soil; see last note.

‡Group symbols from the Unified Soil Classification System.

§No increase in the allowable bearing pressure is allowed for an increase in width of the footing.

For dense or stiff soils, allowable bearing values are generally conservative. For very loose or very soft soils, allowable bearing values may be too high.

Source: Data from *Uniform Building Code* (1997).

capacity equation, with a reduction in the bearing capacity factors to account for the loss of shear strength of the underlying liquefied soil layer (Sec. 8.2.3).

4. *Special considerations:* Special considerations may be required if the structure is subjected to buoyancy or if there is a sloping ground condition.

8.2.2 Punching Shear Analysis

Illustration of Punching Shear. Figure 8.7 illustrates the earthquake-induced punching shear analysis. The soil layer portrayed by dashed lines represents unliquefiable soil which is underlain by a liquefied soil layer. For the punching shear analysis, it is assumed that the load will cause the foundation to punch straight downward through the upper unliquefiable soil layer and into the liquefied soil layer. As shown in Fig. 8.7, this assumption means that there will be vertical shear surfaces in the soil that start at the sides of the footing and extend straight downward to the liquefied soil layer. It is also assumed that the liquefied soil has no shear strength.

Factor of Safety. Using the assumptions outlined above, the factor of safety (FS) can be calculated as follows:
For strip footings:

$$\text{FS} = \frac{R}{P} = \frac{2T\tau_f}{P} \tag{8.1a}$$

For spread footings:

$$\text{FS} = \frac{R}{P} = \frac{2\,(B + L)\,(T\tau_f)}{P} \tag{8.1b}$$

TABLE 8.3 Requirements and Analyses for Soil Susceptible to Liquefaction

Requirements and analyses	Design conditions
Requirements	1. *Bearing location of foundation:* The foundation must not bear on soil that will liquefy during the design earthquake. Even lightly loaded foundations will sink into the liquefied soil. 2. *Surface layer H_1*: As discussed in Sec. 7.3, there must be an adequate thickness of an unliquefiable soil surface layer H_1 to prevent damage due to sand boils and surface fissuring (see Fig. 7.3). Without this layer, there could be damage to shallow foundations, pavements, flatwork, and utilities.
Settlement analysis	Use Figs 7.1 and 7.2 for the following conditions: 1. *Lightweight structures:* Settlement of lightweight structures, such as wood-frame buildings bearing on shallow foundations. 2. *Low net bearing stress:* Settlement of any other type of structure that imparts a low net bearing pressure onto the soil. 3. *Floating foundation:* Settlement of floating foundations, provided the zone of liquefaction is below the bottom of the foundation and the floating foundation does not impart a significant net stress upon the soil. 4. *Heavy structures with deep liquefaction:* Settlement of heavy structures, such as massive buildings founded on shallow foundations, provided the zone of liquefaction is deep enough that the stress increase caused by the structural load is relatively low. 5. *Differential settlement:* Differential movement between a structure and adjacent appurtenances, where the structure contains a deep foundation that is supported by strata below the zone of liquefaction.
Bearing capacity analysis	Use the analyses presented in Secs. 8.2 and 8.3 for the following conditions: 1. *Heavy buildings with underlying liquefied soil:* Use a bearing capacity analysis when there is a soil layer below the bottom of the foundation that will be susceptible to liquefaction during the design earthquake. In this case, once the soil has liquefied, the foundation load could cause it to punch or sink into the liquefied soil, resulting in a bearing capacity failure (see Sec. 8.2). 2. *Check bearing capacity:* Perform a bearing capacity analysis whenever the footing imposes a net pressure onto the soil and there is an underlying soil layer that will be susceptible to liquefaction during the design earthquake (see Sec. 8.2). 3. *Positive induced pore water pressures:* For cases where the soil will not liquefy during the design earthquake, but there will be the development of excess pore water pressures, perform a bearing capacity analysis (see Sec. 8.3).
Special considerations	1. *Buoyancy effects:* Consider possible buoyancy effects. Examples include buried storage tanks or large pipelines that are within the zone of liquefied soil. Instead of settling, the buried storage tanks and pipelines may actually float to the surface when the ground liquefies. 2. *Sloping ground condition:* Determine if the site is susceptible to liquefaction-induced flow slide or lateral spreading (see Chap. 9).

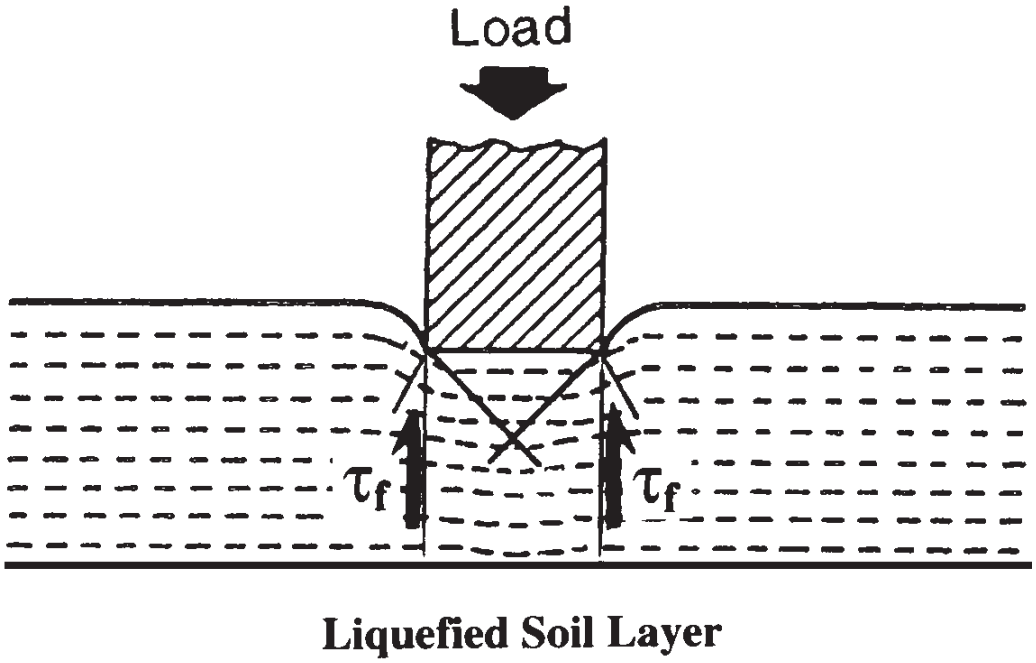

FIGURE 8.7 Illustration of a punching shear analysis. The dashed lines represent unliquefiable soil that is underlain by a liquefied soil layer. In the analysis, the footing will punch vertically downward and into the liquefied soil.

where R = shear resistance of soil. For strip footings, R is the shear resistance per unit length of footing, lb/ft or kN/m. For spread footings, R is the shear resistance beneath entire footing perimeter, lb or kN.
P = footing load. For strip footings, P is the load per unit length of footing, lb/ft or kN/m. For spread footings, P is total load of footing, lb or kN. The footing load includes dead, live, and seismic loads acting on footing as well as weight of footing itself. Typically the value of P would be provided by the structural engineer.
T = vertical distance from the bottom of footing to top of liquefied soil layer, ft or m
τ_f = shear strength of unliquefiable soil layer, lb/ft^2 or kPa
B = width of footing, ft or m
L = length of footing, ft or m

Note in Eq. (8.1*b*) that the term $2(B + L)$ represents the entire perimeter of the spread footing. When this term is multiplied by T, it represents the total perimeter area that the footing must push through in order to reach the liquefied soil layer. For an assumed footing size and given loading condition, the only unknowns in Eqs. (8.1*a*) and (8.1*b*) are the vertical distance from the bottom of the footing to the top of the liquefied soil layer T and the shear strength of the unliquefiable soil layer τ_f. The value of T would be based on the liquefaction analysis (Chap. 6) and the proposed depth of the footing. The shear strength of the unliquefiable soil layer τ_f can be calculated as follows:

1. For an unliquefiable soil layer consisting of cohesive soil (e.g., clays), use a total stress analysis:

$$\tau_f = s_u \tag{8.2a}$$

or

$$\tau_f = c + \sigma_h \tan \phi \tag{8.2b}$$

where s_u = undrained shear strength of cohesive soil (total stress analysis), lb/ft^2 or kPa. As

discussed in Sec. 5.5.1, often undrained shear strength is obtained from unconfined compression tests or vane shear tests.

c, ϕ = undrained shear strength parameters (total stress analysis). As discussed in Sec. 5.5.1, these undrained shear strength parameters are often obtained from triaxial tests, such as unconsolidated undrained triaxial compression test (ASTM D 2850-95, 2000) or consolidated undrained triaxial compression tests (ASTM D 4767-95, 2000).

σ_h = horizontal total stress, lb/ft^2 or kPa. Since vertical shear surfaces are assumed (see Fig. 8.7), normal stress acting on shear surfaces will be the horizontal total stress. For cohesive soil, σ_h is often assumed to be equal to $\frac{1}{2}\sigma_v$.

2. For an unliquefiable soil layer consisting of cohesionless soil (e.g., sands), use an effective stress analysis:

$$\tau_f = \sigma_h' \tan \phi' = k_0 \sigma_{v0}' \tan \phi' \tag{8.2c}$$

where σ_h' = horizontal effective stress, lb/ft^2 or kPa. Since vertical shear surfaces are assumed (see Fig. 8.7), the normal stress acting on the shear surface will be the horizontal effective stress. The horizontal effective stress σ_h' is equal to the coefficient of earth pressure at rest k_0 times the vertical effective stress σ_{v0}', or $\sigma_h' = k_0\, \sigma_{v0}'$.

ϕ' = effective friction angle of cohesionless soil (effective stress analysis). Effective friction angle could be determined from drained direct shear tests or from empirical correlations such as shown in Figs. 5.12 and 5.14.

Example Problems. The following example problems illustrate the use of Eqs. (8.1) and (8.2).

Example Problem for Cohesive Surface Layer (Total Stress Analysis). Use the data from Prob. 6.15, which deals with the subsurface conditions shown in Fig. 6.15 (i.e., the sewage disposal site). Based on the standard penetration test data, the zone of liquefaction extends from a depth of 1.2 to 6.7 m below ground surface. Assume the surface soil (upper 1.2 m) shown in Fig. 6.15 consists of an unliquefiable cohesive soil and during construction, an additional 1.8-m-thick layer of cohesive soil will be placed at ground surface. Use a peak ground acceleration a_{max} of $0.20g$.

Assume that after the 1.8-m-thick layer is placed at ground surface, it is proposed to construct a sewage disposal plant. The structural engineer would like to use shallow strip footings to support exterior walls and interior spread footings to support isolated columns. It is proposed that the bottom of the footings be at a depth of 0.5 m below ground surface. The structural engineer has also indicated that the maximum total loads (including the weight of the footing and the dynamic loads) are 50 kN/m for the strip footings and 500 kN for the spread footings. It is desirable to use 1-m-wide strip footings and square spread footings that are 2 m wide.

For both the existing 1.2-m-thick unliquefiable cohesive soil layer and the proposed additional 1.8-m-thick fill layer, assume that the undrained shear strength s_u of the soil is equal to 50 kPa. Calculate the factor of safety of the footings, using Eq. (8.1).

Solution. The first step is to check the two requirements in Table 8.3. Since the footings will be located within the upper unliquefiable cohesive soil, the first requirement is met. As indicated in the example problem in Sec. 7.3.3, the surface unliquefiable soil layer must be at least 3 m thick to prevent liquefaction-induced ground damage. Since a fill layer equal to 1.8 m is proposed for the site, the final thickness of the unliquefiable soil will be equal to 3 m. Thus the second requirement is met.

To calculate the factor of safety in terms of a bearing capacity failure for the strip and spread footings, the following values are used:

P = 50 kN/m for strip footing and 500 kN for spread footing

T = 2.5 m i.e., total thickness of unliquefiable soil layer minus footing embedment depth = 3 m − 0.5 m = 2.5 m

$\tau_f = s_u$ = 50 kPa = 50 kN/m^2

$B = L$ = 2 m

Substituting the above values into Eqs. (8.1*a*) and (8.1*b*) yields

$$\text{FS} = \frac{2\,T\tau_f}{P} = \frac{2\ (2.5\ \text{m})\ (50\ \text{kN/m}^2)}{50\ \text{kN/m}} = 5.0 \qquad \text{strip footing}$$

$$\text{FS} = \frac{2\ (B + L)\ T\tau_f}{P} = \frac{2\ (2 + 2)\ (2.5\ \text{m})\ (50\ \text{kN/m}^2)}{500\ \text{kN}} = 2.0 \qquad \text{spread footing}$$

For a seismic analysis, a factor of safety of 5.0 would be acceptable, but the factor of safety of 2.0 would probably be too low.

Example Problem for Cohesionless Surface Layer (Effective Stress Analysis). Use the same data, but assume the surface soil and the proposed 1.8-m-thick fill layer are sands with an effective friction angle ϕ' equal to 32° and a coefficient of earth pressure at rest k_0 equal to 0.5. Also assume that instead of the groundwater table being at a depth of 0.4 m (see Fig. 6.15), it is at a depth of 1.2 m below the existing ground surface. Calculate the factor of safety of the footings, using Eq. (8.1).

Solution. To calculate the factor of safety in terms of a bearing capacity failure for the strip and spread footings, the following values are used:

P = 50 kN/m for strip footing and 500 kN for spread footing

T = 2.5 m i.e., total thickness of unliquefiable soil layer minus footing embedment depth = 3 m − 0.5 m = 2.5 m

$\sigma'_{v0} = \sigma_v - u$ Since soil is above groundwater table, assume $u = 0$. Use a total unit weight of 18.3 kN/m^3 (Prob. 6.15) and an average depth of 1.75 m [(0.5 + 3.0)/2 = 1.75 m] or $\sigma'_{v0} = 18.3 \times 1.75 = 32$ kPa.

$\tau_f = k_0\,\sigma'_{v0} \tan \phi' = (0.5)\ (32\ \text{kPa})\ (\tan 32°) = 10\ \text{kPa} = 10\ \text{kN/m}^2$ [Eq. (8.2*c*)]

$B = L$ = 2 m

Substituting the above values into Eqs. (8.1*a*) and (8.1*b*) gives

$$\text{FS} = \frac{2T\tau_f}{P} = \frac{2\ (2.5\ \text{m})\ (10\ \text{kN/m}^2)}{50\ \text{kN/m}} = 1.0 \qquad \text{strip footing}$$

$$\text{FS} = \frac{2\ (B + L)\ T\tau_f}{P} = \frac{2\ (2 + 2)\ (2.5\ \text{m})\ (10\ \text{kN/m}^2)}{500\ \text{kN}} = 0.4 \qquad \text{spread footing}$$

For the seismic bearing capacity analyses, these factors of safety would indicate that both the strip and spread footings would punch down through the upper sand layer and into the liquefied soil layer.

As a final check, the FS calculated from the earthquake-induced punching shear analysis must be compared with the FS calculated from the static bearing capacity analysis (i.e., nonearthquake condition). The reason for this comparison is that FS for the earthquake

punching shear case [Eq. (8.1)] could exceed the FS calculated from the static condition. This often occurs when the liquefied soil layer is at a significant depth below the bottom of the footing, or in other words at high values of *T*/*B*. In any event, the lower value of FS from either the earthquake punching shear analysis or the static bearing capacity analysis would be considered the critical condition.

8.2.3 Terzaghi Bearing Capacity Equation

Introduction. The most commonly used bearing capacity equation is that equation developed by Terzaghi (1943). For a uniform vertical loading of a strip footing, Terzaghi (1943) assumed a shallow footing and general shear failure (Fig. 8.1) in order to develop the following bearing capacity equation:

$$q_{\text{ult}} = \frac{Q_{\text{ult}}}{BL} = cN_c + \tfrac{1}{2}\gamma_t B N_\gamma + \gamma_t D_f N_q \tag{8.3}$$

where q_{ult} = ultimate bearing capacity for a strip footing, kPa or lb/ft^2
Q_{ult} = vertical load causing a general shear failure of underlying soil (Fig. 8.1)
B = width of strip footing, m or ft
L = length of strip footing, m or ft
γ_t = total unit weight of soil, kN/m^3 or lb/ft^3
D_f = vertical distance from ground surface to bottom of strip footing, m or ft
c = cohesion of soil underlying strip footing, kPa or lb/ft^2
N_c, N_γ, and N_q = dimensionless bearing capacity factors

As indicated in Eq. (8.3), three terms are added to obtain the ultimate bearing capacity of the strip footing. These terms represent the following:

cN_c The first term accounts for the cohesive shear strength of the soil located below the strip footing. If the soil below the footing is cohesionless (that is, $c = 0$), then this term is zero.

$\frac{1}{2}\gamma_t B N_\gamma$ The second term accounts for the frictional shear strength of the soil located below the strip footing. The friction angle ϕ is not included in this term, but is accounted for by the bearing capacity factor N_γ. Note that γ_t represents the total unit weight of the soil located below the footing.

$\gamma_t D_f N_q$ This third term accounts for the soil located above the bottom of the footing. The value of γ_t times D_f represents a surcharge pressure that helps to increase the bearing capacity of the footing. If the footing were constructed at ground surface (that is, $D_f = 0$), then this term would equal zero. This third term indicates that the deeper the footing, the greater the ultimate bearing capacity of the footing. In this term, γ_t represents the total unit weight of the soil located above the bottom of the footing. The total unit weights above and below the footing bottom may be different, in which case different values are used in the second and third terms of Eq. (8.3).

As previously mentioned, Eq. (8.3) was developed by Terzaghi (1943) for strip footings. For other types of footings and loading conditions, corrections need to be applied to the bearing capacity equation. Many different types of corrections have been proposed (e.g., Meyerhof 1951, 1953, 1965). One commonly used form of the bearing capacity equation for spread (square footings) and combined footings (rectangular footings) subjected to uniform vertical loading is as follows (NAVFAC DM-7.2, 1982):

$$q_{ult} = \frac{Q_{ult}}{BL} = cN_c\left(1 + 0.3\,\frac{B}{L}\right) + 0.4\gamma_t B N_\gamma + \gamma_t D_f N_q \tag{8.4}$$

Equation (8.4) is similar to Eq. (8.3), and the terms have the same definitions. An important consideration is that for the strip footing, the shear strength is actually based on a plane strain condition (soil is confined along the long axis of the footing). It has been stated that the friction angle ϕ is about 10 percent higher in the plane strain condition than the friction angle ϕ measured in the triaxial apparatus (Meyerhof 1961, Perloff and Baron 1976). Ladd et al. (1977) indicated that the friction angle ϕ in plane strain is larger than ϕ in triaxial shear by 4° to 9° for dense sands. A difference in friction angle of 4° to 9° has a significant impact on the bearing capacity factors. In practice, plane strain shear strength tests are not performed, and thus there is an added factor of safety for the strip footing compared to the analysis for spread or combined footings.

Bearing Capacity Equation for a Cohesive Soil Layer Underlain by Liquefied Soil. For the situation of a cohesive soil layer overlying a sand that will be susceptible to liquefaction, a total stress analysis can be performed. This type of analysis uses the undrained shear strength of the cohesive soil (Sec. 5.5.1). The undrained shear strength s_u could be determined from field tests, such as the vane shear test (VST), or in the laboratory from unconfined compression tests. Using a total stress analysis, $s_u = c$ and $\phi = 0$ for Eqs. (8.3) and (8.4). For $\phi = 0$, the Terzaghi bearing capacity factors are $N_\gamma = 0$ and $N_q = 1$ (Terzaghi 1943). The bearing capacity equations, (8.3) and (8.4), thus reduce to the following:
For strip footings:

$$q_{ult} = cN_c + \gamma_t D_f = s_u N_c + \gamma_t D_f \tag{8.5a}$$

For spread footings:

$$q_{ult} = cN_c\left(1 + 0.3\,\frac{B}{L}\right) + \gamma_t D_f = s_u N_c\left(1 + 0.3\,\frac{B}{L}\right) + \gamma_t D_f \tag{8.5b}$$

In dealing with shallow footings, the second term ($\gamma_t D_f$) in Eq. 8.5 tends to be rather small. Thus by neglecting the second term in Eq. (8.5), the final result is as follows:
For strip footings:

$$q_{ult} = cN_c = s_u N_c \tag{8.6a}$$

For spread footings:

$$q_{ult} = cN_c\left(1 + 0.3\,\frac{B}{L}\right) = s_u N_c\left(1 + 0.3\,\frac{B}{L}\right) \tag{8.6b}$$

In order to use Eq. (8.6) to evaluate the ability of a footing to shear through a cohesive soil layer and into a liquefied soil layer, the undrained shear strength of the cohesive soil must be known (that is, $c = s_u$). In addition, the bearing capacity factor N_c must be determined. The presence of an underlying liquefied soil layer will tend to decrease the values for N_c. Figure 8.8 can be used to determine the values of N_c for the condition of a unliquefiable cohesive soil layer overlying a soil layer that is expected to liquefy during the design earthquake. In Fig. 8.8, the terms are defined as follows:

Layer 1 = upper cohesive soil layer that has a uniform undrained shear strength, lb/ft^2 or kPa, or $s_u = c = c_1$

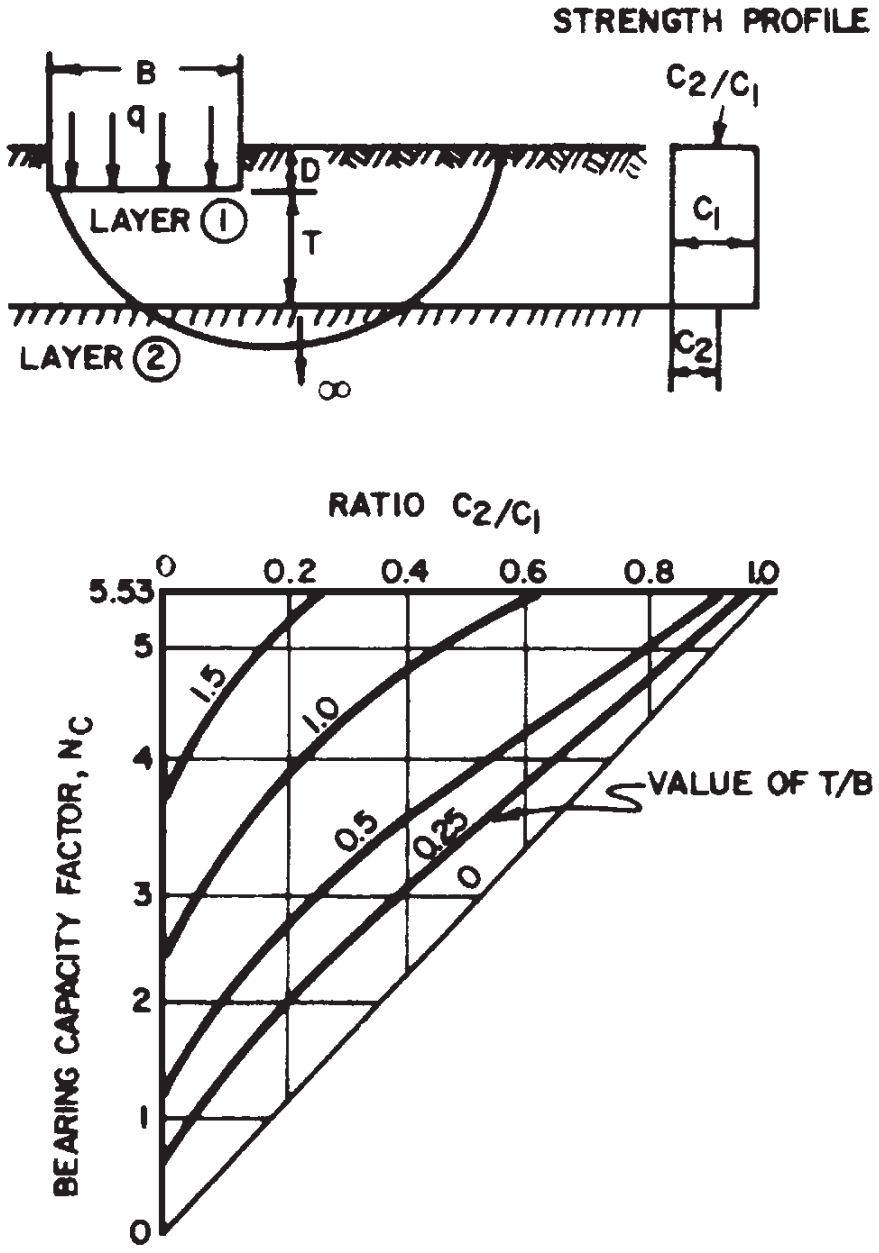

FIGURE 8.8 Bearing capacity factor N_c for two layer soil conditions. (*Reproduced from NAVFAC DM-7.2, 1982.*)

Layer 2 = lower soil layer that will liquefy during the design earthquake. The usual assumption is that the liquefied soil does not possess any shear strength, or $c_2 = 0$.

T = vertical distance from the bottom of the footing to top of the liquefied soil layer, ft or m

B = width of footing, ft or m

Since the liquefied soil layer (i.e., layer 2) has zero shear strength (that is, $c_2 = 0$), the ratio of c_2/c_1 will also be equal to zero. By entering Fig. 8.8 with $c_2/c_1 = 0$ and intersecting the desired *T*/*B* curve, the value of N_c can be determined. Using Fig. 8.8, values of N_c for different *T*/*B* ratios are as follows:

T/B	N_c	Percent reduction in N_c
0	0	100
0.25	0.7	87
0.50	1.3	76
1.00	2.5	55
1.50	3.8	31
∞	5.5	0

Example Problem for Cohesive Surface Layer. This example problem illustrates the use of Eq. (8.6). Use the data from the example problem in Sec. 8.2.2.

Solution. To calculate the factor of safety in terms of a bearing capacity failure for the strip and spread footings, the following values are used:

$P = 50$ kN/m for strip footing and 500 kN for spread footing

$T = 2.5$ m i.e., total thickness of unliquefiable soil layer minus footing embedment depth = 3 m − 0.5 m = 2.5 m

$c_1 = s_u = 50$ kPa $= 50$ kN/m^2 upper cohesive soil layer

$c_2 = 0$ kPa $= 0$ kN/m^2 liquefied soil layer

$B = 1$ m strip footing

$B = \mathrm{L} = 2$ m spread footing

$N_c = 5.5$ for strip footing, using Fig. 8.8 with $T/B = 2.5/1 = 2.5$ and $c_2/c_1 = 0$

$N_c = 3.2$ for spread footing, using Fig. 8.8 with $T/B = 2.5/2 = 1.25$ and $c_2/c_1 = 0$

Substituting the above values into Eqs. (8.6*a*) and (8.6*b*), gives

$$q_{\text{ult}} = cN_c = s_u N_c = (50 \text{ kN/m}^2)\,(5.5) = 275 \text{ kN/m}^2 \quad \text{for strip footing}$$

$$q_{\text{ult}} = s_u N_c \left(1 + 0.3\,\frac{B}{L}\right) = 1.3 s_u N_c = (1.3)\,(50 \text{ kN/m}^2)\,(3.2) = 208 \text{ kN/m}^2 \quad \text{for spread footing}$$

The ultimate load is calculated as follows:

$$Q_{\text{ult}} = q_{\text{ult}} B = (275 \text{ kN/m}^2)\,(1 \text{ m}) = 275 \text{ kN/m} \quad \text{for strip footing}$$

$$Q_{\text{ult}} = q_{\text{ult}} B^2 = (208 \text{ kN/m}^2)\,(2 \text{ m})^2 = 832 \text{ kN} \quad \text{for spread footing}$$

And finally the factor of safety is calculated as follows:

$$\text{FS} = \frac{Q_{\text{ult}}}{P} = \frac{275 \text{ kN/m}}{50 \text{ kN/m}} = 5.5 \quad \text{for strip footing}$$

$$\text{FS} = \frac{Q_{\text{ult}}}{P} = \frac{832 \text{ kN}}{500 \text{ kN}} = 1.7 \quad \text{for spread footing}$$

These values are similar to the values calculated in Sec. 8.2.2 (that is, FS = 5.0 for the strip footing and FS = 2.0 for the spread footing).

8.2.4 Deep Foundations

Deep foundations are used when the upper soil stratum is too soft, weak, or compressible to support the static and earthquake-induced foundation loads. Deep foundations are also used when there is a possibility of undermining of the foundation. For example, bridge piers are often founded on deep foundations to prevent a loss of support due to flood conditions which could cause river bottom scour. In addition, deep foundations are used when the expected settlement is excessive (Chap. 7), to prevent ground surface damage of the structure (Sec. 7.3), or to prevent a bearing capacity failure caused by the liquefaction of an underlying soil deposit.

Types of Deep Foundations. The most common types of deep foundations are piles and piers that support individual footings or mat foundations. Piles are defined as relatively long, slender, columnlike members often made of steel, concrete, or wood that are either driven into place or cast in place in predrilled holes. Common types of piles are as follows:

- *Batter pile:* This pile is driven in at an angle inclined to the vertical to provide high resistance to lateral loads. If the soil should liquefy during an earthquake, then the lateral resistance of the batter pile may be significantly reduced.
- *End-bearing pile:* The support capacity of this pile is derived principally from the resistance of the foundation material on which the pile tip rests. End-bearing piles are often used when a soft upper layer is underlain by a dense or hard stratum. If the upper soft layer should settle or liquefy during an earthquake, the pile could be subjected to downdrag forces, and the pile must be designed to resist these soil-induced forces.
- *Friction pile:* The support capacity of this pile is derived principally from the resistance of the soil friction and/or adhesion mobilized along the side of the pile. Friction piles are often used in soft clays where the end-bearing resistance is small because of punching shear at the pile tip. If the soil is susceptible to liquefaction during an earthquake, then both the frictional resistance and the lateral resistance of the pile may be lost during the earthquake.
- *Combined end-bearing and friction pile:* This pile derives its support capacity from combined end-bearing resistance developed at the pile tip and frictional and/or adhesion resistance on the pile perimeter.

A *pier* is defined as a deep foundation system, similar to a cast-in-place pile, that consists of a columnlike reinforced concrete member. Piers are often of large enough diameter to enable down-hole inspection. Piers are also commonly referred to as drilled shafts, bored piles, or drilled caissons.

There are many other methods available for forming deep foundation elements. Examples include earth stabilization columns, such as (NAVFAC DM-7.2, 1982):

- *Mixed-in-place piles:* A mixed-in-place soil-cement or soil-lime pile.
- *Vibroflotation-replacement stone columns:* Vibroflotation or another method is used to make a cylindrical, vertical hole which is filled with compacted open-graded gravel or crushed rock. The stone columns also have the additional capability of reducing the potential for soil liquefaction by allowing the earthquake-induced pore water pressures to rapidly dissipate as water flows into the highly permeable open-graded gravel or crushed rock.
- *Grouted stone columns:* These are similar to the above but include filling voids with bentonite-cement or water-sand-bentonite cement mixtures.
- *Concrete Vibroflotation columns:* These are similar to stone columns, but concrete is used instead of gravel.

Design Criteria. Several different items are used in the design and construction of piles:

1. *Engineering analysis:* Based on the results of engineering analysis, a deep foundation could be designed and constructed such that it penetrates all the soil layers that are expected to liquefy during the design earthquake. In this case, the deep foundation will derive support from the unliquefiable soil located below the potentially troublesome soil strata. However, the presence of down-drag loads as well as the loss of lateral resistance due to soil liquefaction must be considered in the engineering analysis.

If a liquefiable soil layer is located below the bottom of the deep foundation, then Sec. 8.2.2 could be used to analyze the possibility of the deep foundation's punching into the underlying liquefied soil layer. For end-bearing piles, the load applied to the pile cap can be assumed to be transferred to the pile tips. Then based on the shear strength of the unliquefiable soil below the bottom of the piles as well as the vertical distance from the pile tip to the liquefiable soil layer, the factor of safety can be calculated using Eq. (8.1*b*). Note that B and L in Eq. (8.1*b*) represent the width and length, respectively, of the pile group.

2. *Field load tests:* Prior to the construction of the foundation, a pile or pier could be load-tested in the field to determine its carrying capacity. Because of the uncertainties in the design of piles based on engineering analyses, pile load tests are common. The pile load test can often result in a more economical foundation then one based solely on engineering analyses. Pile load tests can even be performed to evaluate dynamic loading conditions. For example, ASTM provides guidelines on the dynamic testing of piles (for example, D 4945-96, "Standard Test Method for High-Strain Dynamic Testing of Piles" 2000). In this test method, ASTM states:

> This test method is used to provide data on strain or force and acceleration, velocity or displacement of a pile under impact force. The data are used to estimate the bearing capacity and the integrity of the pile, as well as hammer performance, pile stresses, and soil dynamics characteristics, such as soil damping coefficients and quake values.

A limitation of field load tests is that they cannot simulate the response of the pile for those situations where the soil is expected to liquefy during the design earthquake. Thus the results of the pile load tests would have to be modified for the expected liquefaction conditions.

3. *Application of pile driving resistance:* In the past, the pile capacity was estimated based on the driving resistance during the installation of the pile. Pile driving equations, such as the *Engineering News formula* (Wellington 1888), were developed that related the pile capacity to the energy of the pile driving hammer and the average net penetration of the pile per blow of the pile hammer. But studies have shown that there is no satisfactory relationship between the pile capacity from pile driving equations and the pile capacity measured from load tests. Based on these studies, it has been concluded that use of pile driving equations is no longer justified (Terzaghi and Peck 1967).

Especially for high displacement piles that are closely spaced, the vibrations and soil displacement associated with driving the piles will densify granular soil. Thus the liquefaction resistance of the soil is often increased due the pile driving (see compaction piles in Sec. 12.3.3).

4. *Specifications and experience:* Other factors that should be considered in the deep foundation design include the governing building code or agency requirements and local experience. Local experience, such as the performance of deep foundations during prior earthquakes, can be a very important factor in the design and construction of pile foundations.

The use of pile foundations is discussed further in Chap. 13.

8.2.5 Other Design Considerations

There are many other possible considerations in the determination of the bearing capacity of soil that will liquefy during the design earthquake. Some important items are as follows:

Determination of T. An essential part of the bearing capacity analysis is the determination of *T,* which is the distance from the bottom of the footing to the top of the liquefied soil layer. This distance may be easy to determine if the upper unliquefiable soil layer is a cohesive soil, such as a fat clay.

It is much more difficult to determine *T* for soil that is below the groundwater table and has a factor of safety against liquefaction that is slightly greater than 1.0. This is because if a lower layer liquefies, an upward flow of water could induce liquefaction of the layer that has a factor of safety slightly greater than 1.0. In addition, the shear stress induced on the soil by the foundation can actually reduce the liquefaction resistance of loose soil (see Sec. 9.4.2). Because of these effects, considerable experience and judgment are required in the determination of *T.*

Lateral Loads. In addition to the vertical load acting on the footing, it may also be subjected to both static and dynamic lateral loads. A common procedure is to treat lateral loads separately and resist the lateral loads by using the soil pressure acting on the sides of the footing (passive pressure) and by using the frictional resistance along the bottom of the footing.

Moments and Eccentric Loads. It is always desirable to design and construct shallow footings so that the vertical load is applied at the center of gravity of the footing. For combined footings that carry more than one vertical load, the combined footing should be designed and constructed so that the vertical loads are symmetric. For earthquake loading, the footing is often subjected to a moment. This moment can be represented by a load *P* that is offset a certain distance (known as the *eccentricity*) from the center of gravity of the footing.

There are many different methods to evaluate eccentrically loaded footings. Because an eccentrically loaded footing will create a higher bearing pressure under one side than under the opposite side, one approach is to evaluate the actual pressure distribution beneath the footing. The usual procedure is to assume a rigid footing (hence linear pressure distribution) and use the section modulus ($\frac{1}{6} B^2$) in order to calculate the largest and smallest bearing pressures. For a footing having a width *B,* the largest q' and smallest q'' bearing pressures are as follows:

$$q' = \frac{Q\,(B + 6e)}{B^2} \tag{8.7a}$$

$$q'' = \frac{Q\,(B - 6e)}{B^2} \tag{8.7b}$$

where q' = largest bearing pressure underneath footing, which is located along the same side of footing as the eccentricity, kPa or lb/ft^2

q'' = smallest bearing pressure underneath footing, which is located at the opposite side of footing, kPa or lb/ft^2

$Q = P$ = footing load, lb/ft or kN/m. For both strip footings and spread footings, Q is the load per unit length of footing. Footing load includes dead, live, and seismic loads acting on the footing as well as the weight of the footing itself. Typically the value of Q would be provided by the structural engineer.

e = eccentricity of the load Q, that is, the lateral distance from Q to the center of gravity of footing, m or ft
B = width of footing, m or ft

A usual requirement is that the load Q be located within the middle one-third of the footing, and the above equations are valid only for this condition. The value of q' must not exceed the allowable bearing pressure q_{all}.

Figure 8.9 presents another approach for footings subjected to moments. As indicated in Fig. 8.9*a,* the moment M is converted to a load Q that is offset from the center of gravity of the footing by an eccentricity e. This approach is identical to the procedure outlined for Eq. (8.7).

The next step is to calculate a reduced area of the footing. As indicated in Fig. 8.9*b,* the new footing dimensions are calculated as $L' = L - 2e_1$ and $B' = B - 2e_2$. A reduction in footing dimensions in both directions would be applicable only for the case where the footing is subjected to two moments, one moment in the long direction of the footing (hence e_1) and the other moment across the footing (hence e_2). If the footing is subjected to only one moment in either the long or short direction of the footing, then the footing is reduced in only one direction. Similar to Eq. (8.7), this method should be utilized only if the load Q is located within the middle one-third of the footing.

Once the new dimensions L' and B' of the footing have been calculated, the procedure outlined in Sec. 8.2.3 is used by substituting L' for L and B' for B.

Sloping Ground Conditions. Although methods have been developed to determine the allowable bearing capacity of foundations at the top of slopes (e.g., NAVFAC DM-7.2, 1982, page 7.2-135), these methods should be used with caution when dealing with earthquake analyses of soil that will liquefy during the design earthquake. This is because, as shown in Sec. 3.4, the site could be impacted by liquefaction-induced lateral spreading and flow slides. Even if the general vicinity of the site is relatively level, the effect of liquefaction on adjacent slopes or retaining walls must be included in the analysis. For example, Fig. 8.10 shows an example of a warehouse that experienced 2 m of settlement due to lateral movement of a quay wall caused by the liquefaction of a sand layer. If the site consists of sloping ground or if there is a retaining wall adjacent to the site, then in addition to a bearing capacity analysis, a slope stability analysis (Chap. 9) or a retaining wall analysis (Chap. 10) should also be performed.

Inclined Base of Footing. Charts have been developed to determine the bearing capacity factors for footings having inclined bottoms. However, it has been stated that inclined bases should never be constructed for footings (AASHTO 1996). During the earthquake, the inclined footing could translate laterally along the sloping soil or rock contact. If a sloping contact of underlying hard material will be encountered during the excavation of the footing, then the hard material should be excavated in order to construct a level footing that is entirely founded within the hard material.

8.2.6 Example Problem

This example problem for cohesive surface layer illustrates the use of Eq. (8.7) and Fig. 8.9. Use the data from the example problem in Sec. 8.2.2. Assume that in addition to the vertical loads, the strip footing and spread footing will experience an earthquake-induced moment equal to 5 kN·m/m and 150 kN·m, respectively. Furthermore, assume that these moments act in a single direction (i.e., in the B direction).

(A) EQUIVALENT LOADINGS

Resultant force acts at the centroid of the reduced area.

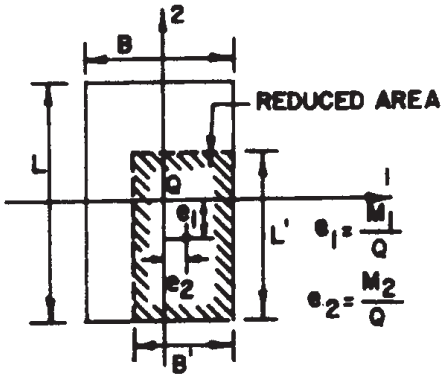

(B) REDUCED AREA-RECTANGULAR FOOTING

For rectangular footings reduce dimension as follows:

$$L' = L - 2e_1 \qquad e_1 = \frac{M_1}{Q}$$

$$B' = B - 2e_2 \qquad e_2 = \frac{M_2}{Q}$$

FIGURE 8.9 Reduced-area method for a footing subjected to a moment. (*Reproduced from NAVFAC DM-7.2, 1982.*)

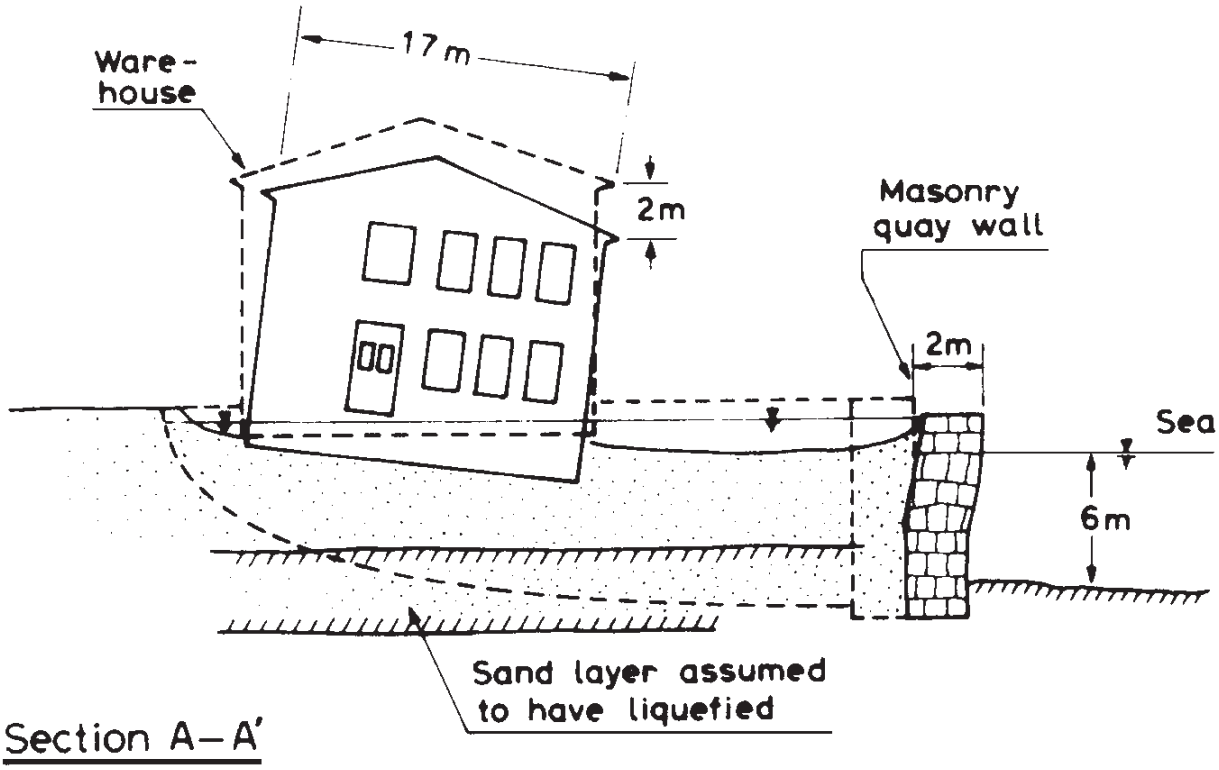

FIGURE 8.10 Damage to a warehouse due to lateral movement of a quay wall in Zelenica. The liquefaction of the sand layer was caused by the Monte Negro earthquake on April 15, 1979. (*Reproduced from Ishihara 1985.*)

Solution for Strip Footing Using Eq. (8.7). To calculate the factor of safety in terms of a bearing capacity failure for the strip footing, the following values are used:

$Q = P = 50$ kN/m for strip footing

$$e = \frac{M}{Q} = \frac{5 \text{ kN} \cdot \text{m/m}}{50 \text{ kN/m}} = 0.10 \text{ m}$$ for middle one-third of footing, e cannot exceed 0.17 m, and therefore e is within middle one-third of footing

$$q' = \frac{Q(B + 6e)}{B^2} = \frac{50\,[1 + (6)\,(0.1)]}{1^2} = 80 \text{ kN/m}^2$$ [Eq. (8.7)]

$T = 2.5$ m i.e., total thickness of unliquefiable soil layer minus footing embedment depth = 3 m − 0.5 m = 2.5 m

$c_1 = s_u = 50$ kPa $= 50$ kN/m^2 upper cohesive soil layer

$c_2 = 0$ kPa $= 0$ kN/m^2 liquefied soil layer

$B = 1$ m

$N_c = 5.5$ using Fig. 8.8 with T/B = 2.5/1.0 = 2.5 and $c_2/c_1 = 0$

Using the Terzaghi bearing capacity equation to calculate q_{ult} yields

$$q_{ult} = cN_c = s_u N_c = (50 \text{ kN/m}^2)\,(5.5) = 275 \text{ kN/m}^2 \qquad \text{[Eq. (8.6}a\text{)]}$$

And finally the factor of safety is calculated as follows:

$$\text{FS} = \frac{q_{ult}}{q'} = \frac{275 \text{ kN/m}^2}{80 \text{ kN/m}^2} = 3.4$$

Solution for Strip Footing Using Fig. 8.9. To calculate the factor of safety in terms of a bearing capacity failure for the strip footing, the following values are used:

$Q = P = 50$ kN/m for strip footing

$e = \dfrac{M}{Q} = \dfrac{5 \text{ kN} \cdot \text{m/m}}{50 \text{ kN/m}} = 0.10$ m for middle one-third of footing, e cannot exceed 0.17 m, and therefore e is within middle one-third of footing

$B' = B - 2e = 1 - 2\,(0.10) = 0.8$ m Fig. 8.9

$T = 2.5$ m i.e., total thickness of unliquefiable soil layer minus footing embedment depth = 3 m − 0.5 m = 2.5 m

$c_1 = s_u = 50$ kPa $= 50$ kN/m^2 upper cohesive soil layer

$c_2 = 0$ kPa $= 0$ kN/m^2 liquefied soil layer

$N_c = 5.5$ using Fig. 8.8 with $T/B = 2.5/1.0 = 2.5$ and $c_2/c_1 = 0$

Using the Terzaghi bearing capacity equation to calculate q_{ult} gives

$$q_{ult} = cN_c = s_u N_c = (50 \text{ kN/m}^2)\,(5.5) = 275 \text{ kN/m}^2 \qquad \text{[Eq. (8.6}a\text{)]}$$

$$Q_{ult} = q_{ult} B' = (275 \text{ kN/m}^2)\,(0.8 \text{ m}) = 220 \text{ kN/m}$$

And finally the factor of safety is calculated as follows:

$$\text{FS} = \frac{Q_{ult}}{Q} = \frac{220 \text{ kN/m}}{50 \text{ kN/m}} = 4.4$$

Solution for Spread Footing Using Eq. (8.7). To calculate the factor of safety in terms of a bearing capacity failure for the spread footing, the following values are used:

$Q = P = 500$ kN for spread footing

$e = \dfrac{M}{Q} = \dfrac{150 \text{ kN} \cdot \text{m}}{500 \text{ kN}} = 0.30$ m for middle one-third of footing, e cannot exceed 0.33 m, and therefore e is within middle one-third of footing

Converting Q to a load per unit length of the footing yields

$$Q = \frac{500 \text{ kN}}{2 \text{ m}} = 250 \text{ kN/m}$$

$$q' = \frac{Q\,(B + 6e)}{B^2} = \frac{250\,[2 + (6)\,(0.3)]}{2^2} = 238 \text{ kN/m}^2 \qquad \text{[Eq. (8.7)]}$$

$T = 2.5$ m i.e., total thickness of unliquefiable soil layer minus footing embedment depth = 3 m − 0.5 m = 2.5 m

$c_1 = s_u = 50$ kPa $= 50$ kN/m^2 upper cohesive soil layer

$c_2 = 0$ kPa $= 0$ kN/m^2 liquefied soil layer

$B = 2$ m

$N_c = 3.2$ for spread footing, using Fig. 8.8 with $T/B = 2.5/2 = 1.25$ and $c_2/c_1 = 0$

Using the Terzaghi bearing capacity equation to calculate q_{ult} results in

$$q_{ult} = s_u N_c \left(1 + 0.3\,\frac{B}{L}\right) = 1.3\,s_u N_c = (1.3)\,(50 \text{ kN/m}^2)\,(3.2) = 208 \text{ kN/m}^2$$

And finally the factor of safety is calculated as follows:

$$\text{FS} = \frac{q_{ult}}{q'} = \frac{208 \text{ kN/m}^2}{238 \text{ kN/m}^2} = 0.87$$

Solution for Spread Footing Using Fig. 8.9. To calculate the factor of safety in terms of a bearing capacity failure for the spread footing, the following values are used:

$Q = P = 500$ kN for spread footing

$e = \dfrac{M}{Q} = \dfrac{150 \text{ kN} \cdot \text{m}}{500 \text{ kN}} = 0.30$ m for middle one-third of footing, e cannot exceed 0.33 m, and therefore e is within middle one-third of footing

$B' = B - 2e = 2 - 2\,(0.30) = 1.4$ m Fig. 8.9

$L' = L = 2$ m moment only in B direction of footing

$T = 2.5$ m i.e., total thickness of unliquefiable soil layer minus footing embedment depth = 3 m − 0.5 m = 2.5 m

$c_1 = s_u = 50$ kPa $= 50$ kN/m^2 upper cohesive soil layer

$c_2 = 0$ kPa $= 0$ kN/m^2 liquefied soil layer

$N_c = 3.2$ for spread footing, using Fig. 8.8 with $T/B = 2.5/2 = 1.25$ and $c_2/c_1 = 0$

Using the Terzaghi bearing capacity equation to calculate q_{ult} gives

$$q_{ult} = s_u N_c \left(1 + 0.3\,\frac{B'}{L'}\right) = 1.2\,s_u N_c = (1.2)\,(50 \text{ kN/m}^2)\,(3.2) = 190 \text{ kN/m}^2$$

$$Q_{ult} = q_{ult} B' L' = (190 \text{ kN/m}^2)\,(1.4 \text{ m})\,(2 \text{ m}) = 530 \text{ kN}$$

And finally the factor of safety is calculated as follows:

$$\text{FS} = \frac{Q_{\text{ult}}}{Q} = \frac{530\ \text{kN}}{500\ \text{kN}} = 1.06$$

In summary, the factors of the safety factor in terms of a bearing capacity failure for the strip and spread footings are as follows:

Method	Factor of safety	
	Strip footing	Spread footing
Using Eq. (8.7*a*)	3.4	0.87
Using Fig. 8.9	4.4	1.06
No moment (i.e., values from Sec. 8.2.3)	5.5	1.7

8.3 GRANULAR SOIL WITH EARTHQUAKE-INDUCED PORE WATER PRESSURES

8.3.1 Introduction

Section 8.2 deals with soil that is weakened during the earthquake due to liquefaction. This section deals with granular soil that does not liquefy; rather, there is a reduction in shear strength due to an increase in pore water pressure. Examples include sands and gravels that are below the groundwater table and have a factor of safety against liquefaction that is greater than 1.0 but less than 2.0. If the factor of safety against liquefaction is greater than 2.0, the earthquake-induced excess pore water pressures will typically be small enough that their effect can be neglected.

8.3.2 Bearing Capacity Equation

Using the Terzaghi bearing capacity equation and an effective stress analysis, and recognizing that sands and gravels are cohesionless (that is, $c' = 0$), we see that Eq. (8.3) reduces to the following:

$$q_{\text{ult}} = \tfrac{1}{2}\gamma_t B N_\gamma + \gamma_t D_f N_q \tag{8.8}$$

For shallow foundations, it is best to neglect the second term ($\gamma_t D_f N_q$) in Eq. 8.8. This is because this term represents the resistance of the soil located above the bottom of the footing, which may not be mobilized for a punching shear failure into the underlying weakened granular soil layer. Thus by neglecting the second term in Eq. (8.8):

$$q_{\text{ult}} = \tfrac{1}{2}\gamma_t B N_\gamma \tag{8.9}$$

Assuming that the location of groundwater table is close to the bottom of the footing, the buoyant unit weight γ_b is used in place of the total unit weight γ_t in Eq. (8.9). In addition, since this is an effective stress analysis, the increase in excess pore water pressures that are generated during the design earthquake must be accounted for in Eq. (8.9). Using Fig. 5.15 can accomplish this, which is a plot of the pore water pressure ratio $r_u = u_e/\sigma'$ versus the factor of safety against liquefaction (Chap. 6). Using the buoyant unit weight γ_b in

place of the total unit weight γ_t and inserting the term $1 - r_u$ to account for the effect of the excess pore water pressures generated by the design earthquake, we get the final result for the ultimate bearing capacity q_{ult} as follows:
For strip footings,

$$q_{ult} = \tfrac{1}{2} (1 - r_u)\, \gamma_b B N_\gamma \tag{8.10a}$$

For spread footings based on Eq. (8.4),

$$q_{ult} = 0.4 (1 - r_u)\, \gamma_b B N_\gamma \tag{8.10b}$$

where r_u = pore water pressure ratio from Fig. 5.15 (dimensionless). To determine r_u, the factor of safety against liquefaction of soil located below the bottom of the footing must be determined (see Chap. 6). As previously mentioned, Eq. (8.10) is valid only if the factor of safety against liquefaction is greater than 1.0. When factor of safety against liquefaction is greater than 2.0, Terzaghi bearing capacity equation can be utilized, taking into account the location of groundwater table (see section 8.2.1 of Day 1999).

γ_b = buoyant unit weight of soil below footing, lb/ft^3 or kN/m^3. As previously mentioned, Eq. (8.10) was developed based on an assumption that the groundwater table is located near the bottom of footing or it is anticipated that the groundwater table could rise so that it is near the bottom of the footing.

B = width of footing, ft or m

N_γ = bearing capacity factor (dimensionless). Figure 8.11 presents a chart that can be used to determine the value of N_γ based on the effective friction angle ϕ' of the granular soil.

8.3.3 Example Problem

This example problem illustrates the use of Eq. (8.10). A site consists of a sand deposit with a fluctuating groundwater table. The proposed development will consist of buildings having shallow strip footings to support bearing walls and interior spread footings to support isolated columns. The expected depth of the footings will be 0.5 to 1.0 m. Assume that the groundwater table could periodically rise to a level that is close to the bottom of the footings. Also assume the following parameters: buoyant unit weight of the sand is 9.7 kN/m^3, the sand below the groundwater table has a factor of safety against liquefaction of 1.3, the effective friction angle of the sand $\phi' = 32°$, and the footings will have a minimum width of 1.5 and 2.5 m for the strip and spread footings, respectively. Using a factor of safety of 5, determine the allowable bearing capacity of the footings.

Solution. We use the following values:

$\gamma_b = 9.7$ kN/m^3

$N_\gamma = 21$ entering Fig. 8.11 with $\phi' = 32°$ and intersecting N_γ curve, the value of N_γ from the vertical axis is 21

$B = 1.5$ m for strip footings and 2.5 m for spread footings

$r_u = 0.20$ entering Fig. 5.15 with a factor of safety against liquefaction of 1.3,

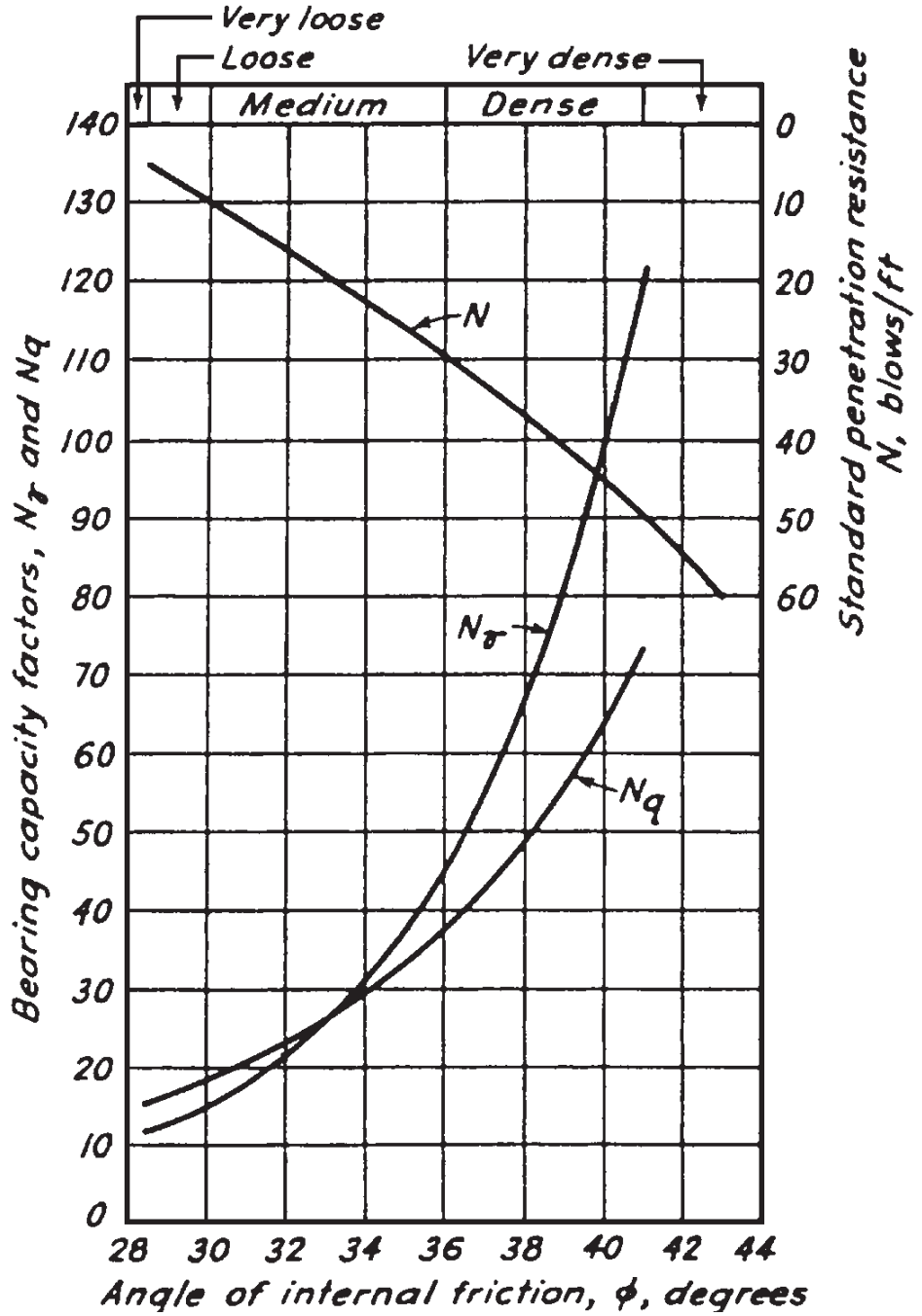

FIGURE 8.11 Bearing capacity factors N_γ and N_q, which automatically incorporate allowance for punching and local shear failure. The standard penetration resistance N value indicated in this chart refers to the uncorrected N value. (*From Peck et al. 1974; reproduced with permission of John Wiley & Sons.*)

value of r_u for sand varies from 0.05 to 0.35. Using an average value, $r_u = 0.20$.

Inserting the above values into Eq. (8.10) yields
For the strip footings:

$$q_{\text{ult}} = \tfrac{1}{2}\,(1 - r_u)\,\gamma_b B N_\gamma = \tfrac{1}{2}\,(1 - 0.20)\,(9.7\ \text{kN/m}^3)\,(1.5\ \text{m})\,(21) = 120\ \text{kPa}$$

And using a factor of safety of 5.0 gives

$$q_{all} = \frac{q_{ult}}{FS} = \frac{120 \text{ kPa}}{5.0} = 24 \text{ kPa}$$

For the spread footings:

$$q_{ult} = 0.4\,(1 - r_u)\,\gamma_b B N_\gamma = 0.4\,(1 - 0.20)\,(9.7 \text{ kN/m}^3)\,(2.5 \text{ m})\,(21) = 160 \text{ kPa}$$

And using a factor of safety of 5.0 gives

$$q_{all} = \frac{q_{ult}}{FS} = \frac{160 \text{ kPa}}{5.0} = 32 \text{ kPa}$$

Thus provided the strip and spread footings are at least 1.5 and 2.5 m wide, respectively, the allowable bearing capacity is equal to 24 kPa for the strip footings and 32 kPa for the spread footings. These allowable bearing pressures would be used to determine the size of the footings based on the anticipated dead, live, and seismic loads.

8.4 BEARING CAPACITY ANALYSIS FOR COHESIVE SOIL WEAKENED BY THE EARTHQUAKE

8.4.1 Introduction

As discussed in Sec. 5.5.1, cohesive soils and organic soils can also be susceptible to a loss of shear strength during the earthquake. Examples include sensitive clays, which lose shear strength when they are strained back and forth. In dealing with such soils, it is often desirable to limit the stress exerted by the footing during the earthquake so that it is less than the maximum past pressure σ'_{vm} of the cohesive or organic soils. This is to prevent the soil from squeezing out or deforming laterally from underneath the footing.

8.4.2 Bearing Capacity Equation

As mentioned in Sec. 7.5, it is often very difficult to predict the amount of earthquake-induced settlement for foundations bearing on cohesive and organic soils. One approach is to ensure that the foundation has an adequate factor of safety in terms of a bearing capacity failure. To perform a bearing capacity analysis, a total stress analysis can be performed by assuming that $c = s_u$. Using Eq. (8.6), and for a relatively constant undrained shear strength versus depth below the footing, the ultimate bearing capacity is as follows:
For strip footings:

$$q_{ult} = cN_c = 5.5 s_u \tag{8.11a}$$

For spread footings:

$$q_{ult} = cN_c \left(1 + 0.3\,\frac{B}{L}\right) = 5.5 s_u \left(1 + 0.3\,\frac{B}{L}\right) \tag{8.11b}$$

For a given footing size, the only unknown in Eq. (8.11) is the undrained shear strength s_u. Table 5.4 presents guidelines in terms of the undrained shear strength that should be uti-

lized for earthquake engineering analyses. These guidelines for the selection of the undrained shear strength s_u as applied to bearing capacity analyses are as follows:

1. *Cohesive soil above the groundwater table:* Often the cohesive soil above the groundwater table will have negative pore water pressures due to capillary tension of the pore water fluid. In some cases, the cohesive soil may even be dry and desiccated. The capillary tension tends to hold together the soil particles and to provide additional shear strength to the soil. For the total stress analysis, the undrained shear strength s_u of the cohesive soil could be determined from unconfined compression tests or vane shear tests.

Because of the negative pore water pressures, a future increase in water content would tend to decrease the undrained shear strength s_u of partially saturated cohesive soil above the groundwater table. Thus a possible change in water content in the future should be considered. In addition, an unconfined compression test performed on a partially saturated cohesive soil often has a stress-strain curve that exhibits a peak shear strength which then reduces to an ultimate value. If there is a significant drop-off in shear strength with strain, it may be prudent to use the ultimate value in the bearing capacity analysis.

2. *Cohesive soil below the groundwater table having low sensitivity:* The *sensitivity* S_t of a cohesive soil is defined as the undrained shear strength of an undisturbed soil specimen divided by the undrained shear strength of a completely remolded soil specimen. The sensitivity thus represents the loss of undrained shear strength as a cohesive soil specimen is remolded. An earthquake also tends to shear a cohesive soil back and forth, much as the remolding process does. For cohesive soil having low sensitivity ($S_t \leq 4$), the reduction in the undrained shear strength during the earthquake should be small. Thus the undrained shear strength from the unconfined compression test or vane shear tests could be used in the bearing capacity analysis (for field vane tests, consider a possible reduction in shear strength due to strain rate and anisotropy effects, see Table 7.13 in Day 2000).

3. *Cohesive soil below the groundwater table having a high sensitivity:* For highly sensitive and quick clays ($S_t > 8$), the earthquake-induced ground shaking will tend to shear the soil back and forth, much as the remolding process does. For these types of soils, there could be a significant shear strength loss during the earthquake shaking.

The stress-strain curve from an unconfined compression test performed on a highly sensitive or quick clay often exhibits a peak shear strength that develops at a low vertical strain, followed by a dramatic drop-off in strength with continued straining of the soil specimen. An example of this type of stress-strain curve is shown in Fig. 8.12. The analysis will need to include the estimated reduction in undrained shear strength due to the earthquake shaking. In general, the most critical conditions exist when the highly sensitive or quick clay is subjected to a high static shear stress (such as the high bearing pressure acting on the soil). If, during the earthquake, the sum of the static shear stress and the seismic induced shear stress exceeds the undrained shear strength of the soil, then a significant reduction in shear strength is expected to occur.

Cohesive soils having a medium sensitivity ($4 < S_t \leq 8$) tend to be an intermediate case.

Some of the other factors that may need to be considered in the bearing capacity analysis are as follows:

1. *Earthquake parameters:* The nature of the design earthquake, such as the peak ground acceleration a_{max} and earthquake magnitude, is a factor. The higher the peak ground acceleration and the higher the magnitude of the earthquake, the greater the tendency for the cohesive soil to be strained and remolded by the earthquake shaking.

2. *Soil behavior:* As mentioned above, the important soil properties for the bearing

capacity analysis are the undrained shear strength s_u, sensitivity S_t, maximum past pressure σ'_{vm}, and the stress-strain behavior of the soil (e.g., Fig. 8.12).

3. *Rocking:* The increase in shear stress caused by the dynamic loads acting on the foundation must be considered in the analysis. Lightly loaded foundations tend to produce the smallest dynamic loads, while heavy and tall buildings subject the foundation to high dynamic loads due to rocking.

Given the many variables as outlined above, it takes considerable experience and judgment in the selection of the undrained shear strength s_u to be used in Eq. (8.11).

8.4.3 Example Problem

This example problem illustrates the use of Eq. (8.13). Assume that a site has a subsoil profile shown in Fig. 8.13. Suppose that a tall building will be constructed at the site. In addition, during the life of the structure, it is anticipated that the building will be subjected to significant earthquake-induced ground shaking.

Because of the desirability of underground parking, a mat foundation will be constructed such that the bottom of the mat is located at a depth of 20 ft (6 m) below ground surface. Assuming that the mat foundation will be 100 ft long and 100 ft wide (30 m by 30 m), determine the allowable bearing pressure that the mat foundation can exert on the underlying clay layer. Further assume that the clay below the bottom of the mat will not be disturbed (i.e., lose shear strength) during construction of the foundation.

Solution. Based on the sensitivity values S_t listed in Fig. 8.11, this clay would be classified as a quick clay. The analysis has been divided into two parts.

Part A. To prevent the soil from being squeezed out or deforming laterally from underneath the foundation due to rocking of the structure during the earthquake, the allowable bearing pressure should not exceed the maximum past pressure (also known as the preconsolidation stress). Recognizing that the building pressure will decrease with depth, the critical condition is just below the bottom of the foundation (i.e., depth = 20 ft). At a depth of 20 ft (6 m), the preconsolidation stress is about 1.2 kg/cm^2 (2500 lb/ft^2), and it increases with depth. Thus the allowable bearing pressure should not exceed 120 kPa (2500 lb/ft^2).

Part B. The next step is to consider a bearing capacity failure. As indicated in Fig. 8.13, the average undrained shear strength s_u from field vane shear tests below a depth of 20 ft (6 m) is about 0.6 kg/cm^2 (1200 lb/ft^2). Field vane shear tests tend to overestimate the undrained shear strength because of the fast strain rate and anisotropy effects, and thus a correction should be applied. Using Bjerrum's (1972) recommended correction (see Fig. 7.19 of Day 2000), the correction factor = 0.85 for a plasticity index = 40 (the plasticity index is from Fig. 8.13, where the liquid limit w_l is about 65 and the plastic limit w_p is about 25). Thus the corrected undrained shear strength is equal to 0.6 kg/cm^2 times 0.85, or s_u = 0.5 kg/cm^2 (50 kPa).

Using Eq. (8.11*b*) gives

$$q_{\text{ult}} = 5.5 s_u \left(1 + 0.3 \frac{B}{L}\right) = 7.1 s_u = (7.1)\,(50 \text{ kPa}) = 350 \text{ kPa}$$

Using a factor of safety of 5.0 to account for the possibility of a loss of shear strength during the earthquake yields

$$q_{\text{all}} = \frac{q_{\text{ult}}}{\text{FS}} = \frac{350 \text{ kPa}}{5.0} = 70 \text{ kPa or } 1400 \text{ lb/ft}^2$$

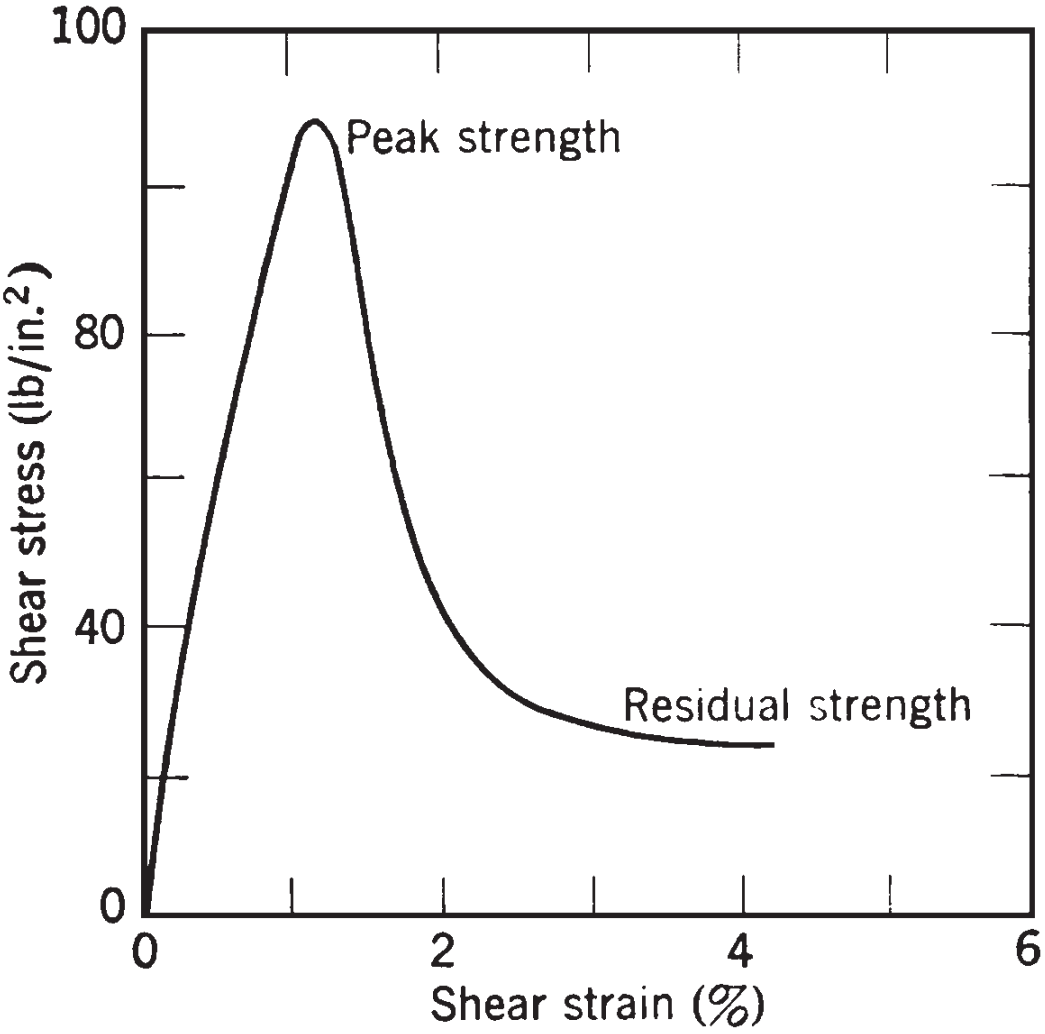

FIGURE 8.12 Stress-strain curve from a shear strength test performed on Cucaracha clay. (*From Lambe and Whitman 1969, reprinted with permission of John Wiley & Sons*)

This allowable bearing pressure does not include any factor to account for the depth of the footing below the ground surface. Usually with shallow foundations, the depth effect is small and could be neglected. However, in this case the bottom of the foundation will be at a depth of 20 ft (6 m). As indicated in Fig. 8.13, the existing vertical effective stress at this depth is equal to 0.5 kg/cm^2 (50 kPa). Thus the allowable pressure that the foundation can exert on the soil is equal to 70 kPa plus 50 kPa, or 120 kPa (2500 lb/ft^2), which is equal to the maximum value calculated from part A.

In summary, the allowable bearing pressure is 120 kPa (2500 lb/ft^2). This allowable bearing pressure is the maximum pressure that the foundation can exert on the soil for the condition of a mat foundation located at a depth below ground surface of 20 ft (6 m). Note that the foundation pressure calculated from the structural dead, live, and seismic loads, as well as any eccentricity of loads caused by rocking of the structure during the earthquake, should not exceed this allowable bearing value.

8.5 REPORT PREPARATION

Based on the results of the settlement analysis (Chap. 7) and the bearing capacity analysis (Chap. 8) for both the static and dynamic conditions, the geotechnical engineer would typ-

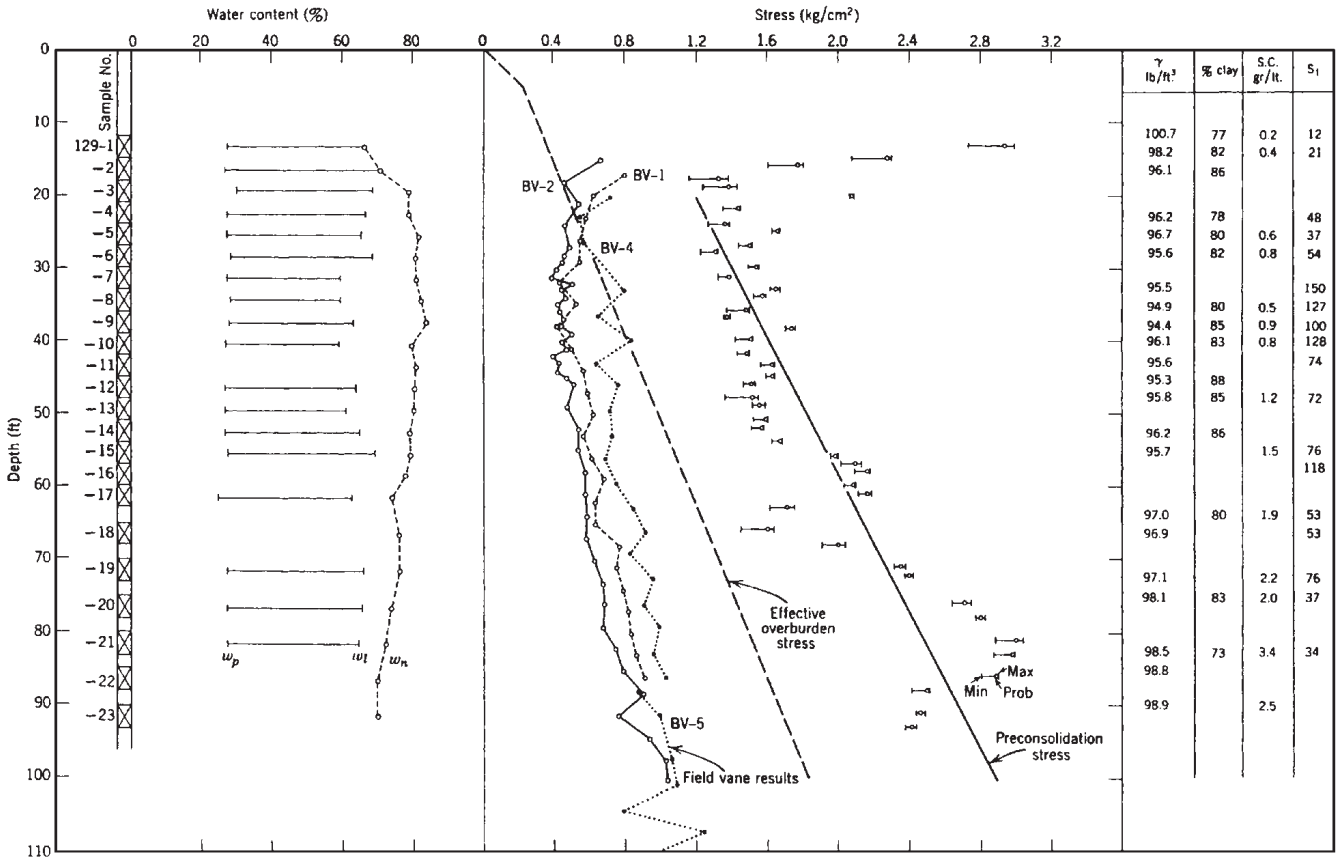

FIGURE 8.13 Subsoil profile, Canadian clay. (*From Lambe and Whitman 1969, reprinted with permission of John Wiley & Sons*)

ically provide design recommendations such as the minimum footing dimensions, embedment requirements, and allowable bearing capacity values. These recommendations would normally be included in a soils report. Appendix D presents an example of a geotechnical engineering report.

An example of typical wording for a bearing material that is not expected to be weakened by the earthquake is as follows:

> The subject site consists of intact Mission Valley formation (siltstone and sandstone) bedrock. For the static design condition, the allowable bearing pressure for spread footings is 8000 lb/ft^2 (400 kPa) provided that the footing is at least 5 ft (1.5 m) wide with a minimum of 2-ft (0.6-m) embedment in firm, intact bedrock. For continuous wall footings, the allowable bearing pressure is 4000 lb/ft^2 (200 kPa) provided the footing is at least 2 ft (0.6 m) wide with a minimum of 2-ft (0.6-m) embedment in firm, intact bedrock. It is recommended that the structures be entirely supported by bedrock.
>
> Because of cut-fill transition conditions, it is anticipated that piers will be needed for the administrative building. Belled piers can be designed for an allowable end-bearing pressure of 12,000 lb/ft^2 (600 kPa) provided that the piers have a diameter of at least 2 ft (0.6 m), length of at least 10 ft (3 m), with a minimum embedment of 3 ft (0.9 m) in firm, intact bedrock. It is recommended that the geotechnical engineer observe pier installation to confirm embedment requirements.
>
> In designing to resist lateral loads, passive resistance of 1200 lb/ft^2 per foot of depth (200 kPa per meter of depth) to a maximum value of 6000 lb/ft^2 per foot of depth (900 kPa per meter of depth) and a coefficient of friction equal to 0.35 may be utilized for embedment within firm bedrock.
>
> For the analysis of earthquake loading, the above values of allowable bearing pressure and passive resistance may be increased by a factor of one-third. This material is not expected to be weakened by the earthquake-induced ground motion.

An example of typical wording for a bearing material that is expected to be weakened by the earthquake is as follows:

> The subject site consists of a 10-ft-thick upper layer of cohesive soil that is underlain by a 15-ft-thick layer of submerged loose sand. Based on our analysis, it is anticipated that the 15-ft-thick sand layer will liquefy during the design earthquake. Since the site is essentially level, lateral movement due to a liquefaction-induced flow failure or lateral spreading is not anticipated to occur. In addition, the upper 10-ft-thick clay layer should be adequate to prevent liquefaction-induced ground damage (i.e., sand boils, surface fissuring, etc.).
>
> It is our recommendation that the lightly loaded structures be supported by the 10-ft-thick upper cohesive soil layer. For the design condition of lightly loaded shallow foundations, the allowable bearing pressure is 1000 lb/ft^2 (50 kPa). It is recommended that the shallow footings be embedded at a depth of 1 ft (0.3 m) below ground surface and be at least 1 ft (0.3 m) wide.
>
> It is anticipated that piles or piers will be needed for the heavily loaded industrial building. The piles or piers should be founded in the unliquefiable soil stratum which is located at a depth of 25 ft. The piles or piers can be designed for an allowable end-bearing pressure of 4000 lb/ft^2 (200 kPa), provided that the piles or piers have a diameter of at least 1 ft (0.3 m) and are embedded at least 5 ft (1.5 m) into the unliquefiable soil strata. It is recommended that the geotechnical engineer observe pile and pier installation to confirm embedment requirements. The piles or piers should also be designed for down-drag loads during the anticipated earthquake-induced liquefaction of the loose sand layer.
>
> In designing to resist lateral loads, the upper 10-ft-thick clay layer can provide passive resistance of 100 lb/ft^2 per foot of depth (equivalent fluid pressure). For seismic analysis, the underlying 15-ft-thick sand layer should be assumed to have zero passive resistance.
>
> The above values of allowable bearing pressure and passive resistance should not be increased for the earthquake conditions. As previously mentioned, the loose sand layer from a depth of 10 to 25 ft below ground surface is expected to liquefy during the design earthquake (i.e., weakened soil conditions).

8.6 PROBLEMS

The problems have been divided into basic categories as indicated below.

Bearing Capacity for Shallow Foundations Underlain by Liquefied Soil

8.1 Use the data from the example problem for the cohesive surface layer in Sec. 8.2.2. Calculate the spread footing size so that the factor of safety is equal to 5. *Answer:* 5-m by 5-m spread footing.

8.2 Use the data from the example problem for the cohesive surface layer in Sec. 8.2.2. Calculate the maximum concentric load that can be exerted to the 2-m by 2-m spread footing such that the factor of safety is equal to 5. *Answer:* $P = 200$ kN.

8.3 Use the data from the example problem for the cohesionless surface layer in Sec. 8.2.2. Calculate the maximum concentric load that can be exerted to the strip footing such that the factor of safety is equal to 5. *Answer:* $P = 10$ kN/m.

8.4 Use the data from the example problem for the cohesionless surface layer in Sec. 8.2.2. Calculate the maximum concentric load that can be exerted to the 2-m by 2-m spread footing such that the factor of safety is equal to 5. *Answer:* $P = 40$ kN.

8.5 Use the data from Prob. 6.12 and the subsoil profile shown in Fig. 6.13. Assume the following: Peak ground acceleration is equal to $0.20g$, the groundwater table is unlikely to rise above its present level, a 1.5-m-thick fill layer will be constructed at the site, the soil above the groundwater table (including the proposed fill layer) is sand with an effective friction angle ϕ' equal to 33° and $k_0 = 0.5$, and the foundation will consist of shallow strip and spread footings that are 0.3 m deep. Using a factor of safety equal to 5 and footing widths of 1 m, determine the allowable bearing pressure for the strip and spread footings. *Answer:* $q_{all} = 10$ kPa for 1-m-wide strip footings and $q_{all} = 20$ kPa for 1-m by 1-m spread footings.

8.6 Solve Prob. 8.5, except assume that the soil above the groundwater table (including the proposed fill layer) is cohesive soil that has undrained shear strength of 20 kPa. *Answer:* $q_{all} = 20$ kPa for the 1-m-wide strip footings, and $q_{all} = 40$ kPa for the 1-m by 1-m spread footings.

8.7 Solve Prob. 8.5, using the Terzaghi bearing capacity equation. What values should be used in the design of the footings? *Answer:* $q_{all} = 48$ kPa for the 1-m-wide strip footings, and $q_{all} = 38$ kPa for the 1-m by 1-m spread footings. For the design of the footings, use the lower values calculated in Prob. 8.5.

8.8 Solve Prob. 8.6, using the Terzaghi bearing capacity equation. What values should be used in the design of the footings? *Answer:* $q_{all} = 22$ kPa for the 1-m-wide strip footings, and $q_{all} = 30$ kPa for the 1-m by 1-m spread footings. For the design of the strip footings, use the value from Prob. 8.6 ($q_{all} = 20$ kPa). For the design of the spread footings, use the lower value calculated in this problem ($q_{all} = 30$ kPa).

8.9 Solve Prob. 8.6, assuming that the spread footing is 3 m by 3 m. Use the methods outlined in Secs. 8.2.2 and 8.2.3. What bearing capacity values should be used in the design of the footings? *Answer:* From Eq. (8.1), $q_{all} = 14$ kPa. From the method in Sec. 8.2.3, $q_{all} = 12$ kPa. Use the lower value of 12 kPa for the design of the 3-m by 3-m spread footing.

Bearing Capacity for Deep Foundations Underlain by Liquefied Soil

8.10 Use the data from Prob. 6.12 and Fig. 6.13. Assume that a 20-m by 20-m mat foundation is supported by piles, with the tip of the piles located at a depth of 15 m. The

piles are evenly spaced along the perimeter and interior portion of the mat. The structural engineer has determined that the critical design load (sum of live, dead, and seismic loads) is equal to 50 MN, which can be assumed to act at the center of the mat and will be transferred to the pile tips. The effective friction angle ϕ' of the sand from a depth of 15 to 17 m is equal to 34° and $k_0 = 0.60$. Calculate the factor of safety [using Eq. (8.1)] for an earthquake-induced punching shear failure into the liquefied soil located at a depth of 17 to 20 m below ground surface. *Answer:* FS = 0.20 and therefore the pile foundation will punch down into the liquefied soil layer located at a depth of 17 to 20 m below ground surface.

8.11 Use the data from Prob. 8.10, but assume that high-displacement friction piles are used to support the mat. The friction piles will densify the upper 15 m of soil and prevent liquefaction of this soil. In addition, the piles will primarily resist the 50-MN load by soil friction along the pile perimeters. Using the 2 : 1 approximation and assuming it starts at a depth of $^2/_3L$ (where L = pile length), determine the factor of safety [using Eq. (8.1)] for an earthquake-induced punching shear failure into the liquefied soil located at a depth of 17 to 20 m below ground surface. *Answer:* FS = 0.27 and therefore the pile foundation will punch down into the liquefied soil layer located at a depth of 17 to 20 m below ground surface.

Eccentrically Loaded Foundations

8.12 Use the data from the example problem in Sec. 8.2.6. Assume that the eccentricity e is 0.10 m for the strip footing and 0.3 m for the spread footing. Determine the values of Q and M for a factor of safety of 5. *Answer:* For the strip footing, $Q = 34$ kN/m and $M = 3.4$ kN·m/m. For the spread footing, $Q = 88$ kN and $M = 26$ kN·m.

8.13 Use the data for the spread footing from the example problem in Sec. 8.2.6. Assume that there are 150 kN·m moments acting in both the B and L directions. Calculate the factor of safety in terms of a bearing capacity failure. *Answer:* FS = 0.82.

8.14 Use the data from the example problem in Sec. 8.4.3. Assume that the structural engineer has determined that the design load (dead, live, plus rocking seismic load) is 15,000 kips with an eccentricity of 5 ft (eccentricity only in the B direction). Is this an acceptable design based on the allowable bearing values provided in Sec. 8.4.3? *Answer:* Yes, the bearing pressure exerted by the mat is less than the allowable bearing pressure.

Granular Soil with Earthquake-Induced Excess Pore Water Pressures

8.15 Using the data from the example problem in Sec. 8.3.3, determine the allowable load (dead, live, plus seismic) that the footings can support. Assume concentric loading conditions (i.e., no eccentricity). *Answer:* $Q = 36$ kN/m for the strip footing and $Q = 200$ kN for the spread footing.

8.16 Solve the example problem in Sec. 8.3.3, but assume that the factor of safety against liquefaction is equal to 1.2. *Answer:* $q_{all} = 21$ kPa for the strip footing and $q_{all} = 28$ kPa for the spread footing.

Cohesive Soil Weakened by the Earthquake

8.17 Assume a tall building will be constructed at a level-ground site. The foundation will consist of a mat constructed near ground surface. The mat foundation will be 75 ft long and 50 ft wide, and the structural engineer has determined that the design vertical load (including seismic effects) is 20,000 kips located at the center of the mat. Assume that the soil located beneath the mat is a clay that has the shear strength properties shown in Fig. 8.12. Determine the factor of safety for a bearing capacity failure using the fully weakened shear strength. *Answer:* FS = 4.5.

Subsoil Profile

8.18 Assume an oil tank will be constructed at a level-ground site, and the subsurface soil conditions are shown in Fig. 8.14. The groundwater table is located at a depth of 1 m below ground surface.

The standard penetration test values shown in Fig. 8.14 are uncorrected N values. Assume a hammer efficiency E_m of 0.6 and a boring diameter of 100 mm, and the length of the drill rods is equal to the depth of the SPT below ground surface. The design earthquake conditions are a peak ground acceleration a_{max} of $0.20g$ and a magnitude of 7.5.

For the materials shown in Fig. 8.14, assume the following:

a. The surface soil layer (0 to 2.3 m) is clay having an undrained shear strength s_u of 50 kPa. The total unit weight of the soil above the groundwater table γ_t is 19.2 kN/m^3, and the buoyant unit weight γ_b is equal to 9.4 kN/m^3.

b. The fine sand with gravel layer (2.3 to 8 m) has a low gravel content and can be considered to be essentially a clean sand (γ_b = 9.7 kN/m^3).

c. The sand layer (8 to 11.2 m) has less than 5 percent fines (γ_b = 9.6 kN/m^3).

d. The silty sand layer (11.2 to 18 m) meets the requirements for a potentially liquefiable soil and has 35 percent fines (γ_b = 9.6 kN/m^3).

e. The Flysh claystone (>18 m) is essentially solid rock, and it is not susceptible to earthquake-induced liquefaction or settlement.

Assume the oil tank will be constructed at ground surface and will have a diameter of 20 m and an internal storage capacity equal to a 3-m depth of oil (unit weight of oil = 9.4 kN/m^3), and the actual weight of the tank can be ignored in the analysis. Determine the factor of safety against liquefaction and the amount of fill that must be placed at the site to prevent liquefaction-induced ground surface fissuring and sand boils. With the fill layer in place, determine the liquefaction-induced settlement of the tank, and calculate the factor of safety against a bearing capacity failure of the tank. Assume that the fill will be obtained from a borrow site that contains clay, and when compacted, the clay will have an undrained shear strength s_u of 50 kPa. *Answer:* Zone of liquefaction extends from 2.3 to 18 m, thickness of required fill layer at site = 0.7 m, liquefaction-induced settlement of the oil tank = 54 to 66 cm based on Figs. 7.1 and 7.2, and factor of safety against a bearing capacity failure = 1.06.

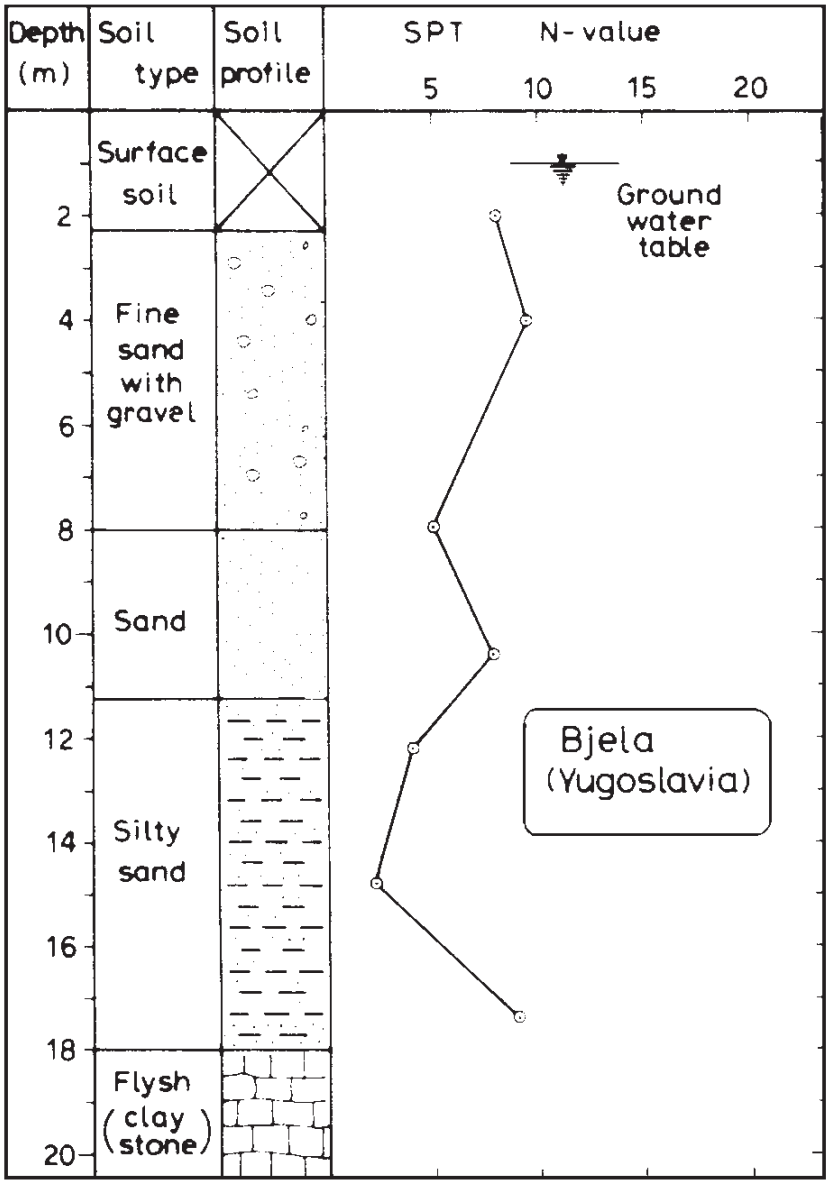

FIGURE 8.14 Subsoil profile, Bjela, Yugoslavia. (*Reproduced from Ishihara 1985.*)

CHAPTER 9

SLOPE STABILITY ANALYSES FOR EARTHQUAKES

The following notation is used in this chapter:

SYMBOL	*DEFINITION*
a	Acceleration
a_{max}	Maximum horizontal acceleration at ground surface (also known as peak ground acceleration)
a_y	Yield acceleration, which is defined as that acceleration that produces a pseudostatic FS = 1.0
c	Cohesion based on total stress analysis
c'	Cohesion based on effective stress analysis
d	Downslope movement caused by earthquake
D_H	Horizontal ground displacement due to lateral spreading
D_r	Relative density of soil
D_{50}	Grain size corresponding to 50 percent finer of soil
F	Fines content of soil comprising layer T
F_h	Pseudostatic lateral force
FS	Factor of safety
FS_L	Factor of safety against liquefaction
g	Acceleration of gravity
h	Depth below ground surface (for calculation of r_u)
H	Height of free face
k_h	Seismic coefficient, also known as pseudostatic coefficient
k_v	Vertical pseudostatic coefficient
K_α	Factor used to adjust factor of safety against liquefaction for sloping ground
L	Length of slip surface
L	Horizontal distance from base of free face to site location (Sec. 9.5.2)
m	Total mass of slide material
M	Magnitude of design earthquake
M_L	Local magnitude of earthquake
N	Normal force on slip surface
N'	Effective normal force on slip surface
$(N_1)_{60}$	N value corrected for field testing procedures and overburden pressure
r_u	Pore water pressure ratio
R	Distance to expected epicenter or nearest fault rupture
s_u	Undrained shear strength of soil
S	Slope gradient
T	Shear force along slip surface
T	Cumulative thickness of submerged sand layers having $(N_1)_{60} < 15$ (Sec. 9.5.2)
u	Pore water pressure

u_e Earthquake-induced pore water pressure
u_i Initial pore water pressure
W Total weight of failure wedge or failure slice
W Free face ratio (Sec. 9.5.2)
α Slope inclination
ß Angular distortion as defined by Boscardin and Cording (1989)
ε_h Horizontal strain of foundation
ϕ Friction angle based on total stress analysis
ϕ' Friction angle based on effective stress analysis
ϕ'_r Drained residual friction angle
γ_t Total unit weight of soil
γ_w Unit weight of water
σ Total stress
σ' Effective stress
σ_n Total normal stress
σ'_n Effective normal stress
σ'_{v0} Vertical effective stress
τ_f Shear strength of soil
$\tau_{h\ \text{static}}$ Static shear stress acting on a horizontal plane

9.1 INTRODUCTION

Section 3.5 presents an introduction to slope movement. Types and examples of earthquake-induced slope movement are discussed in that section. In addition, Sec. 3.4 deals with flow slides and lateral spreading of slopes caused by the liquefaction of soil during the earthquake. Tables 3.1 and 3.2 list the different types of slope movement for rock and soil slopes.

There would appear to be a shaking threshold that is needed to produce earthquake-induced slope movement. For example, as discussed in Sec. 6.3, the threshold values needed to produce liquefaction are a peak ground acceleration $a_{\max}$ of about $0.10g$ and local magnitude M_L of about 5 (National Research Council 1985, Ishihara 1985). Thus, those sites having a peak ground acceleration $a_{\max}$ less than $0.10g$ or a local magnitude M_L less than 5 would typically not require a liquefaction-related flow slide or lateral spreading analysis. Other threshold values for different types of slope movement are summarized in Tables 9.1 and 9.2.

Tables 9.1 and 9.2 also indicate the relative abundance of earthquake-induced slope failures based on a historical study of 40 earthquakes by Keefer (1984). In general, the most abundant types of slope failures during earthquakes tend to have the lowest threshold values and can involve both small and large masses. For example, rockfalls have a low threshold value ($M_L = 4.0$) and can consist of only one or a few individual rocks, such as shown in Figs. 9.1 and 9.2. Other rockfalls during earthquakes can involve much larger masses of rock, such as shown in Fig. 9.3.

Another example of a very abundant type of earthquake-induced slope movement is a rock slide. As indicated in Table 9.1, rock slides also have a low threshold value ($M_L = 4.0$) and can involve small or large masses of rock. Figure 9.4 shows an example of a rock slide at Pacoima Dam, which was triggered by the San Fernando earthquake in California on February 9, 1971.

Those slope failures listed as *uncommon* in Tables 9.1 and 9.2 tend to have higher threshold values and also typically involve larger masses of soil and rock. Because of their large volume, they tend to be less common. For example, in comparing rock slides and rock block slides in Table 9.1, the rock block slides tend to involve massive blocks of rock that remain

FIGURE 9.1 A rockfall that struck a house located at the mouth of Pacoima Gorge. The rockfall was caused by the San Fernando earthquake (magnitude 6.6) in California on February 9, 1971. (*Photograph from the Steinbrugge Collection, EERC, University of California, Berkeley.*)

FIGURE 9.2 Large rocks from a rockfall that rolled onto the road located on the west side of Carroll Summit. The rockfall was caused by the Dixie Valley–Fairview Peaks earthquake (magnitude 7.0) in Nevada on December 16, 1954. (*Photograph from the Steinbrugge Collection, EERC, University of California, Berkeley.*)

FIGURE 9.3 A large rockfall caused by the Hebgen Lake earthquake in Montana on August 17, 1959. (*Photograph from the Steinbrugge Collection, EERC, University of California, Berkeley.*)

FIGURE 9.4 Rock slide at the Pacoima Dam caused by the San Fernando earthquake in California on February 9, 1971. (*Photograph from the Steinbrugge Collection, EERC, University of California, Berkeley.*)

relatively intact during the earthquake-induced slope movement. Another example is a rock avalanche, which by definition implies a large mass of displaced material. Figure 9.5 shows a rock avalanche caused by the Hebgen Lake earthquake, in Montana, which blocked a canyon and created a temporary lake.

As discussed in Sec. 3.5.3, the seismic evaluation of slope stability can be grouped into two general categories: inertia slope stability analysis and weakening slope stability analysis, as discussed in the following sections.

9.1.1 Inertia Slope Stability Analysis

The inertia slope stability analysis is preferred for those materials that retain their shear strength during the earthquake. Examples of these types of soil and rock are as follows:

- Massive crystalline bedrock and sedimentary rock that remain intact during the earthquake, such as earthquake-induced rock block slide (see Tables 3.1 and 9.1).
- Soils that tend to dilate during the seismic shaking, or, for example, dense to very dense granular soil and heavily overconsolidated cohesive soil such as very stiff to hard clays.
- Soils that have a stress-strain curve that does not exhibit a significant reduction in shear strength with strain. Earthquake-induced slope movement in these soils often takes the form of soil slumps or soil block slides (see Tables 3.2 and 9.2).
- Clay that has a low sensitivity.
- Soils located above the groundwater table. These soils often have negative pore water pressure due to capillary action.
- Landslides that have a distinct rupture surface, and the shear strength along the rupture surface is equal to the drained residual shear strength ϕ'_r.

FIGURE 9.5 Rock avalanche caused by the Hebgen Lake earthquake in Montana on August 17, 1959. (*Photograph from the Steinbrugge Collection, EERC, University of California, Berkeley.*)

TABLE 9.1 Earthquake-Induced Slope Movement in Rock

Main type of slope movement	Subdivisions	Material type	Minimum slope inclination	Threshold values	Relative abundance
Falls	Rockfalls	Rocks weakly cemented, intensely fractured, or weathered; contain conspicuous planes of weakness dipping out of slope or contain boulders in a weak matrix	40° (1.2 : 1)	$M_L = 4.0$	Very abundant (more than 100,000 in the 40 earthquakes)
Slides	Rock slides	Rocks weakly cemented, intensely fractured, or weathered; contain conspicuous planes of weakness dipping out of slope or contain boulders in a weak matrix	35° (1.4 : 1)	$M_L = 4.0$	Very abundant (more than 100,000 in the 40 earthquakes)
	Rock avalanches	Rocks intensely fractured and exhibiting one of the following properties: significant weathering, planes of weakness dipping out of slope, weak cementation, or evidence of previous landsliding	25° (2.1 : 1)	$M_L = 6.0$	Uncommon (100 to 1000 in the 40 earthquakes)
	Rock slumps	Intensely fractured rocks, preexisting rock slump deposits, shale, and other rocks containing layers of weakly cemented or intensely weathered material	15° (3.7 : 1)	$M_L = 5.0$	Moderately common (1000 to 10,000 in the 40 earthquakes)
	Rock block slides	Rocks having conspicuous bedding planes or similar planes of weakness dipping out of slopes	15° (3.7 :1)	$M_L = 5.0$	Uncommon (100 to 1000 in the 40 earthquakes)

Note: Also see Table 3.1 for additional comments.
Sources: Keefer (1984) and Division of Mines and Geology (1997).

TABLE 9.2 Earthquake-Induced Slope Movement in Soil

Main type of slope movement	Subdivisions	Material type	Minimum slope inclination	Threshold values	Relative abundance
Falls	Soil falls	Granular soils that are slightly cemented or contain clay binder	40° (1.2 : 1)	$M_L = 4.0$	Moderately common (1000 to 10,000 in the 40 earthquakes)
Slides	Soil avalanches	Loose, unsaturated sands	25° (2.1 : 1)	$M_L = 6.5$	Abundant (10,000 to 100,000 in the 40 earthquakes)
	Disrupted soil slides	Loose, unsaturated sands	15° (3.7 : 1)	$M_L = 4.0$	Very abundant (more than 100,000 in the 40 earthquakes)
	Soil slumps	Loose, partly to completely saturated sand or silt; uncompacted or poorly compacted artificial fill composed of sand, silt, or clay, preexisting soil slump deposits	10° (5.7 : 1)	$M_L = 4.5$	Abundant (10,000 to 100,000 in the 40 earthquakes)
	Soil block slides	Loose, partly or completely saturated sand or silt; uncompacted or slightly compacted artificial fill composed of sand or silt, bluffs containing horizontal or subhorizontal layers of loose, saturated sand or silt	5° (11 : 1)	$M_L = 4.5$	Abundant (10,000 to 100,000 in the 40 earthquakes)
Flow slides and lateral spreading	Slow earth flows	Stiff, partly to completely saturated clay and preexisting earth flow deposits	10° (5.7 : 1)	$M_L = 5.0$	Uncommon (100 to 1000 in the 40 earthquakes)
	Flow slides	Saturated, uncompacted or slightly compacted artificial fill composed of sand or sandy silt (including hydraulic fill earth dams and tailings dams); loose, saturated granular soils	2.3° (25 : 1)	$M_L = 5.0$ $a_{\max} = 0.10g$	Moderately common (1000 to 10,000 in the 40 earthquakes)

TABLE 9.2 Earthquake-Induced Slope Movement in Soil (*Continued*)

Flow slides and lateral spreading (*Continued*)	Subaqueous flows	Loose, saturated granular soils	0.5° (110 : 1)	$M_L = 5.0$ $a_{max} = 0.10g$	Uncommon (100 to 1000 in the 40 earthquakes)
	Lateral spreading	Loose, partly or completely saturated silt or sand, uncompacted or slightly compacted artificial fill composed of sand	0.3° (190 : 1)	$M_L = 5.0$ $a_{max} = 0.10>$	Abundant (10,000 to 100,000 in the 40 earthquakes)

Note: Also see Table 3.2 for additional comments.
Sources: Keefer (1984) and Division of Mines and Geology (1997).

There are many different types of inertia slope stability analyses, and two of the most commonly used are the pseudostatic approach and the Newmark (1965) method. These two methods are described in Secs. 9.2 and 9.3.

9.1.2 Weakening Slope Stability Analysis

The weakening slope stability analysis is preferred for those materials that will experience a significant reduction in shear strength during the earthquake. Examples of these types of soil and rock are as follows:

1. Foliated or friable rock that fractures apart during the earthquake, resulting in rockfalls, rock slides, and rock slumps (see Tables 3.1 and 9.1).
2. Sensitive clays that lose shear strength during the earthquake. An example of a weakening landslide is the Turnagain Heights landslide as described Sec. 3.5.2.
3. Soft clays and organic soils that are overloaded and subjected to plastic flow during the earthquake. The type of slope movement involving these soils is often termed *slow earth flows* (see Tables 3.2 and 9.2).
4. Loose soils located below the groundwater table and subjected to liquefaction or a substantial increase in excess pore water pressure. There are two cases of weakening slope stability analyses involving the liquefaction of soil:
   - ***a.*** *Flow slide:* As discussed in Sec. 3.4.4 and Tables 3.2 and 9.2, flow slides develop when the static driving forces exceed the shear strength of the soil along the slip surface, and thus the factor of safety is less than 1.0. Figures 3.38 to 3.40 show the flow slide of the Lower San Fernando Dam caused by the San Fernando earthquake on February 9, 1971.
   - ***b.*** *Lateral spreading:* As discussed in Sec. 3.4.5 and Tables 3.2 and 9.2, there could be localized or large-scale lateral spreading of retaining walls and slopes. Examples of large-scale lateral spreading are shown in Figs. 3.41 and 3.42. The concept of cyclic mobility is used to describe large-scale lateral spreading of slopes. In this case, the static driving forces do not exceed the shear strength of the soil along the slip surface, and thus the ground is not subjected to a flow slide. Instead, the driving forces only exceed the resisting forces during those portions of the earthquake that impart net inertial forces in the downslope direction. Each cycle of net inertial forces in the downslope direction causes the driving forces to exceed the resisting forces along the slip surface, resulting in progressive and incremental lateral movement. Often

the lateral movement and ground surface cracks first develop at the unconfined toe, and then the slope movement and ground cracks progressively move upslope.

Weakening slope stability analyses are discussed in Secs. 9.4 to 9.6.

9.1.3 Cross Section and Soil Properties

The first step in a slope stability analysis is to develop a cross section through the slope. It is important that cross sections be developed for the critical slope locations, such as those areas that are believed to have the lowest factors of safety. The cross section of the slope and the various soil properties needed for the analysis would be determined during the screening investigation and quantitative evaluation (see Secs. 5.2 to 5.5). Some of the additional items that may need to be addressed prior to performing a slope stability analysis are as follows (adapted from Division of Mines and Geology 1997):

- Do landslides or slope failures, that are active or inactive, exist on or adjacent (either uphill or downhill) to the project?
- Are there geologic formations or other earth materials located on or adjacent to the site that are known to be susceptible to slope movement or landslides?
- Do slope areas show surface manifestations of the presence of subsurface water (springs and seeps), or can potential pathways or sources of concentrated water infiltration be identified on or upslope of the site?
- Are susceptible landforms and vulnerable locations present? These include steep slopes, colluvium-filled swales, cliffs or banks being undercut by stream or water action, areas that have recently slid, and liquefaction-prone areas.
- Given the proposed development, could anticipated changes in the surface and subsurface hydrology (due to watering of lawns, on-site sewage disposal, concentrated runoff from impervious surfaces, etc.) increase the potential for future slope movement or landslides in some areas?

Other considerations for the development of the cross section to be used in the slope stability analysis are discussed in Sec. 9.2.6.

9.2 INERTIA SLOPE STABILITY—PSEUDOSTATIC METHOD

9.2.1 Introduction

As previously mentioned, the inertial slope stability analysis is preferred for those materials that retain their shear strength during the earthquake. The most commonly used inertial slope stability analysis is the pseudostatic approach. The advantages of this method are that it is easy to understand and apply and that the method is applicable for both total stress and effective stress slope stability analyses.

The original application of the pseudostatic method has been credited to Terzaghi (1950). This method ignores the cyclic nature of the earthquake and treats it as if it applied an additional static force upon the slope. In particular, the pseudostatic approach is to apply a lateral force acting through the centroid of the sliding mass, acting in an out-of-slope direction. The pseudostatic lateral force F_h is calculated by using Eq. (6.1), or

$$F_h = ma = \frac{Wa}{g} = \frac{Wa_{max}}{g} = k_h W \tag{9.1}$$

where F_h = horizontal pseudostatic force acting through the centroid of sliding mass, in an out-of-slope direction, lb or kN. For slope stability analysis, slope is usually assumed to have a unit length (i.e., two-dimensional analysis).
m = total mass of slide material, lb or kg, which is equal to W/g
W = total weight of slide material, lb or kN
a = acceleration, which in this case is the maximum horizontal acceleration at ground surface caused by earthquake ($a = a_{max}$), ft/s^2 or m/s^2
a_{max} = maximum horizontal acceleration at ground surface that is induced by the earthquake, ft/s^2 or m/s^2. The maximum horizontal acceleration is also commonly referred to as the peak ground acceleration (see Sec. 5.6).
$a_{max}/g = k_h$ = seismic coefficient, also known as pseudostatic coefficient (dimensionless)

Note that an earthquake could subject the sliding mass to both vertical and horizontal pseudostatic forces. However, the vertical force is usually ignored in the standard pseudostatic analysis. This is because the vertical pseudostatic force acting on the sliding mass usually has much less effect on the stability of a slope. In addition, most earthquakes produce a peak vertical acceleration that is less than the peak horizontal acceleration, and hence k_v is smaller than k_h.

As indicated in Eq. (9.1), the only unknowns in the pseudostatic method are the weight of the sliding mass W and the seismic coefficient k_h. Based on the results of subsurface exploration and laboratory testing, the unit weight of the soil or rock can be determined, and then the weight of the sliding mass W can be readily calculated. The other unknown is the seismic coefficient k_h, which is much more difficult to determine. The next section discusses guidelines for the selection of the seismic coefficient k_h for the pseudostatic method.

9.2.2 Selection of the Seismic Coefficient

The selection of the seismic coefficient k_h takes considerable experience and judgment. Guidelines for the selection of k_h are as follows:

1. *Peak ground acceleration:* Section 5.6 presents an in-depth discussion of the determination of the peak ground acceleration a_{max} for a given site. The higher the value of the peak ground acceleration a_{max}, the higher the value of k_h that should be used in the pseudostatic analysis.
2. *Earthquake magnitude:* The higher the magnitude of the earthquake, the longer the ground will shake (see Table 2.2) and consequently the higher the value of k_h that should be used in the pseudostatic analysis.
3. *Maximum value of k_h:* When items 1 and 2 as outlined above are considered, keep in mind that the value of k_h should never be greater than the value of a_{max}/g.
4. *Minimum value of k_h:* Check to determine if there are any agency rules that require a specific seismic coefficient. For example, a common requirement by many local agencies in California is the use of a minimum seismic coefficient $k_h = 0.15$ (Division of Mines and Geology 1997).
5. *Size of the sliding mass:* Use a lower seismic coefficient as the size of the slope failure mass increases. The larger the slope failure mass, the less likely that during the earthquake the entire slope mass will be subjected to a destabilizing seismic force acting in the out-of-slope direction. Suggested guidelines are as follows:

a. *Small slide mass:* Use a value of $k_h = a_{max}/g$ for a small slope failure mass. Examples would include small rockfalls or surficial stability analyses.

b. *Intermediate slide mass:* Use a value of $k_h = 0.65a_{max}/g$ for slopes of moderate size (Krinitzsky et al. 1993, Taniguchi and Sasaki 1986). Note that this value of 0.65 was used in the liquefaction analysis [see Eq. 6.5)].

c. *Large slide mass:* Use the lowest values of k_h for large failure masses, such as large embankments, dams, and landslides. Seed (1979b) recommended the following:

$k_h = 0.10$ for sites near faults capable of generating magnitude 6.5 earthquakes. The acceptable pseudostatic factor of safety is 1.15 or greater.

$k_h = 0.15$ for sites near faults capable of generating magnitude 8.5 earthquakes. The acceptable pseudostatic factor of safety is 1.15 or greater.

Other guidelines for the selection of the value of k_h include the following:

- Terzaghi (1950) suggested the following values: $k_h = 0.10$ for "severe" earthquakes, $k_h = 0.20$ for "violent and destructive" earthquakes, and $k_h = 0.50$ for "catastrophic" earthquakes.
- Seed and Martin (1966) and Dakoulas and Gazetas (1986), using shear beam models, showed that the value of k_h for earth dams depends on the size of the failure mass. In particular, the value of k_h for a deep failure surface is substantially less than the value of k_h for a failure surface that does not extend far below the dam crest. This conclusion is identical to item 5 (size of sliding mass) as outlined above.
- Marcuson (1981) suggested that for dams $k_h = 0.33a_{max}/g$ to 0.50 a_{max}/g, and consider possible amplification or deamplification of the seismic shaking due to the dam configuration.
- Hynes-Griffin and Franklin (1984), based on a study of the earthquake records from more than 350 accelerograms, use $k_h = 0.50a_{max}/g$ for earth dams. By using this seismic coefficient and having a psuedostatic factor of safety greater than 1.0, it was concluded that earth dams will not be subjected to "dangerously large" earthquake deformations.
- Kramer (1996) states that the study on earth dams by Hynes-Griffin and Franklin (1984) would be appropriate for most slopes. Also Kramer indicates that there are no hard and fast rules for the selection of the pseudostatic coefficient for slope design, but that it should be based on the actual anticipated level of acceleration in the failure mass (including any amplification or deamplification effects).

9.2.3 Wedge Method

The simplest type of slope stability analysis is the wedge method. Figure 9.6 illustrates the free-body diagram for the wedge method. Note in this figure that the failure wedge has a planar slip surface inclined at an angle α to the horizontal. Although the failure wedge passes through the toe of the slope in Fig. 9.6, the analysis could also be performed for the case of the planar slip surface intersecting the face of the slope.

For the pseudostatic wedge analysis, there are four forces acting on the wedge:

$W =$ weight of failure wedge, lb or kN. Usually a two-dimensional analysis is performed based on an assumed unit length of slope (i.e., length of slope = 1 ft or 1 m). Thus the weight of the wedge is calculated as the total unit weight γ_t times the cross-sectional area of the failure wedge.

$F_h = k_h W =$ horizontal psuedostatic force acting through the centroid of the sliding mass, in an out-of-slope direction, lb or kN. The value of the seismic coefficient k_h is discussed in Sec. 9.2.2.

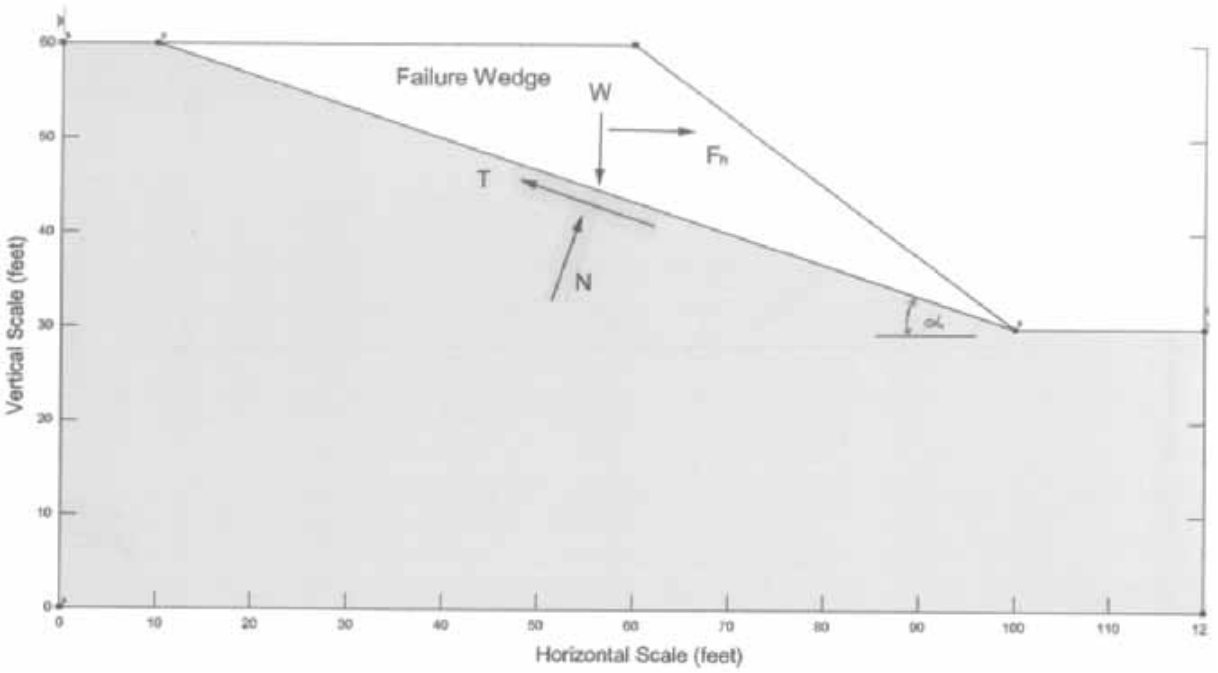

FIGURE 9.6 Wedge method, with the forces acting on the wedge shown in this diagram.

N = normal force acting on the slip surface, lb or kN

T = shear force acting along the slip surface, lb or kN. The shear force is also known as the resisting force because it resists failure of the wedge. Based on the Mohr-Coulomb failure law, the shear force is equal to the following:

For a total stress analysis:

$$T = cL + N \tan \phi$$

or

$$T = s_u L$$

For an effective stress analysis:

$$T = c'L + N' \tan \phi'$$

where L = length of the planar slip surface, ft or m
c, ϕ = shear strength parameters in terms of a total stress analysis
s_u = undrained shear strength of the soil (total stress analysis)
N = total normal force acting on the slip surface, lb or kN
c', ϕ' = shear strength parameters in terms of an effective stress analysis
N' = effective normal force acting on the slip surface, lb or kN

The assumption in this slope stability analysis is that there will be movement of the wedge in a direction that is parallel to the planar slip surface. Thus the factor of safety of the slope can be derived by summing forces parallel to the slip surface, and it is as follows:

Total stress pseudostatic analysis:

$$\text{FS} = \frac{\text{resisting force}}{\text{driving forces}} = \frac{cL + N \tan \phi}{W \sin \alpha + F_h \cos \alpha} = \frac{cL + (W \cos \alpha - F_h \sin \alpha) \tan \phi}{W \sin \alpha + F_h \cos \alpha} \tag{9.2a}$$

Effective stress pseudostatic analysis:

$$\text{FS} = \frac{c'L + N' \tan \phi'}{W \sin \alpha + F_h \cos \alpha} = \frac{c'L + (W \cos \alpha - F_h \sin \alpha - uL) \tan \phi'}{W \sin \alpha + F_h \cos \alpha} \quad (9.2b)$$

where FS = factor of safety for the pseudostatic slope stability (dimensionless parameter)
u = average pore water pressure along the slip surface, kPa or lb/ft^2

Because the wedge method is a two-dimensional analysis based on a unit length of slope (i.e., length = 1 m or 1 ft), the numerator and denominator of Eq. (9.2) are in pounds (or kilonewtons). The resisting force in Eq. (9.2) is equal to the shear strength (in terms of total stress or effective stress) of the soil along the slip surface. The driving forces [Eq. (9.2)] are caused by the pull of gravity and the pseudostatic force and are equal to their components that are parallel to the slip surface.

The total stress pseudostatic analysis is performed in those cases where the total stress parameters of the soil are known. A total stress analysis could be performed by using the consolidated undrained shear strength c and ϕ or the undrained shear strength s_u of the slip surface material. When the undrained shear strength is used, $s_u = c$ and $\phi = 0$ are substituted into Eq. (9.2*a*). A total stress pseudostatic analysis is often performed for cohesive soil, such as silts and clays.

The effective stress pseudostatic analysis is performed in those cases where the effective stress parameters (c' and ϕ') of the soil are known. Note that in order to use an effective stress analysis [Eq. (9.2*b*)], the pore water pressure u along the slip surface must also be known. The effective stress analysis is often performed for cohesionless soil, such as sands and gravels.

9.2.4 Method of Slices

The most commonly used method of slope stability analysis is the *method of slices,* where the failure mass is subdivided into vertical slices and the factor of safety is calculated based on force equilibrium equations. A circular arc slip surface and rotational type of failure mode are often used for the method of slices, and for homogeneous soil, a circular arc slip surface provides a lower factor of safety than assuming a planar slip surface.

The calculations for the method of slices are similar to those for the wedge-type analysis, except that the resisting and driving forces are calculated for each slice and then summed in order to obtain the factor of safety of the slope. For the *ordinary method of slices* [also known as the *Swedish circle method* or *Fellenius method,* (Fellenius 1936)], the equation used to calculate the factor of safety is identical to Eq. (9.2), with the resisting and driving forces calculated for each slice and then summed to obtain the factor of safety.

Commonly used methods of slices to obtain the factor of safety are listed in Table 9.3. The method of slices is not an exact method because there are more unknowns than equilibrium equations. This requires that an assumption be made concerning the interslice forces. Table 9.3 presents a summary of the assumptions for the various methods. For example, for the ordinary method of slices (Fellenius 1936), it is assumed that the resultant of the interslice forces is parallel to the average inclination of the slice α. It has been determined that because of this interslice assumption for the ordinary method of slices, this method provides a factor of safety that is too low for some situations (Whitman and Bailey 1967). As a result, the other methods listed in Table 9.3 are used more often than the ordinary method of slices.

Because of the tedious nature of the calculations, computer programs are routinely used to perform the analysis. Most slope stability computer programs have the ability to perform pseudostatic slope stability analyses, and the only additional item that needs to be input is the seismic coefficient k_h. In southern California, an acceptable minimum factor of safety of the slope is 1.1 to 1.15 for a pseudostatic slope stability analysis.

TABLE 9.3 Assumptions Concerning Interslice Forces for Different Method of Slices

Type of method of slices	Assumption concerning interslice forces	Reference
Ordinary method of slices	Resultant of interslice forces is parallel to average inclination of slice	Fellenius (1936)
Bishop simplified method	Resultant of interslice forces is horizontal (no interslice shear forces)	Bishop (1955)
Janbu simplified method	Resultant of interslice forces is horizontal (a correction factor is used to account for interslice shear forces)	Janbu (1968)
Janbu generalized method	Location of interslice normal force is defined by an assumed line of thrust	Janbu (1957)
Spencer method	Resultant of interslice forces is of constant slope throughout the sliding mass	Spencer (1967, 1968)
Morgenstern-Price method	Direction of resultant interslice forces is determined by using a selected function	Morgenstern and Price (1965)

Sources: Lambe and Whitman (1969) and Geo-Slope (1991).

Duncan (1996) states that the nearly universal availability of computers and much improved understanding of the mechanics of slope stability analyses have brought about considerable change in the computational aspects of slope stability analysis. Analyses can be done much more thoroughly and, from the point of view of mechanics, more accurately than was possible previously. However, problems can develop because of a lack of understanding of soil mechanics, soil strength, and the computer programs themselves, as well as the inability to analyze the results in order to avoid mistakes and misuse (Duncan 1996).

Section 9.2.7 presents an example problem dealing with the use of the pseudostatic slope stability analysis based on the method of slices.

9.2.5 Landslide Analysis

As mentioned in Sec. 9.1.1, the pseudostatic method can be used for landslides that have a distinct rupture surface, and the shear strength along the rupture surface is equal to the drained residual shear strength ϕ_r'. The residual shear strength ϕ_r' is defined as the remaining (or residual) shear strength of cohesive soil after a considerable amount of shear deformation has occurred. In essence, ϕ_r' represents the minimum shear resistance of a cohesive soil along a fully developed failure surface. The drained residual shear strength is primarily used to evaluate slope stability when there is a preexisting shear surface. An example of a preexisting shear surface is shown in Fig. 9.7, which is the Niguel Summit landslide slip surface that was exposed during its stabilization. In addition to landslides, other conditions that can be modeled using the drained residual shear strength include slopes in overconsolidated fissured clays, slopes in fissured shales, and other types of preexisting shear surfaces, such as sheared bedding planes, joints, and faults (Bjerrum 1967, Skempton and Hutchinson 1969, Skempton 1985, Hawkins and Privett 1985, Ehlig 1992).

Skempton (1964) states that the residual shear strength ϕ_r' is independent of the original shear strength, water content, and liquidity index; and it depends only on the size, shape, and mineralogical composition of the constituent particles. The drained residual friction angle ϕ_r' of cohesive soil could be determined by using the direct shear apparatus. For example, a clay specimen could be placed in the direct shear box and then sheared back and

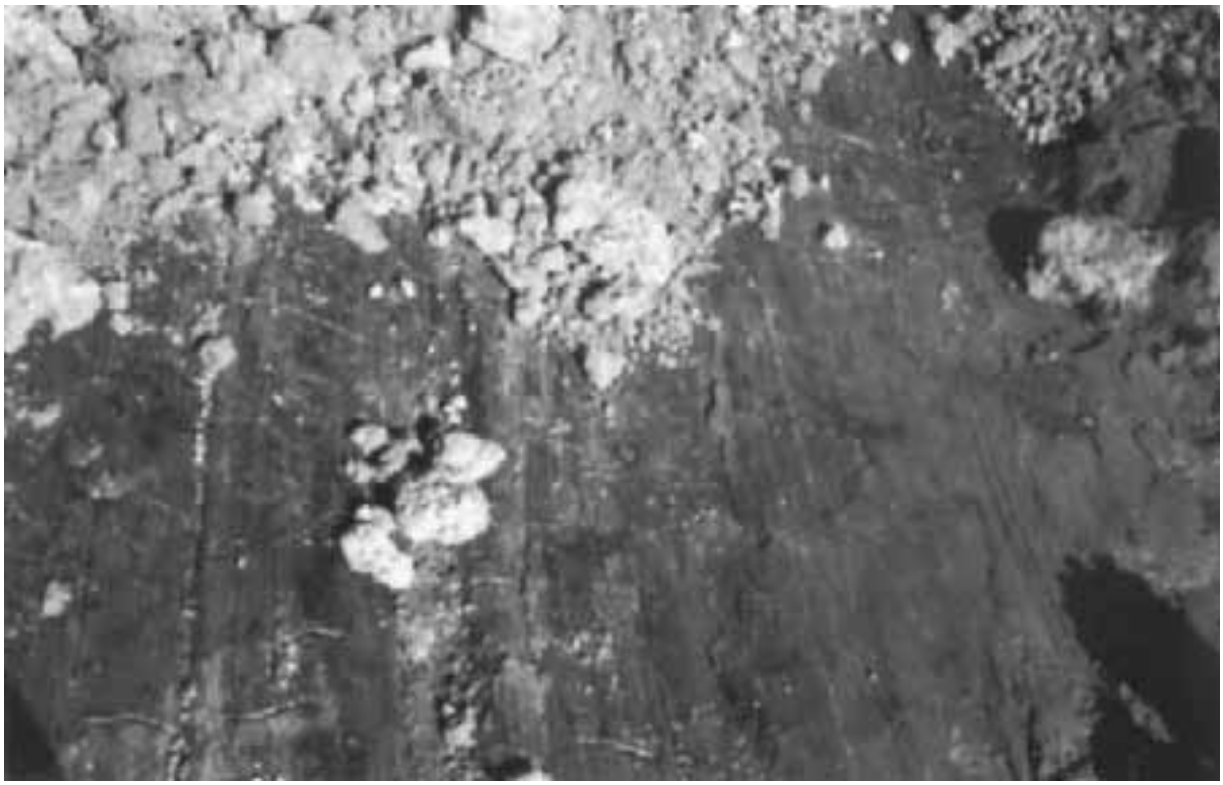

FIGURE 9.7 Photograph of the slide plane, which was exposed during the stabilization of the Niguel Summit landslide. Note that the direction of movement of the landslide can be inferred by the direction of striations in the slide plane.

forth several times to develop a well-defined shear failure surface. By shearing the soil specimen back and forth, the clay particles become oriented parallel to the direction of shear. Once the shear surface is developed, the drained residual shear strength can be determined by performing a final, slow shear of the specimen.

Besides the direct shear equipment, the drained residual shear strength can be determined by using the torsional ring shear apparatus (Stark and Eid 1994). Back calculations of landslide shear strength indicate that the residual shear strength from torsional ring shear tests is reasonably representative of the slip surface (Watry and Ehlig 1995). Test specifications have recently been developed, i.e., "Standard Test Method for Torsional Ring Shear Test to Determine Drained Residual Shear Strength of Cohesive Soils" (ASTM D 6467-99, 2000).

Figures 9.8 and 9.9 present an example of data obtained from torsional ring shear laboratory tests performed on slide plane material of an actual landslide (Day and Thoeny 1998). It can be seen in Fig. 9.8 that the failure envelope is nonlinear, which is a common occurrence for residual soil (Maksimovic 1989). If a linear failure envelope is assumed to pass through the origin and the shear stress at an effective normal stress of 100 kPa (2090 lb/ft^2), the residual friction angle ϕ_r' is 8.2°. If a linear failure envelope is assumed to pass through the origin and the shear stress at an effective normal stress of 700 kPa (14,600 lb/ft^2), the residual friction angle ϕ_r' is 6.2°. These drained residual friction angles are very low and are probably close to the lowest possible drained residual friction angles of soil. Also note in Fig. 9.9 that the stress-strain curve does not exhibit a reduction in shear strength with strain. This is to be expected since it is the lowest possible shear strength the soil can possess.

When the stability of a landslide is evaluated, the first step is to perform a static analysis. Since the drained residual shear strength is being utilized in the analysis (that is, ϕ_r'), an effective stress analysis must be performed. This means that the location of the groundwater table or the pore water pressures must also be known. After the static analysis is com-

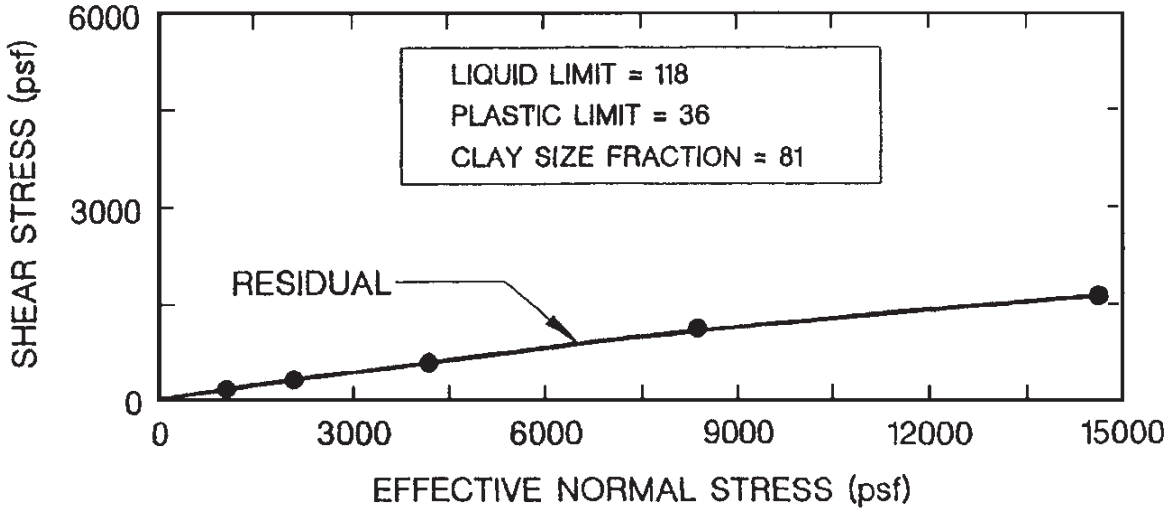

FIGURE 9.8 Drained residual shear strength envelope from torsional ring shear test on slide plane material. Also see Fig. 9.9 for the stress-strain plot.

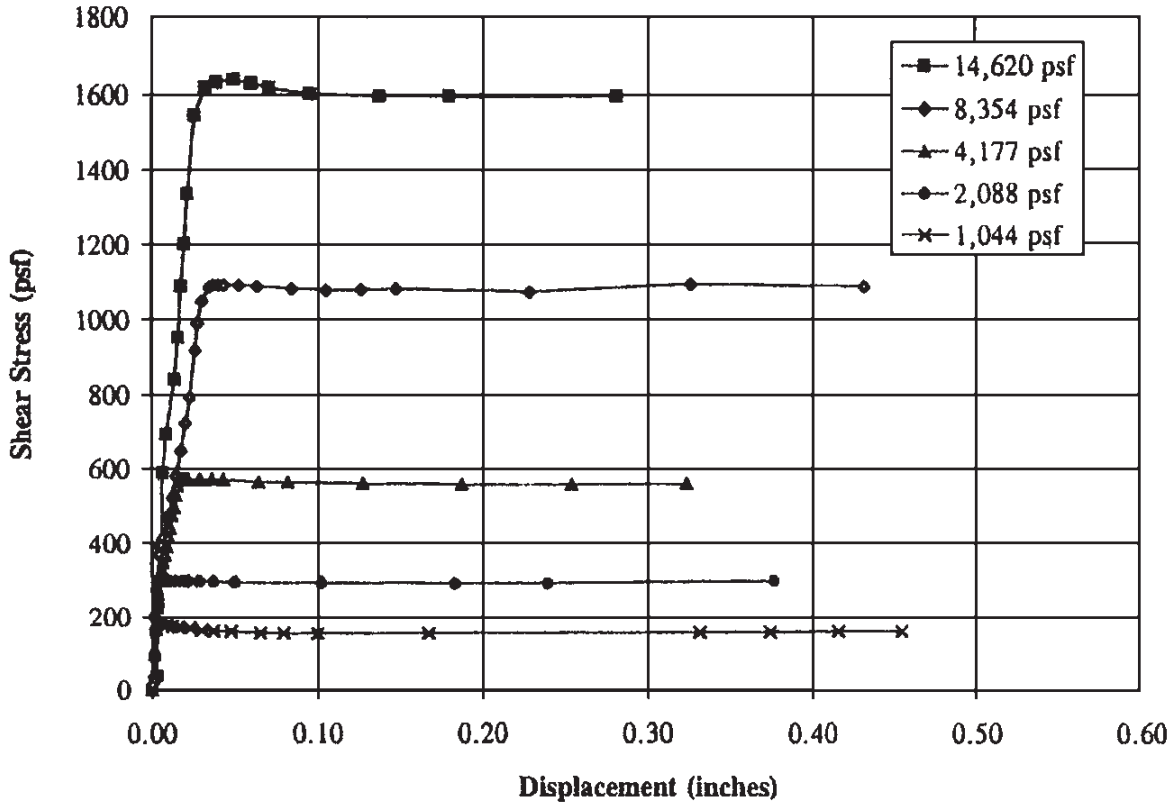

FIGURE 9.9 Shear stress versus displacement from torsional ring shear test on slide plane material. Also see Fig. 9.8 for the shear strength envelope.

pete, a pseudostatic analysis can be performed, and the only additional information that will be needed is the seismic coefficient k_h.

9.2.6 Other Slope Stability Considerations

To perform a pseudostatic slope stability analysis, a cross section must be developed that accurately models the existing or design conditions of the slope. Some of the important

factors that may need to be considered in the development of the cross section to be used for the pseudostatic slope stability analysis are as follows:

Different Soil Layers. If a proposed slope or existing slope contains layers of different soil or rock types with different engineering properties, then these layers must be input into the slope stability computer program. Most slope stability computer programs have this capability. Note that for all the different soil layers, either the effective shear strength (c' and ϕ') or the shear strength in terms of total stress parameters (s_u) must be known. It is important that the horizontal pseudostatic force P_h be specified for every layer that comprises the slope cross section.

Slip Surfaces. In some cases, a planar slip surface or a composite-type slip surface may need to be used for the analysis. Most slope stability computer programs have the capability of specifying various types of failure surfaces.

Tension Cracks. It has been stated that tension cracks at the top of the slope can reduce the factor of safety of a slope by as much as 20 percent and are usually regarded as an early and important warning sign of impending failure in cohesive soil (Cernica 1995b). Slope stability programs often have the capability to model or input tension crack zones. The destabilizing effects of water in tension cracks can also be modeled by some slope stability computer programs. When the pseudostatic approach is used, these features should be included in the slope stability analysis.

Surcharge Loads. There may be surcharge loads (such as a building load) at the top of the slope or even on the slope face. Most slope stability computer programs have the capability of including surcharge loads. In some computer programs, other types of loads, such as due to tie-back anchors, can also be included in the analysis. These permanent surcharge loads should also be included in the pseudostatic method.

Nonlinear Shear Strength Envelope. In some cases, the shear strength envelope for soil or rock is nonlinear (e.g., see Fig. 9.8). If the shear strength envelope is nonlinear, then a slope stability computer program that has the capability of using a nonlinear shear strength envelope should be used in the analysis.

Plane Strain Condition. Similar to strip footings, long uniform slopes will be in a plane strain condition. As discussed in Sec. 8.2.3, the friction angle ϕ is about 10 percent higher in the plane strain condition than the friction angle ϕ measured in the triaxial apparatus (Meyerhof 1961, Perloff and Baron 1976). Since plane strain shear strength tests are not performed in practice, there will be an additional factor of safety associated with the plane strain condition. For uniform fill slopes that have a low factor of safety, it is often observed that the "end" slopes (slopes that make a 90° turn) are the first to show indications of slope movement or the first to fail during an earthquake. This is because the end slope is not subjected to a plane strain condition and the shear strength is actually lower than in the center of a long, continuous slope.

Progressive Failure. For the method of slices, the factor of safety is an average value of all the slices. Some slices, such as at the toe of the slope, may have a lower factor of safety which is balanced by other slices that have a higher factor of safety. For those slices that have a low factor of safety, the shear stress and strain may exceed the peak shear strength. For some soils, such as stiff-fissured and sensitive clays, there may be a significant drop in shear strength as the soil deforms beyond the peak values. This reduction in shear strength will then transfer the load to an adjacent slice, which will cause it to experience the same

condition. Thus the movement and reduction of shear strength will progress along the slip surface, eventually leading to failure of the slope. Because of this weakening of the soil during the earthquake, it is best to use a weakening slope stability analysis (see Sec. 9.6).

Other Structures. Slope stability analysis can be used for other types of engineering structures. For example, the stability of the ground underneath a retaining wall is often analyzed by considering a slip surface beneath the foundation of the wall.

Effective Stress Analysis. The pseudostatic slope stability analysis can be performed using the effective shear strength of the soil. For this type of analysis, the effective shear strength parameters c' and ϕ' are input into the computer program. The pore water pressures must also be input into the computer program. For the pseudostatic method, it is common to assume that the same pore water pressures exist for the static case and the pseudostatic case. Several different options can be used concerning the pore water pressures:

1. *Zero pore water pressure:* A common assumption for those soil layers that are above the groundwater table is to assume zero pore water pressure. This is a conservative assumption since the soil will often have negative pore water pressures due to capillary effects.

2. *Groundwater table:* A second situation concerns those soils located below the groundwater table. If the groundwater table is horizontal, then the pore water pressures below the groundwater table are typically assumed to be hydrostatic. For the condition of seepage through the slope (i.e., a sloping groundwater table), a flow net can be drawn in order to estimate the pore water pressures below the groundwater table. Most slope stability computer programs have the ability to estimate the pore water pressures below a sloping groundwater table.

3. *Pore water pressure ratio r_u:* A third choice for dealing with pore water pressures is to use the pore water pressure ratio. The pore water pressure ratio is $r_u = u/(\gamma_t h)$, where u = pore water pressure, γ_t = total unit weight of the soil, and h = depth below the ground surface. If a value of $r_u = 0$ is selected, then the pore water pressures u are assumed to be equal to zero in the slope.

Suppose an r_u value is used for the entire slope. In many cases the total unit weight is about equal to 2 times the unit weight of water (that is, $\gamma_t = 2\,\gamma_w$), and thus a value of $r_u = 0.25$ is similar to the effect of a groundwater table at midheight of the slope. A value of $r_u = 0.5$ would be similar to the effect of a groundwater table corresponding to the ground surface.

The pore water pressure ratio r_u can be used for existing slopes where the pore water pressures have been measured in the field, or for the design of proposed slopes where it is desirable to obtain a quick estimate of the effect of pore water pressures on the stability of the slope.

In summary, the pseudostatic approach utilizes the same cross section and conditions that apply for the static slope stability case. The only additional information that most computer programs require to perform the pseudostatic method is the seismic coefficient k_h.

9.2.7 Example Problem

The purpose of this section is to present an example problem dealing with the use of the pseudostatic slope stability analysis based on the method of slices. A cross section through the slope is shown in Fig. 9.10. Specific details on the condition of the slope are as follows:

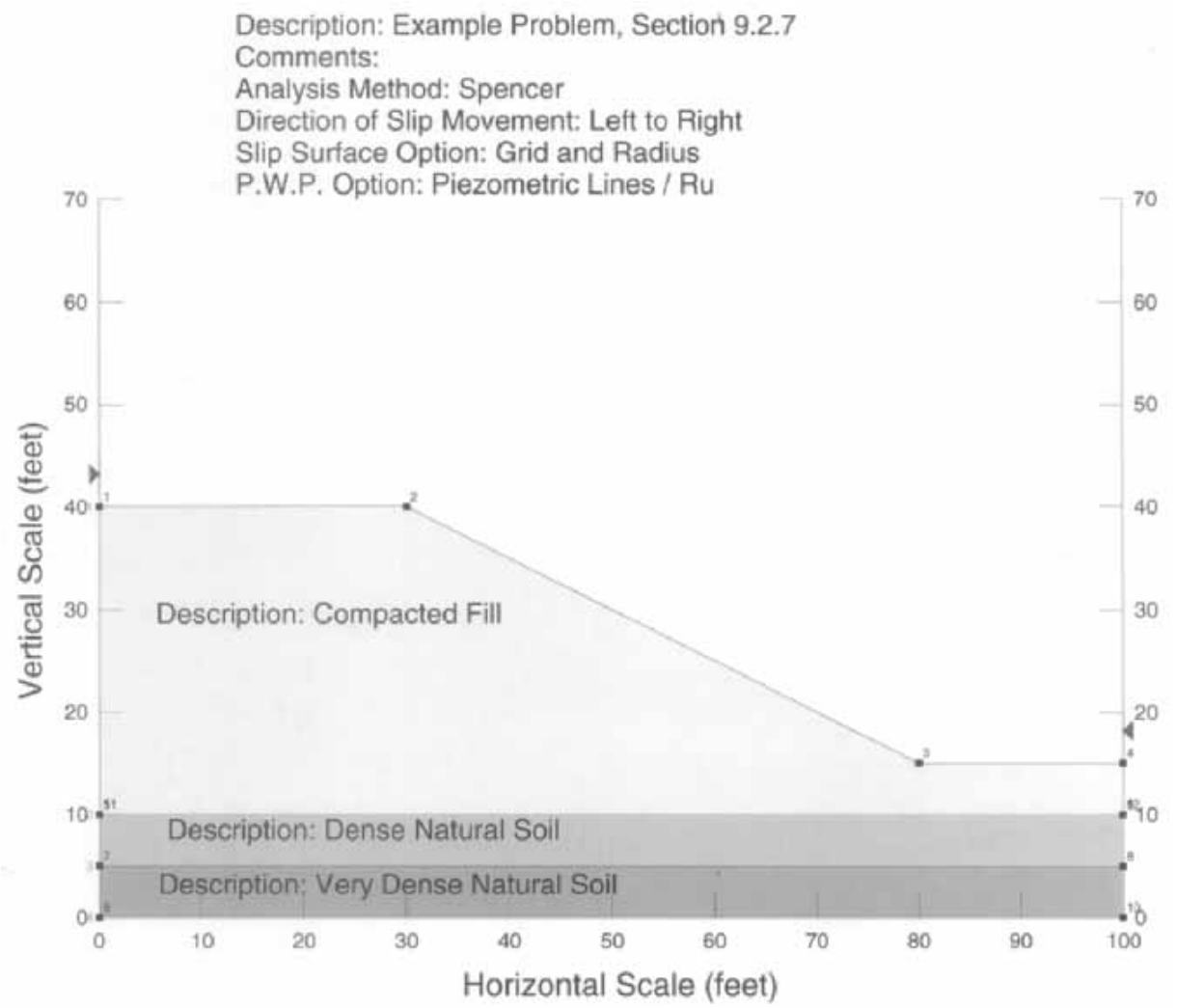

FIGURE 9.10 Cross section of the slope that is used for the example problem.

- Type of analysis: effective stress analysis
- Slope inclination: 2 : 1 (horizontal : vertical)
- Slope height = 25 ft
- Soil types:
  1. *Compacted fill:* It consists of dense granular soil having the following shear strength parameters: $\phi' = 37°$ and $c' = 0$. The total unit weight of the soil $\gamma_t = 125$ lb/ft^3.
  2. *Dense natural soil:* Underlying the fill, there is a 5-ft-thick dense natural soil layer having the following shear strength parameters: $\phi' = 38°$ and $c' = 100$ lb/ft^2. The total unit weight of the soil $\gamma_t = 125$ lb/ft^3.
  3. *Very dense natural soil:* Underlying the dense natural soil, there is a very dense natural soil layer having the following shear strength parameters: $\phi' = 40°$ and $c' = 200$ lb/ft^2. The total unit weight of the soil $\gamma_t = 130$ lb/ft^3.
- Groundwater table: The seasonal high groundwater table is located at the top of the dense natural soil layer. For the compacted fill, the pore water pressures u have been assumed to be equal to zero.

The slope stability analyses for the example problem were performed by using the SLOPE/W (Geo-Slope 1991) computer program. In particular, the slope stability analyses for the cross section shown in Fig. 9.10 were performed for two cases: the static case and the pseudostatic case, as described below:

Static Case. The first slope stability analysis was used to calculate the factor of safety of the slope for the static case (i.e., no earthquake forces). Particular details of the analysis are as follows:

- *Critical slip surface:* For this analysis, the computer program was requested to perform a trial-and-error search for the critical slip surface (i.e., the slip surface having the lowest factor of safety). Note in Fig. 9.11 that a grid of points has been produced above the slope. Each one of these points represents the center of rotation of a circular arc slip surface passing through the base of the slope. The computer program has actually performed about 1300 slope stability analyses, using the Spencer method of slices. In Fig. 9.11, the dot with the number 1.590 indicates the center of rotation of the circular arc slip surface with the lowest factor of safety (i.e., lowest factor of safety = 1.59).

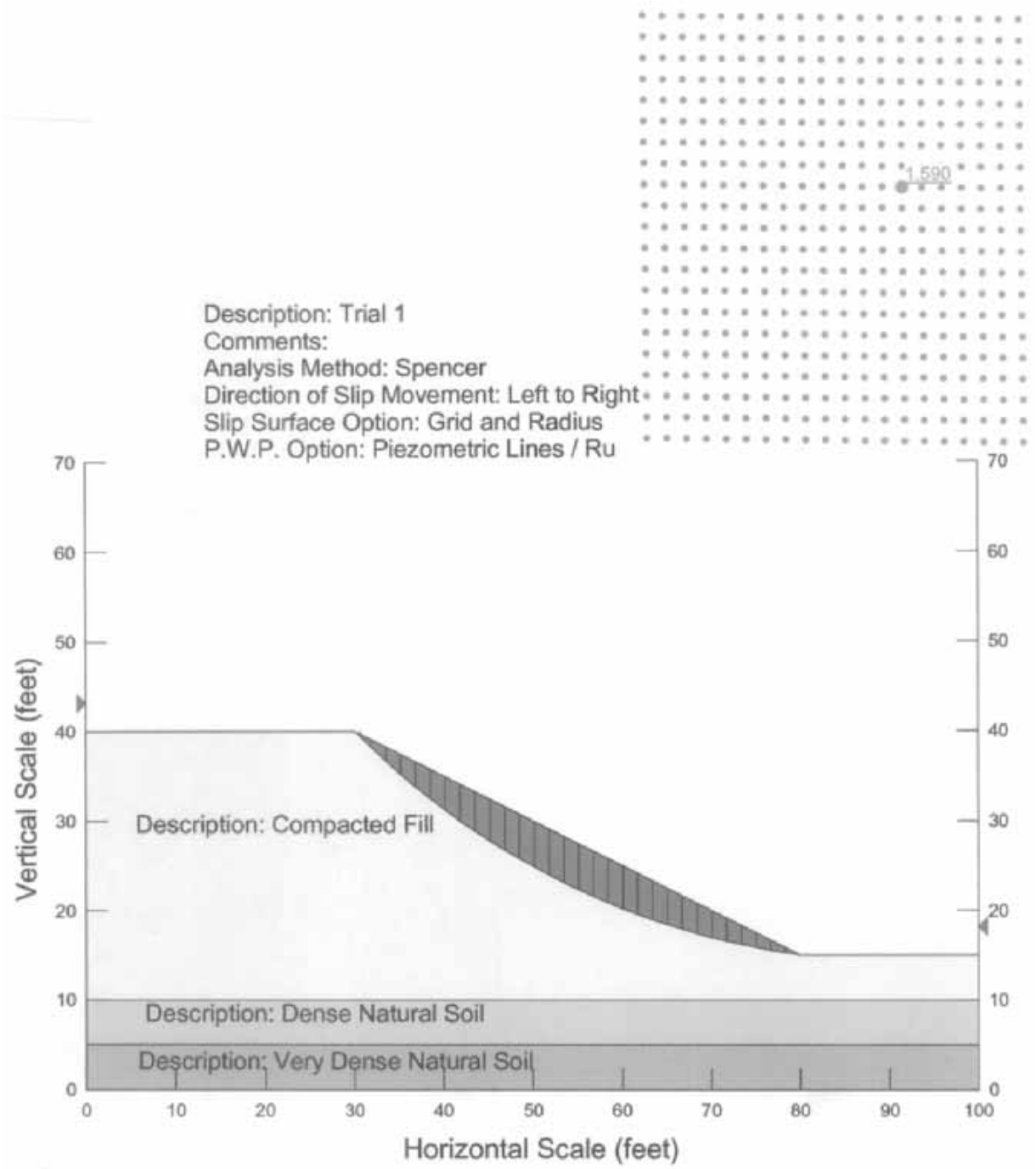

FIGURE 9.11 Slope stability analysis for the static condition using the SLOPE/W computer program (Geo-Slope 1991).

- *Check the results:* It is always a good idea to check the final results from the computer program. For this slope, with $c' = 0$, the factor of safety can be approximated as follows:

$$FS = \frac{\tan \phi'}{\tan \alpha} = \frac{\tan 37°}{\tan 26.6°} = 1.50$$

This value of FS = 1.50 is close to the value calculated by the computer program—1.59—and provides a check on the answer. A factor of safety of 1.5 is typically an acceptable condition for a permanent slope.

- *Shear strength and shear mobilized:* The SLOPE/W (Geo-Slope 1991) computer program has the ability to print out different forces acting on the individual slices that comprise the critical failure mass. For example, Fig. 9.12 shows the shear strength and the mobilized shear along the base of each slice. The distance referred to in Fig. 9.12 is the distance measured along the slip surface, starting at the uppermost slice. Notice in Fig. 9.12 that the shear strength is always greater than the mobilized shear for each slice, which makes sense because the factor of safety is much greater than 1.0.

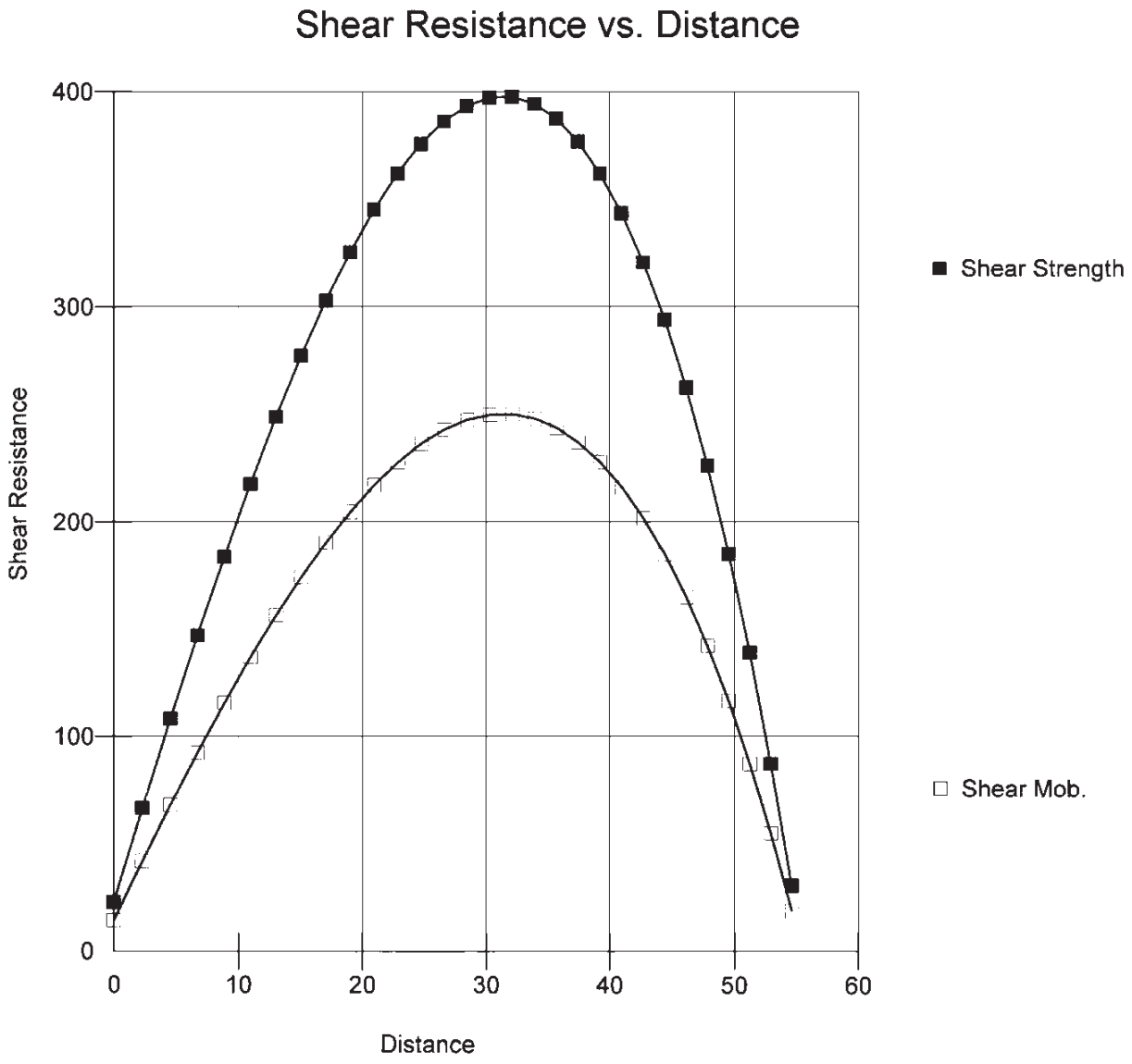

FIGURE 9.12 Shear strength and mobilized shear along the base of each slice for the static slope stability analysis. The SLOPE/W computer program was used to generate the plot (Geo-Slope 1991).

- *Seismic force divided by slice width:* Figure 9.13 shows the seismic force divided by slice width for each slice. Since the first analysis was performed for the static case, the seismic force is equal to zero for all slices.
- *Interslice forces:* Figure 9.14 shows the interslice forces (normal force and shear force). The interslice forces increase and decrease in a similar fashion to the shear forces along the base of the slices (Fig. 9.12). This is to be expected since it is the middle slices that have the greatest depth, and hence greatest shear resistance and highest interslice forces.

Pseudostatic Case. The second slope stability analysis was for the pseudostatic condition. All three soil types for this example problem are in a dense to very dense state and are not expected to lose shear strength during the seismic shaking. Therefore a pseudostatic slope stability analysis can be performed for this slope. The only additional item that needs to be input into the computer program is the seismic coefficient k_h. For this example problem, it was assumed that the seismic coefficient $k_h = 0.40$. Particular details of the analysis are as follows:

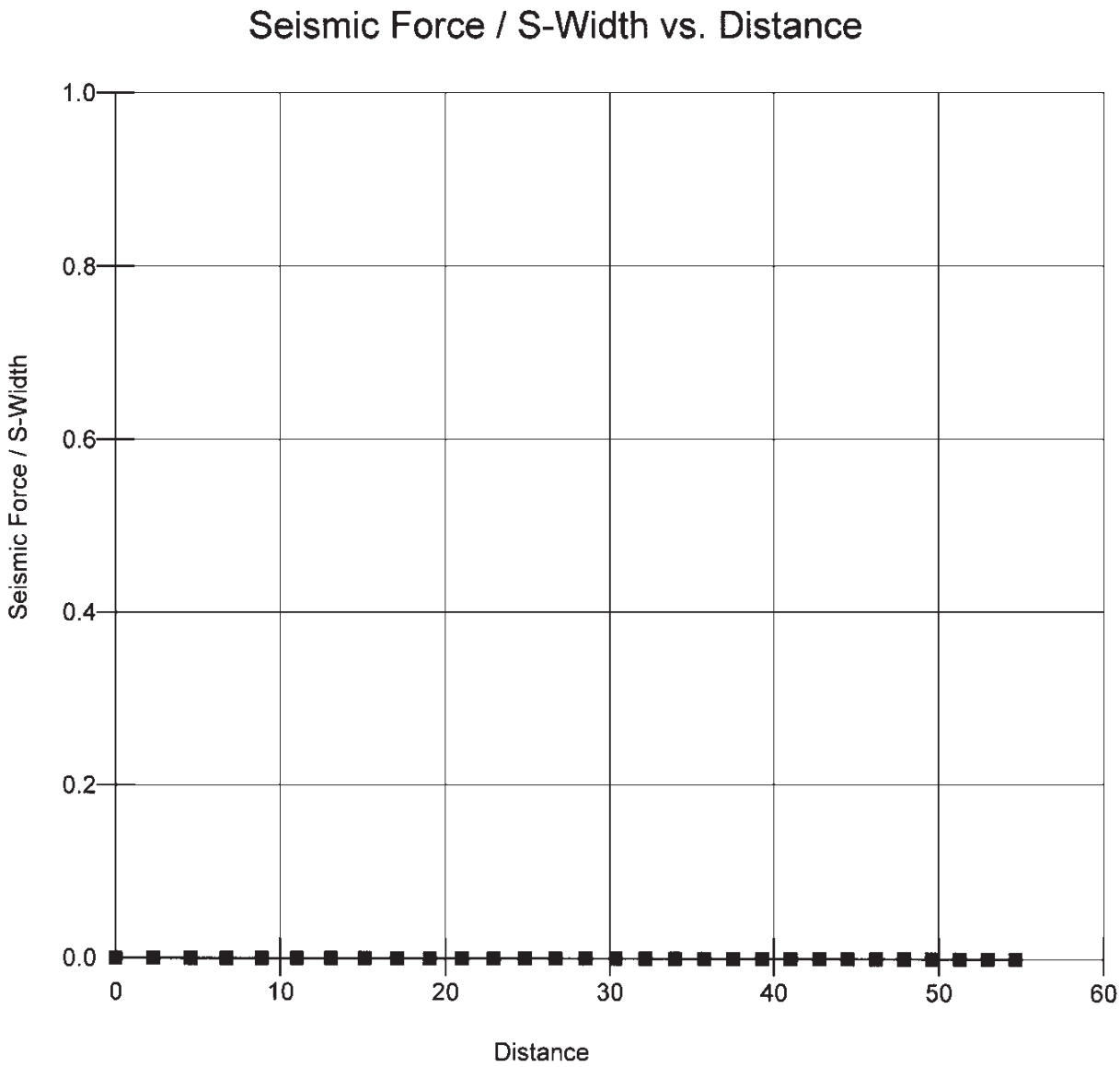

FIGURE 9.13 Seismic force for each slice in the static slope stability analysis. Note that the seismic force must equal zero for the static case. The SLOPE/W computer program was used to generate the plot (GeoSlope 1991).

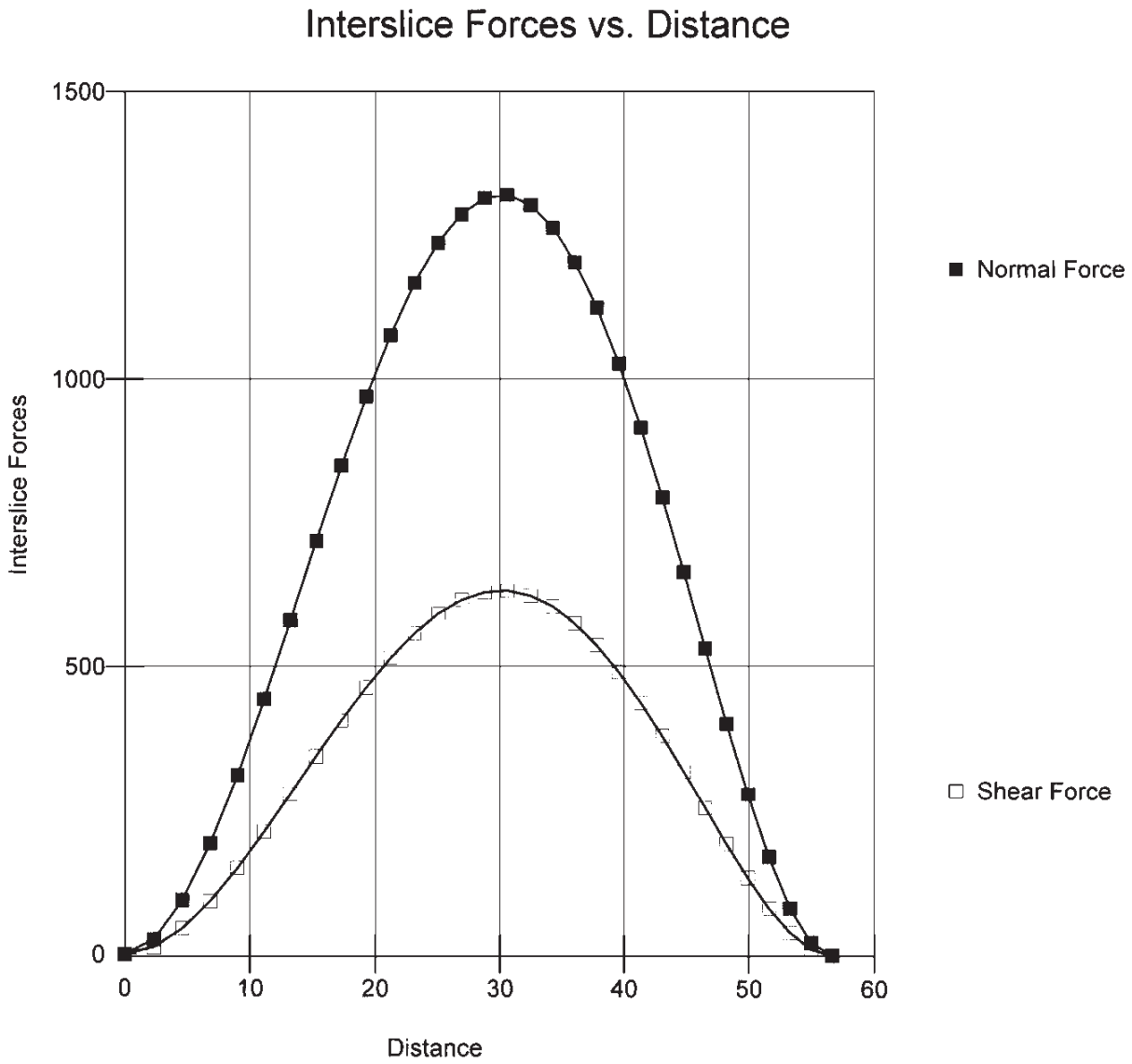

FIGURE 9.14 The shear force and normal force acting between each slice for the static slope stability analysis. These forces are also known as the interslice forces. The SLOPE/W computer program was used to generate the plot (Geo-Slope 1991).

- *Critical slip surface:* Similar to the static analysis, the computer program was requested to perform a trial-and-error search for the critical slip surface (i.e., the slip surface having the lowest factor of safety). In Fig. 9.15, the dot with the number 0.734 indicates the center of rotation of the circular arc slip surface with the lowest factor of safety (i.e., lowest factor of safety = 0.734). Since this factor of safety is less than 1.0, it is expected that the slope will fail during the earthquake.
- *Shear strength and shear mobilized:* Figure 9.16 shows the shear strength and the mobilized shear along the base of each slice. Notice in Fig. 9.16 that the shear strength is always less than the mobilized shear for each slice, which makes sense because the factor of safety is less than 1.0.
- *Seismic force divided by slice width:* Figure 9.17 shows the seismic force divided by the slice width for each slice. The seismic force is higher for the middle slices because they are deeper slices and hence have a larger weight.
- *Interslice forces:* Figure 9.18 shows the interslice forces (normal force and shear force). The interslice forces increase and decrease in a similar fashion to the shear forces along the base of the slices (Fig. 9.16). This is to be expected since it is the middle slices

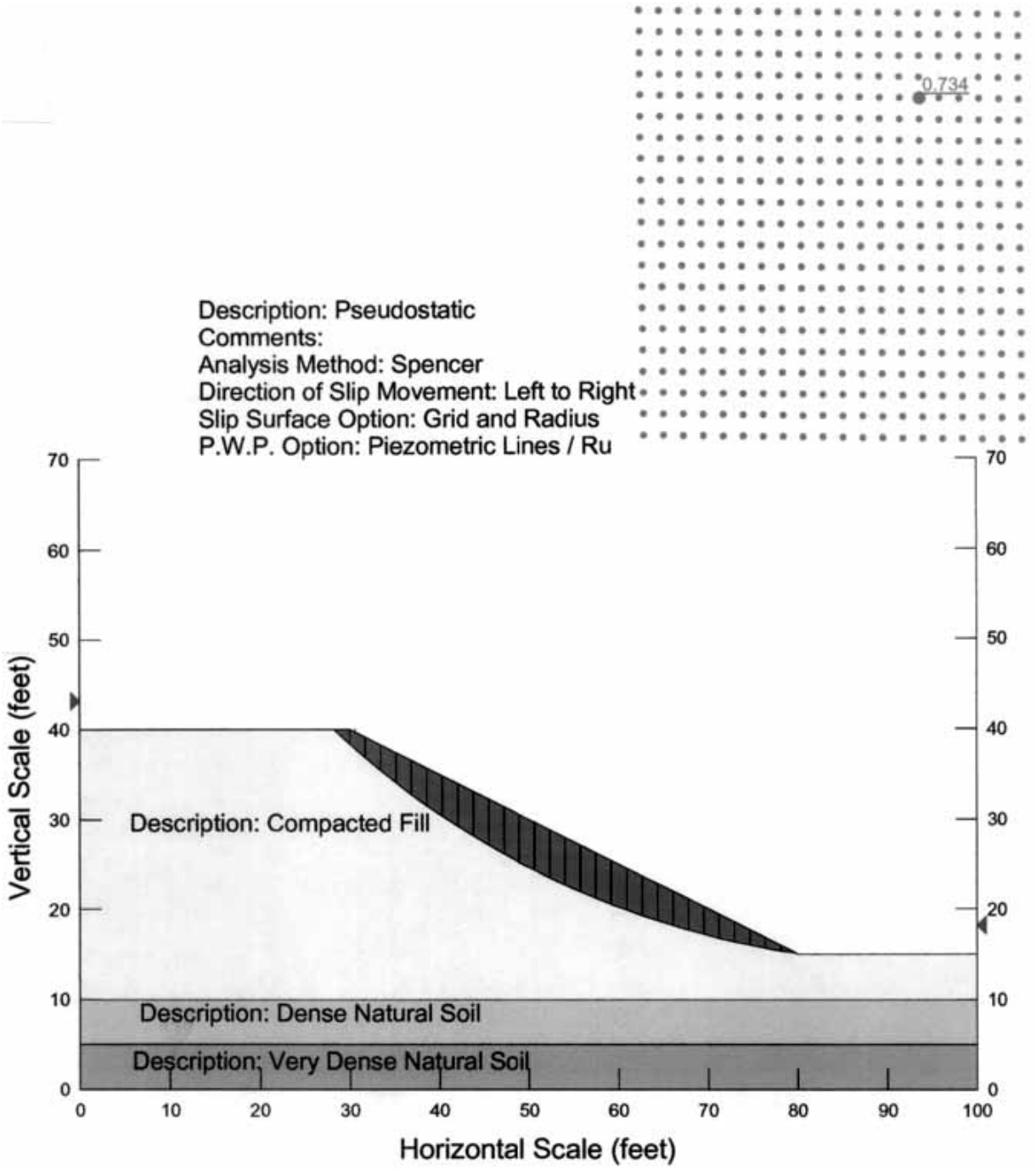

FIGURE 9.15 Slope stability analysis for the pseudostatic condition using the SLOPE/W computer program (Geo-Slope 1991).

that have the greatest depth, and hence greatest shear resistance and highest interslice forces.

- *Extent of slope failure:* The pseudostatic method shows that only the outer face of the slope is most susceptible to failure. The slip surface could be forced farther back into the slope to evaluate the factor of safety versus distance from the top of slope. The extent of the slope that would be subjected to failure could then be determined (i.e., that slip surface that has FS = 1.0).

In summary, the factor of safety of the slope for the pseudostatic condition is less than 1.0, and failure of the slope is expected to occur during the earthquake. Acceptable values of the pseudostatic factor of safety are typically in the range of 1.1 to 1.15.

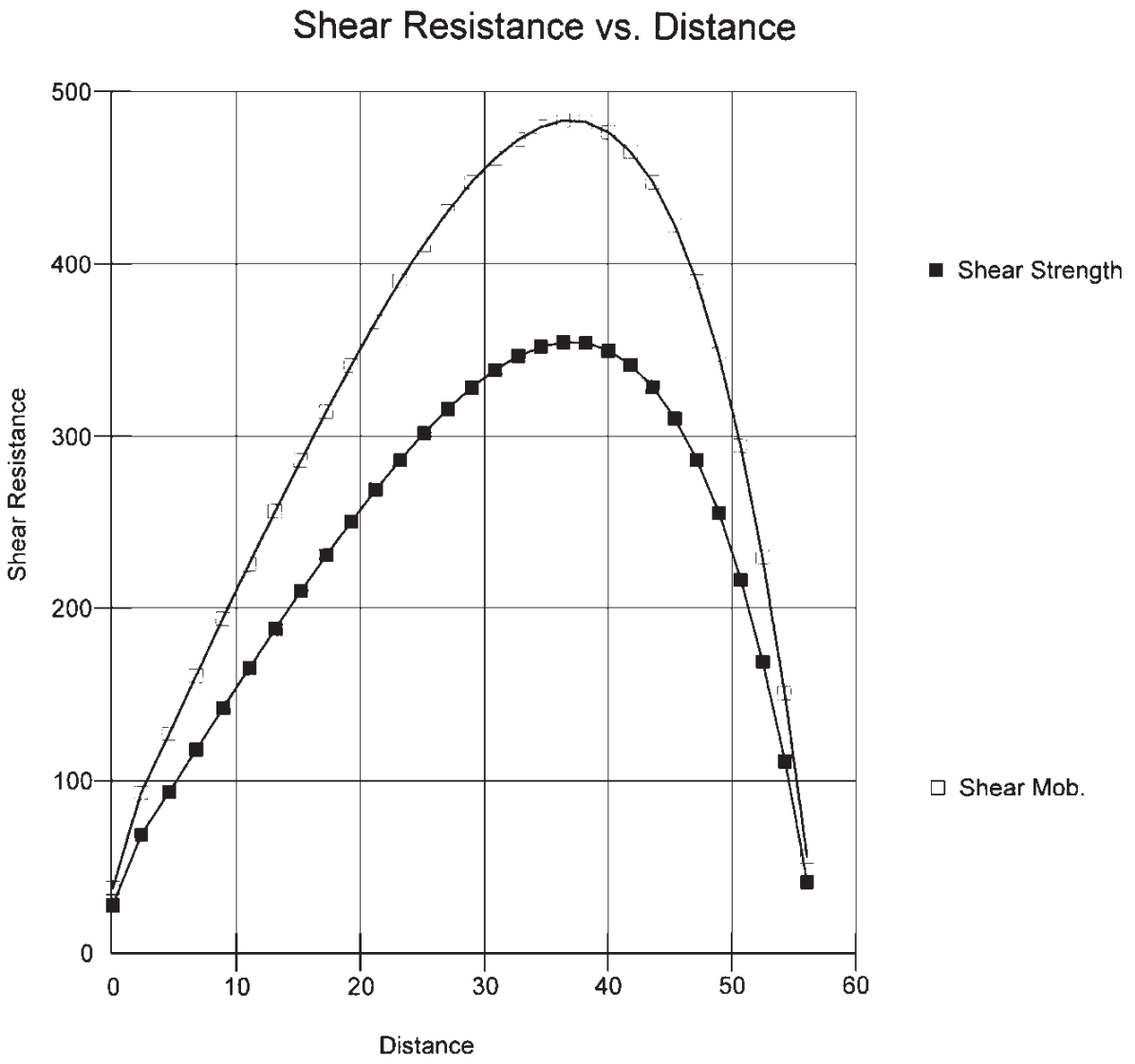

FIGURE 9.16 Shear strength and mobilized shear along the base of each slice for the pseudostatic slope stability analysis. The SLOPE/W computer program was used to generate the plot (Geo-Slope 1991).

9.3 INERTIA SLOPE STABILITY—NEWMARK METHOD

9.3.1 Introduction

The purpose of the Newmark (1965) method is to estimate the slope deformation for those cases where the pseudostatic factor of safety is less than 1.0 (i.e., the failure condition). The Newmark (1965) method assumes that the slope will deform only during those portions of the earthquake when the out-of-slope earthquake forces cause the pseudostatic factor of safety to drop below 1.0. When this occurs, the slope will no longer be stable, and it will be accelerated downslope. The longer that the slope is subjected to a pseudostatic factor of safety below 1.0, the greater the slope deformation. On the other hand, if the pseudostatic factor of safety drops below 1.0 for a mere fraction of a second, then the slope deformation will be limited.

Figure 9.19 can be used to illustrate the basic premise of the Newmark (1965) method. Figure 9.19*a* shows the horizontal acceleration of the slope during an earthquake. Those accelerations that plot above the zero line are considered to be out-of-slope accelerations, while

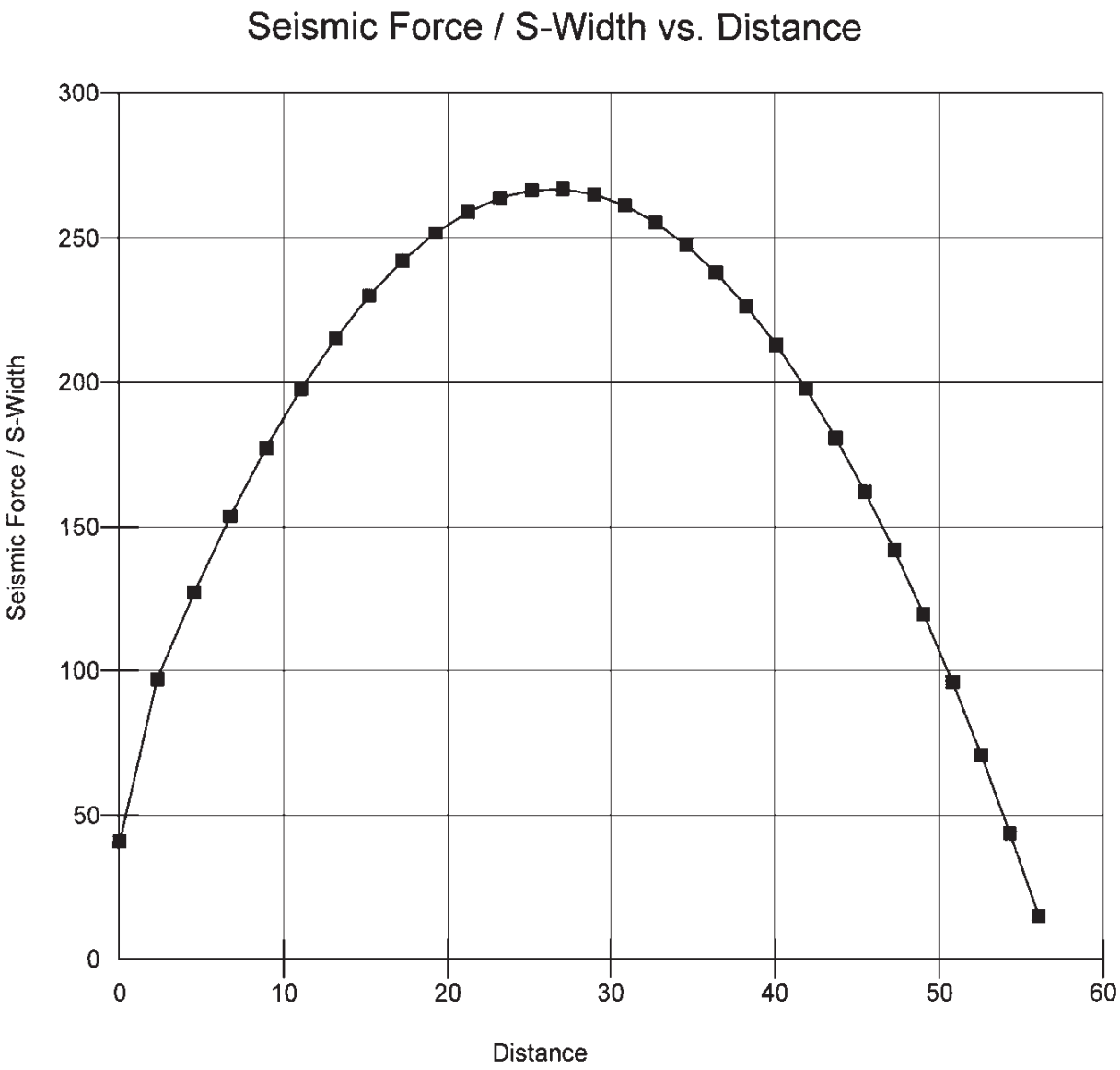

FIGURE 9.17 Seismic force for each slice in the pseudostatic slope stability analysis. The SLOPE/W computer program was used to generate the plot (Geo-Slope 1991).

those accelerations that plot below the zero line are considered to be into-the-slope accelerations. It is only the out-of-slope accelerations that cause downslope movement, and thus only the acceleration that plots above the zero line is considered in the analysis. In Fig. 9.19*a,* a dashed line has been drawn that corresponds to the horizontal yield acceleration, which is designated a_y. This horizontal yield acceleration a_y is considered to be the horizontal earthquake acceleration that results in a pseudostatic factor of safety that is exactly equal to 1.0. The portions of the two acceleration pulses that plot above a_y have been darkened. According to the Newmark (1965) method, it is these darkened portions of the acceleration pulses that will cause lateral movement of the slope.

Figure 9.19*b* and *c* presents the corresponding horizontal velocity and slope displacement that occur in response to the darkened portions of the two acceleration pulses. Note that the slope displacement is incremental and occurs only when the horizontal acceleration from the earthquake exceeds the horizontal yield acceleration a_y. The magnitude of the slope displacement depends on the following factors:

1. *Horizontal yield acceleration a_y:* The higher the horizontal yield acceleration a_y, the more stable the slope is for any given earthquake.

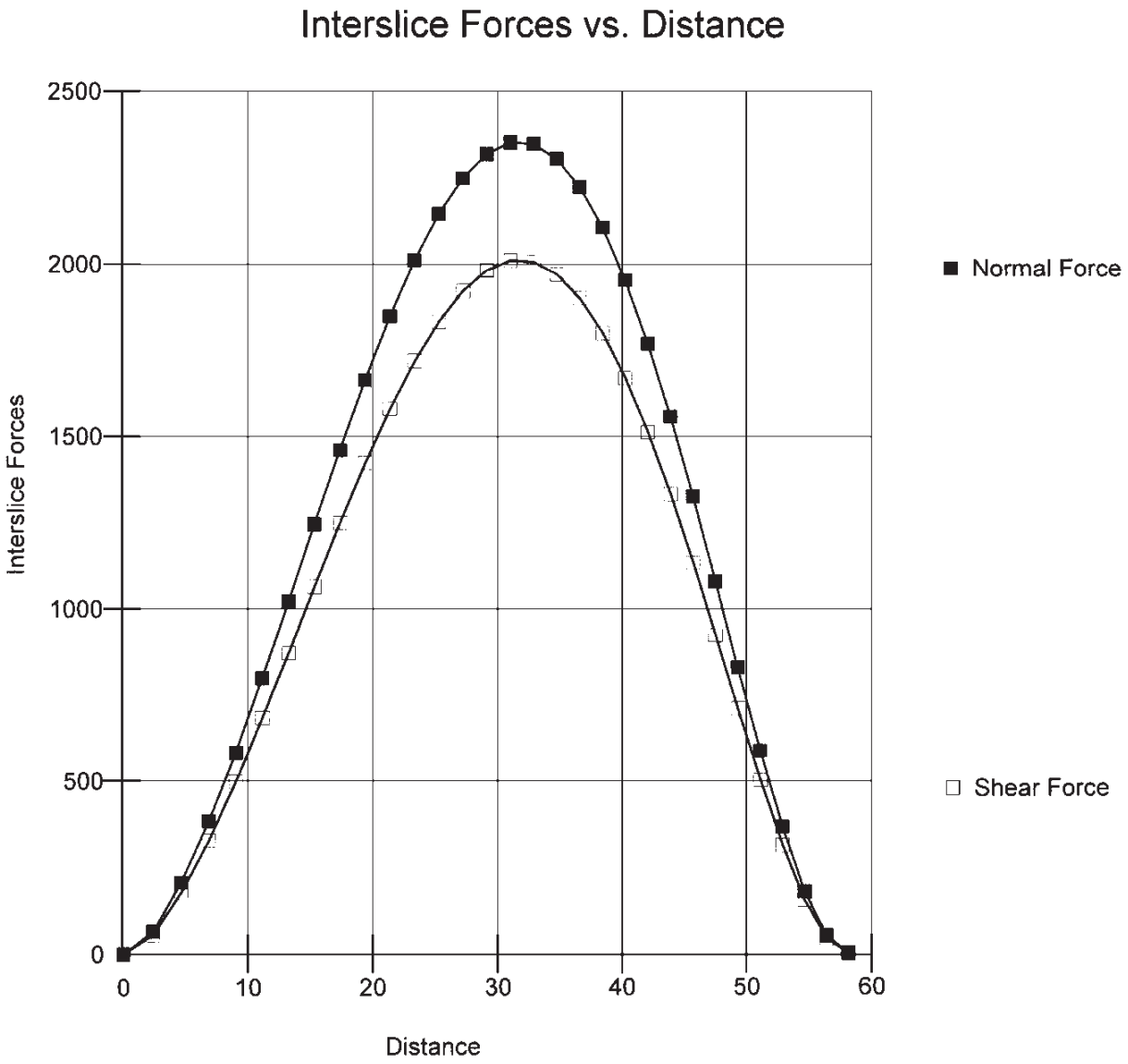

FIGURE 9.18 The shear force and normal force acting between each slice for the pseudostatic slope stability analysis. These forces are also known as the interslice forces. The SLOPE/W computer program was used to generate the plot (Geo-Slope 1991).

2. *Peak ground acceleration* a_{max}: The peak ground acceleration a_{max} represents the highest value of the horizontal ground acceleration. In essence, this is the amplitude of the maximum acceleration pulse. The greater the difference between the peak ground acceleration a_{max} and the horizontal yield acceleration a_y, the larger the downslope movement.
3. *Length of time:* The longer the earthquake acceleration exceeds the horizontal yield acceleration a_y, the larger the downslope deformation. Considering the combined effects of items 2 and 3, it can be concluded that the larger the shaded area shown in Fig. 9.19*a*, the greater the downslope movement.
4. *Number of acceleration pulses:* The larger the number of acceleration pulses that exceed the horizontal yield acceleration a_y, the greater the cumulative downslope movement during the earthquake.

Many different equations have been developed utilizing the basic Newmark (1965) method as outlined above. One simple equation that is based on the use of two of the four main parameters discussed above is as follows (Ambraseys and Menu 1988):

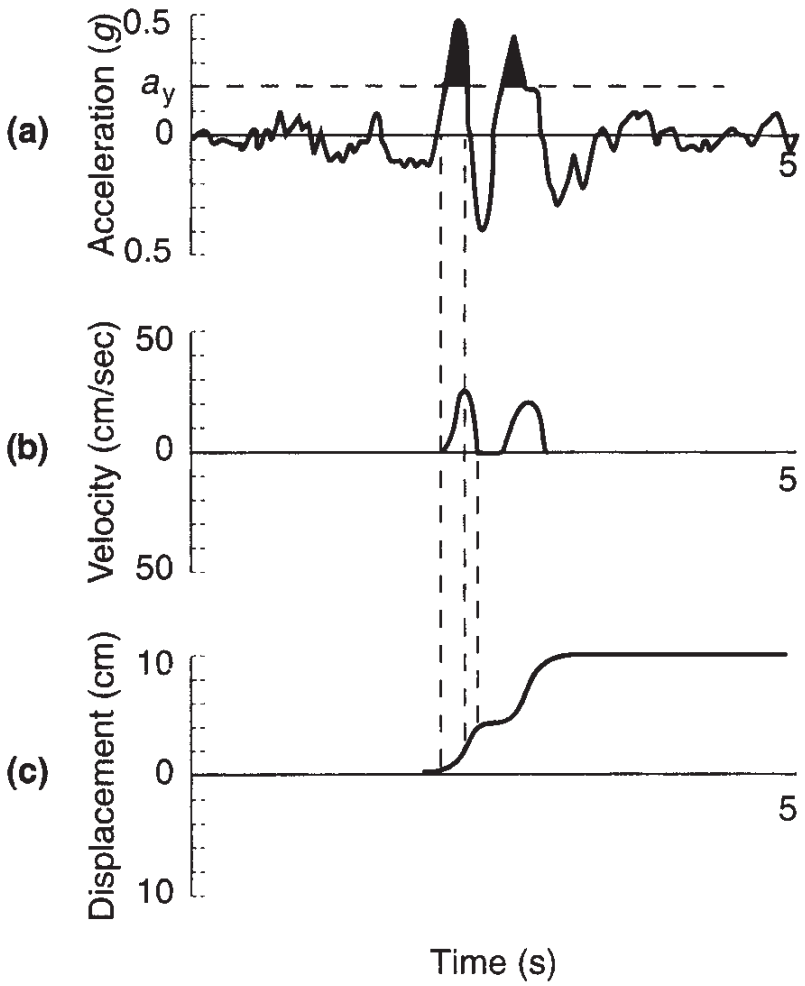

FIGURE 9.19 Diagram illustrating the Newmark method. (*a*) Acceleration versus time; (*b*) velocity versus time for the darkened portions of the acceleration pulses; (*c*) the corresponding downslope displacement versus time in response to the velocity pulses. (*After Wilson and Keefer 1985.*)

$$\log d = 0.90 + \log\left[\left(1 - \frac{a_y}{a_{max}}\right)^{2.53}\left(\frac{a_y}{a_{max}}\right)^{-1.09}\right] \tag{9.3}$$

where d = estimated downslope movement caused by the earthquake, cm
a_y = yield acceleration, defined as the horizontal earthquake acceleration that results in a pseudostatic factor of safety that is exactly equal to 1.0
$a_{\max}$ = peak ground acceleration of the design earthquake

Based on the Newmark (1965) method, Eq. (9.3) is valid only for those cases where the pseudostatic factor of safety is less than 1.0. In essence, the peak ground acceleration $a_{\max}$ must be greater then the horizontal yield acceleration a_y. To use Eq. (9.3), the first step is to determine the pseudostatic factor of safety, using the method outlined in Sec. 9.2. Provided the pseudostatic factor of safety is less than 1.0, the next step is to reduce the value of the seismic coefficient k_h until a factor of safety exactly equal to 1.0 is obtained. This can usually be quickly accomplished when using a slope stability computer program. The value of k_h that corresponds to a pseudostatic factor of safety equal to 1.0 can easily be converted to the yield acceleration [i.e., see Eq. (9.1)]. Substituting the values of the peak ground acceleration $a_{\max}$ and the yield acceleration a_y into Eq. (9.3), we can determine the slope deformation in centimeters.

Because Eq. (9.3) utilizes the peak ground acceleration a_{max} from the earthquake, the analysis tends to be more accurate for small or medium-sized failure masses where the seismic coefficient k_h is approximately equal to a_{max}/g (see Sec. 9.2.2).

9.3.2 Example Problem

Consider the example problem in Sec. 9.2.7. For this example problem, it was determined that the pseudostatic factor of safety = 0.734 for a peak ground acceleration $a_{max} = 0.40g$ (i.e., the seismic coefficient k_h is equal to 0.40). Since the pseudostatic factor of safety is less than 1.0, the Newmark (1965) method can be used to estimate the slope deformation. Although the stability analysis is not shown, the SLOPE/W (Geo-Slope 1991) computer program was utilized to determine the value of k_h that corresponds to a pseudostatic factor of safety of 1.0. This value of k_h is equal to 0.22, and thus the yield acceleration a_y is equal to $0.22g$. Substituting the ratio of $a_y/a_{max} = 0.22g/0.40g = 0.55$ into Eq. (9.3) yields

$$\log d = 0.90 + \log [(1 - 0.55)^{2.53} (0.55)^{-1.09}]$$

or

$$\log d = 0.90 + \log 0.254 = 0.306$$

And solving the above equation reveals the slope deformation d is equal to about 2 cm. Thus, although the pseudostatic factor of safety is well below 1.0 (i.e., pseudostatic factor of safety = 0.734), Eq. (9.3) predicts that only about 2 cm of downslope movement will occur during the earthquake.

9.3.3 Limitation of the Newmark Method

Introduction. The major assumption of the Newmark (1965) method is that the slope will deform only when the peak ground acceleration a_{max} exceeds the yield acceleration a_y. This type of analysis is most appropriate for a slope that deforms as a single massive block, such as a wedge-type failure. In fact, Newmark (1965) used the analogy of a sliding block on an inclined plane to develop the displacement equations.

A limitation of the Newmark (1965) method is that it may prove unreliable for those slopes that do not tend to deform as a single massive block. An example is a slope composed of dry and loose granular soil (i.e., sands and gravels). The individual soil grains that compose a dry and loose granular soil will tend to individually deform, rather than the entire slope deforming as one massive block.

The earthquake-induced settlement of dry and loose granular soil is discussed in Sec. 7.4 (i.e., volumetric compression). As discussed in that section, the settlement of a dry and loose granular soil is primarily dependent on three factors: (1) the relative density D_r of the soil, which can be correlated with the SPT blow count $(N_1)_{60}$ value; (2) the maximum shear strain induced by the design earthquake; and (3) the number of shear strain cycles.

The amount of lateral movement of slopes composed of dry and loose granular soils is difficult to determine. The method outlined in Sec. 7.4 will tend to underestimate the amount of settlement of a slope composed of dry and loose granular soil. This is because in a sloping environment, the individual soil particles not only will settle, but also will deform laterally in response to the unconfined slope face. In terms of initial calculations, the method outlined in Sec. 7.4 could be used to determine the minimum settlement at the top of slope. However, the actual settlement will be greater because of the unconfined slope condition. In addition, it is anticipated that the lateral movement will be the same order of

magnitude as the calculated settlement. The following example problem illustrates these calculations.

Example Problem. To illustrate the analysis for dry and loose sand, assume that a slope has a height of 50 ft (15.2 m) and consists of dry and loose sand that has an $(N_1)_{60}$ value equal to 5. Further assume that the slope has a 22° slope inclination and that the slope is underlain by rock. A cross section illustrating these conditions is presented in Fig. 9.20.

To use the pseudostatic method, the earthquake must not weaken the soil. The pseudostatic slope stability methods can be used for the dry and loose sand because it will not lose shear strength during the earthquake. In fact, as the sand settles during the earthquake, there may even be a slight increase in shear strength. The friction angle ϕ' of well-graded dry and loose sand typically varies from about 30° to 34° (Table 6.12, Day 2001b). Based on an average value, a friction angle ϕ' of the dry and loose sand that is equal to 32° will be used in the slope stability analysis. In addition, for the design earthquake, a peak ground acceleration a_{max} equal to 0.20g will be used. Furthermore, the unit weight of the sand is assumed to be equal to 95 lb/ft^3 (15 kN/m^3).

Figure 9.21 shows the results of the pseudostatic slope stability analysis. For a peak ground acceleration a_{max} of 0.20g, the pseudostatic factor of safety is equal to 1.116. Since the pseudostatic factor of safety is greater than 1.0, there will be no slope deformation per the Newmark (1965) method. However, by using the method by Tokimatsu and Seed presented in Sec. 7.4.3, a 50-ft- (15.2-m-) thick layer of dry and loose sand having an $(N_1)_{60}$ value of 5 will experience about 2 in (5 cm) of settlement (see Prob. 7.25). Thus the minimum amount of downward movement of the top of slope will be 2 in (5 cm). Because of

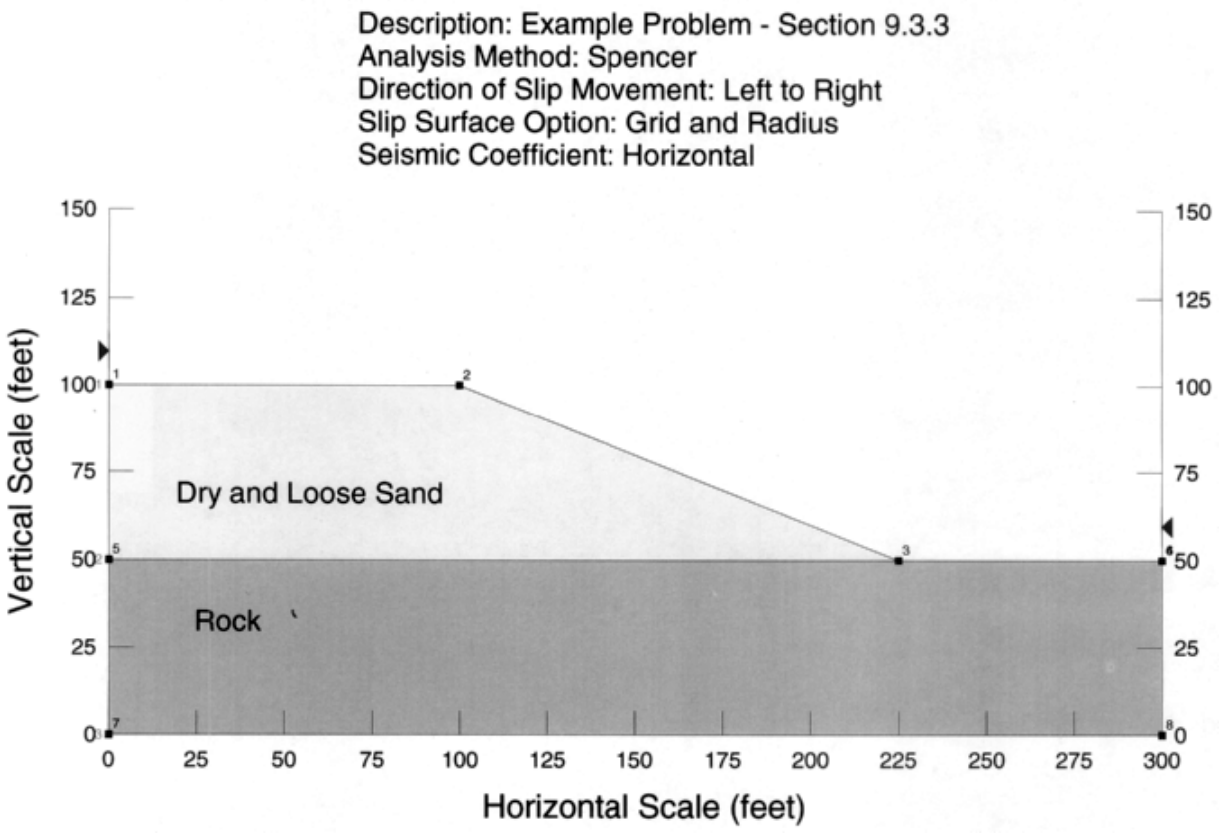

FIGURE 9.20 Cross section of the slope used for the example problem.

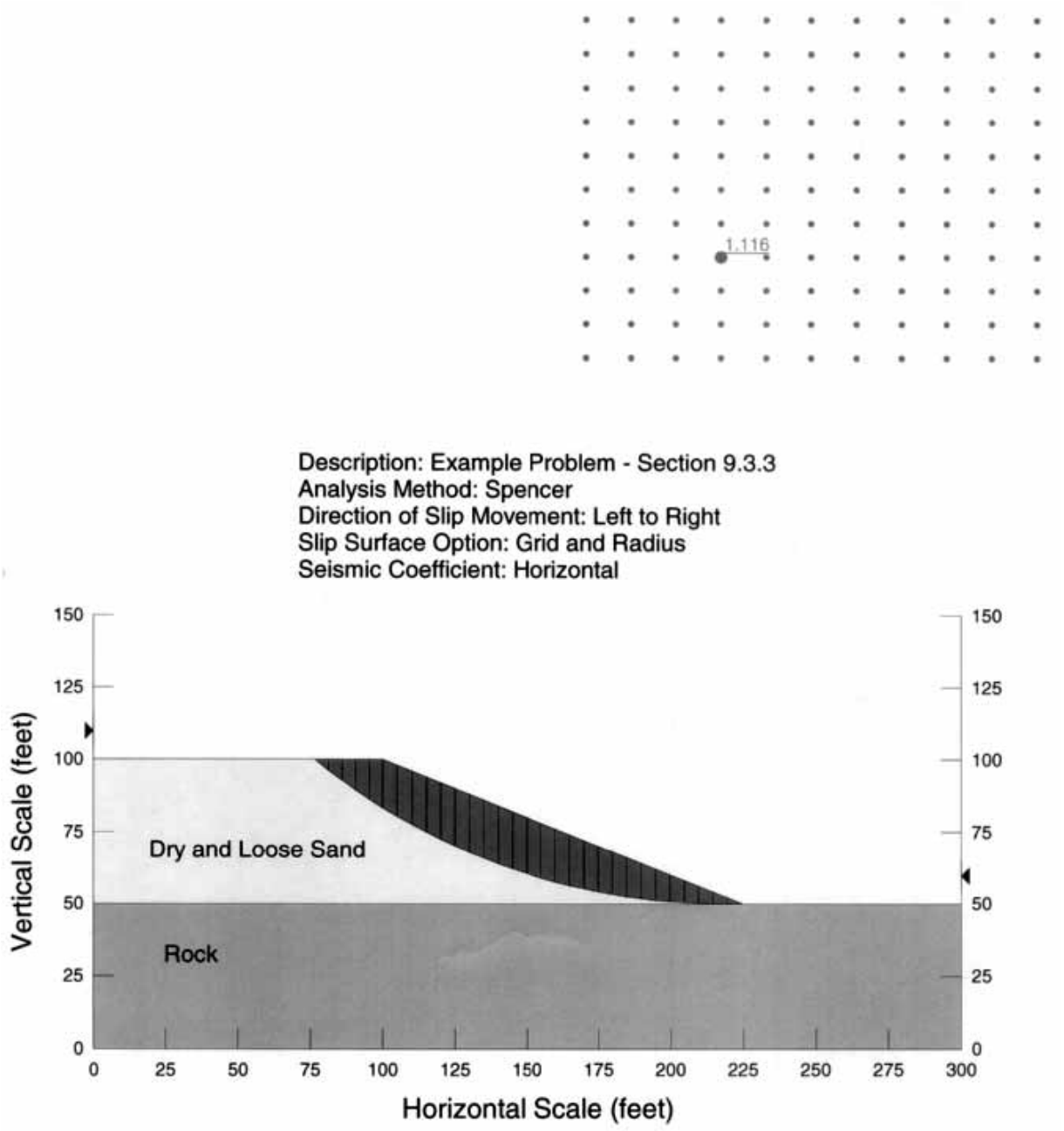

FIGURE 9.21 Slope stability analysis for the pseudostatic condition using the SLOPE/W computer program (Geo-Slope 1991).

the unconfined slope face, it is anticipated that the downward movement will exceed 2 in (5 cm). In addition, there will be lateral movement of the slope, which will also most likely exceed 2 in (5 cm).

Summary. In summary, the Newmark (1965) method assumes no deformation of the slope during the earthquake if the pseudostatic factor of safety is greater than 1.0. However, as indicated by the above example, a slope composed of dry and loose sand could both settle and deform laterally even if the pseudostatic factor of safety is greater than 1.0. Thus the Newmark (1965) method should be used only for slopes that will deform as an intact massive block, and not for those cases of individual soil particle movement (such as a dry and loose granular soil).

CHAPTER 10
RETAINING WALL ANALYSES FOR EARTHQUAKES

The following notation is used in this chapter:

SYMBOL	*DEFINITION*
a	Acceleration (Sec. 10.2)
a	Horizontal distance from W to toe of footing
a_{max}	Maximum horizontal acceleration at ground surface (also known as peak ground acceleration)
A_p	Anchor pull force (sheet pile wall)
c	Cohesion based on total stress analysis
c'	Cohesion based on effective stress analysis
c_a	Adhesion between bottom of footing and underlying soil
d	Resultant location of retaining wall forces (Sec. 10.1.1)
d_1	Depth from ground surface to groundwater table
d_2	Depth from groundwater table to bottom of sheet pile wall
D	Depth of retaining wall footing
D	Portion of sheet pile wall anchored in soil (Fig. 10.9)
e	Lateral distance from P_v to toe of retaining wall
F, FS	Factor of safety
FS_L	Factor of safety against liquefaction
g	Acceleration of gravity
H	Height of retaining wall
H	Unsupported face of sheet pile wall (Fig. 10.9)
k_A	Active earth pressure coefficient
k_{AE}	Combined active plus earthquake coefficient of pressure (Mononobe-Okabe equation)
k_h	Seismic coefficient, also known as pseudostatic coefficient
k_0	Coefficient of earth pressure at rest
k_p	Passive earth pressure coefficient
k_v	Vertical pseudostatic coefficient
L	Length of active wedge at top of retaining wall
m	Total mass of active wedge
M_{max}	Maximum moment in sheet pile wall
N	Sum of wall weights W plus, if applicable, P_v
P_A	Active earth pressure resultant force
P_E	Pseudostatic horizontal force acting on retaining wall
P_{ER}	Pseudostatic horizontal force acting on restrained retaining wall
P_F	Sum of sliding resistance forces (Fig. 10.2)
P_H	Horizontal component of active earth pressure resultant force
P_L	Lateral force due to liquefied soil
P_p	Passive resultant force

P_R Static force acting upon restrained retaining wall
P_v Vertical component of active earth pressure resultant force
P_1 Active earth pressure resultant force ($P_1 = P_A$, Fig. 10.7)
P_2 Resultant force due to uniform surcharge
Q Uniform vertical surcharge pressure acting on wall backfill
R Resultant of retaining wall forces (Fig. 10.2)
s_u Undrained shear strength of soil
W Total weight of active wedge (Sec. 10.2)
W Resultant of vertical retaining wall loads
β Slope inclination behind the retaining wall
δ, ϕ_{cv} Friction angle between bottom of wall footing and underlying soil
δ, ϕ_w Friction angle between back face of wall and soil backfill
ϕ Friction angle based on total stress analysis
ϕ' Friction angle based on effective stress analysis
γ_b Buoyant unit weight of soil
γ_{sat} Saturated unit weight of soil
γ_t Total unit weight of the soil
θ Back face inclination of retaining wall
σ_{avg} Average bearing pressure of retaining wall foundation
σ_{mom} That portion of bearing pressure due to eccentricity of N
ψ Equal to $\tan^{-1}(a_{max}/g)$

10.1 INTRODUCTION

A *retaining wall* is defined as a structure whose primary purpose is to provide lateral support for soil or rock. In some cases, the retaining wall may also support vertical loads. Examples include basement walls and certain types of bridge abutments. The most common types of retaining walls are shown in Fig. 10.1 and include gravity walls, cantilevered walls, counterfort walls, and crib walls. Table 10.1 lists and describes various types of retaining walls and backfill conditions.

10.1.1 Retaining Wall Analyses for Static Conditions

Figure 10.2 shows various types of retaining walls and the soil pressures acting on the walls for static (i.e., nonearthquake) conditions. There are three types of soil pressures acting on a retaining wall: (1) active earth pressure, which is exerted on the backside of the wall; (2) passive earth pressure, which acts on the front of the retaining wall footing; and (3) bearing pressure, which acts on the bottom of the retaining wall footing. These three pressures are individually discussed below.

Active Earth Pressure. To calculate the active earth pressure resultant force P_A, in kilonewtons per linear meter of wall or pounds per linear foot of wall, the following equation is used for granular backfill:

$$P_A = \tfrac{1}{2} k_A \gamma_t H^2 \tag{10.1}$$

where k_A = active earth pressure coefficient, γ_t = total unit weight of the granular backfill, and H = height over which the active earth pressure acts, as defined in Fig. 10.2. In its simplest form, the active earth pressure coefficient k_A is equal to

$$k_A = \tan^2(45° - \tfrac{1}{2}\phi) \tag{10.2}$$

where ϕ = friction angle of the granular backfill. Equation (10.2) is known as the active Rankine state, after the British engineer Rankine who in 1857 obtained this relationship. Equation (10.2) is only valid for the simple case of a retaining wall that has a vertical rear face, no friction between the rear wall face and backfill soil, and the backfill ground surface is horizontal. For retaining walls that do not meet these requirements, the active earth pressure

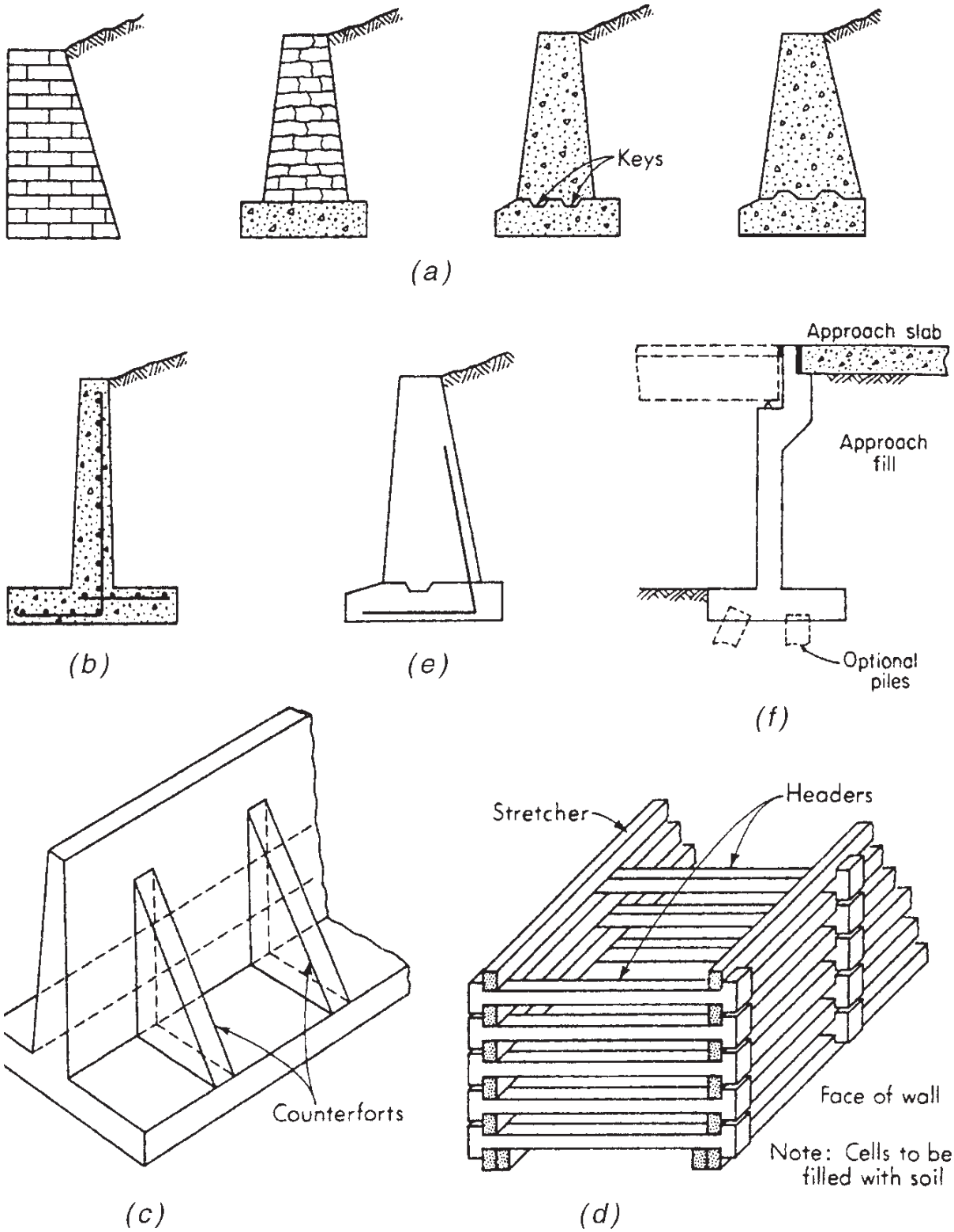

FIGURE 10.1 Common types of retaining walls. (*a*) Gravity walls of stone, brick, or plain concrete. Weight provides overturning and sliding stability. (*b*) Cantilevered wall. (*c*) Counterfort, or buttressed wall. If backfill covers counterforts, the wall is termed a *counterfort.* (*d*) Crib wall. (*e*) Semigravity wall (often steel reinforcement is used). (*f*) Bridge abutment. (*Reproduced from Bowles 1982 with permission of McGraw-Hill, Inc.*)

TABLE 10.1 Types of Retaining Walls and Backfill Conditions

Topic	Discussion
Types of retaining walls	As shown in Fig. 10.1, some of the more common types of retaining walls are gravity walls, counterfort walls, cantilevered walls, and crib walls (Cernica 1995a). Gravity retaining walls are routinely built of plain concrete or stone, and the wall depends primarily on its massive weight to resist failure from overturning and sliding. Counterfort walls consist of a footing, a wall stem, and intermittent vertical ribs (called counterforts) which tie the footing and wall stem together. Crib walls consist of interlocking concrete members that form cells which are then filled with compacted soil. Although mechanically stabilized earth retaining walls have become more popular in the past decade, cantilever retaining walls are still probably the most common type of retaining structure. There are many different types of cantilevered walls, with the common feature being a footing that supports the vertical wall stem. Typical cantilevered walls are T-shaped, L-shaped, or reverse L-shaped (Cernica 1995a).
Backfill material	Clean granular material (no silt or clay) is the standard recommendation for backfill material. There are several reasons for this recommendation: 1. *Predictable behavior:* Import granular backfill generally has a more predictable behavior in terms of earth pressure exerted on the wall. Also, expansive soil-related forces will not be generated by clean granular soil. 2. *Drainage system:* To prevent the buildup of hydrostatic water pressure on the retaining wall, a drainage system is often constructed at the heel of the wall. The drainage system will be more effective if highly permeable soil, such as clean granular soil, is used as backfill. 3. *Frost action:* In cold climates, frost action has caused many retaining walls to move so much that they have become unusable. If freezing temperatures prevail, the backfill soil can be susceptible to frost action, where ice lenses form parallel to the wall and cause horizontal movements of up to 0.6 to 0.9 m (2 to 3 ft) in a single season (Sowers and Sowers 1970). Backfill soil consisting of clean granular soil and the installation of a drainage system at the heel of the wall will help to protect the wall from frost action.
Plane strain condition	Movement of retaining walls (i.e., active condition) involves the shear failure of the wall backfill, and the analysis will naturally include the shear strength of the backfill soil. Similar to the analysis of strip footings and slope stability, for most field situations involving retaining structures, the backfill soil is in a plane strain condition (i.e., the soil is confined along the long axis of the wall). As previously mentioned, the friction angle ϕ is about 10 percent higher in the plane strain condition compared to the friction angle ϕ measured in the triaxial apparatus. In practice, plane strain shear strength tests are not performed, which often results in an additional factor of safety for retaining wall analyses.

coefficient k_A for Eq. (10.1) is often determined by using the Coulomb equation (see Fig. 10.3). Often the wall friction is neglected ($\delta = 0°$), but if it is included in the analysis, typical values are $\delta = \frac{3}{4}\phi$ for the wall friction between granular soil and wood or concrete walls and $\delta = 20°$ for the wall friction between granular soil and steel walls such as sheet pile walls. Note in Fig. 10.3 that when the wall friction angle δ is used in the analysis, the active

earth pressure resultant force P_A is inclined at an angle equal to δ. Additional important details concerning the active earth pressure follow.

1. *Sufficient movement:* There must be sufficient movement of the retaining wall in order to develop the active earth pressure of the backfill. For dense granular soil, the amount of wall translation to reach the active earth pressure state is usually very small (i.e., to reach active state, wall translation $\geq 0.0005H$, where H = height of wall).

2. *Triangular distribution:* As shown in Figs. 10.2 and 10.3, the active earth pressure is a triangular distribution, and thus the active earth pressure resultant force P_A is located at a distance equal to $^1/_3H$ above the base of the wall.

3. *Surcharge pressure:* If there is a uniform surcharge pressure Q acting upon the entire ground surface behind the wall, then an additional horizontal pressure is exerted upon the retaining wall equal to the product of k_A and Q. Thus the resultant force P_2, in kilonewtons per linear

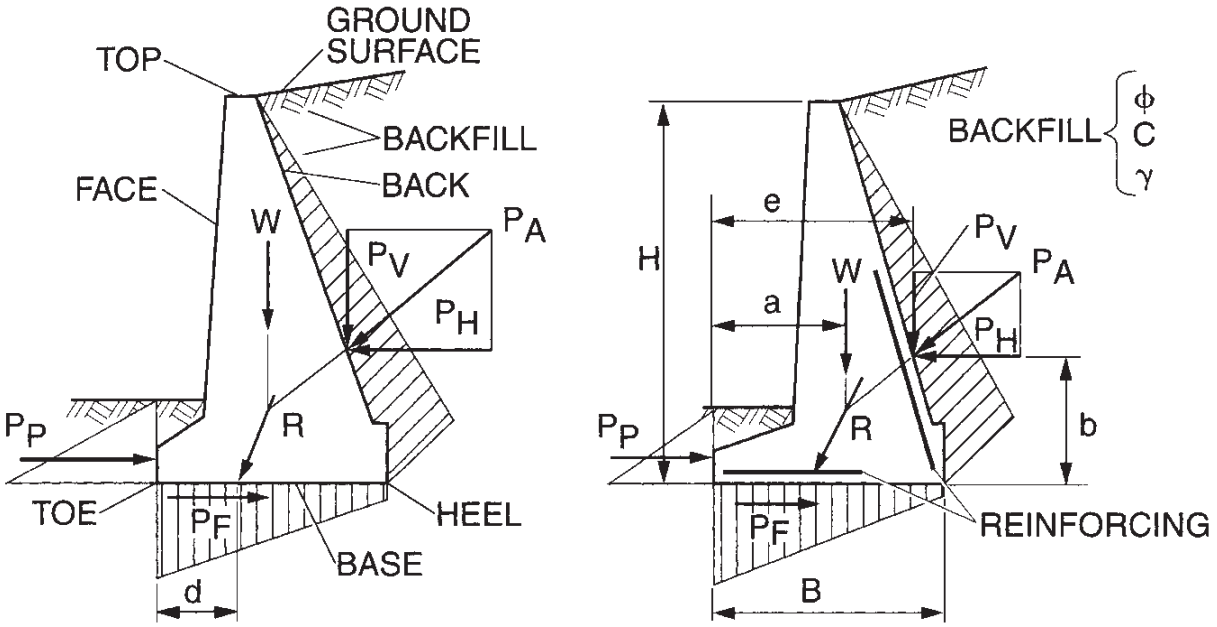

FIGURE 10.2a Gravity and semigravity retaining walls. (*Reproduced from NAVFAC DM-7.2, 1982.*)

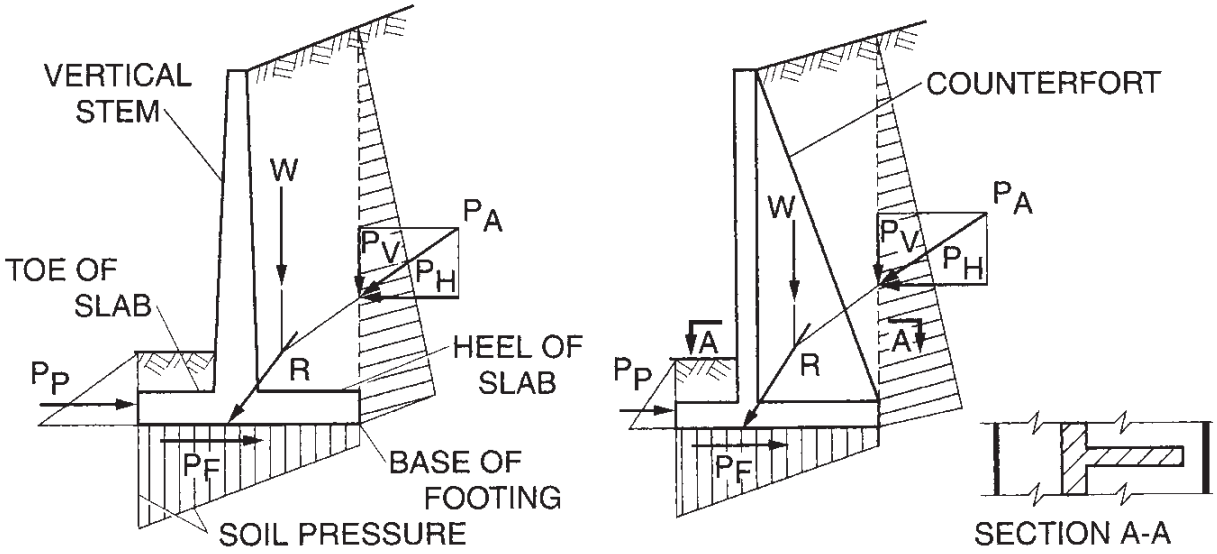

FIGURE 10.2b Cantilever and counterfort retaining walls. (*Reproduced from NAVFAC DM-7.2, 1982.*)

LOCATION OF RESULTANT

MOMENTS ABOUT TOE:

$$d = \frac{Wa + P_V e - P_H b}{W + P_V}$$

ASSUMING $P_P = 0$

OVERTURNING

MOMENTS ABOUT TOE:

$$F = \frac{W_a}{P_H b - P_V e} \geqq 1.5$$

IGNORE OVERTURNING IF R IS WITHIN MIDDLE THIRD (SOIL), MIDDLE HALF (ROCK).
CHECK R AT DIFFERENT HORIZONTAL PLANES FOR GRAVITY WALLS.

RESISTANCE AGAINST SLIDING

$$F = \frac{(W + P_V) \text{ TAN } \delta + C_a B}{P_H} \geqq 1.5$$

$$F = \frac{(W+P_V) \text{ TAN } \delta + C_a B + P_P}{P_H} \geqq 2.0$$

$$P_F = (W + P_V) \text{ TAN } \delta + C_a B$$

C_a = ADHESION BETWEEN SOIL AND BASE

TAN δ = FRICTION FACTOR BETWEEN SOIL AND BASE

W = INCLUDES WEIGHT OF WALL AND SOIL IN FRONT FOR GRAVITY AND SEMIGRAVITY WALLS.
INCLUDES WEIGHT OF WALL AND SOIL ABOVE FOOTING, FOR CANTILEVER AND COUNTERFORT WALLS.

FIGURE 10.2c Design analysis for retaining walls shown in Fig. 10.2*a* and *b*. (*Reproduced from NAVFAC DM-7.2, 1982.*)

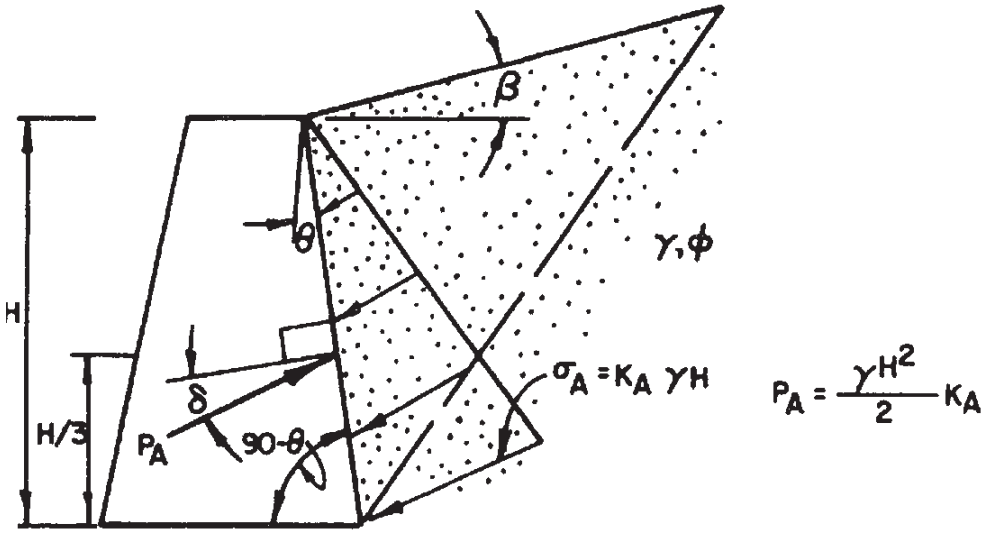

A) Coulomb's Equation (Static Condition):

$$K_A = \frac{\cos^2(\phi - \theta)}{\cos^2\theta \cos(\delta + \theta)\left[1 + \sqrt{\dfrac{\sin(\delta + \phi)\sin(\phi - \beta)}{\cos(\delta + \theta)\cos(\beta - \theta)}}\right]^2}$$

B) Mononobe-Okabe Equation (Earthquake Condition):

$$K_{AE} = \frac{\cos^2(\phi - \theta - \psi)}{\cos\psi \cos^2\theta \cos(\delta + \theta + \psi)\left[1 + \sqrt{\dfrac{\sin(\delta + \phi)\sin(\phi - \beta - \psi)}{\cos(\delta + \theta + \psi)\cos(\beta - \theta)}}\right]^2}$$

FIGURE 10.3 Coulomb's earth pressure (k_A) equation for static conditions. Also shown is the Mononobe-Okabe equation (k_{AE}) for earthquake conditions. (*Figure reproduced from NAVFAC DM-7.2, 1982, with equations from Kramer 1996.*)

meter of wall or pounds per linear foot of wall, acting on the retaining wall due to the surcharge Q is equal to $P_2 = QHk_A$, where Q = uniform vertical surcharge acting upon the entire ground surface behind the retaining wall, k_A = active earth pressure coefficient [Eq. (10.2) or Fig. 10.3], and H = height of the retaining wall. Because this pressure acting upon the retaining wall is uniform, the resultant force P_2 is located at midheight of the retaining wall.

4. *Active wedge:* The *active wedge* is defined as that zone of soil involved in the development of the active earth pressures upon the wall. This active wedge must move laterally to develop the active earth pressures. It is important that building footings or other

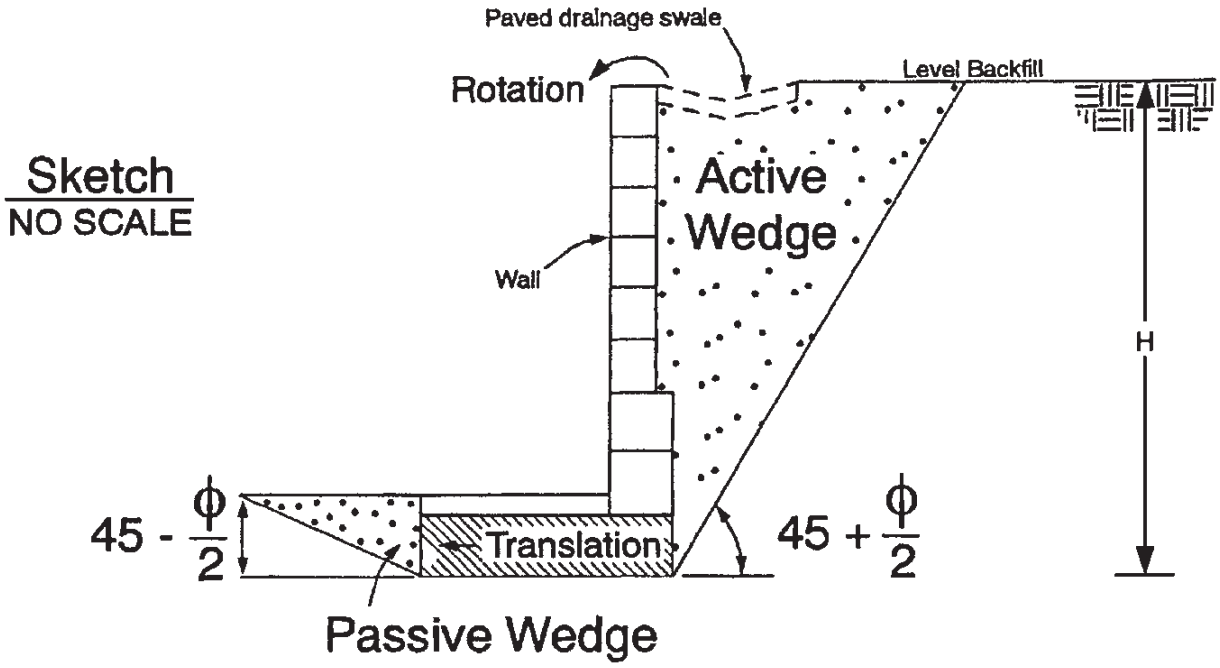

FIGURE 10.4 Active wedge behind retaining wall.

load-carrying members not be supported by the active wedge, or else they will be subjected to lateral movement. The active wedge is inclined at an angle of $45° + \phi/2$ from the horizontal, as indicated in Fig. 10.4.

Passive Earth Pressure. As shown in Fig. 10.4, the passive earth pressure is developed along the front side of the footing. Passive pressure is developed when the wall footing moves laterally into the soil and a passive wedge is developed. To calculate the passive resultant force P_p, the following equation is used, assuming that there is cohesionless soil in front of the wall footing:

$$P_p = \tfrac{1}{2} k_p \gamma_t D^2 \tag{10.3}$$

where P_p = passive resultant force in kilonewtons per linear meter of wall or pounds per linear foot of wall, k_p = passive earth pressure coefficient, γ_t = total unit weight of the soil located in front of the wall footing, and D = depth of the wall footing (vertical distance from the ground surface in front of the retaining wall to the bottom of the footing). The passive earth pressure coefficient k_p is equal to

$$k_p = \tan^2 (45° + \tfrac{1}{2}\phi) \tag{10.4}$$

where ϕ = friction angle of the soil in front of the wall footing. Equation (10.4) is known as the passive Rankine state. To develop passive pressure, the wall footing must move laterally into the soil. The wall translation to reach the passive state is at least twice that required to reach the active earth pressure state. Usually it is desirable to limit the amount of wall translation by applying a reduction factor to the passive pressure. A commonly used reduction factor is 2.0. The soil engineer routinely reduces the passive pressure by one-half (reduction factor = 2.0) and then refers to the value as the allowable passive pressure.

Footing Bearing Pressure. To calculate the footing bearing pressure, the first step is to sum the vertical loads, such as the wall and footing weights. The vertical loads can be represented by a single resultant vertical force, per linear meter or foot of wall, that is offset by a distance (eccentricity) from the toe of the footing. This can then be converted to a pressure distribution by using Eq. (8.7). The largest bearing pressure is routinely at the toe of the footing, and it should not exceed the allowable bearing pressure (Sec. 8.2.5).

Retaining Wall Analyses. Once the active earth pressure resultant force P_A and the passive resultant force P_p have been calculated, the design analysis is performed as indicated in Fig. 10.2*c*. The retaining wall analysis includes determining the resultant location of the forces (i.e., calculate *d,* which should be within the middle third of the footing), the factor of safety for overturning, and the factor of safety for sliding. The adhesion c_a between the bottom of the footing and the underlying soil is often ignored for the sliding analysis.

10.1.2 Retaining Wall Analyses for Earthquake Conditions

The performance of retaining walls during earthquakes is very complex. As stated by Kramer (1996), laboratory tests and analyses of gravity walls subjected to seismic forces have indicated the following:

1. Walls can move by translation and/or rotation. The relative amounts of translation and rotation depend on the design of the wall; one or the other may predominate for some walls, and both may occur for others (Nadim and Whitman 1984, Siddharthan et al. 1992).
2. The magnitude and distribution of dynamic wall pressures are influenced by the mode of wall movement, e.g., translation, rotation about the base, or rotation about the top (Sherif et al. 1982, Sherif and Fang 1984a, b).
3. The maximum soil thrust acting on a wall generally occurs when the wall has translated or rotated toward the backfill (i.e., when the inertial force on the wall is directed toward the backfill). The minimum soil thrust occurs when the wall has translated or rotated away from the backfill.
4. The shape of the earthquake pressure distribution on the back of the wall changes as the wall moves. The point of application of the soil thrust therefore moves up and down along the back of the wall. The position of the soil thrust is highest when the wall has moved toward the soil and lowest when the wall moves outward.
5. Dynamic wall pressures are influenced by the dynamic response of the wall and backfill and can increase significantly near the natural frequency of the wall-backfill system (Steedman and Zeng 1990). Permanent wall displacements also increase at frequencies near the natural frequency of the wall-backfill system (Nadim 1982). Dynamic response effects can also cause deflections of different parts of the wall to be out of phase. This effect can be particularly significant for walls that penetrate into the foundation soils when the backfill soils move out of phase with the foundation soils.
6. Increased residual pressures may remain on the wall after an episode of strong shaking has ended (Whitman 1990).

Because of the complex soil-structure interaction during the earthquake, the most commonly used method for the design of retaining walls is the pseudostatic method, which is discussed in Sec. 10.2.

10.1.3 One-Third Increase in Soil Properties for Seismic Conditions

When the recommendations for the allowable soil pressures at a site are presented, it is common practice for the geotechnical engineer to recommend that the allowable bearing pressure

and the allowable passive pressure be increased by a factor of one-third when performing seismic analyses. For example, in soil reports, it is commonly stated: "For the analysis of earthquake loading, the allowable bearing pressure and passive resistance may be increased by a factor of one-third." The rationale behind this recommendation is that the allowable bearing pressure and allowable passive pressure have an ample factor of safety, and thus for seismic analyses, a lower factor of safety would be acceptable.

Usually the above recommendation is appropriate if the retaining wall bearing material and the soil in front of the wall (i.e., passive wedge area) consist of the following:

- Massive crystalline bedrock and sedimentary rock that remains intact during the earthquake.
- Soils that tend to dilate during the seismic shaking or, e.g., dense to very dense granular soil and heavily overconsolidated cohesive soil such as very stiff to hard clays.
- Soils that have a stress-strain curve that does not exhibit a significant reduction in shear strength with strain.
- Clay that has a low sensitivity.
- Soils located above the groundwater table. These soils often have negative pore water pressure due to capillary action.

These materials do not lose shear strength during the seismic shaking, and therefore an increase in bearing pressure and passive resistance is appropriate.

A one-third increase in allowable bearing pressure and allowable passive pressure should not be recommended if the bearing material and/or the soil in front of the wall (i.e., passive wedge area) consists of the following:

- Foliated or friable rock that fractures apart during the earthquake, resulting in a reduction in shear strength of the rock.
- Loose soil located below the groundwater table and subjected to liquefaction or a substantial increase in pore water pressure.
- Sensitive clays that lose shear strength during the earthquake.
- Soft clays and organic soils that are overloaded and subjected to plastic flow.

These materials have a reduction in shear strength during the earthquake. Since the materials are weakened by the seismic shaking, the static values of allowable bearing pressures and allowable passive resistance should not be increased for the earthquake analyses. In fact, the allowable bearing pressure and the allowable passive pressure may actually have to be reduced to account for the weakening of the soil during the earthquake. Sections 10.3 and 10.4 discuss retaining wall analyses for the case where the soil is weakened during the earthquake.

10.2 PSEUDOSTATIC METHOD

10.2.1 Introduction

The most commonly used method of retaining wall analyses for earthquake conditions is the pseudostatic method. The pseudostatic method is also applicable for earthquake slope stability analyses (see Sec. 9.2). As previously mentioned, the advantages of this method are that it is easy to understand and apply.

Similar to earthquake slope stability analyses, this method ignores the cyclic nature of the earthquake and treats it as if it applied an additional static force upon the retaining wall. In particular, the pseudostatic approach is to apply a lateral force upon the retaining wall. To derive the lateral force, it can be assumed that the force acts through the centroid of the active wedge. The pseudostatic lateral force P_E is calculated by using Eq. (6.1), or

$$P_E = ma = \frac{W}{g}\, a = W\, \frac{a_{\max}}{g} = k_h W \tag{10.5}$$

where P_E = horizontal pseudostatic force acting upon the retaining wall, lb or kN. This force can be assumed to act through the centroid of the active wedge. For retaining wall analyses, the wall is usually assumed to have a unit length (i.e., two-dimensional analysis)
m = total mass of active wedge, lb or kg, which is equal to W/g
W = total weight of active wedge, lb or kN
a = acceleration, which in this case is maximum horizontal acceleration atground surface caused by the earthquake ($a = a_{\max}$), ft/s^2 or m/s^2
$a_{\max}$ = maximum horizontal acceleration at ground surface that is induced by the earthquake, ft/s^2 or m/s^2. The maximum horizontal acceleration is also commonly referred to as the peak ground acceleration (see Sec. 5.6)
$a_{\max}/g = k_h$ = seismic coefficient, also known as pseudostatic coefficient (dimensionless)

Note that an earthquake could subject the active wedge to both vertical and horizontal pseudostatic forces. However, the vertical force is usually ignored in the standard pseudostatic analysis. This is because the vertical pseudostatic force acting on the active wedge usually has much less effect on the design of the retaining wall. In addition, most earthquakes produce a peak vertical acceleration that is less than the peak horizontal acceleration, and hence k_v is smaller than k_h.

As indicated in Eq. (10.5), the only unknowns in the pseudostatic method are the weight of the active wedge W and the seismic coefficient k_h. Because of the usual relatively small size of the active wedge, the seismic coefficient k_h can be assumed to be equal to $a_{\max}/g$. Using Fig. 10.4, the weight of the active wedge can be calculated as follows:

$$W = \tfrac{1}{2} HL\gamma_t = \tfrac{1}{2} H\,[H \tan (45^\circ - \tfrac{1}{2}\phi)]\,\gamma_t = \tfrac{1}{2} k_A^{1/2}\, H^2 \gamma_t \tag{10.6}$$

where W = weight of the active wedge, lb or kN per unit length of wall
H = height of the retaining wall, ft or m
L = length of active wedge at top of retaining wall. Note in Fig. 10.4 that the active wedge is inclined at an angle equal to $45^\circ + \frac{1}{2}\phi$. Therefore the internal angle of the active wedge is equal to $90^\circ - (45^\circ + \frac{1}{2}\phi) = 45^\circ - \frac{1}{2}\phi$. The length L can then be calculated as $L = H \tan (45^\circ - \frac{1}{2}\phi) = H k_A^{1/2}$
γ_t = total unit weight of the backfill soil (i.e., unit weight of soil comprising active wedge), lb/ft^3 or kN/m^3

Substituting Eq. (10.6) into Eq. (10.5), we get for the final result:

$$P_E = k_h W = \tfrac{1}{2} k_h k_A^{1/2}\, H^2 \gamma_t = \tfrac{1}{2} k_A^{1/2} \left(\frac{a_{\max}}{g} \right) (H^2 \gamma_t) \tag{10.7}$$

Note that since the pseudostatic force is applied to the centroid of the active wedge, the location of the force P_E is at a distance of $\frac{2}{3}H$ above the base of the retaining wall.

10.2.2 Method by Seed and Whitman

Seed and Whitman (1970) developed an equation that can be used to determine the horizontal pseudostatic force acting on the retaining wall:

$$P_E = \frac{3}{8}\,\frac{a_{\max}}{g}\,H^2\gamma_t \tag{10.8}$$

Note that the terms in Eq. (10.8) have the same definitions as the terms in Eq. (10.7). Comparing Eqs. (10.7) and (10.8), we see the two equations are identical for the case where $\frac{1}{2}k_A^{1/2} = \frac{3}{8}$. According to Seed and Whitman (1970), the location of the pseudostatic force from Eq. (10.8) can be assumed to act at a distance of $0.6H$ above the base of the wall.

10.2.3 Method by Mononobe and Okabe

Mononobe and Matsuo (1929) and Okabe (1926) also developed an equation that can be used to determine the horizontal pseudostatic force acting on the retaining wall. This method is often referred to as the Mononobe-Okabe method. The equation is an extension of the Coulomb approach and is

$$P_{AE} = P_A + P_E = \tfrac{1}{2}k_{AE}H^2\gamma_t \tag{10.9}$$

where P_{AE} = the sum of the static (P_A) and the pseudostatic earthquake force (P_E). The equation for k_{AE} is shown in Fig. 10.3. Note that in Fig. 10.3, the term ψ is defined as

$$\psi = \tan^{-1}k_h = \tan^{-1}\,\frac{a_{\max}}{g} \tag{10.10}$$

The original approach by Mononobe and Okabe was to assume that the force P_{AE} from Eq. (10.9) acts at a distance of $\frac{1}{3}H$ above the base of the wall.

10.2.4 Example Problem

Figure 10.5 (from Lambe and Whitman 1969) presents an example of a proposed concrete retaining wall that will have a height of 20 ft (6.1 m) and a base width of 7 ft (2.1 m). The wall will be backfilled with sand that has a total unit weight γ_t of 110 lb/ft^3 (17.3 kN/m^3), friction angle ϕ of 30°, and an assumed wall friction $\delta = \phi_w$ of 30°. Although $\phi_w = 30°$ is used for this example problem, more typical values of wall friction are $\phi_w = \frac{3}{4}\phi$ for the wall friction between granular soil and wood or concrete walls, and $\phi_w = 20°$ for the wall friction between granular soil and steel walls such as sheet pile walls. The retaining wall is analyzed for the static case and for the earthquake condition assuming $k_h = 0.2$. It is also assumed that the backfill soil, bearing soil, and soil located in the passive wedge are not weakened by the earthquake.

Static Analysis

Active Earth Pressure. For the example problem shown in Fig. 10.5, the value of the active earth pressure coefficient k_A can be calculated by using Coulomb's equation (Fig. 10.3) and inserting the following values:

- Slope inclination: $\beta = 0$ (no slope inclination)
- Back face of the retaining wall: $\theta = 0$ (vertical back face of the wall)

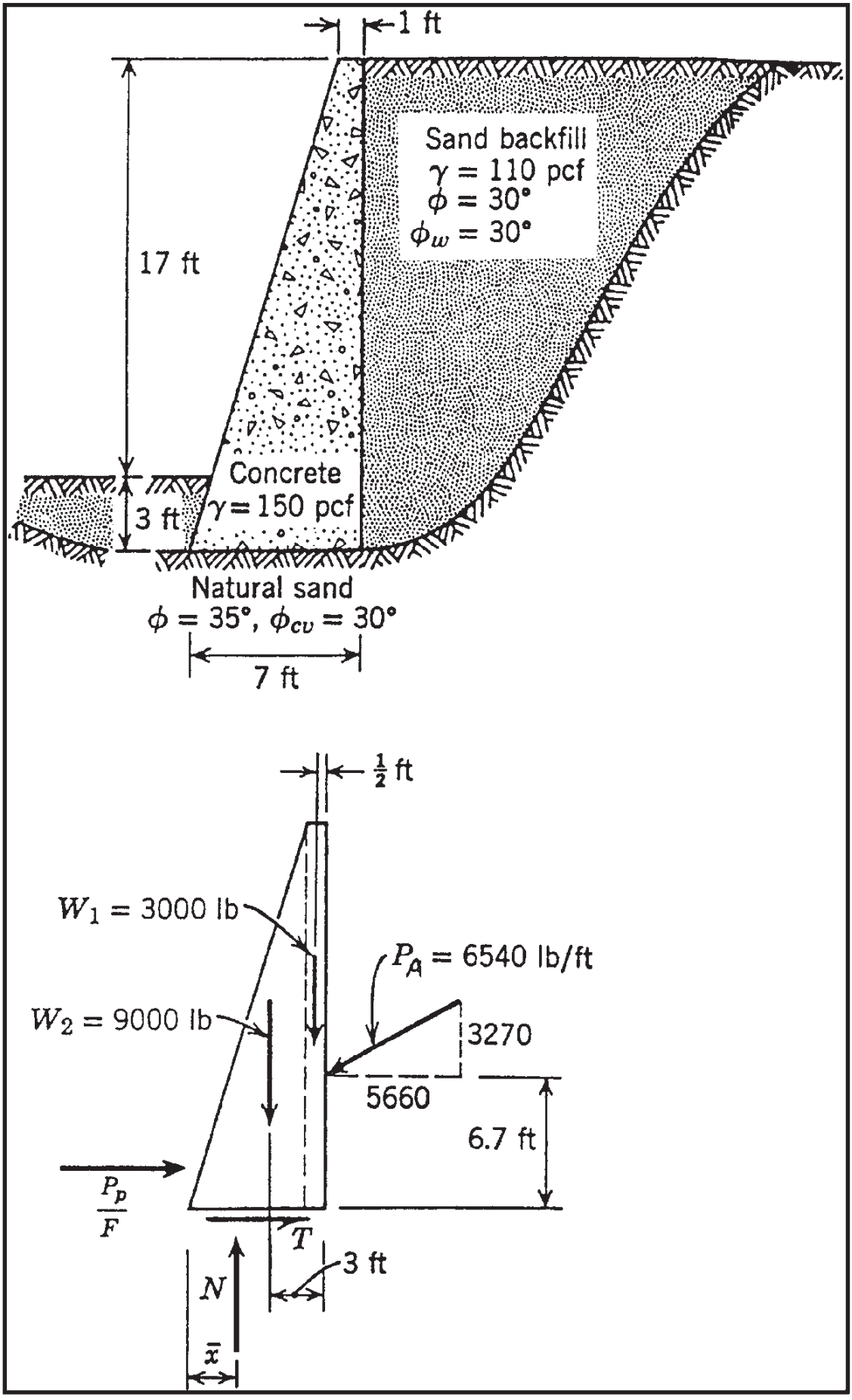

FIGURE 10.5a Example problem. Cross section of proposed retaining wall and resultant forces acting on the retaining wall. (*From Lambe and Whitman 1969; reproduced with permission of John Wiley & Sons.*)

Find. Adequacy of wall.
Solution. The first step is to determine the active thrust;
The next step is to compute the weights:

$$W_1 = (1)(20)(150) = 3000 \text{ lb/ft}$$

$$W_2 = \tfrac{1}{2}(6)(20)(150) = 9000 \text{ lb/ft}$$

Next N and $\bar{x}$ are computed:

$$N = 9000 + 3000 + 3270 = 15{,}270 \text{ lb/ft}$$

$$\text{Overturning moment} = 5660(6.67) - 3270(7) = 37{,}800 - 22{,}900 = 14{,}900$$

$$\text{Moment of weight} = (6.5)(3000) + (4)(9000) = 19{,}500 + 36{,}000 = 55{,}500$$

$$\text{Ratio} = 3.73 \qquad \underline{\text{OK}}$$

$$\bar{x} = \frac{55{,}500 - 14{,}900}{15{,}270} = \frac{40{,}600}{15{,}270} = 2.66 \text{ ft} \qquad \underline{\text{OK}}$$

The location of N

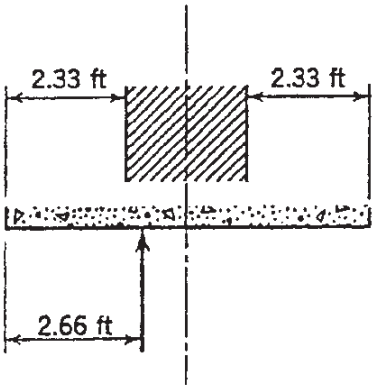

FIGURE 10.5b Example problem (*continued*). Calculation of the factor of safety for overturning and the location of the resultant force *N*. (*From Lambe and Whitman 1969; reproduced with permission of John Wiley & Sons.*)

- Friction between the back face of the wall and the soil backfill: $\delta = \phi_w = 30°$
- Friction angle of backfill sand: $\phi = 30°$

Inputting the above values into Coulomb's equation (Fig. 10.3), the value of the active earth pressure coefficient $k_A = 0.297$.

By using Eq. (10.1) with $k_A = 0.297$, total unit weight $\gamma_t = 110$ lb/ft^3 (17.3 kN/m^3), and the height of the retaining wall $H = 20$ ft (see Fig. 10.5*a*), the active earth pressure resultant force $P_A = 6540$ lb per linear foot of wall (95.4 kN per linear meter of wall). As indicated in Fig. 10.5*a,* the active earth pressure resultant force $P_A = 6540$ lb/ft is inclined at an angle of 30° due to the wall friction assumptions. The vertical ($P_v = 3270$ lb/ft) and horizontal ($P_H = 5660$ lb/ft) resultants of P_A are also shown in Fig. 10.5*a.* Note in Fig. 10.3 that even

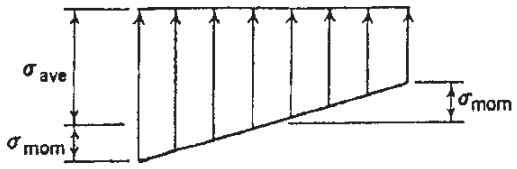

Next the bearing stress is computed. The average bearing stress is 15,270/7 = 2180 psf. Assuming that the bearing stress is distributed linearly, the maximum stress can be found

$$\sigma_{mom} = \frac{M}{S}$$

where

M = moment about ℄ = 15,270(3.5 − 2.66) = 12,820 lb-ft/ft

S = section modulus = $\frac{1}{6}B^2 = \frac{1}{6}(7)^2 = 8.17$ ft²

where B is width of base

$$\sigma_{mom} = \frac{12{,}820}{8.17} = 1570 \text{ psf}$$

Maximum stress = 2180 + 1570 = 3750 psf

Finally, the resistance to horizontal sliding is checked. Assuming passive resistance without wall friction,

$$K_p = 3$$

$$P_p = \tfrac{1}{2}(110)(3^2)(3) = 1500 \text{ lb/ft}$$

With reduction factor of 2,

$$\frac{P_p}{F} = 750 \text{ lb/ft}$$

$$T = 5660 - 750 = 4910 \text{ lb/ft}$$

$$N \tan 30^\circ = 8810 \text{ lb/ft}$$

$$\frac{N \tan \phi_{cv}}{T} = 1.79 < 2 \qquad \underline{\text{not OK}}$$

Ignoring passive resistance

$$T = 5660 \text{ lb/ft}$$

$$\frac{N \tan \phi_{cv}}{T} = 1.55 > 1.5 \qquad \underline{\text{OK}}$$

FIGURE 10.5c Example problem (*continued*). Calculation of the maximum bearing stress and the factor of safety for sliding. (*From Lambe and Whitman 1969, reproduced with permission of John Wiley & Sons.*)

with wall friction, the active earth pressure is still a triangular distribution acting upon the retaining wall, and thus the location of the active earth pressure resultant force P_A is at a distance of $\frac{1}{3}H$ above the base of the wall, or 6.7 feet (2.0 m).

Passive Earth Pressure. As shown in Fig. 10.5*a,* the passive earth pressure is developed by the soil located at the front of the retaining wall. Usually wall friction is ignored for the passive earth pressure calculations. For the example problem shown in Fig. 10.5, the passive resultant force P_p was calculated by using Eqs. (10.3) and (10.4) and neglecting wall friction and the slight slope of the front of the retaining wall (see Fig. 10.5*c* for passive earth pressure calculations).

Footing Bearing Pressure. The procedure for the calculation of the footing bearing pressure is as follows:

1. *Calculate N:* As indicated in Fig. 10.5*b,* the first step is to calculate N (15,270 lb/ft), which equals the sum of the weight of the wall, footing, and vertical component of the active earth pressure resultant force (that is, $N = W + P_A \sin \phi_w$).
2. *Determine resultant location of N*: The resultant location of N from the toe of the retaining wall (that is, 2.66 ft) is calculated as shown in Fig. 10.5*b.* The moments are determined about the toe of the retaining wall. Then the location of N is equal to the difference in the opposing moments divided by N.
3. *Determine average bearing pressure:* The average bearing pressure (2180 lb/ft^2) is calculated in Fig. 10.5*c* as N divided by the width of the footing (7 ft).
4. *Calculate moment about the centerline of the footing:* The moment about the centerline of the footing is calculated as N times the eccentricity (0.84 ft).
5. *Section modulus:* The section modulus of the footing is calculated as shown in Fig. 10.5*c.*
6. *Portion of bearing stress due to moment:* The portion of the bearing stress due to the moment (σ_{mom}) is determined as the moment divided by the section modulus.
7. *Maximum bearing stress:* The maximum bearing stress is then calculated as the sum of the average stress (σ_{avg} = 2180 lb/ft^2) plus the bearing stress due to the moment (σ_{mom} = 1570 lb/ft^2).

As indicated in Fig. 10.5*c,* the maximum bearing stress is 3750 lb/ft^2 (180 kPa). This maximum bearing stress must be less than the allowable bearing pressure (Chap. 8). It is also a standard requirement that the resultant normal force N be located within the middle third of the footing, such as illustrated in Fig. 10.5*b.* As an alternative to the above procedure, Eq. (8.7) can be used to calculate the maximum and minimum bearing stress.

Sliding Analysis. The factor of safety (FS) for sliding of the retaining wall is often defined as the resisting forces divided by the driving force. The forces are per linear meter or foot of wall, or

$$\text{FS} = \frac{N \tan \delta + P_p}{P_H} \tag{10.11}$$

where $\delta = \phi_{cv}$ = friction angle between the bottom of the concrete foundation and bearing soil; N = sum of the weight of the wall, footing, and vertical component of the active earth pressure resultant force (or $N = W + P_A \sin \phi_w$); P_p = allowable passive resultant force [P_p from Eq. (10.3) divided by a reduction factor]; and P_H = horizontal component of the active earth pressure resultant force ($P_H = P_A \cos \phi_w$).

There are variations of Eq. (10.11) that are used in practice. For example, as illustrated in Fig. 10.5*c,* the value of P_p is subtracted from P_H in the denominator of Eq. (10.11), instead of P_p being used in the numerator. For the example problem shown in Fig. 10.5, the factor of safety for sliding is FS = 1.79 when the passive pressure is included and FS = 1.55 when the passive pressure is excluded. For static conditions, the typical recommendations for minimum factor of safety for sliding are 1.5 to 2.0 (Cernica 1995b).

Overturning Analysis. The factor of safety for overturning of the retaining wall is calculated by taking moments about the toe of the footing and is

$$\text{FS} = \frac{Wa}{\frac{1}{3}P_H H - P_v e} \tag{10.12}$$

where a = lateral distance from the resultant weight W of the wall and footing to the toe of the footing, P_H = horizontal component of the active earth pressure resultant force, P_v = vertical component of the active earth pressure resultant force, and e = lateral distance from the location of P_v to the toe of the wall. In Fig. 10.5*b,* the factor of safety (ratio) for overturning is calculated to be 3.73. For static conditions, the typical recommendations for minimum factor of safety for overturning are 1.5 to 2.0 (Cernica 1995b).

Settlement and Stability Analysis. Although not shown in Fig. 10.5, the settlement and stability of the ground supporting the retaining wall footing should also be determined. To calculate the settlement and evaluate the stability for static conditions, standard settlement and slope stability analyses can be utilized (see chaps. 9 and 13, Day 2000).

Earthquake Analysis. The pseudostatic analysis is performed for the three methods outlined in Secs. 10.2.1 to 10.2.3.

Equation (10.7). Using Eq. (10.2) and neglecting the wall friction, we find

$$k_A = \tan^2 (45° - \tfrac{1}{2}\phi) = \tan^2 (45° - \tfrac{1}{2}30°) = 0.333$$

Substituting into Eq. (10.7) gives

$$P_E = \tfrac{1}{2}\, k_A^{1/2} \left(\frac{a_{\max}}{g} \right) (H^2 \gamma_t)$$

$$= \tfrac{1}{2}\, (0.333)^{1/2}\, (0.2)\, (20 \text{ ft})^2\, (110 \text{ lb/ft}^3) = 2540 \text{ lb per linear foot of wall length}$$

This pseudostatic force acts at a distance of $\frac{2}{3}H$ above the base of the wall, or $\frac{2}{3}H = \frac{2}{3}(20 \text{ ft}) = 13.3$ ft. Similar to Eq. (10.11), the factor of safety for sliding is

$$\text{FS} = \frac{N \tan \delta + P_p}{P_H + P_E} \tag{10.13}$$

Substituting values into Eq. (10.13) gives

$$\text{FS} = \frac{15{,}270 \tan 30° + 750}{5660 + 2540} = 1.17$$

Based on Eq. (10.12), the factor of safety for overturning is

$$\text{FS} = \frac{Wa}{\frac{1}{3}P_H H - P_v e + \frac{2}{3}HP_E} \tag{10.14}$$

Inserting values into Eq. (10.14) yields

$$\text{FS} = \frac{55{,}500}{\frac{1}{3}(5660)(20) - 3270(7) + \frac{2}{3}(20)(2540)} = 1.14$$

Method by Seed and Whitman (1970). Using Eq. (10.8) and neglecting the wall friction, we get

$$P_E = \frac{3}{8} \left(\frac{a_{\max}}{g} \right) H^2 \gamma_t$$

$$= \tfrac{3}{8}\, (0.2)\, (20 \text{ ft})^2\, (110 \text{ lb/ft}^3) = 3300 \text{ lb per linear foot of wall length}$$

This pseudostatic force acts at a distance of $0.6H$ above the base of the wall, or $0.6H = (0.6)(20 \text{ ft}) = 12$ ft. Using Eq. (10.13) gives

$$\text{FS} = \frac{N \tan \delta + P_p}{P_H + P_E} = \frac{15{,}270 \tan 30° + 750}{5660 + 3300} = 1.07$$

Similar to Eq. (10.14), the factor of safety for overturning is

$$\text{FS} = \frac{Wa}{\frac{1}{3}P_H H - P_v e + 0.6HP_E} \tag{10.15}$$

Substituting values into Eq. (10.15) gives

$$\text{FS} = \frac{55{,}500}{\frac{1}{3}(5660)(20) - 3270(7) + 0.6(20)(3300)} = 1.02$$

Mononobe-Okabe Method. We use the following values:

θ (wall inclination) = 0°

ϕ (friction angle of backfill soil) = 30°

β (backfill slope inclination) = 0°

$\delta = \phi_w$ (friction angle between the backfill and wall) = 30°

$$\psi = \tan^{-1} k_h = \tan^{-1} \frac{a_{\max}}{g} = \tan^{-1} 0.2 = 11.3°$$

Inserting the above values into the K_{AE} equation in Fig. 10.3, we get $K_{AE} = 0.471$. Therefore, using Eq. (10.9) yields

$$P_{AE} = P_A + P_E = \tfrac{1}{2}k_{AE}H^2\gamma_t$$
$$= \tfrac{1}{2}(0.471)(20)^2(110) = 10{,}400 \text{ lb per linear foot of wall length}$$

This force P_{AE} is inclined at an angle of 30° and acts at a distance of $0.33H$ above the base of the wall, or $0.33H = (0.33)(20 \text{ ft}) = 6.67$ ft. The factor of safety for sliding is

$$\text{FS} = \frac{N \tan \delta + P_p}{P_H} = \frac{(W + P_{AE} \sin \phi_w) \tan \delta + P_p}{P_{AE} \cos \phi_w} \tag{10.16}$$

Substituting values into Eq. (10.16) gives

$$\text{FS} = \frac{(3000 + 9000 + 10{,}400 \sin 30°)(\tan 30°) + 750}{10{,}400 \cos 30°} = 1.19$$

The factor of safety for overturning is

$$\text{FS} = \frac{Wa}{\frac{1}{3} H P_{AE} \cos \phi_w - P_{AE} \sin \phi_w e} \tag{10.17}$$

Substituting values into Eq. (10.17) produces

$$\text{FS} = \frac{55{,}500}{\frac{1}{3}(20)(10{,}400)(\cos 30°) - (10{,}400)(\sin 30°)(7)} = 2.35$$

Summary of Values. The values from the static and earthquake analyses using $k_h = a_{max}/g = 0.2$ are summarized below:

Type of condition		P_E or P_{AE}, lb/ft	Location of P_E or P_{AE} above base of wall, ft	Factor of safety for sliding	Factor of safety for overturning
Static		$P_E = 0$	—	1.69*	3.73
Earthquake ($k_h = 0.2$)	Equation (10.7)	$P_E = 2{,}540$	$\frac{2}{3}H = 13.3$	1.17	1.14
	Seed and Whitman	$P_E = 3{,}300$	$0.6H = 12$	1.07	1.02
	Mononobe-Okabe	$P_{AE} = 10{,}400$	$\frac{1}{3}H = 6.7$	1.19	2.35

*Factor of safety for sliding using Eq. (10.11).

For the analysis of sliding and overturning of the retaining wall, it is common to accept a lower factor of safety (1.1 to 1.2) under the combined static and earthquake loads. Thus the retaining wall would be considered marginally stable for the earthquake sliding and overturning conditions.

Note in the above table that the factor of safety for overturning is equal to 2.35 based on the Mononobe-Okabe method. This factor of safety is much larger than that for the other two methods. This is because the force P_{AE} is assumed to be located at a distance of $\frac{1}{3}H$ above the base of the wall. Kramer (1996) suggests that it is more appropriate to assume that P_E is located at a distance of $0.6H$ above the base of the wall [that is, $P_E = P_{AE} - P_A$, see Eq. (10.9)].

Although the calculations are not shown, it can be demonstrated that the resultant location of N for the earthquake condition is outside the middle third of the footing. Depending on the type of material beneath the footing, this condition could cause a bearing capacity failure or excess settlement at the toe of the footing during the earthquake.

10.2.5 Mechanically Stabilized Earth Retaining Walls

Introduction. Mechanically stabilized earth (MSE) retaining walls are typically composed of strip- or grid-type (geosynthetic) reinforcement. Because they are often more economical to construct than conventional concrete retaining walls, mechanically stabilized earth retaining walls have become very popular in the past decade.

A mechanically stabilized earth retaining wall is composed of three elements: (1) wall facing material, (2) soil reinforcement, such as strip- or grid-type reinforcement, and (3) compacted fill between the soil reinforcement. Figure 10.6 shows the construction of a mechanically stabilized earth retaining wall.

The design analyses for a mechanically stabilized earth retaining wall are more complex than those for a cantilevered retaining wall. For a mechanically stabilized earth retaining wall, both the internal and external stability must be checked, as discussed below.

External Stability—Static Conditions. The analysis for the external stability is similar to that for a gravity retaining wall. For example, Figs. 10.7 and 10.8 present the design analysis for external stability for a level backfill condition and a sloping backfill condition. In both

FIGURE 10.6 Installation of a mechanically stabilized earth retaining wall. The arrow points to the wall facing elements, which are in the process of being installed.

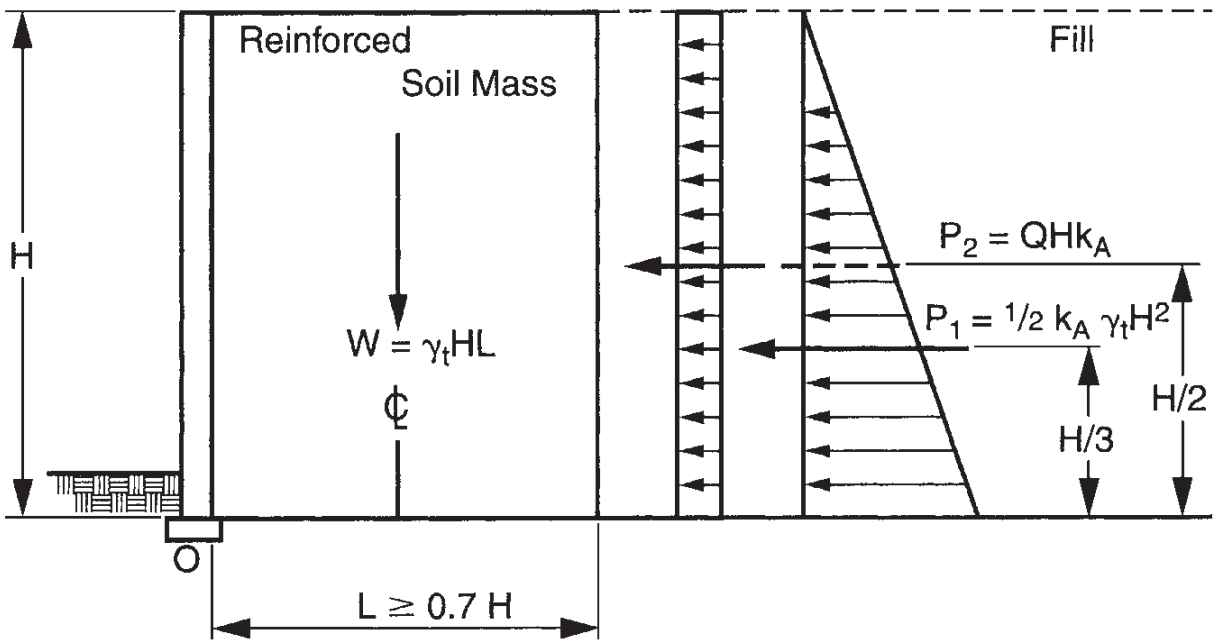

FIGURE 10.7 Static design analysis for mechanically stabilized earth retaining wall having horizontal backfill. (*Adapted from Standard Specifications for Highway Bridges, AASHTO 1996.*)

Figs. 10.7 and 10.8, the zone of mechanically stabilized earth mass is treated in a similar fashion as a massive gravity retaining wall. For static conditions, the following analyses must be performed:

1. *Allowable bearing pressure:* The bearing pressure due to the reinforced soil mass must not exceed the allowable bearing pressure.

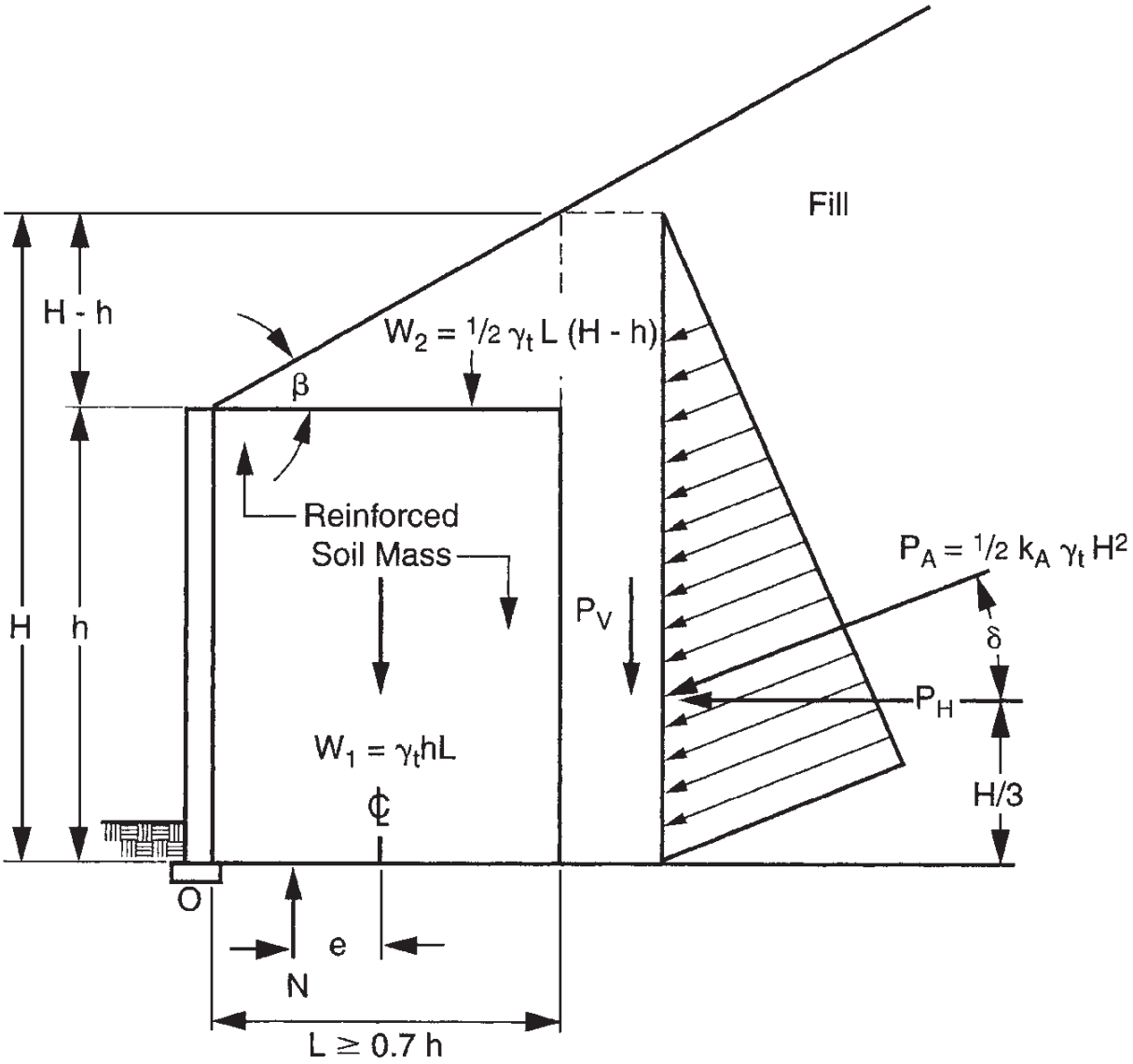

FIGURE 10.8 Static design analysis for mechanically stabilized earth retaining wall having sloping backfill. (*Adapted from Standard Specifications for Highway Bridges, AASHTO 1996.*)

2. *Factor of safety for sliding:* The reinforced soil mass must have an adequate factor of safety for sliding.
3. *Factor of safety for overturning:* The reinforced soil mass must have an adequate factor of safety for overturning about point *O*.
4. *Resultant of vertical forces:* The resultant of the vertical forces *N* must be within the middle one-third of the base of the reinforced soil mass.
5. *Stability of reinforced soil mass.* The stability of the entire reinforced soil mass (i.e., shear failure below the bottom of the wall) should be checked.

Note in Fig. 10.7 that two forces P_1 and P_2 are shown acting on the reinforced soil mass. The first force P_1 is determined from the standard active earth pressure resultant equation [Eq. (10.1)]. The second force P_2 is due to a uniform surcharge Q applied to the entire ground surface behind the mechanically stabilized earth retaining wall. If the wall does not have a surcharge, then P_2 is equal to zero.

Figure 10.8 presents the active earth pressure force for an inclined slope behind the retaining wall. As shown in Fig. 10.8, the friction δ of the soil along the backside of the reinforced soil mass has been included in the analysis. The value of k_A would be obtained

from Coulomb's earth pressure equation (Fig. 10.3). As a conservative approach, the friction angle δ can be assumed to be equal to zero, and then $P_H = P_A$. As indicated in both Figs. 10.7 and 10.8, the minimum width of the reinforced soil mass must be at least 7/10 times the height of the reinforced soil mass.

External Stability—Earthquake Conditions. For earthquake conditions, the most commonly used approach is the pseudostatic method. The pseudostatic force can be calculated from Eqs. (10.7), (10.8), or (10.9). Once the pseudostatic force and location are known, then the five items listed in "External Stability—Static Conditions" would need to be checked. Acceptable values of the factors of safety for sliding and overturning are typically in the range of 1.1 to 1.2 for earthquake conditions.

Internal Stability. To check the static stability of the mechanically stabilized zone, a slope stability analysis can be performed in which the soil reinforcement is modeled as horizontal forces equivalent to its allowable tensile resistance. For earthquake conditions, the slope stability analysis could incorporate a pseudostatic force (i.e., Sec. 9.2.4). In addition to calculating the factor of safety for both the static and earthquake conditions, the pullout resistance of the reinforcement along the slip surface should be checked.

Example Problem. Using the mechanically stabilized earth retaining wall shown in Fig. 10.7, let $H = 20$ ft, the width of the mechanically stabilized earth retaining wall = 14 ft, the depth of embedment at the front of the mechanically stabilized zone = 3 ft, and there is a level backfill with no surcharge pressures (that is, $P_2 = 0$). Assume that the soil behind and in front of the mechanically stabilized zone is a clean sand having a friction angle $\phi = 30°$, a total unit weight of $\gamma_t = 110$ lb/ft^3, and there will be no shear stress (that is, $\delta = 0°$) along the vertical back and front sides of the mechanically stabilized zone. For the mechanically stabilized zone, assume the soil will have a total unit weight $\gamma_t = 120$ lb/ft^3 and $\delta = 23°$ along the bottom of the mechanically stabilized zone. For earthquake design conditions, use $a_{max} = 0.20g$. Calculate the factor of safety for sliding and for overturning for both the static and earthquake conditions.

Solution: Static Analysis

$$k_A = \tan^2 (45° - \tfrac{1}{2}\phi) = \tan^2 [45° - \tfrac{1}{2}(30°)] = 0.333$$

$$k_p = \tan^2 (45° + \tfrac{1}{2}\phi) = \tan^2 [45° + \tfrac{1}{2}(30°)] = 3.0$$

$$P_A = \tfrac{1}{2}k_A\gamma_t H^2 = \tfrac{1}{2}(0.333)(110)(20)^2 = 7330 \text{ lb/ft}$$

$$P_p = \tfrac{1}{2}k_p\gamma_t D^2 = \tfrac{1}{2}(3.0)(110)(3)^2 = 1490 \text{ lb/ft}$$

With reduction factor = 2,

$$\text{Allowable } P_p = 740 \text{ lb/ft}$$

For sliding analysis:

$$\text{FS} = \frac{N \tan \delta + P_p}{P_A} \qquad \text{Eq. (10.11)}, \text{ where } P_A = P_H$$

$$W = N = HL\gamma_t = (20)(14)(120 \text{ lb/ft}^3) = 33{,}600 \text{ lb per linear foot of wall length}$$

$$\text{FS} = \frac{33{,}600 \tan 23^\circ + 740}{7330} = 2.05$$

For overturning analysis: Taking moments about the toe of the wall gives

$$\text{Overturning moment} = P_A \frac{H}{3} = 7330 \frac{20}{3} = 48{,}900$$

$$\text{Moment of weight} = 33{,}600 \frac{14}{2} = 235{,}000$$

$$\text{FS} = \frac{235{,}000}{48{,}900} = 4.81$$

Solution: Earthquake Analysis. Using Eq. (10.7), we get

$$P_E = \tfrac{1}{2} k_A^{1/2} (a_{\max}/g)(H^2 \gamma_t) = \tfrac{1}{2} (0.333)^{1/2} (0.20)(20)^2 (110) = 2540 \text{ lb/ft}$$

For sliding analysis, use Eq. (10.13):

$$\text{FS} = \frac{N \tan \delta + P_p}{P_H + P_E} = \frac{33{,}600 \tan 23^\circ + 740}{7330 + 2540} = 1.52$$

For overturning analysis, use Eq. (10.14) with $P_v = 0$.

$$\text{FS} = \frac{Wa}{\tfrac{1}{3} P_H H + \tfrac{2}{3} H P_E} = \frac{33{,}600(7)}{\tfrac{1}{3}(7330)(20) + \tfrac{2}{3}(20)(2540)} = 2.84$$

In summary,

Static conditions:

$$\text{FS sliding} = 2.05$$

$$\text{FS overturning} = 4.81$$

Earthquake conditions ($a_{\max} = 0.20g$):

$$\text{FS sliding} = 1.52$$

$$\text{FS overturning} = 2.84$$

10.3 RETAINING WALL ANALYSES FOR LIQUEFIED SOIL

10.3.1 Introduction

Retaining walls are commonly used for port and wharf facilities, which are often located in areas susceptible to liquefaction. Many of these facilities have been damaged by earthquake-induced liquefaction. The ports and wharves often contain major retaining structures, such

as seawalls, anchored bulkheads, gravity and cantilever walls, and sheet pile cofferdams, that allow large ships to moor adjacent to the retaining walls and then load or unload cargo. Examples of liquefaction-induced damage to retaining walls are presented in Sec. 3.4.3.

There are often three different types of liquefaction effects that can damage the retaining wall:

1. *Passive wedge liquefaction:* The first is liquefaction of soil in front of the retaining wall. In this case, the passive resistance in front of the retaining wall is reduced.

2. *Active wedge liquefaction:* In the second case, the soil behind the retaining wall liquefies, and the pressure exerted on the wall is greatly increased. Cases 1 and 2 can act individually or together, and they can initiate an overturning failure of the retaining wall or cause the wall to progressively slide outward (localized lateral spreading) or tilt toward the water. Another possibility is that the increased pressure exerted on the wall could exceed the strength of the wall, resulting in a structural failure of the wall.

Liquefaction of the soil behind the retaining wall can also affect tieback anchors. For example, the increased pressure due to liquefaction of the soil behind the wall could break the tieback anchors or reduce their passive resistance.

3. *Liquefaction below base of wall:* The third case is liquefaction below the bottom of the wall. Many waterfront retaining walls consist of massive structures, such as the concrete box caissons shown in Fig. 3.31. In this case, the bearing capacity or slide resistance of the wall is reduced, resulting in a bearing capacity failure or promoting lateral spreading of the wall.

10.3.2 Design Pressures

The first step in the analysis is to determine the factor of safety against liquefaction for the soil behind the retaining wall, in front of the retaining wall, and below the bottom of the wall. The analysis presented in Chap. 6 can be used to determine the factor of safety against liquefaction. The retaining wall may exert significant shear stress into the underlying soil, which can decrease the factor of safety against liquefaction for loose soils (i.e., see Fig. 9.24). Likewise, there could be sloping ground in front of the wall or behind the wall, in which case the factor of safety against liquefaction may need to be adjusted (see Sec. 9.4.2).

After the factor of safety against liquefaction has been calculated, the next step is to determine the design pressures that act on the retaining wall:

1. *Passive pressure:* For those soils that will be subjected to liquefaction in the passive zone, one approach is to assume that the liquefied soil has zero shear strength. In essence, the liquefied zones no longer provide sliding or overturning resistance.

2. *Active pressure:* For those soils that will be subjected to liquefaction in the active zone, the pressure exerted on the face of the wall will increase. One approach is to assume zero shear strength of the liquefied soil (that is, $\phi' = 0$). There are two possible conditions:

a. *Water level located only behind the retaining wall:* In this case, the wall and the ground beneath the bottom of the wall are relatively impermeable. In addition, there is a groundwater table behind the wall with dry conditions in front of the wall. The thrust on the wall due to liquefaction of the backfill can be calculated by using Eq. (10.1) with $k_A = 1$ [i.e., for $\phi' = 0$, $k_A = 1$, see Eq. (10.2)] and $\gamma_t = \gamma_{sat}$ (i.e., γ_{sat} = saturated unit weight of the soil).

b. *Water levels are approximately the same on both sides of the retaining wall:* The more common situation is that the elevation of the groundwater table behind the wall is approximately the same as the water level in front of the wall. The thrust on the wall due to liquefaction of the soil can be calculated by using Eq. (10.1) with $k_A = 1$ [i.e., for $\phi' = 0$, $k_A = 1$, see Eq. (10.2)] and using γ_b (buoyant unit weight) in place of γ_t.

The only difference between the two cases is that the first case includes the unit weight of water ($\gamma_{sat} = \gamma_b + \gamma_w$), while the second case does not include γ_w because it is located on both sides of the wall and hence its effect is canceled out.

In addition to the increased pressure acting on the retaining wall due to liquefaction, consider a reduction in support and/or resistance of the tieback anchors.

3. *Bearing soil:* For the liquefaction of the bearing soil, use the analysis in Sec. 8.2.

10.3.3 Sheet Pile Walls

Introduction. Sheet pile retaining walls are widely used for waterfront construction and consist of interlocking members that are driven into place. Individual sheet piles come in many different sizes and shapes. Sheet piles have an interlocking joint that enables the individual segments to be connected together to form a solid wall.

Static Design. Many different types of static design methods are used for sheet pile walls. Figure 10.9 shows the most common type of static design method. In Fig. 10.9, the term *H* represents the unsupported face of the sheet pile wall. As indicated in Fig. 10.9, this sheet pile wall is being used as a waterfront retaining structure, and the elevation of the water in front of the wall is the same as that of the groundwater table behind the wall. For highly permeable soil, such as clean sand and gravel, this often occurs because the water can quickly flow underneath the wall in order to equalize the water levels.

In Fig. 10.9, the term *D* represents that portion of the sheet pile wall that is anchored in soil. Also shown in Fig. 10.9 is a force designated as A_P. This represents a restraining force on the sheet pile wall due to the construction of a tieback, such as by using a rod that has a

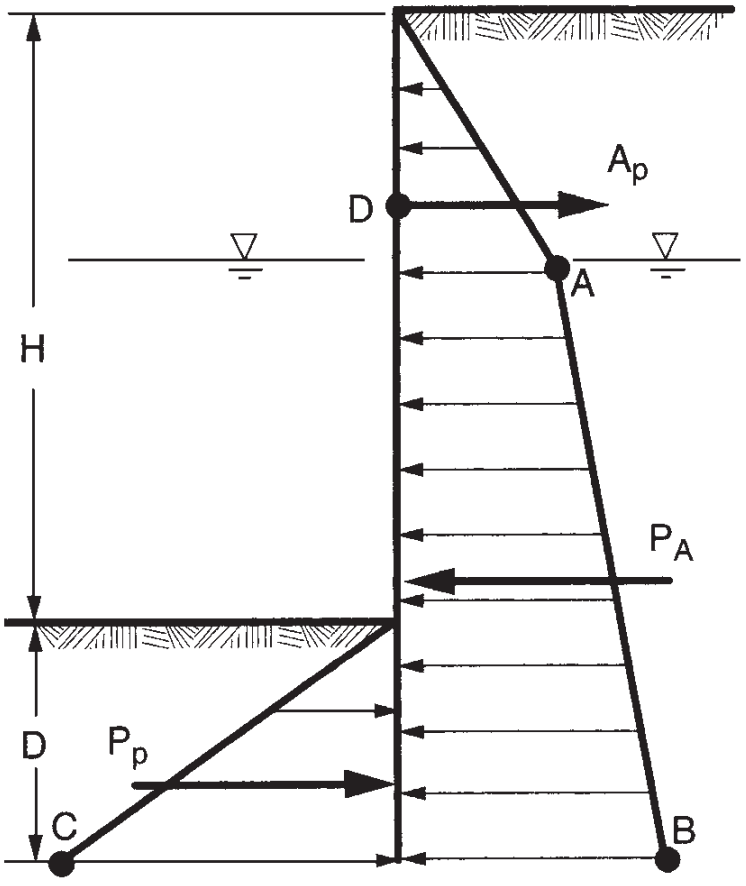

FIGURE 10.9 Earth pressure diagram for static design of sheet pile wall. (*From NAVFAC DM-7.2, 1982.*)

grouted end or is attached to an anchor block. Tieback anchors are often used in sheet pile wall construction to reduce the bending moments in the sheet pile. When tieback anchors are used, the sheet pile wall is typically referred to as an anchored bulkhead, while if no tiebacks are utilized, the wall is called a cantilevered sheet pile wall.

Sheet pile walls tend to be relatively flexible. Thus, as indicated in Fig. 10.9, the design is based on active and passive earth pressures. The soil behind the wall is assumed to exert an active earth pressure on the sheet pile wall. At the groundwater table (point *A*), the active earth pressure is equal to

$$\text{Active earth pressure at point } A, \text{ kPa or lb/ft}^2 = k_A \gamma_t d_1 \tag{10.18}$$

where k_A = active earth pressure coefficient from Eq. (10.2) (dimensionless parameter). Friction between sheet pile wall and soil is usually neglected in design analysis
γ_t = total unit weight of the soil above the groundwater table, kN/m^3 or lb/ft^3
d_1 = depth from the ground surface to the groundwater table, m or ft

In using Eq. (10.18), a unit length (1 m or 1 ft) of sheet pile wall is assumed. At point *B* in Fig. 10.9, the active earth pressure equals

$$\text{Active earth pressure at point } B, \text{ kPa or lb/ft}^2 = k_A \gamma_t d_1 + k_A \gamma_b d_2 \tag{10.19}$$

where γ_b = buoyant unit weight of the soil below the groundwater table and d_2 = depth from the groundwater table to the bottom of the sheet pile wall. For a sheet pile wall having assumed values of *H* and *D* (see Fig. 10.9) and using the calculated values of active earth pressure at points *A* and *B,* the active earth pressure resultant force P_A, in kilonewtons per linear meter of wall or pounds per linear foot of wall, can be calculated.

The soil in front of the wall is assumed to exert a passive earth pressure on the sheet pile wall. The passive earth pressure at point *C* in Fig. 10.9 is

$$\text{Passive earth pressure at point } C, \text{ kPa or lb/ft}^2 = k_p \gamma_b D \tag{10.20}$$

where the passive earth pressure coefficient k_p can be calculated from Eq. (10.4). Similar to the analysis of cantilever retaining walls, if it is desirable to limit the amount of sheet pile wall translation, then a reduction factor can be applied to the passive pressure. Once the allowable passive pressure is known at point *C,* the passive resultant force P_p can be readily calculated.

As an alternative solution for the passive pressure, Eq. (10.3) can be used to calculate P_p with the buoyant unit weight γ_b substituted for the total unit weight γ_t and the depth *D* as shown in Fig. 10.9.

Note that a water pressure has not been included in the analysis. This is because the water level is the same on both sides of the wall, and water pressure cancels and thus should not be included in the analysis.

The static design of sheet pile walls requires the following analyses: (1) evaluation of the earth pressures that act on the wall, such as shown in Fig. 10.9; (2) determination of the required depth *D* of piling penetration; (3) calculation of the maximum bending moment $M_{\max}$ which is used to determine the maximum stress in the sheet pile; and (4) selection of the appropriate piling type, size, and construction details.

A typical design process is to assume a depth *D* (Fig. 10.9) and then calculate the factor of safety for toe failure (i.e., toe kick-out) by the summation of moments at the tieback anchor (point *D*). The factor of safety is defined as the moment due to the passive force divided by the moment due to the active force. Values of acceptable FS for toe failure are 2 to 3. An alternative solution is to first select the factor of safety and then develop the active and passive resultant forces and moment arms in terms of *D.* By solving the equation, the value of *D* for a specific factor of safety can be directly calculated.

Once the depth D of the sheet pile wall is known, the anchor pull A_p must be calculated. The anchor pull is determined by the summation of forces in the horizontal direction, or

$$A_p = P_A - \frac{P_p}{\text{FS}} \tag{10.21}$$

where P_A and P_p are the resultant active and passive forces (see Fig. 10.9) and FS is the factor of safety that was obtained from the toe failure analysis. Based on the earth pressure diagram (Fig. 10.9) and the calculated value of A_p, elementary structural mechanics can be used to determine the maximum moment in the sheet pile wall. The maximum moment divided by the section modulus can then be compared with the allowable design stresses of the sheet piling.

Some other important design considerations for the static design of sheet pile walls include the following:

1. *Soil layers:* The active and passive earth pressures should be adjusted for soil layers having different engineering properties.

2. *Penetration depth:* The penetration depth D of the sheet pile wall should be increased by at least an additional 20 percent to allow for the possibility of dredging and scour. Deeper penetration depths may be required based on a scour analysis.

3. *Surcharge loads:* The ground surface behind the sheet pile wall is often subjected to surcharge loads. The equation $P_2 = QHk_A$ can be used to determine the active earth pressure resultant force due to a uniform surcharge pressure applied to the ground surface behind the wall. Note in this equation that the entire height of the sheet pile wall (that is, $H + D$, see Fig. 10.9) must be used in place of H. Typical surcharge pressures exerted on sheet pile walls are caused by railroads, highways, dock loading facilities and merchandise, ore piles, and cranes.

4. *Unbalanced hydrostatic and seepage forces:* The previous discussion has assumed that the water levels on both sides of the sheet pile wall are at the same elevation. Depending on factors such as the watertightness of the sheet pile wall and the backfill permeability, it is possible that the groundwater level could be higher than the water level in front of the wall, in which case the wall would be subjected to water pressures. This condition could develop when there is a receding tide or a heavy rainstorm that causes a high groundwater table. A flow net can be used to determine the unbalanced hydrostatic and upward seepage forces in the soil in front of the sheet pile wall.

5. *Other loading conditions:* The sheet pile wall may have to be designed to resist the lateral loads due to ice thrust, wave forces, ship impact, mooring pull, and earthquake forces. If granular soil behind or in front of the sheet pile wall is in a loose state, it could be susceptible to liquefaction during an earthquake.

Earthquake Analysis. In the case of liquefaction of soil, the earthquake design pressures must be modified. As indicated in Sec. 10.3.2, higher pressures will be exerted on the back face of the wall if this soil should liquefy. Likewise, there will be less passive resistance if the soil in front of the sheet pile wall will liquefy during the design earthquake. Section 10.3.2 should be used as a guide in the selection of the pressures exerted on the sheet pile wall during the earthquake. Once these earthquake-induced pressures behind and in front of the wall are known, then the factor of safety for toe failure and the anchor pull force can be calculated in the same manner as outlined in the previous section.

Example Problems. Using the sheet pile wall diagram shown in Fig. 10.9, assume that the soil behind and in front of the sheet wall is uniform sand with a friction angle $\phi' = 33°$, buoyant unit weight $\gamma_b = 64$ lb/ft^3, and above the groundwater table, the total unit weight

$\gamma_t = 120$ lb/ft^3. Also assume that the sheet pile wall has $H = 30$ ft and $D = 20$ ft, the water level in front of the wall is at the same elevation as the groundwater table which is located 5 ft below the ground surface, and the tieback anchor is located 4 ft below the ground surface. In the analysis, neglect wall friction.

Static Design. Calculate the factor of safety for toe kick-out and the tieback anchor force. Equation (10.2):

$$k_A = \tan^2 (45° - \tfrac{1}{2}\phi) = \tan^2 [45° - \tfrac{1}{2}(33°)] = 0.295$$

Equation (10.4):

$$k_p = \tan^2 (45° + \tfrac{1}{2}\phi) = \tan^2 [45° + \tfrac{1}{2}(33°)] = 3.39$$

From 0 to 5 ft:

$$P_{1A} = \tfrac{1}{2}k_A\gamma_t(5)^2 = \tfrac{1}{2}(0.295)(120)(5)^2 = 400 \text{ lb/ft}$$

From 5 to 50 ft:

$$P_{2A} = k_A\gamma_t(5)(45) + \tfrac{1}{2}k_A\gamma_b(45)^2 = 0.295(120)(5)(45) + \tfrac{1}{2}(0.295)(64)(45)^2$$

$$= 8000 + 19{,}100 = 27{,}100$$

$$P_A = P_{1A} + P_{2A} = 400 + 27{,}100 = 27{,}500 \text{ lb/ft}$$

Equation (10.3) with γ_b:

$$P_p = \tfrac{1}{2}k_p\gamma_b D^2 = \tfrac{1}{2}(3.39)(64)(20)^2 = 43{,}400 \text{ lb/ft}$$

$$\text{Moment due to passive force} = 43{,}400(26 + \tfrac{2}{3}20) = 1.71 \times 10^6$$

Neglecting P_{1A},

Moment due to active force (at tieback anchor)

$$= 8000\left(1 + \frac{45}{2}\right) + 19{,}100[1 + \tfrac{2}{3}(45)] = 7.8 \times 10^5$$

$$\text{FS} = \frac{\text{resisting moment}}{\text{destabilizing moment}} = \frac{1.71 \times 10^6}{7.8 \times 10^5}$$

$$= 2.19$$

$$A_p = P_A - \frac{P_p}{\text{FS}} = 27{,}500 - \frac{43{,}400}{2.19} = 7680 \text{ lb/ft}$$

For a 10-ft spacing, therefore,

$$A_p = 10(7680) = 76{,}800 \text{ lb} = 76.8 \text{ kips}$$

Earthquake Analysis, Pseudostatic Method. For the first earthquake analysis, assume that the sand behind, beneath, and in front of the wall has a factor of safety against liquefaction that is greater than 2.0. The design earthquake condition is $a_{max} = 0.20g$. Using the pseudostatic approach [i.e., Eq. (10.7)], calculate the factor of safety for toe kick-out and the tieback anchor force.

Since the effect of the water pressure tends to cancel on both sides of the wall, use Eq. (10.7) and estimate P_E based on the buoyant unit weight $\gamma_b = 64$ lb/ft^3, or

$$P_E = \tfrac{1}{2}k_A^{1/2}\left(\frac{a_{\max}}{g}\right)(H^2\gamma_b) = \tfrac{1}{2}(0.295)^{1/2}(0.20)(50)^2(64) = 8690 \text{ lb/ft}$$

And P_E acts at a distance of $\frac{2}{3}(H + D)$ above the bottom of the sheet pile wall.

$$\text{Moment due to } P_E = 8690[\tfrac{1}{3}(50) - 4] = 1.10 \times 10^5$$

$$\text{Total destabilizing moment} = 7.80 \times 10^5 + 1.10 \times 10^5 = 8.90 \times 10^5$$

$$\text{Moment due to passive force} = 1.71 \times 10^6$$

$$\text{FS} = \frac{\text{resisting moment}}{\text{destabilizing moment}} = \frac{1.71 \times 10^6}{8.90 \times 10^5} = 1.92$$

$$A_p = P_A + P_E - \frac{P_p}{\text{FS}} = 27{,}500 + 8690 - \frac{43{,}400}{1.92} = 13{,}600 \text{ lb/ft}$$

For a 10-ft spacing, therefore

$$A_p = 10\ (13{,}600) = 136{,}000 \text{ lb} = 136 \text{ kips}$$

Earthquake Analysis, Liquefaction of Passive Wedge. For the second earthquake analysis, assume that the sand located behind the retaining wall has a factor of safety against liquefaction greater than 2.0. Also assume that the upper 10 ft of sand located in front of the retaining wall will liquefy during the design earthquake, while the sand located below a depth of 10 ft has a factor of safety greater than 2.0. Calculate the factor of safety for toe kick-out and the tieback anchor force.

For the passive wedge:

- 0 to 10 ft: Passive resistance = 0
- At 10-ft depth: Passive resistance $= k_p\gamma_b d = 3.39(64)(10) = 2170$ lb/ft^2
- At 20-ft depth: Passive resistance $= k_p\gamma_b d = 3.39(64)(20) = 4340$ lb/ft^2

$$\text{Passive force} = \frac{(2170 + 4340)}{2}(10) = 32{,}600 \text{ lb/ft}$$

$$\text{Moment due to passive force} = 2170(10)(45 - 4) + \frac{4340 - 2170}{2}(10)[40 + \tfrac{2}{3}(10) - 4]$$

$$= 890{,}000 + 463{,}000 = 1.35 \times 10^6$$

Including a pseudostatic force in the analysis gives these results:

$$P_E = \tfrac{1}{2}k_A^{1/2}\left(\frac{a_{\max}}{g}\right)(H^2\gamma_b) = \tfrac{1}{2}(0.295)^{1/2}(0.20)(50)^2(64) = 8690 \text{ lb/ft}$$

And P_E acts at a distance of $\frac{2}{3}(H + D)$ above the bottom of the sheet pile wall.

$$\text{Moment due to } P_E = 8690[\tfrac{1}{3}(50) - 4] = 1.10 \times 10^5$$

$$\text{Total destabilizing moment} = 7.80 \times 10^5 + 1.10 \times 10^5 = 8.90 \times 10^5$$

$$\text{Moment due to passive force} = 1.35 \times 10^6$$

$$\text{FS} = \frac{\text{resisting moment}}{\text{destabilizing moment}} = \frac{1.35 \times 10^6}{8.90 \times 10^5}$$

$$= 1.52$$

$$A_p = P_A + P_E - \frac{P_p}{\text{FS}} = 27{,}500 + 8690 - \frac{32{,}600}{1.52} = 14{,}700 \text{ lb/ft}$$

For a 10-ft spacing, therefore,

$$A_p = 10\ (14{,}700) = 147{,}000 \text{ lb} = 147 \text{ kips}$$

Earthquake Analysis, Liquefaction of Active Wedge. For the third earthquake analysis, assume that the sand located in front of the retaining wall has a factor of safety against liquefaction greater than 2.0. However, assume that the submerged sand located behind the retaining will liquefy during the earthquake. Further assume that the tieback anchor will be unaffected by the liquefaction. Calculate the factor of safety for toe kick-out.

As indicated in Sec. 10.3.2, when the water levels are approximately the same on both sides of the retaining wall, use Eq. (10.1) with $k_A = 1$ [i.e., for $\phi' = 0$, $k_A = 1$, see Eq. (10.2)] and use γ_b (buoyant unit weight) in place of γ_t.

As an approximation, assume that the entire 50 ft of soil behind the sheet pile wall will liquefy during the earthquake. Using Eq. (10.1), with $k_A = 1$ and $\gamma_b = 64$ lb/ft^3,

$$P_L = \tfrac{1}{2} k_A \gamma_b (\text{H} + \text{D})^2 = \tfrac{1}{2}(1.0)(64)(50)^2 = 80{,}000 \text{ lb/ft}$$

$$\text{Moment due to liquefied soil} = 80{,}000[\tfrac{2}{3}(50) - 4] = 2.35 \times 10^6$$

$$\text{Moment due to passive force} = 1.71 \times 10^6$$

$$\text{FS} = \frac{\text{resisting moment}}{\text{destabilizing moment}} = \frac{1.71 \times 10^6}{2.35 \times 10^6}$$

$$= 0.73$$

Summary of Values

Example problem		Factor of safety for toe kick-out	A_p, kips
Static analysis		2.19	76.8
Earthquake	Pseudostatic method [Eq. (10.7)]	1.92	136
	Partial passive wedge liquefaction*	1.52	147
	Liquefaction of soil behind wall	0.73	—

*Pseudostatic force included for the active wedge.

As indicated by the values in this summary table, the sheet pile wall would not fail for partial liquefaction of the passive wedge. However, liquefaction of the soil behind the retaining wall would cause failure of the wall.

10.3.4 Summary

As discussed in the previous sections, the liquefaction of soil can affect the retaining wall in many different ways. It is also possible that even with a factor of safety against liquefaction greater than 1.0, there could be still be significant weakening of the soil, leading to a retaining wall failure. In summary, the type of analysis should be based on the factor of safety against liquefaction FS_L as follows:

1. $FS_L \leq 1.0$: In this case, the soil is expected to liquefy during the design earthquake, and thus the design pressures acting on the retaining wall must be adjusted (see Sec. 10.3.2).
2. $FS_L > 2.0$: If the factor of safety against liquefaction is greater than about 2.0, the pore water pressures generated by the earthquake-induced contraction of the soil are usually small enough that they can be neglected. In this case, it could be assumed that the earthquake does not weaken the soil, and the pseudostatic analyses outlined in Sec. 10.2 could be performed.
3. $1.0 < FS_L \leq 2.0$: For this case, the soil is not anticipated to liquefy during the earthquake. However, as the loose granular soil contracts during the earthquake, there could still be a substantial increase in pore water pressure and hence weakening of the soil. Figure 5.15 can be used to estimate the pore water pressure ratio r_u for various values of the factor of safety against liquefaction FS_L. The analysis would vary depending on the location of the increase in pore water pressure as follows:
   - *Passive wedge:* If the soil in the passive wedge has a factor of safety against liquefaction greater than 1.0 but less than 2.0, then the increase in pore water pressure would decrease the effective shear strength and the passive resisting force would be reduced [i.e., passive resistance $= P_p(1 - r_u)$].
   - *Bearing soil:* For an increase in the pore water pressure in the bearing soil, use the analysis in Sec. 8.3.
   - *Active wedge:* In addition to the pseudostatic force P_E and the active earth pressure resultant force P_A, include a force that is equivalent to the anticipated earthquake-induced pore water pressure.

10.4 RETAINING WALL ANALYSES FOR WEAKENED SOIL

Besides the liquefaction of soil, many other types of soil can be weakened during the earthquake. In general, there are three cases:

1. *Weakening of backfill soil:* In this case, only the backfill soil is weakened during the earthquake. An example would be backfill soil that is susceptible to strain softening during the earthquake. As the backfill soil weakens during the earthquake, the force exerted on the back face of the wall increases. One design approach would be to estimate the shear strength corresponding to the weakened condition of the backfill soil and then use this strength to calculate the force exerted on the wall. The bearing pressure, factor of safety for sliding, factor of safety for overturning, and location of the resultant vertical force could then be calculated for this weakened backfill soil condition.

2. *Reduction in the soil resistance:* In this case, the soil beneath the bottom of the wall or the soil in the passive wedge is weakened during the earthquake. For example, the bearing soil could be susceptible to strain softening during the earthquake. As the bearing soil weakens during the earthquake, the wall foundation could experience additional settlement, a bearing capacity failure, sliding failure, or overturning failure. In addition, the weakening of

the ground beneath or in front of the wall could result in a shear failure beneath the retaining wall. One design approach would be to reduce the shear strength of the bearing soil or passive wedge soil to account for its weakened state during the earthquake. The settlement, bearing capacity, factor of safety for sliding, factor of safety for overturning, and factor of safety for a shear failure beneath the bottom of the wall would then be calculated for this weakened soil condition.

3. *Weakening of the backfill soil and reduction in the soil resistance:* This is the most complicated case and would require combined analyses of both items 1 and 2 as outlined above.

10.5 RESTRAINED RETAINING WALLS

10.5.1 Introduction

As mentioned in Sec. 10.1.1, in order for the active wedge to be developed, there must be sufficient movement of the retaining wall. In many cases movement of the retaining wall is restricted. Examples include massive bridge abutments, rigid basement walls, and retaining walls that are anchored in nonyielding rock. These cases are often described as *restrained retaining walls.*

10.5.2 Method of Analysis

To determine the static earth pressure acting on a restrained retaining wall, Eq. (10.1) can be utilized where the coefficient of earth pressure at rest k_0 is substituted for k_A. For static design conditions of restrained retaining walls that have granular backfill, a commonly used value of k_0 is 0.5. Restrained retaining walls are especially susceptible to higher earth pressures induced by heavy compaction equipment, and extra care must be taken during the compaction of backfill for restrained retaining walls.

For earthquake conditions, restrained retaining walls will usually be subjected to larger forces compared to those retaining walls that have the ability to develop the active wedge. One approach is to use the pseudostatic method to calculate the earthquake force, with an increase to compensate for the unyielding wall conditions, or

$$P_{ER} = \frac{P_E k_0}{k_A} \tag{10.22}$$

where P_{ER} = pseudostatic force acting upon a restrained retaining wall, lb or kN
P_E = pseudostatic force assuming wall has the ability to develop the active wedge, i.e., use Eq. (10.7), (10.8), or (10.9), lb or kN
k_0 = coefficient of earth pressure at rest
k_A = active earth pressure coefficient, calculated from Eq. (10.2) or using the k_A equation in Fig. 10.3

10.5.3 Example Problem

Use the example problem from Sec. 10.2.4 (i.e., Fig. 10.5), but assume that it is an unyielding bridge abutment. Determine the static and earthquake resultant forces acting on the restrained retaining wall. Neglect friction between the wall and backfill ($\delta = \phi_w = 0$).

Static Analysis. Using a value of $k_0 = 0.5$ and substituting k_0 for k_A in Eq. (10.1), we see the static earth pressure resultant force exerted on the restrained retaining wall is

$$P_R = \tfrac{1}{2}k_0\gamma_t H^2 = \tfrac{1}{2}(0.5)(110)(20)^2 = 11{,}000 \text{ lb per linear foot of wall}$$

The location of this static force is at a distance of $\frac{1}{3}H = 6.7$ ft above the base of the wall.

Earthquake Analysis. Using the method outlined in Sec. 10.2.1, we find the value of $k_A = 0.333$ and $P_E = 2540$ lb per linear foot of wall length (see Sec. 10.2.4). Therefore, using Eq. (10.22), we have

$$P_{ER} = P_E \frac{k_0}{k_A} = 2540 \frac{0.5}{0.333} = 3800 \text{ lb per linear foot of wall}$$

The location of this pseudostatic force is assumed to act at a distance of $\frac{2}{3}H = 13.3$ ft above the base of the wall.

In summary, the resultant earth pressure forces acting on the retaining wall are static $P_R = 11{,}000$ lb/ft acting at a distance of 6.7 ft above the base of the wall and earthquake $P_{ER} = 3800$ lb/ft acting at a distance of 13.3 ft above the base of the wall.

10.6 TEMPORARY RETAINING WALLS

10.6.1 Static Design

Temporary retaining walls are often used during construction, such as for the support of the sides of an excavation that is made below grade to construct the building foundation. If the temporary retaining wall has the ability to develop the active wedge, then the basic active earth pressure principles described in Sec. 10.1.1 can be used for the design of the temporary retaining walls.

Especially in urban areas, movement of the temporary retaining wall may have to be restricted to prevent damage to adjacent property. If movement of the retaining wall is restricted, the earth pressures will typically be between the active (k_A) and at-rest (k_0) values.

For some projects, temporary retaining walls may be constructed of sheeting (such as sheet piles) that are supported by horizontal braces, also known as *struts.* Near or at the top of the temporary retaining wall, the struts restrict movement of the retaining wall and prevent the development of the active wedge. Because of this inability of the retaining wall to deform at the top, earth pressures near the top of the wall are in excess of the active (k_A) pressures. At the bottom of the wall, the soil is usually able to deform into the excavation, which results in a reduction in earth pressure. Thus the earth pressures at the bottom of the excavation tend to be constant or even decrease, as shown in Fig. 10.10.

The earth pressure distributions shown in Fig. 10.10 were developed from actual measurements of the forces in struts during the construction of braced excavations. In Fig. 10.10, case *a* shows the earth pressure distribution for braced excavations in sand and cases *b* and *c* show the earth pressure distribution for clays. In Fig. 10.10, the distance H represents the depth of the excavation (i.e., the height of the exposed wall surface). The earth pressure distribution is applied over the exposed height H of the wall surface with the earth pressures transferred from the wall sheeting to the struts (the struts are labeled with forces F_1, F_2, etc.).

Any surcharge pressures, such as surcharge pressures on the ground surface adjacent to the excavation, must be added to the pressure distributions shown in Fig. 10.10. In addition, if the sand deposit has a groundwater table that is above the level of the bottom of the excavation, then water pressures must be added to the case *a* pressure distribution shown in Fig. 10.10.

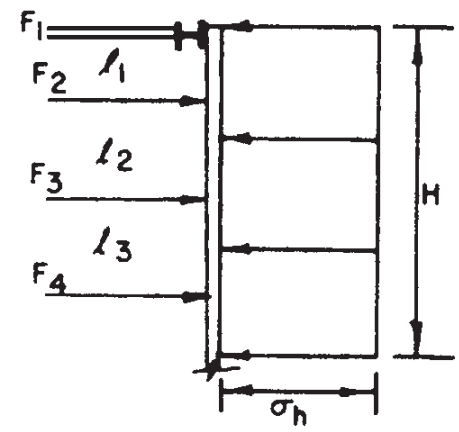

(a) SAND

$\sigma_h = 0.65\ K_A \cdot \gamma H$

WHERE $K_A = \tan^2(45 - \phi/2)$

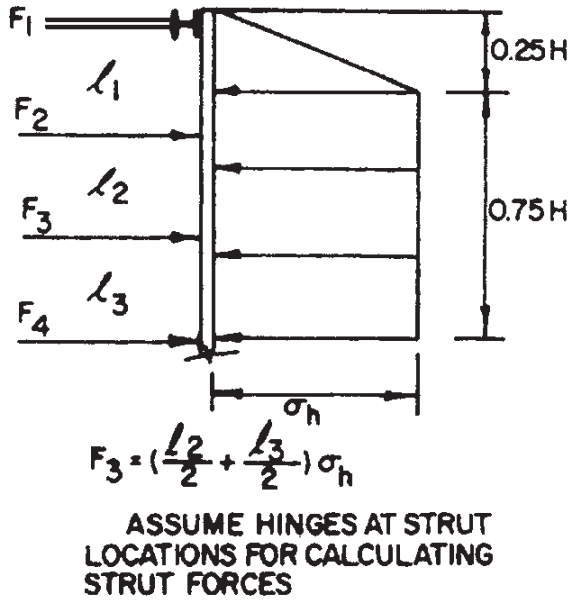

(b) SOFT TO MEDIUM CLAY
($N_o > 6$)

For clays base the selection on
$N_o = \gamma H/c$

$\sigma_h = K_A \cdot \gamma \cdot H$

$K_A = 1 - m\frac{4c}{\gamma H}$;
m = 1 except where cut is underlain by deep soft normally consolidated clay, then m = 0.4

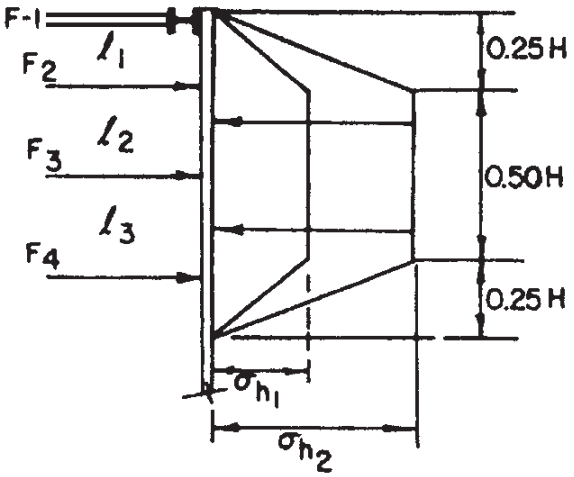

(c) STIFF CLAY
($N_o < 4$)
For $4 < N_o < 6$, use larger of diagrams (b) and (c).
$\sigma_{h1} = 0.2\gamma H$; $\sigma_{h2} = 0.4\gamma H$
Use lower value when movements are minimal and short construction period.

FIGURE 10.10 Earth pressure distribution on temporary braced walls. (*From NAVFAC DM-7.2 1982, originally developed by Terzaghi and Peck 1967.*)

Because the excavations are temporary (i.e., short-term condition), the undrained shear strength ($s_u = c$) is used for the analysis of the earth pressure distributions for clay. The earth pressure distributions for clay (i.e., cases *b* and *c*) are not valid for permanent walls or for walls where the groundwater table is above the bottom of the excavation.

10.6.2 Earthquake Analysis

Since temporary retaining walls are usually only in service for a short time, the possibility of earthquake effects is typically ignored. However, in active seismic zones or if the consequence of failure could be catastrophic, it may be prudent to perform an earthquake analysis. Depending on whether the wall is considered to be yielding or restrained, the analysis would be based on the data in Sec. 10.2 or Sec. 10.5. Weakening of the soil during the design earthquake and its effects on the temporary retaining wall should also be included in the analysis.

10.7 PROBLEMS

The problems have been divided into basic categories as indicated below.

Pseudostatic Method

10.1 Using the retaining wall shown in Fig. 10.4, assume $H = 4$ m, the thickness of the reinforced concrete wall stem = 0.4 m, the reinforced concrete wall footing is 3 m wide by 0.5 m thick, the ground surface in front of the wall is level with the top of the wall footing, and the unit weight of concrete = 23.5 kN/m^3. The wall backfill will consist of sand having $\phi = 32°$ and $\gamma_t = 20$ kN/m^3. Also assume that there is sand in front of the footing with these same soil properties. The friction angle between the bottom of the footing and the bearing soil $\delta = 38°$. For the condition of a level backfill and neglecting the wall friction on the backside of the wall and the front side of the footing, determine the resultant normal force N and the distance of N from the toe of the footing, the maximum bearing pressure q' and the minimum bearing pressure q'' exerted by the retaining wall foundation, factor of safety for sliding, and factor of safety for overturning for static conditions and earthquake conditions [using Eq. (10.7)] if $a_{max} = 0.20g$. *Answer:* Static conditions: $N = 68.2$ kN/m and location = 1.16 m from toe, $q' = 37.9$ kPa and $q'' = 7.5$ kPa, FS for sliding = 1.17, and FS for overturning = 2.2. Earthquake conditions: $P_E = 17.7$ kN/m, N is not within the middle third of the footing, FS for sliding = 0.86, FS for overturning = 1.29.

10.2 Solve Prob. 10.1, using Eq. (10.8). *Answer:* Static values are the same. Earthquake conditions: $P_E = 24$ kN/m, N is not within the middle third of the footing, FS for sliding = 0.78, FS for overturning = 1.18.

10.3 Solve Prob. 10.1, but include wall friction in the analysis (use Coulomb's earth pressure equation, Fig. 10.3). Assume the friction angle between the backside of the retaining wall and the backfill is equal to $\frac{3}{4}$ of ϕ (that is, $\phi_w = \frac{3}{4}\phi = 24°$). Use Eq. (10.9) for the earthquake analysis. *Answer:* Static condition: $N = 86.1$ kN/m and location = 1.69 m from toe, $q' = 39.6$ kPa and $q'' = 17.8$ kPa, FS for sliding = 1.78, and FS for overturning = ∞. Earthquake conditions: $P_{AE} = 68.5$ kN/m, N is 1.51 m from the toe of the footing, $q' = q'' = 32.0$ kPa, FS for sliding = 1.26, FS for overturning = ∞.

10.4 Using the retaining wall shown at the top of Fig. 10.2*b* (i.e., a cantilevered retaining wall), assume $H = 4$ m, the thickness of the reinforced concrete wall stem = 0.4 m and the

wall stem is located at the centerline of the footing, the reinforced concrete wall footing is 2 m wide by 0.5 m thick, the ground surface in front of the wall is level with the top of the wall footing, and the unit weight of concrete = 23.5 kN/m^3. The wall backfill will consist of sand having $\phi = 32°$ and $\gamma_t = 20$ kN/m^3. Also assume that there is sand in front of the footing with these same soil properties. The friction angle between the bottom of the footing and the bearing soil $\delta = 24°$. For the condition of a level backfill and assuming total mobilization of the shear strength along the vertical plane at the heel of the wall, calculate the resultant normal force N and the distance of N from the toe of the footing, the maximum bearing pressure q' and the minimum bearing pressure q'' exerted by the retaining wall foundation, factor of safety for sliding, and factor of safety for overturning for static conditions and earthquake conditions [using Eq. (10.9)] if $a_{max} = 0.20g$. *Answer:* Static conditions: $N = 136$ kN/m and location = 1.05 m from toe, $q' = 78.1$ kPa and $q'' = 57.8$ kPa, FS for sliding = 1.72, and FS for overturning = 47. Earthquake conditions: $P_{AE} = 71.2$ kN/m, N is 0.94 m from the toe of the footing, $q' = 88.6$ kPa and $q'' = 61.5$ kPa, FS for sliding = 1.17, FS for overturning = 29.

10.5 For the example problem shown in Fig. 10.5, assume that there is a vertical surcharge pressure of 200 lb/ft^2 located at ground surface behind the retaining wall. Calculate the factor of safety for sliding and the factor of safety for overturning, and determine if N is within the middle third of the retaining wall foundation for the static conditions and earthquake conditions [using Eq. (10.9)] if $a_{max} = 0.20g$. *Answer:* Static conditions: FS for sliding = 1.48, FS for overturning = 2.64, and N is not within the middle third of the retaining wall foundation. Earthquake conditions: FS for sliding = 1.02, FS for overturning = 0.91, and N is not within the middle third of the retaining wall foundation.

10.6 For the example problem shown in Fig. 10.5, assume that the ground surface behind the retaining wall slopes upward at a 3:1 (horizontal:vertical) slope inclination. Calculate the factor of safety for sliding and factor of safety for overturning, and determine if N is within the middle third of the retaining wall foundation for the static conditions and earthquake conditions [using Eq. (10.9)] if $a_{max} = 0.20g$. *Answer:* Static conditions: FS for sliding = 1.32, FS for overturning = 2.73, and N is not within the middle third of the retaining wall foundation. Earthquake conditions: FS for sliding = 0.72, FS for overturning = 1.06, and N is not within the middle third of the retaining wall foundation.

10.7 Use the data from the example problem in Sec. 10.2.5, and assume that there is a vertical surcharge pressure of 200 lb/ft^2 located at ground surface behind the mechanically stabilized earth retaining wall. Calculate the factor of safety for sliding, factor of safety for overturning, and maximum pressure exerted by the base of the mechanically stabilized earth retaining wall for static and earthquake conditions. *Answer:* Static conditions: FS for sliding = 1.73, FS for overturning = 3.78, and maximum pressure $q' = 4300$ lb/ft^2. Earthquake conditions: FS for sliding = 1.29, FS for overturning = 2.3, and N is not within the middle third of the base of the wall.

10.8 Use the data from the example problem in Sec. 10.2.5, and assume that the ground surface behind the mechanically stabilized earth retaining wall slopes upward at a 3:1 (horizontal:vertical) slope inclination. Also assume that the 3:1 slope does not start at the upper front corner of the rectangular reinforced soil mass (such as shown in Fig. 10.8), but instead the 3:1 slope starts at the upper back corner of the rectangular reinforced soil mass. Calculate the factor of safety for sliding, factor of safety for overturning, and maximum pressure exerted by the retaining wall foundation for the static and earthquake conditions, using the equations in Fig. 10.3. *Answer:* Static conditions: FS for sliding = 1.60, FS for overturning = 3.76, and maximum pressure $q' = 4310$ lb/ft^2. Earthquake conditions: FS for sliding = 0.81, FS for overturning = 1.91, and N is not within the middle third of the base of the wall.

10.9 For the example problem in Sec. 10.2.5, the internal stability of the mechanically stabilized zone is to be checked by using wedge analysis. Assume a planar slip surface that

is inclined at an angle of 61° (that is, $\alpha = 61°$) and passes through the toe of the mechanically stabilized zone. Also assume that the mechanically stabilized zone contains 40 horizontal layers of Tensar SS2 geogrid which has an allowable tensile strength = 300 lb/ft of wall length for each geogrid. In the wedge analysis, these 40 layers of geogrid can be represented as an allowable horizontal resistance force = 12,000 lb/ft of wall length (that is, 40 layers times 300 lb). If the friction angle ϕ of the sand = 32° in the mechanically stabilized zone, calculate the factor of safety for internal stability of the mechanically stabilized zone, using the wedge analysis for static and earthquake conditions. *Answer:* Static conditions: $F = 1.82$; earthquake conditions: FS = 1.29.

Sheet Pile Wall Analyses for Liquefied Soil

10.10 For the example problem in Sec. 10.3.3, assume that there is a uniform vertical surcharge pressure = 200 lb/ft^2 applied to the ground surface behind the sheet pile wall. Calculate the factor of safety for toe kick-out and the anchor pull force for the static condition and the earthquake conditions, using the pseudostatic method, and for partial liquefaction of the passive wedge. *Answer:* See App. E for solution.

10.11 For the example problem in Sec. 10.3.3, assume that the ground surface slopes upward at a 3:1 (horizontal:vertical) slope ratio behind the sheet pile wall. Calculate the factor of safety for toe kick-out and the anchor pull force for the static condition and the earthquake conditions, using the pseudostatic method, and for partial liquefaction of the passive wedge. *Answer:* See App. E for solution.

10.12 For the example problem in Sec. 10.3.3, assume that the ground in front of the sheet pile wall (i.e., the passive earth zone) slopes downward at a 3:1 (horizontal:vertical) slope ratio. Calculate the factor of safety for toe kick-out for the static condition and the earthquake conditions, using the pseudostatic method. *Answer:* Static condition: FS for toe kick-out = 1.18; earthquake condition: FS for toe kick-out = 1.04.

10.13 For the example problem in Sec. 10.3.3, assume that the anchor block is far enough back from the face of the sheet pile wall that it is not in the active zone. Also assume that the anchor block is located at a depth of 3 to 5 ft below ground surface, it is 5 ft by 5 ft in plan dimensions, and it consists of concrete that has a unit weight of 150 lb/ft^3. Further assume that the tieback rod is located at the center of gravity of the anchor block. For friction on the top and bottom of the anchor block, use a friction coefficient = $^2/_3\phi$, where ϕ = friction angle of the sand. Determine the lateral resistance of the anchor block for static conditions and for earthquake conditions, assuming that all the soil behind the retaining wall will liquefy during the earthquake. *Answer:* Static condition: lateral resistance = 26.6 kips; earthquake conditions: lateral resistance = 0.

Braced Excavations

10.14 A braced excavation will be used to support the vertical sides of a 20-ft-deep excavation (that is, $H = 20$ ft in Fig. 10.10). If the site consists of a sand with a friction angle $\phi = 32°$ and a total unit weight $\gamma_t = 120$ lb/ft^3, calculate the earth pressure σ_h and the resultant earth pressure force acting on the braced excavation for the static condition and the earthquake condition [using Eq. (10.7)] if $a_{max} = 0.20g$. Assume the groundwater table is well below the bottom of the excavation. *Answer:* Static condition: $\sigma_h = 480$ lb/ft^2 and the resultant force = 9600 lb per linear foot of wall length. Earthquake condition: $P_E = 2700$ lb per linear foot of wall length.

10.15 Solve Prob. 10.14, but assume the site consists of a soft clay having an undrained shear strength $s_u = 300$ lb/ft^2 (that is, $c = s_u = 300$ lb/ft^2) and use Eq. (10.8).

Answer: Static condition: $\sigma_h = 1200$ lb/ft^2, and the resultant force = 21,000 lb per linear foot of wall length. Earthquake condition: $P_E = 3600$ lb per linear foot of wall length.

10.16 Solve Prob. 10.15, but assume the site consists of a stiff clay having an undrained shear strength $s_u = 1200$ lb/ft^2 and use the higher earth pressure condition (that is, σ_{h2}). *Answer:* Static condition: $\sigma_{h2} = 960$ lb/ft^2, and resultant force = 14,400 lb per linear foot of wall length. Earthquake condition: $P_E = 3600$ lb per linear foot of wall length.

Subsoil Profiles

10.17 Use the data from Prob. 6.15 and Fig. 6.15 (i.e., sewage site at Niigata). Assume the subsoil profile represents conditions behind a retaining wall. Also assume that the type of retaining wall installed at the site is a concrete box structure, having height = 8 m, width = 5 m, and total weight of the concrete box structure = 823 kilonewtons per linear meter of wall length. The soil behind the retaining wall is flush with the top of the concrete box structure. The water level in front of the retaining wall is at the same elevation as the groundwater table behind the wall. The effective friction angle ϕ' of the soil can be assumed to be equal to 30°, wall friction along the back face of the wall can be neglected, and the coefficient of friction along the bottom of the wall = $^2/_3\phi'$. In addition, the ground in front of the wall is located 1 m above the bottom of the wall, and the subsoil profile in Fig. 6.15 starting at a depth of 7 m can be assumed to be applicable for the soil in front of the wall. For the static conditions and earthquake conditions, determine the resultant normal force N and the distance of N from the toe of the wall, the maximum bearing pressure q' and the minimum bearing pressure q'' exerted by the retaining wall foundation, factor of safety for sliding, and factor of safety for overturning. *Answer:* Static conditions: $N = 450$ kN/m and location = 1.89 m from toe, $q' = 156$ kPa and $q'' = 24$ kPa, FS for sliding = 1.66, and FS for overturning = 4.1. Earthquake conditions: $N = 450$ kN/m, N is not within the middle third of the footings, FS for sliding = 0.55, FS for overturning = 1.36.

Submerged Backfill Condition

10.18 A cantilevered retaining wall (3 m in height) has a granular backfill with $\phi = 30°$ and $\gamma_t = 20$ kN/m^3. Neglect wall friction, and assume the drainage system fails and the water level rises 3 m above the bottom of the retaining wall (i.e., the water table rises to the top of the retaining wall). Determine the initial active earth pressure resultant force P_A and the resultant force (due to earth plus water pressure) on the wall due to the rise in water level. For the failed drainage system condition, also calculate the total force on the wall if the soil behind the retaining wall should liquefy during the earthquake. For both the static and earthquake conditions, assume that there is no water in front of the retaining wall (i.e., only a groundwater table behind the retaining wall). *Answer:* Static condition: $P_A = 30$ kN/m (initial condition). With a rise in water level the force acting on the wall = 59.4 kN/m. Earthquake condition: $P_L = 90$ kN/m.

CHAPTER 11

OTHER GEOTECHNICAL EARTHQUAKE ENGINEERING ANALYSES

The following notation is used in this chapter:

SYMBOL	*DEFINITION*
a	Acceleration
a_{max}	Maximum horizontal acceleration at ground surface (also known as peak ground acceleration)
A, B, C	Seismic source types
B	Width of pipeline (for trench conditions B = width of trench at top of pipeline)
C_a, C_v	Seismic coefficients needed for development of a response spectrum
C_w	Coefficient used to calculate load on a pipeline for trench or jacked condition
D	Diameter of pipeline
E'	Modulus of soil resistance
F_v	Vertical pseudostatic force (pipeline design)
g	Acceleration of gravity
H	Height of soil above top of pipeline
k_h	Horizontal seismic coefficient
k_v	Vertical seismic coefficient
K_b	Bedding coefficient
m	Total mass of soil bearing on pipeline
N_a, N_v	Near-source factors
$(N_1)_{60}$	N value corrected for field testing procedures and overburden pressure
s_u	Undrained shear strength
S_A, S_B, etc.	Soil profile types
T	Period of vibration
T_0, T_s	Periods needed for determination of response spectrum
V_{s1}	Corrected shear wave velocity [Equation (6.9)]
W	Total weight of soil bearing on top of pipeline
W_{min}	Minimum vertical load on rigid pipeline
γ_t	Total unit weight of soil

11.1 INTRODUCTION

The prior chapters in Part 2 have described field investigation, liquefaction analyses, earthquake-induced settlement, bearing capacity, slope stability, and retaining wall analyses. There are many other types of earthquake analyses that may be required by the geotechnical

engineer. This final chapter of Part 2 describes some of these analyses. Items included in this chapter are:

- Surface rupture zone
- Groundwater
- Pavement design
- Pipeline design
- Response spectrum

11.2 SURFACE RUPTURE ZONE

11.2.1 Introduction

Section 3.2 presents an introduction into surface rupture. Examples of damage caused by surface rupture are shown in Figs. 3.3 to 3.13.

The best individual to determine the location and width of the surface rupture zone is the engineering geologist. Seismic study maps, such as the *State of California Special Studies Zones Maps* (1982), which were developed as part of the Alquist-Priolo Special Studies Zones Act, delineate the approximate location of active fault zones that require special geologic studies. These maps also indicate the approximate locations of historic fault offsets, which are indicated by year of earthquake-associated event, as well as the locations of ongoing surface rupture due to fault creep. There are many other geologic references, such as the cross section shown in Fig. 5.2, that can be used to identify active fault zones. Trenches, such as shown in Fig. 5.8, can be excavated across the fault zone to more accurately identify the width of the surface rupture zone.

11.2.2 Design Approach

Since most structures will be unable to resist the shear movement associated with surface rupture, one design approach is to simply restrict construction in the fault shear zone. Often the local building code will restrict the construction in fault zones. For example, the *Southern Nevada Building Code Amendments* (1997) state the following:

> Minimum Distances to Ground Faulting:
>
> **1.** No portion of the foundation system of any habitable space shall be located less than five feet to a fault.
> **2.** When the geotechnical report establishes that neither a fault nor a fault zone exists on the project, no fault zone set back requirements shall be imposed.
> **3.** If through exploration, the fault location is defined, the fault and/or the no-build zone shall be clearly shown to scale on grading and plot plan(s).
> **4.** When the fault location is not fully defined by explorations but a no build zone of potential fault impact is established by the geotechnical report, no portion of the foundation system of any habitable space shall be constructed to allow any portion of the foundation system to be located within that zone. The no build zone shall be clearly shown to scale on grading and plot plan(s).
> **5.** For single lot, single family residences, the fault location may be approximated by historical research as indicated in the geotechnical report. A no build zone of at least 50 feet each side of the historically approximated fault edge shall be established. The no build zone shall be clearly shown to scale on grading and plot plan(s).

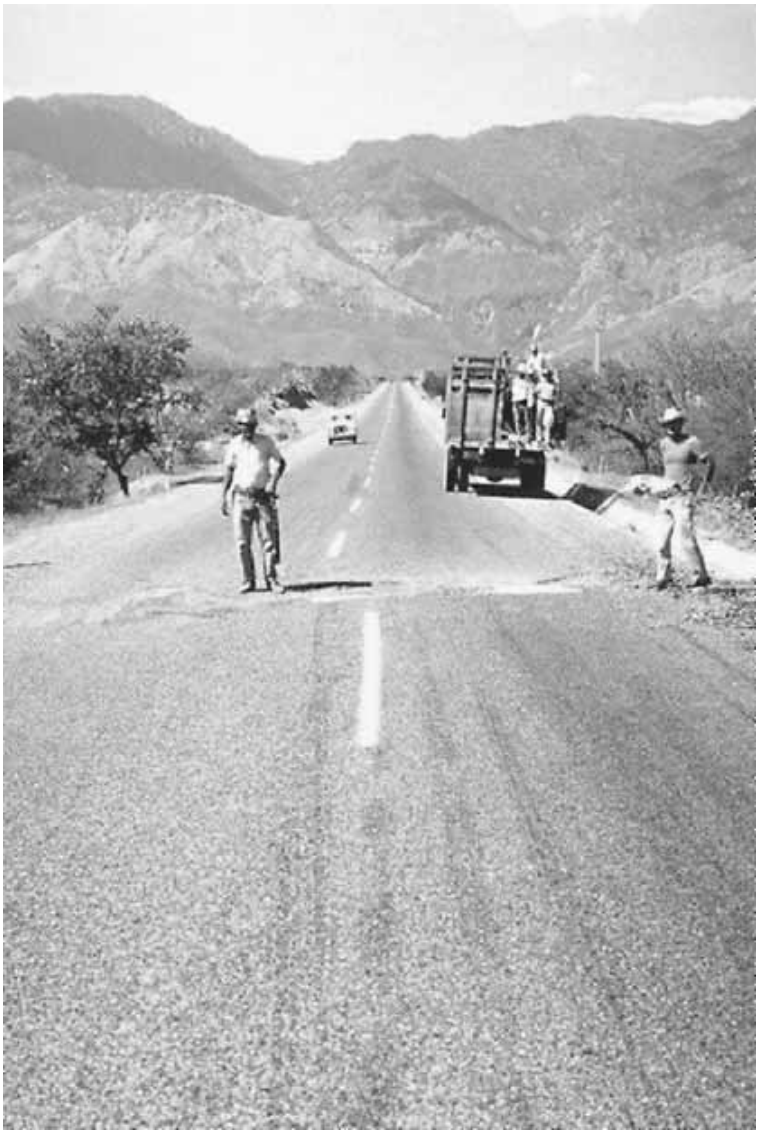

FIGURE 11.1 Offset of a road north of Zacapa caused by the Guatemala (Gualan) earthquake (magnitude 7.5) on February 4, 1976. (*Photograph from the Steinbrugge Collection, EERC, University of California, Berkeley.*)

In many cases, structures will have to be constructed in the surface rupture zone. For example, transportation routes may need to cross the active shear fault zones. One approach is to construct the roads such that they cross the fault in a perpendicular direction. In addition, it is desirable to cross the surface rupture zone at a level ground location so that bridges or overpasses need not be constructed in the surface rupture zone. Probably the best type of pavement material to be used in the fault zone is asphalt concrete, which is relatively flexible and easy to repair. For example, Fig. 11.1 shows an asphalt concrete road that crosses a surface rupture zone. The damage shown in Fig. 11.1 was caused by the surface rupture associated with the Guatemala (Gulan) earthquake. This damage will be relatively easy to repair. In fact, the road was still usable even in its sheared condition.

Pipelines also must often pass through surface rupture zones. Similar to pavements, it is best to cross the fault rupture zone in a perpendicular direction and at a level ground site. There are many different types of design alternatives for pipelines that cross the rupture zone. For example, a large tunnel can be constructed with the pipeline suspended within the center of the tunnel. The amount of open space between the tunnel wall and the pipeline would be based on the expected amount of surface rupture. Another option is to install automatic

shutoff valves that will close the pipeline if there is a drop in pressure. With additional segments of the pipeline stored nearby, the pipe can then be quickly repaired.

11.2.3 Groundwater

The fault plane often contains of a thin layer of *fault gouge,* which is a clayey seam that has formed during the slipping or shearing of the fault and often contains numerous striations. For example, Fig. 11.2 shows surface rupture associated with the August 31, 1968, Kakh earthquake in Iran. Figure 11.3 shows a close-up view of the fault gouge. The cracks in the fault gouge are due to the drying out of the clay upon exposure. The fault gouge tends to act as a barrier to the migration of water, and it can have a strong influence on the regional groundwater table.

Earthquakes can also change the quality of the groundwater. For example, after the Gujarat earthquake (magnitude 7.9) in India on January 23, 2001, it was reported that black saline water was oozing from cracks in the ground and that farm animals were dying of thirst because they refused to drink the black water. It was also reported that near the Indian cities of Bhuj and Bhachau, which were among the worst hit by the tremor, the normally saline well water now tastes better. According to the M. S. Patel, Irrigation Secretary (*Earthweek* 2001), "Sweet water is coming from wells, and traces are seeping from the ground in several places. In some villages, where we could only find salty water at around 100–150 meters deep, we are now finding sweet water at 20 meters." This change in quality of the groundwater is usually attributed to fracturing of the ground during the earthquake which can alter the groundwater flow paths.

FIGURE 11.2 Surface rupture caused by the Kakh earthquake (magnitude 7.3) in Iran on August 31, 1968. The view is to the east along the Dasht-i-bayaz fault, located east of Baskobad. There was about 6 ft of lateral slip and about 2 ft of vertical movement. (*Photograph from the Steinbrugge Collection, EERC, University of California, Berkeley.*)

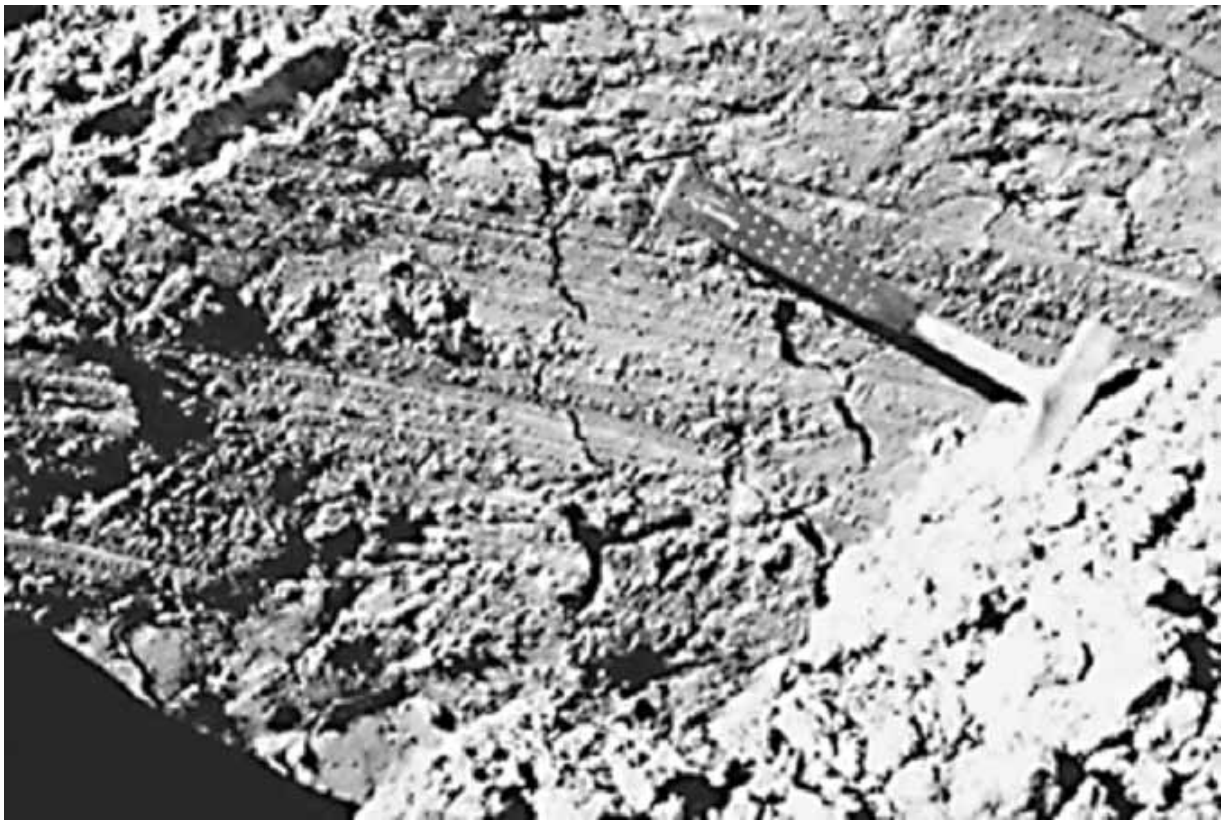

FIGURE 11.3 Close-up view of the fault plane. The striations indicate predominantly horizontal movement with some vertical movement. (*Photograph from the Steinbrugge Collection, EERC, University of California, Berkeley.*)

11.3 PAVEMENT DESIGN

11.3.1 Introduction

In terms of pavement design, one of the main objectives is to provide an adequate pavement thickness in order to prevent a bearing capacity failure. For example, unpaved roads and roads with a weak subgrade can be susceptible to bearing capacity failures caused by heavy wheel loads. The heavy wheel loads can cause a general bearing capacity failure or a punching-type shear failure. These bearing capacity failures are commonly known as *rutting,* and they develop when the unpaved road or weak pavement section is unable to support the heavy wheel load.

Because the thickness of the pavement design is governed by the shear strength of the soil supporting the road, usually the geotechnical engineer tests the soil and determines the pavement design thickness. The transportation engineer often provides design data to the geotechnical engineer, such as the estimated traffic loading, required width of pavement, and design life of the pavement.

Pavements are usually classified as either *rigid* or *flexible* depending on how the surface loads are distributed. A rigid pavement consists of Portland cement concrete slabs, which tend to distribute the loads over a fairly wide area. Flexible pavements are discussed in the next section.

11.3.2 Flexible Pavements

A *flexible pavement* is defined as a pavement having a sufficiently low bending resistance, yet having the required stability to support the traffic loads, e.g., macadam, crushed stone, gravel, and asphalt (California Division of Highways 1973).

The most common type of flexible pavement consists of the following:

- *Asphalt concrete:* The uppermost layer (surface course) is typically *asphalt concrete* that distributes the vehicle load in a cone-shaped area under the wheel and acts as the wearing surface. The ingredients in asphalt concrete are asphalt (the cementing agent), coarse and fine aggregates, mineral filler (i.e., fines such as limestone dust), and air. Asphalt concrete is usually hot-mixed in an asphalt plant and then hot-laid and compacted by using smooth-wheeled rollers. Other common names for asphalt concrete are *black-top, hot mix,* or simply *asphalt* (Atkins 1983).
- *Base:* Although not always a requirement, in many cases there is a base material that supports the asphalt concrete. The base typically consists of aggregates that are well graded, hard, and resistant to degradation from traffic loads. The base material is compacted into a dense layer that has a high frictional resistance and good load distribution qualities. The base can be mixed with up to 6 percent Portland cement to give it greater strength, and this is termed a *cement-treated base* (CTB).
- *Subbase:* In some cases, a subbase is used to support the base and asphalt concrete layers. The subbase often consists of a lesser-quality aggregate that is lower-priced than the base material.
- *Subgrade:* The subgrade supports the pavement section (i.e., the overlying subbase, base, and asphalt concrete). The subgrade could be native soil or rock, a compacted fill, or soil that has been strengthened by the addition of lime or other cementing agents. Instead of strengthening the subgrade, a geotextile could be placed on top of the subgrade to improve its load-carrying capacity.

Many different types of methods can be used for the design of the pavements. For example, empirical equations and charts have been developed based on the performance of pavements in actual service. For the design of flexible pavements in California, an empirical equation is utilized that relates the required pavement thickness to the anticipated traffic loads, shear strength of the materials (R value), and gravel equivalent factor (California Division of Highways 1973; ASTM Standard No. D 2844-94, 2000). Instead of using the R value, some methods utilize the *California bearing ratio* (CBR) as a measure of the shear strength of the base and subgrade. Numerous charts have also been developed that relate the shear strength of the subgrade and the traffic loads to a recommended pavement thickness (e.g., Asphalt Institute 1984). When designing pavements, the geotechnical engineer should always check with the local transportation authority for design requirements as well as the local building department or governing agency for possible specifications on the type of method that must be used for the design.

11.3.3 Earthquake Design

The design of an asphalt concrete road typically does not include any factors to account for earthquake conditions. The reason is that usually the surface course, base, and subbase are in a compacted state and are not affected by the ground shaking. In addition, the cumulative impact and vibration effect of cars and trucks tends to have greater impact than the shaking due to earthquakes.

Concrete pavement and concrete median barriers are often damaged at their joints, or they are literally buckled upward. This damage frequently develops because the concrete sections are so rigid and there are insufficient joint openings to allow for lateral movement during the earthquake. For example, Fig. 11.4 shows compressional damage to the roadway and at the median barrier caused by the Northridge earthquake, in California, on January 17, 1994. In additional to rigid pavements, flexible pavements can be damaged by localized compression, such as shown in Fig. 11.5.

FIGURE 11.4 View to the north along northbound Interstate 405, 250 yards south of Rinaldi Overcrossing. The compressional damage to the roadway and at the median barrier was caused by the Northridge earthquake, in California, on January 17, 1994. (*Photograph from the Northridge Collection, EERC, University of California, Berkeley.*)

FIGURE 11.5 Localized compression feature and pavement damage caused by the Northridge earthquake, in California, on January 17, 1994. (*Photograph from the Northridge Collection, EERC, University of California, Berkeley.*)

Other common causes of damage to roadways are the following:

- Surface rupture, such as shown in Fig. 11.1.
- Slope instability, such as shown in Figs. 3.54, 9.35, and 9.36.
- Liquefaction flow slides or lateral spreading, such as shown in Fig. 3.42.
- Settlement of soft soils. For example, Fig. 11.6 shows the failure of a concrete surface highway during the Chile earthquake in May 1960. The highway was constructed on top of a marshy region.
- Collapse of underlying structures. For example, Fig. 11.7 shows street damage caused by the collapse of the Daikai subway station during the Kobe earthquake.

In summary, the pavement design typically is not based on seismic conditions or modified for earthquake effects. Common causes of damage are due to localized compression and movement of the underlying ground, such as earthquake-induced slope instability, settlement, or collapse of underlying structures.

11.4 PIPELINE DESIGN

11.4.1 Introduction

Similar to pavements, pipelines are often damaged due to surface rupture or movement of the underlying soil caused by earthquake-induced slope movement, liquefaction flow slides or lateral spreading, and earthquake-induced settlement of soft soils.

FIGURE 11.6 This picture shows the failure of a concrete surfaced highway due to an earthquake-induced foundation failure. This area was observed to be a marshy region. This main highway is located 6 km north of Perto Montt. The May 1960 Chile earthquake (moment magnitude = 9.5) caused the highway damage. (*Photograph from the Steinbrugge Collection, EERC, University of California, Berkeley.*)

FIGURE 11.7 This picture shows street damage caused by the underlying collapse of the Daikai subway station. The January 17, 1995, Kobe earthquake (moment magnitude = 6.9) in Japan caused this damage. (*Photograph from the Kobe Geotechnical Collection, EERC, University of California, Berkeley.*)

The pipeline can also be crushed by the dynamic soil forces exerted upon the pipeline. The pseudostatic approach is often utilized in the design of the pipeline. As previously mentioned, this method ignores the cyclic nature of the earthquake and treats it as if it applied an additional static force upon the pipeline. In particular, the pseudostatic approach is to apply a vertical force acting through the centroid of the mass of soil bearing on the top of the pipeline. The pseudostatic vertical force F_v is calculated by using Eq. (6.1), or

$$F_v = ma = \frac{\mathrm{W}}{\mathrm{g}}\, a = W\,\frac{\mathrm{a}}{\mathrm{g}} = k_v W \tag{11.1}$$

where F_v = vertical pseudostatic force acting through the centroid of the mass of soil bearing on top of the pipeline, lb or kN. For pipeline analysis, the pipe is usually assumed to have a unit length (i.e., two-dimensional analysis)

m = total mass of soil bearing on top of the pipeline, lb or kg, which is equal to W/g

W = total weight of soil bearing on top of the pipeline, lb or kN

a = acceleration, which in this case is the vertical acceleration at ground surface caused by the earthquake, ft/s^2 or m/s^2

$a/g = k_v$ = vertical seismic coefficient (dimensionless). The vertical seismic coefficient k_v is often assumed to be equal to $\frac{2}{3}k_h$. As previously mentioned, $k_h = a_{\max}/g$, where $a_{\max}$ is the maximum horizontal acceleration at ground surface that is induced by the earthquake, ft/s^2 or m/s^2. The maximum horizontal acceleration is also commonly referred to as peak ground acceleration (see Sec. 5.6).

Note that an earthquake could subject the soil to both vertical and horizontal pseudostatic forces. However, the horizontal force is usually ignored in the standard pipeline pseudostatic analysis. This is because the vertical pseudostatic force acting on the soil

mass supported by the pipeline will usually cause a more critical design condition than the addition of a horizontal pseudostatic force acting on the sides of the pipeline.

As indicated in Eq. (11.1), the only unknowns in the pseudostatic method are the weight of the soil mass bearing on the top of the pipeline W and the seismic coefficient k_v. As previously mentioned, the seismic coefficient k_v can be assumed to be equal to $\frac{2}{3}(a_{max}/g)$. The determination of W is described in the next section.

11.4.2 Static Design

For static design, the external load on a pipeline depends on many different factors. One important factor is the type of pipeline (rigid versus flexible). Another important factor is the placement conditions, i.e., whether the pipeline is constructed under an embankment, in a trench, or is pushed or jacked into place. Figure 11.8 illustrates the three placement conditions of trench, embankment, and tunnel (or pushed or jacked condition).

Other factors that affect the external load on a pipeline for the static design include the unit weight and thickness of overburden soil, the surface loads such as applied by traffic, compaction procedures, and the presence of groundwater (i.e., buoyant conditions on an empty pipeline).

Rigid Pipeline Design for Static Conditions. Examples of rigid pipelines include precast concrete, cast-in-place concrete, and cast iron. Design pressures due to the overlying soil pressure are as follows:

Minimum Design Load. In general, the minimum vertical load W on a rigid pipeline is equal to the unit weight of soil γ_t times the height H of soil above the top of the pipeline times the diameter of the pipe D, or

$$W_{min} = \gamma_t HD \tag{11.2}$$

As an example, suppose the pipeline has a diameter D of 24 in (2 ft) and a depth of overburden H of 10 ft, and the backfill soil has a total unit weight γ_t of 125 lb/ft^3. Therefore, the minimum vertical load W_{min} acting on the pipeline is

$$W_{min} = (125 \text{ lb/ft}^3)\ (10 \text{ ft})\ (2 \text{ ft}) = 2500 \text{ lb per linear foot of pipe length}$$

Embankment Condition. Different types of embankment conditions are shown in Fig. 11.8. In many cases, compaction of fill or placement conditions will impose vertical loads greater than the minimum values calculated above. Also, because the pipe is rigid, the arching effect of soil adjacent to the pipe will tend to transfer load to the rigid pipe.

Figure 11.9*a* shows the recommendations for a pipeline to be constructed beneath a fill embankment. In Fig. 11.9*a*, W = vertical dead load on the pipeline, D = diameter of the pipeline, and B = width of the pipeline (that is, $B = D$). Note that Fig. 11.9*a* was developed for an embankment fill having a total unit weight γ_t = 100 lb/ft^3 and an adjustment is required for conditions having different unit weights.

As an example, use the same conditions as before ($B = D = 2$ ft, $H = 10$ ft, and $\gamma_t = 125$ lb/ft^3). Figure 11.9*a* is entered with $H = 10$ ft, the curve marked 24 in (2 ft) is intersected, and the value of W read from the vertical axis is about 3800 pounds. Therefore,

$$W = 3800\ \frac{125}{100} = 4750 \text{ lb per linear foot of pipeline length}$$

Note that this value of 4750 pounds is greater than the minimum dead load (2500 lb), and the above value (4750 lb) would be used for the embankment condition.

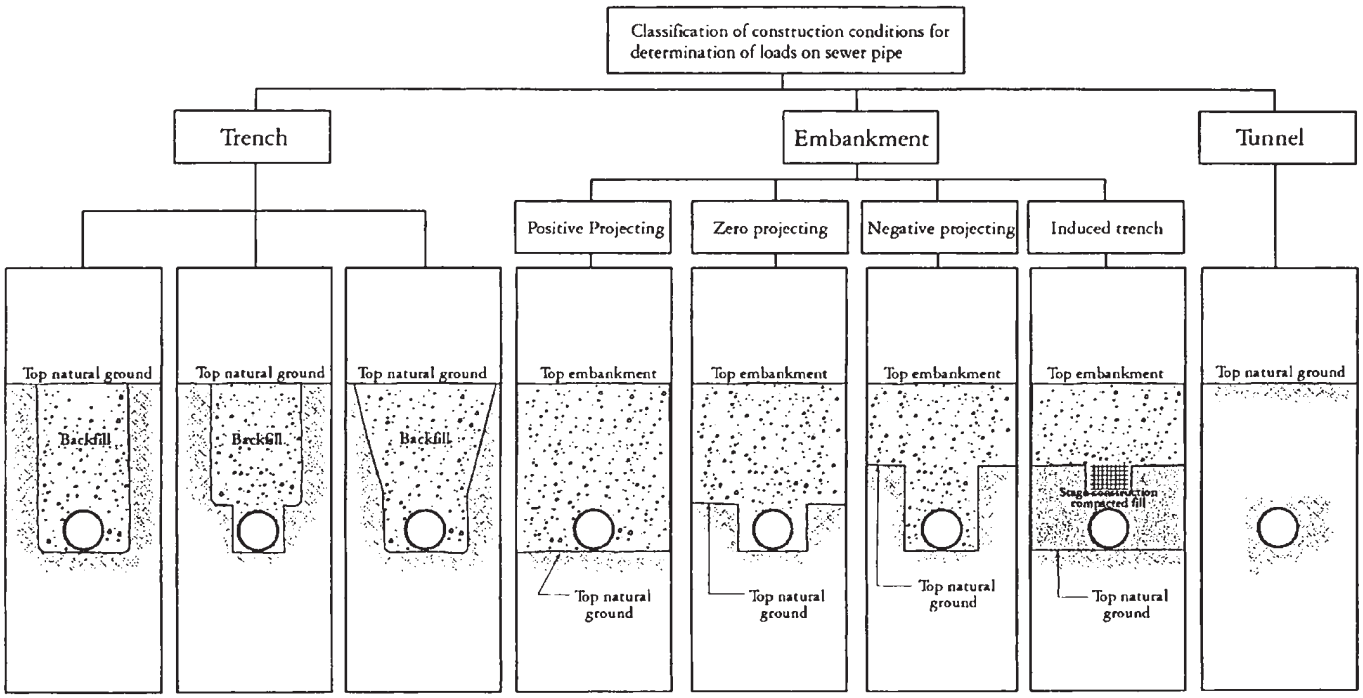

FIGURE 11.8 Classification of construction conditions for buried pipelines. (*From ASCE 1982, reprinted with permission of the American Society of Civil Engineers.*)

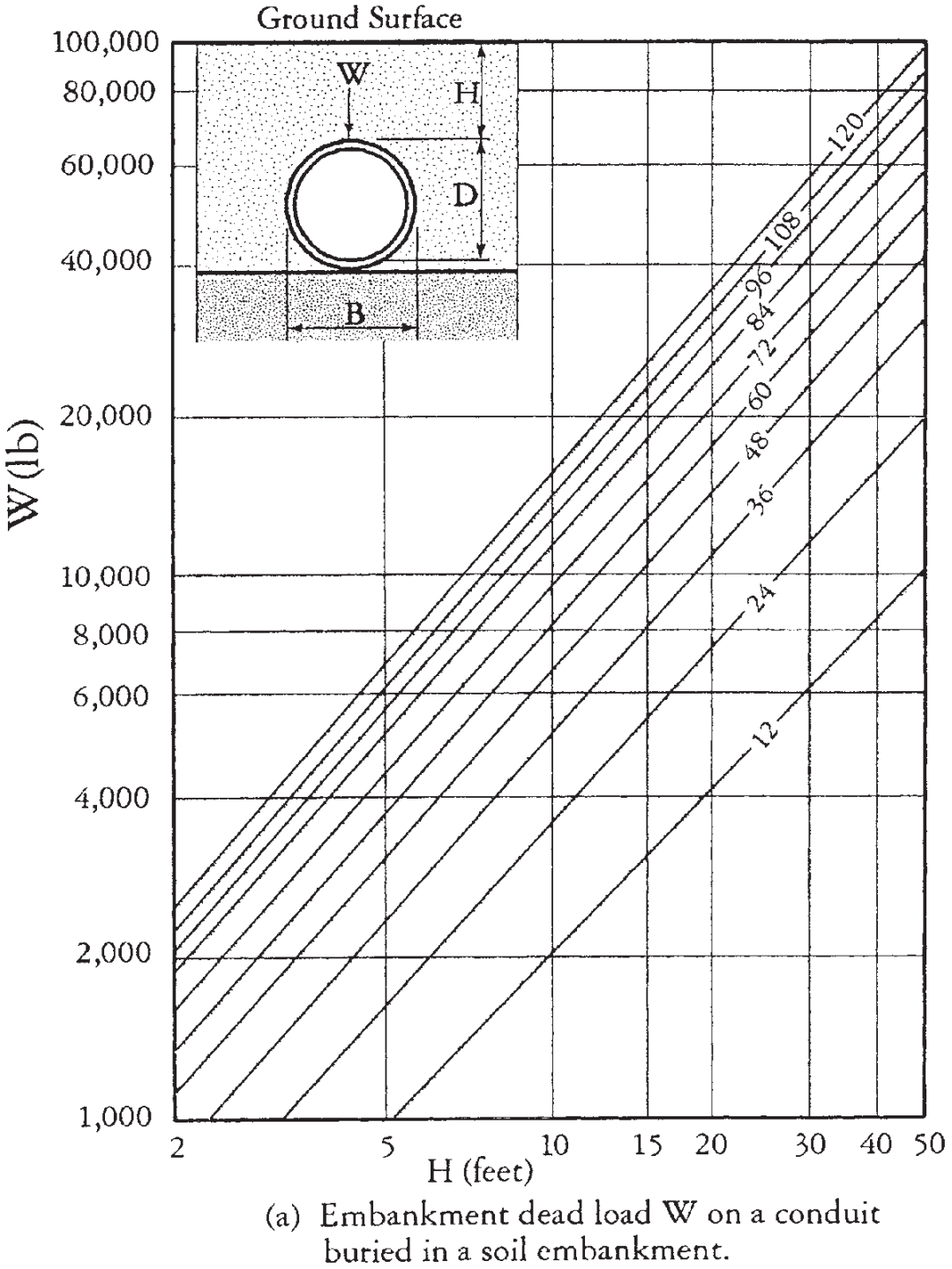

FIGURE 11.9 Embankment load W for rigid pipelines buried in a soil embankment. (*Reproduced from NAVFAC DM-7.1, 1982.*)

Trench Condition. Different types of trench conditions are shown in Fig. 11.8. Figure 11.9*b* shows the recommendations for a pipeline to be constructed in a trench. Note that in Fig. 11.9*b* the dimension B is *not* the diameter of the pipeline, but rather is the width of the trench at the top of the pipeline. This is because studies have shown that if the pipeline is rigid, it will carry practically all the load on the plane defined by B (Marston 1930, ASCE 1982). Curves are shown for both sand and clay backfill in Fig. 11.9*b*. The procedure is to enter the chart with the H/B ratio, intersect the "sands" or "clays" curve, and then determine C_w. Once C_w is obtained, the vertical load W on the pipeline is calculated from

$$W = C_w \gamma_t B^2 \tag{11.3}$$

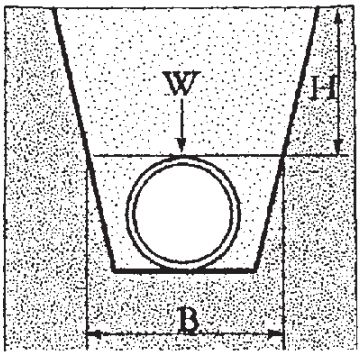

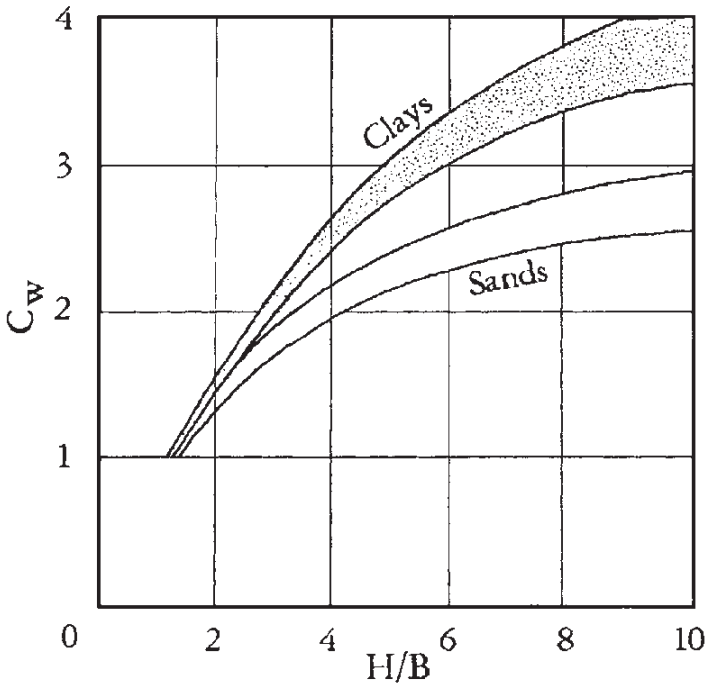

(b) C_w for conduit in a trench

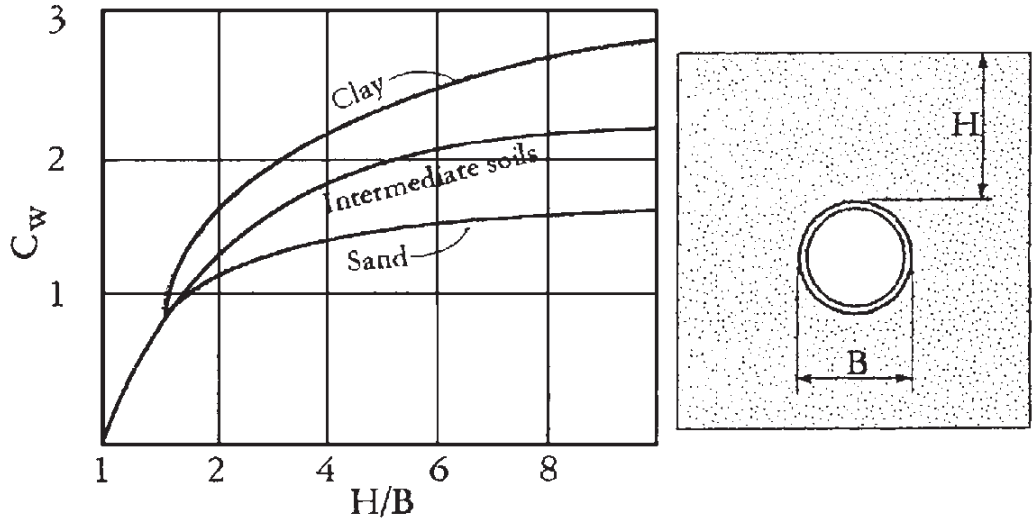

(c) C_w for jacked conduit

FIGURE 11.9 (*Continued*) Embankment load W and backfill coefficient C_w for rigid pipelines in a trench or for a jacked condition. (*Reproduced from NAVFAC DM-7.1, 1982.*)

As an example, use the same conditions as before ($D = 2$ ft, $H = 10$ ft, and $\gamma_t = 125$ lb/ft^3). Also assume that the trench width at the top of the pipeline will be 4 ft (that is, $B = 4$ ft) and the trench will be backfilled with sand. Figure 11.9*b* is entered with $H/B = 10/4 = 2.5$, the curve marked "sands" is intersected, and the value of C_w of about 1.6 is obtained from the vertical axis. Therefore,

$$W = C_w \gamma_t B^2 = (1.6)\ (125)\ (4)^2 = 3200 \text{ lb per linear foot}$$

Note this value of 3200 lb is greater than the minimum value (2500 lb), and thus 3200 lb would be used for the trench condition.

It should be mentioned that as the width of the trench increases, the values from this section may exceed the embankment values. If this occurs, the embankment condition should be considered to be the governing loading condition.

Jacked or Driven Pipelines. The jacked or driven pipeline condition (i.e., tunnel condition) is shown in Fig. 11.8. Figure 11.9*c* shows the recommendations for a jacked or driven pipeline. Note in Fig. 11.9*c* that the dimension B is equal to the diameter of the pipeline ($B = D$). The curves shown in Fig. 11.9*c* are for pipelines jacked or driven through sand, clay, or intermediate soils. The procedure is to enter the chart with the H/B ratio, intersect the appropriate curve, and then determine C_w. Once C_w is obtained, the vertical load W on the pipeline is calculated from

$$W = C_w \gamma_t B^2 \tag{11.4}$$

As an example, use the same conditions as before ($D = B = 2$ ft, $H = 10$ ft, and $\gamma_t = 125$ lb/ft^3), and the pipeline will be jacked through a sand deposit. Figure 11.9*c* is entered with $H/B = 10/2 = 5$, the curve marked "sand" is intersected, and the value of C_w of about 1.5 is obtained from the vertical axis. Therefore,

$$W = C_w \gamma_t B^2 = (1.5)\ (125)\ (2)^2 = 750 \text{ lb per linear foot}$$

Note this value of 750 lb is less than the minimum load value (2500 lb), and thus the value of 2500 lb would be used for the jacked or driven pipe condition. Basic soil mechanics indicates that the long-term load for rigid pipelines will be at least equal to the overburden soil pressure (i.e., the minimum design load).

Factor of Safety. A factor of safety should be applied to the static design dead load W calculated above. The above values also consider only the vertical load W on the pipeline due to soil pressure. Other loads, such as traffic or seismic loads, may need to be included in the static design of the pipeline. For pressurized pipes, rather than the exterior soil load W, the interior fluid pressure may govern the design.

Flexible Pipeline Design for Static Conditions. Flexible pipelines under embankments or in trenches derive their ability to support loads from their inherent strength plus the passive resistance of the soil as the pipe deflects and the sides of the flexible pipe move outward against the soil. Examples of flexible pipes are ductile iron pipe, ABS pipe, polyvinyl chloride (PVC) pipe, and corrugated metal pipe (CMP). Proper compaction of the soil adjacent to the sides of the flexible pipe is essential in its long-term performance. Flexible pipes often fail by excessive deflection and by collapse, buckling, and cracking, rather than by rupture, as in the case of rigid pipes.

The design of flexible pipelines depends on the amount of deflection considered permissible, which in turn depends on the physical properties of the pipe material and the project use. Because flexible pipe can deform, the dead load on the pipe W is usually less than that calculated for rigid pipes. Thus as a conservative approach, the value of the design dead load W calculated from the rigid pipe section can be used for the flexible pipeline design.

To complete the static design of flexible pipelines, the designer will need to calculate the deflection of the pipeline. The deflection depends on the applied vertical dead load W as well as other factors, such as the modulus of elasticity of the pipe, pipe diameter and thickness, modulus of soil resistance (E', see ASCE 1982, Table 9-10), and bedding constant K_b. Per ASCE (1982, Table 9-11), the values of the bedding constant K_b vary from 0.110 (bedding angle = 0°) to about 0.083 (bedding angle = 180°). The bedding angle may vary along the trench, and thus a conservative value of 0.10 is often recommended.

11.4.3 Earthquake Design

Once the weight W of the soil bearing on top of the pipeline is known [i.e., Eqs. (11.2), (11.3), and (11.4)], the pseudostatic force can be calculated by using Eq. (11.1)]. As an example, use the same data from Sec. 11.4.2 ($B = 2$ ft, $H = 10$ ft, and $\gamma_t = 125$ lb/ft^3), and assume that for the design earthquake, the peak ground acceleration $a_{max} = 0.30g$. Using $k_v = \frac{2}{3}k_h = \frac{2}{3}(0.30) = 0.20$, the pseudostatic forces are as follows [Eq. (11.1)]:

Minimum pseudostatic force:

$$F_v = k_v W_{min} = 0.20\ (2500) = 500 \text{ lb per linear foot}$$

Embankment condition:

$$F_v = k_v W = 0.20\ (4750) = 950 \text{ lb per linear foot}$$

Trench condition:

$$F_v = k_v W = 0.20\ (3200) = 640 \text{ lb per linear foot}$$

Jacked or driven pipeline:

$$F_v = k_v W = 0.20\ (750) = 150 \text{ lb per linear foot}$$

For jacked or driven pipeline, use the minimum value of $F_v = 500$ lb per linear foot.

In summary, for the example problem of a 2-ft-diameter pipeline having 10 ft of overburden soil with a total unit weight of 125 lb/ft^3, the soil loads are as follows:

Pipeline design	Minimum design load, lb/ft	Embankment condition, lb/ft	Trench condition, lb/ft	Jacked or driven pipeline, lb/ft
Static load W	2500	4750	3200	2500*
Pseudostatic load F_v	500	950	640	500*

*Using minimum design values.

11.5 RESPONSE SPECTRUM

11.5.1 Introduction

As discussed in Sec. 4.6, a response spectrum can be used to directly assess the nature of the earthquake ground motion on the structure. A response spectrum is basically a plot of the maximum displacement, velocity, or acceleration versus the natural period of a

single-degree-of-freedom system. Different values of system damping can be used, and thus a family of such curves could be obtained. The structural engineer can then use this information for the design of the building.

The geotechnical engineer may be required to provide a response spectrum to the structural engineer. The response spectrum could be based on site-specific geology, tectonic activity, seismology, and soil characteristics. As an alternative, a simplified response spectrum can be developed based on the seismic zone and the site soil profile. This method is described in the following section.

11.5.2 Response Spectrum per the *Uniform Building Code*

One easy approach for the preparation of a response spectrum is to use the method outlined in the *Uniform Building Code* (1997). Figure 11.10 shows the elastic response spectrum in terms of the spectral acceleration g versus the period of vibration (in seconds) for 5 percent system damping. To prepare the response spectra shown in Fig. 11.10, only two parameters are needed: the seismic coefficients C_a and C_v. The steps in determining C_a and C_v are as follows:

1. *Determine seismic zone:* Figure 5.17 presents the seismic zone map for the United States. By using Fig. 5.17, the seismic zone (i.e., 0, 1, 2A, 2B, 3, or 4) can be determined for the

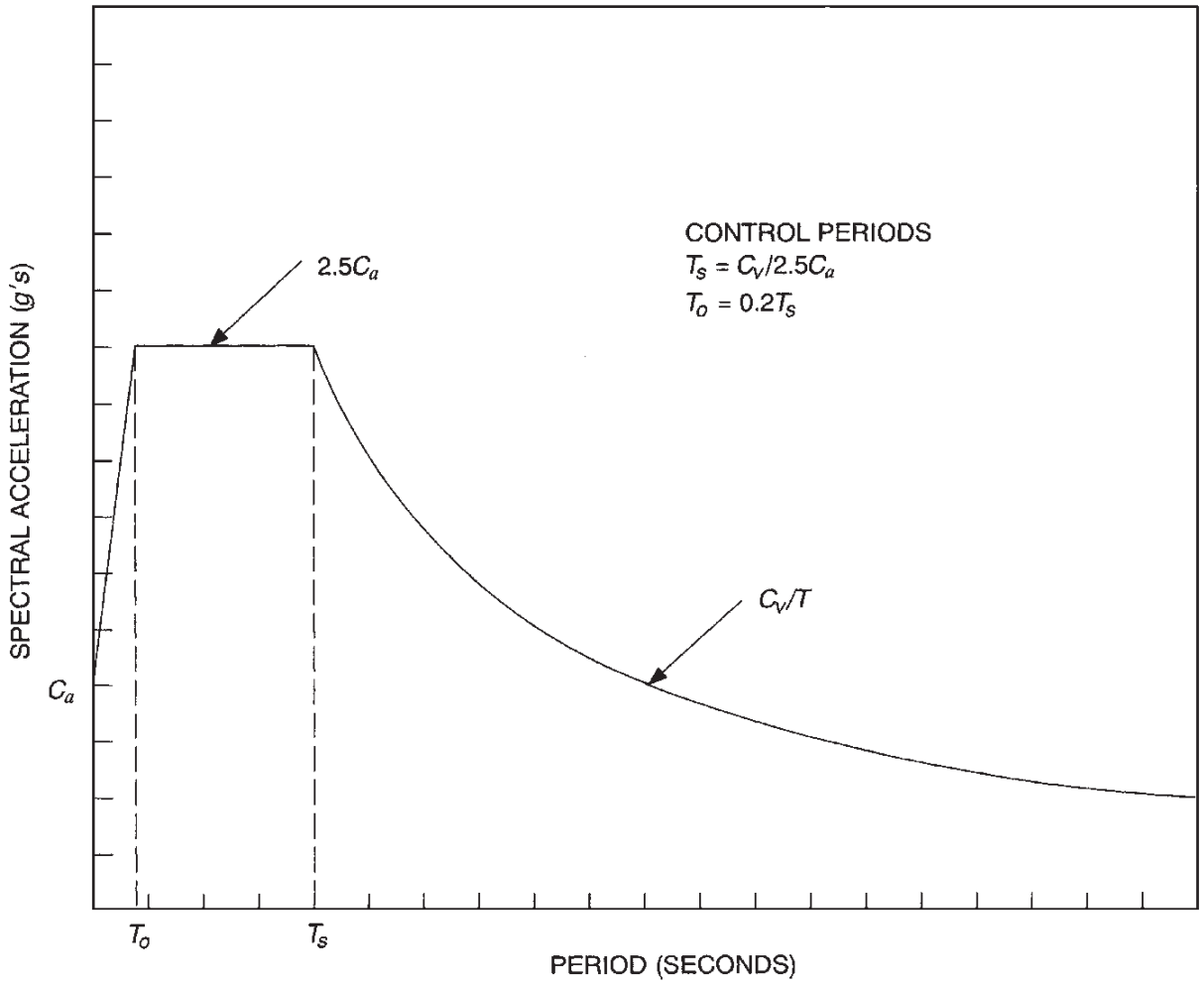

FIGURE 11.10 Response spectrum in terms of the spectral acceleration g versus the period of vibration (in seconds) for 5 percent system damping. (*Reproduced from the Uniform Building Code, 1997, with permission from the International Conference of Building Officials.*)

TABLE 11.1 Soil Profile Types

Soil profile type	Material descriptions	Average soil properties from ground surface to a depth of 100 ft (30 m): Shear wave velocity V_{s1} [see Eq. (6.9)], ft/s (m/s)	Granular soil: $(N_1)_{60}$ value [see Eq. (5.2)], blows per foot	Cohesive soil: undrained shear strength s_u, lb/ft^2 (kPa)
S_A	Hard rock	>5000 (>1500)	—	—
S_B	Rock	2500–5000 (760–1500)	—	—
S_C	Soft rock, very dense granular soil, very stiff to hard cohesive soil	1200–2500 (360–760)	>50	>2000 (>100)
S_D	Dense granular soil, stiff cohesive soil	600–1200 (180–360)	15–50	1000–2000 (50–100)
S_E*	Granular soil having a loose to medium density; cohesive soil having a soft to medium consistency	<600 (<180)	<15	<1000 (<50)
S_F		Soil requiring a site-specific evaluation (see Sec. 11.5.2)		

*Soil profile S_E also includes any subsoil profile having more than 10 ft (3 m) of soft clay, defined as a soil with a plasticity index > 20, water content ≥ 40 percent, and s_u < 500 lb/ft^2 (24 kPa).

Data obtained from the *Uniform Building Code* (1997).

site. The *Uniform Building Code* (1997) also provides the seismic zone values for other countries. A response spectrum would usually not be needed for sites that have a seismic zone = 0.

2. *Soil profile type:* Using Table 11.1, the next step is to determine the soil type profile (i.e., S_A, S_B, S_C, S_D, S_E, or S_F), as follows:

a. *Soil profile types S_A, S_B, S_C, and S_D:* For the first four soil profile types, the classification is based on the average condition of the material that exists at the site from ground surface to a depth of 100 ft (30 m). If the ground surface will be raised or lowered by grading operations, then the analysis should be based on the final as-built conditions. As indicated in Table 11.1, the selection of the first four soil profile types is based on the material type and engineering properties, such as shear wave velocity, standard penetration test $(N_1)_{60}$ values, and the undrained shear strength.

b. *Soil profile type S_E:* Similar to the first four soil profiles, the classification for S_E is based on material type and engineering properties, such as shear wave velocity, standard penetration test $(N_1)_{60}$ values, and the undrained shear strength. In addition, any site that contains a clay layer that is thicker than 10 ft and has a plasticity index > 20, water content ≥ 40 percent, and undrained shear strength s_u < 500 lb/ft^2 (24 kPa) would be considered to be an S_E soil profile.

c. *Soil profile type S_F:* The definition of this last soil profile is as follows:

- Soils vulnerable to potential failure or collapse under seismic loading such as liquefiable soil, quick and highly sensitive clays, and collapsible weakly cemented soils

TABLE 11.2 Seismic Coefficient C_a

Soil profile type	Seismic zone (see Fig. 5.17)				
	Zone 1	Zone 2A	Zone 2B	Zone 3	Zone 4
S_A	0.06	0.12	0.16	0.24	0.32 N_a
S_B	0.08	0.15	0.20	0.30	0.40 N_a
S_C	0.09	0.18	0.24	0.33	0.40 N_a
S_D	0.12	0.22	0.28	0.36	0.44 N_a
S_E	0.19	0.30	0.34	0.36	0.44 N_a
S_F	Soil requiring a site-specific evaluation (see Sec. 11.5.2)				

Data obtained from the *Uniform Building Code* (1997). Data for soil profile type S_E at zone 4 adjusted to be more consistent with published data. Obtain N_a from Table 11.3.

TABLE 11.3 Near-Source Factor N_a

Seismic source type (see Table 11.4)	Closest distance to known seismic source		
	≤1.2 mi (≤2 km)	3 mi (5 km)	≥6 mi (≥10 km)
A	1.5	1.2	1.0
B	1.3	1.0	1.0
C	1.0	1.0	1.0

Notes: Data obtained from the *Uniform Building Code* (1997). Near-source factor N_a is only needed if the seismic zone = 4 (see Table 11.2). The near-source factor may be based on the linear interpolation of values for distances other than those shown in the table. The location and type of seismic sources to be used for design can be based on geologic data, such as recent mapping of active faults by the U.S. Geological Survey or the California Division of Mines and Geology. The closest distance to the known seismic source can be calculated as the minimum distance between the site and the surface location of the fault plane (or the surface projection of the fault plane). If there are several sources of seismic activity, then the closest one to the site should be considered to be the governing case.

- Greater than 10-ft (3-m) thickness of peats and/or highly organic clays
- Greater than 25-ft (8-m) thickness of very highly plastic clays having a plasticity index >75
- Greater than 120-ft (37-m) thickness of soft, medium, or stiff clays. If the soil at a site meets any one of these criteria, then a site-specific analysis is required and the method outlined in this section is not applicable.

3. *Seismic coefficient C_a:* Given the seismic zone and the soil profile type, the seismic coefficient C_a can be obtained from Table 11.2. If the seismic zone is equal to 4, then the near-source factor N_a must be known. To calculate the near-source factor N_a, use Table 11.3 as follows:

a. *Closest distance to known seismic source:* The location and type of seismic sources to be used for design can be based on geologic data, such as recent mapping of active faults by the U.S. Geological Survey or the California Division of Mines and Geology. The closest distance to the known seismic source can be calculated as the minimum distance between the site and the surface location of the fault plane (or the

TABLE 11.4 Seismic Source Type

Seismic source type	Seismic source definition		
	Seismic source description	Maximum moment magnitude M_w	Slip rate, mm/yr
A	Faults that are capable of producing large-magnitude events and that have a high rate of seismic activity	$M_w \geq 7$	SR ≥ 5
B	All faults other than types A and C	$M_w \geq 7$ $M_w < 7$ $M_w \geq 6.5$	SR < 5 SR > 2 SR < 2
C	Faults that are not capable of producing large-magnitude earthquakes and that have a relatively low rate of seismic activity	$M_w < 6.5$	SR ≤ 2

Notes: Data obtained from the *Uniform Building Code* (1997). Seismic source type is only needed if the seismic zone = 4 (see Table 11.2). Subduction sources shall be evaluated on a site-specific basis. For the seismic source definition, both the maximum moment magnitude M_w and slip rate (SR) conditions must be satisfied concurrently when determining the seismic source type.

TABLE 11.5 Seismic Coefficient C_v

Soil profile type	Seismic zone (see Fig. 5.17)				
	Zone 1	Zone 2A	Zone 2B	Zone 3	Zone 4
S_A	0.06	0.12	0.16	0.24	$0.32N_v$
S_B	0.08	0.15	0.20	0.30	$0.40N_v$
S_C	0.13	0.25	0.32	0.45	$0.56N_v$
S_D	0.18	0.32	0.40	0.54	$0.64N_v$
S_E	0.26	0.50	0.64	0.84	$0.96N_v$
S_F	Soil requiring a site-specific evaluation (see Sec. 11.5.2)				

Data obtained from the *Uniform Building Code* (1997). Obtain N_v from Table 11.6.

surface projection of the fault plane). If there are several sources of seismic activity, then the closest one to the site should be considered to be the governing case.

b. *Seismic source type:* The data in Table 11.4 can be used to determine the seismic source type (A, B, or C).

c. *Near-source factor N_a:* Given the seismic source type and the closest distance to a known seismic source, the near-source factor N_a can be determined from Table 11.3.

4. *Seismic coefficient C_v:* Given the seismic zone and the soil profile type, the seismic coefficient C_v can be obtained from Table 11.5. If the seismic zone is equal to 4, then the near-source factor N_v must be known. To calculate the near-source factor N_v, the following steps are performed:

a. *Closest distance to known seismic source:* As outlined in step 3*a,* the closest distance to the known seismic source must be determined.

TABLE 11.6 Near-Source Factor N_v

Seismic source type (see Table 11.4)	Closest distance to known seismic source			
	≤1.2 mi (≤2 km)	3 mi (5 km)	6 mi (10 km)	≥9 mi (≥15 km)
A	2.0	1.6	1.2	1.0
B	1.6	1.2	1.0	1.0
C	1.0	1.0	1.0	1.0

Notes: Data obtained from the *Uniform Building Code* (1997). Near-source factor N_v is only needed if the seismic zone = 4 (see Table 11.5). The near-source factor may be based on the linear interpolation of values for distances other than those shown in the table. The location and type of seismic sources to be used for design can be based on geologic data, such as recent mapping of active faults by the U.S. Geological Survey or the California Division of Mines and Geology. The closest distance to the known seismic source can be calculated as the minimum distance between the site and the surface location of the fault plane (or the surface projection of the fault plane). If there are several sources of seismic activity, then the closest one to the site should be considered to be the governing case.

b. *Seismic source type:* As indicated in step 3*b,* the data in Table 11.4 can be used to determine the seismic source type (A, B, or C).

c. *Near-source factor N_v:* Given the seismic source type and the closest distance to a known seismic source, the near-source factor N_v can be determined from Table 11.6.

Once the seismic coefficients C_a and C_v are known, then the response spectrum shown in Fig. 11.10 can be developed. The first step is to determine the periods T_s and T_0, defined as follows:

$$T_s = \frac{C_v}{2.5C_a} \tag{11.5}$$

$$T_0 = 0.2T_s \tag{11.6}$$

At a period of 0 s, the spectral acceleration is equal to C_a. The spectral acceleration then linearly increases to a value of $2.5C_a$ at a period of T_0. As shown in Fig. 11.10, the spectral acceleration is constant until a period equal to T_s has been reached. For any period greater than T_s, the spectral acceleration is equal to C_v/T, where T = period of vibration, in seconds, corresponding to the horizontal axis in Fig. 11.10.

11.5.3 Alternate Method

In Fig. 11.10, the seismic coefficient C_a determines the highest value of the spectral acceleration. It is expected that the spectral acceleration will increase when (1) the intensity of the earthquake increases and (2) as the ground becomes softer (see Sec. 4.6.1). This is why the values of the seismic coefficient C_a in Table 11.2 increase as the seismic zone increases. In addition, the values of C_a in Table 11.2 increase for softer ground conditions.

In Fig. 11.10, a period of zero would correspond to a completely rigid structure. Thus when $T = 0$, the spectral acceleration is equal to the peak ground acceleration (that is, $C_a = a_{max}$). The geotechnical engineer will often need to determine a_{max} in order to perform liquefaction, settlement, slope stability, and retaining wall analyses. Once the peak ground acceleration a_{max} has been determined, it can be used in place of C_a to construct the response spectrum (i.e., in Fig. 11.10, use $C_a = a_{max}$). Since a_{max} is based on site-specific conditions (see Sec. 5.6), the use of $C_a = a_{max}$ would seem to be an appropriate revision to the method outlined in Sec. 11.5.2.

11.5.4 Example Problem

For this example problem, assume the following:

- The subsurface exploration revealed that the site is underlain by soft sedimentary rock that has an average shear wave velocity $V_{s1} = 2300$ ft/s.
- Seismic zone = 4.
- Design earthquake conditions: maximum moment magnitude $M_w = 7$, SR = 5 mm/yr, and distance to seismic source = 3 mi.

To develop the response spectrum, the following data are utilized:

1. *Soil profile type* (*Table 11.1*): For soft sedimentary rock that has an average shear wave velocity $V_{s1} = 2300$ ft/s, the soil profile type is S_C (see Table 11.1).
2. *Seismic source type* (*Table 11.4*): Since the maximum moment magnitude $M_w = 7$ and SR = 5 mm/yr, the seismic source type is A (see Table 11.4).
3. *Seismic coefficient* C_a (*Table 11.2*): Entering Table 11.2 with soil profile type = S_C and zone 4, the value of $C_a = 0.40N_a$. Entering Table 11.3 with seismic source type = A and distance to the seismic source = 3 mi, the value of $N_a = 1.2$. Therefore, the value of the seismic coefficient $C_a = 0.40N_a = 0.40(1.2) = 0.48$.
4. *Seismic coefficient* C_v (*Table 11.5*): Entering Table 11.5 with soil profile type = S_C and zone 4, the value of $C_v = 0.56N_v$. Entering Table 11.6 with seismic source type = A and distance to the seismic source = 3 mi, the value of $N_v = 1.6$. Therefore, the value of the seismic coefficient $C_v = 0.56N_v = 0.56(1.6) = 0.90$.
5. *Values of* T_s *and* T_0 *[Eqs. (11.5) and (11.6)]:* The values of T_s and T_0 can be calculated as follows:

$$T_s = \frac{C_v}{2.5C_a} = \frac{0.90}{2.5\ (0.48)} = 0.75 \text{ s}$$

$$T_0 = 0.2T_s = 0.20\ (0.75) = 0.15 \text{ s}$$

By using Fig. 11.10 and the values of $C_a = 0.48$, $C_v = 0.90$, $T_s = 0.75$ s, and $T_0 = 0.15$ s, the response spectrum can be developed such as shown in Fig. 11.11.

11.6 PROBLEMS

11.1 Solve the example problem in Secs. 11.4.2 and 11.4.3, but assume that the pipe is located 20 ft below ground surface. *Answer:* See App. E for the solution.

11.2 Solve the example problem in Sec. 11.5.4, but assume that the seismic zone = 1. Compare the results with the solution to the example problem in Sec. 11.5.4. *Answer:* See App. E for the solution and Fig. 11.12 for the response spectrum.

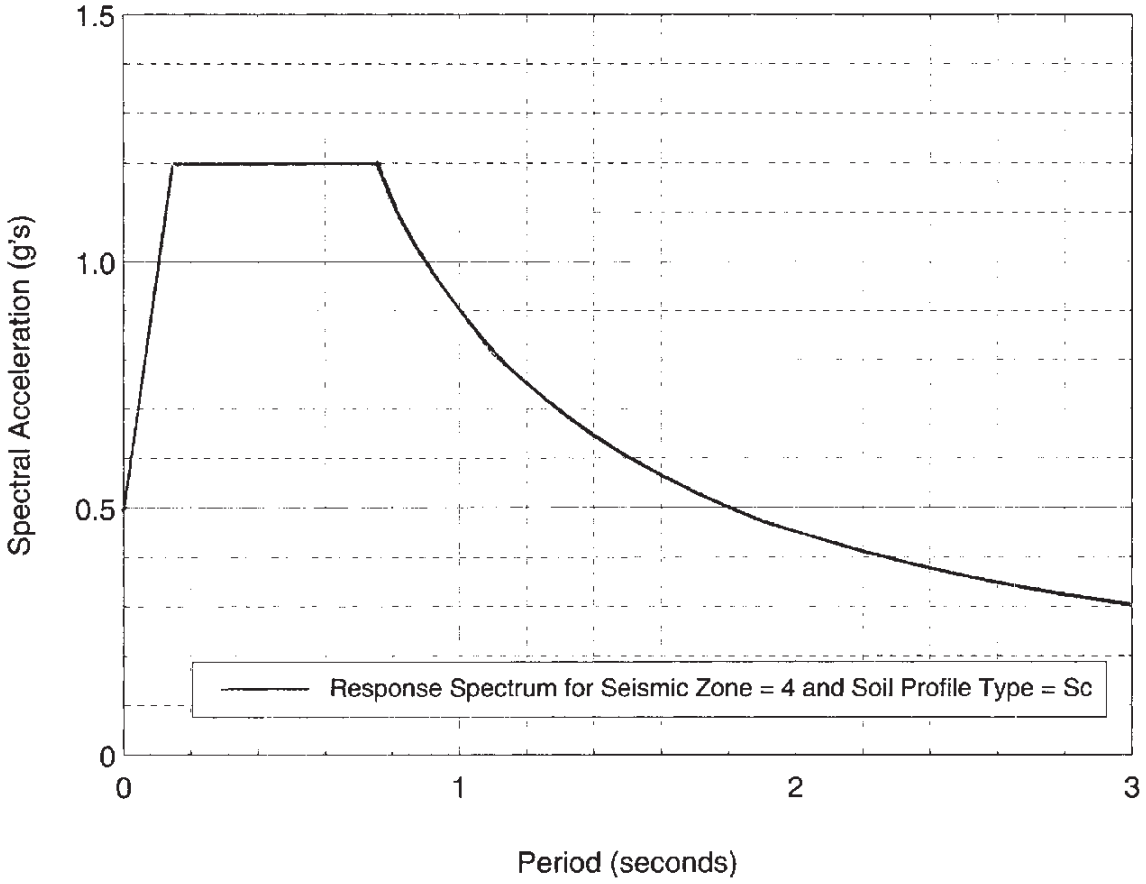

FIGURE 11.11 Response spectrum in terms of the spectral acceleration g versus the period of vibration (in seconds) for 5 percent system damping using the data from the example problem in Sec. 11.5.4.

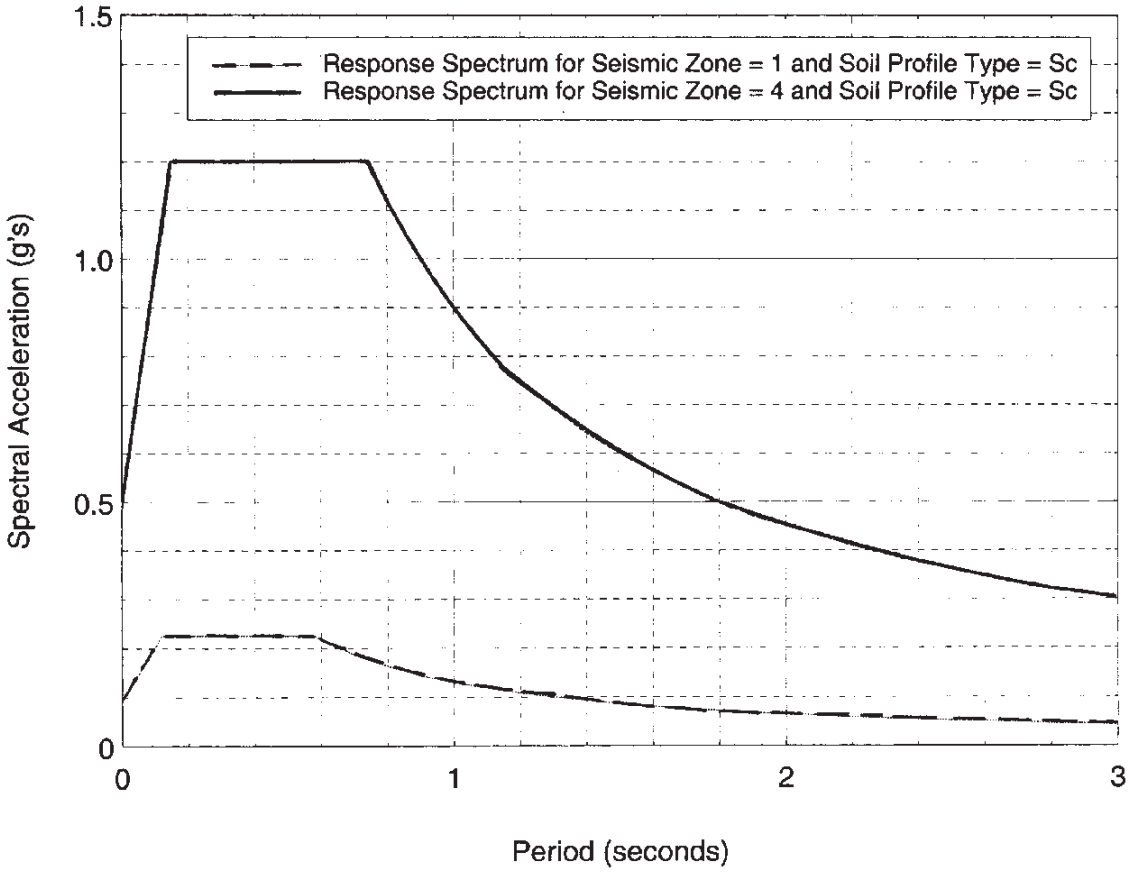

FIGURE 11.12 Answer to Prob. 11.2. Response spectrum in terms of the spectral acceleration g versus the period of vibration (in seconds) for 5 percent system damping using the data from the example problem in Sec. 11.5.4 and seismic zones 1 and 4.

P · A · R · T · 3

SITE IMPROVEMENT METHODS TO MITIGATE EARTHQUAKE EFFECTS

CHAPTER 12
GRADING AND OTHER SOIL IMPROVEMENT METHODS

12.1 INTRODUCTION

Part 3 of the book (Chaps. 12 and 13) discusses the various methods that can be used to mitigate the effects of the earthquake on the structure. The next two chapters deal with site mitigation methods such as grading and soil improvement (Chap. 12) and foundation alternatives to resist the earthquake effects (Chap. 13).

The mitigation of slope hazards has already been discussed in Sec. 9.7.2. Options include avoiding the slope failure, protecting the site from the failure mass, and reducing the risk to an acceptable level by increasing the factor of safety of the slope. For slope hazards dealing with liquefaction-induced flow slides and lateral spreading, Seed (1987) states:

> It is suggested that, at the present time, the must prudent method of minimizing the hazards associated with liquefaction-induced sliding and deformations is to plan new construction or devise remedial measures in such a way that either high pore water pressures cannot build up in the potentially liquefiable soil, and thus liquefaction cannot be triggered, or, alternatively, to confine the liquefiable soils by means of stable zones so that no significant deformations can occur; by this means, the difficult problems associated with evaluating the consequences of liquefaction (sliding or deformations) are avoided.

Types of stable zones that can be used to confine the liquefiable soils include robust edge containment structures and shear keys (i.e., compacted soil zones). Examples of robust edge containment structures that are capable of resisting failure or excessive displacement under the seismic loading include compacted berms and dikes as well as massive seawalls or retaining structures (R. B. Seed 1991). The construction of stable zones may need to be used in conjunction with other methods that mitigate liquefaction-induced settlement, bearing capacity, and ground damage (surface cracking and sand boils).

Other options for dealing with liquefaction hazards are as follows (Federal Emergency Management Agency 1994):

> Four general approaches apply to the mitigation of liquefaction hazards (avoidance, prevention, engineered design, and post earthquake repairs). A prime way to limit the damage due to liquefaction is to avoid areas susceptible to liquefaction. This approach is not always possible

because some facilities such as transportation routes, irrigation canals, pipelines, etc., commonly must cross susceptible areas. In some instances ground can be stabilized by compaction, dewatering or replacement of soil. In other cases, structures can be designed to resist liquefaction by attachment to the soil strata below all liquefiable layers.

These general approaches for the mitigation of liquefaction hazards when designing or constructing new buildings or other structures such as bridges, tunnels, and roads can be summarized as follows:

1. *Avoid liquefaction-susceptible soils:* The first option is to avoid construction on liquefaction-susceptible soils. Those sites that have thick deposits of soils that have a low factor of safety against liquefaction can be set aside as parks or open-space areas. Buildings and other facilities would be constructed in those areas that have more favorable subsurface conditions.
2. *Remove or improve the soil:* The second option involves mitigation of the liquefaction hazards by removing or improving the soil. For example, the factor of safety against liquefaction can be increased by densifying the soil and/or by improving the drainage characteristics of the soil. This can be done using a variety of soil improvement techniques; such as removal and replacement of liquefiable soil; in situ stabilization by grouting, densification, and dewatering; and buttressing of lateral spread zones. These various options are discussed in Secs. 12.2 to 12.4.
3. *Build liquefaction-resistant structures:* For various reasons, such as the lack of available land, a structure may need to be constructed on liquefaction-prone soils. It may be possible to make the structure liquefaction-resistant by using mat or deep foundation systems. This is discussed further in Chap. 13.

12.2 GRADING

Since most building sites start out as raw land, the first step in site construction work usually involves the grading of the site. *Grading* is defined as any operation consisting of excavation, filling, or a combination thereof. The glossary (App. A, Glossary 4) presents a list of common construction and grading terms and their definitions. Most projects involve grading, and it is an important part of geotechnical engineering.

The geotechnical engineer often prepares a set of grading specifications for the project. These specifications are then used to develop the grading plans, which are basically a series of maps that indicate the type and extent of grading work to be performed at the site. Often the grading specifications will be included as an appendix in the preliminary or feasibility report prepared by the geotechnical engineer and engineering geologist (see App. B of Day 2000 for an example of grading specifications).

An important part of the grading of the site often includes the compaction of fill. *Compaction* is defined as the densification of a fill by mechanical means. This physical process of getting the soil into a dense state can increase the shear strength, decrease the compressibility, and decrease the permeability of the soil.

Some examples of activities that can be performed during grading to mitigate earthquake effects include the following:

1. *Slope stabilization:* Examples are the flattening of the slope, decreasing the height of the slope, or increasing the factor of safety of the slope by constructing a fill buttress or shear key.

2. *Liquefaction-prone soils:* If the liquefaction-prone soils are shallow and the groundwater table can be temporarily lowered, then these soils can be removed and replaced with different soil during the grading operations. Another option is to remove the potentially liquefiable soil, stockpile the soil and allow it to dry out (if needed), and then recompact the soil as structural fill.

3. *Earthquake-induced settlement:* As discussed in Sec. 7.3, one approach for level-ground sites that can be used to reduce the potential for liquefaction-induced ground damage, such as surface fissuring and sand boils, is to add a fill layer to the site. This operation could be performed during the grading of the site. It should be mentioned that this method will provide relatively little benefit for sloping ground since it will not prevent structural damage and surface fissuring due to lateral spreading.

4. *Volumetric settlement and rocking settlement:* Loose soils and those types of soils that are susceptible to plastic flow or strain softening can be removed and replaced during the grading operations. Another option is to remove the soil, stockpile the soil and allow it to dry out, and then recompact the soil as structural fill.

Instead of removing and recompacting the soil during grading, another approach is to use precompression, which is often an effective method of soil improvement for soft clays and organic soils. The process consists of temporarily surcharging the soils during the grading operations in order to allow the soils to consolidate, which will reduce their compressibility and increase their shear strength.

5. *Earthquake-induced bearing capacity:* Similar to the options for settlement, poor bearing soils can be removed and replaced or surcharged during the grading operations.

6. *Drainage and dewatering systems:* Drainage systems could be installed during the grading operations. Drainage and dewatering are discussed in Sec. 12.4.

12.3 OTHER SITE IMPROVEMENT METHODS

12.3.1 Soil Replacement

As discussed in the previous section, soil replacement typically occurs during grading. As indicated in Table 12.1, there are basically two types of soil replacement methods: (1) removal and replacement and (2) displacement. The first method is the most common approach, and it consists of the removal of the compressible soil layer and replacement with structural fill during the grading operations. Usually the remove-and-replace grading option is only economical if the compressible soil layer is near the ground surface and the groundwater table is below the compressible soil layer, or the groundwater table can be economically lowered.

12.3.2 Water Removal

Table 12.1 lists several different types of water removal site improvement techniques. If the site contains an underlying compressible cohesive soil layer, the site can be surcharged with a fill layer placed at ground surface. Vertical drains (such as wick drains or sand drains) can be installed in the compressible soil layer to reduce the drainage path and to speed up the consolidation process. Once the compressible cohesive soil layer has had sufficient consolidation, the fill surcharge layer is removed and the building is constructed.

TABLE 12.1 Site Improvement Methods

Method	Technique	Principles	Suitable soils	Remarks
Soil replacement methods	Remove and replace	Excavate weak or undesirable material and replace with better soils	Any	Limited depth and area where cost-effective; generally $\leq$ 30 ft
	Displacement	Overload weak soils so that they shear and are displaced by stronger fill	Very soft	Problems with mud waves and trapped compressible soil under the embankment; highly dependent on specific site
Water removal methods	Trenching	Allows water drainage	Soft, fine-grained soils and hydraulic fills	Effective depth up to 10 ft; speed dependent on soil and trench spacing; resulting desiccated crust can improve site mobility
	Precompression	Loads applied prior to construction to allow soil consolidation	Normally consolidated fine-grained soil, organic soil, fills	Generally economical; long time may be needed to obtain consolidation; effective depth only limited by ability to achieve needed stresses
	Precompression with vertical drains	Shortens drainage path to speed consolidation	Same as above	More costly; effective depth usually limited to $\leq$ 100 ft
	Electroosmosis	Electric current causes water to flow to cathode	Normally consolidated silts and silty clays	Expensive; relatively fast; usable in confined area; not usable in conductive soils; best for small areas
Site strengthening methods	Dynamic compaction	Large impact loads applied by repeated dropping of a 5- to 35-ton weight; larger weights have been used	Cohesionless best; possible use for soils with fines; cohesive soils below groundwater table give poorest results	Simple and rapid; usable above and below the groundwater table; effective depths up to 60 ft; moderate cost; potential vibration damage to adjacent structures

TABLE 12.1 Site Improvement Methods

Method	Technique	Principles	Suitable soils	Remarks
	Vibrocompaction	Vibrating equipment densifies soils	Cohesionless soils with <20 percent fines	Can be effective up to 100-ft depth; can achieve good density and uniformity; grid spacing of holes critical, relatively expensive
	Vibroreplacement	Jetting and vibration used to penetrate and remove soil; compacted granular fill then placed in hole to form support columns surrounded by undisturbed soil	Soft cohesive soils (s_u = 15 to 50 kPa)	Relatively expensive
	Vibrodisplacement	Similar to vibroreplacement except soil is displaced laterally rather than removed from the hole	Stiffer cohesive soils (s_u = 30 to 60 kPa)	Relatively expensive
Grouting	Injection of grout	Fill soil voids with cementing agents to strengthen and reduce permeability	Wide spectrum of coarse- and fine-grained soils	Expensive; more expensive grouts needed for finer-grained soils; may use pressure injection, soil fracturing, or compaction techniques
	Deep mixing	Jetting or augers used to physically mix stabilizer and soil	Wide spectrum of coarse- and fine-grained soils	Jetting poor for highly cohesive clays and some gravelly soils; deep mixing best for soft soils up to 165 ft deep
Thermal	Heat	Heat used to achieve irreversible strength gain and reduced water susceptibility	Cohesive soils	High energy requirements; cost limits practicality
	Freezing	Moisture in soil frozen to hold particles together and increase shear strength and reduce permeability	All soils below the groundwater table; cohesive soils above the groundwater table	Expensive; highly effective for excavations and tunneling; high groundwater flows troublesome; slow process
Geosynthetics	Geogrids, geotextiles, geonets, and geomembranes	Use geosynthetic materials for filters, erosion control, water barriers, drains, or soil reinforcing	Effective filters for all soils; reinforcement often used for soft soils	Widely used to accomplish a variety of tasks; commonly used in conjunction with other methods (e.g., strip drain with surcharge or to build a construction platform for site access)

Source: Rollings and Rollings (1996).

12.3.3 Site Strengthening

Many different methods can be used to strengthen the on-site soil (see Table 12.1). Examples are as follows:

- *Dynamic compaction methods:* For example, heavy tamping consists of using a crane that repeatedly lifts and drops a large weight onto the ground surface in order to vibrate the ground and increase the density of near-surface granular soils. Although this method can increase the density of soil to a depth of 60 ft (18 m), it is usually only effective to depths of approximately 20 to 30 ft (6 to 9 m). In addition, this method requires the filling of impact craters and releveling of the ground surface.
- *Compaction piles:* Large-displacement piles, such as precast concrete piles or hollow steel piles with a closed end, can be driven into the ground to increase the density of the soil. The soil is densified by both the actual displacement of the soil and the vibration of the ground that occurs during the driving process. The piles are typically left in place, which makes this method more expensive than the other methods. In addition, there must be relatively close spacing of the piles in order to provide meaningful densification of soil between the piles.
- *Blasting:* Deep densification of the soil can be accomplished by blasting. This method has a higher risk of injury and damage to adjacent structures. There may be local restrictions on the use of such a method.
- *Compaction with vibratory probes:* Deep vibratory techniques, such as illustrated in Fig. 12.1, are often used to increase the density of loose sand deposits. This method is considered to be one of the most reliable and comprehensive methods for the mitigation of liquefaction hazard when liquefiable soils occur at depth (R. B. Seed 1991). Some techniques can be used to construct vertical gravel drains (discussed below).
- *Vertical gravel drains:* Vibroflotation or other methods are used to make a cylindrical vertical hole, which is filled with compacted gravel or crushed rock. These columns of gravel or crushed rock have a very high permeability and can quickly dissipate the earthquake-induced pore water pressures in the surrounding soil. This method can be effective in reducing the loss of shear strength, but it will not prevent overall site settlements. In addition, the method can be effective in relatively free-draining soils, but the vertical columns must be closely spaced to provide meaningful pore pressure dissipation. If the drain capacity is exceeded by the rate of pore pressure increase, there will be no partial mitigation (R. B. Seed 1991).

12.3.4 Grouting

There are many types of grouting methods that can be used to strengthen the on-site soil (see Table 12.1). For example, to stabilize the ground, fluid grout can be injected into the ground to fill in joints, fractures, or underground voids (Graf 1969, Mitchell 1970). For the releveling of existing structures, one option is *mudjacking,* which has been defined as a process whereby a water and soil-cement or soil-lime cement grout is pumped beneath the slab, under pressure, to produce a lifting force which literally floats the slab to the desired position (Brown 1992). Other site improvement grouting methods are as follows:

- *Compaction grouting:* A commonly used site improvement technique is compaction grouting, which consists of intruding a mass of very thick consistency grout into the soil, which both displaces and compacts the loose soil (Brown and Warner 1973; Warner 1978, 1982). Compaction grouting has proved successful in increasing the density of

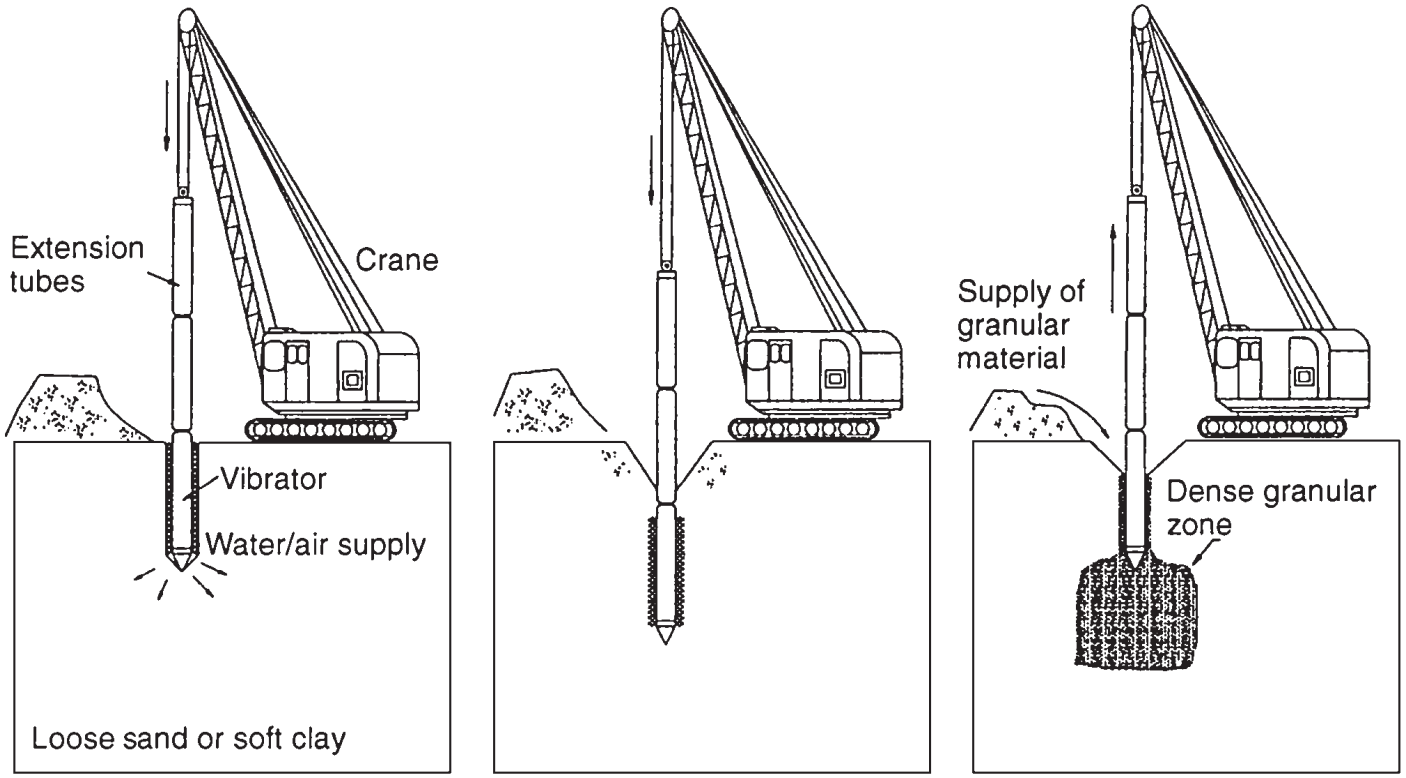

FIGURE 12.1 Equipment used for deep vibratory techniques. (*From Rollings and Rollings 1996, reprinted with permission of McGraw-Hill, Inc.*)

poorly compacted fill, alluvium, and compressible or collapsible soil. The advantages of compaction grouting are less expense and disturbance to the structure than foundation underpinning, and it can be used to relevel the structure. The disadvantages of compaction grouting are that it is difficult to analyze the results, it is usually ineffective near slopes or for near-surface soils because of the lack of confining pressure, and there is the danger of filling underground pipes with grout (Brown and Warner 1973).

- *Jet grouting* (*columnar*): This process is used to create columns of grouted soil. The grouted columns are often brittle and may provide little or no resistance to lateral movements and may be broken by lateral ground movements (R. B. Seed 1991).
- *Deep mixing:* Jetting or augers are used to physically mix the stabilizer and soil. There can be overlapping of treated columns in order to create a more resistant treated zone.

12.3.5 Thermal

As indicated in Table 12.1, the thermal site improvement method consists of either heating or freezing the soil in order to improve its shear strength and reduce its permeability. These types of soil improvement methods are usually very expensive and thus have limited uses.

12.3.6 Summary

Figure 12.2 presents a summary of site improvement methods as a function of soil grain size. Whatever method of soil improvement is selected, the final step should be to check the results in the field, using such methods as the cone penetration test (CPT) or standard penetration test (SPT). For example, Fig. 6.11 shows actual field test data, where standard penetration tests were performed before and after soil improvement. If the soil improvement is unsatisfactory, then it should be repeated until the desired properties are attained.

12.4 GROUNDWATER CONTROL

12.4.1 Introduction

The groundwater table (also known as the phreatic surface) is the top surface of underground water, the location of which is often determined from piezometers, such as an open standpipe. A perched groundwater table refers to groundwater occurring in an upper zone separated from the main body of groundwater by underlying unsaturated rock or soil.

Groundwater can affect all types of civil engineering projects. Probably more failures in geotechnical earthquake engineering are either directly or indirectly related to groundwater than to any other factor. Groundwater can cause or contribute to failure because of excess saturation, seepage pressures, uplift forces, and loss of shear strength due to liquefaction. It has been stated that uncontrolled saturation and seepage cause many billions of dollars yearly in damage. Examples of geotechnical and foundation problems due to groundwater are as follows (Cedergren 1989):

- Piping failures of dams, levees, and reservoirs
- Seepage pressures that cause or contribute to slope failures and landslides
- Deterioration and failure of roads due to the presence of groundwater in the base or subgrade
- Highway and other fill foundation failures caused by perched groundwater

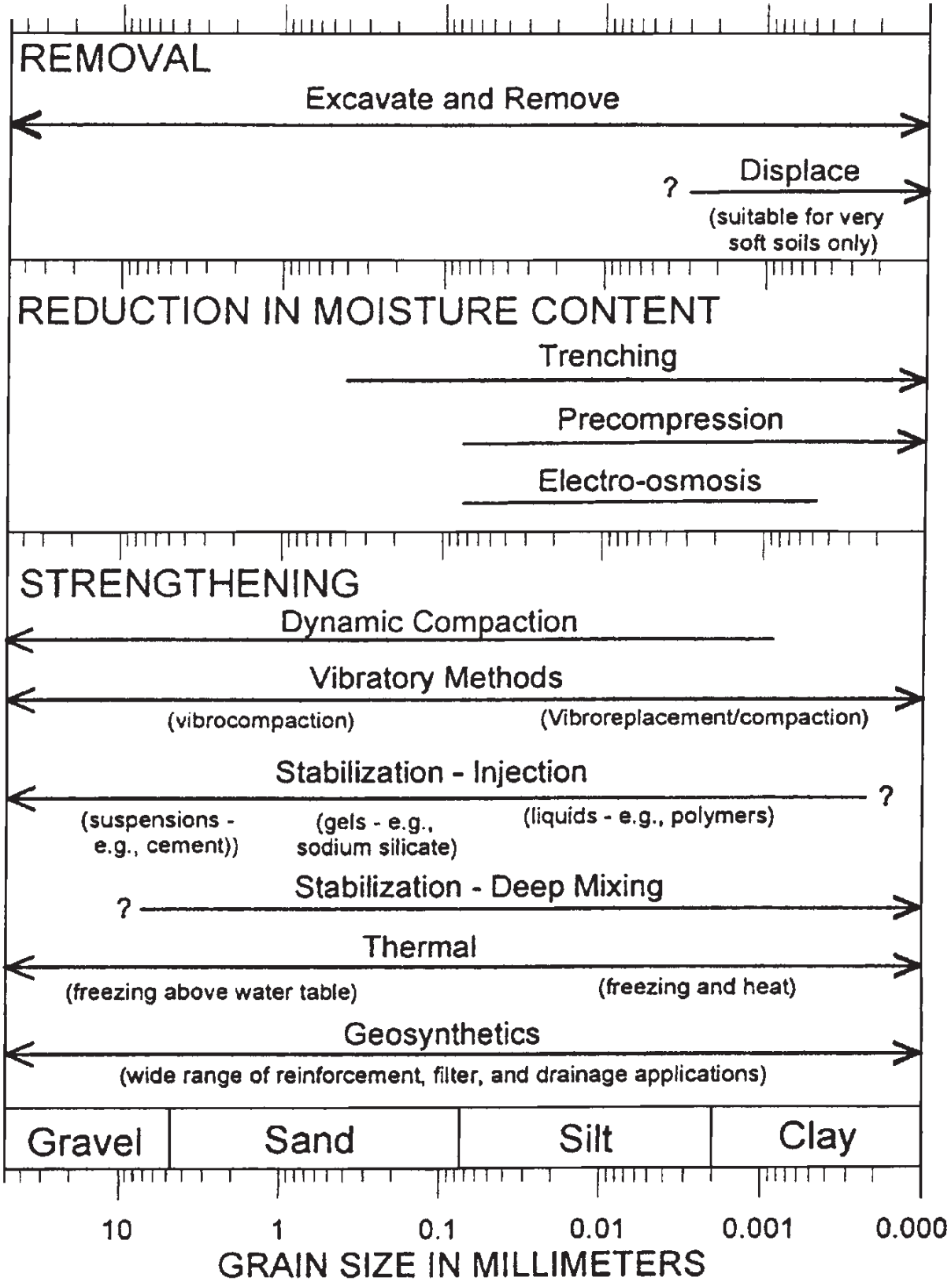

FIGURE 12.2 Site improvement methods as a function of soil grain size. (*From Rollings and Rollings 1996, reprinted with permission of McGraw-Hill, Inc.*)

- Earth embankment and foundation failures caused by excess pore water pressures
- Retaining wall failures caused by hydrostatic water pressures
- Canal linings, dry docks, and basement or spillway slabs uplifted by groundwater pressures
- Soil liquefaction, caused by earthquake shocks, because of the presence of loose granular soil that is below the groundwater table

Proper drainage design and construction of drainage facilities can mitigate many of these groundwater problems. For example, for canyon and drainage channels where fill is to be placed, a canyon subdrain system should be installed to prevent the buildup of groundwater in the canyon fill. The drain consists of a perforated pipe (perforations on the underside of the pipe), an open graded gravel around the pipe, with the gravel wrapped in a geofabric that is used to prevent the gravel and pipe from being clogged with soil particles.

12.4.2 Methods of Groundwater Control

For sites that have highly permeable soil and that are adjacent to a large body of water, such as coastal areas, it is usually not economical to permanently lower the groundwater table. However, for other sites, it may be possible to use groundwater control to mitigate earthquake effects. Table 12.2 lists various methods of groundwater control.

One commonly used method of lowering the groundwater table is to install a well point system with suction pumps. The purpose of this method is to lower the groundwater table by installing a system of perimeter wells. As illustrated in Fig. 12.3, this method is often utilized for temporary excavations, but it can also be used as a permanent groundwater control system. The well points are small-diameter pipes having perforations at the bottom ends. Pumps are used to extract water from the pipes, which then lowers the groundwater table, as illustrated in Fig. 12.3. It is important to consider the possible damage to adjacent structures caused by the lowering of the groundwater table at the site. For example, lowering of the groundwater table could lead to consolidation of soft clay layers or rotting of wood piling.

Another type of system that can be installed for groundwater control consists of a sump. Figure 12.4 illustrates the basic elements of this system.

12.4.3 Groundwater Control for Slopes

Groundwater can affect slopes in many different ways. Table 12.3 presents common examples and the influence of groundwater on slope failures. The main destabilizing factors of groundwater on slope stability are as follows (Cedergren 1989):

1. Reducing or eliminating cohesive strength
2. Producing pore water pressures which reduce effective stresses, thereby lowering shear strength
3. Causing horizontally inclined seepage forces which increase the driving forces and reduce the factor of safety of the slope
4. Providing for the lubrication of slip surfaces
5. Trapping of groundwater in soil pores during earthquakes or other severe shocks, which leads to liquefaction failures

There are many different construction methods that can be used to mitigate the effects of groundwater on slopes. During construction of slopes, built-in drainage systems can be installed. For existing slopes, drainage devices such as trenches or galleries, relief wells, or horizontal drains can be installed. Another common slope stabilization method is the construction of a drainage buttress at the toe of a slope. In its simplest form, a drainage buttress can consist of cobbles or crushed rock placed at the toe of a slope. The objective of the drainage buttress is to be as heavy as possible to stabilize the toe of the slope and also have a high permeability so that seepage is not trapped in the underlying soil.

TABLE 12.2 Methods of Groundwater Control

Method	Soils suitable for treatment	Uses	Comments
Sump pumping	Clean gravels and coarse sands	Open shallow excavations	Simplest pumping equipment. Fines easily removed from the ground. Encourages instability of formation. See Fig. 12.4
Well-point system with suction pump	Sandy gravels down to fine sands (with proper control can also be used in silty sands)	Open excavations including utility trench excavations	Quick and easy to install in suitable soils. Suction lift limited to about 18 ft (5.5 m). If greater lift needed, multistage installation is necessary. See Fig. 12.3
Deep wells with electric submersible pumps	Gravels to silty fine sands, and water-bearing rocks	Deep excavation in, through, or above water-bearing formations	No limitation on depth of drawdown. Wells can be designed to draw water from several layers throughout its depth. Wells can be sited clear of working area
Jetting system	Sands, silty sand, and sandy silts	Deep excavations in confined space where multistage well points cannot be used	Jetting system uses high-pressure water to create vacuum as well as to lift the water. No limitation on depth of drawdown
Sheet piling cutoff wall	All types of soil (except boulder beds)	Practically unrestricted use	Tongue-and-groove wood sheeting utilized for shallow excavations in soft and medium soils. Steel sheet piling for other cases. Well-understood method and can be rapidly installed. Steel sheet piling can be incorporated into permanent works or recovered. Interlock leakage can be reduced by filling interlock with bentonite, cement, grout, or similar materials
Slurry trench cutoff wall	Silts, sands, gravels, and cobbles	Practically unrestricted use; extensive curtain walls around open excavations	Rapidly installed. Can be keyed into impermeable strata such as clays or soft shales. May be impractical to key into hard or irregular bedrock surfaces, or into open gravels

TABLE 12.2 Methods of Groundwater Control (*Continued*)

Method	Soils suitable for treatment	Uses	Comments
Freezing: ammonium and brine refrigerant	All types of saturated soils and rock	Formation of ice in void spaces stops groundwater flow	Treatment is effective from a working surface outward. Better for large applications of long duration. Treatment takes longer time to develop
Freezing: liquid nitrogen refrigerant	All types of saturated soils and rock	Formation of ice in void spaces stops groundwater flow	Better for small applications of short duration where quick freezing is required. Liquid nitrogen is expensive and requires strict site control. Some ground heave could occur
Diaphragm structural walls: structural concrete	All soil types including those containing boulders	Deep basements, underground construction, and shafts	Can be designed to form a part of the permanent foundation. Particularly efficient for circular excavations. Can be keyed into rock. Minimum vibration and noise. Can be used in restricted space. Also can be installed very close to the existing foundation
Diaphragm structural walls: bored piles or mixed-in-place piles	All soil types, but penetration through boulders may be difficult and costly	Deep basements, underground construction, and shafts	A type of diaphragm wall that is rapidly installed. Can be keyed into impermeable strata such as clays or soft shales

Sources: NAVFAC DM-7.2 (1982), based on the work by Cashman and Harris (1970).

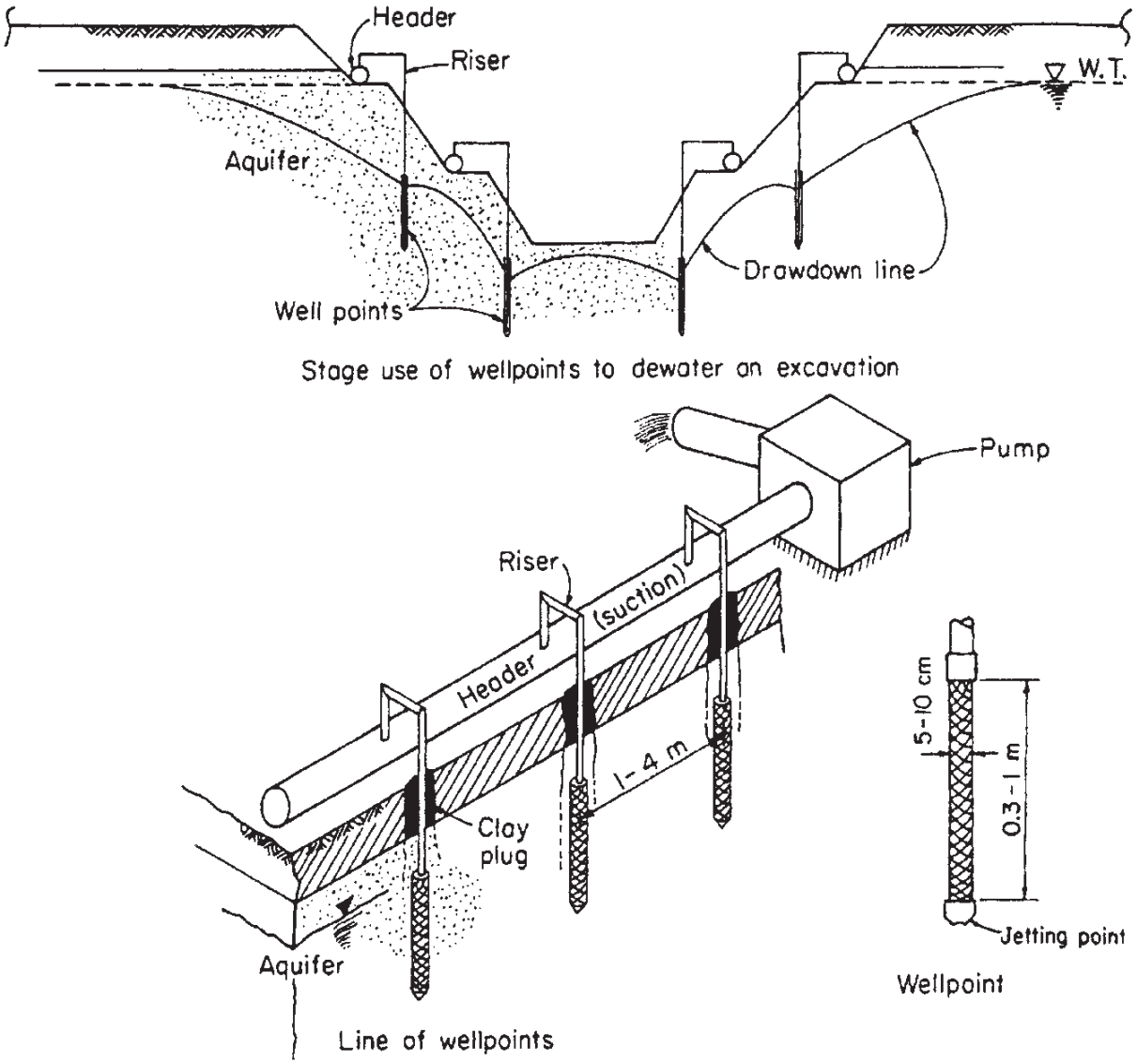

FIGURE 12.3 Groundwater control: well point system with suction pump. (*From Bowles 1982, reprinted with permission of McGraw-Hill, Inc.*)

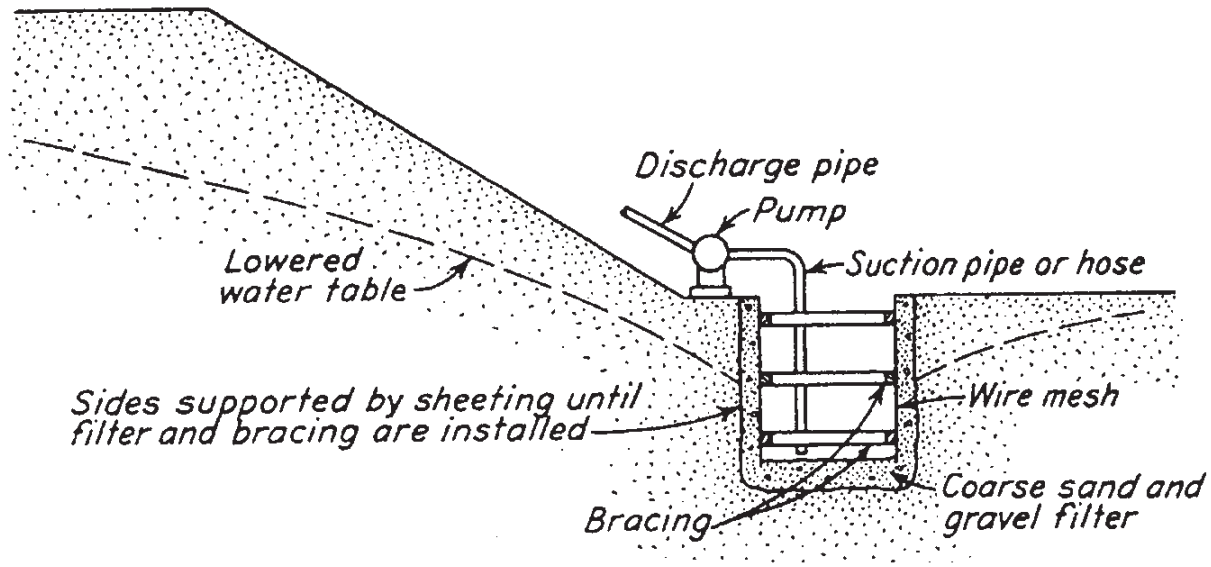

FIGURE 12.4 Groundwater control: example of a sump being used to lower the groundwater table. (*From Peck, Hanson, and Thornburn 1974, reprinted with permission of John Wiley & Sons.*)

TABLE 12.3 Common Groundwater Conditions Causing Slope Failures

Kind of slope	Conditions leading to failure	Type of failure and its consequences
Natural earth slopes above developed land areas (homes, industrial)	Earthquake shocks, heavy rains, snow, freezing and thawing, undercutting at toe, mining excavations	Mud flows, avalanches, landslides; destroying property, burying villages, damming rivers
Natural earth slopes within developed land areas	Undercutting of slopes, heaping fill on unstable slopes, leaky sewers and water lines, lawn sprinkling	Usually slow creep type of failure; breaking water mains, sewers, destroying buildings, roads
Reservoir slopes	Increased soil and rock saturation, raised water table, increased buoyancy, rapid drawdown	Rapid or slow landslides, damaging highways, railways, blocking spillways, leading to over-topping of dams, causing flood damage with serious loss of life
Highway or railway cut or fill slopes	Excessive rain, snow, freezing, thawing, heaping fill on unstable slopes, undercutting, trapping groundwater	Cut slope failures blocking roadways, foundation slipouts removing roadbeds or tracks, property damage, some loss of life
Earth dams and levees, reservoir ridges	High seepage levels, earthquake shocks; poor drainage	Sudden slumps leading to total failure and floods downstream, much loss of life, property damage
Excavations	High groundwater level, insufficient groundwater control, breakdown of dewatering systems	Slope failures or heave of bottoms of excavations; largely delays in construction, equipment loss, property damage

Source: Cedergren 1989.